PB84-105329

Study of Aftertreatment and Fuel Injection Variables for Particulate Control in Heavy-Duty Diesel Engines

Michigan Technological Univ., Houghton.

Prepared for

Environmental Protection Agency, Ann Arbor, MI.
Emission Control Technology Div.

30 Nov 82

U.S. Department of Commerce
National Technical Information Service
NTIS

TECHNICAL REPORT DATA

(Please read Instructions on the reverse before completing)

1. REPORT NO.
EPA 460/3-83-002

2.

3. RECIPIENT'S ACCESSION NO.
PB8 4 105329

4. TITLE AND SUBTITLE
Study of Aftertreatment and Fuel Injection Variables for Particulate Control In Heavy-Duty Diesel Engines.

5. REPORT DATE
November 30, 1982

6. PERFORMING ORGANIZATION CODE

7. AUTHOR(S)
Jackson P. School, Susan T. Bagley, David G. Leddy and John H. Johnson.

8. PERFORMING ORGANIZATION REPORT NO.

9. PERFORMING ORGANIZATION NAME AND ADDRESS
Michigan Technological University
Houghton, Michigan 49931

10. PROGRAM ELEMENT NO.

11. CONTRACT/GRANT NO.
68-03-2794

12. SPONSORING AGENCY NAME AND ADDRESS
U.S. Environmental Protection Agency
Office of Mobile Sources
Emission Control Technology Division
Ann Arbor, MI 48105

13. TYPE OF REPORT AND PERIOD COVERED
FINAL

14. SPONSORING AGENCY CODE

15. SUPPLEMENTARY NOTES

16. ABSTRACT

This report summarizes the results of a multiyear project funded by the Environmental Protection Agency (EPA) to provide data on the impact of engine operating parameters, fuels, and exhaust aftertreatment devices on the physical, chemical and biological character of diesel particulates. These data are useful for determining whether various control technologies can minimize the health and welfare impact of diesel particulates on society. Two main studies are emphasized: 1) the results of varying fuel injection parameters and 2) the evaluation and characterization of available (current technology) as well as aftertreatment devices, including catalysts and particulate traps. A brief study of an adiabatic engine is also examed.

17. KEY WORDS AND DOCUMENT ANALYSIS

a. DESCRIPTORS		b. IDENTIFIERS/OPEN ENDED TERMS	c. COSATI Field/Group
Catalysts	Motor Vehicles	EPA	
Diesel Engines	Traps	Heavy Duty Vehicles	
Diesel Particulates		Engines	
Exhaust Emissions			
Fuel Injection			
Particulate Traps			
Particles			

18. DISTRIBUTION STATEMENT
release unlimited

19. SECURITY CLASS *(This Report)*
unclassified

20. SECURITY CLASS *(This page)*
unclassified

21. NO. OF PAGES
388

22. PRICE

EPA Form 2220-1 (9-73)

United States
Environmental Protection
Agency

Office of Mobile Sources
Emission Control Technology Division
2565 Plymouth Road
Ann Arbor, MI 48105

EPA 460/3-83-002

PB84-105329

Air

EPA

Study of Aftertreatment and Fuel Injection Variables for Particulate Control in Heavy-duty Diesel Engines

REPRODUCED BY
NATIONAL TECHNICAL
INFORMATION SERVICE
U.S. DEPARTMENT OF COMMERCE
SPRINGFIELD, VA 22161

EPA-460/3-83-002

FINAL REPORT

STUDY OF AFTERTREATMENT AND FUEL INJECTION VARIABLES FOR PAPTICULATE CONTROL IN HEAVY-DUTY DIESEL ENGINES

November 30, 1982

by

Jackson P. Scholl
Susan T. Bagley
David G. Leddy
John H. Johnson

Contract No. 68-03-2794

Michigan Technological University
Houghton, Michigan 49931

This report was furnished to the Environmental Protection Agency by Michigan Technological University, Houghton, Michigan, in fulfillment of Contract No. 68-03-2794. The contents of this report are reproduced herein as received from Michigan Technological University. The opinions, findings, and conclusions expressed are those of the authors and not necessarily those of the Environmental Protection Agency. Mention of company or product names is not to be considered as an endorsement by the Environmental Protection Agency.

Publication No. EPA 460/3-83-002

CONTENTS

Page

Nomenclature iv
Executive Summary v

1. INTRODUCTION 1

General Background. 1
Injection Parameter Modifications 3
Aftertreatment Devices. 8
Oxidation Catalysts 8
Particulate Traps and Filtration Theory 10

2. EXPERIMENTAL 19

Sample Collection and Emissions Measurements. 19
Chemical Characterization 28
Biological Characterization 34

3. RESULTS AND DISCUSSION 37

Mack ENDT-676 - Fuel Injection Parameter Study. 37
Engine and Injection Equipment 37
Effect of Piston Bowl and Nozzle Orifice Diameter/Number. . . 45
Effect of Increased Rate of Injection 53
Effect of Static Port Closure Timing 62
Injection Rate vs. Injection Timing 71
Effect of Higher Sac-Volume Nozzles 77
Effect of Timing and Ultra-High Injection Rate 78
Recommended Fuel Injection Characteristics 84

Caterpillar 3208 - Aftertreatment Device Study. 95
Engine Specifications 95
Englehard PTX Oxidation Catalyst 95
Engine Test Set-up 95
Effects of Catalyst on Mass Emissions 101
Ames Bioassay Variability and Strain Differences 125
Effect of Catalyst on Ames Biological Activity 129
Effect of Shale Fuel on PTX Catalyst Operation 137
Johnson-Matthey Close-Coupled Port Catalysts 142
Effects on Engine Operating Conditions and Gaseous Emissions - Number 2 Fuel 152
Effects on Particulate Emissions - Number 2 Fuel 152
Effects on Emissions - Shale Fuel. 165
Ames Bioassay Results 169
Corning EX-47 Uncatalyzed Particulate Traps 174
Effects on Engine Operating Conditions 174
Effects on Gaseous and Particulate Emissions 176
Ames Bioassay Results 193
Discussion of Trap Behavior. 193

Adsorption and SOF/SOLID Ratio. 216
Johnson-Matthey Cylindrical Mesh Trap 217

Cummins Adiabatic Engine - Alternate Fuel Samples 223
Effects of Operating Conditions on Ames Bioassay Results . 225

4. CONCLUSIONS 227

Mack ENDT-676 - Fuel Injection Parameter Study. 227
Caterpillar 3208 - Aftertreatment Device Study. 229
Cummins Adiabatic Engine - Alternate Fuel Samples 236

5. RECOMMENDATIONS FOR FUTURE RESEARCH 237

References 240

Appendix A. - Engine Test Summary. 247

Appendix B. - Ames Bioassay Variability and Data Quantification 285
Sensitivity Analysis Experiments. 285
Quantification of Ames Data 293
Reproducibility of Ames Data. 311
Ames Bioassay Results of Selected Data. 318
Bioassay Test Summary. 336

Appendix C. - Non-Routine Chemical Investigations 342
CRC Round-Robin 342
Sephadex LH-20 Lipophilic Gel 346
Sulfate Analysis by Ion Chromatography versus the Barium Chloranilate Method 353
SOF Subfraction Summary. 357

NOMENCLATURE

SOF - soluble organic fraction
DI - direct injection
Φ - equivalence ratio = $(\text{fuel/air})_{\text{actual}}/(\text{fuel/air})_{\text{stoichiometric}}$
HFID - heated flame ionization detector
HC - hydrocarbons
DCM - dichloromethane
TDC - top dead center
TPM - total particulate matter
CRC - Coordinating Research Council
BS - Brake - specific (referenced to engine power output)
FC - Fuel Consumption
SA_{SL} - Specific Activity, Semilog Transformation
SA_{LL} - Specific Activity, Log-Log Transformation
SOLID - defined as TPM -SOF -sulfate
BTC - Before Top Center
NO - Nitric Oxide
NO_2 - Nitrogen Dioxide
NO_x - Oxides of Nitrogen
EIN - Ether Insoluble Subfraction
BAS - Basic Subfraction
ACD - Acidic Subfraction
PRF - Paraffin Subfraction
ARM - Aromatic Subfraction
TRN - Transitional Subfraction
OXY - Oxygenated Subfraction
HIN - Hexane Insoluble Subfraction
OMMP - Order of Magnitude Mutagenic Potential
SRCII - Solvent-refined coal-derived fuel, middle distillate

EXECUTIVE SUMMARY

Particulate control technologies for heavy-duty diesel engines were investigated experimentally. This research was performed as part of a multiyear project funded by the United States Environmental Protection Agency (USEPA) to provide data on the impact of engine operating parameters, fuels, and exhaust aftertreatment devices on the physical, chemical, and biological character of diesel particulates. These data are useful for determining whether various control technologies can minimize the health and welfare impact of diesel particulates on society.

This report emphasizes two main studies: (1) the result of varying fuel injection parameters and (2) the evaluation and characterization of presently available (current technology) as well as advanced aftertreatment devices, including catalysts and particulate traps. A brief study of an adiabatic engine was carried out in cooperation with the Cummins Engine Co. The background, experimental plan followed, results of the experiments, and conclusions relative to each control strategy are presented in the report.

Fuel injection parameters were studied using a Mack ENDT-676 diesel engine equipped with several advanced high-injection-rate fuel injection systems. The effects of load, engine speed, increased fuel injection rates, retarded injection timing, and injector nozzle sac volume were evaluated. Aftertreatment devices were characterized using a Caterpillar 3208 engine. An Englehard PTX oxidation catalyst, a Johnson-Matthey close-coupled port catalyst, a Corning particulate trap, and a Johnson-Matthey trap were all evaluated. Fuel effects on catalyst performance were examined using No. 1, No. 2, and a shale-derived fuel.

Particulate samples which had been collected by Cummins from an experimental adiabatic engine were also examined. The effects of mode and fuel on the biological activity of the particulates were studied.

The engines were mounted on a dynamometer and operated over the EPA 13-mode cycle. Particulate samples were collected from the exhaust using the Michigan Tech dilution tunnel. Particulates were characterized by measuring (1) total particulates generated, (2) soluble organic fraction, (3) composition of subfractions of the soluble organic fraction, (4) percent sulfates in the particulates, (5) percent solids in the particulates, and (6) biological activity (as determined by the Ames Salmonella/microsome bioassay). Gas-phase composition of NO_2, NO, and hydrocarbons was constantly monitored in the experiments. The results of all physical and chemical measurements have been reported as mass per cubic meter of exhaust, as well as in brake-specific terms. Biological activities are reported as revertants per microgram, as well as in brake-specific terms.

The results of the fuel-injection parameter studies showed that increased fuel injection rates (at constant timing) reduced solids formation, soluble organic fraction, and brake-specific fuel consumption, while NO and NO_2 increased. Increased biological activity of the soluble organic fraction at high injection rates offset the corresponding reduction of the soluble organic fraction in terms of the brake-specific revertants from the Ames test.

Retarded injection timing (at higher injection rates) increased solid particulates and brake-specific fuel consumption, but decreased the soluble organic fraction, NO, and NO_2. The acidic fraction of the soluble organic fraction increased, while the ether-insoluble fraction decreased (the other subfractions did not always decrease as might be expected.) A larger injector sac volume increased hydrocarbons, solids, and the soluble organic fraction. There was little reduction in NO_x.

The use of the Englehard PTX catalyst had little impact on total NO_x, but converted NO to NO_2 in most modes. The catalyst decreased the soluble organic fraction and hydrocarbons for all cases, while sulfate emissions increased. The increase in solid particulates in most cases is thought to be due to the dehydrogenation of organic compounds on the catalyst surface to create new species with a very high molecular weight and a low hydrogen-to-carbon ratio. Biological activity of the soluble organic fraction is generally increased by the PTX catalyst.

The Johnson-Matthey close-coupled catalyst decreased hydrocarbons and the soluble organic fraction in all cases, while the sulfates increased, although less so than for the PTX catalyst. Solid particulates did not change significantly except for mode 11. Rated-speed modes showed the largest increases in this parameter, due to increases in sulfate formation and dehydrogenation of organic compounds. Biological activity increased at all intermediate-speed modes and decreased at rated-speed modes. A reduction in brake-specific revertants was found at all modes with the greatest reductions at rated speed.

Corning particulate traps decreased hydrocarbons at all speeds with the greatest reductions at rated speed. Sulfates were reduced significantly at all speeds and loads. Solids emissions and, consequently, total particulates were reduced significantly, especially at rated speed. Biological activity of the soluble organic fraction increased at all modes but mode 3. Brake-specific revertants were dramatically reduced for most modes, but very high biological activities of certain subfractions of the soluble organic fraction suggested that certain compounds produced in the trap might be potentially toxic. This trap also showed increased back pressure with time, and an operating temperature of about 500°C was necessary for continuous regeneration.

The use of the Johnson-Matthey trap resulted in increased brake-specific fuel consumption and NO_2 at most modes with large reductions in hydrocarbons. Total particulates, as the result of increased sulfate emissions, increased at most modes. The pressure drop across the trap increased with time, with the greatest increases at modes 3 and 11 and slight increases for the other modes.

In summary, each control technology has its strong and weak points. The selection of the appropriate method depends upon a number of factors, such as the availability of fuel with a uniform composition, the way the engine will be operated, whether or not the engine and/or the device will be properly operated and maintained, and the initial and operating cost of the device.

A fuel injection system with ideal injection characteristics could theoretically be an effective means for controlling diesel NO_x and particulate emissions. In practice, however, this effectiveness is not easily obtained. The control of injection rate and timing is difficult, although electronically controlled fuel injection systems should be able to do this in the future. In addition, sophisticated high-pressure, high-rate injection systems could be more expensive.

Particulate traps promise the most economical means of emission control, and the Corning ceramic traps discussed here were superior to the other three devices tested. Still, the variability of fuels and operating conditions necessitates use of this device only under continuous particulate burn-off (regeneration) conditions to avoid localized release of material possibly more hazardous than untreated exhaust. Further investigation of organic gaseous emissions from these traps is also needed before their general use is advised.

For new production engines, adiabatic or insulated components may offer greater fuel economy, but the production of durable ceramics and other materials for the general market using such a control strategy may not be competitive in the near term.

INTRODUCTION

Diesel engines have distinct advantages over spark-ignition engines due to their lower fuel consumption and gaseous hydrocarbon and carbon monoxide emissions. The prime disadvantages of diesel engines are the atmospheric visibility and soiling degradation (1)* and possible adverse health effects (2) caused by much higher particulate emissions than spark ignition engines. Present control technology for diesel particulate includes a variety of aftertreatment devices as well as engine and fuel modifications.

The main objectives of this contract were: a) to evaluate and characterize various presently available aftertreatment devices that may be applicable for the control or minimization of diesel particulate, b) to evaluate advanced aftertreatment devices or methods which could minimize diesel particulate, and c) to ascertain the size, characteristics, and magnitude of diesel engine particulate. In this report, a brief background on each emission control strategy employed during the course of this contract will be presented, followed by the experimental, results, and conclusions sections, each of which is subdivided according to control strategy.

GENERAL BACKGROUND

Diesel particulate is composed of liquid and solid components and may be roughly described as agglomerates of carbonaceous particles (solid) upon which is layered liquid organic material (SOF or the soluble organic fraction), and liquid sulfuric acid. The SOF contains a wide variety of compounds, many of which arise from the combustion process (3). Table 1.1 gives the major compound classes present in diesel SOF, as well as typical compounds for each class. Because of the correlation between compounds that are mutagenic in bacterial test systems and those that are carcinogenic in mammalian test systems (4,5,6) microbial assays are used to screen particulate SOF samples as a first step to assess potential adverse health effects (7,8,9,10). The aromatic and transitional classes have shown the most potential for being harmful to health; however, many of the other compounds as yet unidentified in diesel exhaust may be responsible for much of the observed mutagenic activity (11). The great variety of compounds present in diesel SOF suggests that no single compound or class of compounds should account for the total observed mutagenic activity. The resolution and identification of the mutagenic compounds would require extensive analytical separation work and biological characterization.

---

*Numbers in brackets are references

The sulfuric acid component of diesel particulate arises from oxidation of the sulfur present in diesel fuel, which is converted into sulfate to the extent of 2-4% of the fuel sulfur by mass for engines without an exhaust aftertreatment device (14). The majority of sulfur not converted to sulfuric acid is primarily SO_2, although a small portion of that not converted appears as elemental sulfur in the particulate (15).

Table 1.1 Typical Compounds Found in Diesel SOF Subfractions (4,11,12,13)

Paraffinic Compounds	Aromatic Compounds	Acidic Compounds
n-Tetradecane	Ethyl naphthalene	Cresol
n-Hexadecane	Phenanthrene	Phenylphenols
n-Eicosane	Fluoranthene*	Naphthols
	Benzo(a)pyrene*	Naphthoic acid
	Methyl phenanthrene*	Benzoic acids
	Dibenzanthracenes	
Basic Compounds	**Transitional Compounds**	**Oxygenated Compounds**
Benzacridine	1-Nitropyrene*	9, 10-Anthraquinone
Methyl aniline	9-Fluorenone	Hydroquinone
o-Toluidine	2-Methyl-9-anthrone	Benzanthrone
Dibenzo(c,g)carbazole	1,8-Naphthalic acid anhydride	Dinitro-o-cresol

*Known mutagens

The gaseous emissions in diesel exhaust include CO (usually quite low), hydrocarbons, and oxides of nitrogen. Hydrocarbons, as measured in the raw exhaust, contribute to the SOF appearing with the particulate, and the fraction of hydrocarbons measured as particulate SOF is a function of exhaust temperature, HC concentration and dilution ratio, as well as mixture temperature at the filter. Oxides of nitrogen, primarily NO and NO_2, are formed during the highest temperature portion of the combustion cycle (16) and are directly involved in atmospheric oxidation and (with traces of nitric acid) nitration of organic material (17). The presence of nitro aromatics in diesel SOF, or perhaps in noncondensed diesel hydrocarbons, is of concern because of the high mutagenic potency of these compounds (11). Long-term health effects of such compounds are unknown and deserve serious attention.

INJECTION PARAMETER MODIFICATIONS

Most of the work done on diesel emissions has shown that combustion and pollutant formation is highly dependent on fuel-air mixing. Diesel combustion is complicated by the fact that the fuel is injected into the combustion chamber as a liquid. The atomization into droplets, dispersion, and vaporization of fuel largely precede combustion, but both homogeneous (gas-phase) and heterogeneous (liquid-phase) combustion take place. Figure 1.1a is a schematic showing the fuel spray in a typical DI diesel engine (18). This shows the spray divided into three main regions based on values of Φ (equivalence ratio). Region 1 (the spray core) contains large droplets which have not sufficiently atomized and mixed with air to support a flame. Region 2 contains fuel droplets and combustible fuel-air mixture of $\Phi \simeq 1$.

This is the region in which combustion begins and proceeds as fuel from region 1 evaporates and mixes with air from region 3, where the mixture is too lean to support combustion. The wall jets (Figure 1.1b) which reflect fuel

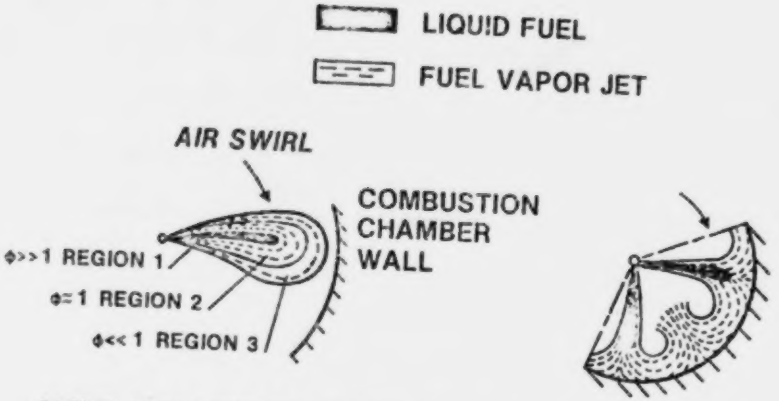
LIQUID FUEL
FUEL VAPOR JET
AIR SWIRL
COMBUSTION CHAMBER WALL
$\phi >> 1$ REGION 1
$\phi \approx 1$ REGION 2
$\phi << 1$ REGION 3

A) FUEL SPRAY DIVIDED INTO REGIONS BASED ON EQUIVALENCE RATIO

B) FORMATION OF WALL JETS, NO WET IMPINGEMENT

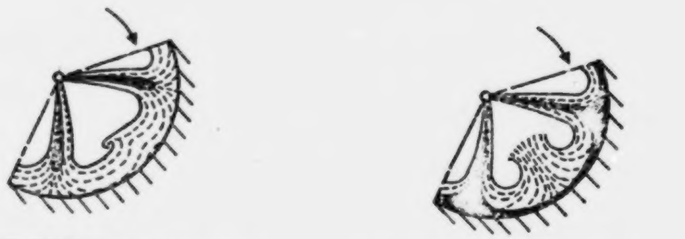

C) FUEL VAPOR IMPINGEMENT

D) WET FUEL IMPINGEMENT WITH WALL JETS

Fig. 1.1 - Schematic of fuel injection regions based on equivalence ratio (ϕ) (reference 18)

vapor away from the cylinder wall act to remove vapor from quench areas near the wall and complete fuel-air mixing. If these wall jets do not form (Figure 1.1c), air swirl must supply the mixing necessary for good combustion. If fuel spray penetration is too great, wet fuel can impinge upon the wall (Figure 1.1d) and will be a source of particulate and HC if air swirl cannot vaporize and mix it sufficiently. Of the sprays depicted here, Figures 1.1a and 1.1b will respond to an increase in fuel injection rate; the others will not, as increased rates of injection merely deposit more fuel on the wall (18). The zones for emission formation include regions 1 (where carbonaceous solids are likely to originate) and 3 (where very low equivalence ratios lead to unburned HC emissions). Region 2 is the premixed region where ignition occurs and does not contribute significantly to emissions.

In a diesel engine the start of ignition is controlled largely by the temperature of the air-fuel charge. A finite time period, the ignition delay, is required for physical mixing and atomization plus chemical pre-ignition reactions to occur before combustion begins. The cylinder charge temperature is at a maximum just a few degrees before TDC, where heat loss to the walls begins to cool the charge faster than compression raises it. The maximum cylinder charge temperature corresponds to minimum ignition delay, and advancing fuel injection timing from this point lengthens the ignition delay; however, this increase is somewhat less than injection advance (19), leading to auto-ignition occurring earlier in the cycle. Thus, peak temperature of a burning air-fuel mixture is actually somewhat before minimum ignition delay, and more complete combustion is achieved by advancing the timing. Another advantage of advancing the timing is the increased opportunity for air swirl to effect fuel evaporation and mixing, leading to lower HC and particulate emissions.

Although advanced timing leads to more complete combustion, the increased peak temperature is a source of NO_x emissions. Aoyagi et al. (16) found that formation of NO did not occur until some 15 crank angle degrees after initial formation of particulate. Since carbon formation occurs in temperature regions between 2000° and 2400°F, one way to decrease both carbon and NO formation would be to mix the air-fuel charge very rapidly after injection at minimum ignition delay, achieving very high cylinder temperatures, then cool the mixture by expansion to avoid NO formation. The noise and durability problems associated with such an injection strategy may limit its usefulness but a certain amount of this rapid, retarded injection may be allowable and beneficial if used in conjunction with certain design modifications. These include 1) reduction of nozzle orifice volume, 2) air inlet port design optimization to ensure rapid, adequate mixing, and 3) spray geometries which avoid wet fuel impingement under high injection pressures. It should be noted, however, that excessive mixing must be avoided because it could inhibit auto-ignition or lead to formation of quench regions if it exceeds the combustion rate. Thus, advanced fuel injection systems are preferable to air swirl modification to control emissions.

Greeves (18) has defined a rate parameter, representing the value of air entrainment completed in a given crank angle since the start of fuel injection:

$$RP = \frac{F}{\theta} \frac{d_o}{d} \left[\frac{n_o}{n}\right]^{1/3} \left[\frac{F_o}{F}\right]^{2/3} \left[\frac{\rho}{\rho_o}\right]^{1/3} ,$$

where

RP = rate parameter (mm^3 fuel/°CA)

d = orifice dia. (mm)

d_o = reference orifice dia. (0.28mm)

F = quantity fuel injected (mm^3/stroke)

F_o = reference quantity fuel injected (60mm^3/stroke)

Θ = period of fuel injection (°CA)

n = number of nozzle holes

n_o = reference number of nozzle holes (4)

ρ = charge density (kg/m^3)

ρ_o = reference charge density at end of compression for an NA engine with 16:1 compression ratio (18.7 kg/m^3)

This parameter can be used to help relate the rate of fuel injection to the rate of fuel-air mixing. Solid particulate emissions should result from a higher value of this parameter, which is used in this report to help correlate particulate and NO_x emissions to the mixing rate.

Table 1.2 summarizes effects of engine speed and load on selected engine parameters and resultant emissions. Increased engine speed should reduce ignition delay by accelerating pre-ignition reactions (increased gas wall temperatures) and lead to more fuel being burned by diffusion combustion (heterogeneously). Although this may lead to higher particulate, the more rapid rates of mixing should increase oxidation. Brysik and Smith (20) saw an increase in solid emissions with speed, while other workers (21,22) found a decrease. While it appears that NO should increase with the higher temperatures associated with higher speeds, it is actually decreased (21,22,23,24) probably due to the reduced residence time. Increased load should lead to an increase in solids and NO and NO_2 formation due to higher Φ and cycle temperatures with no accompanying mixing rate increase.

Table 1.2: The General Effects of Engine Speed and Load on Selected Emissions

Engine Speed ↑(a)	HC and SOF	Solids Formation	Solids Oxidation	NO and NO_2 Formation	NO_2 Survival
Mixing rates ↑	↑	↓	↑	↓	↑
Cycle temperature ↑	↓	↑	↑	↑	↓
Ignition delay ↓	↓	↑	–	–	–
Time for reactions ↓	↑	–	↓	–	↑
Overall effect	↑	↑	↑	↓(b)	↑
Engine Load ↑					
Cycle temperature ↑	↓	↑	↑	↑	↓
Φ ↑	↑	↑	↓	↓	↓
Overall effect	↓	↑	↓	↑	↓

(a) ↑ indicates an increase, ↓ indicates a decrease, – indicates no change.

(b) While it appears that NO should increase, experimental results show it decreases; the increase in mixing rate probably affects NO most by reducing the residence time in the reaction zones.

AFTERTREATMENT DEVICES

Of the various aftertreatment devices for control of diesel particulate emissions, two main categories may be distinguished: those that collect particulate as it passes (traps); and those that oxidize particulate as it passes the device without collection (oxidation catalysts). Each type of device will be discussed separately.

Oxidation Catalysts

Oxidation catalysts have had limited use on diesel engines until recently. Their prime purpose has been to oxidize CO to CO_2 and HC to CO_2 and H_2O where diesels are used in enclosed environments, such as on underground mining vehicles. One consequence of an oxidation catalyst on spark-ignition engine emissions is the oxidation of SO_2 and SO_3 and release as sulfate (25,26). Despite its ability to reduce particulate or SOF, a catalyst may increase the biological activity of the remaining emissions above that of the exhaust without the catalyst. Low sulfur fuel may be required because of increased oxidation of

SO_2 to SO_3. Increases in NO or NO_2 emissions may also occur (27,28,29). The evaluation of any emission control modifications should be based not only on the desired reduction of a specified pollutant, but also on the total effect which the modification has on the entire exhaust. This report describes the first major parametric study of the effect of two basically different types of oxidation catalysts on diesel engine operation.

The first catalyst investigated was a canister-type, laminar flow downstream catalyst manufactured by Englehard Corporation. This catalyst was composed of Cordierite with an alumina wash coat and platinum oxidizing agent. It was selected because it was the only device available at the time, and was useful for developing our methods for characterization of particulate emissions. The large size of this catalyst should allow relatively efficient treatment of the HC despite the diffusion-limited nature of laminar flow. Its placement downstream of the exhaust manifold will, however, allow heat transfer to occur between the exhaust and the surroundings, with possible loss of efficiency. To take advantage of the high exhaust temperatures at the exhaust port, a catalyst placed directly next to the combustion chamber in the exhaust port is another approach.

An example of this type of small-volume, high-temperature catalyst is the close-coupled exhaust port catalyst manufactured by Johnson-Matthey, Inc. and utilized experimentally as an insert in each exhaust port of the Caterpillar 3208. The insert is a honeycomb type cross section monolith made of Fecralloy and coated with a platinum-based oxidation catalyst. The Johnson-Matthey catalyst inserts have a total volume which is 82% less than the two Englehard PTX catalysts which Hunter et al. investigated (30,31) and therefore would yield residence times 82% less. The operating temperatures of the Johnson-Matthey insert would be higher than the PTX downstream catalyst experienced due to the location in the exhaust port as opposed to the exhaust manifold outlet. This operating temperature difference would increase nonlinearly with increasing load because of the radiative (nonlinear) heat transfer occurring between the exhaust port location and the exhaust manifold outlet location.

Both catalysts should ideally oxidize the gaseous and particulate carbon in the exhaust stream completely; this ideal is only approachable, due in part to incomplete theory regarding the nature of catalyzed exhaust oxidation. A more complete theory of particle removal mechanisms has been developed for the second type of aftertreatment device used in this investigation, which will be discussed next.

Particulate Traps and Filtration Theory

The collection of particulate by a trap requires disposal of particulate, usually by incineration. The main problem of particulate traps is the accumulation of particulate faster than oxidation of particulate, leading to pressure buildup, with reduced engine efficiency and vehicle driveability. Turbocharged engines are worse in this respect due to the cooler temperature of exhaust than that of a naturally aspirated engine of equal displacement and loading conditions. Since most light-duty and some heavy-duty vehicles operate over low-load duty cycles, a practical regeneration system is the major barrier to widespread trap utilization. To be successful on the general market, a regeneration system must be safe, reliable, inexpensive, and require no attention from the driver. Any regeneration system must maintain the fuel economy benefit derived from the diesel combustion system to ensure the diesel's penetration into the vehicle market.

A number of researchers (25,32,33,34,35) have performed fundamental studies of trap regeneration. Wade et al. (33) used intake air throttling with a 2.3 L diesel engine and a Corning ceramic trap. It was found that overthrottling to less than 2% exhaust oxygen prohibited regeneration, and that intake air throttling would not be an adequate regeneration method for most light-duty vehicles at 55 mph or less. Mogaka (34) used intake air throttling and found that a minimum loading parameter, M (equal to ratio of the pressure drop across the trap over the "clean trap" pressure drop) of 2.7 may be acceptable for continuous running conditions due to the relatively short throttling time necessary to reach this value, compared to the throttling time necessary to clean the trap completely. Any trap system should then be designed to allow acceptable engine performance at a minimum M value somewhat greater than 1.

Hillenbrand and Trayser (32) added metal salts to diesel fuel and reduced the particulate ignition temperature by up to 250°C; likewise Wade et al. (33) showed that lead in diesel fuel could reduce the ignition temperature by 150°C. A second catalytic approach would be to apply a catalyst directly to the trapping surfaces. Enga et al. (35) have reportedly accomplished this successfully without forming excessive amounts of sulfate from fuel sulfur, at light-duty cycles. Wade et al. (33) found that use of catalyst-impregnated Corning traps offered no reduction in trap regeneration temperature, probably due to insufficient contact between exhaust particulate and the catalyst because of an isolating layer of trapped particulate.

A third method of approaching trap regeneration temperatures in the exhaust stream involves adding energy to the exhaust just before it enters the trap. Wade et al. (33) used a number of burner systems successfully at steady state, but did not investigate their reliability during the transients of normal driving. It was estimated in this study that 5% additional fuel would be required during the period of regeneration with either an air throttle system or a burner system.

Of the types of particulate filters currently available, two were utilized in the present study. The filtration theory of each will now be discussed.

The knitted metal mesh trap developed by Johnson-Matthey belongs to the fibrous filter type of particulate trap. Oh et al. (36) reviewed the theory of particulate collection on fibrous filters and described three particle collection mechanisms: direct interception, inertial impaction, and diffusion (Figure 1.2). The interception mechanism occurs when the distance between the gas streamline and a single fiber becomes smaller than the particle radius. The inertial impaction mechanism occurs when a relatively massive particle deviates from the gas streamlines and impacts on a fiber. The diffusion mechanism occurs when random motions of a particle caused by collisions with gas molecules (Brownian movement) causes deposition on the fiber. The dimensionless numbers characterizing these mechanisms are:

INTERCEPTION - Interception Parameter, $R = \frac{d_p}{d_f}$

INERTIAL IMPACTION - Stokes Number, $Stk = \frac{C\rho_p \; d_p^2}{9\mu_g \; d_f}$

DIFFUSION - Peclet Number, $Pe = \frac{v \; d_f}{D}$

where

$D = \frac{C \; k_b \; T}{3\pi\mu_g \; d_p}$ = particle diffusivity

d_p = particle diameter	v = approach velocity
d_f = fiber diameter	μ_g = exhaust gas viscosity
ρ_p = particle density	k_b = Boltzmann constant
C = Cunningham factor	T = absolute gas temperature

Some simplifying assumptions include: 1) spherical equivalent particles; 2) cylindrical fibers perpendicular to the flow; 3) uniform packing in the filter; 4) sticking probability of particles equal to one; and 5) flow field not influenced by particles. Single fiber efficiencies, plotted versus particle

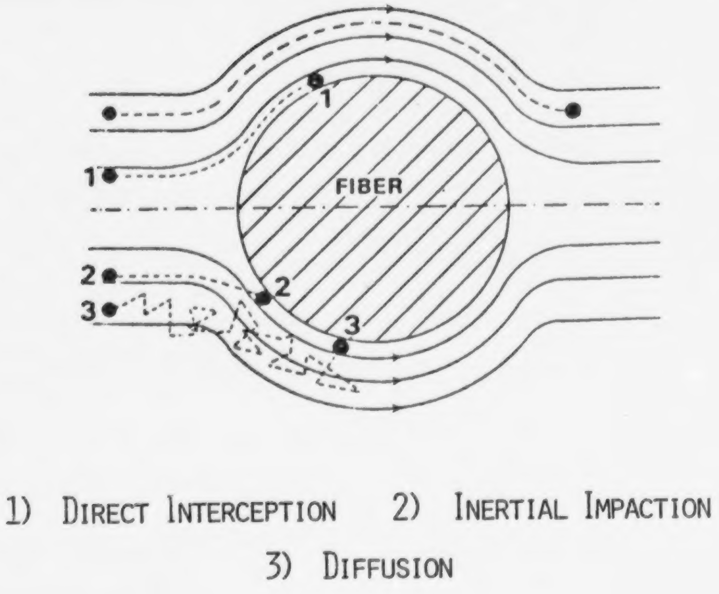
1
FIBER
1
2
2
3
3
1) Direct Interception 2) Inertial Impaction
3) Diffusion

Fig. 1.2 - Particle collection mechanisms
by a single fiber (reference 36)

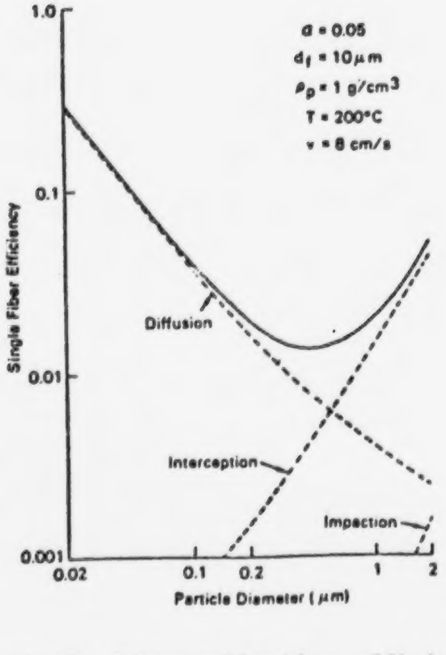

Fig. 1.3 - Single fiber collection efficiency as a
function of particle diameter for the
various collection mechanisms (reference 36)

diameter using these assumptions and constant values of packing density, fiber diameter, particle density, exhaust temperature, and gas velocity, give a plot as shown in Figure 1.3. The relative importance of the impaction mechanism and great importance of the diffusion mechanism for diesel particulate (with a mean diameter near or below 0.1 micrometer) is apparent.

MacDonald and Vaneman (37) conducted experiments using a number of filter configurations, fiber size distributions, and particle size distributions. With relatively clean traps, the theoretical and experimental trapping efficiencies agreed quite well. Figure 1.4 illustrates the trade-off between trap thickness and face area with lines of constant trap volume, filtering efficiency, and pressure drop. Their work shows that larger face area is desirable to maximize filtering efficiency and minimize pressure drop. This was accomplished by use of a radial-flow filter design, as used in the Johnson-Matthey filter described in the present report, and by Enga et al. (35).

The mesh filter trap studied here was initially subject to particle blow-off, due to accelerations, temperature changes, or for no obvious reason. The trap was redesigned so that the packing density and surface-to-volume ratio of the knitted metal mesh resulted in the outer diameter trapping the largest particles while progressively finer particles were trapped as the exhaust flowed radially inward. Such a graduated filter structure has reportedly eliminated the blow-off problem in tests consisting of low-speed operation for an extended time, followed by repeated accelerations.

The porous wall flow filter manufactured by Corning was described by Howitt and Montierth (38). The Corning design is based on the extruded cellular ceramic monoliths used as catalyst supports for catalytic converters used on light-duty gasoline-engine vehicles. By placing ceramic plugs at the inlet and outlet ends of alternate cells, the filtered exhaust is forced through the cell

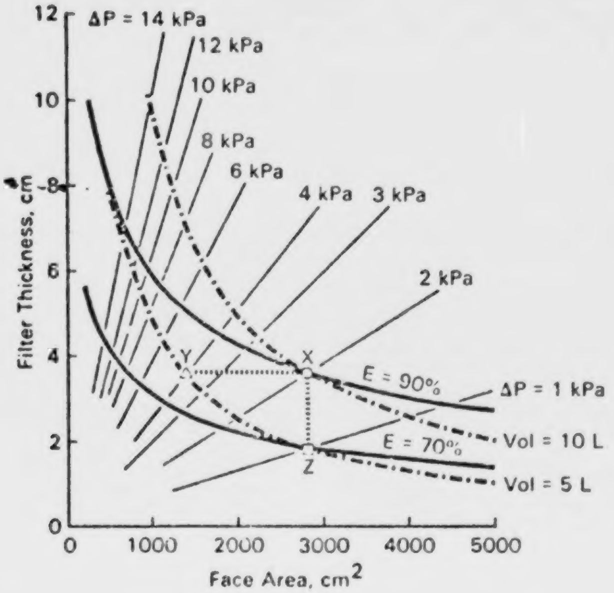

Fig. 1.4 - Dependence of filter performance on filter thickness and face area (reference 37)

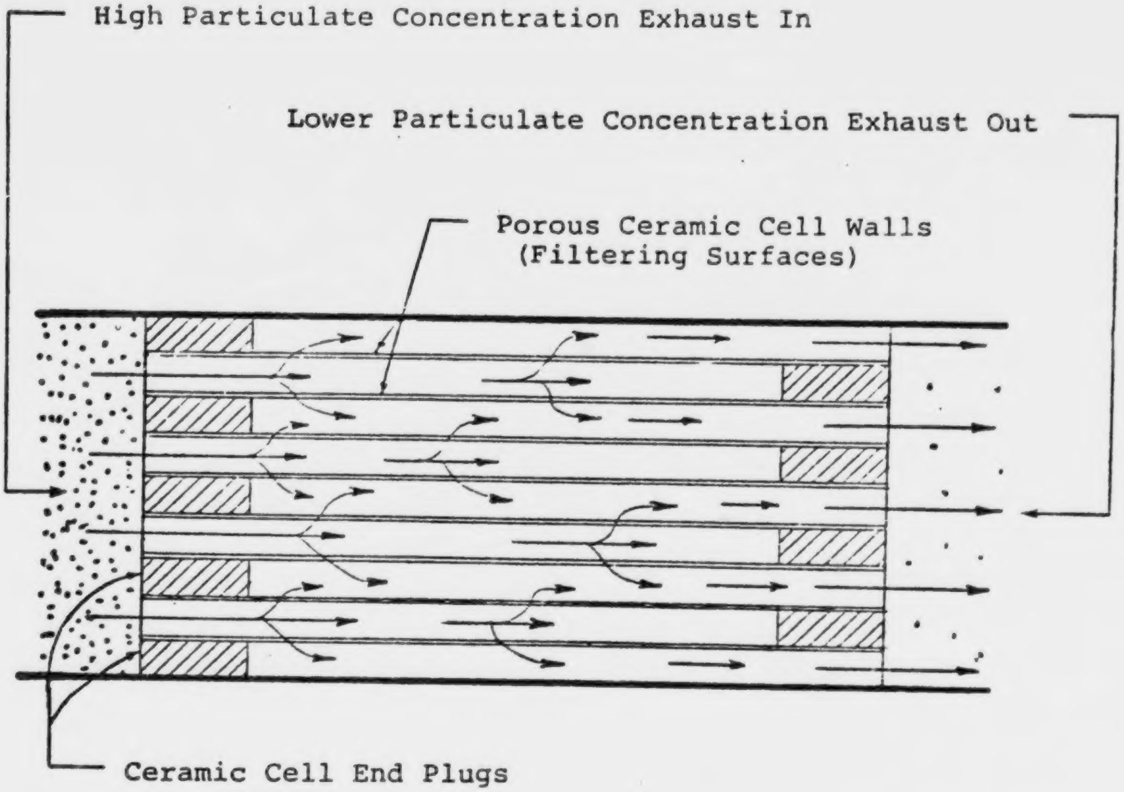
High Particulate Concentration Exhaust In
Lower Particulate Concentration Exhaust Out
Porous Ceramic Cell Walls
(Filtering Surfaces)
Ceramic Cell End Plugs

Fig. 1.5 - Schematic of flow situation in the Corning trap

walls and directed toward the outlet end of the trap. This arrangement cleverly fits a sufficient filtering area into a reasonable-sized volume (see Figure 1.5).

Little theory has been published on wall flow filters in the context of diesel particulate control. Using the general gas filtration theory of Orr (39,40), the porous wall flow filter could be modeled as a membrane filter. As with fiber filters, the mechanisms of diffusion, direct interception, and inertial impaction are operative trapping mechanisms for a wall flow filter, but their formulations in this theory are somewhat different (41,42):

INTERCEPTION - Interception Parameter, $N_R = \frac{d_{particle}}{d_{pore}}$

E_R = Direct interception filtering efficiency,

$= N_R \, (2-N_R)$, if $N_R < 1$

$= 1$, if $N_R \geq 1$

INERTIAL IMPACTION - Impaction Parameter, N_I

where $N_I = (1+\alpha)^{-1}[4\mathrm{Stk}\sqrt{\alpha}+8\mathrm{Stk}^2\alpha\exp(-1/2\mathrm{Stk}\sqrt{\alpha}) - 8\ \mathrm{Stk}^2]$

ε = porosity fraction of filter material and $\alpha = \sqrt{\varepsilon}/(1-\sqrt{\varepsilon})$;

Stokes number = $\mathrm{Stk} = \frac{U_o m}{3\pi\mu_g\, d_{part}\, d_{pore}}$ and

U_o = superficial approach velocity = flowrate/filter area

m = particle mass based on particle diameter and bulk density

μ_g = exhaust gas viscosity

d_{part} = particle diameter

d_{pore} = pore diameter

INERTIAL IMPACTION FILTERING EFFICIENCY = $E_I = 2N_I - N_I^2$

DIFFUSION - Diffusion Parameter $N_D = \dfrac{4DL}{{d_p}^2 \, \overline{U}}$

D = previously defined particle diffusivity

L = filter thickness (pore length)

d_p = particle diameter

$\overline{U}$ = mean pore flow velocity

DIFFUSION FILTERING EFFICIENCY, E_D

$$= 2.57 \, {N_D}^{2/3} \ \underline{\text{if}} \ N_D \leq 0.03$$

$$= 1 - 0.819 \, e^{-3-6568N_D} - 0.097 \, e^{-22.304N_D} - 0.032 \, e^{-56.95N_D} - 0.0157 \, e^{-107.6N_D}, \ \underline{\text{if}} \ N_D > 0.03$$

Since the Stokes number formulation here uses particle mass, and diesel particulate is normally an agglomeration of spherical particles, one must approximate the bulk density and use it with the average diameter of the agglomeration to calculate particle mass.

The combined efficiency of all three mechanisms for a wall flow filter may be given by:

$$E = E_I \, (1-E_I) \, (E_D + \sigma^{(1-N_R)} \, E_R),$$

where

$$\sigma \cong 0.6$$

This expression would have to be integrated over the particle size distribution and pore size distribution for the desired flow conditions.

Mogaka et al. (34) developed a loading parameter for the Corning trap using both fundamental aspects of fluid flow and bench tests of the Corning EX-47 material. The total pressure drop across the trap was considered as the sum of end losses (due to abrupt area changes, accounting for about 5% of the pressure drop), frictional losses along the cell walls (accounting for 12% of the pressure drop), and frictional losses due to restriction of flow through the cell walls (accounting for the remainder of the pressure drop). Given the hydraulic diameter of cells in the trap configuration used here, a loading parameter was developed, defined as the ratio of the dimensionless pressure drop to the pressure drop that should exist for a clean trap under the same flow conditions.

$$M = \frac{(\Delta P)_{\text{loaded}}}{(\Delta P)_{\text{clean}}}$$

A correlation between loading parameter and estimated particle accumulation was found which could be used in the design of a trap configuration with a given particulate level, exhaust flow, and acceptable pressure buildup characteristics.

2

EXPERIMENTAL

A total of 3 engines, in various configurations, were used in this work. The experimental procedures used for the Mack ENDT-676 (a heavy-duty, turbocharged engine, used for investigation of injection parameters) and the Caterpillar 3208 (a medium-duty, naturally aspirated engine, used for investigation of aftertreatment devices) will be discussed here. The Cummins NTC-400 engine (an experimental, single-cylinder, turbocharged engine) received testing on a limited basis for this project at Cummins Engine Company. The experimental procedures used with this engine will be discussed together with the results of its testing.

SAMPLE COLLECTION AND EMISSIONS MEASUREMENTS

For all tests utilizing investigating fuel injection parameter and aftertreatment systems, the Michigan Technological University (MTU) dynamometer cell and dilution tunnel were employed for particulate collection. The engines were connected to an Eaton Dynamatic 500 horsepower water-gap, eddy-current dynamometer. Fuel consumption measurements were obtained using an AVL fuel balance and electronic counter. Engine intake air flow was measured by a Meriam laminar flow element in conjunction with an inclined water manometer. Inlet air conditions were not controlled during testing. All engine temperatures were measured using Omega type K (chromel/alumel) thermocouples. Thermocouples were positioned in the intake manifold, coolant outlet, oil sump, and both exhaust manifolds. The specifications of the dilution tunnel are listed in Table 2 .1, and a complete description is given in reference 27. EPA procedures were followed during the study; additional precautions of trying to maintain constant dilution ratio were taken in order to help maintain repeatability in particulate measurements.

Table 2.1: Dilution Tunnel Specifications

Material	304 Stainless Steel
Diameter	.305 m
Distance from Injection to Sample	4.57 m
Flow	15.29 m^3/min
Transient Time	1.34 s
Reynolds Number	47,000
Injection	Counter Current
Exhaust Utilized	Variable
Intended Use	Diesel Emissions

The dilution ratio was monitored by using engine NO_x emissions as a tracer gas. A Beckman Instruments model 951H chemiluminescence analyzer was used to measure NO and NO_x emissions. Samples from the raw exhaust were drawn through a heated (121°C) sample line, while dilution tunnel samples were drawn though a heated filter to remove any particulate matter before introduction into the analyzer. The volume dilution ratio was determined by the equation:

$$DR = \text{raw } NO_x / \text{ dilute } NO_x \qquad (1)$$

The recorded values for NO_x and NO concentrations were those that were directly measured by the instrument used. The value for equivalent NO_2 concentration was found by the equation:

$$NO_2 \text{ (ppm)} = NO_x \text{ (ppm)} - NO \text{ (ppm)} \qquad (2)$$

The NO_x, NO, and equivalent NO_2 emissions were adjusted for humidity and air-fuel ratio using SAE J177 procedures (28). No corrections for NO_2 readings due to undetermined types and amounts of other forms of nitrogen oxides or other compounds which may affect the instrument response were attempted (29).

The brake-specific NO_x emissions were calculated by assuming the molecular weight of NO_x is that of NO_2, i.e., 46 kg/kmol. The brake-specific NO_2 and NO emissions were calculated using the appropriate molecular weights of each species, 46 kg/kmol and 30 kg/kmol, respectively.

Measurements of gaseous HC emissions were made using a Beckman model 402 heated flame ionization detector (HFID) hydrocarbon analyzer. The sample line and pre-filter of this instrument were both operated at 191°C. The brake-specific HC emissions were calculated by assuming an average atomic hydrogen/carbon ratio of 1.85 for the exhaust HC (30).

Engine exhaust opacity was measured by Celesco model 107 green light, water-cooled opacity meter.

Pallflex Corporation 47 mm EMFAB TX40HI20WW Teflon-coated glass fiber filters were used to determine total particulate mass (TPM), SOF, and sulfate emissions. The sampling procedure and equipment used for the 47 mm filter tests are described in Frisch et al. (14). Although for the particulate size range found in diesel exhaust isokinetic sampling is not critical (14,31), an effort was made to sample within 20% of the isokinetic rate.

After testing, the filters were placed in a desiccator with the plastic container tops ajar and exposed to an ammonia atmosphere for one hour. This ammoniation converted all of the sulfates collected on the filter (primarily sulfuric acid (26)) to ammonium sulfate. Ammoniation changed all of the extremely hygroscopic sulfuric acid to the less hygroscopic ammonium sulfate, which allowed for more repeatable weighing by eliminating changes in filter mass due to water pick-up by the sulfuric acid.

The ammoniated filters were placed back into the humidity chamber and allowed to equilibrate for 24 hours before being weighed for total particulate mass analysis.

The filter was then extracted for 4 hours in a glass Soxhlet microextractor (50 ml reflux volume) using dichloromethane (DCM) as the solvent. The extracted filters were then allowed to equilibrate an additional 24 hours in the humidity chamber before being weighed to determine the amount of SOF that was present on the filter.

The filters were then analyzed for sulfate. Many of the sulfate analyses were performed using the EPA barium chloranilate method (44). These filters were re-extracted using a 60/40 water/isopropyl alcohol solution. Samples collected after March, 1981, or those that were believed to contain sulfate levels below the detection limit of the EPA barium chloranilate method ($< 100\mu g$ per filter) were analyzed using ion chromatography using a Dionex Model 10 ion chromatograph(See Appendix C). These filters were extracted using distilled, de-ionized water. Because ammonium sulfate has a higher molecular weight than the sulfate ion, the total particulate mass collected must be corrected to account for this difference.

The solid (unextractable) portion of the particulate was defined using Equation 3:

$$\text{SOLID} = \text{TPM} - \text{SOF} - \text{SO}_4^{=} \quad (3)$$

Samples for chemical and biological characterization were collected on either Pallflex Corporation 20in x 20in type T60A20 filters (for injection parameter or aftertreatment modification tests), or on Pallflex 110 mm round filters (for single-cylinder engine tests). The 20 x 20 filters consist of a non-woven glass fiber with a Teflon coating applied over it. The Teflon coating provides a relatively inert surface for sample collection, minimizing artifact formation due to surface reactions catalyzed by the collection media (45). All the handling of the 20 x 20 filters was done under yellow light (Kodak type 908 filters) to eliminate the effects of ultraviolet radiation on the SOF.

The ultra-high volume (UHV) sampler shown in Figure 2.1 was used in conjunction with these filters to collect large mass samples for chemical and biological analysis. The sampling rate of this unit was 4.25 Act.m^3/min. which

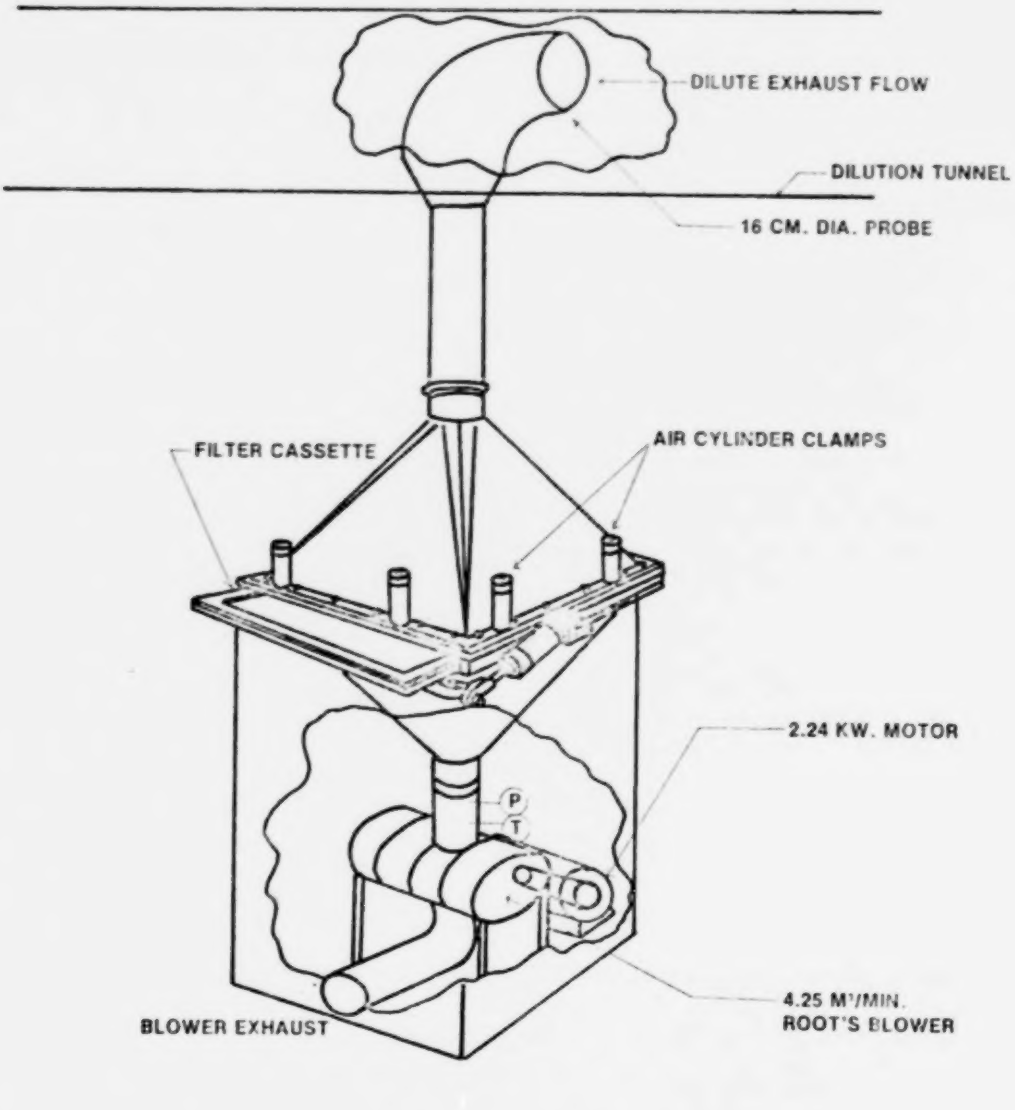
DILUTE EXHAUST FLOW
DILUTION TUNNEL
16 CM. DIA. PROBE
FILTER CASSETTE
AIR CYLINDER CLAMPS
2.24 KW. MOTOR
P
T
4.25 M³/MIN.
ROOT'S BLOWER
BLOWER EXHAUST

Fig. 2.1 - Schematic of ultra-high volume sampler used to collect greater than 50 mg amounts of particulate for chemical and biological characterization

drastically reduced the sample time required to collect the needed amounts of SOF. The plans for the filter holder portion of this sampler were obtained from EPA (46), while the sample pump system was designed and constructed at MTU. The sample system consists of a Roots blower type positive displacement pump (PDP) driven at a constant speed by a 2.24 kW electric motor. The exhaust from the blower is fed back into the dilution tunnel downstream of the sample section in order to maintain a constant flowrate in the dilution tunnel whether or not the UHV is in use. The sample volume/blower revolution was determined to 1.863×10^{-3} Act.m^3/rev using a laminar flow element and a digital revolution counter mounted on the blower shaft. The total volume of diluted exhaust sampled may be calculated by multiplying the number of blower revolutions by this factor.

Ideally, 130 mg of SOF were required for each individual chemical fractionation, and 100 mg were required for an Ames mutagenicity bioassay. The total sample time required to collect enough mass of SOF for chemical and biological characterization was determined from the 20 x 20 test time nomograph shown in Figure 2.2. Because the time required for sampling with the 20 x 20 filters was usually longer than the sample time of the 47 mm filters, some of the 20 x 20 filters were run without sampling simultaneously with the 47 mm filters. Sampling with the 47 mm filters was done during the mid-point of the 20 x 20 sample period. All total particulate, SOF, and sulfate emission rates reported were determined from samples collected on 47 mm filters. The assumption made was that the particulate mass emissions did not greatly change throughout the 20 x 20 sample time period and that the results obtained using the 47 mm filters were representative of the entire sampling period.

To begin sampling with the 20 x 20 filter, the filter was first loaded into the filter cassette. This was done by placing the 20 x 20 filter face up on the filter cassette back-up screen and then placing the cassette lid on top of the

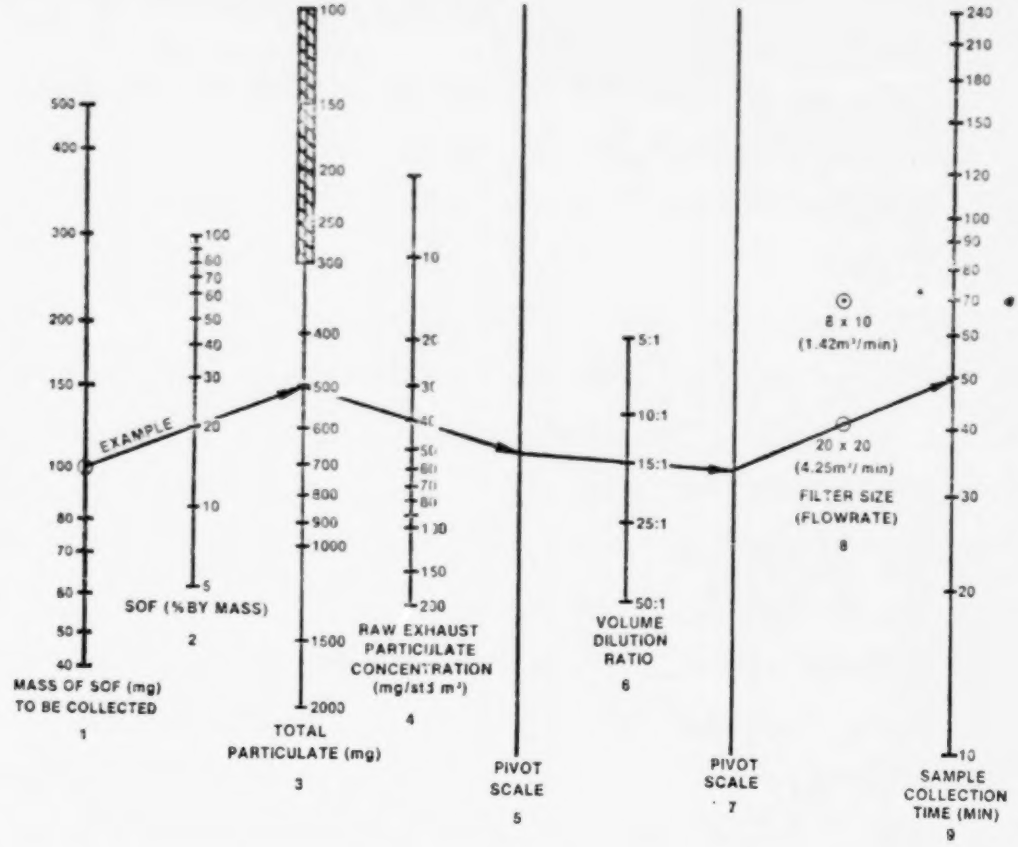

Fig. 2.2 - 20x20 sample time nomograph. Select on scale 1 the desired amount of SOF to be collected. Draw line from point on scale 1 through approximate % SOF (scale 2) to determine amount of total particulate required (scale 3). Shaded area depicts insufficient particulate/filter and should be avoided. Draw line from point on scale 3 through approximate raw exhaust particulate concentration to scale 5. From scale 5, a line is drawn through the desired dilution ratio (scale 6) to scale 7. Draw a line from scale 7 through the appropriate filter size to determine the required sample time (scale 9)

filter. The filter cassette was then loaded into the UHV sampler through the air-actuated access door and the cylinder cassette clamps were actuated at the same time the Roots blower PDP was started. It was important to start the sample pump as quickly as possible when the cassette was in place to prevent the slight vacuum in the dilution tunnel (approximately 0.25-0.75 kPa) from pulling the filter out of the cassette and ruining it.

Filter plugging was also a problem at most modes with the 20 x 20 filters. A 20 x 20 filter was arbitrarily considered plugged when a vacuum of approximately 14 kPa gage was created across the filter. The pressure drop at plugging was different for the 20 x 20 filters and 47 mm filters because of the different types of sample pumps used with each filter.

At the end of the sample period or when the filter became plugged, the access door and air cylinder clamps were released and the cassette removed. The filter was then removed from the cassette and folded in sixths. The filter was placed in a folder and then sealed in an autoclave bag; the bag was then placed in a freezer until the filter was to be extracted.

The 20 x 20 filters were extracted in a 200 ml Soxhlet extractor using DCM for 24 hours. The extended extraction time was required because of the longer cycling time of the larger extractor. The extractors were covered with aluminum foil as insulation in order to decrease siphoning time, as well as to protect the compounds from photodecomposition. After extraction the solvent was removed from the SOF using a rotary evaporator to a volume of approximately 10 ml. The samples were then taken to dryness under a stream of nitrogen at room temperature and stored at -5°C until further use.

The fuel used throughout this study (unless indicated otherwise) was Amoco Premier No.2 diesel fuel; fuel properties are listed in Table 2.2, along with the properties of two other fuels used in selected portions of the study.

Table 2.2 Fuel Properties

Fuel Classification	No. 2*	No. 1	Shale
Cetane Index	52	47	51.5
API Gravity	39.1	43.6	37.8
Distillation Profile °C:			
% Recovered			
0	146	NA	208
5	191	NA	226
10	NA	177	233
50	248	204	266
90	307	246	293
95	323	258	299
EP	338	272	305
Elemental Analysis %:			
C	86.2	86.1	86.7
H	13.52	13.9	13.7
S	0.26	0.04	0.00051(a)
O	0.00	0.04	0.008
N	0.02	0.01	0.000137(a)
Ash	0.00	NA	NA
Hydrocarbon Analysis Vol %:			
Saturates	72.3(b)	83.3(c)	79.0(c)
Paraffins	NA	35.6	43.4
Naphthenes	NA	47.7	35.6
Olefins	2.9	0.0	0.0
Aromatics	24.3	16.7	21.0

NA = Not Available

(a) Analysis by DOE

(b) No. 2 fuel analysis by FIA Method

(c) No. 1 fuel and shale oil analysis by mass spectrometry

*AMOCO Premier

CHEMICAL CHARACTERIZATION

Compound class characterization of the SOF was performed using a fractionation method developed by Huisingh et al. (47), as modified by Funkenbusch et al. (12). Pooled SOF from a number of filters corresponding to the same engine test mode and exhaust aftertreatment was divided into at least three portions after removal of 60-120 mg for biological testing. Each portion was then re-dissolved in DCM and filtered through a 0.45 micron membrane filter just prior to fractionation, in order to eliminate any insoluble degradation products which may have accumulated during storage. The SOF sample was then placed in a tared 50 ml round bottom flask and the DCM removed until the flask obtained constant weight. The SOF mass used as the basis for fractionation was typically 100 to 150 mg.

The fractionation procedure used to obtain SOF compound classes is described in Funkenbusch et al. (12). Basic and acidic subfractions were obtained using liquid-liquid extraction with strong acid and strong base, respectively. Paraffins, aromatics, transitionals, and oxygenates were eluted from a 1 cm x 10 cm silica gel chromatographic column using hexane, 1% ether in hexane, and acetone:methanol (1:1), sequentially. Ether insoluble and hexane insoluble subfractions were also obtained.

Detailed analysis of an aromatic subfraction was performed using a Hewlett-Packard model 5840 gas chromatograph/FID using a 30 m x 0.25 mm ID open tubular glass capillary column, wall coated with SP-2100 methyl silicone fluid. Compounds were identified by combined gas chromatography-mass spectrometry with a Hewlett-Packard model 5985 GC-MS data system. The same capillary column conditions were 3°C/min from 100-250°C, after an initial 10 minute hold. The final temperature was held for 20 minutes.

The Hewlett-Packard probability based search program was used to select matches for spectra generated during the chromatographic run. The National Bureau of Standards library of nearly 30,000 spectra was used as the data base, and the three most probable spectral matches for each chromatographic peak were obtained for comparison with the sample spectra. Identification of the molecular weight was deemed necessary information for tentative assignment of compound identities.

In addition to the routinely-used fractionation method of Funkenbusch et al. (12), two other methods of SOF chemical fractionation were used on a limited basis. The first of these was a high pressure liquid chromatographic procedure developed by Ford Motor Research Laboratories and the second was a low pressure gel permeation procedure adapted from a method used by Lovelace Inhalation Toxicology Research Laboratory (7).

The Ford Motor Company procedure was employed as part of a Coordinating Research Council inter-laboratory round robin. Two diesel SOF samples supplied by EPA were fractionated using a microparticulate silica gel column (Bio-Sil A, 20-44 micron) 25 cm long by 4.6 mm i.d. A 25 µl sample of extract (approximate concentration 1 mg/ml) was injected into the column using 5% DCM in hexane as eluent, flowing at 2 ml/min. After 17 minutes, a programmed gradient of 5%/minute increasing DCM was started. At 36 minutes, the solvent was 100% DCM. This was continued for 17 more minutes, when 200 ml acetonitrile was injected to elute the final chromatographic peak. The instruments used for this procedure were a Hewlett-Packard 1084B liquid chromatograph, coupled to a Schoeffel Model 970 fluorescence detector; the fluorescence excitation wavelength was 313 nm, and emission cutoff was 418 nm.

The second procedure for chemical fractionation employed Sephadex LH-20 lipophilic gel (7). The use of a 1 meter x 1.5 cm column of gel afforded separation of up to 500 mg SOF at a time into seven subfractions. The column (pyrex glass) was filled with Sephadex LH-20 soaked overnight in tetrahydrofuran. The first five fractions (total volume 200 ml) were eluted with tetrahydrofuran, and the last two fractions (total volume 300 ml) were eluted with methanol. Fractions were collected using Buchler Alpha 200 fraction collector and pooled as shown in Table 2.3. The results of this fractionation are given in Table 2.3.

Table 2.3: Sephadex LH-20 Lipophilic Gel Chromatography of Diesel Soluble Organic Fraction

Fraction Number	Eluent	Volume	Typical Compounds
1	THF	80-93 ml	May be high molecular weight alkylaromatics or non-substituted aromatics.
(a) *2	THF	94-107 ml (paraffinic)	Hexadecane
(a) *3	THF	94-107 ml (non-paraffinic)	Low molecular weight alkyl aromatics
4	THF	108-132 ml	Phenyloctane
5	THF	133-198 ml	Pyrene, nitropyrene, dibenzothiophene
6	Methanol	199-356 ml	Esters, acids
7	Methanol	357-500 ml	Esters, acids, perhaps some organometallics

(a) Separated on a post-run silica gel column, 1.0 x 20 cm, using 10 ml hexane for fraction 2 and 20 ml THF followed by 20 ml methanol for fraction 3.

As mentioned previously, the EPA barium chloranilate sulfate method was employed prior to March, 1981. This method was supplanted by use of the Dionex Model 10 ion chromatograph after a comparison of the two methods (to be discussed in a later section of this report) demonstrated the utility of ion chromatography to the analysis of diesel sulfate. A schematic of the barium chloranilate system is shown in Figure 2.3. Due to high levels of condensed hydrocarbons which absorb light at 310 nm, the valving system in this modification (48) of the EPA procedure was modified as shown in Figure 2.3 so that corrections for the HC interferences in the sample could be made. Any

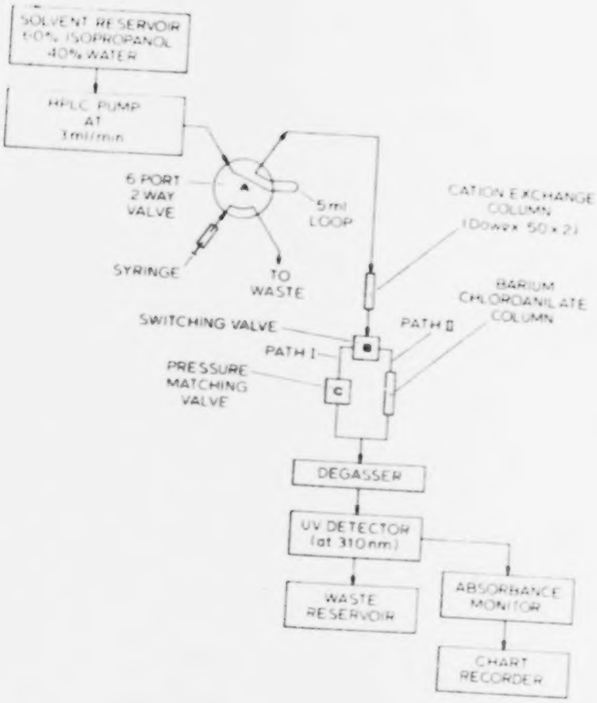
SOLVENT RESERVOIR
60% ISOPROPANOL
40% WATER
HPLC PUMP
AT
3ml/min
6 PORT
2 WAY
VALVE
A
5ml
LOOP
SYRINGE
TO
WASTE
CATION EXCHANGE
COLUMN
(Dowex 50×2)
BARIUM
CHLOROANILATE
COLUMN
SWITCHING VALVE
PATH II
PATH I
PRESSURE
MATCHING
VALVE
C
DEGASSER
UV DETECTOR
(at 310nm)
WASTE
RESERVOIR
ABSORBANCE
MONITOR
CHART
RECORDER

Fig. 2.3 - Barium chloranilate sulfate analysis system
(reference 48)

absorbances due to hydrocarbons must be subtracted from sulfate (chloranilate) absorbance. This is accomplished by running each sample twice. Path I in Figure 2.3 yields a strip chart output whose peak area represents that of hydrocarbons, while running the sample through path II yields a peak whose area corresponds to sulfate and hydrocarbons. The difference in peak areas (determined planimetrically) represents sulfate. A standard curve of four or more points was used with a least-squares curve fit to obtain unknown concentrations.

The Dionex Model 10 ion chromatograph is schematically illustrated in Figure 2.4. Since conductimetric rather than colorimetric detection is used, there was no need to correct for hydrocarbons in the filter extract as in the barium chloranilate method. The ion chromatograph is capable of detecting other common ions, including nitrate, in the configuration used for sulfate analysis. Levels of nitrate on the 47 mm Pallflex filters always were much lower than sulfate levels, but were not routinely quantified. Due to the higher volatility of HNO_3 relative to H_2SO_4, and the tendency for HNO_3 to be produced as an artifact on particulate filters (49), no attempt to relate nitrate measured by ion chromatography to particulate nitrate levels was made.

The sulfate concentration as determined by ion chromatography was proportional to peak height. At least three standards, whose range of values bracketed those of samples to be run, were measured on any day that sulfate determinations were made. As with the barium chloranilate method, a least-squares curve fit of concentration versus peak size (in this case, height) was employed, and sample concentration was calculated using the resulting regression equation.

The total amount of sulfate on each filter (for both methods) was calculated using the equation:

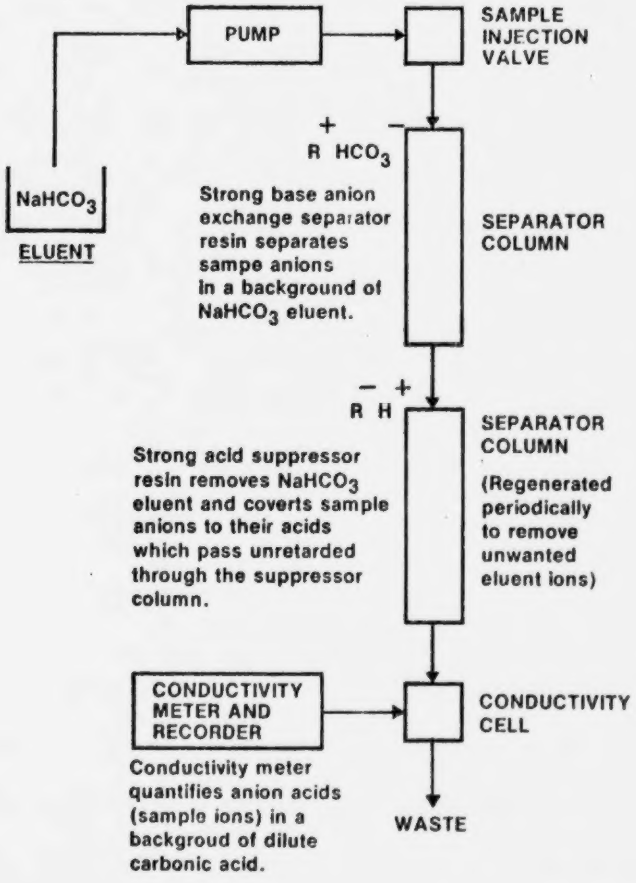
PUMP
SAMPLE INJECTION VALVE
NaHCO$_3$
ELUENT
$R^+ HCO_3^-$
SEPARATOR COLUMN
$R^- H^+$
SEPARATOR COLUMN
CONDUCTIVITY METER AND RECORDER
CONDUCTIVITY CELL
WASTE

Strong base anion exchange separator resin separates sampe anions in a background of NaHCO$_3$ eluent.

(Regenerated periodically to remove unwanted eluent ions)

Strong acid suppressor resin removes NaHCO$_3$ eluent and coverts sample anions to their acids which pass unretarded through the suppressor column.

Conductivity meter quantifies anion acids (sample ions) in a backgroud of dilute carbonic acid.

Fig. 2.4 - Ion chromatography flow scheme (anion analysis illustrated)

$$\text{mg SO}_4^{=} = \text{mg SO}_4^{=}/\text{ml} \times V_o \times D_s,$$

where

V_o = total volume of original sample extract (usually 25 ml) and

D_s = dilution factor used in analysis of original extract

BIOLOGICAL CHARACTERIZATION

The SOF or subfractions to be used for the Ames mutagenicity bioassay were prepared by dissolving a filtered amount of the sample in DCM and removing the DCM using a rotary evaporator until constant weight was obtained. The sample was then either dissolved directly in DMSO to a known concentration or dissolved in a small amount of DCM to which a measured amount of DMSO was added. Removal of DCM from samples prepared in the latter manner was accomplished using a rotary evaporator with water bath no greater than 35°C, assuming negligible lose of DMSO (DMSO B.P. @ 189°C; DCM B.P. @ 40°C). It was usually possible to dissolve SOF or subfraction samples directly into DMSO; however, paraffins and some oxygenated subfractions often remained as a second phase in concentrated DMSO solutions. Samples so prepared were transferred to 15 ml Teflon vials and stored at -10°C or below until use.

The SOF and subfractions were tested for biological activity using the Salmonella/microsome mutagenicity bioassay developed by Ames et al. (4). This test was chosen because it is the most commonly used bacterial bioassay for determining any type of potential mutagenicity (5,10). It is also possible to rapidly screen SOF and subfraction samples for biological activity (e.g., mutagenicity or toxicity). By use of the Ames bioassay, a quantitative dose-response curve can be obtained depicting the overall biological activity of the test samples.

The Ames bioassay utilizes several mutant strains of Salmonella typhimurium for defining the mutation produced by a sample or compound. Mutagenicity, as defined by the Ames bioassay, is the ability of a sample compound to revert the Salmonella typhimurium histidine-dependent mutants to their histidine-independent wild types. Salmonella typhimurium mutant strains TA98, TA100, TA1535, TA1537, and TA1538 were used as the indicator strains in the tests. All strains were obtained directly from Dr. B. N. Ames, University of California, Berkeley. Strains TA98, TA1537, and TA1538 respond to frameshift mutagens; strain TA1535 responds to base-pair substitution mutagens; and strain TA100 will respond to both base-pair and frameshift substitution mutagens. Base-pair substitution mutations in the Ames tester strains occur when a nucleotide is substituted by a different nucleotide thus causing a change in the reading of the codon. A frameshift mutation in the Ames tester strains occurs when one or two nucleotides are deleted from or added to the DNA, thus causing a change in the reading of subsequent codons.

Plate incorporation tests were performed on all samples under a laminar flow hood. The protocol followed that established by Ames et al. (50) except that the Petri plates containing the tester strain and the test samples were incubated for 60 hours instead of 48 hours (51). In order to determine if any of the samples' mutagenic response was direct-acting or required metabolic activation (9), some of the SOF samples were tested in conjunction with a mammalian-microsome (S-9) activation mixture.

A variety of measures were employed to ensure the accuracy and repeatability of the Ames test results, including the following:

1) Use of forced air incubators with internal temperature measured to be 37±0.2°C;
2) use of an automatic colony counter with routine checks on counter accuracy using a calibration slide;
3) routine performance of strain identification checks and top agar sterility

checks;

4) use of tester strain density of 1-2 x 10^8 cells/ml monitored by routine viability counts;

5) holding of cells and top agar mixture at 43°C for no more than 2 minutes before pouring;

6) use of a vortex to thoroughly mix the top agar suspension;

7) dilution of positive controls and sample not more than 2 hours before each test;

8) conducting all test procedures at the same time of day for each series of tests;

9) testing several concentrations of each appropriate positive control to ensure that each tester strain was responding properly;

10) running plates in duplicate or triplicate; and

11) testing the samples on the same day to eliminate any experimental differences when comparing SOF or subfractions from the same mode but with and without an aftertreatment device installed.

For an initial screening test, all five Salmonella typhimurium strains were tested using at least five sample concentrations over a thousand-fold range, in order to establish the linear portion of the dose-response curve (plotted in linear-log form). The most responsive strains were then tested using at least five sample concentrations within the linear dose-response range. The two tester strains used most routinely were TA98 and TA100, without metabolic activation (7,8,9,47). The number of revertants was recorded for each dose tested; data analysis was performed using techniques described in Appendix B.

RESULTS AND DISCUSSION

The physical, chemical, and biological (mutagenic) characteristics of particulate from three basic diesel engine systems are discussed here. These systems include:

1. A Mack ENDT-676 heavy-duty engine, used in conjunction with the dilution tunnel and sampling system discussed in the experimental section of this report; the Mack engine was used for investigation of fuel-injection parameters.
2. A Caterpillar 3208 medium-duty engine, also used in conjunction with the dilution tunnel and sampling system previously described; this engine was used for investigation of exhaust aftertreatment devices.
3. A Cummins NTC-400 experimental single-cylinder engine, used with a mini-dilution tunnel and sampling system at Cummins Engine Company; this engine was used for investigation of fuel, mode, and timing effects on SOF mutagenic activity.

MACK ENDT-676 - FUEL INJECTION PARAMETER STUDY

Engine and Injection Equipment

For this study, we wanted to make use of an engine representative of a heavy-duty diesel turbocharged DI truck engine. To simplify the experimental portion of the study, the engine to be tested should allow changing of the fuel injection rate and timing with a minimum of effort. It was desired that such an engine could be modified using existing components and hence keep the development aspect of the experiment to a minimum. The Mack ENDT-676 engine satisfied both of these requirements. The specifications for the 1980 production baseline engine are listed in Table 3.1.1. The American Bosch fuel injection components for this engine could be quickly changed which allowed the variables of interest to be parametrically studied.

Although it was desired to study the effects of a range of fuel injection rates, the availability of fuel injection components restricted the study to two changes of injection rate. The three pumps tested are listed in Table 3.1.2 with the APE-BB pump being the baseline 1980 production "low rate" pump and the APE-6G pump being the "high rate" 1981 version. The APS shuttle "ultra-high rate" pump is a prototype injection pump. The terms "low" and "high" rates are used merely for convenience to differentiate between the two injection pumps and their respective cams/components. They imply only that the injection rates are low or high relative to one another. Physical characterization and NO/NO_x measurements were made at modes 3, 4, 5, 9, 10, and 11 of the EPA 13 mode cycle as it was felt that these modes represented truck operating conditions. The modes correspond to 25, 50, and 75% of peak torque at intermediate speed and 75, 50, and 25% of rated torque at rated speed, respectively. The engine performance data corresponding to these modes are listed in Table A-1 of the appendix.

Table 3.1.1 - Mack Engine Specifications

Manufacturer and Model:	Mack ENDT - 676
Type:	I-6, Direct Injection, turbocharged, after-cooled
Bore x Stroke:	123.8 mm x 152.4 mm (4.875 in x 6.0 in)
Displacement:	11.0 liter (672 in^3)
Compression Ratio:	14.9:1 (3.3 in piston bowl)
Rated Power:	212 KW (285 hp) @ 2100rpm
Rated Torque:	1465 N-M (1080 ft-lbf)
Turbocharger,	
Compressor A/R;	0.55
Turbine A/R:	0.87

Table 3.1.2 - American Bosch Fuel Injection Equipment Specifications

Pump Model	APE-BB ("low rate")	APE-6G ("high rate")	Shuttle ("ultra-high rate")
Plunger diameter (mm)	11	11	11
Cam, maximum lift (mm/degree)	11.61	12.23	18.0
Nozzle orifice (number x diameter, mm)	5x.32	6x.29	6x.29
Nozzle valve opening pressure (MPa)	29.3	29.3	29.3
The following characteristics are for EPA mode 3 engine operation, 1260 rpm, 70 mm^3/stroke:			
Peak injection pressure (MPa)	40.0	46.5	65.5
Injection duration (°CA)	9	9	3
Injection rate (mm^3/°CA)	7.7	7.7	21.8
Rate parameter (mm^3/°CA)	5.6	5.6	17.7
Helix characteristics	constant beginning, variable ending of injection (all pumps)		

The engine was tested in its 1980 production configuration before any modifications were made to establish the baseline levels of performance and emissions. The engine was then systematically modified with the performance and emissions measured at each step. The second engine-fuel injection system (high rate pump) represented what Mack and American Bosch believed would be the most likely configuration to be produced in 1981. This configuration had shown indications of reduced smoke levels while maintaining acceptable NO_x emissions.

The modifications needed to obtain this configuration were made in several steps to allow parametric evaluation of each of the changes. The first modification consisted of replacing the original pistons (1980 production) with pistons having a larger combustion bowl diameter. Because of the larger diameter, the bowl depth was shallower to avoid reducing the compression ratio. As a result, the larger diameter piston bowl has a higher compression ratio (17 as compared to 14.9 for the smaller bowl). The profiles of these piston bowls are compared in Figure 3.1.1. Injector nozzles also were replaced to match the bowl profile. For brevity, this system is denoted as the "3.8 in. bowl, low rate" system.

The second modification was to replace the fuel pump with one of a higher velocity cam profile and other components designed to increase the rate and pressure of injection. This system is referred to hereafter as the "3.8 in. bowl, high rate" system. This "high rate" system was tested at various port closure timings to study the effect of retarded timing in conjunction with the increased injection rates obtained with the new pump. The long sample times required for collection of the large samples for chemical and biological characterization and the time required for these characterizations made it necessary to limit this type of analysis to a few selected engine conditions. EPA modes 3 and 9 were selected as they were representative of city and highway operation, respectively. The last modification was to install the shuttle fuel injection pump. The above modifications and the test matrix followed during the study are summarized in Table 3.1.3.

The APS "shuttle" pump has three inline plungers which supply fuel to all six engine cylinders (52). Each plunger has hydraulically switched gates which shuttle back and forth directing the fuel to one of the two cylinders supplied by that plunger. This enables the pump to run at engine speed, as opposed to one half engine speed for conventional pumps. As a result, the increased cam and plunger velocities enable the use of much higher injection pressures and

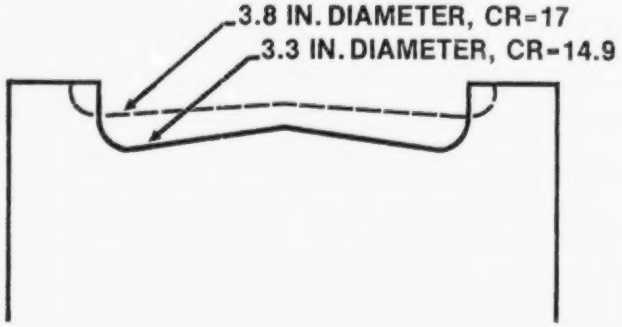
3.8 IN. DIAMETER, CR=17
3.3 IN. DIAMETER, CR=14.9

Fig. 3.1.1 - Schematic of piston bowl profiles

rates. Because of these high rates of injection, this pump will be denoted as the "ultra-high rate" and/or "shuttle" pump. The specifications of the pump are listed in Table 3.1.2.

The high fuel supply pressures required by the shuttle pump were obtained with an external electrically powered gear pump. The supply pressure was controlled by adjusting the amount of fuel flowing through a by-pass circuit which returned the fuel to the supply pump. This continuous flow through the pump generated excessive heat, which was removed by fuel-to-water heat exchangers.

The tendency of the shuttle pump to cause pressure reflections in the injector lines was thought to be responsible for breaking springs within the injectors. These springs held the "needle" in place and thus closed the nozzles. A pressure pickup had to be installed in the injector lines to monitor this reflection. The supply pressure was then adjusted until this reflection was minimized. The supply pressures required at various engine speed and load conditions were then recorded for future use.

Being a prototype, the shuttle pump has undergone limited development work and, as a result, it was not very reliable. Also, the extreme pressures generated at high speeds and loads caused the injector lines to leak and/or pull out of the fittings. This limited complete testing of the shuttle pump to mode 3 only. The injection timing was varied at this mode and physical, chemical, and biological characterization of the particulate was performed at each timing. Gaseous and particulate data at selected timings for modes 4, 5, and 11 were also measured, and are tabulated in Appendix A.

The fuel used throughout the Mack Engine study was Amoco Premier No.2 diesel fuel, whose properties were listed in Table 2.2.

Table 3.1.3 - Test Matrix Used for the Mack Engine Study

Fuel Inj. System (nozzle)	Piston Bowl dia. (in.)	Static Inj. Timing (°BTC)	EPA Mode	Test No.	TPM, SOF, $SO_4^=$ NO, NO_x	Ames on SOF	Chemical Fractionation	Ames on Chemical Sub-fractions
APE-BB (5x 0.29 mm) "low rate"	3.3	19	3	3B	x	x	x	x
			4	4B	x	x		
			5	5B	x	x		
			9	9B	x	x	x	
			10	10B	x	x		
			11	11B	x	x		
APE-BB (6x0.32 mm) "low rate"	3.8	19	3	3.8-3	x	x		
			4	3.8-4	x			
			5	3.8-5	x			
			9	3.8-9	x	x		
			10	3.8-10	x			
			11	3.8-11	x			
APE-6G (6x0.32 mm) "high rate"	3.8	19	3	G-19-3	x	x	x	x
			4	G-19-4	x			
			5	G-19-5	x			
			9	G-19-9	x	x	x	
			10	G-19-10	x			
			11	G-19-11	x			
		12	3	G-12-3	x	x	x	x
			4	G-12-4	x			
			5	G-12-5	x			
			5	G2-12-5(a)	x		x	
			9	G-12-9	x	x	x	
			10	G-12-10	x			
			11	G-12-11	x			
			11	G2-12-11(a)	x		x	

Table 3.1.3 continued

Fuel Inj. System (nozzle)	Piston Bowl dia. (in.)	Static Inj. Timing (°BTC)	EPA Mode	Test No.	TPM, SOF, $SO_4^=$ NO, NO_x	Ames on SOF	Chemical Fractionation	Ames on Chemical Sub-fractions
		17	3	G-17-3	x	x	x	x
			4	G-17-4	x			
			5	G-17-5	x			
			5	G2-17-5[(a)]	x		x	
			9	G-17-9	x	x	x	
			10	G-17-10	x			
			11	G-17-11	x			
			11	G2-17-11[(a)]	x		x	
		22	3	G-22-3	x	x	x	x
			4	G-22-4	x			
			5	G-22-5	x			
			5	G2-22-5[(a)]	x		x	
			9	G-22-9	x	x	x	
			10	G-22-10	x			
			11	G-22-11	x			
	3.8		11	G2-22-11[(a)]	x		x	
		22	11	G3-22-11	x		x	
(6x0.32 mm; 0.77mm^3 sac Volume)	3.8	17	3	S-17-3	x	x	x	
		14	3	S-14-3	x	x	x	
Shuttle (6x0.29 mm) "ultra-high rate"		12	3	S-12-3	x	x	x	
		8	3	S-8-3	x	x	x	
			4	S-17-4	x			
		17	5	S-17-5	x			
		14	5	S-14-5	x			
		12	5	S-12-5	x			
		12	11	S-12-11	x			

(a) Tests designated "G2" are repeats of similar tests designated "G". These repeats were conducted to provide additional SOF for chemical characterization.

Effect of Piston Bowl and Nozzle Orifice Diameter/Number

The BSFC, BSNO$_x$, BSSOLIDS, BSSOF and BSTPM emissions (before and after the piston bowl and nozzle orifice change) for the intermediate speed (1260 rpm), APE-BB "low rate" pump are plotted in Figure 3.1.2a. Similarly, the same variables for the rated speed (2100 rpm) are plotted in Figure 3.1.2b. The modification resulted in increased solids, TPM, and slightly increased BSFC at rated speed. Also, the NO$_x$ was reduced for both speeds while SOF was reduced at intermediate speed. These trends would indicate that the overall fuel-air mixing rates have been lowered.

The effects of increasing engine load and/or speed can be determined by comparing Figures 3.1.2a and b. While engine load is not the same for each figure, both cover similar load ranges and thus may be used for determining general trends. The figures show that when load is increased at constant speed, NO$_x$ concentration increases while SOF and BSFC decrease. The changes in NO$_x$ and SOF are due to shorter ignition delays and higher cylinder temperatures. The solid particulate emissions are expected to increase at both speeds as the load is increased due to the fact that: 1) the amount of fueling is increased, 2) intake manifold volume flow rate is constant (± 3%), therefore air swirl should remain constant, 3) fuel injection duration increases, therefore the luminosity duration should increase, and 4) fuel injection rate increases, but the rate parameter decreases slightly. All of the above factors hold for both engine speeds; however, only the intermediate speed shows an increase in solids and smoke with load. The rated-speed solid emissions do not show this increase. In light of the above factors, the only apparent reason for this trend at rated speed is that the flame temperature, at some point, exceeds the carbon formation range.

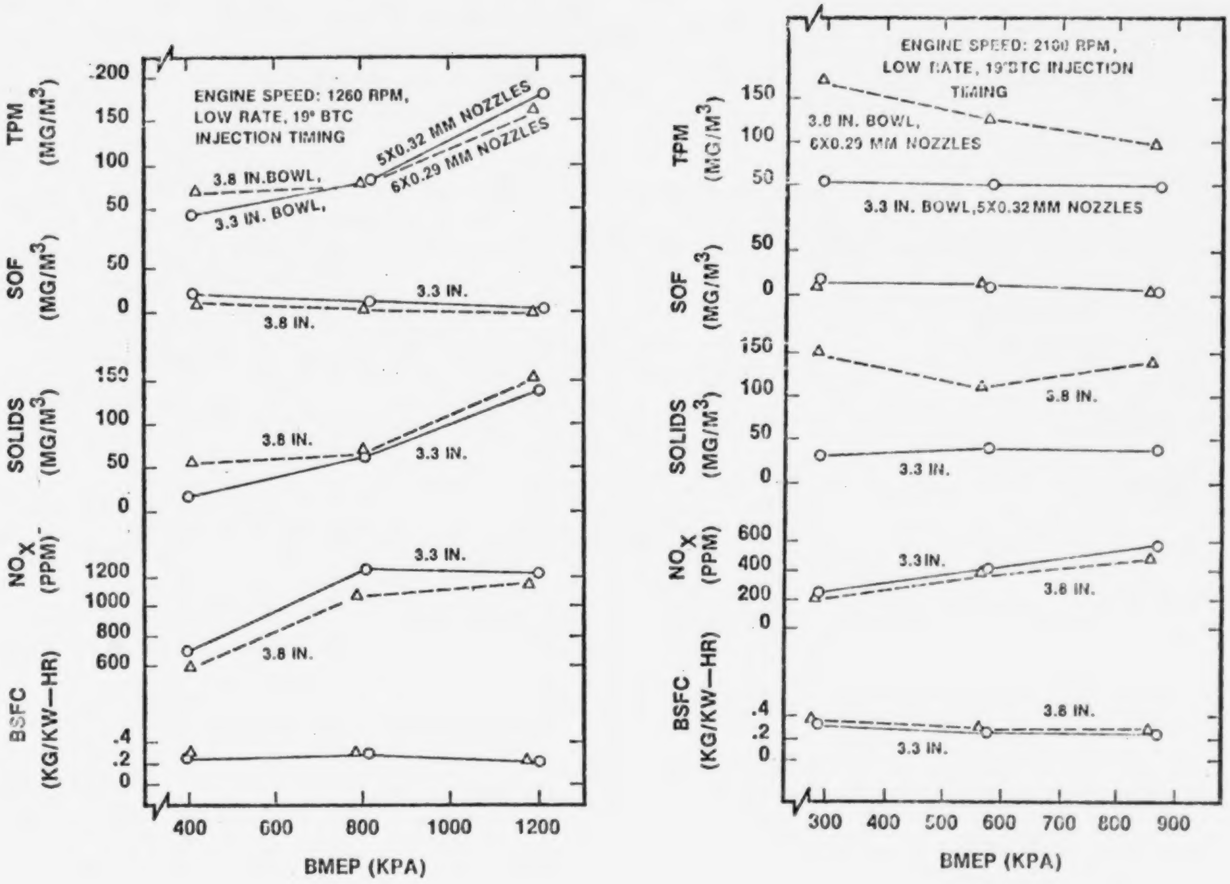

a) 1260 rpm

b) 2100 rpm

Fig. 3.1.2 - Effect of piston bowl/nozzle orifice on BSFC and emissions, low rate, 19° BTC injection timing

As fuel is injected into the combustion chamber after the ignition delay, the local temperatures are expected to steadily increase. At some point in the cycle these temperatures will exceed the carbon formation range; past this point any additional injected fuel, due to increased load, should burn without producing additional solid particulate.

From Table A1 of the Appendix A, it can be seen that both NO and NO_2 concentrations increase with load. NO_2 formation should follow the same trends as NO formation, with the final NO_2 concentrations being dependent upon both formation and survival rates. While it was expected that NO_2 levels would decrease with load, due to less survival at the higher temperatures, increased formation probably offsets the reduced survival to yield higher NO_2 levels with increasing load.

Increased engine speed also had the effect of reducing NO and NO_2 and increasing BSFC and SOF. As mentioned earlier, NO_2 concentrations are dependent on both formation and survival. The NO_2 reduction at rated speed is most likely due to reduced formation rates resulting from reduced residence time. The solids were decreased with the 3.3 in. piston bowl diameter at rated speed, probably due to a combination of increased mixing and temperatures exceeding the carbon formation range. With the 3.8 in. diameter bowl, solids increased at rated speed.

An examination of the brake-specific particulate emissions (Fig. 3.1.3a and b) shows that BSSolids have increased with the piston/bowl nozzle orifice change. This is another indication of decreased fuel-air mixing rates. The rated speed results (Fig. 3.1.3b) showed a more pronounced effect on the BSSolids due to this modification than did the intermediate speed results (Fig. 3.1.3a). (Note: The effect of injection rate was included in these figures, but will be discussed in the next section.)

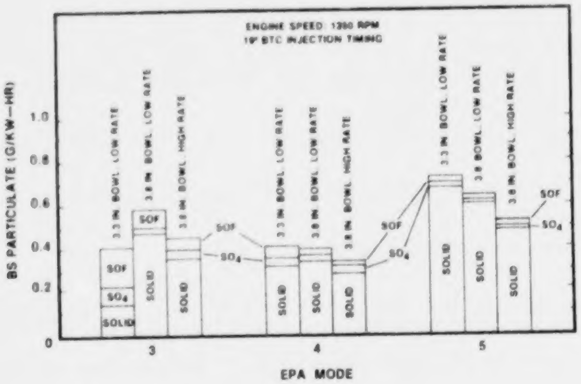

a) 1260 rpm

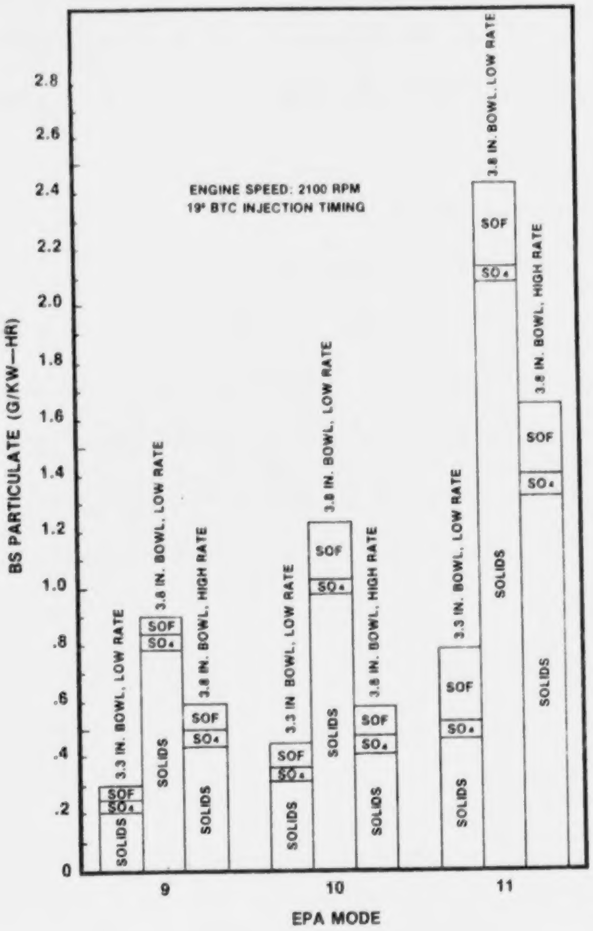

b) 2100 rpm

Fig. 3.1.3 - Effect of piston bowl/nozzle orifice and injection rate on brake specific particulate emissions, low rate, 19° BTC injection timing

The 3.8 inch diameter, shallow piston bowl has the effect of reduced air motion within the combustion chamber (53). Since the air swirl at bottom dead center (BDC) is constant at a given speed and load, the swirl at TDC is controlled by combustion chamber (piston bowl) geometry. Due to the conservation of angular momentum, larger diameter bowls would yield lower air swirl velocities. However, with the bowl diameters used in this study the change in swirl should be fairly small.

The nozzle modification has the effect of reducing the penetration, thus decreasing the total area available for fuel-air mixing. When the 5 x 0.32 mm orifice nozzle was replaced with a 6 x 0.29 mm nozzle, the total orifice area of the nozzle was not changed significantly. Also, for given engine operating conditions, the total volume flow rate of fuel through the nozzle was approximately unchanged. Therefore, injection velocities from each orifice and the resultant atomization should also not have changed significantly. However, the smaller diameter jet would have a lower momentum because of reduced mass flow. This causes the jet to be more susceptible to air friction effects and thus would result in decreased penetration.

The reduced fuel-air mixing rates are then the combined results of reduced air motion and spray penetration with the reduced mixing rates leading to longer burn times and hence to increased BSFC. However, the rated speed results (Fig. 3.1.3b) show a pronounced increase in BSSOLIDS and BSSOF emissions while the intermediate speed results (Fig. 3.1.3a) show a much lower increase in BSSOLIDS and a reduction in BSSOF.

The fuel injection pumps used in this study have the characteristic of a triangular shaped pressure (and hence rate) pulse. From Figure 3.1.4 it can be seen that the injection pressure (measured just before entering the injector) increases steadily until mid injection and then decreases steadily to the end of

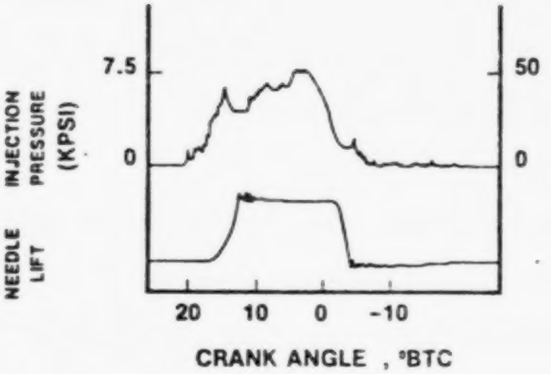

Fig. 3.1.4 - Injection pressure trace and needle lift - typical of low rate and high rate injection pumps, 1260 rpm, 188 mm³/stroke APE-BB 'low rate' pump

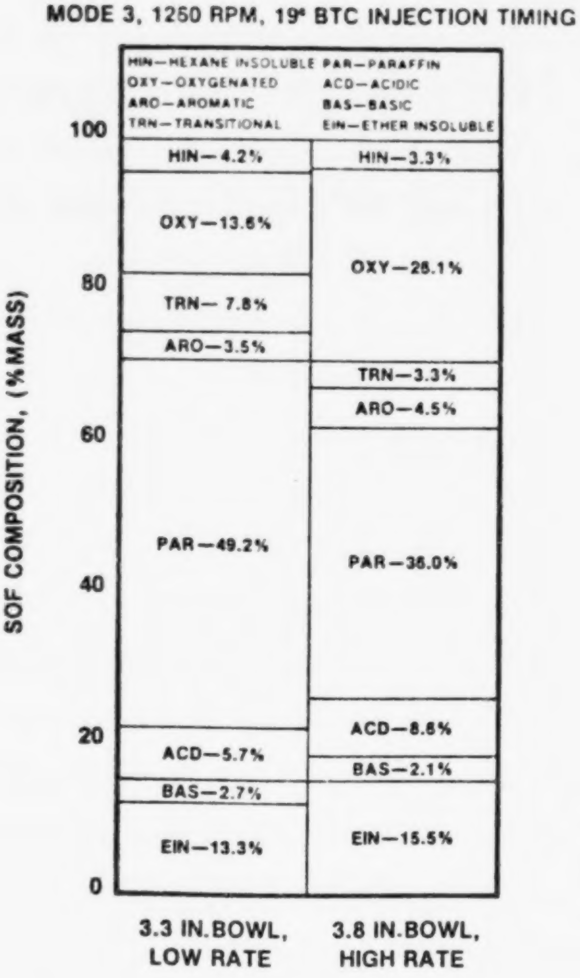

Fig. 3.1.5 - Chemical subfractions of the SOF for low rate - 3.3 in. bowl and high rate - 3.8 in. bowl, 19°BTC injection timing

injection. As the load or fueling is increased, the peak injection pressure also increases. However, an increase in pump speed has a more pronounced effect on the pressure increase than does the load. This pressure increase will increase the injection velocity and spray atomization which would tend to both increase and decrease the penetration, respectively. Thus, it is difficult to predict whether penetration will increase or decrease with speed. However, with non-quiescent engines the air swirl is proportional to the engine speed while the injection pressure rise is less than proportional. The combined effect then would be to reduce penetration as speed increases.

If penetration is sufficient to reach the combustion chamber wall, without wet fuel impingement, the formation of wall jets due to reflection of fuel vapor may occur. Decreased penetration would decrease the action of these wall jets and thus reduce overall fuel-air mixing. Increasing the distance from the nozzle to the wall would have the same effect. The bowl and nozzle change would act to decrease the action of these jets. The reduced wall jet action would be more pronounced as the speed is increased if there is a tendency for spray under-penetration at high speeds. The pronounced increase in solids at rated speed with the bowl and nozzle change can then be attributed to under-penetration. At intermediate speed, the solids were increased slightly, probably due to the reduced air motion within the piston bowl. Also the increased compression ratio with the 3.8 in. bowl would increase the compression temperature by about 50°K and reduce the ignition delay by approximately 25%, thus explaining the reduced SOF at intermediate speed. The increased SOF at rated speed would be the result of more fuel being exposed to the quench areas near the wall due to reduced wall jet action. The chemical and biological characteristics for the bowl modification are shown in Figures 3.1.5 and 3.1.6, respectively. However, due

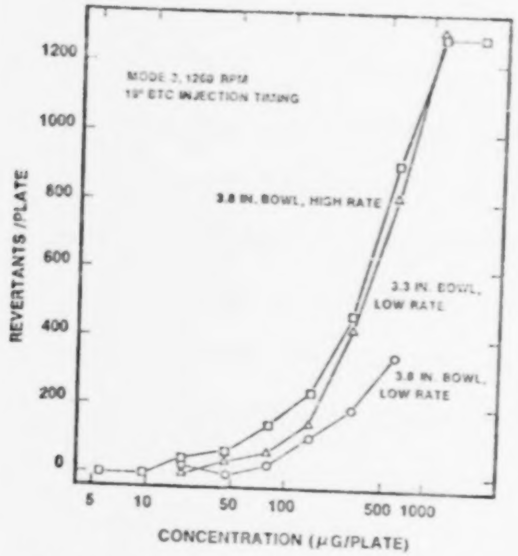

Fig. 3.1.6 - Effect of piston bowl/nozzle orifice and injection rate on biological activity, mode 3, Ames tester strain TA100 without S-9, 19° BTC injection timing

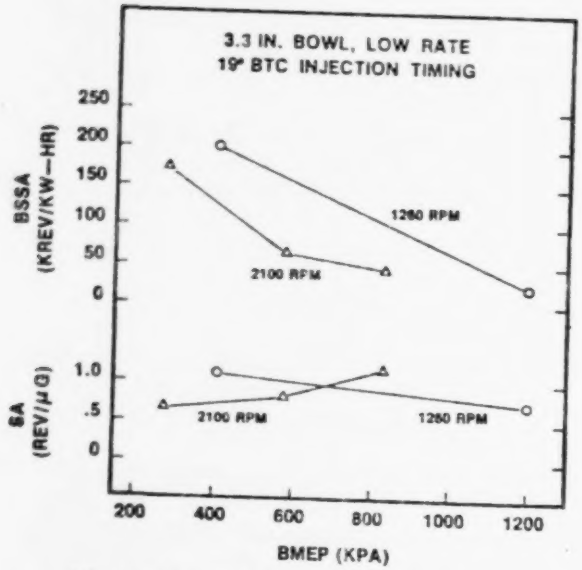

Fig. 3.1.7 - Effect of engine speed and load on biological activity, Ames tester strain TA100 without S-9, 3.3 in. bowl, low rate, 19°btc injection timing

to the limited data, they will be analyzed later when they can be compared with the effects of changing injection rate.

The effect of speed and load on the biological activity of the SOF is shown in Figure 3.1.7. The SA does not appear to follow any general trends due to speed or load changes. At intermediate speed the SA decreases with load, while at rated speed it increases. The BSSA, however, shows a marked reduction as the load is increased at both speeds. BSSA is proportional to the product of SA and BSSOF, therefore these trends may be attributed to the reduced BSSOF emissions at increased loads. The effect of increased engine speed was to reduce the BSSA emissions, again due to generally lower BSSOF emissions.

Effect of Increased Rate of Injection

The increased rate of injection and higher pressure with the APE-6G "high rate" pump was produced by the modified pump components and increased plunger velocity used with this pump. As shown in Figures 3.1.8a and b, solids and TPM are reduced while NO_x is increased with the increased rate/pressure at both speeds. SOF was also reduced at all conditions except mode 9. The smoke, TPM, and NO_x trends may be attributed to increased fuel-air mixing rates. An increased mixing rate will also shorten burn time and explain the slightly improved BSFC at rated speed. When the injection rate was increased, the effect of speed and load on gaseous emissions were relatively unchanged. However, the solids decreased with increased load at rated speed, probably due the higher temperatures exceeding the carbon formation range.

The effect of the increased rate/pressure was primarily to reduce the BSSolids, although the BSSOF was reduced also (Fig. 3.1.3a and b). The decreased BSSolids are due to the increased mixing rate. It should be noted that the greatest reduction in BSSolids was found at rated speed, indicating that the under-penetration hypothesized for the piston bowl and nozzle change

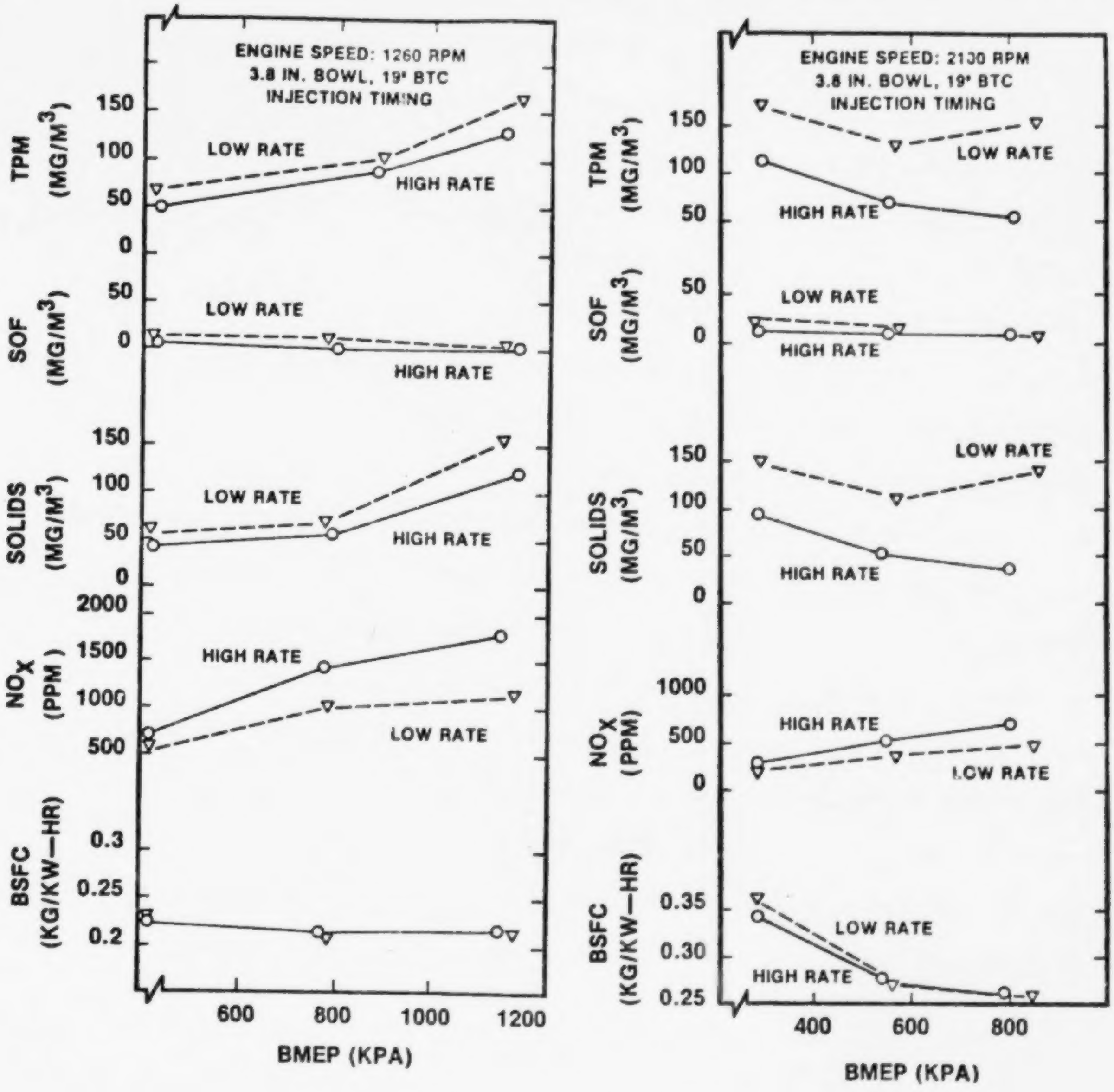

a) 1260 rpm

b) 2100 rpm

Fig. 3.1.8 - Effect of injection rate on BSFC and emissions, 3.8 in. bowl, 19°BTC injection timing

had been changed by the increased injection rate. The reduction of BSSOF at rated speed with the high rate of injection (Fig. 3.1.3b) may also be attributed to improved fuel-air mixing from the wall jets, resulting in less fuel in the wall quench areas. The mixing rate is quantified by the Greeves rate parameter, and increases in the parameter resulted in definite changes in the emissions of BSSOLIDS, $BSNO_x$, and $BSNO_2$, while the BSFC was fairly stable (Table 3.1.4). These findings show that while BSFC, BSCO, and smoke opacity may become constant for Greeves' parameter values greater than a certain value (18), the particulate emissions do not appear to follow this trend.

The chemical character of mode 3 baseline (3.3 in. bowl, low rate) and the 3.8 in. bowl, high rate system SOF was presented in Figure 3.1.5. The paraffin and oxygenated fractions are the largest fractions under both test conditions. Both the acidic and oxygenated fractions were increased over the baseline engine conditions while the paraffin and transitional subfractions decreased.

The acidic, oxygenated, and transitional subfractions of the SOF are formed when fuel molecules undergo thermal decomposition and/or partial oxidation. Injection rate would affect the amount of fuel exposed to these reactions by changing the amount of fuel in the wall quench and/or lean limit regions. Increased injection rates should affect the chemical composition of the SOF only by increasing the lean limit and/or wall quench regions. The increased amounts of acidic oxygenated fractions at mode 3 are then the result of increased amounts of fuel undergoing thermal decomposition in these regions.

Figure 3.1.9 compares typical dose response curves resulting from the biological activity of the chemical subfractions from mode 3. The transitional, acidic, ether insoluble, oxygenated, and basic subfractions are (respectively) the most active fractions (per unit mass) of the SOF. The remaining subfractions (hexane insoluble, aromatic, and paraffin) show very little

Table 3.1.4 - Effect of Injection on Rate Parameter, Engine Emissions, and Fuel Consumption, 3.8 in. Bowl, 19° BTC Injection Timing

EPA Mode	Relative Injection Rate	Rate Parameter $\frac{mm^3}{°CA}$	BSFC $\frac{kg}{kw-hr}$	BSsolids $\frac{g}{kw-hr}$	BSSOF $\frac{g}{kw-hr}$	$BSNO_x$ $\frac{g}{kw-hr}$	$BSNO_2$ $\frac{g}{kw-hr}$
3	low	4.2	0.231	0.50	0.08	9.42	0.40
	high	5.9	0.228	0.38	0.05	10.12	0.57
4	low	4.2	0.213	0.36	0.03	9.52	0.28
	high	5.3	0.214	0.29	0.02	11.71	0.76
5	low	3.7	0.216	0.60	0.02	7.90	0.22
	high	4.8	0.216	0.48	0.02	11.50	0.77
9	low	2.9	0.261	0.84	0.05	6.05	0.16
	high	3.8	0.262	0.34	0.02	7.66	0.40
10	low	3.6	0.276	1.11	0.12	5.45	0.10
	high	4.4	0.278	0.46	0.10	6.89	0.27
11	low	4.2	0.356	2.16	0.28	5.68	0.16
	high	4.8	0.346	1.39	0.24	7.07	0.28

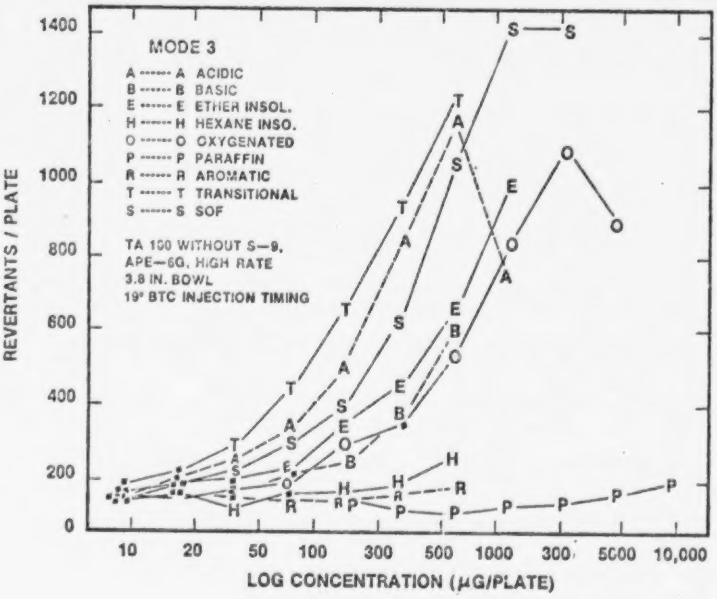

Fig. 3.1.9 - Typical dose-response for SOF chemical subfraction, mode 3, Ames tester strain TA100 without S-9, high rate, 3.8 in. bowl, 19°BTC injection timing

biological activity. This is typical of most of the particulate matter tested throughout the study.

The dose-response curves of the biological activity for SOF obtained from using the 3.3 in. and 3.8 in. diameter bowls with the low rate pump as well as the 3.8 in. diameter bowl with the high rate pump were shown in Figure 3.1.6. The spontaneous revertant levels have been subtracted from each of the response curves to allow direct comparison of the revertant levels. The effect of increasing the piston bowl diameter (at the low rate) was to decrease the biological activity. Increasing the rate of injection, however, increased the response levels until they were slightly greater than the 3.3 in. bowl-low rate results. However, the difference was less than the standard deviation and is therefore not considered to be significant. Table B-2 of the appendix contains values of SA and BSSA for these modifications.

Although the SOF was reduced with the high rate of injection, this reduction was not enough to offset the increased specific activity; thus the BSSA was also increased. Note that the air-fuel mixing also follows the same trends as SA, indicating a correlation between the mixing rate and the biological activity. However, there is not sufficient data to substantiate this.

Figure 3.1.10 shows the relative magnitudes of the brake-specific emissions for modes 3 and 9, and how they change when the bowl size and injection rate/pressure are increased. Generally, when a change is made which reduces the BSTPM and BSFC, the $BSNO_x$ is increased. Similarly, decreases in $BSNO_x$ generally lead to increased BSTPM and BSFC. This relationship is shown in Figure 3.1.11 where $BSNO_x$ and BSFC have been plotted vs. BSTPM. Each of the six points on a given curve represents one of the six modes tested. Therefore, each curve encompasses a range of speed and load conditions, but does not follow any

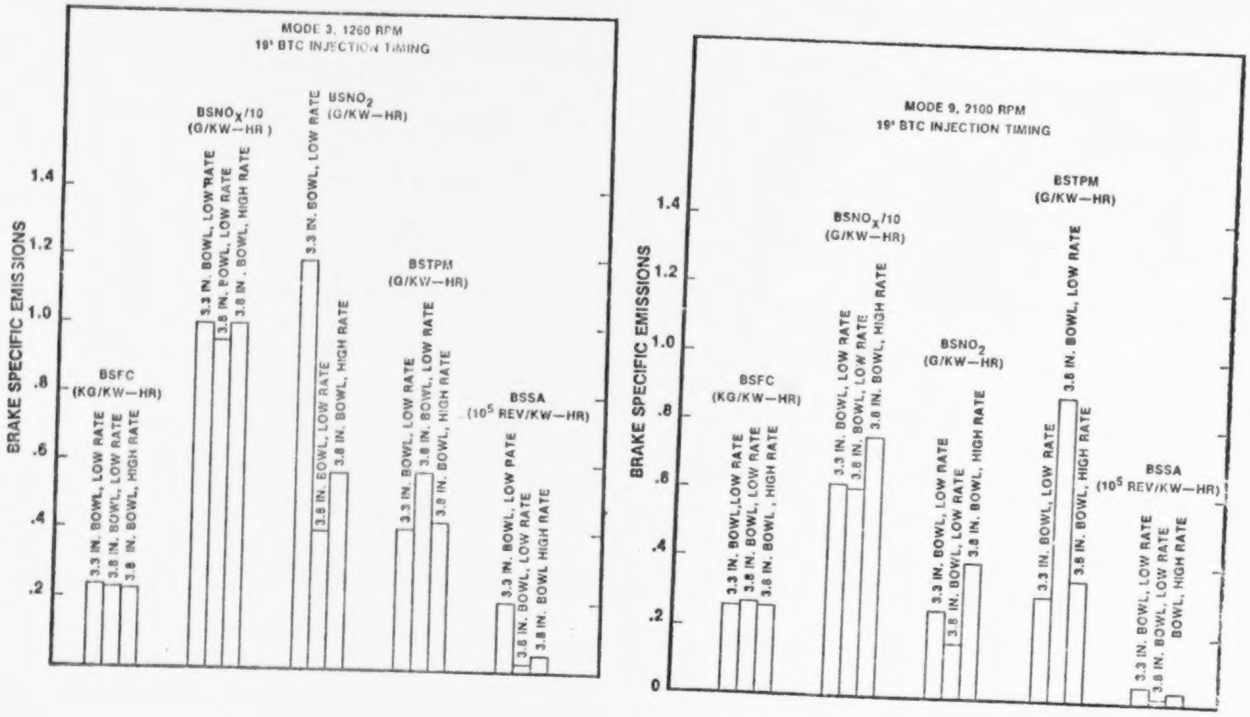

a) mode 3

b) mode 9

Fig. 3.1.10 - Effect of piston bowl/nozzle orifice and injection rate on relative magnitudes of BSFC and brake specific emissions, 19° BTC injection timing

general speed and load trends. As engine conditions are changed to reduce BSTPM, the $BSNO_x$ increases while the BSFC decreases. The BSTPM and $BSNO_x$, therefore, appear to be inversely related while the BSFC and BSTPM are more directly related. None of the modifications improved these relationships. The bowl/nozzle change reduced $BSNO_x$ but increased BSTPM; increasing the rate of injection did return the BSTPM to lower levels, but did so by increasing $BSNO_x$.

To further analyze these relationships one should plot all three variables on one graph with the relative (i.e., percent) changes in any one variable weighted the same as changes in any other variable. This is accomplished by normalizing variables to be plotted on the same axis by dividing the variable by its average value. TPM and BSFC tend to vary with each other. Hence, these two variables are combined on the same axis. In Figure 3.1.12, the BSTPM-BSFC-$BSNO_2$ relationship is shown. The ordinate is the combination of the normalized values of BSTPM and BSFC. Similarly, Figure 3.1.13 shows the BSTPM-BSFC-$BSNO_x$ relationship. In each of these figures the curve closest to the origin represents the engine-fuel injection system with the lowest BSFC-BSTPM-$BSNO_x$ (or $BSNO_2$) emissions. As an aid for determining the curve closest to the origin, Table 3.1.5 contains the average distance of the points on each curve from the origin. This distance would be analogous to the average distance of the curve from the origin on a three-dimensional plot. From the table it is clear that even though the piston bowl/nozzle orifice and injection rate changes have changed the positioning of these curves, the average distance from the origin is almost constant. Recalling that all the variables have been normalized and weighted equally, these relationships could be drastically changed by varying this weighting.

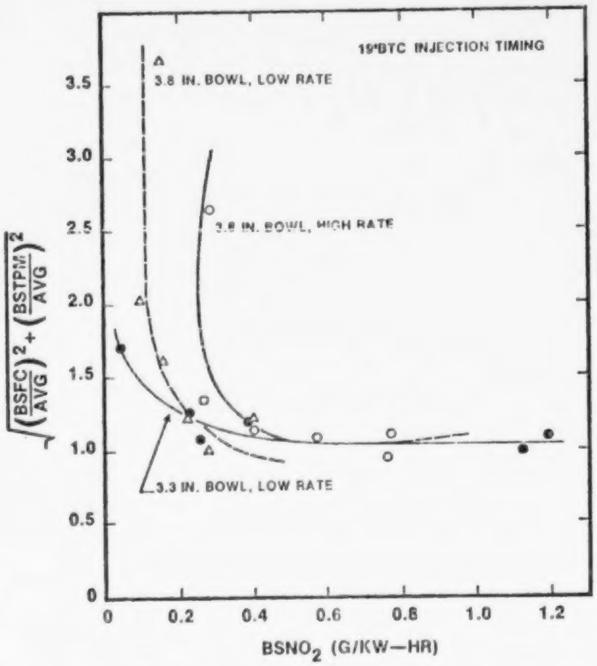

Fig. 3.1.12 - Effect of piston bowl/nozzle orifice and injection rate on BSTPM-BSFC-BSNO$_2$ tradeoff, 19°BTC injection timing. Each curve contains points from all 6 modes

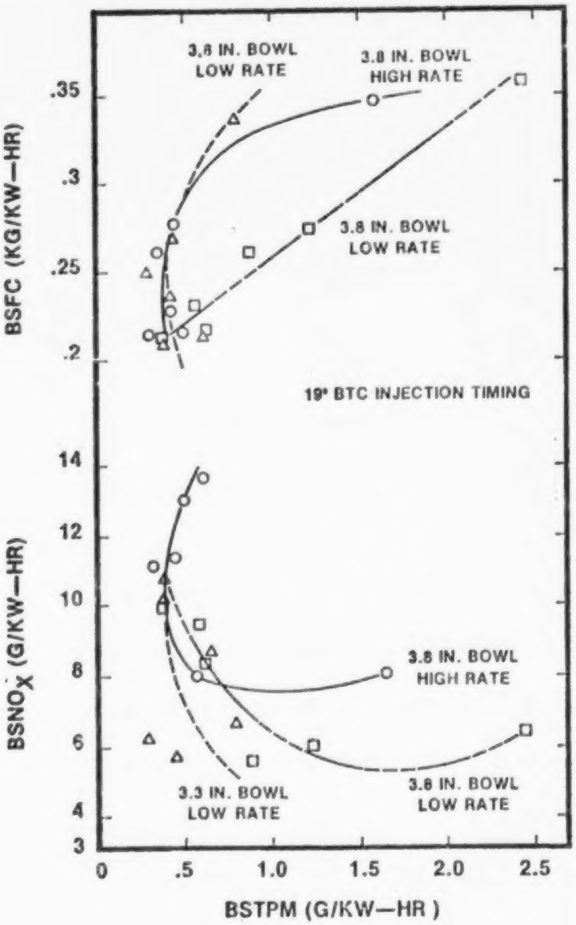

Fig. 3.1.11 - Effect of piston bowl/nozzle orifice and injection rate on BSTPM, BSNO$_x$ and BSFC relationships, 19°BTC injection timing. Each curve contains points from all 6 modes

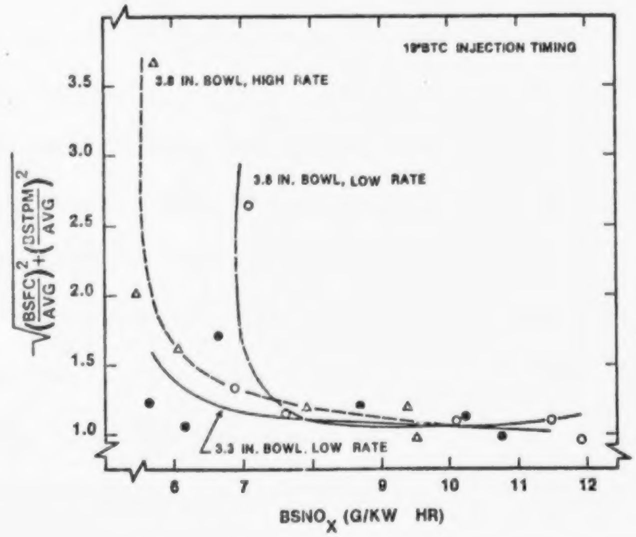

Fig. 3.1.13 - Effect of piston bowl/nozzle orifice and injection rate on BSTPM-BSFC-BSNO$_x$ tradeoff, 19°BTC injection timing. Each curve contains points from all 6 modes

Table 3.1.5 - Effect of Piston Bowl Diameter/Nozzle Orifice and Injection Rate on Combined Performance & Emissions, 19°BTC Injection Timing

Bowl Dia. (in)	Relative Inj. Rate	Combined BSFC, BSTPM, BSNO$_2$ Parameter(a)	BSFC, BSTPM, BSNO$_x$ Parameter (b)
3.3	low	1.95	1.65
3.8	low	1.91	2.07
3.8	high	1.93	1.83

(a) $$\text{parameter} = \frac{1}{n} \sum_{i=1}^{n} \sqrt{\frac{(\text{BSFC})_i^2}{\text{Avg}} + \frac{(\text{BSTPM})_i^2}{\text{Avg}} + \frac{(\text{BSNO}_2)_i^2}{\text{Avg}}}$$

(b) $$\text{parameter} = \frac{1}{n} \sum_{i=1}^{n} \sqrt{\frac{(\text{BSFC})_i^2}{\text{Avg}} + \frac{(\text{BSTPM})_i^2}{\text{Avg}} + \frac{(\text{BSNO}_x)_i^2}{\text{Avg}}}$$

If the objective is to minimize the emissions relationship, with equal weighting given to BSFC-BSTPM-BSNO$_x$ (or BSNO$_2$), then these data show that the rate of mixing can be used to achieve this goal. Increased mixing rates, either by smaller bowl diameter or increased rate of injection, have shown a tendency to reduce the BSTPM-BSFC-BSNO$_x$ combination. The BSTPM-BSFC-BSNO$_2$ combination, however, appears to increase slightly as mixing rates increase. If it is desired to minimize the health effects (low BSNO$_2$ and BSSA as well as BSTPM and BSFC), it would seem that reduced mixing rates are favored. However, based on existing and proposed regulated emissions, i.e., BSNO$_x$, BSTPM, and low BSFC, one would favor increased mixing rates.

The Effect of Static Port Closure Timing

The effects of static port closure timing on BSFC, NO$_x$, solids, SOF and TPM emissions for the 3.8 in. bowl with increased rate of injection are shown in

Figure 3.1.14. The figure contains data from mode 9 only, as the TPM showed both an increase and a decrease with timing retard. The TPM trends are discussed in detail in the next paragraph, but the other emissions trends are typical of all modes tested. As the injection timing is retarded, the solids and BSFC are increased while NO_x and SOF are decreased. The trends were expected and, as explained previously, are due to shorter ignition delays which reduce fuel-air mixing before ignition.

Figures 3.1.15a and b are a comparison of the brake-specific particulate emissions for various injection timings for intermediate and rated speed, respectively. It is apparent that with retarded timing, the BSSOLIDS are increased and BSSOF reduced, again due to ignition delay effects. The BSTPM, being dependent upon both BSSOF and BSSOLIDS, may increase or decrease with timing depending on the relative changes in these emissions. However, for the conditions tested, injection timing had the greatest effect on BSSOLIDs, thus BSTPM was generally increased as the timing was retarded.

The chemical characteristics of the SOF for various injection timings at modes 3 and 9 are presented in Figures 3.1.16a and b. For the separation scheme used at MTU, the paraffins are the largest fraction and account for approximately half of the SOF. This is typical of most of the particulate SOF analyzed at MTU (12,30). As the timing is retarded, the acidic fraction is increased while the ether insolubles are somewhat reduced. At mode 9 the oxygenated fraction is increased with timing retard while at mode 3 it is reduced with timing retard.

Retarded injection timing reduces the amount of fuel in the lean limit region and, as a result, reduces the amount of fuel undergoing thermal decomposition. This should result in a decrease in the acidic, oxygenated, and transitional chemical subfractions. However, Figure 3.1.16b shows that

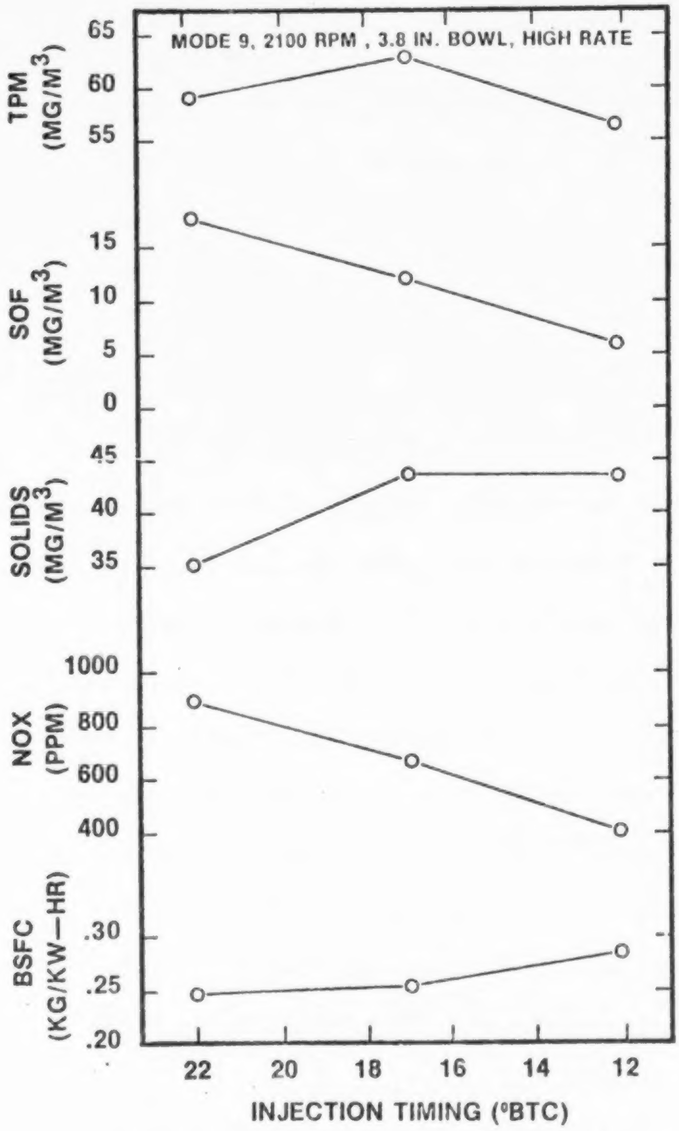

Fig. 3.1.14 - Effect of injection timing on BSFC and emissions, high rate, 3.8 in. bowl, mode 9, 2100 rpm

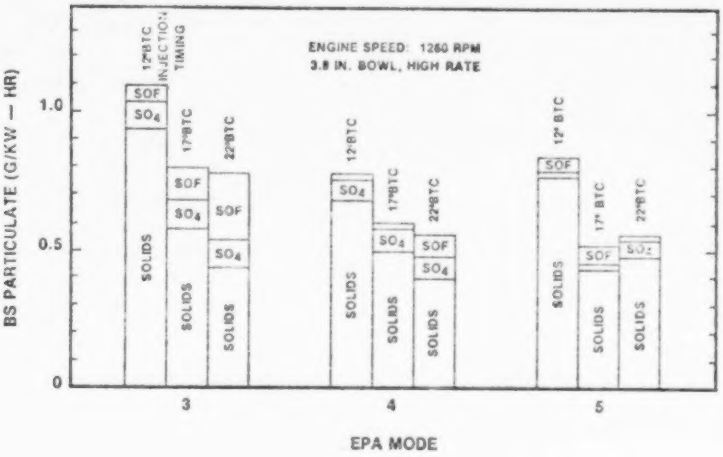

a) 1260 rpm

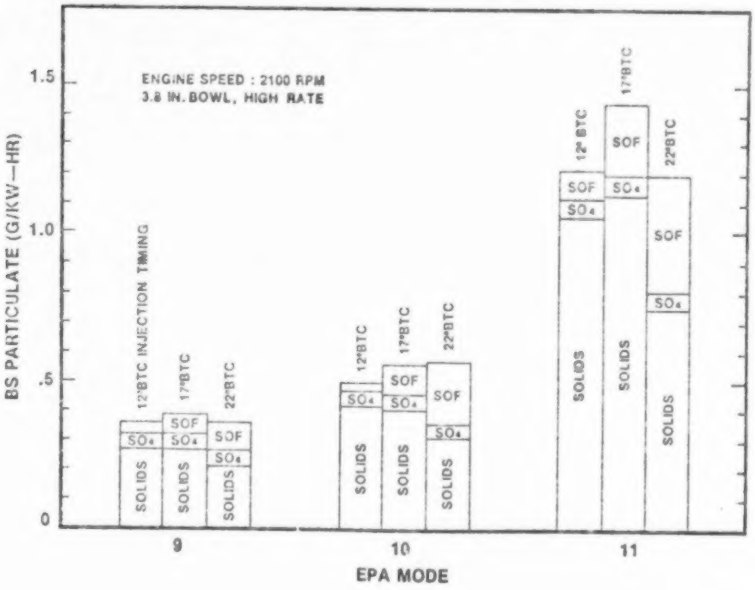

b) 2100 rpm

Fig. 3.1.15 - Effect of injection timing on brake specific particulate emissions, high rate, 3.8 in. bowl

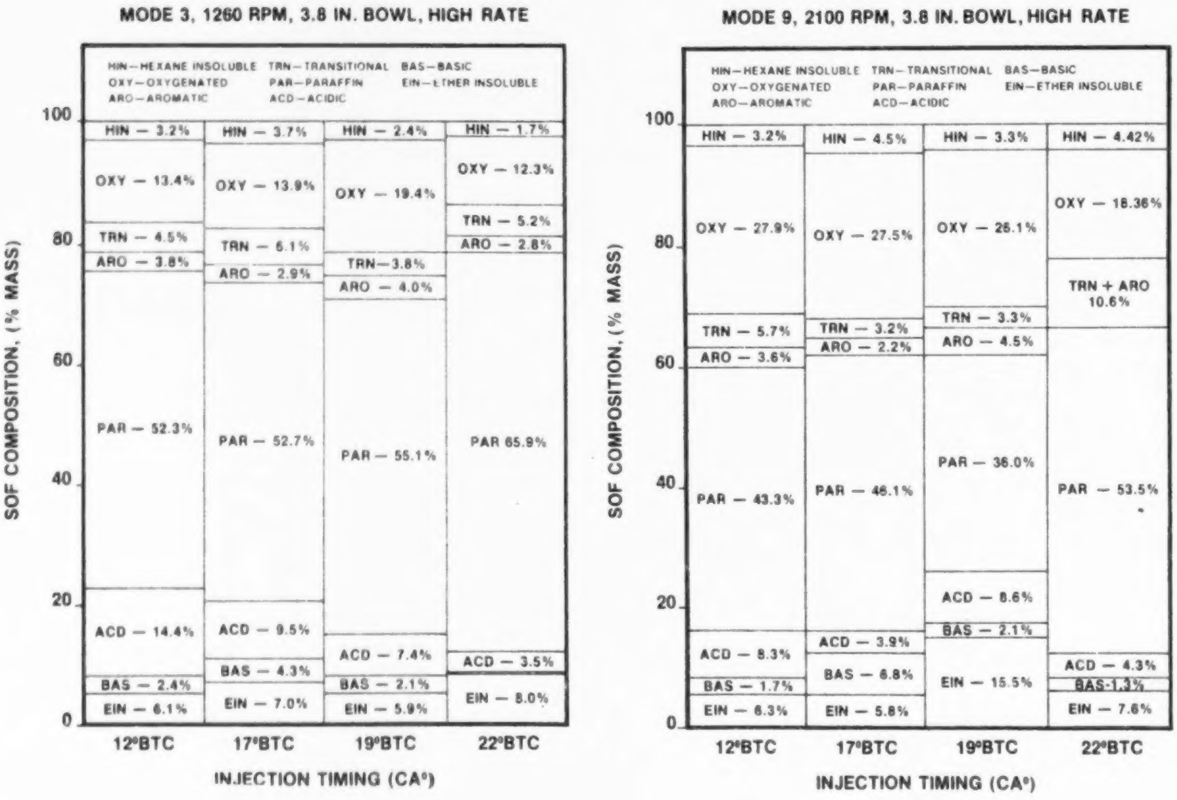

a) 1260 rpm

b) 2100 rpm

Fig. 3.1.16 - Effect of injection timing on the SOF chemical subfractions, 3.8 in. bowl, high rate

transitional and oxygenated fractions actually increase with injection retard. One possible explanation of this discrepancy could be that when fuel molecules thermally decompose, free radicals can be formed. These radicals readily combine with monatomic oxygen to form the acidic, oxygenated, and transitional subfractions. At high temperatures, N_2 will dissociate to N free radicals which have a higher affinity for O radicals than the organics. Thus two competing reactions can take place:

1) $O + N \rightarrow NO$

2) $O + 'R' \rightarrow ACD, TRN, OXY$

where 'R' denotes an organic radical and ACD, TRN, and OXY are, respectively, the acidic, oxygenated, and transitional subfractions. Since monatomic nitrogen has a higher heat of formation than monatomic oxygen, 473 MJ/kmol as opposed to 250 MJ/kmol, N_2 will dissociate at higher temperatures than O_2. Reduced temperatures, by retarded injection, would decrease the relative amounts of N and make more O available for the second reaction. This is evidenced by the reduced NO emissions at retarded injection timings. Therefore, even though the reactions are much more involved than indicated here, the increase in oxygenated and transitional fractions at mode 9 can be explained simplistically by the idea of the competition for monatomic oxygen between N and organic radicals.

The effect of injection timing on the biological activity of the SOF is shown in Figure 3.1.17. The SA of the mode 3 fraction is increased as timing is retarded, while at mode 9 the SA decreases. As mentioned earlier, these changes in SA magnitude are considered to be slight and may not represent significant differences. Both modes show reduced BSSA at retarded timings due to decreased SOF emissions.

The relative magnitudes of the $BSNO_x$, BSFC, BSTPM, BSSA, and $BSNO_2$ for various injection timings for modes 3 and 9 are shown in Figures 3.1.18a and

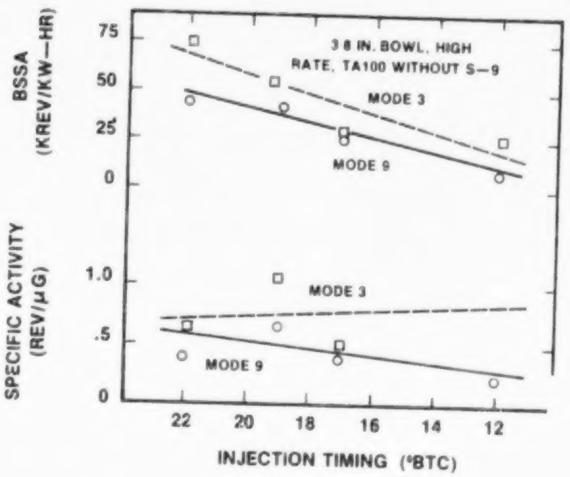

Fig. 3.1.17 - Effect of injection timing on biological activity, Ames tester strain TA100 without S-9, high rate, 3.8 in. bowl

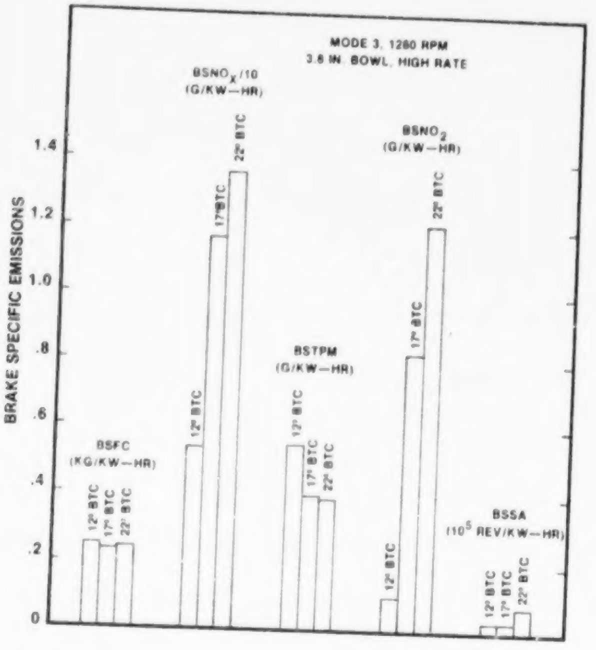

a) mode 3, 1260 rpm

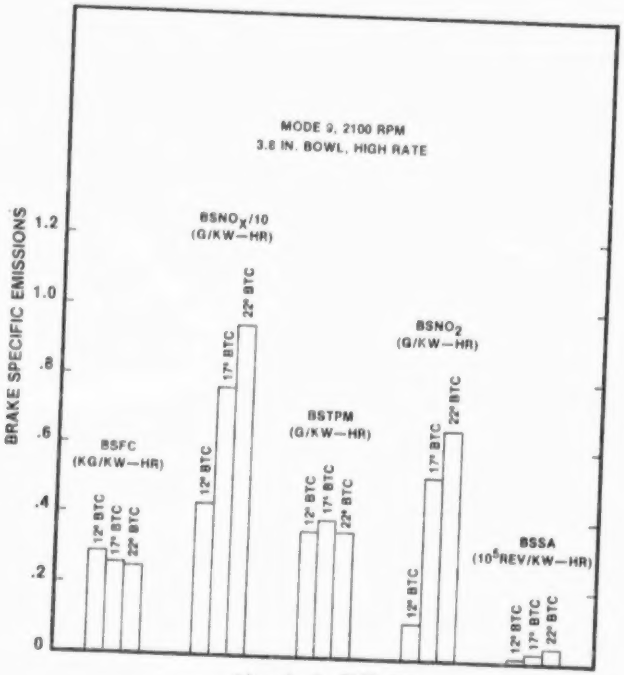

b) mode 9, 2100 rpm

Fig. 3.1.18 - Effect of injection timing on relative magnitudes of BSFC and brake specific emissions, 3.8 in. bowl, high rate

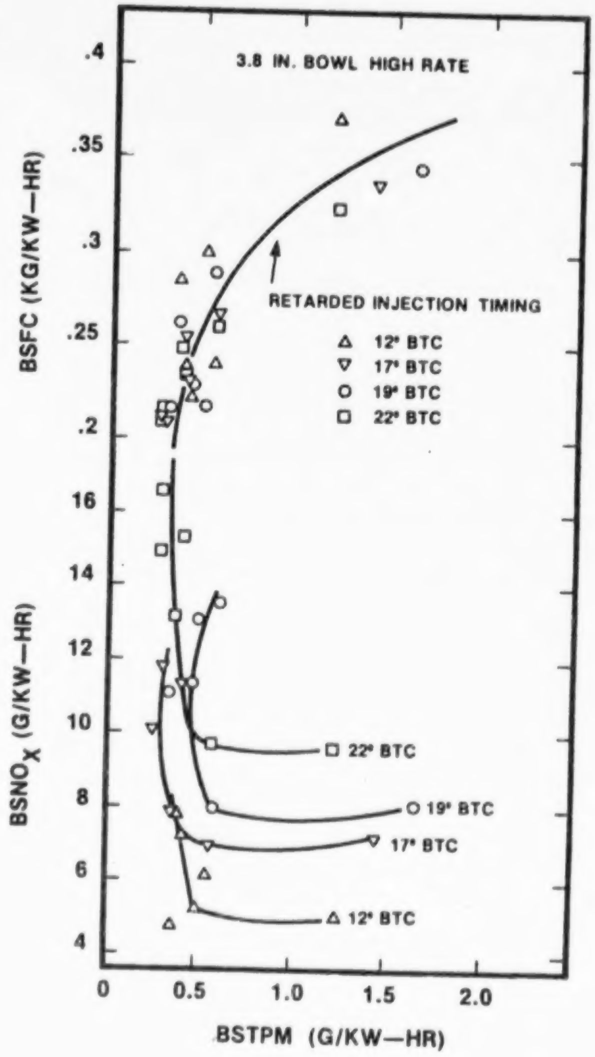

Fig. 3.1.19 - Effect of injection timing on BSTPM and BSNO$_x$ and BSFC relationships, 3.8 in. bowl, high rate. Each curve contains points from all 6 modes

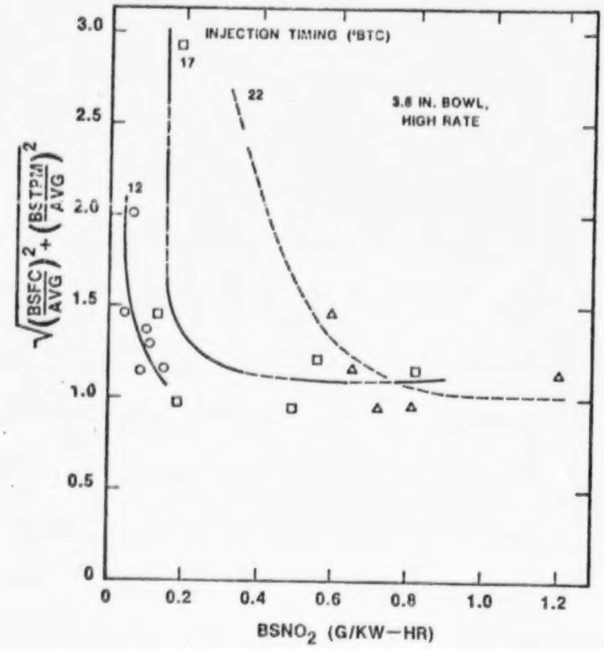

Fig. 3.1.20 - Effect of injection timing on BSTPM-BSFC-BSNO$_2$ tradeoff, high rate, 3.8 in. bowl. Each curve contains points from all 6 modes

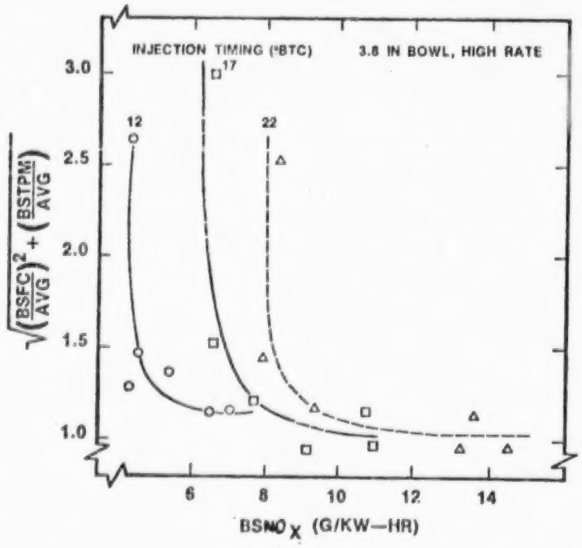

Fig. 3.1.21 - Effect of injection timing on BSTPM-BSFC-BSNO$_x$ tradeoff, 3.8 in. bowl, high rate. Each curve contains points from all 6 modes

3.1.18b. The mode 3 results show that as BSFC and BSTPM are reduced, the $BSNO_x$ and $BSNO_2$ are increased. These trends were shown for most of the modes tested. However, under certain conditions, such as at mode 10, $BSNO_x$, $BSNO_2$, and BSTPM increase together while BSFC decreases.

Figure 3.1.19 contains plots of $BSNO_x$ and BSFC vs. BSTPM. Each curve in this and the following figures contains six points at a given timing which correspond to the six modes tested. The major effects of retarding the injection timing were to lower the $BSNO_x$ levels while the BSTPM and BSFC changed only slightly. To further analyze these relationships, all three variables should be plotted on the same graph. The normalized values of BSFC and BSTPM were combined and are plotted vs. $BSNO_2$ and $BSNO_x$ in Figures 3.1.20 and 3.1.21. The curve closest to the origin represents the timing which results in the lowest BSTPM-BSFC-$BSNO_2$ or BSTPM-BSFC-$BSNO_x$ relationship for these variables. Another method of determining the injection timing which has the lowest BSFC-BSTPM-$BSNO_x$ (and $BSNO_2$) combination would be to find the average normalized distance of the data points from the origin. From the examination of these data (Table 3.1.6), it is apparent that the system approaches the optimum conditions as the static timing is retarded. This is due to the pronounced effect of timing on the $BSNO_x$ and $BSNO_2$ emissions.

Table 3.1.6 - Effect of Injection Timing on Combined Emissions and Performance, 3.8 in. Bowl, High Rate

Static Injection Timing (°BTC)	Combined BSFC, BSTPM, $BSNO_2$ Parameter [a]	Combined BSFC, BSTPM, BSNO Parameter [a]
12	1.55	1.66
17	2.18	1.84
22	2.19	1.98

(a) See Table 3.1.5 for explanation of parameter

Injection Rate vs. Injection Timing

The relative effects of injection rate vs. timing can be examined by comparing the percent change of emissions and BSFC resulting from increased rate of injection to those resulting from changes in injection timing. This is best accomplished by selecting an interval of injection timing which produces the same relative change in one of the measured variables as does a change in the rate of injection. It was found that a five degree advance in injection timing had about the same effect as the increased rate of injection. That is, a five degree advance in timing increased $BSNO_x$ emissions by an average of 28%, while a 21% increase in the mean injection rate increased $BSNO_x$ by an average of 25%. Note that the average percent change represents the value obtained when averaging over all six modes tested. The effect of injection timing on the average percent change of $BSNO_x$ was nearly linear, but the effect was non-linear for BSSolids, BSSOF, $BSNO_2$ and BSSA. Figures 3.1.22 and 3.1.23 illustrate the percent change in the above variables for retardation of timing from 22°BTC. The individual points plotted at a given timing each represent a different engine mode. Table 3.1.7 is a listing of the values of the average percentages as well as those due to the change in injection rate. From these data it was

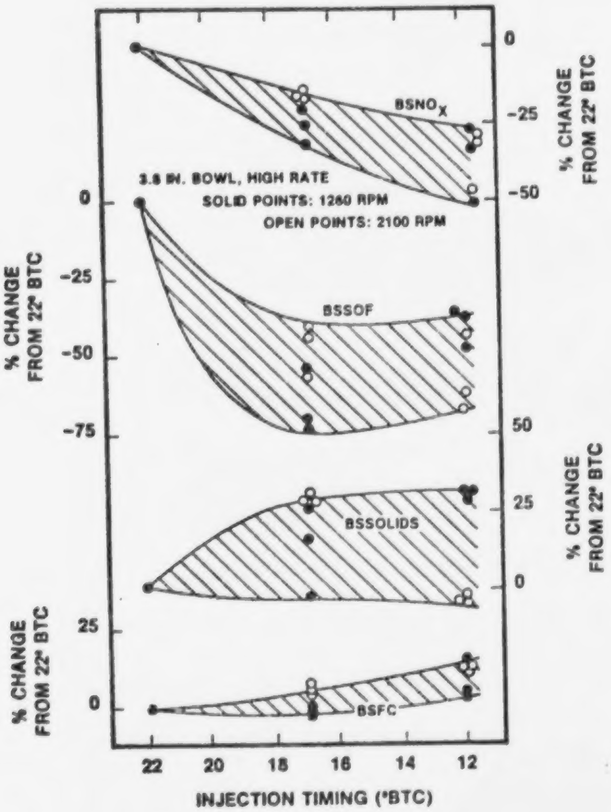

Fig. 3.1.22 - Effect of injection timing on changes in BSFC and emissions when retarded from 22°BTC, 3.8 in. bowl, high rate

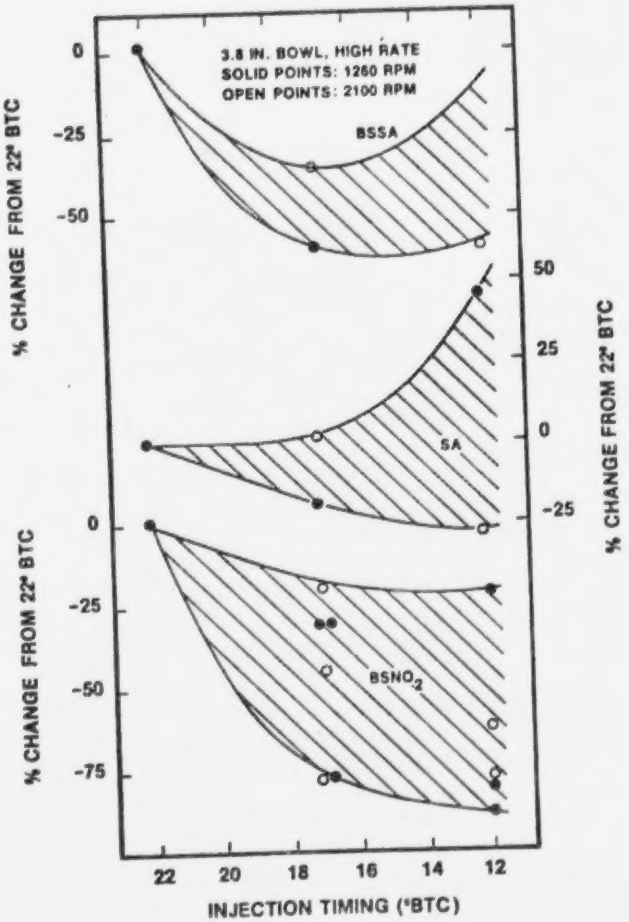

Fig. 3.1.23 - Effect of injection timing on changes in emissions and biological activity when retarded from 22°BTC, 3.8 in. bowl, high rate

determined that for a given change in $BSNO_x$, the effect of injection timing was greater than the increase in rate of injection for BSFC, BSSOF, and BSSA. Timing has a lesser effect than injection rate for BSSOLIDS and $BSNO_2$. Although the biological activity was affected more by injection rate, this was offset by changes in the amount of SOF. Thus the BSSA (which is the product of SA and BSSOF), showed a greater effect due to injection timing.

The effect of increased rate of injection was to reduce BSFC and TPM while increasing NO_x and NO_2. The effect of retarded injection timing was to increase BSFC and TPM while reducing NO_x and NO_2. As previously discussed, an increase in the rate of injection combined with a retard in injection timing could be used to improve the particulate characteristics of an engine without adversely affecting the $BSNO_x$, $BSNO_2$, or BSFC. Data from the engine for the 3.8 in. bowl with the low rate of injection are plotted in Figures 3.1.24a and b. The rate of injection was then increased and the timing retarded. The figure shows that the BSFC and $BSNO_x$ data from the low rate system lie between the values

Table 3.1.7 - Effect of Fuel Injection Rate and Timing on Percent Change in Engine Performance and Emissions; Values are Averages for all 6 EPA Modes Tested

	Rate Increased 21 ± 9.1%	Timing Retarded from 22° to 17°BTC	Timing Retarded from 17° to 12°BTC
BSFC	-0.4 ± 1.4	3.4 ± 2.5	9.3 ± 3.8
BSSOLIDS	-36.4 ± 19	25 ± 17	23.5 ± 29
BSSOF	-27 ± 21	-59 ± 24	-38 ± 31
$BSNO_x$	25 ± 12	-21 ± 5	-37 ± 8
$BSNO_2$	143 ± 75	-47 ± 24	-68 ± 24
BSSA	88 ± 34	-47.8 ± 17	-34 ± 34

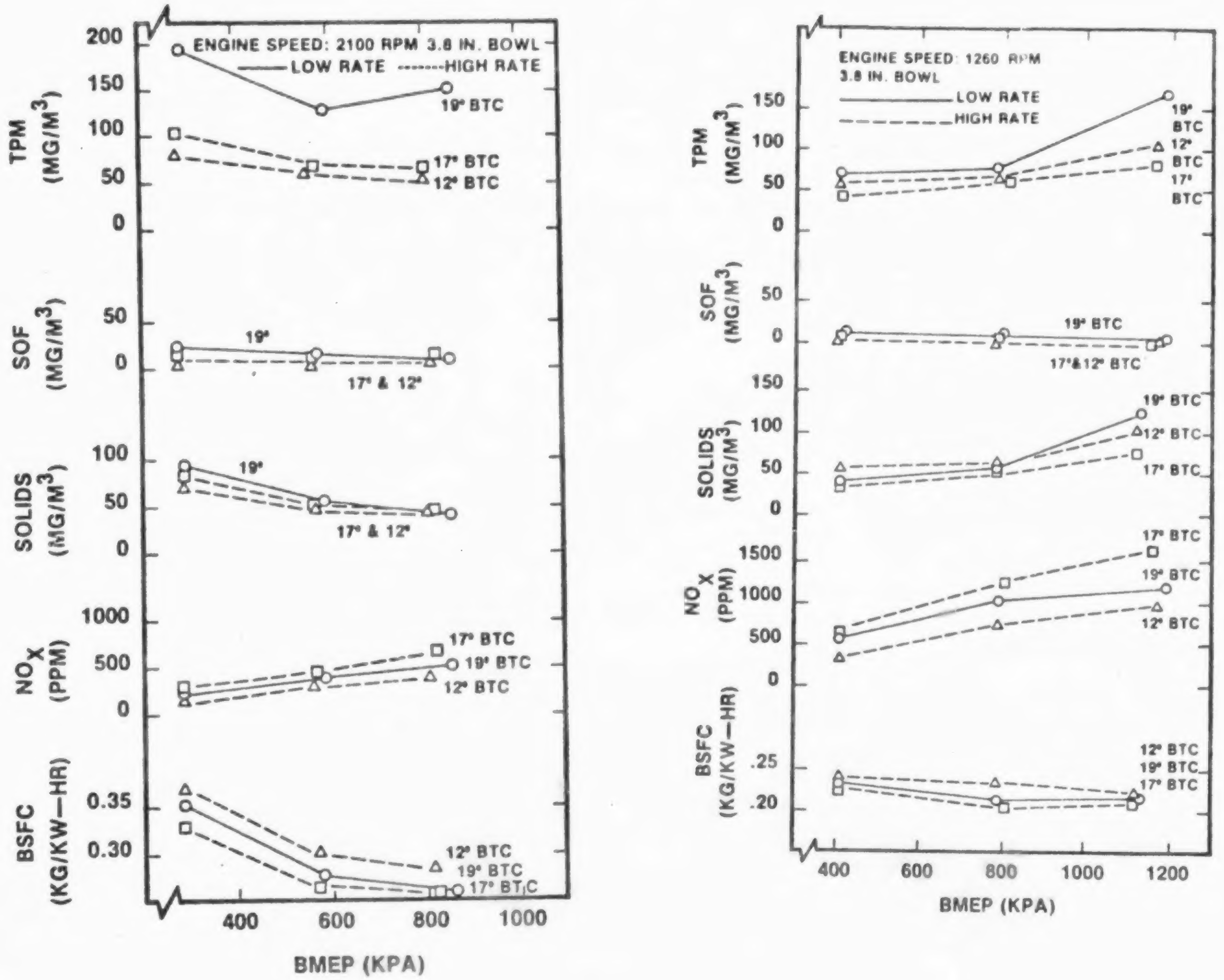

a) 1260 rpm

b) 2100 rpm

Fig. 3.1.24 - Effect of increased rate of injection and retarded injection timing, 3.8 in. bowl

corresponding to the high rate of injection data. Also, the smoke and TPM are lower for the latter data. Thus, it appears that the rate of injection, or more appropriately the rate of air-fuel mixing, has a greater effect on particulate than static injection timing. Similarly, NO_x is affected more by injection timing than by mixing rates.

Up to this point the emphasis has been on the effects of various factors on the trends and relationships experienced by the engine performance and emissions for individual modes. However, one must also be concerned about the magnitude of the composite emissions from a number of modes. Table 3.1.8 contains the weighted brake-specific emissions for all six EPA modes for several combinations of variables. Each mode was weighted equally (16.7%). The table shows that the overall emissions follow the same trends as were discussed earlier, i.e., the increased bowl diameter increases particulate and BSFC, but lowered $BSNO_x$ and BSSA; the increased injection rate lowered BSTPM and BSFC, but increased $BSNO_x$ and BSSA; and retarded timing increased BSTPM and BSFC while reducing $BSNO_x$ and BSSA. However, due to the difference in the magnitudes of the BSTPM and $BSNO_x$ emissions, one could consider the effect of timing on BSTPM to be minimal. For fixed injection timing, the $BSNO_x$ is highest at low engine speeds and decreases as speed is increased, with load having little effect (Table A1 of Appendix A). A variable timing advance unit that would advance timing at higher speeds could be used to yield fairly flat $BSNO_x$ levels. This would allow the rates of injection to be increased for particulate control with a minimum of timing retard at low speeds to provide acceptable $BSNO_x$ levels and good BSFC.

Table 3.1.8 - Weighted Brake Specific Emissions for all 6 EPA Modes Tested, (Unless Otherwise Noted) Each Weighted 16.7%

Engine/Inj. System	Baseline - Low rate, 3.3 in.bowl(a)	Low rate, 3.8 in.bowl(b)	High rate, 3.8 in.bowl (c)			
Static Timing (°BTC)	19	19	22	19	17	12
BSFC (kg/kw-hr)	0.252	0.258	0.248	0.257	0.251	0.276
Mode 5 Smoke (% Opacity)	9.5	7.4	3.5	6.8	3.5	6.1
BSSolids (g/kw-hr)	0.34	0.84	0.32	0.51	0.43	0.49
BSSOF (g/kw-hr)	0.09	0.09	0.14	0.08	0.08	0.03
BSO_4 (g/kw-hr)	0.04	0.02	0.04	0.04	0.05	0.04
BSTPM (g/kw-hr)	0.49	1.03	0.51	0.63	0.55	0.57
$BSNO_x$ (g/kw-hr)	8.00	7.34	11.18	9.15	8.58	5.39
BSNO (g/kw-hr)	4.88	4.65	6.81	5.64	5.34	3.45
$BSNO_2$ (g/kw-hr)	0.54	0.22	0.72	0.51	0.40	0.09
BSSA(d)	123.0	25.0	60.0	47.0	29.5	19.5

(a) APE-BB 'low rate' pump, 3.3 in bowl, 5x.32 mm nozzle
(b) APE-BB 'low rate' pump, 3.8 in bowl, 6x.29 mm nozzle
(c) APE-6G 'high rate' pump, 3.8 in bowl, 6x.29 mm nozzle
(d) Average includes modes 3 and 9 only, each weighted 50%

Effect of Higher Sac-Volume Nozzles

As mentioned in the Background section on fuel injection modifications, the nozzle orifice volume is a design parameter which affects particulate emissions. To observe the effect of this change, the Mack engine with the high rate (6G) pump was outfitted with injector nozzles of 0.77 mm^3 sac volume for comparison with the baseline volume nozzles of 0.32 mm^3. The orifice number (6) and their diameter (0.29 mm) remained unchanged with the new nozzles.

Table 3.1.9 gives the brake-specific emissions for both sets of injector nozzles. These tests were run in close succession to guarantee that ambient test conditions were a negligible factor in creating observed differences. The increase in HC caused by the change in sac volume was over 100%, while the particulate solids increase was 78%. The SOF increased much less than either of these (only 10%). This suggests that the molecular weight of the excess carbonaceous emissions is either in the volatile hydrocarbon region or in the

Table 3.1.9 - Performance Comparison between 0.32 mm^3 and 0.77 mm^3 Sac Volume Nozzles. Mack ENDT-676 No. 2 Fuel, APE-6G Pump, 22° BTC Timing, EPA Mode 3 (all units in grams/kw-hr ± 1 standard deviation)

Parameter	0.32 mm^3 nozzles	0.77 mm^3 nozzles
BSFC	330 ± 2	338 ± 1
$BSNO_x$	9.80 ± 0.17	9.46 ± 0.18
$BSNO_2$	.06 ± 0.00	.06 ± 0.00
BSNO	6.35 ± 0.11	6.13 ± 0.11
BSHC	1.20 ± 0.02	2.58 ± 0.15
BSTPM	1.138 ± 0.056	1.815 ± 0.053
BSSOLIDS	0.873 ± 0.043	1.551 ± 0.043
BSSOF	0.1768 ± 0.0173	0.1949 ± 0.0161
$BSSO_4^=$	0.064 ± 0.002	0.069 ± 0.003

highly polymerized solid carbon region. A comparison of the chemical subfractions present in the SOF (Table 3.1.10) shows that the paraffinic fraction decreased both in absolute amount and in percentage of SOF, while acidics, transitionals, and oxygenates all increased. These results show that unburned fuel from larger sac volume nozzles leaves the engine after considerable oxidation, cracking and dehydrogenation.

Table 3.1.10 - Fraction results for standard (0.32 mm^3) and high sac-volume (0.77 mm^3) injector nozzles; same test conditions as in Table 3.1.9

Subfraction	0.32 mm % of SOF	0.77 mm % of SOF	0.32 mm^3 mg/m^3	0.77 mm^3 mg/m^3
Ether insoluble	7.5	6.6	0.80	0.77
Basic	1.6	1.6	0.17	0.18
Acidic	14.7	17.3	1.56	2.01
Parrafin	53.8	44.5	5.71	5.16
Aromatic	4.0	4.9	0.42	0.60
Transitional	1.2	2.9	0.13	0.33
Oxygenated	12.4	16.2	1.31	1.88
Hexane Insoluble	5.0	5.9	0.53	0.68

The Effect of Injection Timing and Ultra-High Injection Rates

Figure 3.1.25 shows the effects of the ultra-high-rate shuttle pump on BSFC, NO_x, SOLIDS, SOF, and TPM emissions. The increase of 200% in injection rate and 32% in peak injection pressure at mode 3 resulted in a 5% increase in BSFC over the high rate of injection. Advanced injection timing reduced BSFC somewhat, but not to the level experienced with the lower injection rate. Increased BSFC is likely due to the excessive work required to generate the high injection rates, as well as possible spray overpenetration and impingement on

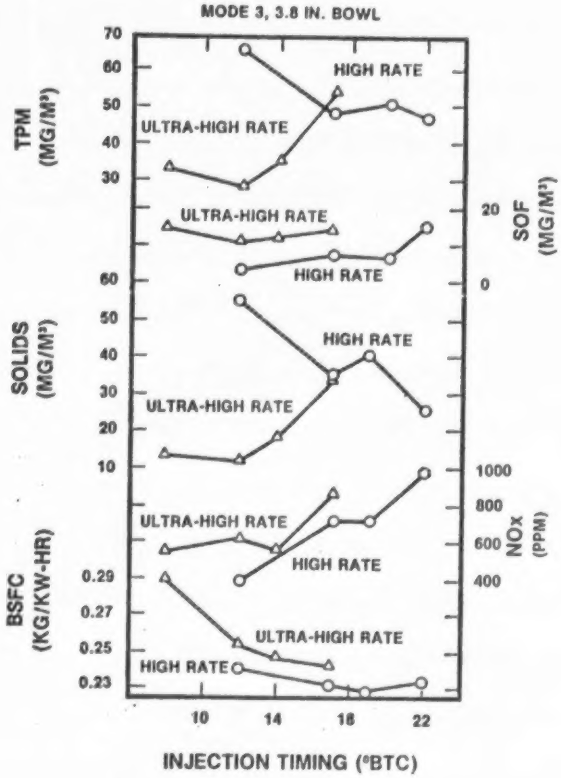

Fig. 3.1.25 - Effect of ultra-high injection rate and timing on BSFC and emissions, 3.8 in. bowl

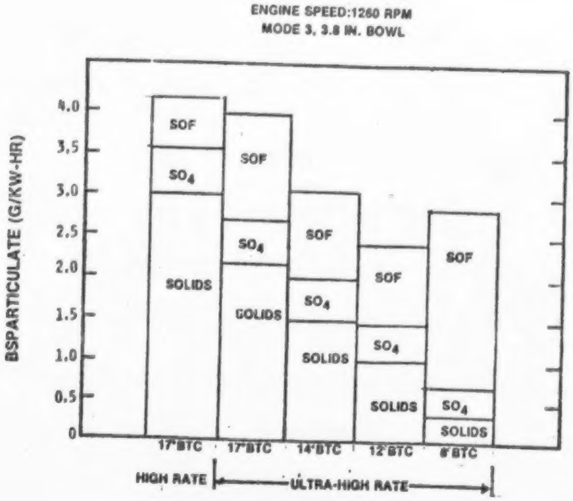

Fig. 3.1.26 - Effect of ultra-high injection rate and timing on brake specific particulate emissions, 3.8 in. bowl

the combustion chamber wall; such fuel should contribute to increased SOF and HC emissions, but this was not observed.

A more likely reason for increased BSFC may be an increase in the amount of fuel injected during the ignition delay, since this should result in more premixed combustion and less diffusion combustion, yielding lower SOF and HC. Although this rate increase will also raise the amount of fuel premixed past the lean limit of combustion, the decrease in SOF and HC with the ultra-high rate suggest that increased premixed combustion predominates over mixture over-leaning.

Figure 3.1.26 shows that the decrease in BSTPM with the ultra-high injection rate is due largely to much decreased BSSolids, with BSSOF actually increasing over that experienced with the high rate. Retarded injection timing reduced both BSSOF and BSSOLIDS, except for the 8°BTC point, which resulted in very high SOF levels, probably due to retarding the injection past the minimum ignition delay. Excessive combustion-generated noise experienced with this timing supports the premise that high SOF levels originate from excessive fuel detonating due to accumulation after the end of ignition delay.

The decrease in solids emissions with timing retard, rather than advance, as for lower injection rates, may be due to both the higher degree of premixed combustion and lower cycle temperatures at retarded timings. Khan et al. (21) found similar results when investigating the effects of injection timing on smoke. With the Mack engine, however, the minimum ignition delay appears between 8° and 12° BTC, and a more plausible explanation for lower solids near maximum retard could be the injection of fuel into an increasingly dense air charge. Increased air density would counteract any overpenetration effects caused by the extremely high injection pressures experienced with the shuttle pump.

The effect of ultra-high rates of injection on sulfate levels with timing retard is minimal. This indicates that a high-sulfur fuel might give sulfate levels approximating the total mass of the TPM at an injection timing of minimum TPM emissions.

Figure 3.1.27 shows that the ultra-high injection rates had little effect on the paraffinic subfraction; there is little change in the total percentage of subfractions containing oxygen, while amounts of individual oxygen-containing subfractions were either increased or decreased with the ultra-high rate. In terms of total SOF, however, the 17° timing gave a greater amount of all subfractions except the aromatics and transitionals with the ultra-high rate pump than with the high rate pump (Figure 3.1.28). A notable feature of the SOF for the ultra-high rate at the 8° timing is the extremely high ether insoluble content. While detailed characterization of this subfraction was not performed, the character of this subfraction in previous work (12) suggests that it may be high molecular weight material containing oxygen and aliphatic as well as aromatic character.

Figures C2 through C12 of the Appendices show the trend in chemical subfractions for the high rate (6G) pump at modes 3, 5, 9, and 11, and for the ultra-high rate (shuttle) pump at mode 3, as a function of injection timing. These figures give percent concentration of total SOF for eight subfractions as a function of timing (Figures C2-C6) and as a function of load (Figures C7-C12).

It should be mentioned that the fractionation procedure is described by Funkenbusch et al. (12) is a manual procedure and is prone to subjective variability which decreases measurement accuracy. Additionally, the measurement of SOF by particulate extraction adds a variability. Still, there are obvious similarities between the high rate and ultra-high rate pumps as timing is retarded at mode 3. Paraffins were generally decreased, both as a proportion of

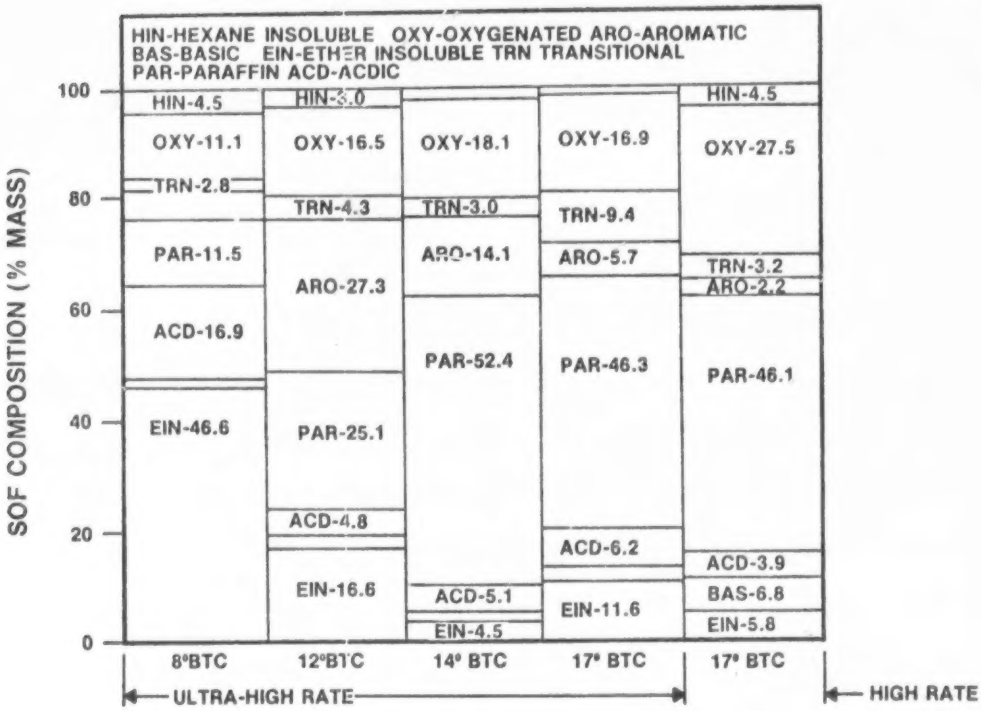

Fig. 3.1.27 - Effect of ultra-high injection rate and timing on the chemical composition of the SOF, 3.8 in. bowl, mode 3

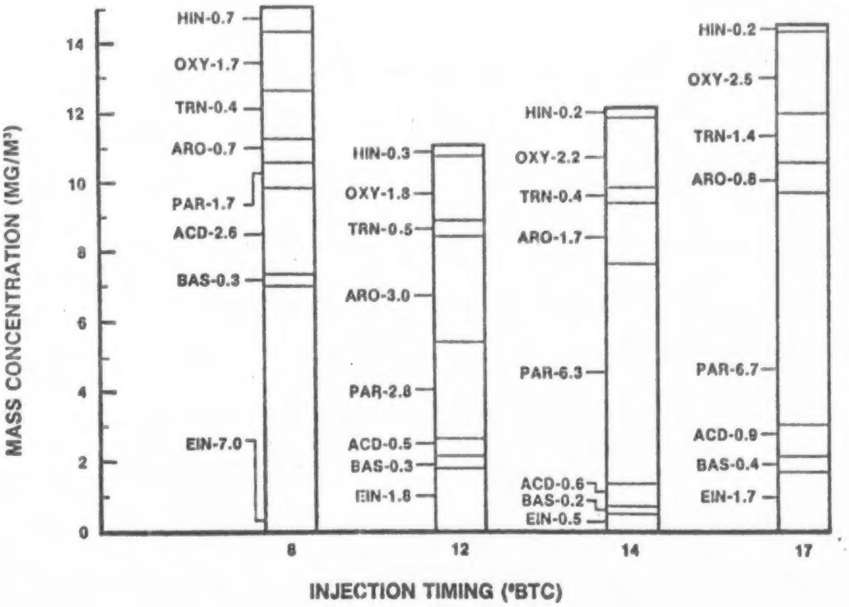

Fig. 3.1.28 - Effect of injection timing on the mass emissions of the chemical subfractions, mode 3, 3.8 in. bowl, ultra-high rate

total SOF, and in terms of total mass and power-normalized emissions, as timing was retarded. This is consistent with less fuel mixed past the lean combustion limit, to leave the cylinder unchanged; injection rate does not seem to affect this phenomenon greatly. Oxygenated compounds are also decreased as timing is retarded for both pumps, which is contrary to the mode 9 observation with the high-rate (6G) pump. This suggests that mode 3 conditions are characterized by less fuel mixed past the lean combustion limit than mode 9 (due largely to less air swirl), and the phenomenon of fewer lean regions with timing retard predominates over the competition of free radicals for monatomic oxygen mentioned previously for mode 9 conditions.

Another similarity between the two injection rates at mode 3 include a general increase in ether insolubles with retard past 14°. This subfraction could represent partially pyrolyzed fuel that originates from incomplete atomization due to relatively poorer mixing at retarded timings. It is not pyrolyzed completely to carbon because peak temperatures do not remain in the solids formation region (2000°-2400°F) long enough for this to occur.

If one observes the trends of subfraction percentages as a function of mode for the 6G (high rate) pump, one sees that the oxygenated fraction is relatively independent of injection timing. Percent oxygenates in the SOF was generally highest at mode 9, with modes 11, 3 and 5 showing decreasing amounts of oxygenates. This independence of percent composition with timing was not observed with any other subfraction and may be due in part to more reproducible mass determination for this subfraction.

Although only two points are available for the load-composition trends, the consistency of decreased transititonals and oxygenateds as well as increased hexane insolubles and aromatics with increased load at intermediate speed (Figures C7-C9) is surprising. This suggests that timing is relatively unimportant in the direct relationship between increased load and increased dehydrogenation of SOF precursors. The dehydrogenation of fuel should increase insoluble and aromatic subfractions, while addition of oxygen (favored at lighter loads) will increase transitional and oxygenated subfractions. Rated speed modes (figures C10-C12) did not show these trends.

The biological activity of the SOF with ultra-high injection rates was increased over that with high rates, and was increased as timing was retarded (Figure 3.1.29). This is contrary to the timing-specific activity trend of the high injection rates. For both pumps, however, the SA follows the same trends as NO_2 concentrations, which supports the hypothesis that nitration of organics may increase the activity of the SOF. As before, the acidic and transitional were the most active subfractions, while paraffins and aromatics were essentially unresponsive.

Figures 3.1.30 and 3.1.31 show the relationship between NO_x and NO_2, respectively, with the BSFC and BSTPM as well as the BSFC-BSTPM combination parameter for both pumps, as timing is varied. The $BSNO_x$ and $BSNO_2$ trade-off with BSFC and BSTPM shows the ultra-high rate pump to be better from an overall standpoint; but if fuel consumption alone is considered, the ultra-high rate pump is inferior to the high rate pump.

Recommended Fuel Injection Characteristics

Theoretically, increased mean injection rates and pressures, by allowing retarded timings, can improve BSFC by permitting the thermodynamic ideal of constant volume combustion to be approached. Additionally, high injection pressures result in: short ignition delays, leading to reduced "lean limit" HC's; reduced peak cylinder temperatures and NO_x emissions; and reduced smoke/particulate levels.

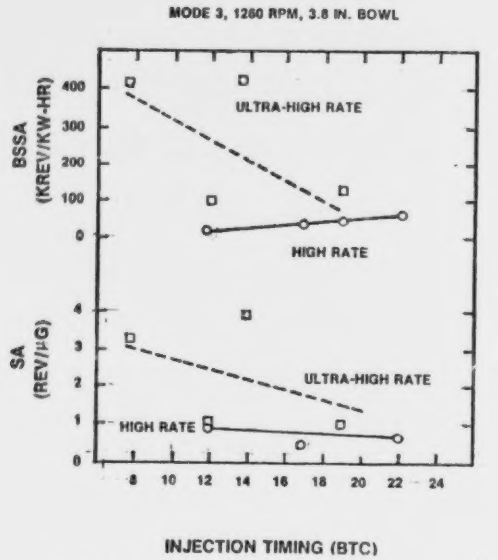

Fig. 3.1.29 - Effect of ultra-high injection rate and timing on biological activity, 3.8 in. bowl, mode 3, tester strain TA100, without S-9

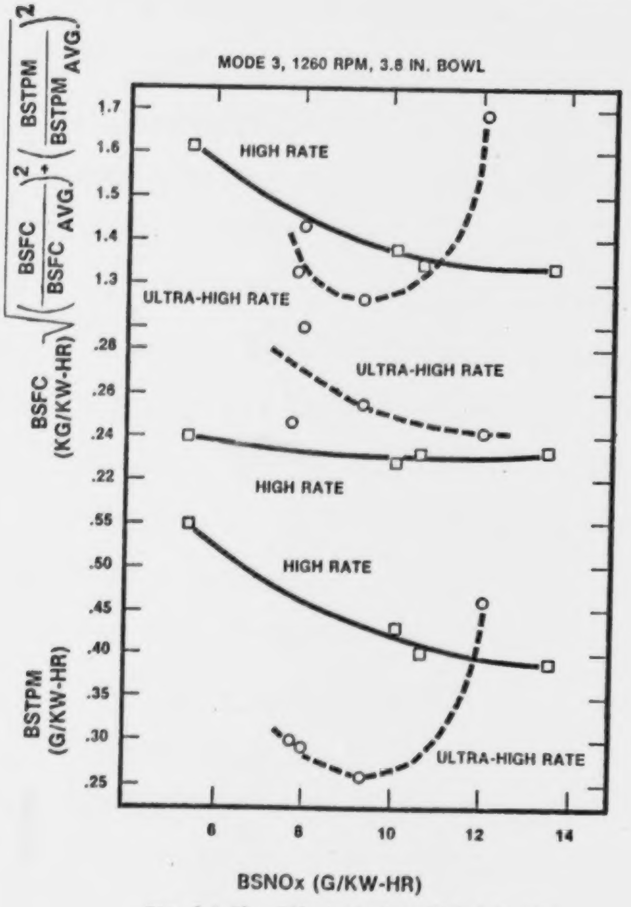

Fig. 3.1.30 - Effect of ultra-high injection rate and timing on BSTPM, $BSNO_x$, and BSFC relationships, 3.8 in. bowl, timing variable

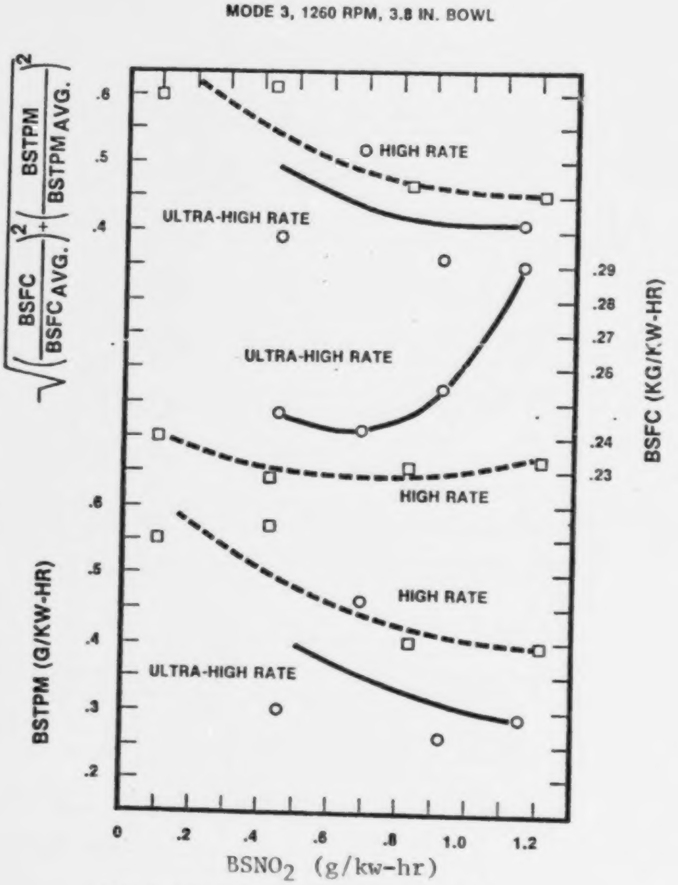

Fig. 3.1.31 - Effect of injection rate on BSTPM, $BSNO_2$, and BSFC relationships, 3.8 in. bowl, timing variable

If mean injection rates are important, the instantaneous rates are perhaps even more important. The instantaneous rates may be analyzed using a rate vs. time curve, as in Figure 3.1.32. This shows the two injection rate shapes generally used in fuel injection systems. Advantages of the triangular shape (Figure 3.1.32a) are low HC and noise due to low initial rates, while disadvantages include smoke and solids contributed by initial and final rates. The square rate shape (Figure 3.1.32b) provides lower peak pressures (and NO_x), and can reduce HC's by providing a rapid final cut-off; however, it has the disadvantage of a high initial rate of injection, leading to noise, HC emissions, and structural loading.

Figure 3.1.33 shows the local histories of ϕ, temperature, solids, HC, and NO masses expected to be contained in an infinitesimal packet of injected fuel. This approach for combustion analysis was developed as a basis for computer modeling (22, 24), and these histories have been based on information gained throughout the study. Histories of three different fuel packets are shown, each formed during a different phase of the injection process. Fuel injected during the initial stages of injection will follow either path 1 or path 1', depending upon initial injection pressures. If the initial pressure is too high, path 1 will be followed. The packet mixes past the lean limit of combustion, does not ignite, and contributes to HC emissions. Packet 1' is followed if initial pressures are too low. This packet fails to mix well and ϕ remains high. The packet contributes to solids formation since its temperature never rises into the solids oxidation region.

Packet 2 is formed during the main period of injection. Since it is injected during the peak cycle temperature, it is heated well above the solids formation region and particulate oxidation occurs. At this point, NO formation

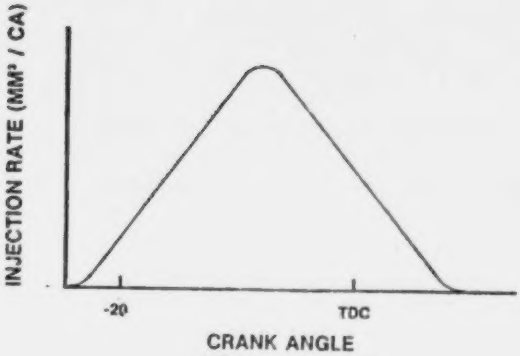

a) Triangular Pulse

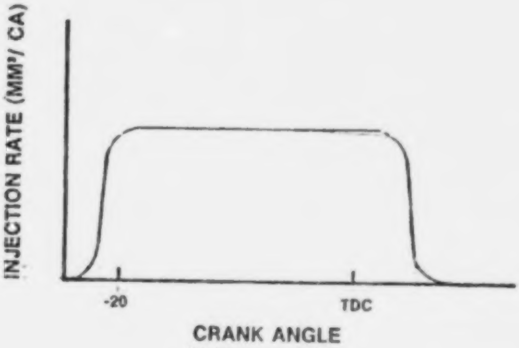

b) Square Pulse

Fig. 3.1.32 - Schematic of the two general rate shapes of the injection rate vs. crank angle curve

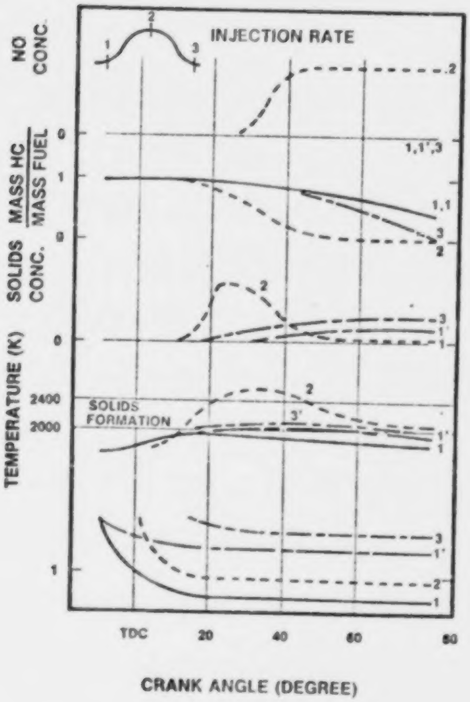

Fig. 3.1.33 - Histories of infinitesimal fuel-air packets formed at various stages of injection

begins until the temperature drops below 2000°F. Due to the high temperatures and $\phi \cong 1$, this packet does not contribute to HC or SOF emissions.

Packet number 3 is formed near the end of injection under conditions of low injection rate and pressure. Solids form rapidly due to low ϕ and high temperatures; these solids will be exhausted from the cylinder. Little or no HC or SOF emissions result from this packet due to high temperatures.

This discussion demonstrates the importance of temperature on HC, solids, and NO_x emissions. Temperature, however, is dependent upon rates of fuel delivery and mixing. Figure 3.1.34 shows the ideal rate shape based upon fundamental considerations, while Figure 3.1.35 is a schematic of ideal temperature histories resulting from this ideal rate shape; packet numbers refer to the same injection period as they did in the previous discussion.

It has been found, for the Mack engine, that injection of fuel at pressures less than about 40 mPa will result in excessive smoke levels (54). Therefore, the initial injection period should just exceed this level until after ignition, to ensure atomization. A packet of fuel injected during this period will follow path 1 and autoignite at the end of the ignition delay. The temperature rises rapidly and then falls due to relatively cool surroundings, contributing little to solids and NO formation. Since peak temperatures are very high, all HC emissions should be consumed. The duration of initial injection corresponds approximately to the ignition delay period, and may be reduced relative to the total injection duration as load is increased for a turbocharged engine.

Parker (55) has suggested a maximum injection pressure during the main injection period of 100 mPa. Peak pressures should be as high as possible to minimize the total injection period, but should not cause loss in efficiency due to excessive energy requirements. At light loads, Parker has suggested mean injection pressure of 50 mPa to avoid overpenetration, with pressures increasing

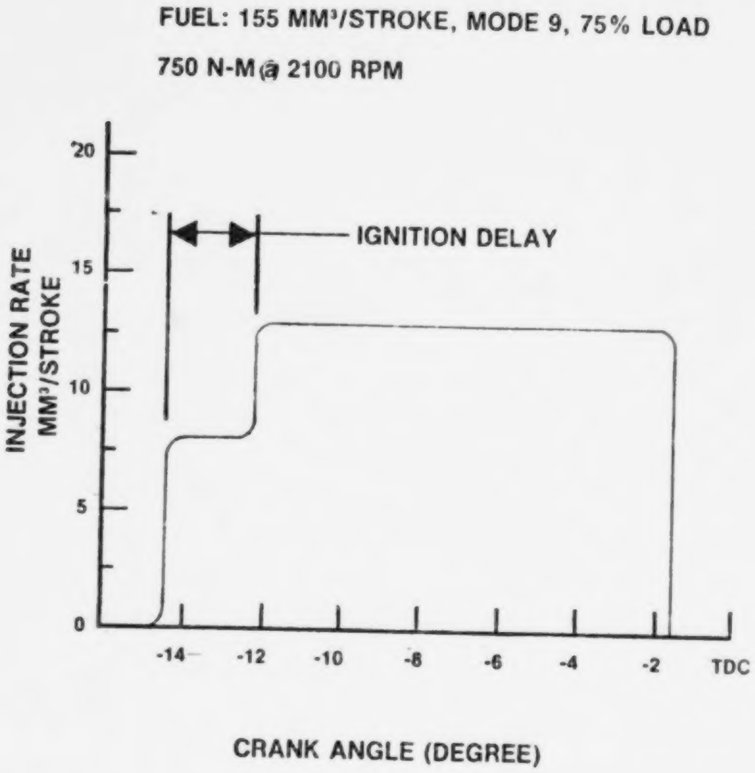

Fig. 3.1.34 - Ideal injection rate for providing optimum BSFC and emissions, mode 9, 155 mm^3/stroke, 6 x 0.29 mm nozzle orifice

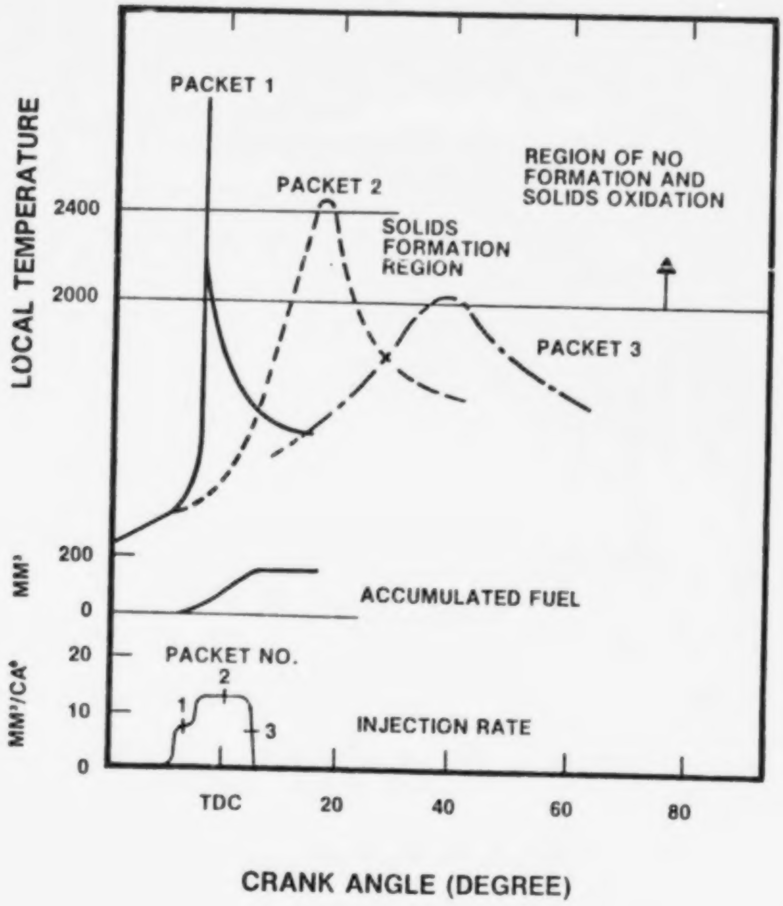

Fig. 3.1.35 - Proposed temperature ranges for optimum BSFC and emissions

rapidly with speed and/or load exceeding 40% of the rated value. Fuel injected during the peak of such an injection cycle will follow path 2 and pass through the solids formation region. If air-fuel mixing is sufficient to give a rapid decrease in ϕ, little net solids formation should result. By retarding the timing as late as possible without reducing the packet's expansion ratio, peak temperature and NO_x emissions are reduced.

The cut-off during the final period of injection would ideally be instantaneous, and should not exceed one degree crank angle (55). Fuel injected during this period will follow path 3 and will always form solids due to high cylinder temperature. Perhaps the only way to reduce solids formation from such packets is to decrease their number by as rapid an injection cut-off as possible.

Injector nozzle orifice number and their size determine spray geometry, and higher swirl speeds at higher speeds and loads may require more nozzles of smaller diameter to maximize air utilization and reduce spray overpenetration. A variable orifice nozzle should enable one to use constant injection pressures over a wider speed range and maintain optimum mixing and penetration characteristics. If the same injector nozzle orifices are used with the ideal injection rate curve as were used for the low rate and shuttle pumps during this study, the recommended injection rates (as calculated from coefficients of discharge of the nozzles) would be 9.4 and 13.3 mm^3/°CA. These rates correspond to 40 and 100 mPa injection pressure, respectively. Although the nozzles used were not variable-orifice in nature, these pressures should give spray geometries appropriate for swirl conditions experienced during a moderate portion of the load cycle.

Optimum Injection Characteristics

With the recommended injection rate shape as shown in Figure 3.1.34, BSFC should be kept low by minimizing energy required to generate injection pressures. Particulate emissions may be controlled by: 1) using a zero sac volume nozzle in combination with a minimum of fuel injected before ignition to reduce SOF; and 2) injecting as quickly as possible with rapid mixing to reduce solids. Since initial rates of injection largely determine the SOF-solids trade off, the initial rate should be just high enough to avoid poor mixing yet not so high as to contribute to solids. To reduce NO_x emissions, lower maximum cycle temperatures should be reached. This is achieved by retarded timing and by injection rates high enough to avoid particulate formation but low enough to maintain reasonable fuel consumption.

While a variable orifice nozzle may not be necessary, its elimination would require variable injection pressure for varying speeds, and would reduce control over the solids. Variable timing control may not be critical, but it would allow better control of NO_x. Achieving so high a degree of control over the injection characteristics may not be possible without a set of electronically triggered, hydraulic actuated unit injectors. This type of injector uses a high-pressure ($<$ 20 mPa) fuel supply to operate a differential area piston, and the injection pressure is a function of the differential areas of the piston and the supply pressure. Although the shuttle pump used in this study approached the mean pressures required, it used a triangular pulse. Although a square-rate cam might improve BSTPM and HC by giving a fast injection cutoff, the hydraulic actuated injectors might still be the best system.

Assuming that the ignition delay, in crank angle degrees, is constant (56), one may use the measured fuel consumption of the various modes to predict the injection duration and hence the mean injection rates the ideal system would supply. Also, assuming that equal changes in injection rate result in similar emissions characteristics, one may predict the increase in $BSNO_x$ that is expected. This would allow predicting the amount of injection timing retard necessary to reduce the $BSNO_x$ to the desired level. Next, by assuming the emissions trends to remain similar to those tested previously, one could calculate the BSSolids and BSFC that would result from this system.

This has been done, and the results are shown in Table 3.1.11. One should be very cautious when using these predicted values, as many assumptions have been made. These assumptions greatly simplify the complex process of diesel combustion, and are based on a limited amount of experimental data.

Table 3.1.11 - Fuel Injection Rates, Injection Timing, and Emissions Expected to Result from Proposed Ideal Rate Characteristics

Mode	Fuel (mm^3)	(°CA)	F/Θ_{mean} (mm^3/°CA)	F/Θ[a] (% increase)	Expected BSNOx @19 BTC (g/kw-hr)	Timing for BSNOx ≈10 (g/kw-hr)	Expected solids (g/kw-hr)	Expected BSFC (kg/kw-hr)
3	69	7.3	9.4	22	12.65	14	.27	.228
4	124	10	12.5	29	15.1	13	.20	.220
5	180	14	12.8	20	13.8	14	.42	.221
9	155	12.2	12.7	63	12.5	15	.02	.264
10	110	8.9	12.4	79	12.3	16	0	.278
11	77	8.2	9.4	59	9.9	19	0	.337

(a) relative to the high-rate, 3.8 inch bowl system at 19°BTC

The injection timings were selected so as to yield a flat $BSNO_x$ level over the EPA modes listed. The BSSOLIDS and BSFC values are the predicted values resulting from the ideal mean rates of injection and the injection timing. These values have been averaged over the six modes and compared to the averages resulting from the 3.8 in. bowl, high rate system at 19°BTC timing. The overall result is that for a $BSNO_x$ level of 10 g/kW-hr, the recommended injection characteristics resulted in a 70% reduction in BSSolids and should also reduce the SOF significantly. This would then yield an overall reduction in the TPM.

The BSFC should remain almost constant, as compared to the high rate system. It should be noted that these BSSOLIDS levels were predicted based on past trends, but if the correlation for Dent's mixing rate is used (84), similar BSSOLIDS are predicted.

It is expected, however, that the elimination of the high peak injection rates and pressures will yield lower NO_x levels than those indicated. This would allow advancing the injection timing until NO_x reaches the maximum desired level and result in improving the predicted BSSOLIDS and $BSNO_x$ levels.

CATERPILLAR 3208 - AFTERTREATMENT DEVICE STUDY

Engine Specifications

The engine used for all studies of exhaust aftertreatment was a Caterpillar 3208 medium-duty diesel truck engine. The engine was received new and was run-in for a total of 50 hours prior to emissions measurements. The engine specifications are given in Table 3.2.1.

Table 3.2.1. Caterpillar Engine Specifications

Engine Manufacturer and Model: Caterpillar 3208
Engine Type: V-8, Direct Injection, Naturally Aspirated
Bore X Stroke: 114mm x 127mm (4.5 in. x 5.0 in.)
Displacement: 10.4 liter (636 cu.in.)
Rated Power: 157 KW (210 hp) at 2800 rpm
Rated Torque: 654 N M (485 FT LBF) at 1400 rpm

A total of four different aftertreatment devices were utilized with this engine. These will be discussed separately, and the relative merits of each device will be discussed in the second section of the conclusions.

Englehard PTX Oxidation Catalyst

Engine Test Set-Up - The first aftertreatment device (an oxidation catalyst) chosen for evaluation was an Engelhard Corporation model PTX-D-616-300NKG platinum exhaust gas purifier. The specifications of the catalyst are given in Table 3.2.2. This catalytic converter is considered typical of oxidation catalysts that could possibly be used on diesel powered vehicles in the near future. Since the Caterpillar 3208 engine is a V-8, a separate catalytic converter was installed for each bank of cylinders.

Table 3.2.2. Oxidation Catalyst Specifications (57)

Manufacturer	Engelhard Industries Div. Engelhard Corp.
Model	PTX-D 616-300NKG
Catalytic Agent	Platinum
Catalyst Loading	<3500 gm/m^3
Wash Coat	Alumina
Substrate Material	Cordierite
Substrate Type	Laminar Flow Monolith
Substrate Cell Size	46.5 cells/cm^2
Substrate Size	14.6 cm dia x 15.24 cm long

The Engelhard PTX catalysts were installed as close as possible to the exhaust manifolds of the engine. This was done to allow the exhaust to enter the catalyst at the highest possible temperature. Blank tubes were fabricated to replace the catalytic converters for baseline testing. Uncatalyzed monoliths had been furnished by Engelhard to be used for baseline testing, but it was felt that their use would not result in an accurate evaluation of the catalyst and substrate as a system. The addition of an uncatalyzed monolith to the exhaust system would have resulted in a large increase in surface area that the exhaust components would have been subjected to, and may have resulted in the catalysis or quenching of reactions occurring in the exhaust system. Approximately 80 hours of use were accumulated on the catalysts before actual testing was begun, as recommended by the catalyst manufacturer (57).

It was discovered during preliminary testing that the exhaust system can act as a large storage place for diesel particulates. Of interest was the amount of sulfates stored when operating with the catalyst installed. Large variations in total mass and sulfate concentrations were observed during early testing when tests without the oxidation catalysts were conducted soon after tests with the catalyst had been completed. It is believed that these variations were caused by the re-entrainment of particulate matter (probably sulfates (25,26)) that had been deposited on the exhaust system walls from prior tests with the catalysts installed. Exhaust system conditioning times were then increased when tests were to be conducted at different conditions than those run immediately prior to allow for system equilibrium to be obtained at the new test conditions. The conditioning time was increased to at least 2 hours when a mode change was made and to at least 8 hours when the catalysts were either removed or installed.

The three fuels used for this evaluation were AMOCO Premier No. 2 (58), a specially blended No. 1 fuel supplied by Chevron Research Company (59), and shale-derived fuel oil supplied by the Department of Energy (DOE). The properties of these fuels were given in Table 2.2. All of the shale oil properties were determined by Chevron (59), except for the percent sulfur and nitrogen (by DOE). AMOCO Premier No. 2 fuel was chosen because it represents a typical No. 2 grade fuel with approximately the national average sulfur content of 0.23% by weight (60). The Chevron No. 1 fuel was chosen for this evaluation because its lower sulfur content (0.04% by weight) may be desirable for use in a catalytic converter equipped diesel-powered vehicle. These two fuels were similar to those used by Frisch et al. in a previous study of fuel effects done at MTU (12,14). The shale oil represents a highly refined fuel which could become a future alternative to the extensive use of petroleum products in diesel-powered vehicles. This particular fuel was refined from Paraho crude shale oil by Standard Oil of Ohio as part of a joint program with DOE and the U.S. Navy (61). In general, it meets military specifications and has good storage capabilities.

A test matrix was devised to allow for comparison of the three test fuels. Because of the limited quantity of shale fuel available for evaluation, testing was limited to Mode 4 of the EPA 13-mode steady-state cycle. Results reported earlier (31) indicated that the oxidation catalyst used for the evaluation had

Table 3.2.3. Test Matrix for PTX Oxidation Catalyst Evaluation

EPA MODE	3		4		5		9		10		11		3		4		5		4	
SPEED (rpm)	1680		1680		1680		2800		2800		2800		1680		1680		1680		1680	
LOAD (N·m)	160		320		480		399		266		133		160		320		480		320	
BMEP (kPa)	192		383		575		485		322		161		192		383		575		383	
FUEL	No. 2		No. 2		No. 2		No. 2		No. 2		No. 2		No. 1		No. 1		No. 1		Shale	
CATALYST	w/o	with	w/o	with	w/o	with	w/o	with	w/o	with	w/o	with	w/o	with	w/o	with	w/o	with	w/o	with
Total particulate, SOF, and SO_4 mass emissions	X	X	X	X	X	X	X	X	X	X	X	X	X	X	X	X	X	X	X	X
HC, NO, and NO_x mass emissions	X	X	X	X	X	X	X	X	X	X	X	X	X	X	X	X	X	X	X	X
Chemical characterization of SOF	X	X	X	X	X	X	X	X	X	X	X	X	X	X	X	X	X	X	X	X
Ames mutagenicity bioassay on SOF	X	X	X	X	X	X	X	X	X	X	X	X	X	X	X	X	X	X	X	X
Ames mutagenicity bioassay on subfractions			X	X								X			X	X			X	X

the greatest effect on the physical, chemical, and biological character of the emissions at Mode 4. This condition (50% rated load and 1680 rpm) was chosen for the fuel evaluation. The quantity of No. 1 fuel available was also limited, allowing for tests with and without the catalyst for this fuel only at Modes 3, 4, and 5. Sufficient quantities of No. 2 fuel were available for testing at modes 9, 10, and 11 in addition to modes 3, 4, and 5.

The experimental test matrix is given in Table 3.2.3. Due to the failure of an injection pump during testing of shale fuel, the baseline emissions with which shale fuel emissions should be compared are those run prior to testing of the close-coupled catalyst, discussed in the next subsection. The dilution and filter sampling parameters observed with No. 2 fuel are listed in Tables 3.2.5 to 3.2.7. The divergence of the mode 9, without catalyst test from the EPA specified maximum sampling temperature of 52°C was due to unusually high dilution tunnel inlet temperature. Since the sample temperature was not too far above 52°C, the results obtained are acceptable for research purposes.

Table 3.2.4. Ambient Test Conditions

	Ambient Temp. (^{o}C)		Barometric Pressure (kPa)		Specific Humidity (g H_2O/kg air)	
MODE	unc.	cat.	unc.	cat.	unc.	cat.
3	29	30	98.9	99.9	4.5	3.0
4	31	32	99.2	99.6	2.0	2.7
5	31	31	99.0	100.3	3.1	2.4
9	37	22	99.4	98.6	6.2	7.4
10	25	27	101.5	98.9	2.1	4.3
11	32	27	99.4	98.8	9.8	2.3

Table 3.2.5. Dilution Tunnel Conditions

MODE	Volume Dilution Ratio unc.	Volume Dilution Ratio cat.	Dilution Temp. (°C) unc.	Dilution Temp. (°C) cat.	NO_x @Filter (ppm) unc.	NO_x @Filter (ppm) cat.	NO_2 @Filter (ppm) unc.	NO_2 @Filter (ppm) cat.
3	15.0	15.1	39	40	32.7	33.4	2.0	1.4
4	14.7	14.7	48	47	64.2	60.6	1.3	19.5
5	14.9	14.4	51	50	84.3	80.9	1.3	8.4
9	15.3	15.0	60	52	63.5	73.7	0.5	1.1
10	14.9	15.0	50	51	48.1	48.4	1.0	1.7
11	15.0	14.2	49	48	29.8	28.7	0.9	3.9

Table 3.2.6. 47mm Filter Operating Conditions

MODE	Sample Time (min.) unc.	Sample Time (min.) cat.	Sample Rate (% Isokinetic) unc.	Sample Rate (% Isokinetic) cat.	Face Velocity (m/s) unc.	Face Velocity (m/s) cat.	Filter Loading $\frac{mg\ TPM}{cm^2\ stain}$ unc.	Filter Loading $\frac{mg\ TPM}{cm^2\ stain}$ cat.	Total Mass (mg) unc.	Total Mass (mg) cat.
3	32	30	73	84	0.28	0.33	0.175	0.122	2.54	1.77
4	42	53	86	84	0.33	0.32	0.201	1.299	2.92	18.86
5	40	32	83	83	0.32	0.31	0.216	1.324	3.14	19.22
9	11	15	81	61	0.31	0.24	0.218	0.493	3.17	7.16
10	39	10	79	98	0.30	0.35	0.424	0.268	6.16	3.89
11	21	16	81	59	0.31	0.23	0.318	0.341	4.62	4.95

Table 3.2.7. Engine & Catalyst Operating Conditions

MODE	A/F unc.	A/F cat.	Exh. Temp[(a)] (°C) unc.	Exh. Temp[(a)] (°C) cat.	Back Pressure (kPa) unc.	Back Pressure (kPa) cat.	Exh. O_2[(b)] (%)	Cat. Temp[(c)] (°C)	Space Vel. x 10^{-3} (hr^{-1})
3	66	67	252	258	101	104	16.1	269	167
4	41	41	365	372	101	104	13.1	383	200
5	29	31	499	481	102	105	10.8	498	242
9	24	25	642	666	104	108	8.4	695	450
10	36	35	474	490	105	106	11.9	507	349
11	51	51	377	374	104	106	14.7	391	295

(a) Measured at exhaust manifold (inlet to catalyst)
(b) Calculated assuming ideal combustion
(c) Measured at center of catalyst monolith

Effect of Catalyst on Mass Emissions - As shown in Table 3.2.7 and in Figures 3.2.1 and 3.2.2, the use of the catalyst had little effect on the operating parameters of the engine. The greatest effects the catalyst had were a slight increase in exhaust backpressure and an increase in exhaust opacity at modes 4 and 10 (50% rated load at intermediate and rated speeds) because of increased particulate emissions. The use of the catalyst had no effect on the brake specific fuel consumption or on the air/fuel (A/F) ratio of the engine.

Figures 3.2.3a and b show the effect of fuel on NO_x, NO and equivalent NO_2 emissions measured with and without the catalysts, respectively using No. 1 and No. 2 fuels. Figure 3.2.3c shows these same emissions for rated speed modes, with No. 2 fuel only. In general, the NO_x, NO, and equivalent NO_2 emissions using the No. 1 fuel follow the same trends as those observed using the No. 2 fuel for both catalyzed and uncatalyzed tests. The NO_x, NO, and NO_2 emissions measured both with and without the catalysts using No. 1 fuel were all lower than those measured using the No. 2 fuel. This difference is probably due to changes in the characteristics of the fuels. For example, although both fuels had similar cetane indexes (indicating similar ignition delay times assuming the cetane index approximates the true cetane number), the No. 1 fuel contains a lower percentage of aromatic than the No. 2 fuel. Fuel aromatic content has been shown to affect NO_x emissions of diesel engines (62,63,64).

The brake specific NO_x and NO_x concentrations by volume (ppm) were unchanged by the catalyst. The levels of NO_2 emissions were, with the exception of mode 3, increased by the catalyst, depending on the engine operating condition. This increase in NO_2 was at the expense of NO emission rates and concentrations, which were reduced.

The changes in conversion of NO to NO_2 by the catalyst (neglecting other changes in exhaust gas composition) as related to catalyst temperature are shown in Figure 3.2.4. The conversion of NO to NO_2 by the catalyst (calculated as the

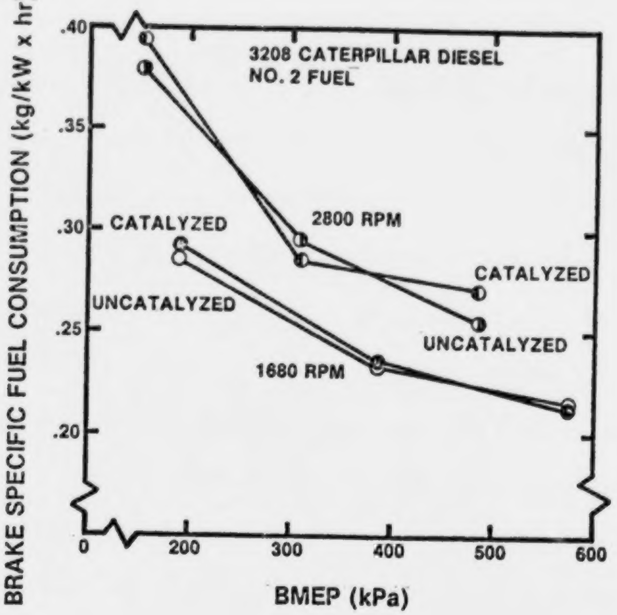

Fig. 3.2.1 - Brake specific fuel consumption, Englehard PTX catalysts

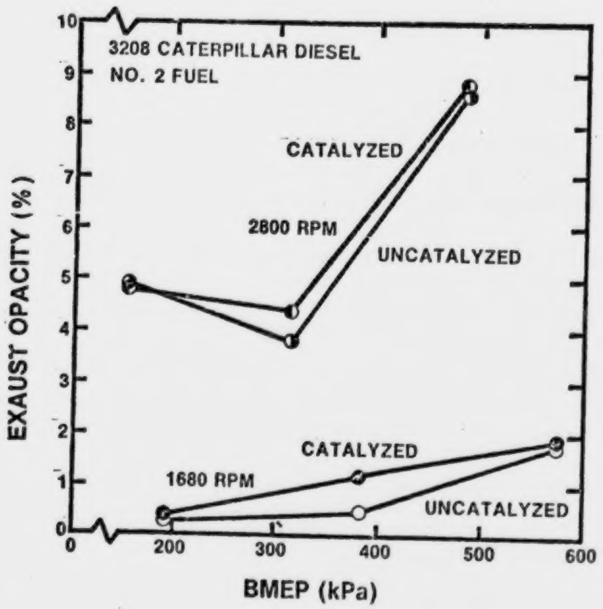

Fig. 3.2.2 - Effect of the PTX oxidation catalysts on the exhaust opacity

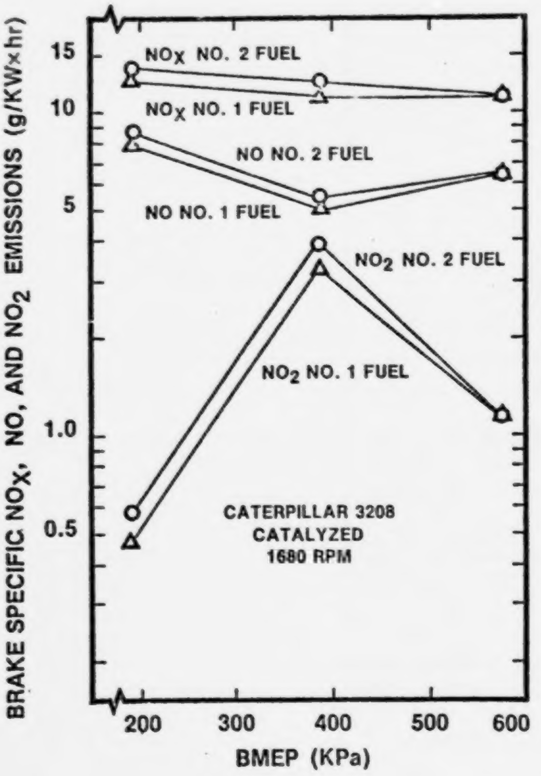

Fig. 3.2.3a – Effect of fuel on brake-specific NO_x, NO, and NO_2 with the PTX oxidation catalysts

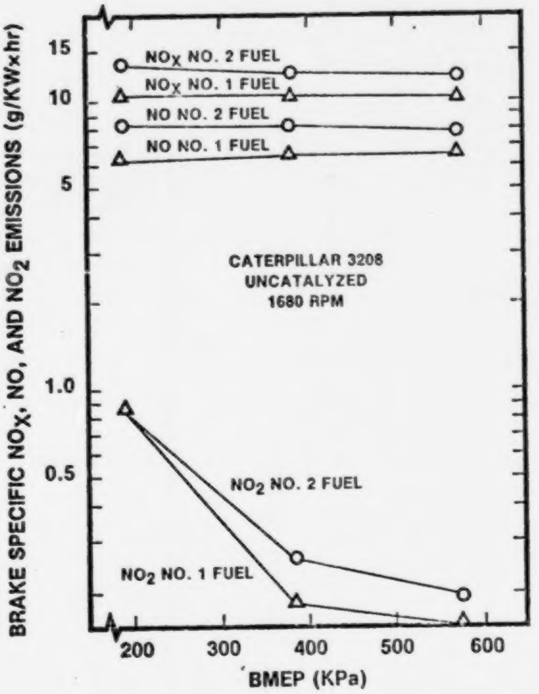

Fig. 3.2.3b – Effect of fuel on brake-specific NO_x, NO, and NO_2 without the PTX oxidation catalysts

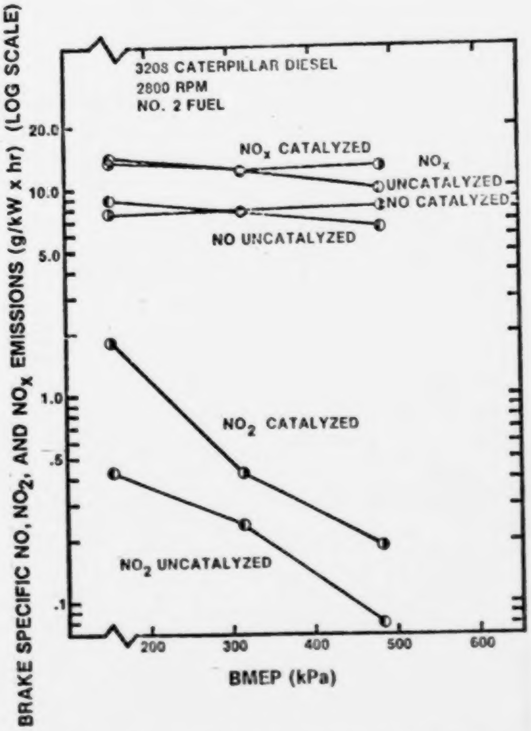

Fig. 3.2.3c – Brake specific NO, NO_2, and NO_x emissions with and without oxidation catalysts, rated speed (2800 rpm)

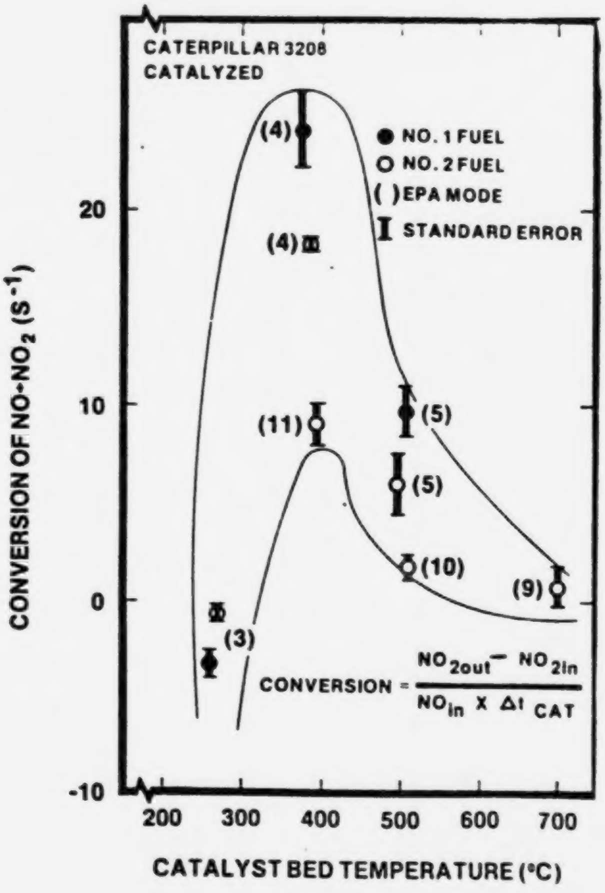

Fig. 3.2.4 – Conversion of NO → NO_2 by catalyst as a function of temperature at the center of the the monolith, Δt_{cat} based on space velocity using gross catalyst volume, NO_{2out} normalized by the factor NO_{xunc}/NO_{xcat} to account for effect of changes in NO_x concentration

fractions of NO converted per unit time)* peaks at approximately 400°C. The catalyst actually reduces some NO_2 back to NO at temperatures below 275°C.

Fuel change effect on HC emissions (with and without the catalysts) is shown in Figure 3.2.5a, while Figure 3.2.5b shows the effect of the oxidation catalyst at the rated-speed modes using No. 2 fuel only. The catalyst was effective in reducing the HC emissions of the engine for all modes and both fuels. There was no change in fuel-metering components or calibration, as the same nozzles were used with each fuel. The uncatalyzed brake-specific HC emissions were lower when No. 1 fuel was used. This is possibly due to the higher volatility of the fuel resulting in more complete combustion because of a higher rate of mixing of the more volatile No. 1 fuel. The brake-specific HC emissions when the catalysts were used were higher for the No. 1 fuel than the No. 2 fuel, indicating the percent reduction in HC emissions was not as great with the No. 1 fuel as compared to No. 2 fuel. This indicates that some physical or chemical characteristic of the No. 1 fuel affects the conversion of gaseous HC in the catalysts.

The brake-specific particulate emissions measured at 1680 and 2800 rpm are shown in Figures 3.2.6a and b, respectively. For both uncatalyzed and catalyzed tests, the use of No. 1 fuel resulted in lower TPM, sulfate, and solid emissions than No. 2 when the catalysts were used. This follows the similar trend in HC emissions discussed above.

---

*A more elegant method of expressing this quantity would be the form

$$\frac{\text{gm moles NO reacted}}{\text{sec-gm Pt}}$$

However, this does not account for the changes in inlet NO concentration and mass flux. The gram of Pt term is not included because it is constant throughout these tests and is a proprietary value. We believe the method of presentation used adequately illustrates the general effects of temperature on the conversion of species on or above the catalytic surfaces.

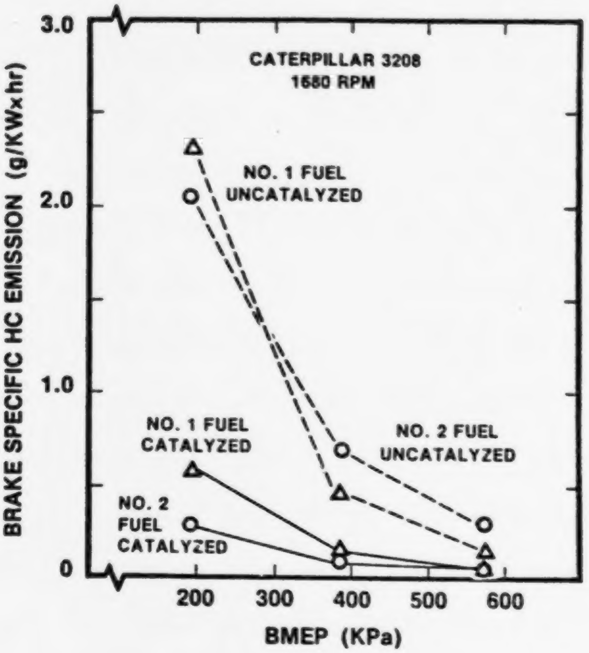

Fig. 3.2.5a - Effect of fuel on brake specific HC emissions, Englehard PTX oxidation catalysts

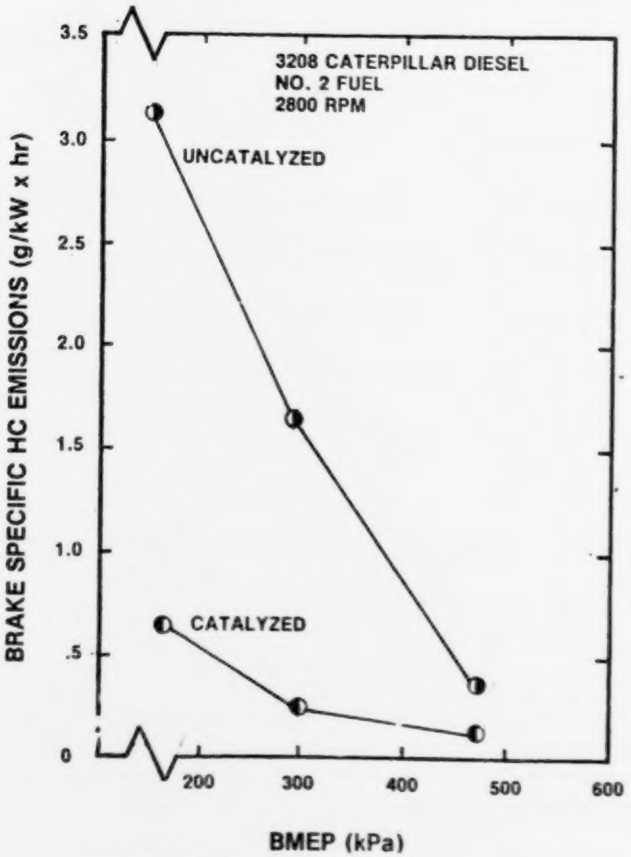

Fig. 3.2.5b - Effect of the PTX oxidation catalyst on brake specific HC emissions, rated speed

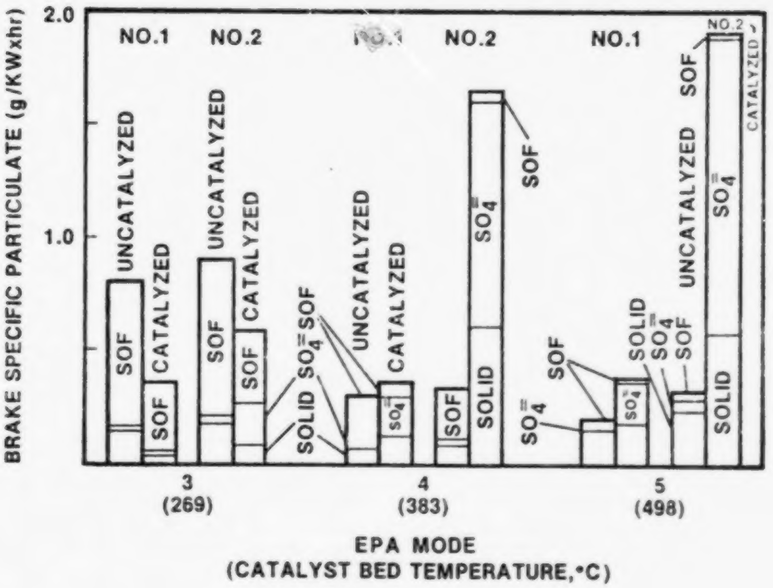

Fig. 3.2.6a - Effect of fuel and PTX oxidation catalysts on brake specific particulate emissions, 1680 rpm

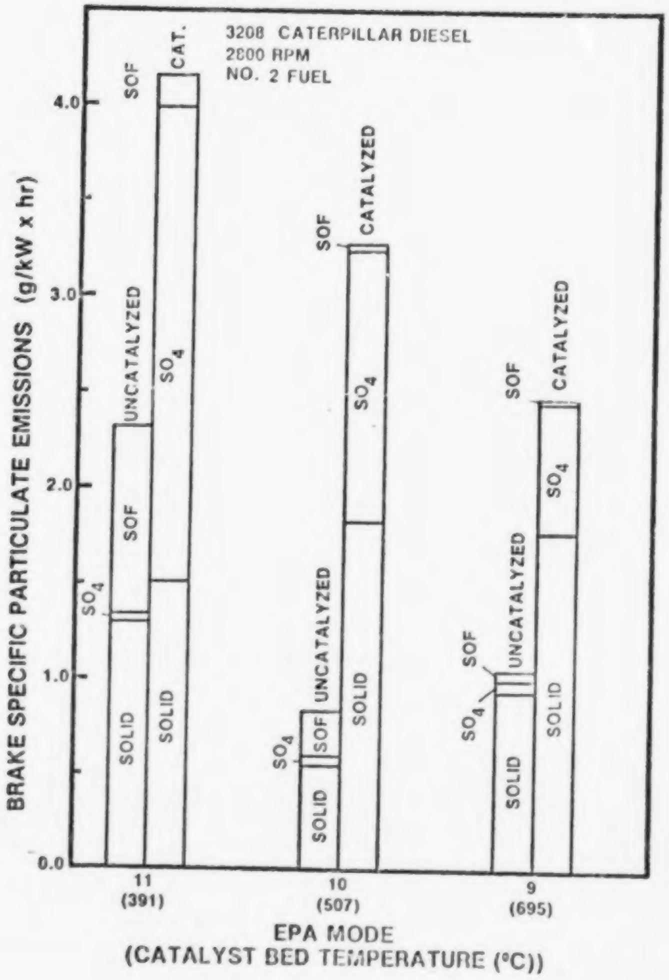

Fig. 3.2.6b - Effect of the PTX oxidation catalysts on brake specific particulate emissions, 2800 rpm

The effects of the oxidation catalyst on the mass emission rates of particulate matter are also given in Figures 3.2.6a and b. As discussed earlier, the total particulate emissions are composed of the sum of the SOF, sulfate, and solids emitted by the engine.

The use of the catalyst reduces the amount of SOF emissions of the engine at all of the test modes. Since the amount of SOF found in the particulate at a given engine speed and load is a function of the dilution parameters and raw exhaust HC concentration, the reduction in particulate SOF is related to the reduction in HFID HC emissions by the catalyst.

As shown in Figures 3.2.6a and b, the amounts of sulfate emissions are increased with the catalyst installed. This phenomenon has been observed with both catalyst equipped spark ignition and diesel engines. The percent conversion of fuel sulfur to exhaust sulfate on a mole basis is shown in Figure 3.2.7.

The use of the catalyst also increases the amounts of total particulate emissions at 5 of the 6 modes tested. The only mode that showed a decrease in total particulate emissions is mode 3. This mode is characterized by a low exhaust temperature, which reduces the catalyst's activation of the oxidation of SO_2 to SO_3, and also by a relatively high baseline SOF emission rate, which causes even a moderate reduction in SOF (61%) to result in a significant decrease in total particulate emissions.

Close examination of Figures 3.2.6a and b reveals that the increase in total particulate emissions is not due entirely to the observed increase in sulfate emissions alone. An increase in the unextractable residue (largely solid) of the particulate at most of the modes of the test cycle used was observed.

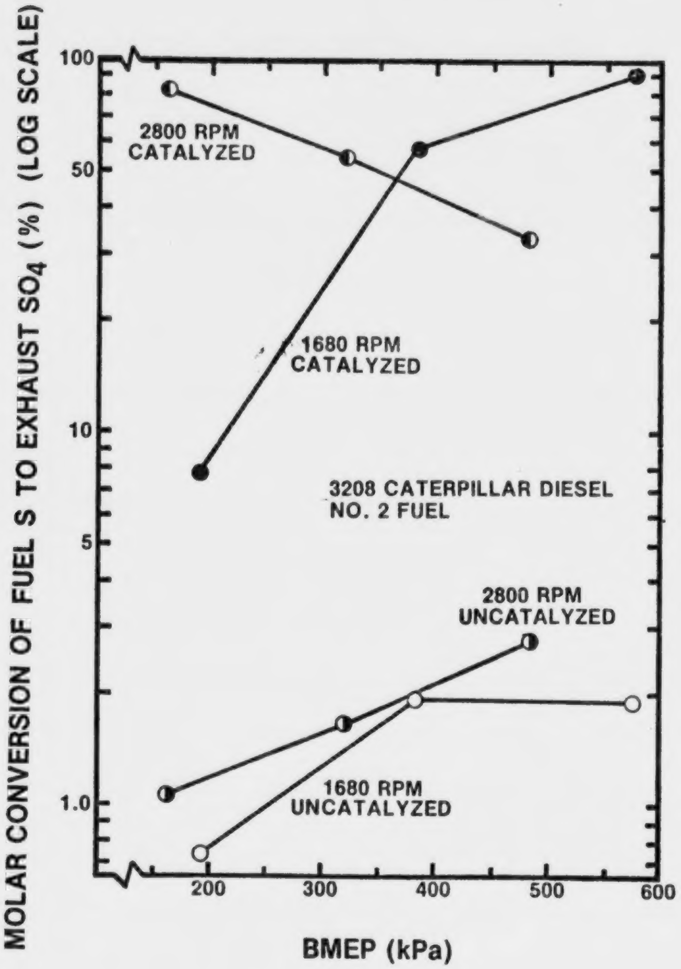

Fig. 3.2.7 - Percent conversion of fuel sulfur to exhaust sulfate (on a mole basis) with and without the PTX oxidation catalysts

The solid portion may contain species such as graphitic carbon, high molecular weight hydrocarbons, and other compounds that are insoluble in DCM, and that may or may not be soluble in the water/isopropyl alcohol solution used for the sulfate extraction. Some of these compounds might be liquids, but the bulk of them are expected to be solid. The increase in opacity observed at modes 4 and 10 with the catalyst installed would suggest that the measured increase in "solid" emissions could be due to an increase in these types of compounds.

The increase in backpressure with the catalyst installed (Table 3.2.7) might cause the increase in solids. It is not felt that the backpressure increase was large enough to account for the measured change in solids. If the backpressure increase was acting to increase the solid portion, the effect should be similar to that of exhaust gas recirculation (EGR). The effects of EGR on a diesel engine include a decrease in the air/fuel ratio and a decrease in NO_x emissions; these phenomena were not observed in these tests. Therefore we feel that the slight increase in backpressure caused by the catalyst was insignificant to the results.

The increase in solids caused by the catalyst may be due to dehydrogenation of the organic compounds present in the exhaust resulting in the formation of solid carbon and low H/C ratio hydrocarbons. The definition of oxidation of an organic compound includes both the addition of oxygen to the molecule (oxygenation) or the removal of hydrogen from the molecule (dehydrogenation). An order of magnitude study was performed to determine if the change due to the installation of the catalyst in the amounts of HC measured in the raw exhaust was sufficient to account for the increased amount of solids measured at modes 4, 5, 9, 10, and 11. The HC measurements done with the HFID both with and without the catalyst at each of these modes were used for this study. Since the response of a HFID is in ppm carbon present in the gas phase HC, the difference in HFID response from uncatalyzed to catalyzed exhaust should be related to, and not more than, the measured increase in solids due to the catalyst. The solid portion of the particulate is probably composed of very low H/C ratio compounds, therefore a H/C ratio of 0.014 by weight (65) was assigned to the compounds measured by the change in HFID response. This available "carbonaceous material" which would be measured as increased solid particulate matter due to the catalyst was then calculated from the change in HFID response and compared to the actual measured increase in solids (as defined by Equation 3 of the Experimental Section), as shown in Figure 3.2.8. With the exception of mode 9, there was enough available gaseous phase HC's in the exhaust to account for the increase in solids due to dehydrogenation in the catalytic converters.

The formation and subsequent condensation of aromatic free radicals above the catalyst sites would result in the formation of low H/C ratio compounds (66) that would be detected as solids. The formation of these radicals is an endothermic process (67), with the required heat being supplied by exothermic reactions occurring on the catalyst sites. The oxidations of NO, SO_2, CO, and HC's on the catalyst sites are all highly exothermic. The formation of benzene radicals by hydrogen dissociation and subsequent condensation to diphenyl has been studied and found to occur both with and without the presence of oxygen over platinum catalysts (68).

Figure 3.2.9 repeats the mode 4 and 5 data of Figure 14 in addition to showing the effect of fuels on the measured increase in solids due to the catalyst, for modes 4 and 5, without regard for other changes in exhaust composition. The use of No. 2 fuel resulted in a greater increase in solid emissions. The No. 2 fuel has a higher aromatic content as well as a higher sulfur content than the No. 1 fuel (Table 2.2). We believe that the increase in

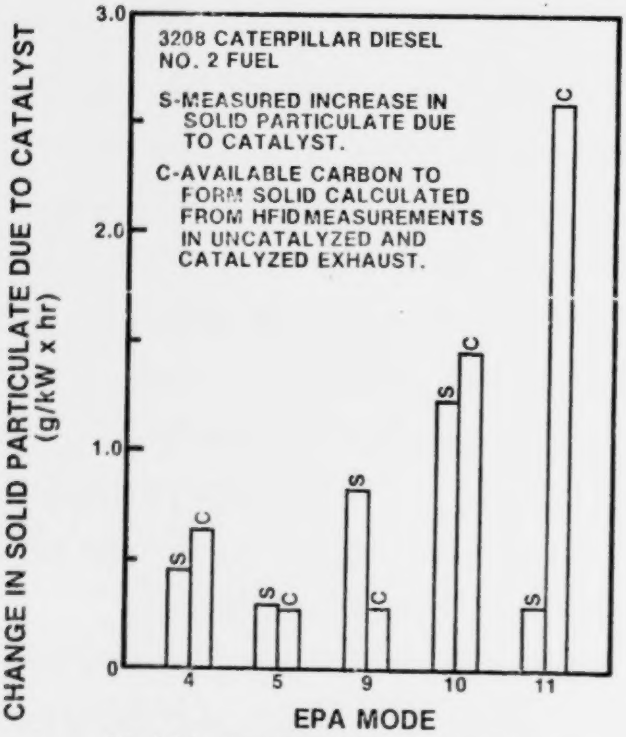

Fig. 3.2.8 - Comparison of measured increase in unextractable residue (solids) with the PTX catalysts to the calculated increase due to HFID HC decrease assuming .014 ratio compounds

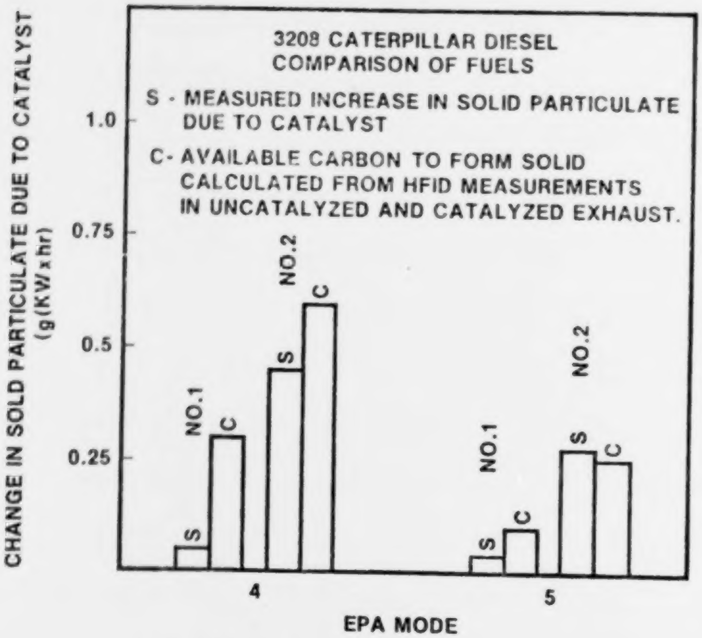

Fig. 3.2.9 - Comparison of measured increase in unextractable residue (solids) with the PTX catalysts to the calculated increase due to HFID HC decrease, showing effects of fuels

solid emissions is primarily due to the formation of aromatic free radicals above the catalyst and the subsequent condensation of these radicals into very high weight polynuclear aromatics.

The data in Figure 3.2.10 show a slightly higher catalyst temperature from the inlet to the center of the monolith for all modes of operation for No. 2 fuel than for No. 1 fuel. Since No. 2 fuel has a higher sulfur content than No. 1 fuel, this temperature increase could be partly attributed to SO_2 oxidation. A three degree temperature increase over the entire catalyst bed would not likely promote any radical formation. It is likely, however, that at the active catalyst sites local temperatures are much higher than the average catalyst temperature that one would measure with a thermocouple.

An increase in solids emissions from the formation of insoluble metal sulfates has been suggested. While this might contribute a small amount to the solids increase, it is unlikely that it is significant since approximately 90 percent of the fuel sulfur not emitted as gaseous compounds can be accounted for by analysis as soluble sulfate in the particulate (15).

The conversion of exhaust HC to solid in the catalytic converters using each fuel is shown in Figure 3.2.11, neglecting the influence of other changes in exhaust composition. The conversion of HC to solids was greater for the No. 2 fuel than for the No. 1 fuel. For both fuels, the conversion of HC to solids increased with temperature; and at catalyst bed temperatures below 275°C, the catalytic converters apparently reduced the amount of solid emissions. The effect of the oxidation of SO_2 to SO_3 in the catalysts on the formation of solids was determined by dividing the fraction of HC converted to solids by the amount of SO_3 per unit volume (as ppm) formed in the catalysts. As shown in Figure 3.2.12, this normalization results in similar conversions of HC to solids for both fuels, which shows that the amount of heat released in the catalyst by

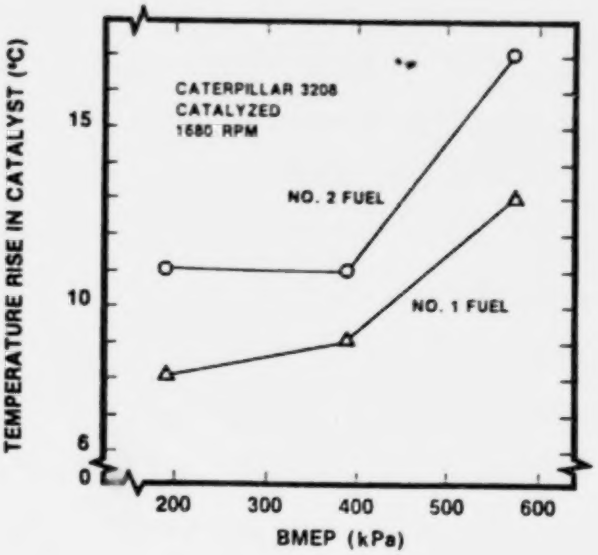

Fig. 3.2.10 - Effect of fuel changes in the temperature rise from the exhaust manifold to center of PTX catalyst monolith

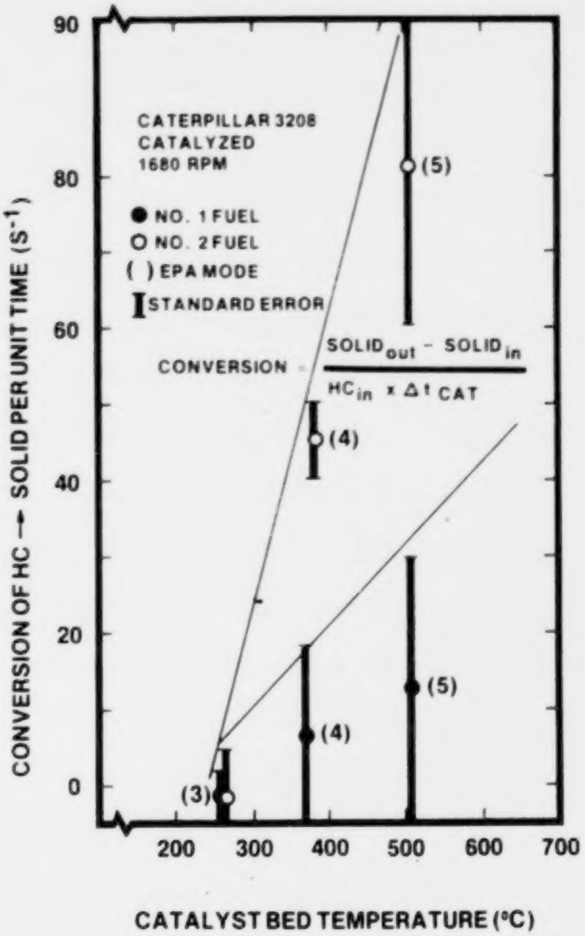

Fig. 3.2.11 - Solid formation by PTX catalysts. Calculated assuming an H/C ratio of .014 by weight for solid and HC, Δt_{cat} based on space velocity using gross catalyst volume

the oxidation of SO_2 to SO_3 possibly affects the formation of solids in the catalytic converters. The conversion of HC to solids normalized to SO_3 production for all test conditions using No. 1 and No. 2 fuels is shown in Figure 3.2.13.

Although, as shown in Figure 3.2.14, the percent conversion of fuel sulfur to sulfate was similar for both fuels with and without the catalysts, the lower sulfur content of the No. 1 resulted in lower sulfate emissions both with and without the catalysts in use.

The effect of catalyst bed temperature on the conversion of exhaust SO_2 to sulfate (neglecting other changes in exhaust composition) is shown in Figure 3.2.15. Because the actual concentration of SO_2 in the raw exhaust entering the catalysts was not measured, it was calculated by assuming that except for the percent of fuel sulfur in the form of sulfate measured without the catalysts installed, the entire fuel sulfur content of the fuel was in the form of SO_2. The conversion of SO_2 to SO_3 in the catalyst peaked at $500^\circ C$, which coincides with the peak conversion temperature of SO_2 to sulfuric acid used in the contact process (69).

Figures 3.2.16a and b show the SOF composition for the modes investigated, using No. 1 and No. 2 fuels, respectively. Use of the oxidation catalyst caused an increase in the percentage oxygenates for 5 of the 6 modes tested. The only mode for which oxygenated compounds were a smaller percentage of the total in catalyzed exhaust was mode 9. This may be due to a long storage time (greater than 3 months) for a portion of the mode 9 filters. Even though the samples were stored frozen, they were thawed and opened repeatedly for the addition of SOF as it became available. This was necessary due to the small amount of SOF collectible on each filter before plugging, requiring addition of SOF from a

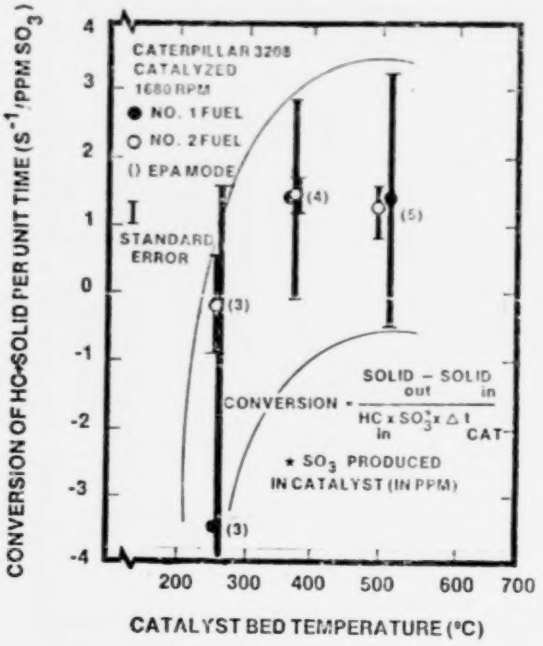

Fig. 3.2.12 - Solid formation in PTX catalyst normalized to amount of SO_3 formed. Calculated assuming an H/C ratio of .014 by weight for solid and HC, Δt_{cat} based on space velocity using gross catalyst volume

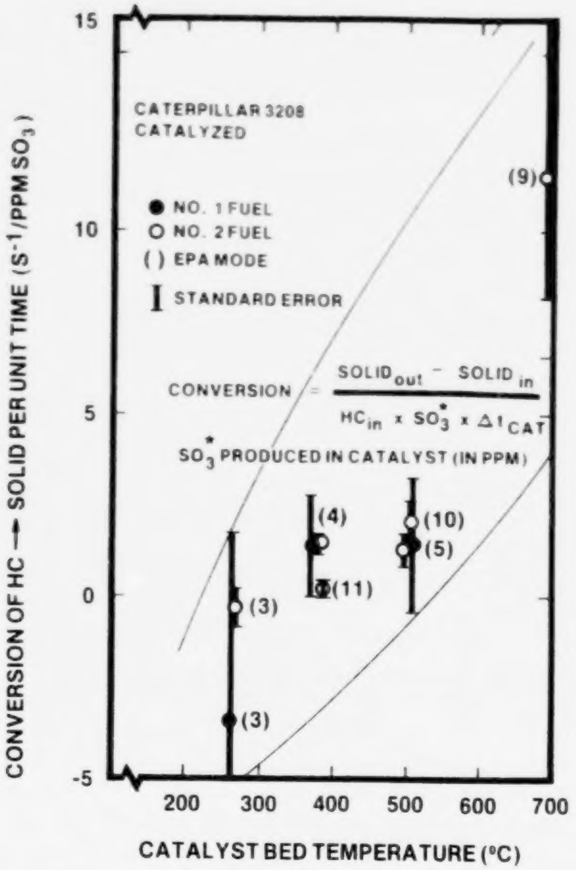

Fig. 3.2.13 - Solid formation in PTX catalyst normalized to amount of SO_3 formed for all tests. Calculated assuming an H/C ratio of .014 by weight for solid and HC, Δt_{cat} based on space velocity using gross catalyst volume

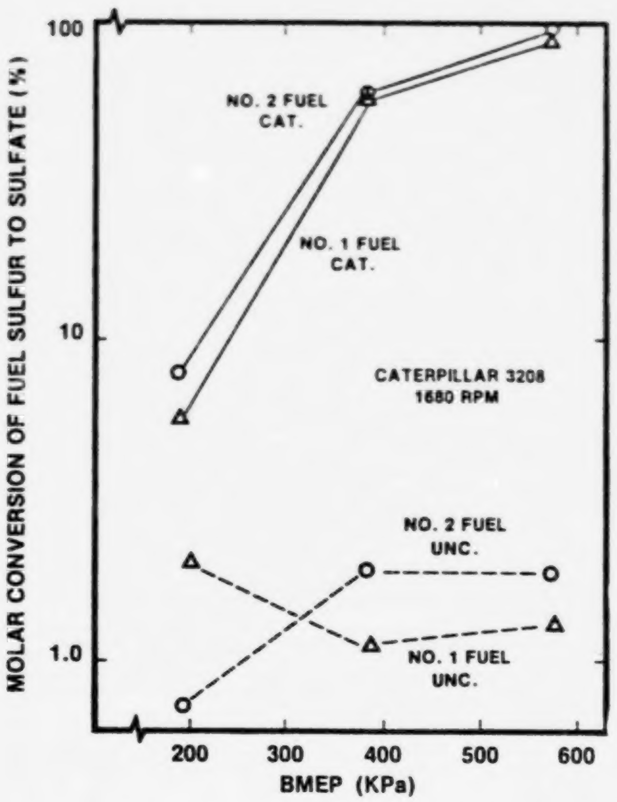

Fig. 3.2.14 - Effect of fuel on the molar conversion of fuel sulfur to $SO_4^=$

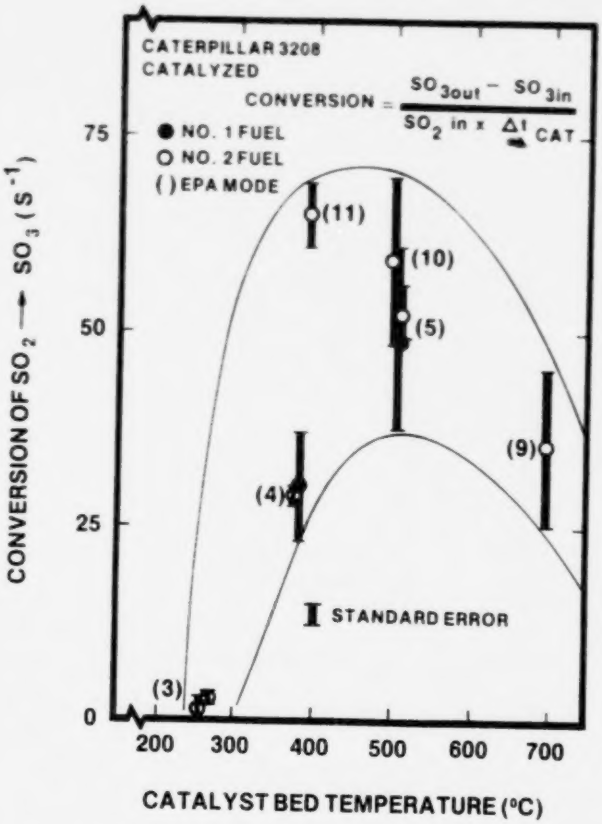

Fig. 3.2.15 - Conversion of SO_2 (calculated) → SO_3 by catalyst as a function of temperature, Δt_{cat}, based on space velocity using gross catalyst volume.

large number of filters. Otherwise, no reasonable explanation is available for this discrepancy.

Another effect of the oxidation catalyst on the SOF was the general decrease in the percentage of paraffins and increase in the percentage of aromatic compounds with its use. The only modes for which this was not observed were the 50% load modes (modes 4 and 10), and mode 5 with No. 1 fuel. With the exception of the 25% load modes (modes 3 and 11), an increase in the percentage of the acidic compounds present in the SOF was observed with the catalyst in use. Since acidic compounds are also partially oxygenated, one might expect the high load modes (higher exhaust and catalyst bed temperature) to produce the greatest total increase in oxygenates and acidics. This was not observed, but the differences in residence time in the catalysts from mode to mode (higher load results in decreased residence time; see Table 3.2.7), and the difficulty encountered with the mode 9 sample may have obscured this trend.

The effects of fuel changes for fuel No. 1 and No. 2 on the percent composition of the eight fractions composing the SOF for tests with and without the catalysts are also given in Figures 3.2.16a and b respectively. Figures 3.2.17 a, b, and c present these data on a mass emissions basis. The concentrations of SOF in the exhaust are independent of the fuel type for fuels 1 and 2 and depends only on the mode and whether or not the catalyst is used. This independence of the effect of fuel properties on the eight fractions that make up the SOF is also apparent.

The percent reductions of the major components of the SOF by the oxidation catalyst are listed in Table 3.2.8. The aromatic and paraffinic fractions show that fuel No. 1 and No. 2 have identical trends toward higher percent reductions going from mode 3 to mode 5. The percent reductions of the transitional fraction and acidic fractions show no consistent trends, while the percent

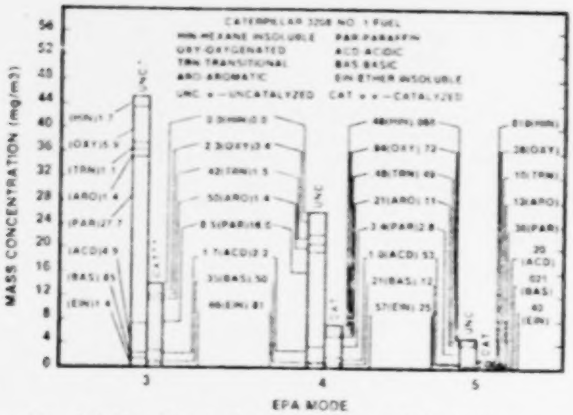

Fig. 3.2.17a- Effect of PTX oxidation catalysts on mass emissions of SOF fractions at 1680 rpm with No. 1 fuel

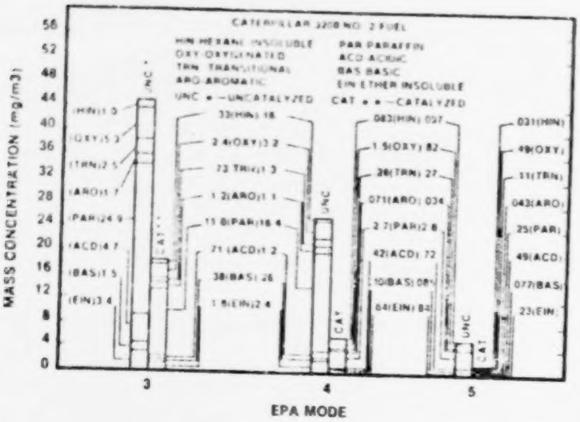

Fig. 3.2.17b - Effect of PTX oxidation catalysts on mass emissions of SOF fractions at 1680 rpm with No. 2 fuel

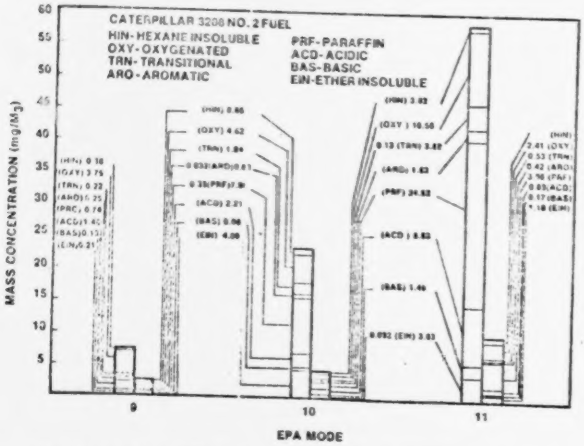

Fig. 3.2.17c - Effect of PTX oxidation catalysts on mass emissions of SOF fractions at 2800 rpm with No. 2 fuel

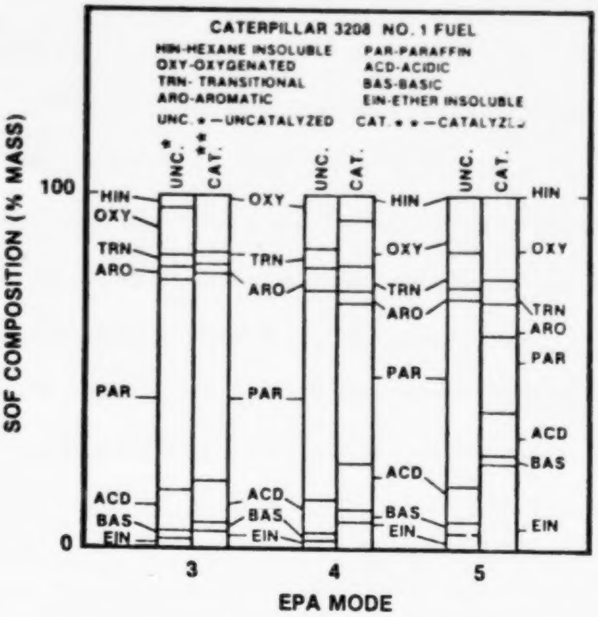

Fig. 3.2.16a - Effect of PTX oxidation catalysts on SOF composition at 1680 rpm, with No. 1 fuel

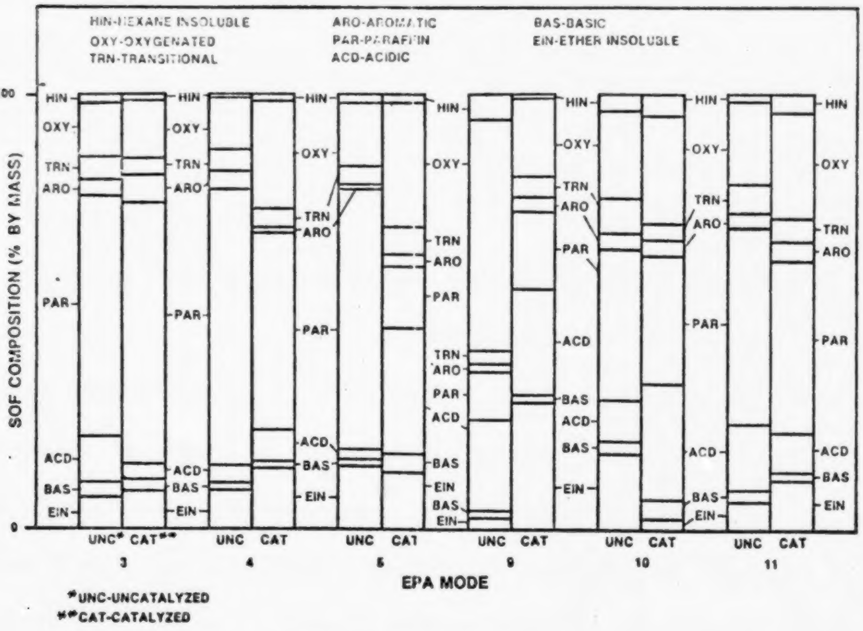

Fig. 3.2.16b - Effect of PTX oxidation catalysts on compostion of SOF with No. 2 fuel

Reproduced from best available copy.

reduction of the oxygenated fraction decreases going from mode 3 to mode 5. The results are consistent for these two fuels also with the greater ease of oxidation of the paraffinic and aromatic fractions over the already partially oxidized transitional, oxygenated and acidic fractions. Some of the aromatic and paraffinic material will be converted to transitional, oxygenated or acidic material leading to apparent lower percent reduction of these fractions.

The similarity in behavior of the aromatic and paraffinic fractions for these two fuels is somewhat surprising. Evidently the effectiveness of the catalyst is sufficient to negate differences in the thermodynamic stabilities of aromatics and alkanes.

Table 3.2.8. Percent Reduction by Mass of SOF Fractions by Oxidation Catalysts

		Fraction					
No. 1	Mode	HIN	OXY	TRN	ARO	PAR	ACD
	3	100	60	62	65	70	65
	4	(a)	72	68	85	69	55
	5	71	27	80	89	87	62
No. 2	3	67	55	70	29	56	74
	4	49	53	80	94	84	65
	5	68	40	59	(a)	91	32
Shale Oil	4	80	88	85	36	89	94

(a) Measured amounts too small for meaningful calculations

Figure 3.2.18 is a gas chromatogram of the No. 2 fuel, mode 11 uncatalyzed aromatic subfraction. Numbered peaks correspond to compounds identified by mass spectrometry, as listed in Table 3.2.9. Compounds no. 1 and no. 17 are possibly not derived from engine particulate samples. Compound no. 1 is a preservative in the diethyl ether used for fractionation, while compound no. 17 is a component of many plastic materials. The compounds listed have been previously

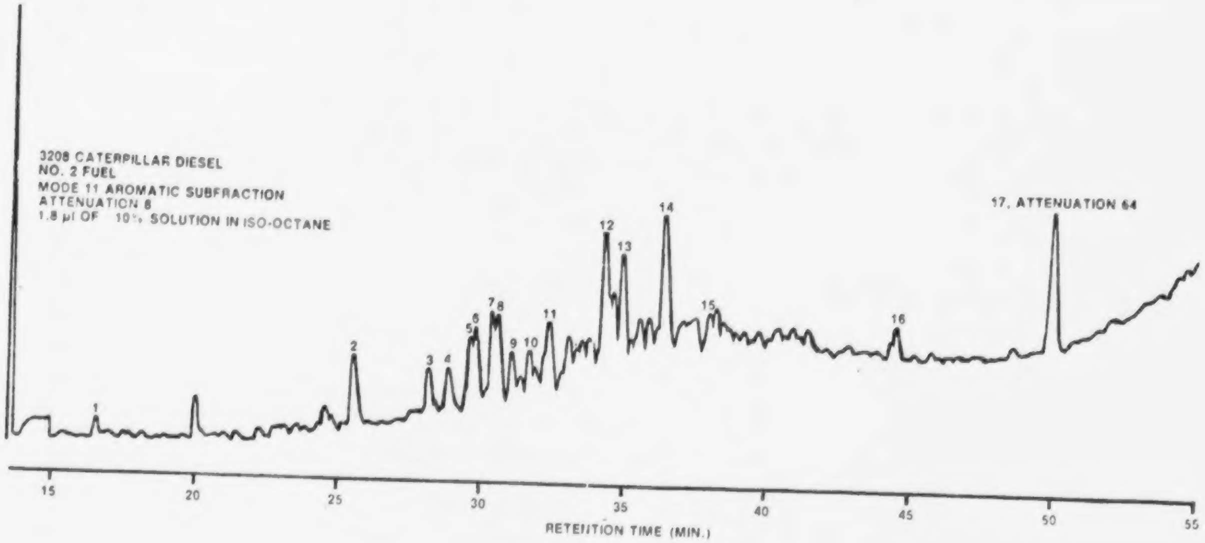

Fig. 3.2.18 - Gas chromatogram of mode 11 uncatalyzed aromatic subfraction. Numbered peaks correspond to compounds listed in table 3.2.9

Table 3.2.9. Tentative Identities of Compounds in Mode 11 Aromatic Subfraction (No. 2 fuel) as Determined by Gas Chromatography-Mass Spectrometry

Peak Number (figure)	Retention Time (min.)	Compound	Molecular Weight
1	19.2	2,6-di(*t*-butyl)-4-methyl phenol	220
2	28.6	Phenanthrene	178
3	31.2	Monomethyl dibenzothiophene isomer	198
4[a]	32.0	Monomethyl dibenzothiophene isomer	198
5[a]	32.8	Monomethyl phenanthrene isomer	192
6[a]	33.0	Monomethyl phenanthrene isomer	192
7[a]	33.6	Monomethyl phenanthrene isomer	192
8[a]	33.8	Monomethyl phenanthrene isomer	192
9	34.8	Dimethyl naphthothiophene isomer	212
10	35.6	Dimethyl naphthothiophene isomer	212
11	36.3	Dimethyl naphthothiophene isomer	212
12	37.6	Dimethyl phenanthrene isomer	206
13(a,b)	38.3	Fluoranthene	202
14(b)	39.9	Pyrene	202
15	41.2	Trimethyl phenanthrene isomer	220
16	48.0	Benzo(ghi)fluoranthene	226
17	53.0	Phthalate ester (insignificant mass ion)	-

(a) Known mutagens (13)

(b) Despite nearly identical mass spectra, identity of these compounds was confirmed by retention times identified by Brooks et al. (7) and Schuetzle et al. (11). Compounds 4-8 and 13 are known mutagens (7), but the mutagenic activity of this aromatic subfraction was not fully determined.

Ames Bioassay Variability and Strain Differences - The statistical analysis of the effect of different assay dates upon the Ames assay data for the same extract is presented in Table 3.2.10. Mode 5 catalyzed SOF and mode 11 catalyzed oxygenated subfraction, both without the S-9 activation mixture, were each assayed on two different dates using identical concentrations within each sample and the Ames tester strain types TA98, TA100, TA1537 and TA1538.

For each strain/mode/date combination a dose-response curve was established and the slope of its linear portion (in Cartesian form) calculated. The two slopes from the different dates within a strain and mode were then compared using the two sample t-statistics. The null hypothesis (H_o) of no difference between the two slopes from the two assay dates within each strain/mode was tested against the alternate hypothesis (H_a), which states that a difference does exist between the slopes from the different assay dates with each strain/mode. For Table 3.2.10 (and Table 3.2.11), the linear model $R = a + b \cdot C$ was used for the testing of differences between slopes. The analyses involved a t-statistic that was calculated based on the differences of the two slopes divided by their pooled residual mean square.

In addition to each date's slope and the calculated t-statistic for each pair of dates within a strain and mode, Table 3.2.10 gives the probability that the differences which exist between the slopes being compared are due to chance. Also shown in Table 3.2.10 is the value of the 5% two-tailed t-statistic with 14 degrees of freedom. The Ha was rejected at the 5% level for all comparisons except for the TA100 mode 11 catalyzed oxygenated subfraction.

Table 3.2.10. Effect of Assay Date on Ames Test Results

Hypotheses Tested: H_o = No difference between experimental dates within sample and strain.
H_a = There is a difference between experiment dates within sample and strain.

Ames Strain[a]	TA98				TA100				TA1537				TA1538			
Mode[b]	5		11		5		11		5		11		5		11	
Extract	SOF		OXY[c]		SOF		OXY		SOF		OXY		SOF		OXY	
Date of Experiment	072980	081480	072380	080780	072080	081480	072380	080780	072980	081480	072380	080780	072980	081480	072380	080780
Slope[d] $\frac{REV}{\mu g}$	4.45	4.64	1.64	1.39	4.61	4.01	2.03	1.66	2.90	2.59	.807	.749	4.44	4.41	1.97	1.68
t-statistic	.1295		.9470		.9640		2.9105		.6800		.7266		.0333		.9288	
Probability	.50<P		.20<P<.50		.20<P<.50		.01<P<.02		.50<P		.20<P<.50		.50<P		.20<P<.50	
$T^{e}_{.05(2),14}$	2.404		2.404		2.404		2.404		2.404		2.404		2.404		2.404	

---

[a] Without S-9 activation system
[b] All samples collected with catalyst installed
[c] OXY - Oxygenated subfraction
[d] Colony counter sensitivity was increased for this study which increased relative slope
[e] Two-tailed t-statistic for 14 degrees of freedom

Table 3.2.11. Effect of Experimental System Variability on Ames Test Results

Hypotheses Tested: H_o = No difference between samples collected and extracted on different days within strains.
H_a = There is a difference between samples collected and extracted on different days within strains.

Ames Strain[a]	TA98				TA100				TA1537				TA1538			
Mode	3		11		3		11		3		11		3		11	
Sample[b]	1	2	1	2	1	2	1	2	1	2	1	2	1	2	1	2
Slope[c] $\frac{REV}{\mu g}$	.469	.541	.506	.605	.809	1.036	.954	.936	.115	.102	.033	.082	.337	.338	.321	.191
t-statistic	1.385		1.251		.1010		.1610		1.258		3.155		.001		2.404	
Probability	.10<P<.20		.20<P<.50		.20<P<.50		.10<P<.20		.20<P<.50		.005<P<.01		.50<P		.02<P<.05	
$t^{d}_{.05(2),14}$	2.404		2.404		2.404		2.404		2.404		2.404		2.404		2.404	

---

[a] Without S-9 activation system

[b] Total SOF collected and extracted from engine on different days, without catalyst

[c] Colony counter sensitivity was increased for this study which increased relative slope

[d] Two-tailed t-statistic for 14 degrees of freedom

Table 3.2.11 shows the effect of varying all phases (collection, extraction, and assaying) of diesel exhaust particulate testing. Samples 3-1 and 3-2 were collected at mode 3 while samples 11-1 and 11-2 were collected at mode 11. The distinction between samples 3-1 and 3-2 (also samples 11-1 and 11-2) is that they were collected on different days, extracted on different days, and assayed in separate experiments.

For each strain and mode combination (without the S-9 activation system), a dose-response curve was obtained and the slope of its linear portion (in Cartesian form) was calculated. For each strain, sample 3-1 was compared with 3-2 and sample 11-1 with 11-2 for significant differences between their slopes. The two sample t-statistic is used for testing the null hypothesis of no difference against the alternate hypothesis that a difference exists.

In addition to the calculated t-statistic, Table 4.2.11 gives the probability that the differences which exist between the slopes are due to chance. Also shown is the tabulated t-value of the 5% two-tailed t-statistic with 14 degrees of freedom. The H_a was rejected at the 5% level for all cases except for strain TA1537 with samples 11-1 and 11-2.

The statistical analysis therefore indicates that the Ames bioassay data were reproducible in 14 of 16 comparisons, whether the same SOF samples were repeated or whether SOF samples from different engine runs were tested. The difference found with strain TA1537 tested against two mode 11 uncatalyzed SOF samples (Table 3.2.11) may be due to the fact that this strain has relatively low-level response (compared to strains TA98, TA100, and TA1538). The slope differences were therefore likely due to natural variation in the Ames bioassay. Strain TA100 provides high-level response with usually good reproducibility. The slopes presented in Table 3.2.10 for repeats of mode 11 catalyzed SOF oxygenated subfraction were not significant at the $\alpha = 0.1$ significance level and therefore the differences probably also represent natural variation in the test results.

Figure 3.2.19 shows the response of all five Salmonella typhimurium tester strain genotypes to the catalyzed mode 11 SOF. Dose-response data indicate the mutagenic components of the diesel SOF are not base-pair substitution mutagens as no mutagenic response was demonstrated by strain TA1535, which is the only strain used responding solely to base-pair substitution mutagens. The greatest response was observed with strains TA100 and TA98, followed by strains TA1538 and TA1537. All of these strains are frameshift mutagen detectors. Similar results have been reported by other investigators working with a variety of diesel and gasoline engines (8,9,49,70). For the purpose of further discussion, only the TA100 tester strain data are presented in graphical form. All test results are listed in Appendix B.

Effect of Catalyst on Ames Biological Activity - The dose-response curves presented in Figure 3.2.20 for strain TA100 and mode 11 SOF (without S-9 activation) indicate that the catalyzed mode 11 SOF (on a revertant/μg of SOF basis) resulted in a greater mutagenic response than the uncatalyzed mode 11 SOF sample. This effect was generally observed with other engine modes, as demonstrated by the dose-response results from modes 4 and 10 catalyzed and uncatalyzed (Figure 3.2.21). The only exception occurred with mode 3, where the catalyzed SOF produced fewer revertants/μg of SOF than the uncatalyzed SOF. Additionally, the SOF from the catalyzed engine modes often displayed a toxic effect which was not found with the uncatalyzed modes (Figure 3.2.21, modes 4 uncatalyzed and 4 catalyzed).

Some of the SOF samples were tested for mutagenic activity in the presence of the S-9 activation mixture. As demonstrated by strain TA100 in Figure 3.2.20, the results from mode 11 and mode 11 catalyzed, with and without the S-9

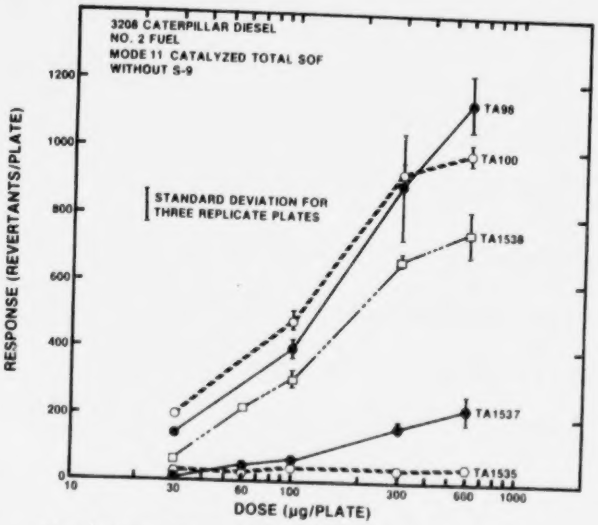

Fig. 3.2.19 - Response of all five Ames tester strains to mode 11 catalyzed SOF

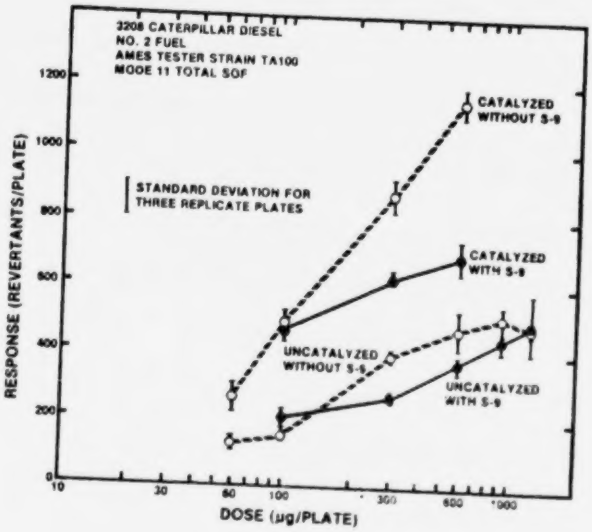

Fig. 3.2.20 - Effects of PTX catalyst and S-9 mammalian activation system on mode 11 SOF

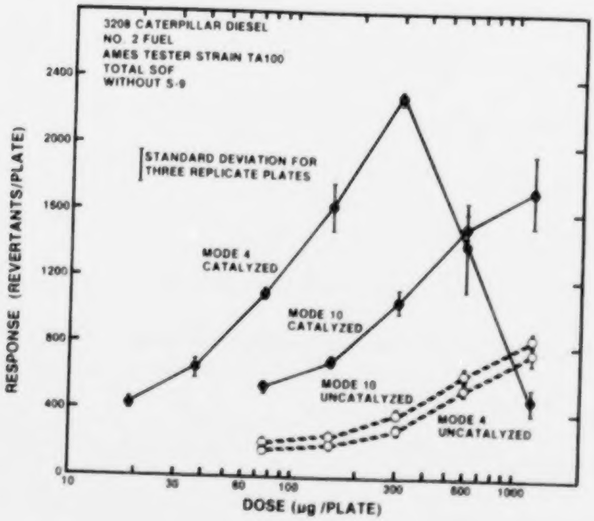

Fig. 3.2.21 - Response of Ames tester strain TA100 to SOF from modes 4 and 11 PTX catalyzed and uncatalyzed

mixture, indicate that the mutagenic activity is direct-acting (i.e., metabolic activation is not required) and the addition of the S-9 mixture causes a general decrease in mutagenic response. These responses have also been noted for SOF from other diesel and fuel systems (7,9,47,70). Tests with other samples and tester strains showed similar results (Appendix B).

The effects of fuel changes on the TA98-SOF dose-response curves with and without the oxidation catalyst at modes 3, 4, and 5 using No. 2 and 1 fuels are shown in Figures 3.2.22a, b, and c, respectively. Figure 3.2.23 shows the effect of the catalyst at rated-speed (2800 rpm) modes for No. 2 fuel. (It should be noted that, in order to reduce variability in the Ames bioassay results, catalyzed and uncatalyzed SOF samples from the same fuel and mode were tested on the same day. A similar format was used when testing the subfractions.) The mode 3 dose-response curves in Figure 3.2.22a are unique with respect to their response to the oxidation catalyst. Only at mode 3 is the biological activity of the No. 1 and No. 2 fuels catalyzed SOF dose-response curves lower than their uncatalyzed SOF dose-response curves. The No. 1 fuel catalyzed SOF has the lowest activity at mode 3, while the uncatalyzed SOF from the No. 2 fuel has the highest activity. The No. 2 fuel's catalyzed and uncatalyzed SOF appears to produce a higher response than does the No. 1 fuel at mode 3.

At modes 4 and 5 (Figures 3.2.22b and c), the catalyzed SOF displayed far greater mutagenic activity than did the uncatalyzed SOF. At all rated speed (2800 rpm) modes, the catalyzed SOF also displayed greater mutagenic activity than did the uncatalyzed SOF (Figure 3.2.23). When comparing within modes, the No. 2 fuel (catalyzed or uncatalyzed) is generally more active than the No. 1 fuel.

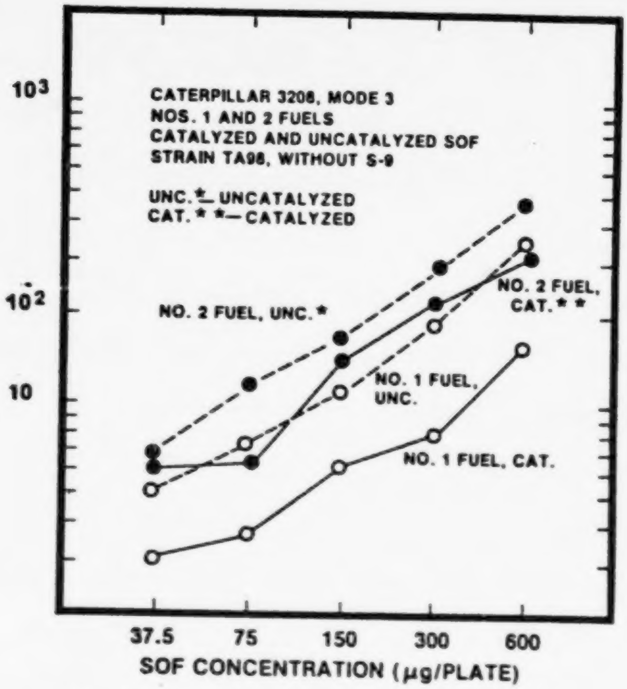

Fig. 3.2.22a- Comparison of No. 1 and No. 2 fuel SOF from Mode 3 uncatalyzed and Mode 3 PTX catalyzed using TA98 without S-9 activation

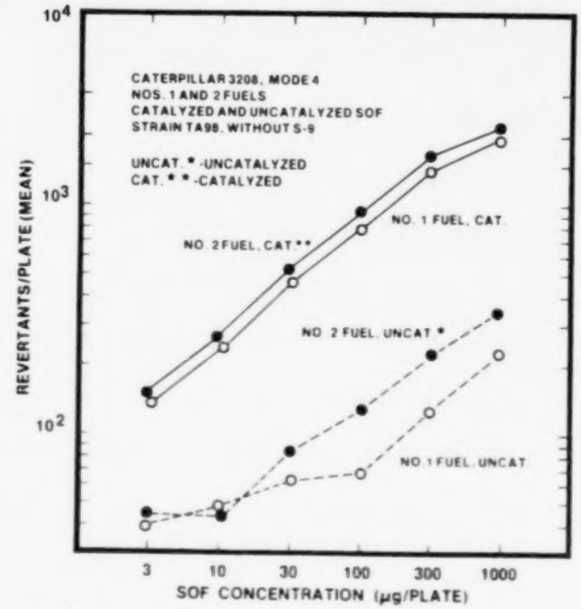

Fig. 3.2.22b - Comparison of No. 1 and No. 2 fuel from Mode 4 uncatalyzed and Mode 4 PTX catalyzed using TA98 without S-9 activation

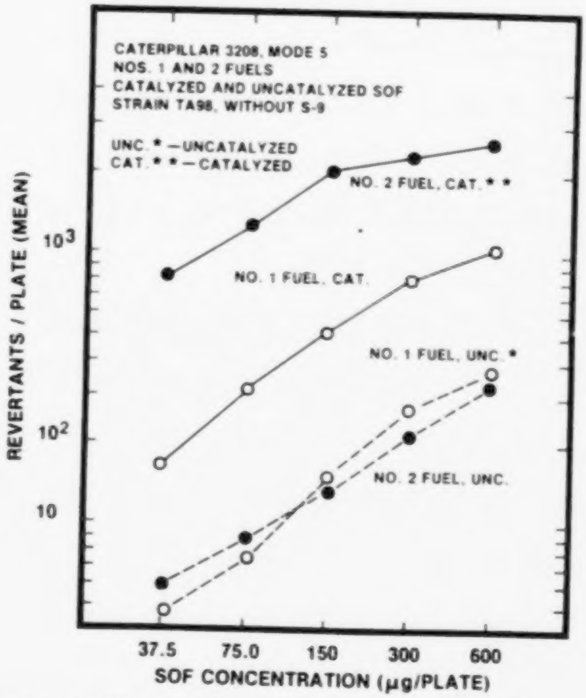

Fig. 3.2.22c - Comparison of No. 1 and No. 2 fuel SOF from Mode 5 uncatalyzed and Mode 5 PTX catalyzed using TA 98 without S-9 activation

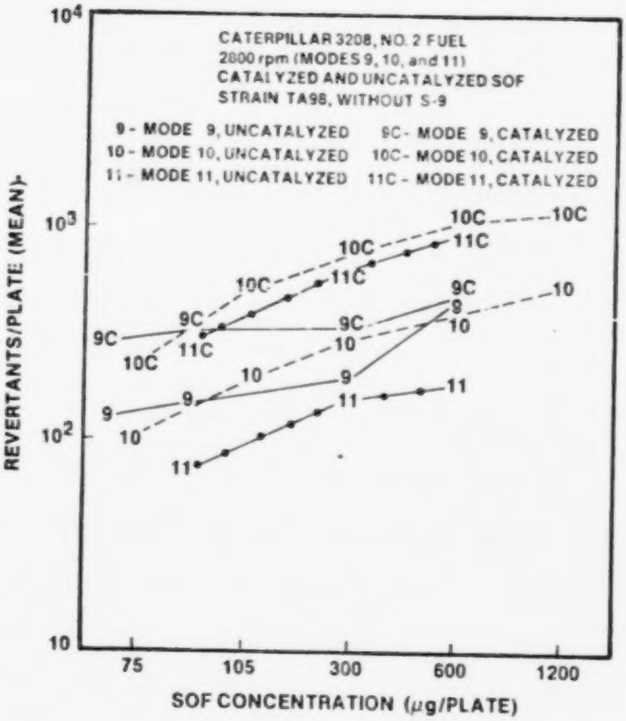

Fig. 3.2.23 - Comparison of No. 2 fuel SOF from 2800 rpm modes uncatalyzed and PTX catalyzed using TA98 without S-9 activation

Figure 3.2.24 shows the effect of the catalyst on the mutagenic SA of the SOF and on the BSSA at 2800 rpm (rated speed). While the SA of the SOF is only slightly increased with increasing engine load at this speed, the BSSA are decreased due to much lower SOF emissions at higher loads, with and without the catalyst.

Figures 3.2.25a and b show the effect of fuel changes on the mutagenic-SA of the SOF and on the BSSA emissions with and without the catalyst. (Specific activity calculations were performed using the log dose-revertant transformation of the liner regression model, and were not standardized with respect to lower and upper doses taken in the regression.) The use of the No. 1 fuel resulted in lower SOF mutagenic-SA and in lower BSSA compared to the No. 2 fuel. Fuel changes have been shown to affect SOF mutagenic-specific activity (47).

A study was conducted to determine whether various sampling and exhaust system variables could be empirically correlated to the specific activity as determined by the Ames bioassay. The quantity SA*, defined as non-paraffinic SOF specific activity, was calculated using the following equation:

$$SA^* = SA \frac{100}{100 - \% \text{ Paraffins}}$$

This value was used rather than the specific activity (SA) of the SOF because paraffins comprise a large portion of the SOF and are inactive using the Ames bioassay. Table 3.2.12 lists the SA* for Strains TA98 and TA100 along with the respective sampling and exhaust system variables. Using the STATJOB subroutine REGAN2 (71), the correlation between a number of independent variables and one dependent variable can be determined, as well as those variables which are significant to the correlation. For the TA100 data, only the raw NO_2 concentration displays significance at the $\alpha = .05$ level. The TA98 data showed that exhaust volume flowrate, raw exhaust temperature and HC concentration in the raw exhaust are significant factors at the $\alpha = .05$ level, while raw NO_2

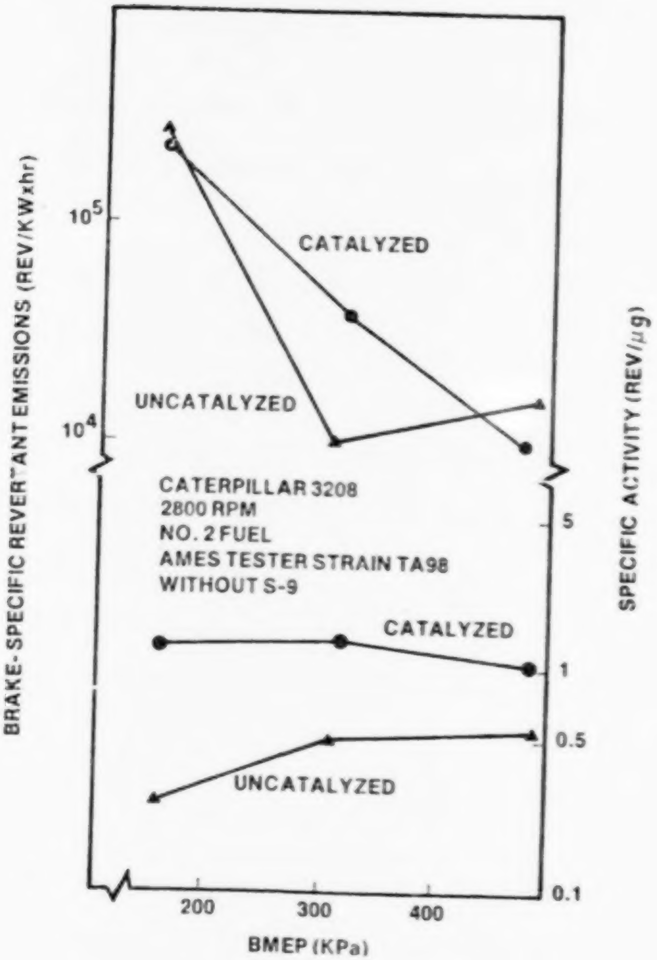

Fig. 3.2.24 - Effect of PTX catalysts on SOF mutagenic-specific activity and brake specific revertant emissions, 2800 rpm

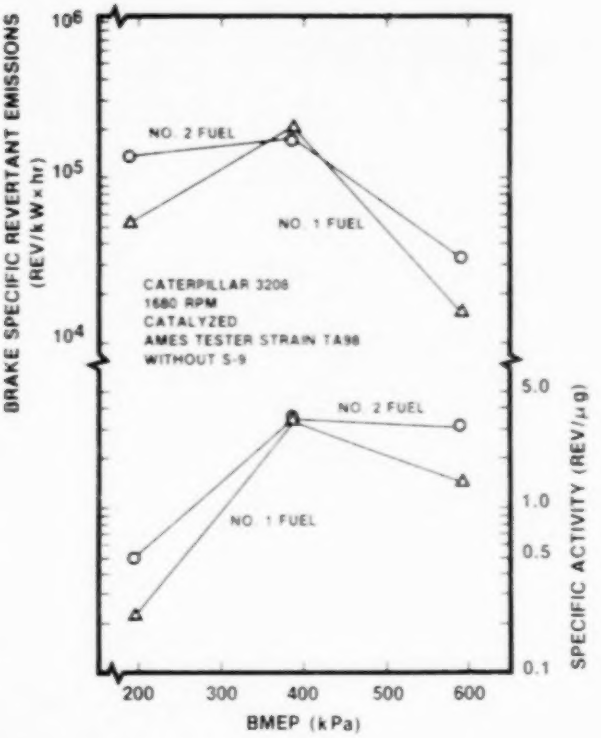

Fig. 3.2.25a - Effect of fuel changes on SOF mutagenic-specific activity and brake specific revertant emissions with PTX oxidation catalysts

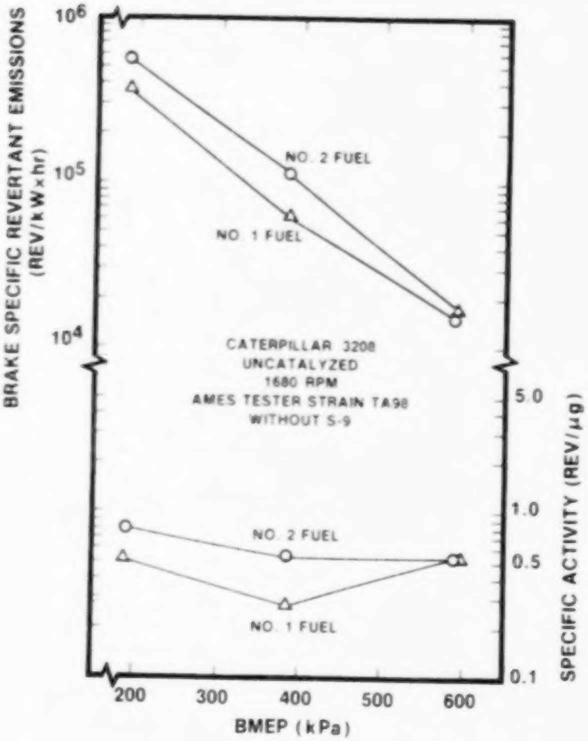

Fig. 3.2.25b - Effect of fuel changes of SOF mutagenic-specific activity and brake specific revertant emissions without PTX oxidation catalysts

Table 3.2.12. Sampling and Exhaust System Variables Associated with Non-Paraffin Specific Activities (SA*) No. 2 Fuel

MODE	PTX	TA98 SA* (Rev/μg)	TA100 SA* (Rev/μg)	NO_{2dil} (ppm)	NO_{2raw} (ppm)	SO_{4dil} ($mg/Actm^3$)	SO_{4raw} ($mg/Actm^3$)	$\dot{V}_{exh}$ $(\frac{m^3\ act.}{min})$	T_{dil}(K)	T_{raw}(K)	Sample Time (min)	HC_{raw} (ppmC)
3		1.07	2.07	2.0	30.1	.1	.9	14	312	525	60	210
3	X	1.08	1.06	1.4	20.6	.7	5.8	14	313	531	120	55
4		0.92	1.37	1.3	19.1	.2	2.1	17	321	638	240	150
4	X	8.20	9.50	19.3	286	7.9	58.5	17	320	645	45	25
5		1.82	1.53	1.3	19.3	.4	23	21	324	772	45	100
5	X	6.01	4.91	8.4	12.0	16.8	107.6	21	323	754	30	17
9		0.61	0.90	0.5	8.0	.6	3.5	34	333	915	30	115
9	X	1.27	3.82	1.1	16.3	7.0	36.6	34	324	939	15	25
10		0.74	0.78	1.0	14.3	.3	2.0	29	323	747	120	320
10	X	2.22	2.98	1.7	25.8	10.1	64.2	29	324	763	10	40
11		0.47	1.17	0.9	13.6	.1	1.0	24	322	650	20	310
11	X	2.14	4.90	3.9	55	9.3	64.1	24	321	647	20	60
3		1.13	1.21	8.2	41	.6	1.9	14	335	523	45	210
3		.95	0.89	2.5	38	.2	1.8	14	314	532	90	210
3		NA	0.2	1.2	33	.1	1.0	15	308	528	135	210
11		1.26	1.53	2.5	13	.7	2.0	23	358	652	10	310
11		.77	1.17	0.5	8	.13	1.0	24	322	650	20	310
11		.45	1.15	0.3	8	.1	1.2	25	315	674	40	310

concentration is significant at the $\alpha = .1$ level. This study tended to show that the raw exhaust variables that would be associated with exhaust system reactions to be more significant than diluted variables and sampling time which might be associated with artifact formation.

Effects of Shale Fuel on PTX Catalyst Operation - As mentioned previously, the emissions data from the PTX catalyst run with shale fuel are not strictly comparable to the baseline emissions used for No. 1 and No. 2 fuels due to the replacement of a failed injection pump in early 1981. Table 3.2.13 compares engine data for the two baselines at modes 3, 4, and 5, although the only mode for which shale fuel data were obtained using the PTX catalyst was mode 4. An appreciable decrease in NO_x levels was seen for the more recent baseline, with lesser increases or decreases in various particulate components of the exhaust.

Figure 3.2.26 shows the change in brake-specific NO_x, NO_2, and NO emissions for the shale fuel with and without the PTX catalyst. As with the No. 1 and No. 2 fuels, the catalyst had little effect on NO_x emissions but increased NO_2 emissions, with resultant decrease in NO emissions. Figure 3.2.27 shows BSHC and BSTPM (including SOF and solids; sulfate was negligible) for mode 4 using shale fuel. As with the other fuels, the HC and SOF were reduced with the shale fuel by use of the oxidation catalyst; however, the TPM was also reduced despite an increase in the solids content with the oxidation catalyst, due primarily to the extremely low sulfur content of the shale fuel.

Figure 3.2.28 illustrates the SOF composition of samples collected using shale fuel with and without the oxidation catalysts at mode 4. The uncatalyzed baseline values obtained with No. 2 fuel after the injection pump change are shown for comparison. Use of shale fuel resulted in lower percentage paraffins, oxygenates, and transitionals; and higher aromatics and acidics for both catalyzed and uncatalyzed shale fuel, compared with uncatalyzed No. 2 fuel. The percentage of aromatics using shale fuel and the oxidation catalyst was higher

Table 3.2.13. Baseline Emissions Comparison
Caterpillar 3208, No. 2 Fuel (all units in grams/kw-hr ± 1 standard deviation)

Mode	Emission	March-April 1980	July 1981
3	BS NO_x	13.65 ± 0.26	10.24 ± 0.03
	BS NO_2	0.84 ± 0.09	1.16 ± 0.22
	BS NO	8.36 ± 0.21	5.92 ± 0.16
	BS HC	2.01 ± 0.00	1.92 ± 0.21
	BSTPM	0.889 ± 0.034	1.047 ± 0.031
	BS Solids	0.117	0.084
	BS SOF	0.753 ± 0.03	0.932 ± 0.030
	BS $SO_4^=$	0.019 ± 0.003	0.031 ± 0.001
4	BS NO_x	12.69 ± 0.18	10.39 ± 0.13
	BS NO_2	0.26 ± 0.03	0.85 ± 0.05
	BS NO	8.11 ± 0.11	6.22 ± 0.07
	BS HC	NA	0.77 ± 0.02
	BS TPM	0.331 ± 0.009	0.482 ± 0.030
	BS Solids	0.086	0.069
	BS SOF	0.215 ± 0.003	0.377 ± 0.024
	BS $SO_4^=$	0.035 ± 0.008	0.036 ± 0.002
5	BS NO_x	12.07 ± 0.36	9.69 ± 0.08
	BS NO_2	0.18 ± 0.05	0.36 ± 0.01
	BS NO	7.75 ± 0.27	6.08 ± 0.05
	BS HC	NA	0.25 ± 0
	BS TPM	0.266 ± 0.006	0.241 ± 0.005
	BS Solids	0.202	0.172
	BS SOF	0.032 ± 0.004	0.038 ± 0.001
	BS $SO_4^=$	0.032 ± 0.013	0.031 ± 0.002

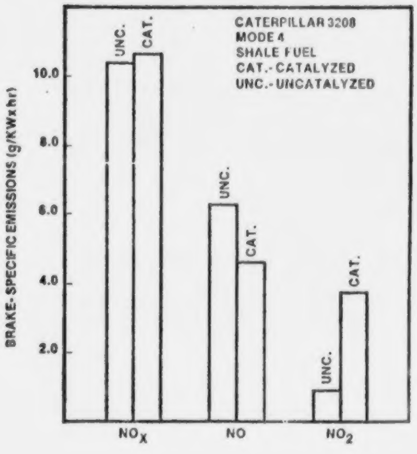

Fig. 3.2.26 - Effect of the PTX oxidation catalysts on $BSNO_x$, BSNO, and $BSNO_2$ with shale fuel

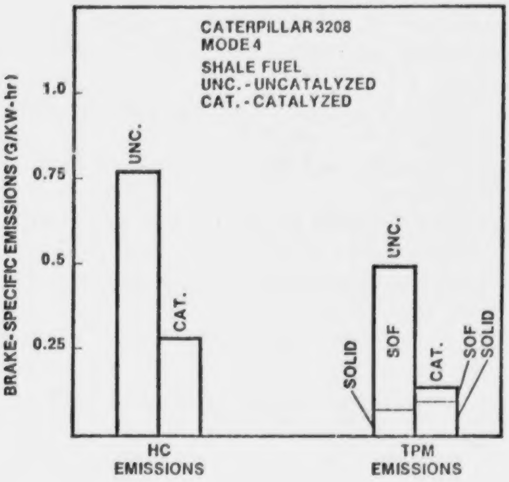

Fig. 3.2.27 - Effect of the PTX oxidation catalysts on HC and particulate emissions with shale fuel

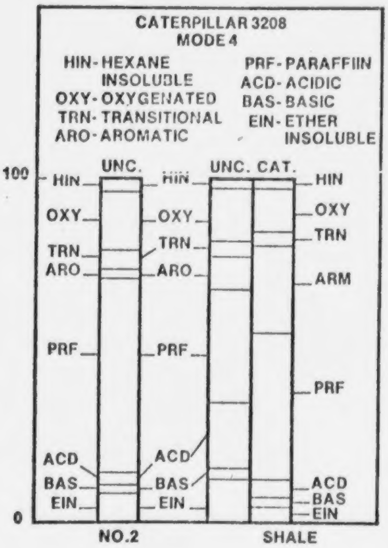

Fig. 3.2.28 - Effect of fuel changes and PTX catalysts on SOF composition with shale fuel, compared with No. 2 fuel uncatalyzed

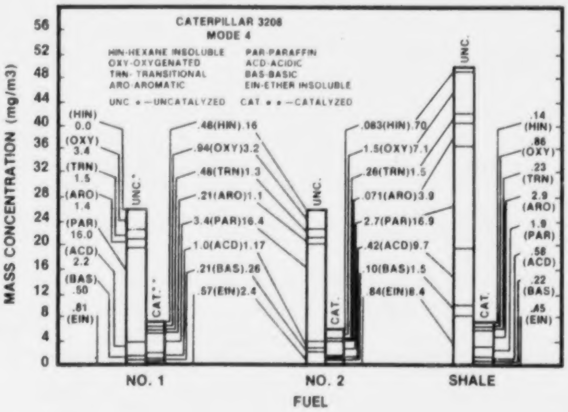

Fig. 3.2.29 - Effect of fuel changes on mass emissions of SOF fractions with and without PTX oxidation catalysts

than for most SOF examined. A different analysis of this data, as shown in Figure 3.2.29 and the last line in Table 3.2.8, also demonstrates the stability of shale fuel aromatics at mode 4. With shale fuel, every fraction but the aromatic fraction is reduced by the catalyst to a greater percentage than for fuels No. 1 and No. 2. The reason for the lower percent reduction of the aromatics must be due to more stable types of aromatics in the SOF. The lower percent conversion of the aromatics to oxygenated, transitional and acidic fractions for the shale fuel is indicated by the higher percent reduction of each of these three fractions. The paraffinic fraction of the shale fuel is reduced by the same percentage as for fuels No. 1 and No. 2.

The mode 4 results in Table B7 of the appendix show that the SA of SOF from all these fuels is similar, and may not be statistically different when using the catalyst; however, the uncatalyzed sample shows the shale fuel to have a noticeably higher SA than the No. 1 or No. 2 fuels. Figure 3.2.30 is a comparison of the Ames dose-response curves for these fuels. The catalyzed samples showed higher SA than the uncatalyzed samples for all these fuels, with No. 1 fuel showing the lowest activity for either catalyzed or uncatalyzed SOF.

The biological activity of the acidic and oxygenated SOF subfractions from the Nos. 1 and 2 fuels and shale oil fuel at EPA mode 4, with and without the oxidation catalyst, are shown in Figures 3.2.31a and b, respectively. Dose-response curves for the other subfractions and all SA calculations are presented in Appendix B Figures B2 - B7 and Table B4. In all cases, except one, the use of an oxidation catalyst increased the SA of the mode 4 SOF subfractions from the three fuels. The exception is the No. 2 fuel's aromatic subfraction; (Figure B2) however, little confidence can be placed on the aromatic subfraction data because of its poor r value (Table B4). In most cases, the No. 2 fuel and the shale fuel had a higher SA than did the No. 1 fuel.

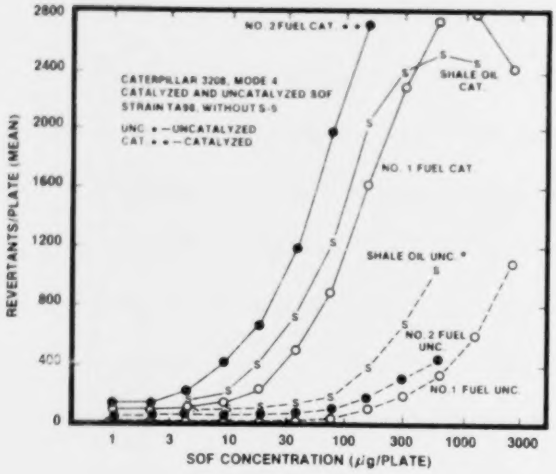

Fig. 3.2.30 - Comparison of fuel effects on dose-response curves of Ames tester strain TA98, with and without PTX catalysts

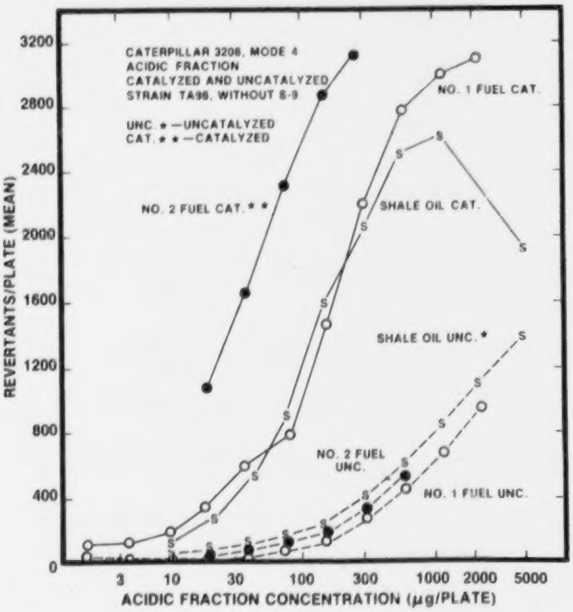

Fig. 3.2.31a - Fuel effects on dose-response curves for Ames tester strain TA98 without S-9 activation for acidic fraction of SOF, with and without PTX catalysts

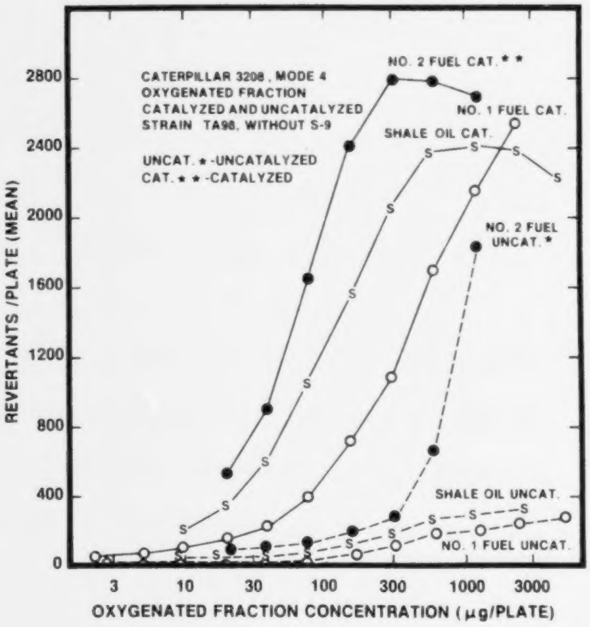

Fig. 3,2.31b - Fuel effects on dose-response curves for Ames tester strain TA98 without S-9 activation for oxygenated fraction of SOF, with and without PTX catalysts

Johnson-Matthey Close-Coupled Port Catalysts

The second aftertreatment device investigated was a close-coupled exhaust port catalyst. The specifications of this catalyst are given in Table 3.2.14 Caterpillar Engine Company donated a set of modified cylinder heads with these catalysts installed for evaluation (one per cylinder, eight in all). Modes 3, 4, 5, 9, 10 and 11 of the EPA 13 mode cycle were investigated using these catalysts and the same No. 2 fuel as was used in the evaluation of the PTX oxidation catalyst; shale fuel was also employed at modes 3, 4, and 5. Table 3.2.15 is the test matrix used for evaluation of these catalysts.

Table 3.2.14 Close Coupled Exhaust Port Catalyst Specifications

Manufacturer	Johnson-Matthey
Catalytic Agent	Platinum
Substrate	Fecralloy
Substrate Type	Laminar Flow Monolith
Substrate Size	1.8" Diameter x 2.0" Long
Substrate Cell Size	0.8 mm x 1.5 mm
Effective Open Volume	89%

Effects of the Close-Coupled Catalysts on Engine Operating Conditions (Both Fuels) and Gaseous Emissions(No. 2 Fuel) - After installing the close-coupled catalyst heads, the engine was run-in using No. 2 fuel until emissions stability was reached, which required 20 hours. An additional 8 hours of running at mode 4 was performed to confirm the stability of emissions.

Table 3.2.16 gives catalyst operating conditions at all 6 EPA modes tested, along with BSFC and exhaust temperature measured just outside the exhaust manifold. The catalyst temperature was measured on the outer face, rather than the center of the monolith, as was the case for the PTX downstream

Table 3.2.15 Test Matrix for Close-Coupled Port Catalyst Evaluation

EPA Mode	3		4		5		9		10		11		3		4		5	
Speed (RPM)	1680		1680		1680		2800		2800		2800		1680		1680		1680	
Load (N-M)	160		320		480		399		266		133		160		320		480	
BMEP (kPa)	192		383		575		485		372		161		192		383		575	
Fuel	No. 2		No. 2		No. 2		No. 2		No. 2		No. 2		Shale		Shale		Shale	
Catalyst	w/o	w	w/o	w	w/o	w	w/o	w	w/o	w	w/o	w	w/o	w	w/o	w	w/o	w
Total Particulate SOF, and $SO_4^=$ mass emissions	x	x	x	x	x	x	x	x	x	x	x	x	x	x	x	x	x	x
HC, NO, and No_x mass emissions	x	x	x	x	x	x	x	x	x	x	x	x	x	x	x	x	x	x
Chemical Characterization of SOF	x	x	x	x	x	x	x	x	x	x	x	x						
Ames Mutagenicity Bioassay on SOF	x	x	x	x	x	x	x	x	x	x	x	x						
Ames Mutagenicity Bioassay on subfractions			x	x														

Table 3.2.16 Engine and Catalyst Operating Parameters, Close-Coupled Catalyst

EPA Mode, Fuel	Exhaust Temperature °C	Catalyst Temperature °C	Catalyst Space Velocity Volumes/sec	Catalyst Residence Time msec	Exhaust Opacity %	Baseline Exhaust Opacity %	BSFC kg/kw-hr	Baseline BSFC kg/kw-hr
3, No. 2	243	288	404	2.48	0.3	0.3	0.291	0.287
4, No. 2	353	406	488	2.05	0.5	0.9	0.229	0.231
5, No. 2	483	530	582	1.72	1.4	1.9	0.218	0.217
9, No. 2	587	690	1093	0.92	5.5	4.9	0.272	0.252
10, No. 2	477	545	901	1.11	3.5	3.8	0.290	0.282
11, No. 2	363	454	773	1.29	4.6	3.2	0.399	0.371
3, Shale	269	286	393	2.54	0.3	N.A.[a]	0.283	N.A.[a]
4, Shale	380	409	484	2.07	0.7	0.4	0.226	0.229
5, Shale	514	558	584	1.71	2.0	N.A.	0.215	N.A.

(a) Not Available

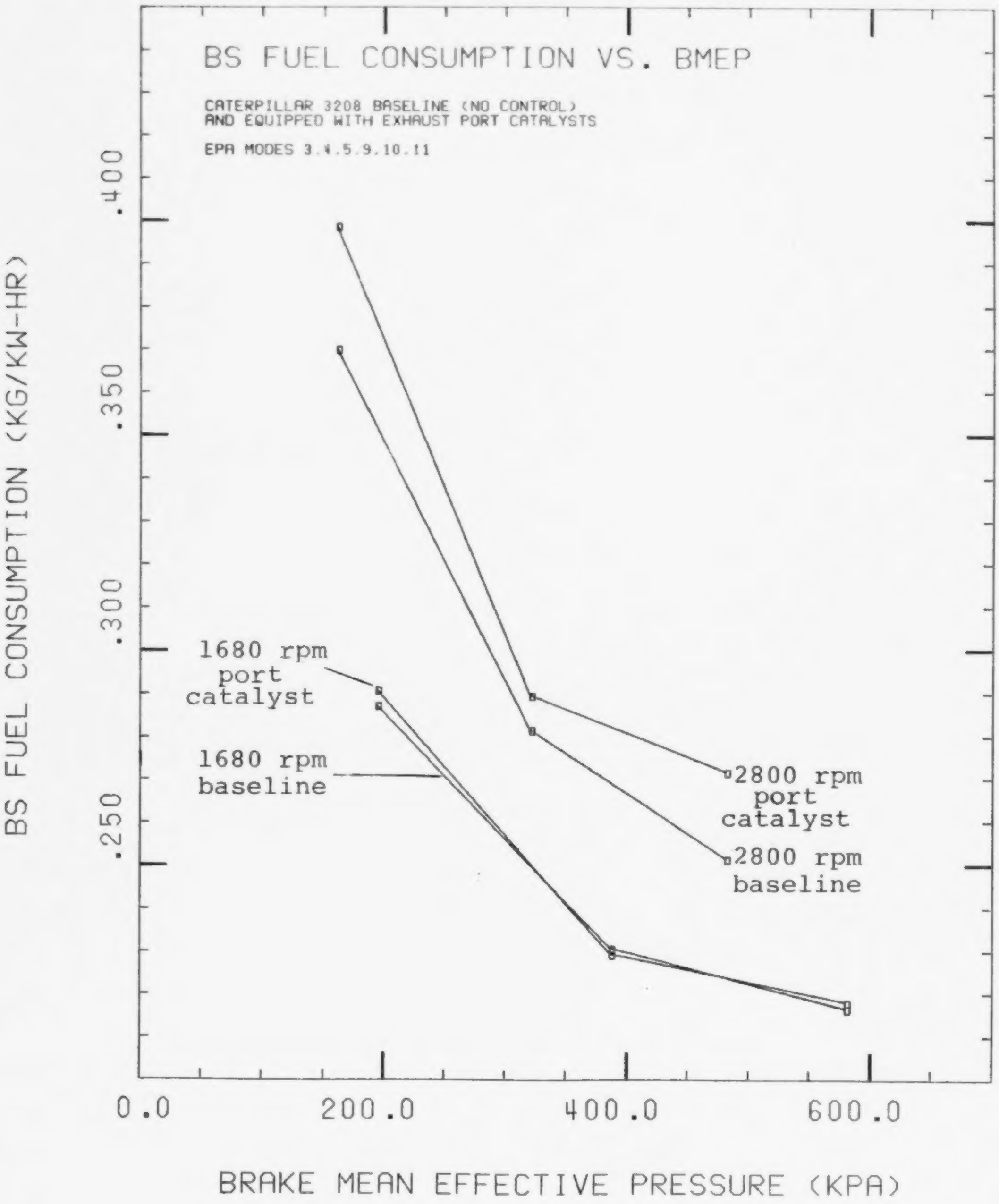

FIG. 3.2.32 THE EFFECT OF EXHAUST PORT CATALYSTS ON BS FUEL CONSUMPTION OF THE CAT 3208. CATALYSTS: JOHNSON-MATTHEY FECRALLOY SUPPORTED OXIDATION PORT CATALYSTS

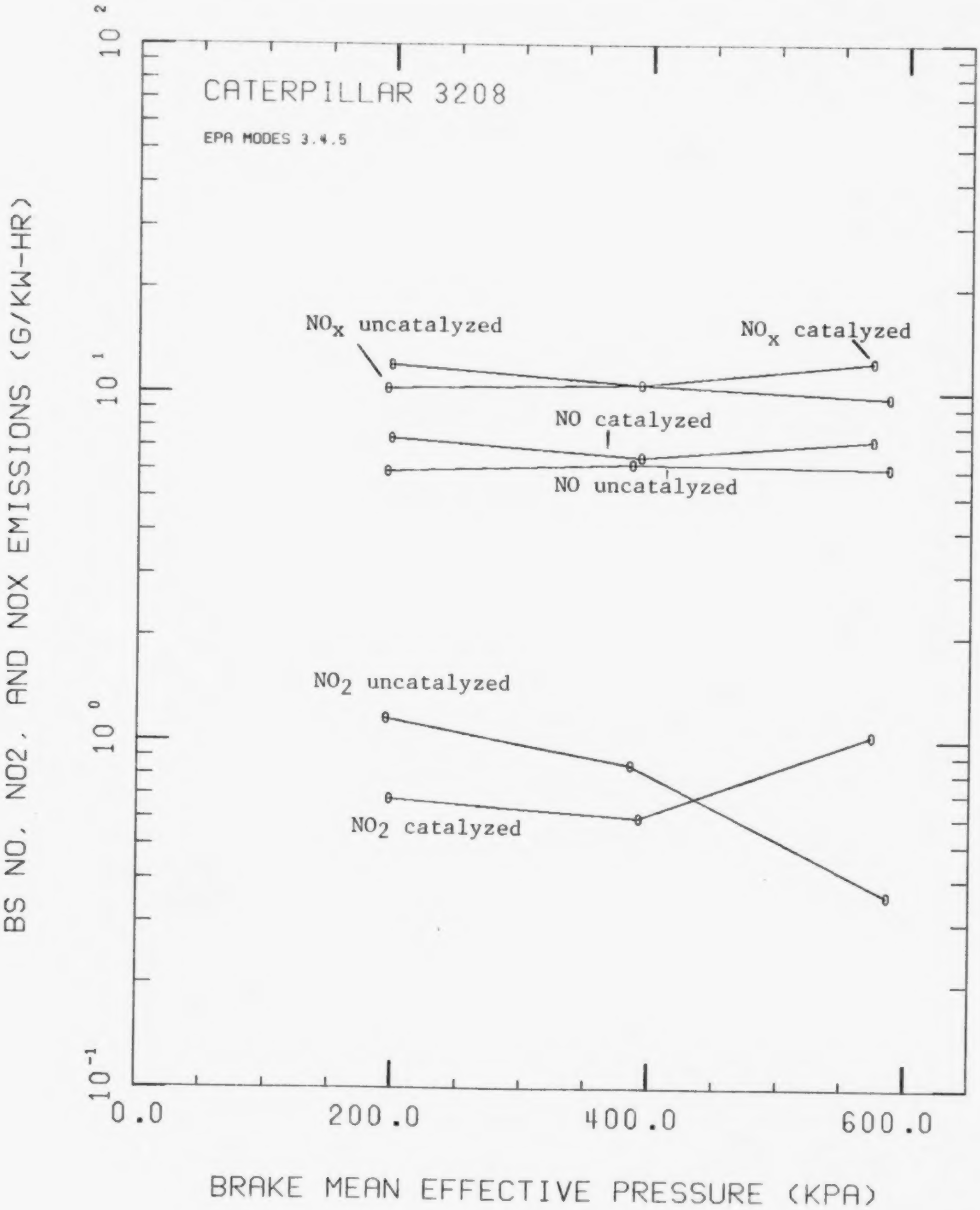

FIG.3.2.33a BRAKE SPECIFIC NO, NO2, AND NOX WITH AND WITHOUT CLOSED-COUPLED CATALYSTS
NO.2 FUEL

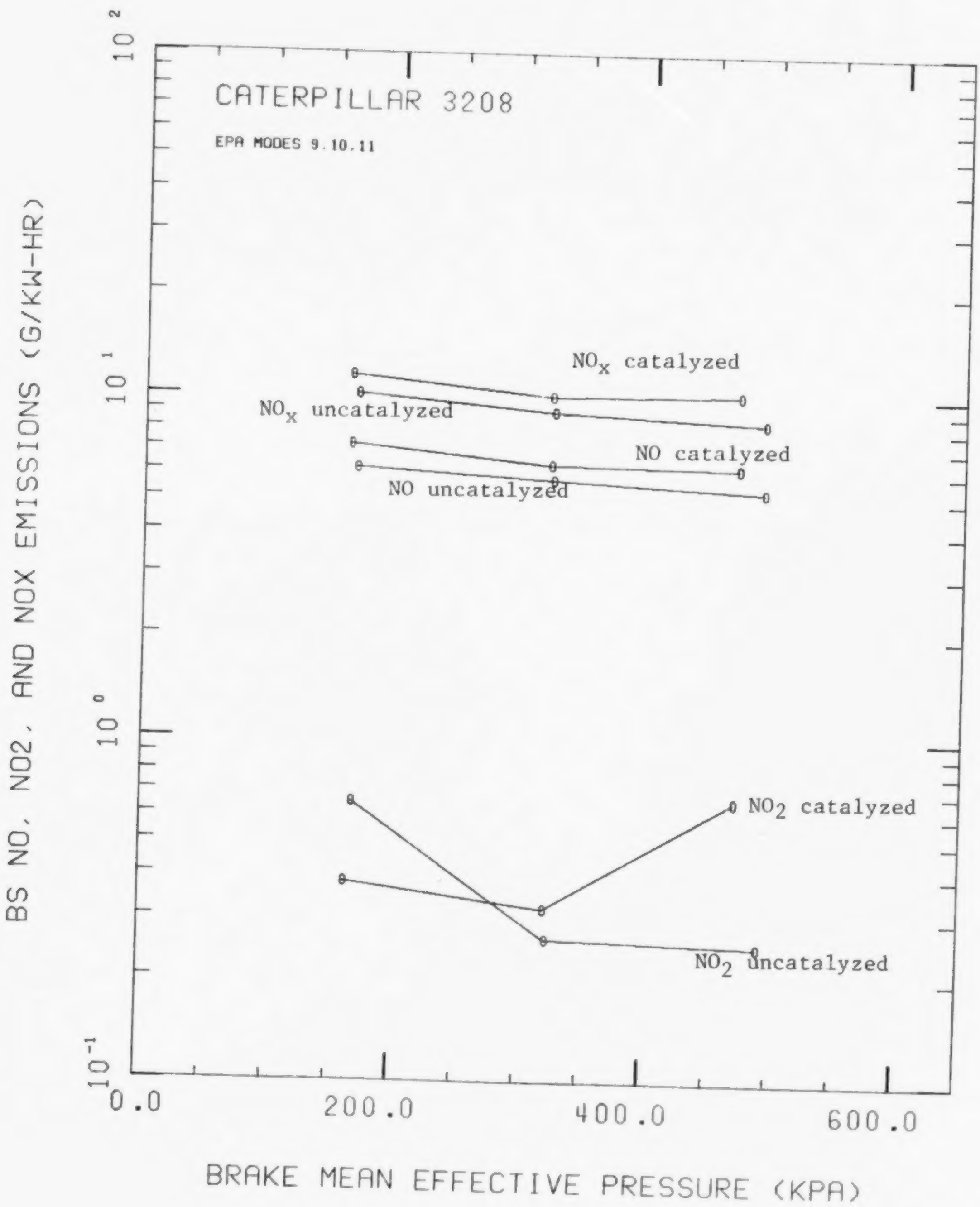

FIG.3.2.33b BRAKE SPECIFIC NO, NO2, AND NOX WITH AND WITHOUT CLOSED-COUPLED CATALYSTS NO.2 FUEL

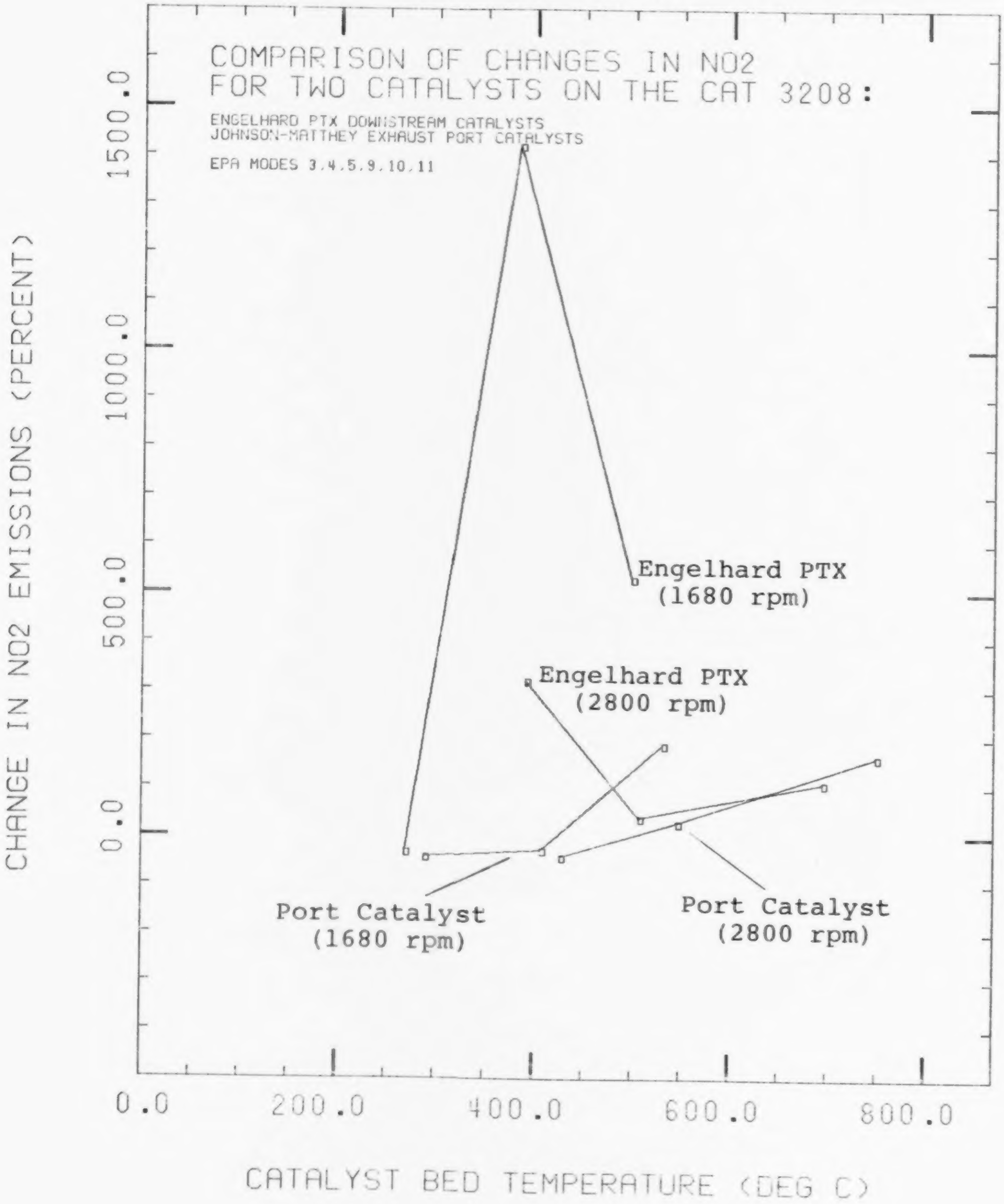

FIG.3.2.34a COMPARISON OF CHANGES IN NO2
FOR TWO CATALYSTS ON THE CAT 3208:
ENGELHARD PTX DOWNSTREAM CATALYSTS AND
JOHNSON-MATTHEY EXHAUST PORT CATALYSTS

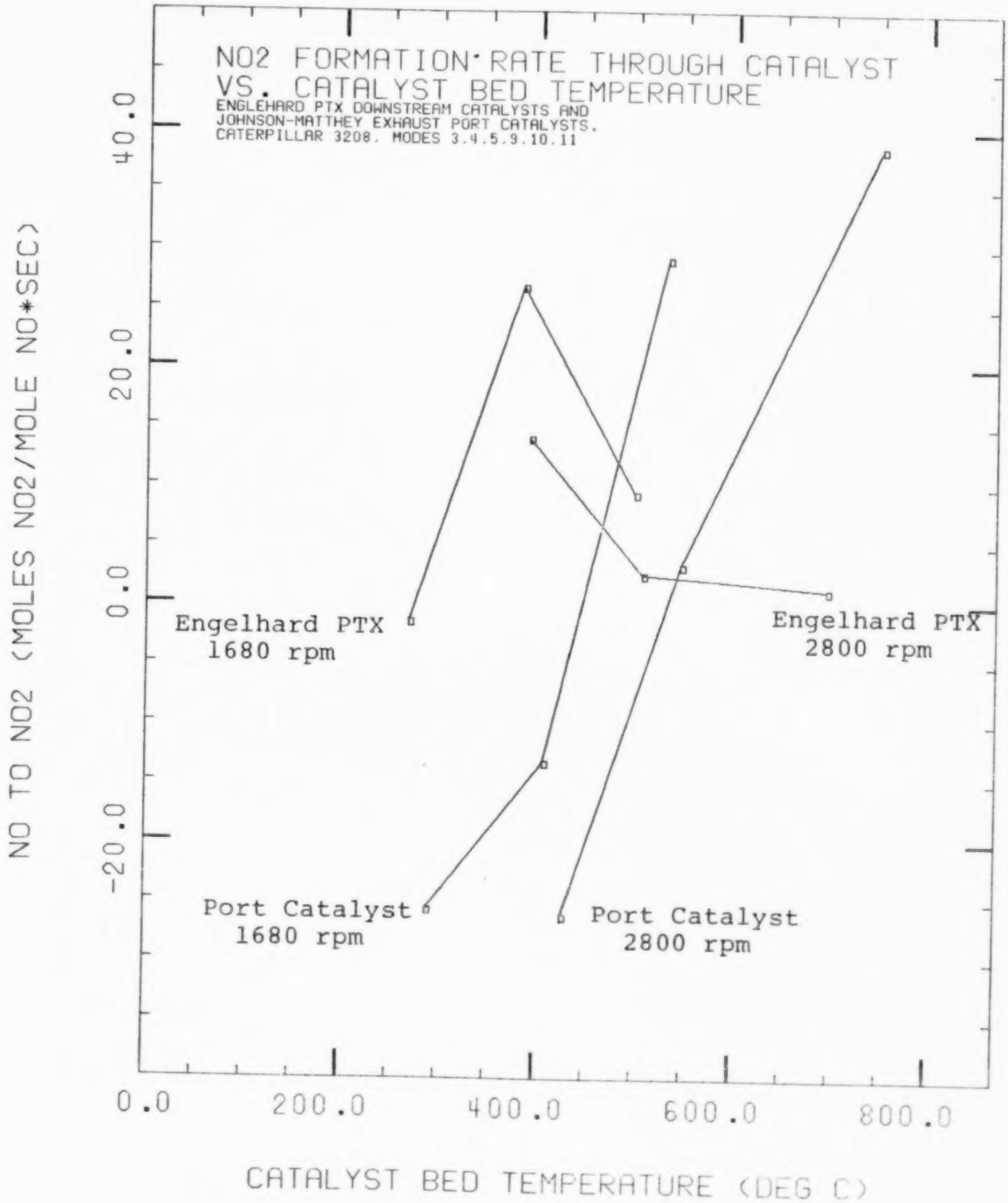

FIG.3.2.34b FORMATION RATES OF NO2 IN CATALYSTS: ENGLEHARD PTX CATALYSTS AND JOHNSON-MATTHEY EXHAUST PORT CATALYSTS ON THE CAT 3208. EPA MODES 3.4.5.9.10.11

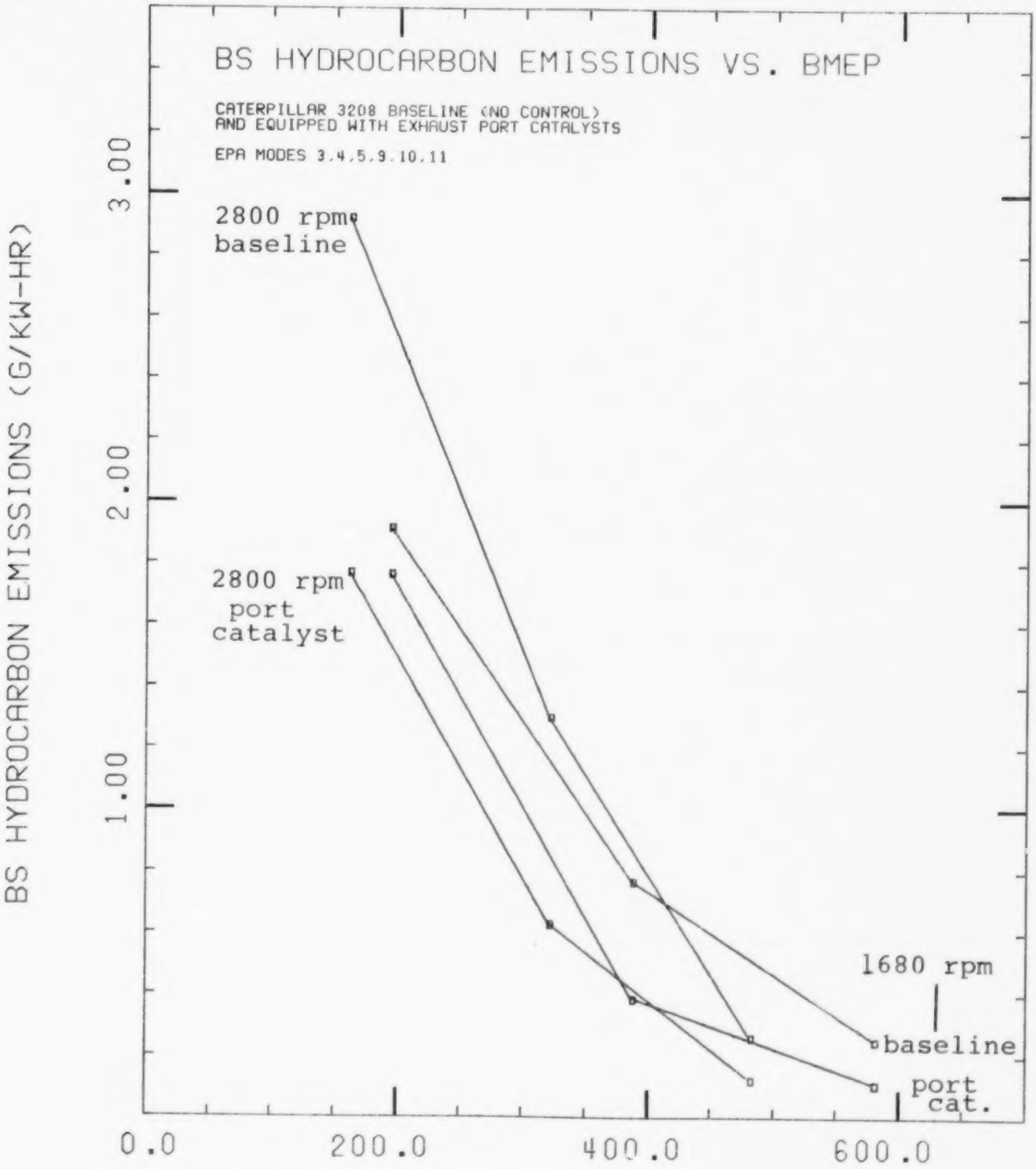

FIG.3.2.35 THE EFFECT OF EXHAUST PORT CATALYSTS ON HYDROCARBON EMISSIONS FROM THE CAT 3208. CATALYSTS: JOHNSON-MATTHEY FECRALLOY SUPPORTED OXIDATION PORT CATALYSTS

catalyst. Fuel consumption at intermediate speed modes was 2% or less higher than that of the baseline, probably due to the relatively small increase in exhaust in back pressure of the engine with the close-coupled catalysts installed (Figure 3.2.32). Rated speed modes showed a 5-8% increase in BSFC relative to the baseline engine, due to likely higher back pressure increases resulting from increased exhaust flowrate. Exhaust opacity was decreased or unchanged by use of the catalysts at all modes but 9 and 11.

Figure 3.2.33a and 3.2.33b show the effect of the catalyst on brake-specific NO_x, NO_2 and NO emissions, with No. 2 fuel. The NO_x and NO levels were only slightly higher at all six modes using the port catalysts, while NO_2 levels were higher for modes 5, 9 and 10 (the high-temperature modes) only. This compares favorably with PTX downstream catalysts, where NO_2 was higher for catalyzed exhaust for all modes but mode 3. The trend for both intermediate and rated speeds for the port catalyst was a decrease in NO_2 at light loads, changing with load so that NO_2 is increased at high load. This contrasts with the Englehard PTX, which showed large increases in all modes except mode 3. Figure 3.2.34a shows the percent increase in NO_2 for both catalysts, and figure 3.2.34b demonstrates the fundamental difference in NO oxidation behavior between the PTX and port catalysts. Only at modes 5 and 9 do the port catalysts show a significant increase in NO oxidation rate over the PTX catalysts. This may be related to the non-linear operating temperature difference between the two devices, to be discussed later. Figure 3.2.35 shows the BSHC emissions for the baseline engine and engine with port catalysts. Reduction of HC at the high-speed modes was greater than at the low-speed modes, with HC levels showing a much greater reduction at mode 11 than at mode 3 despite the two-fold greater residence time at mode 3. This suggests that the catalyst temperature may be more important in hydrocarbon oxidation than catalyst residence time. Figure 3.2.36 shows that the PTX catalyst was much more effective at reducing hydrocarbons despite its slightly lower operating temperature. The increase in port catalyst effectiveness at higher load (temperatures) is shown by comparing temperature differences between the catalysts, as in Figure 3.2.37. Since radiative heat transfer is proportional to absolute temperature raised to the fourth power, the oxidative advantage of close-coupled catalyst over a downstream catalyst is fully realized for hottest running conditions.

Effects on Particulate Emissions - No. 2 Fuel - Brake-specific particulate emissions for the close-coupled catalysts are shown with corresponding baseline emissions in figures 3.2.38a and 3.2.38b. The changes in total particulate emissions ranged from a 25 percent decrease at mode 3 to a 178 percent increase at mode 5.

The solid fraction emission trend was generally opposite the total particulate trend as the range was from a 36 percent decrease at mode 5 (apparent oxidation of some of the solid) to a 65 percent increase at mode 3. The supposed dehydrogenation of gas-phase hydrocarbons to solid, as observed with the PTX catalysts, was not observed to a significant extent with the port catalysts. Mode 5 showed a measurable decrease in solids, and it can be surmised that oxidation to CO_2 and H_2O predominates over dehydrogenation to solid at this mode, while other modes show only slight predominance of the dehydrogenation observed with the PTX catalysts.

The SOF emission reductions were generally less than those of the PTX catalyst (paralleling the gas phase hydrocarbon trend). The sulfate fraction emissions were greatly increased as expected due to the oxidation of SO_2 to SO_3 through the catalyst and subsequent hydrolysis of SO_3 to sulfuric acid. However,

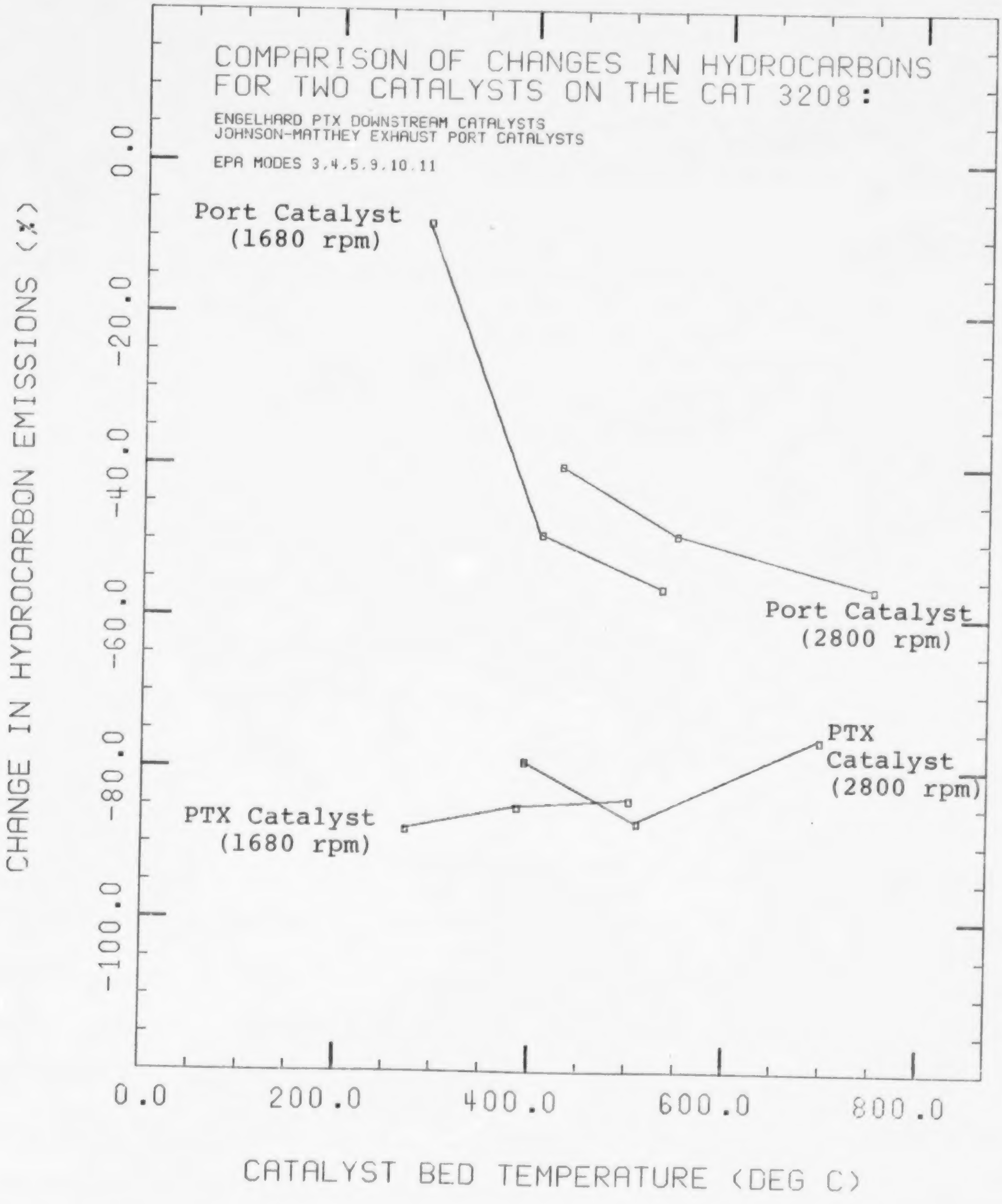

FIG.3.2.36 COMPARISON OF CHANGES IN HYDROCARBONS FOR TWO CATALYSTS ON THE CAT 3208: ENGELHARD PTX DOWNSTREAM CATALYSTS AND JOHNSON-MATTHEY EXHAUST PORT CATALYSTS

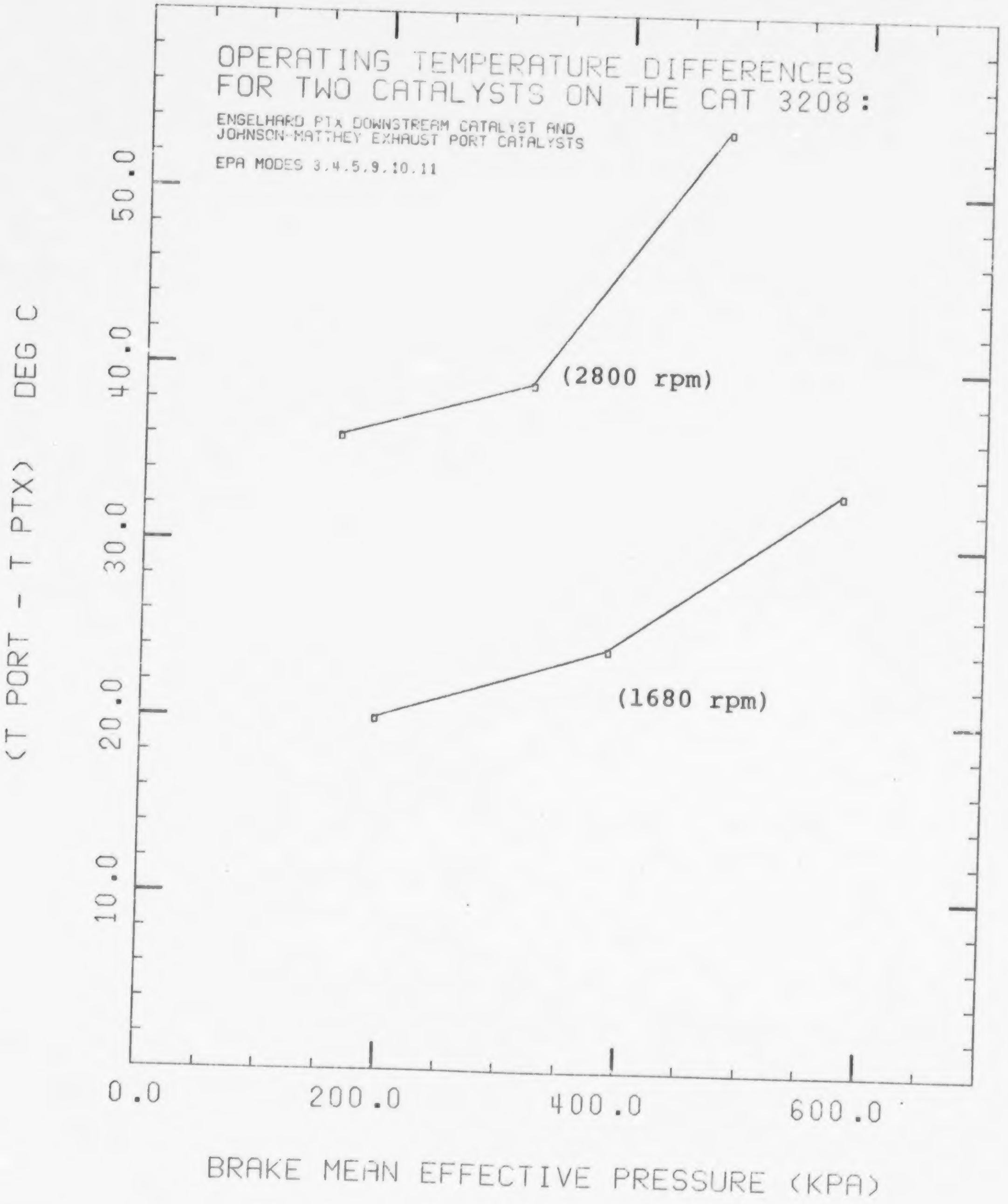

FIG.3.2.37 OPERATING TEMPERATURE DIFFERENCES FOR TWO CATALYSTS ON THE CAT 3208: ENGELHARD PTX DOWNSTREAM CATALYST AND JOHNSON-MATTHEY EXHAUST PORT CATALYSTS

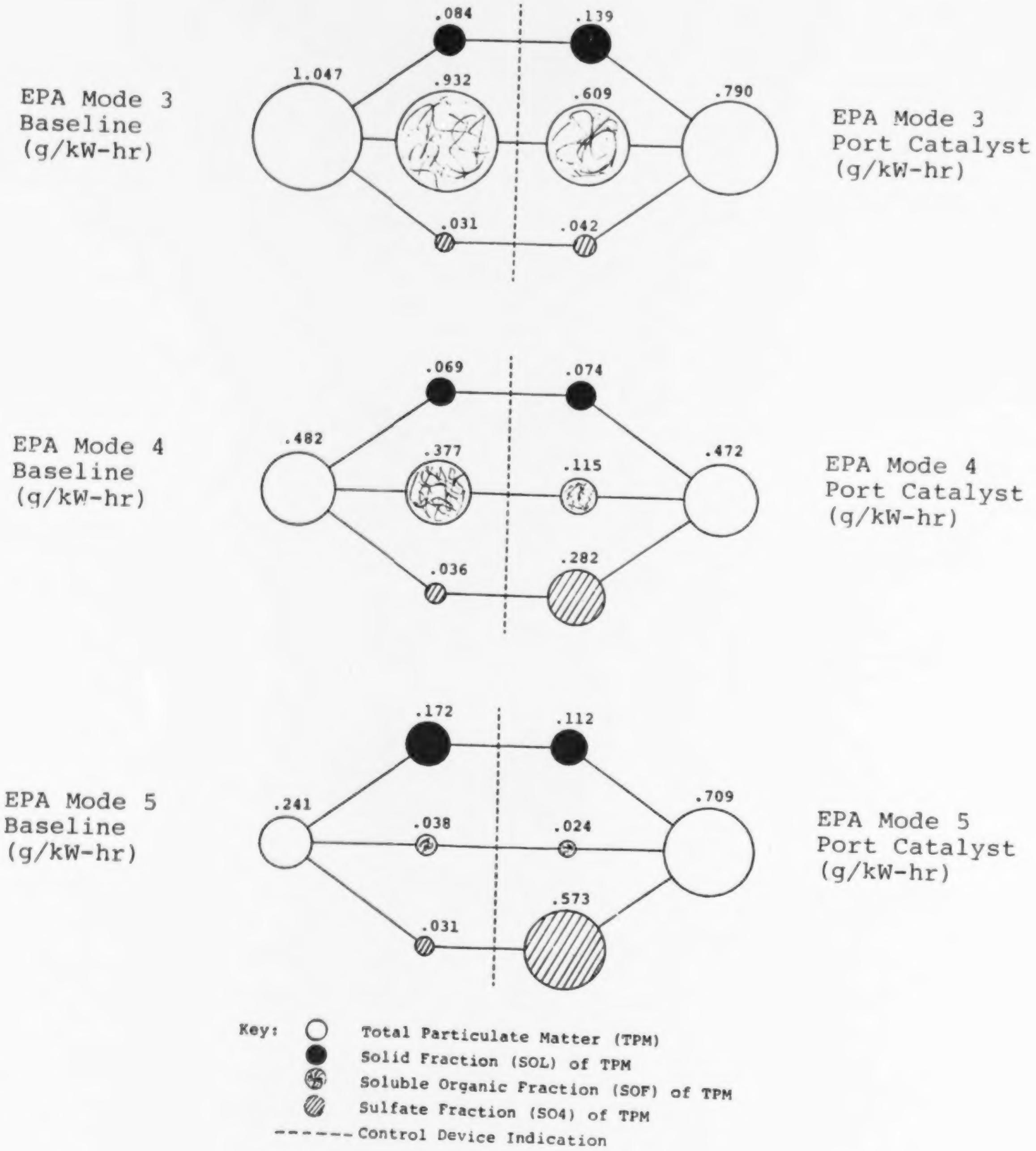

Fig3.2.38a The Effect of Johnson-Matthey Exhaust Port Catalysts on Caterpillar 3208 Particulate Emissions at 1680 rpm (1 Fecralloy based Oxidation Catalyst per Exhaust Port)

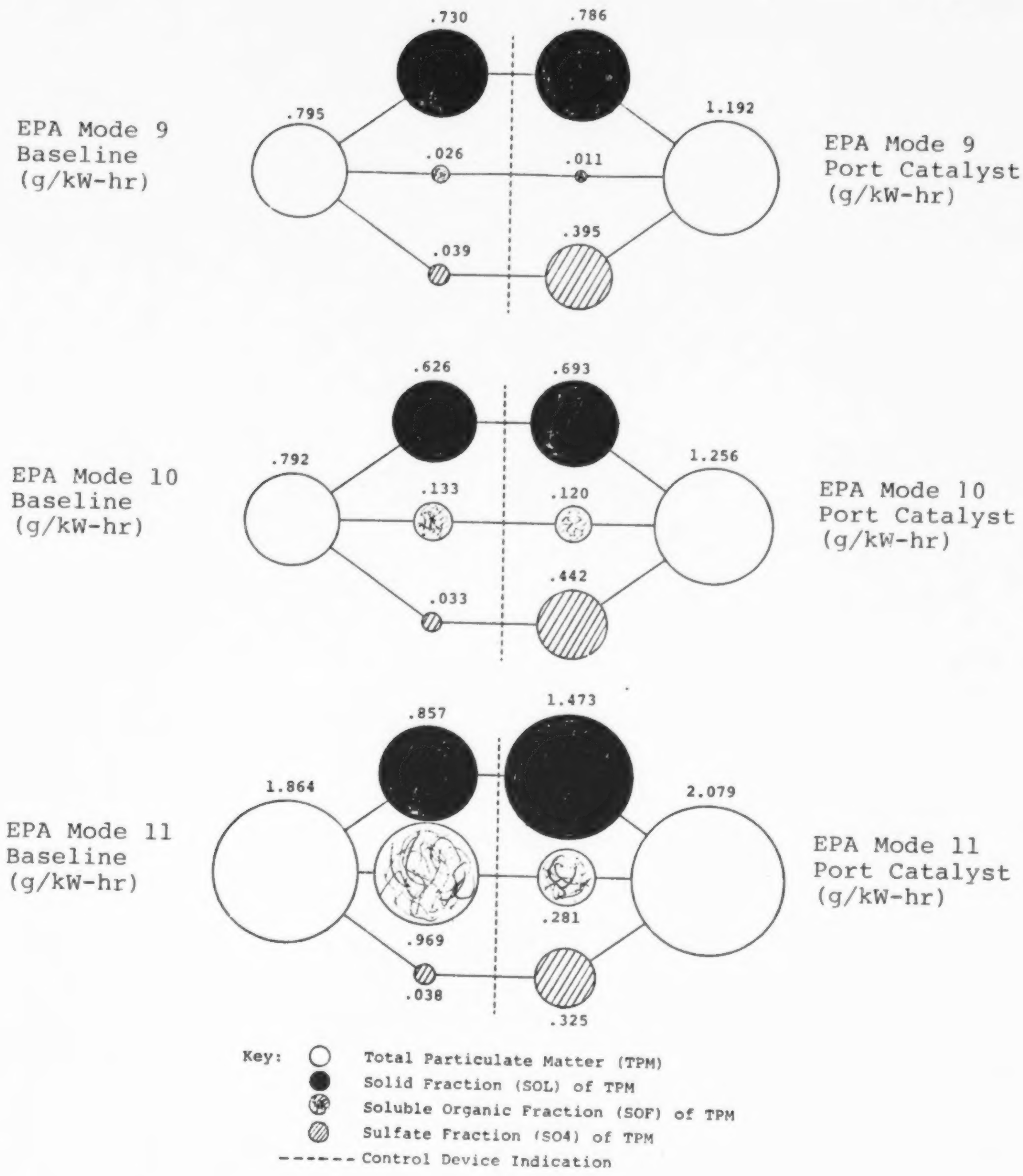

Fig.3.2.38b The Effect of Johnson-Matthey Exhaust Port Catalysts on Caterpillar 3208 Particulate Emissions at 2800 rpm (1 Fecralloy based Oxidation Catalyst per Exhaust Port)

the increases in sulfates were never as large as with the PTX catalysts. Figure 3.2.39 shows the molar percent conversion of fuel sulfur to sulfate for the two catalysts. Both catalysts show the same character of reaching a maximum at a similar intermediate temperature but the port catalyst shows significantly lower conversion. Figure 3.2.40a plots the same variable (molar conversion of fuel sulfur) against catalyst residence time. One can envision a response surface (molar conversion of fuel sulfur as a function of catalyst residence time and catalyst temperature) which would consist of a diagonal ridge (see Figure 3.2.41b). A summary of the effects of both catalysts on fuel consumption and emissions is given in Table 3.2.17.

The chemical fractionation results are presented in Figures 3.2.42 and 3.2.43 and Table C-4 of the Appendix as the brake specific emissions (mg/kw-hr) for each subfraction. This table also gives percent composition of the SOF for the fractions. From the data it can be seen that the catalyst is very selective with respect to the subfractions. A comparison of the selectivity with respect to the subfractions of the port catalysts and PTX catalysts is given in Table 3.2.18. There are many cases where there are differences between the two catalysts such as one catalyst showing an increase in a subfraction while the other showed a decrease. The most unusual case is mode 10 with the port catalysts which as Figure 3.2.43 shows had an unusually small decrease in total SOF. The data of Table 3.2.18 shows this to be the result of the reaction of hydrocarbons to other types of hydrocarbons rather than to CO_2 and H_2O. An increase was observed in the ether insoluble and acidic subfractions with an four-and-a-half-fold increase in the aromatic subfractions. Although the solid and SOF were nearly unchanged at mode 10 with respect to the baseline emissions,

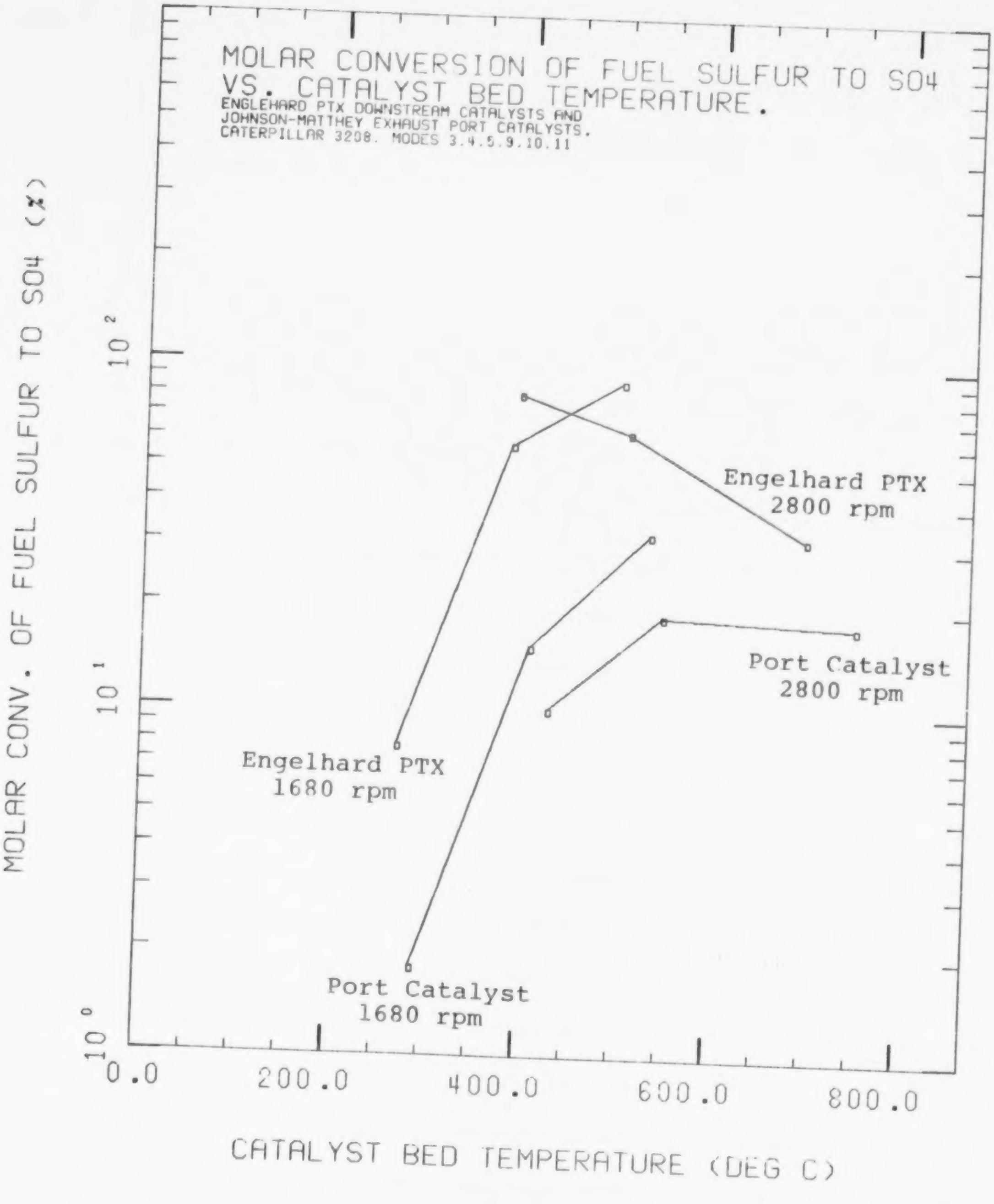

FIG.3.2.39 SULFUR TO SULFATE % VS. CATALYST TEMP.
ENGLEHARD PTX CATALYSTS AND JOHNSON-MATTHEY EXHAUST PORT CATALYSTS ON THE CAT 3208, EPA MODES 3,4,5,9,10,11

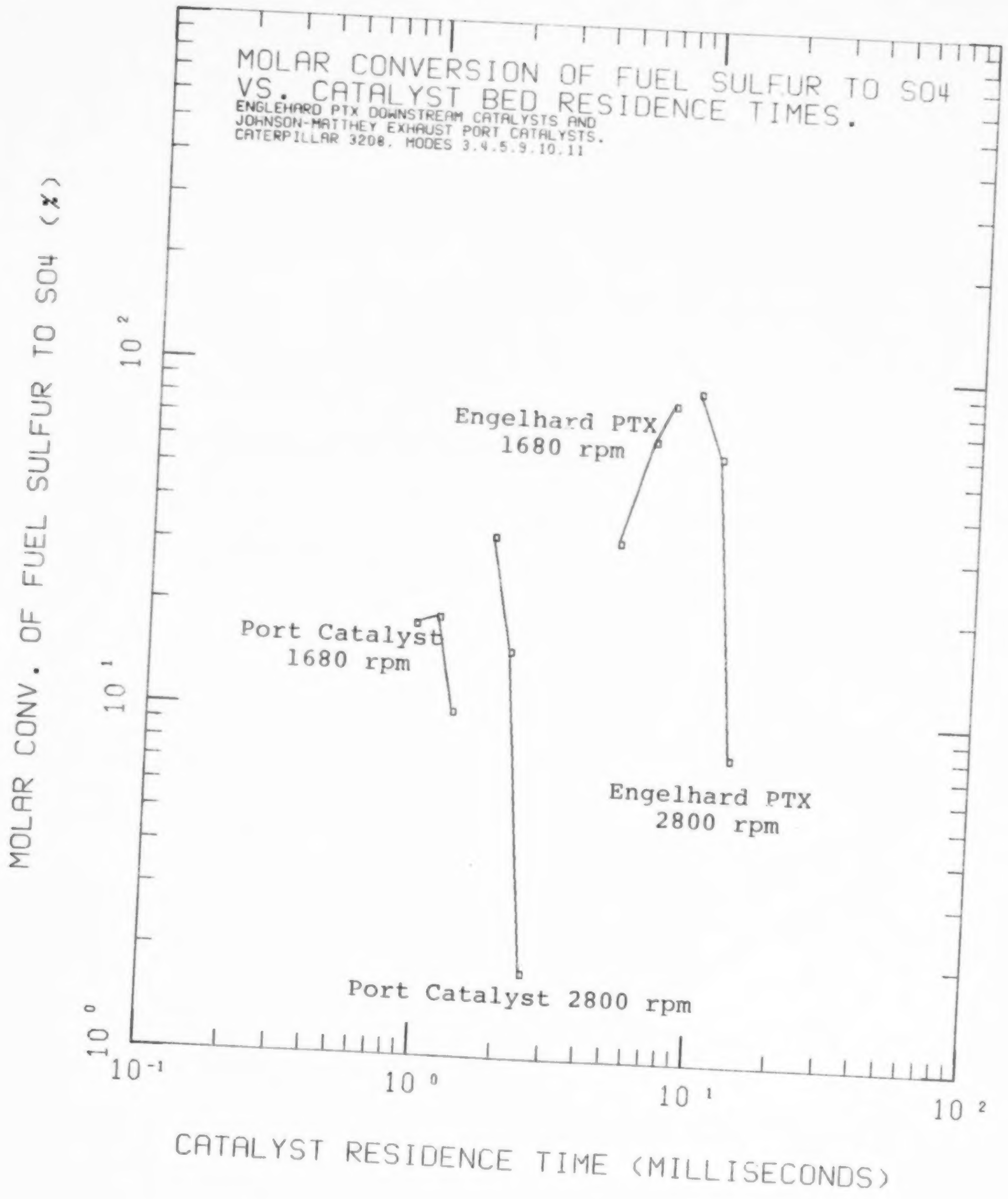

FIG.3.2.40 SULFUR TO SULFATE % VS. RESIDENCE TIME. ENGLEHARD PTX CATALYSTS AND JOHNSON-MATTHEY EXHAUST PORT CATALYSTS ON THE CAT 3208, EPA MODES 3,4,5,9,10,11

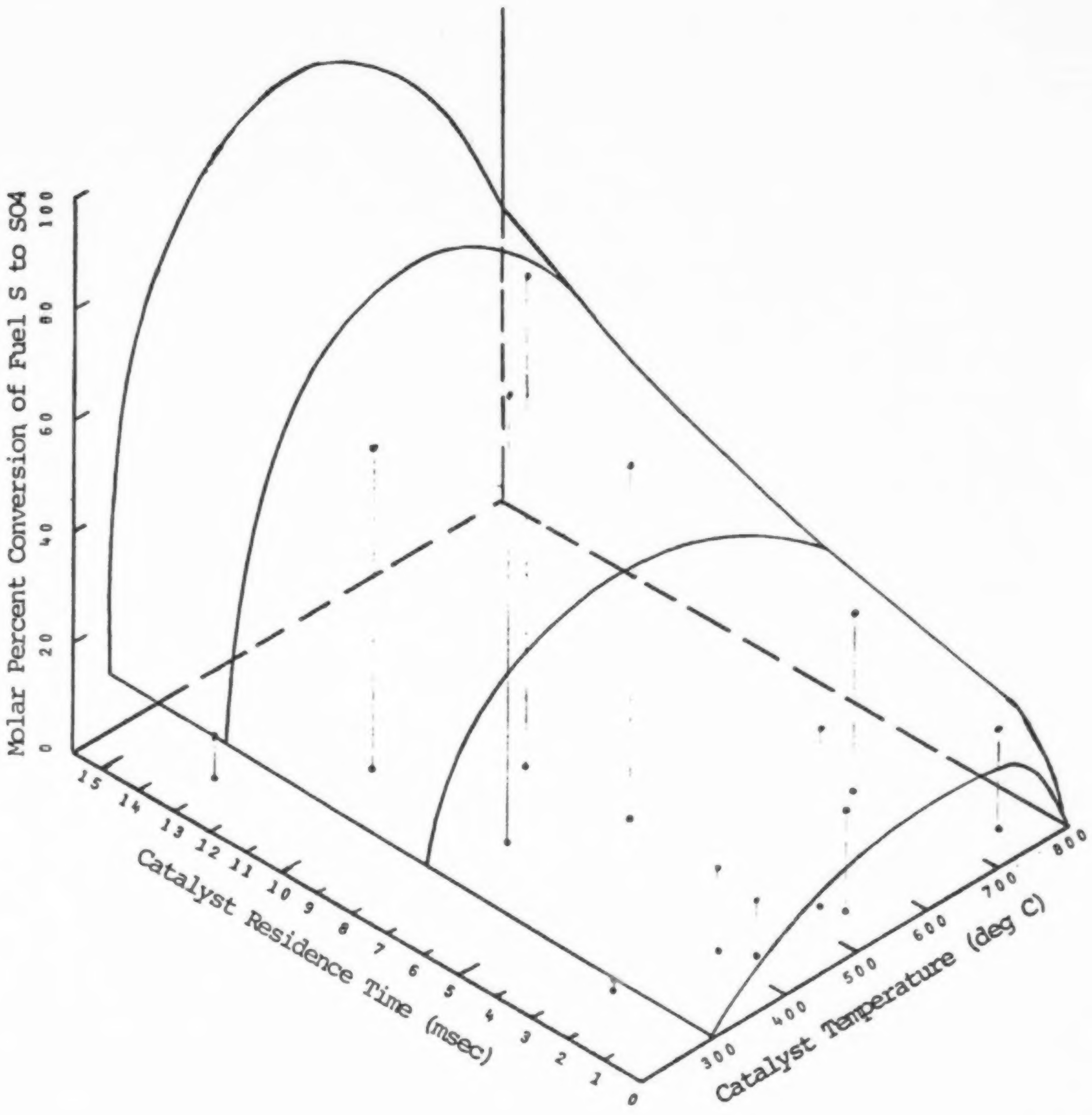

Fig. 3.2.41 Response Surface of Molar Percent Conversion of Fuel Sulfur to Sulfate Through an Oxidation Catalyst on a Diesel Engine, Data from a Cat 3208 with two types of Catalysts: Engelhard PTX Downstream Catalyst & Johnson-Matthey Close-Coupled Exhaust Port Catalyst.

Table 3.2.17 Comparison of Two Catalysts for Diesel Emission Control: Englehard PTX (Downstream) and Johnson-Matthey Close-Coupled (exhaust port)

PERCENT CHANGE (FROM BASELINE) IN
BRAKE SPECIFIC FUEL CONSUMPTION AND EMISSIONS, No.2 FUEL

			Particulate								Gaseous							
	Brake Specific Fuel Consumption		Total		Solid Fraction		Soluble Organic Fraction		Sulfate Fraction		NO_x		NO_2		NO		Gas Phase Hydrocarbons	
EPA Mode	PTX	Port	PTX	Port	PTX	Port	PTX	Port	PTX	Port	PTX	Port	PTX	Port	PTX	Port	PTX	Port
3	+2.4	+1.3	-36	-25	-27	+65	-59	-35	+800	+36	+1	+17	-32	-41	+4	+25	-88	-8
4	+1.3	-0.6	+415	-1	+533	+8	-76	-69	+3500	+700	-4	+2	+1420	-29	-33	+5	-85	-49
5	-1.4	+0.6	+637	+178	+138	-36	-67	-40	+4833	+1630	-7	+27	+530	+189	-15	+20	-84	-56
9	+6.3	+8.0	+137	+38	+88	-1	-75	-61	+1033	+826	-31	+21	+110	+164	+30	+17	-76	-56
10	-3.7	+2.8	+289	+50	+227	+5	-88	-14	+3425	+1180	+2	+16	+39	+28	+1	+16	-87	-49
11	-9.8	+7.7	+79	+5	+15	+61	-84	-73	+8167	+796	-11	+13	+320	-42	-21	+17	-79	-40

PTX - Caterpillar 3208 with Engelhard PTX downstream catalysts

Port - Caterpillar 3208 with Johnson-Matthey Close-Coupled Exhaust Port Catalysts

Table 3.2.18 Comparison of the Selectivity of Catalysts with Respect to Soluble Organic Fraction
Catalysts: Englehard PTX (downstream) and Johnson-Matthey Close-Coupled (exh. Port)
Engine: Caterpillar 3208 Operated at EPA Modes 3, 4, 5, 9, 10, 11 (Dilution Ratio 15:1)

Percent Change in Mass Concentration

	EPA MODE											
	3		4		5		9		10		11	
Subfraction	PTX	Port	PTX	Port	PTX	Port	PTX	Port	PTX	Port	PTX	Port
Ether Insoluble	-59	+55	-65	-46	-79	-28	+125	+35	-99	+36	-72	+10
Basic	-87	+7	-63	-92	-48	-85	-68	+17	-76	-72	-91	-90
Acidic	-78	-19	-60	-53	-31	+31	-74	-83	-85	+42	-90	-75
Paraffin	-63	-47	-83	-74	-93	-46	-54	-80	-93	-37	-86	-79
Aromatic	-42	-42	-93	+12	-8	+86	-38	-60	-92	+462	-80	-46
Transitional	-76	-31	-79	-78	-69	-67	+60	-48	-97	-56	-87	-80
Oxygenated	-62	-22	-52	-76	-54	-57	-91	-55	-90	+4	-80	-80
Hexane Insoluble	-73	+11	-45	-25	-75	-86	-95	-89	-89	-46	-57	-43

PTX - Cat 3208 with Engelhard PTX downstream catalysts
Port - Cat 3208 with Johnson-Matthey Close-Coupled Exhaust Port Catalysts

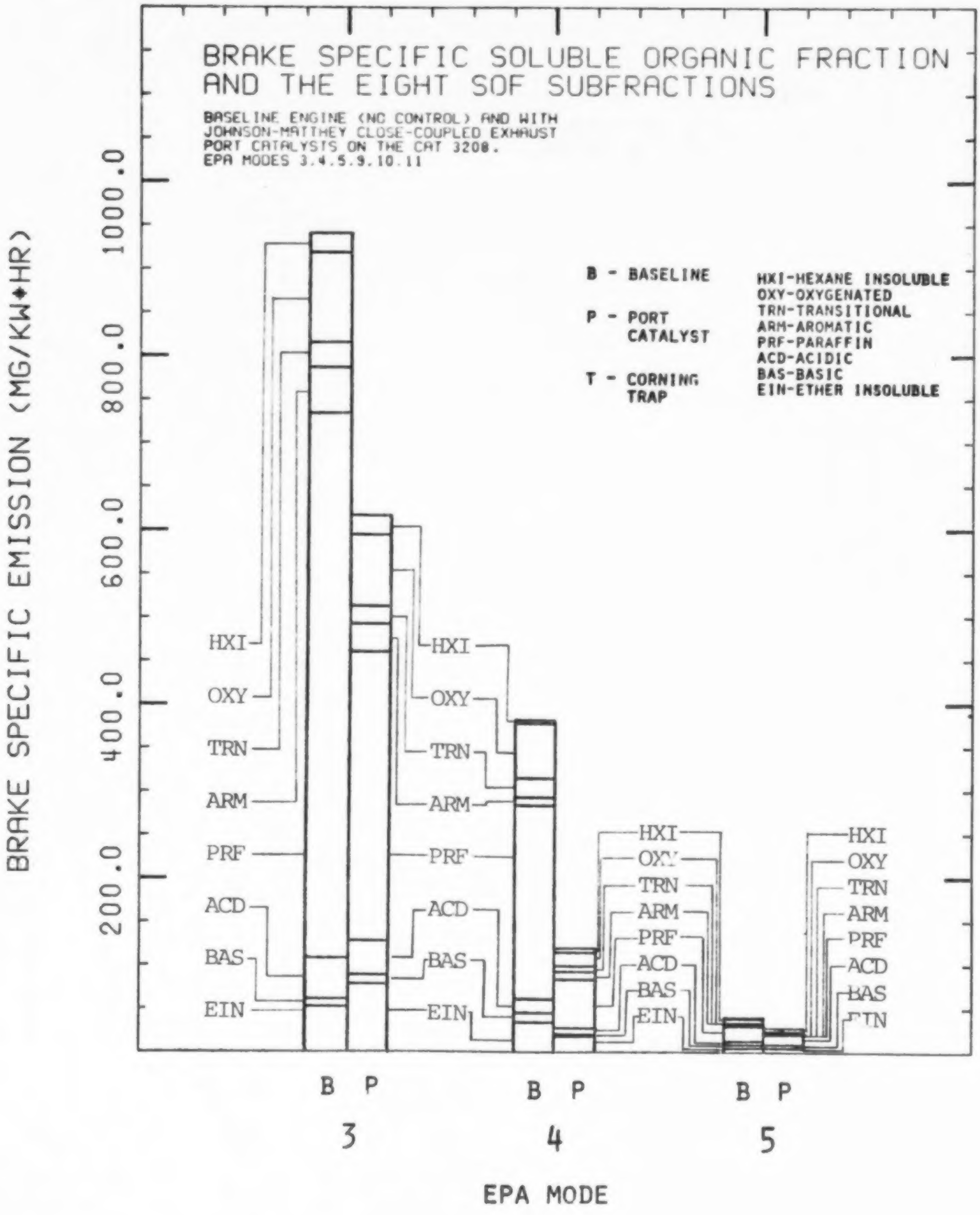

FIG.3.2.42 THE EFFECT OF EXHAUST PORT CATALYSTS ON THE CHEMICAL COMPOSITION OF THE SOLUBLE ORGANIC FRACTION OF CAT 3208 PARTICULATE MATTER.

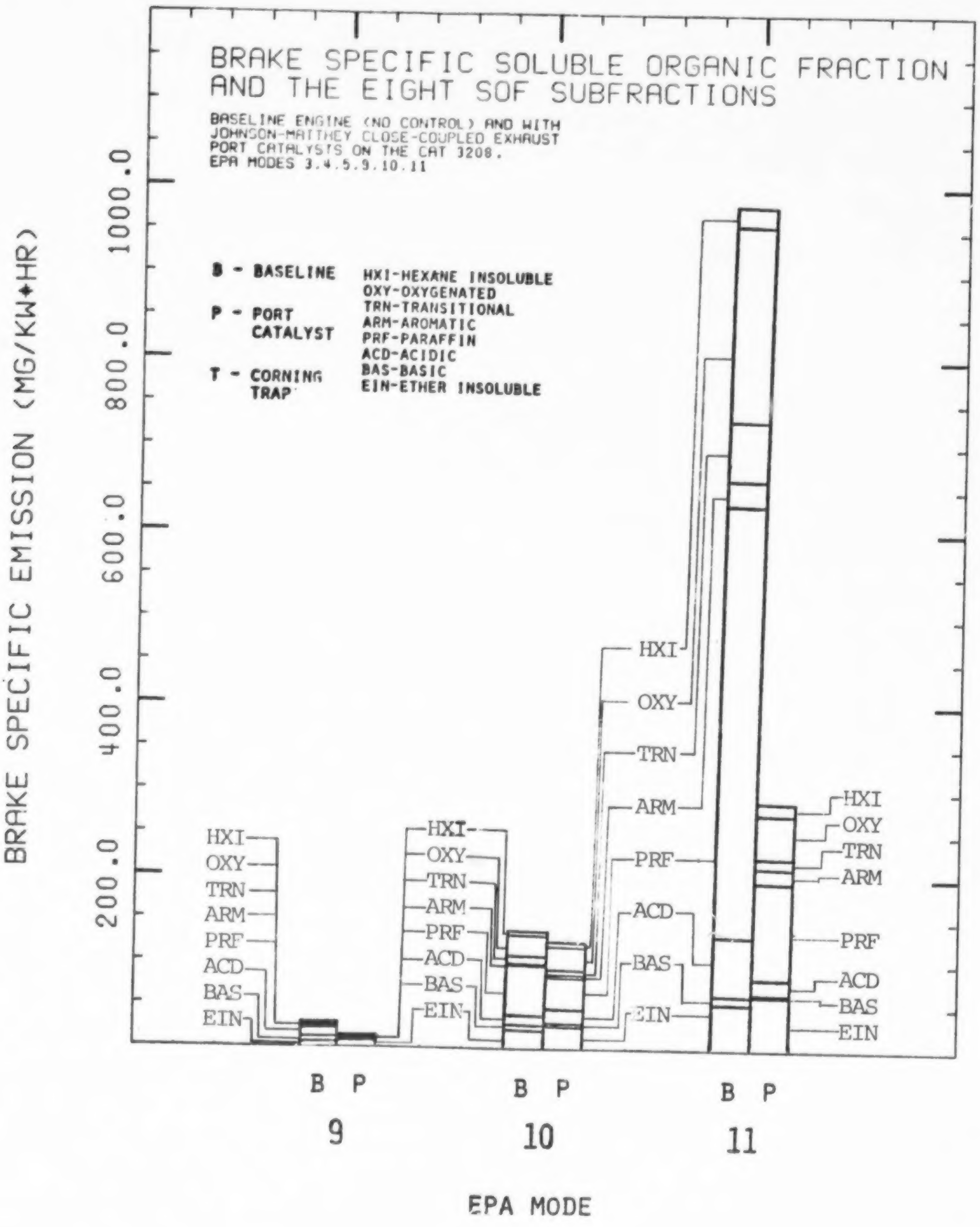

FIG.3.2.43 THE EFFECT OF EXHAUST PORT CATALYSTS ON THE CHEMICAL COMPOSITION OF THE SOLUBLE ORGANIC FRACTION OF CAT 3208 PARTICULATE MATTER.

an increase in both aromatics and ether insolubles suggests that dehydrogenation to solid may predominate over oxidation to CO_2 and H_2O (or other, oxygenated subfractions) at this mode.

Effects on Emissions - Shale Fuel - Figure 3.2.44 shows brake-specific NO_x, NO, and NO_2 emissions for the close-coupled port catalysts at modes 3, 4, and 5 using shale fuel. Baseline (uncatalyzed) values were obtained at mode 4 only. Shale fuel appears to give $BSNO_x$ and BSNO values slightly lower than No. 2 fuel, with $BSNO_2$ emissions higher than No. 2 fuel, except for mode 5. Baseline emissions with No. 2 fuel at mode 4 were essentially unchanged from those experienced with the port catalysts.

Figures 3.2.45 and 3.2.46 show BSHC and BSTPM for shale fuel at modes 3, 4 and 5 compared with the same modes using No. 2 fuel, for the port catalysts. Shale fuel gave slightly higher HC emissions at all 3 modes, and the SOF was higher at modes 3 and 4 (mode 5 SOF was insignificantly lower for shale fuel). Neglecting sulfate, the total particulate was lower at modes 3 and 4 for shale than for No. 2 fuel. Significantly lower solid emissions at mode 5 for the No. 2 fuel were not enough to offset the very high sulfate emissions at mode 5 for the No. 2 fuel and BSTPM for shale fuel was approximately half the No. 2 fuel emissions. The significantly higher solids emissions at mode 5 for shale fuel could be due to a 28°C higher catalyst temperature, but is more likely due to fuel properties. As discussed previously, the only mode for which solids showed a significant decrease over baseline emissions using No. 2 fuel was mode 5. Also, it was mentioned in the discussion of the PTX catalyst that aromatic compounds may be much more stable in the shale fuel than in the No. 2 fuel.

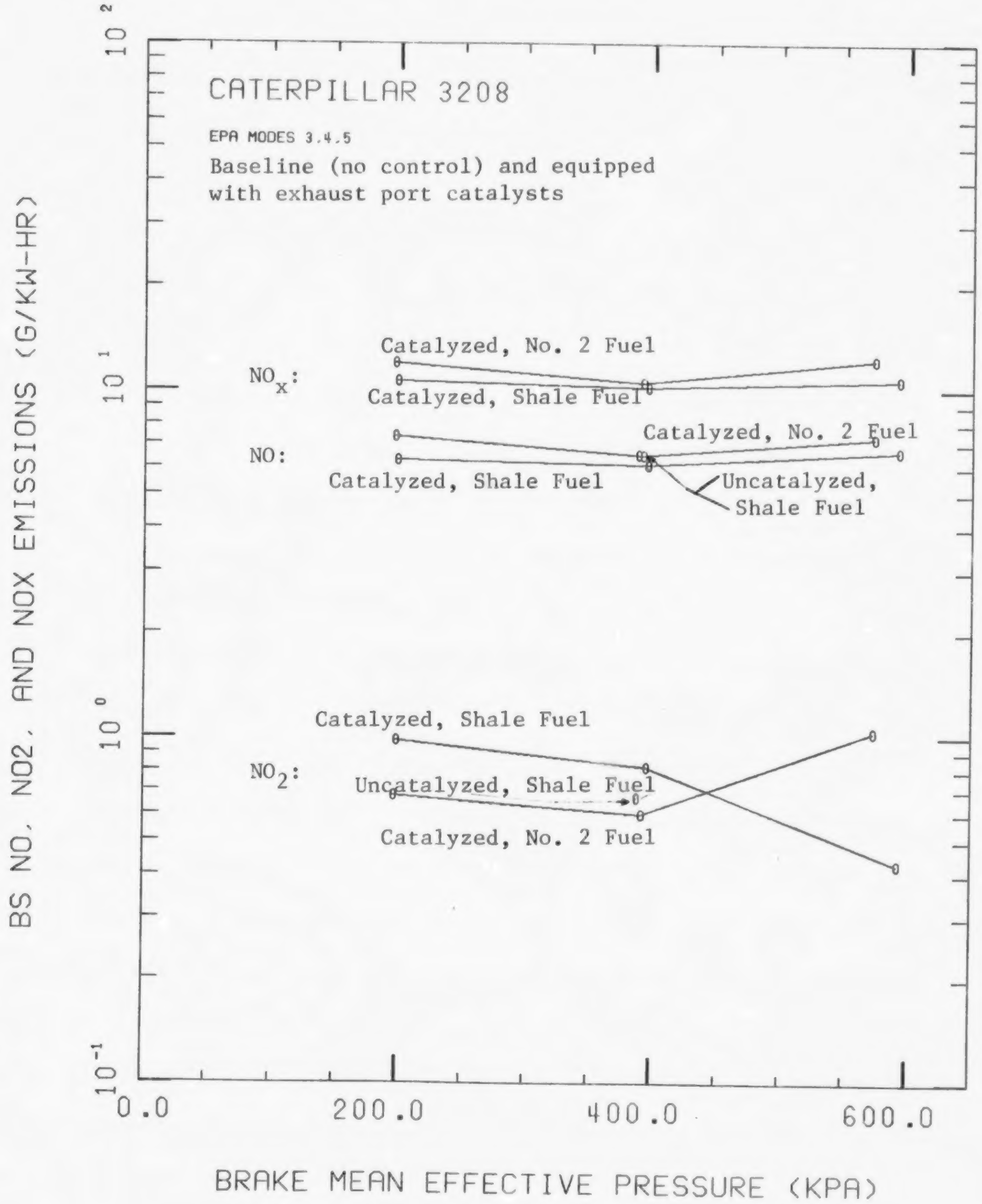

FIG.3.2.44 BRAKE SPECIFIC NO, NO2, AND NOX WITH AND WITHOUT CLOSE-COUPLED CATALYSTS SHALE FUEL; NO.2 FUEL

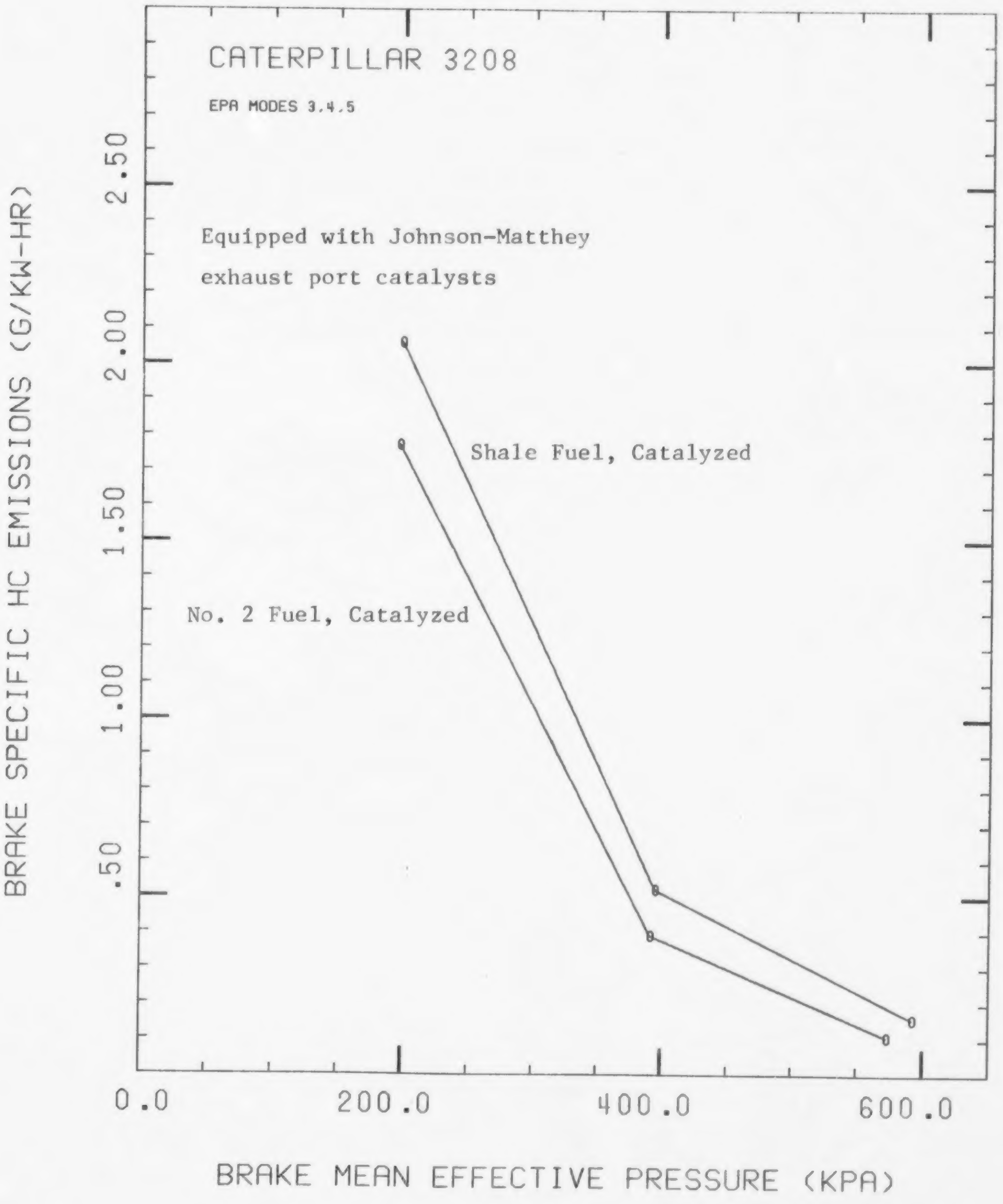

FIG. 3.2.45 EFFECT OF SHALE FUEL ON HYDROCARBON EMISSIONS USING CLOSED-COUPLED PORT CATALYSTS

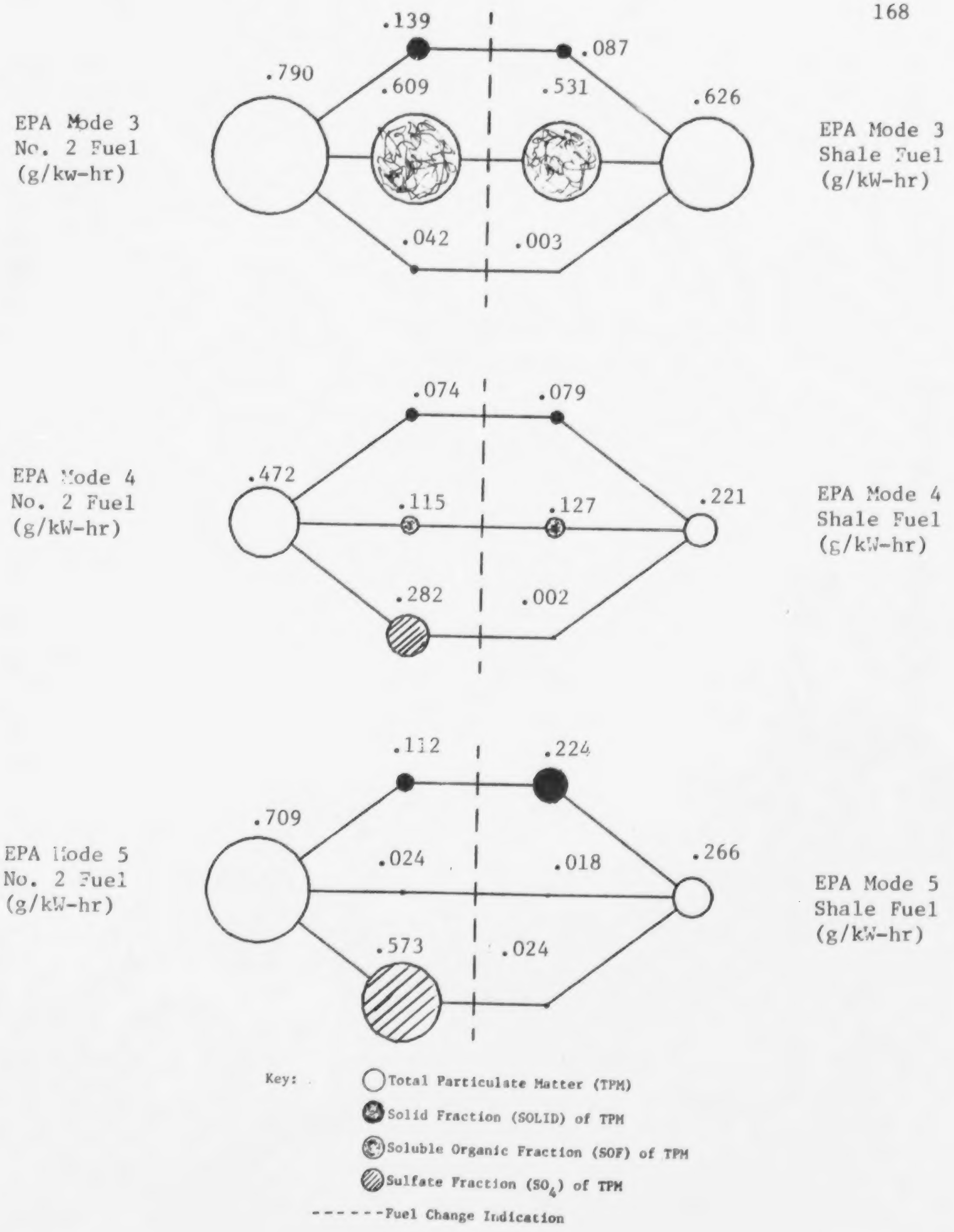
EPA Mode 3
No. 2 Fuel
(g/kw-hr)
.790
.139
.609
.042
.087
.531
.003
.626
EPA Mode 3
Shale Fuel
(g/kW-hr)
EPA Mode 4
No. 2 Fuel
(g/kW-hr)
.472
.074
.115
.282
.079
.127
.002
.221
EPA Mode 4
Shale Fuel
(g/kW-hr)
EPA Mode 5
No. 2 Fuel
(g/kW-hr)
.709
.112
.024
.573
.224
.018
.024
.266
EPA Mode 5
Shale Fuel
(g/kW-hr)
Key:
Total Particulate Matter (TPM)
Solid Fraction (SOLID) of TPM
Soluble Organic Fraction (SOF) of TPM
Sulfate Fraction (SO4) of TPM
------Fuel Change Indication

Fig. 3.2.46 The Effect of Shale Fuel, Relative to No. 2 Fuel, on Caterpillar 3208 Particulate Emissions at 1680 rpm (1 Fecralloy based Oxidation Catalyst per Exhaust Port)

This premise is supported by the observation of predominantly dehydrogenation (to solid) in the case of shale fuel, as opposed to predominantly oxidation (to CO_2 and H_2O) for No. 2 fuel. The very slight reduction of solids using shale fuel with the port catalysts at modes 3 and 4 suggests that there is a threshold temperature (near 500°C) above which catalysis of fuel-dependent oxidation and dehydrogenation occurs.

Ames Bioassay Results - The mutagenic specific activities for both the baseline and the port catalyst SOF using No. 2 fuel are plotted in Figure 3.2.47. The port catalysts produced SOF of higher specific activity at all intermediate speed modes but produced a decrease in SOF specific activity at all rated speed modes. This is contrary to the PTX catalyst which produced increases at all modes.

The results of Ames tests on the subfractions of the SOF for both baseline and port catalysts at mode 4 are given in Table 3.2.19. The log-log SA parameter is compared with the SA calculated from a log-linear dose-response curve; little difference is seen. There is an increase in SA for most of the subfractions of the SOF due to the port catalyst which is consistent with the significant increase in SA of the total port catalyst SOF.

Specific activities for the SOF at all 6 EPA modes tested are shown in Table 3.2.20. BSSA (shown graphically in Figure 3.2.48) are calculated based upon log-log SA parameters. Limits of the linear dose-response region were chosen uniformly at $C_1 = 18.75$ and $C_2 = 600$ μg/plate except for the mode 4 basic subfraction, where sample mass limited C_2 to 300 μg/plate. Mode 5 SA with the port catalysts was much higher than that for any other mode, with or without the catalysts. This indicates that temperature and residence time are sufficient at this mode to produce significantly higher levels of mutagenic compounds.

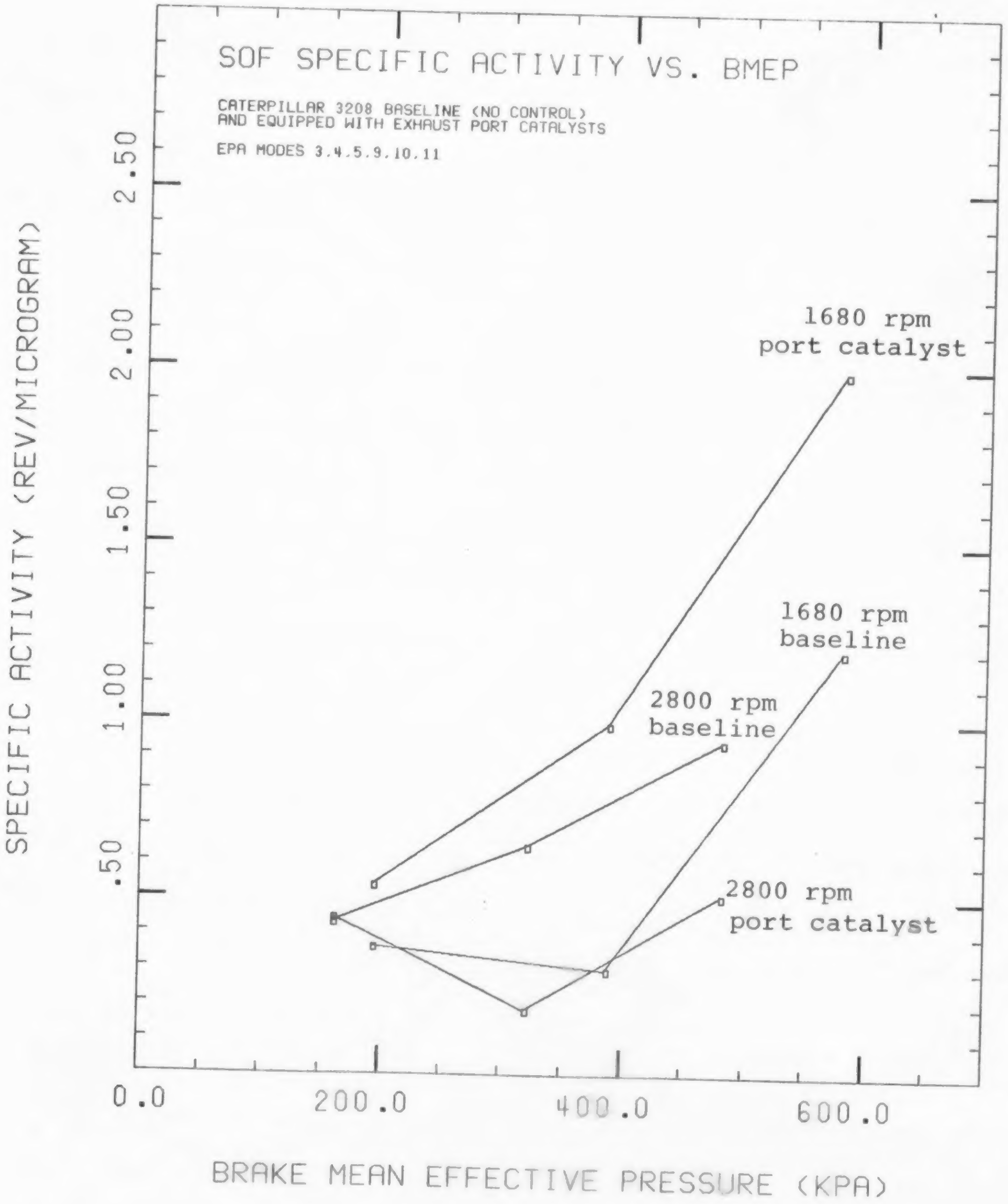

FIG. 3.2.47 THE EFFECT OF EXHAUST PORT CATALYSTS ON SPECIFIC ACTIVITY OF THE CAT 3208 SOF. CATALYSTS: JOHNSON-MATTHEY FECRALLOY SUPPORTED OXIDATION PORT CATALYSTS

Table 3.2.19 Ames Dose-Response Statistics for EPA Mode 4 Subfractions, No. 2 fuel. C_1 = 18.75 µg/plate; C_2 = 600 µg/plate except Basic-Port Catalyst (C_2 = 300). Assayed 11/03/81; TA-98 w/o S-9.

Subfraction	Device	SA_{SL}(c) Rev/µg	SA_{LL}(d), Rev/µg	% of Total SOF
EIN	B(a)	0.5343	0.5459	8.4
EIN	P(b)	1.0449	1.1231	15.1
BAS	B	0.0849	0.0876	2.6
BAS	P	0.4565	0.4780	0.7
ACD	B	1.4749	1.5909	4.1
ACD	P	2.5373	2.8736	6.5
PRF	B	0.0616	0.0548	56.6
PRF	P	0.0177	0.0187	48.5
ARM	B	0.3843	0.3954	2.3
ARM	P	0.0587	0.0563	8.7
TRN	B	0.1234	0.1830	5.5
TRN	P	0.3055	0.2982	4.0
OXY	B	0.4442	0.4678	16.2
OXY	P	0.6541	0.6629	13.1
HIN	B	0.5647	0.4641	1.4
HIN	P	0.4403	0.4210	3.4

(a) Baseline Engine (no control)

(b) Johnson-Matthey Close-coupled port catalyst

(c) $SA_{SL} = \frac{b}{C_2 - C_1} \log_{10} \frac{C_2}{C_1}$, Model: Rev = a + b $\log_{10}$ (mass)

(d) $SA_{LL} = \frac{10^a (C_2^b - C_1^b)}{C_2 - C_1}$, Model: Rev = $a(\text{mass})^b$

Table 3.2.20 Ames Dose-Response Statistics for Total SOF; $C_1 = 18.75$, $C_2 = 600$ μg/plate throughout. Assayed 1/11/82; TA-98 without S-9. See Previous Table for Explanation of Parameters.

EPA Mode	Control Device	SA_{SL} Rev/μg	SA_{LL} Rev/μg	BSSOF g/kw-hr	BSSA[a] kRev/kw-hr
3	B	0.4393	0.4116	0.932	383.6
3	P	0.5709	0.5369	0.609	327.0
4	B	0.3696	0.3296	0.377	124.3
4	P	1.0957	1.0355	0.115	119.1
5	B	1.2247	1.3224	0.38	50.3
5	P	1.9416	2.1738	0.124	52.2
9	B	0.8372	0.8211	0.026	21.4
9	P	0.4602	0.5094	0.011	5.6
10	B	0.7456	0.7367	0.133	9.8
10	P	0.1845	0.1733	0.120	20.8
11	B	0.4433	0.4450	0.969	431.2
11	P	0.3959	0.3873	0.281	108.8

(a) BSSA = (SA_{LL}) (BSSOF) (10^6 μg/g) (kRev/1000Rev)

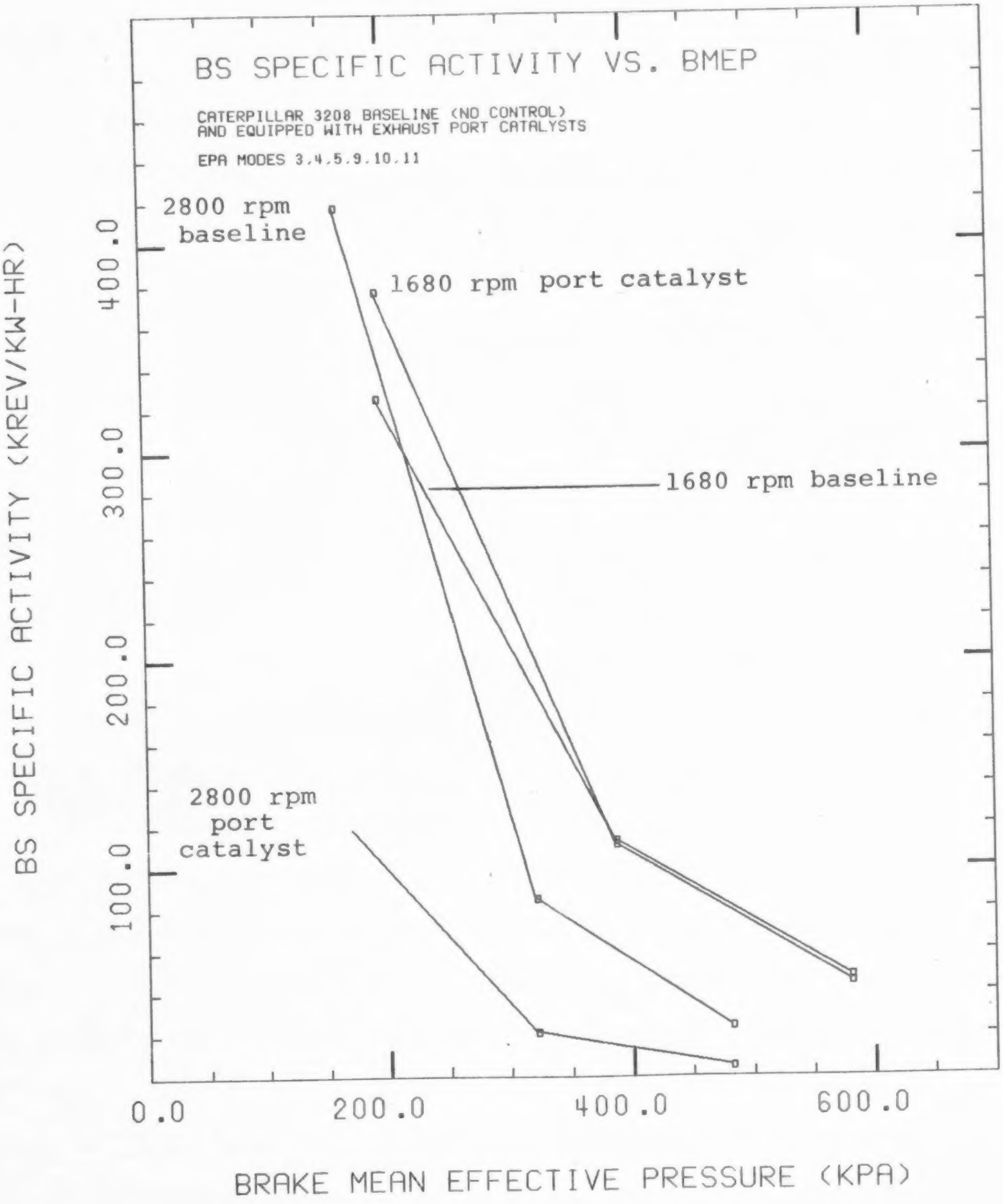

FIG.3.2.48 THE EFFECT OF EXHAUST PORT CATALYSTS ON BS SPECIFIC ACTIVITY OF THE CAT 3208. CATALYSTS: JOHNSON-MATTHEY FECRALLOY SUPPORTED OXIDATION PORT CATALYSTS

Corning Ceramic Trap

The third aftertreatment device investigated was a ceramic trap, from Corning Glass, material designation EX-47. Table 3.2.20 gives the specifications of the traps.

Table 3.2.20 Corning Ceramic Trap Specifications

Manufacturer	Corning Glass Company
Material	Modified Cordierite ($2MgO \cdot 2Al_2O_3 \cdot 5SiO_2$)
Porosity	0.50
Cell Wall Thickness	0.017"
Mean Pore Diameter	12 - 13 μm
Cell Size	15.5 cells/cm^2
Nominal Dimensions	14.37 cm dia x 30.48 cm long

Six Corning traps were obtained from Corning Glass Works (three of the six uncatalyzed, three of the six catalyzed), which were fitted and sealed in metal containers with 3M Interam which is a mat material (heat expanding) developed for automotive catalytic converters (72). The metal containers (one trap per cylinder bank) were easily removable from the exhaust system to permit regeneration in an oven if necessary. Due to durability problems and anticipated high sulfate output, the catalyzed traps were not utilized for test purposes.

Table 3.2.21 is the test matrix utilized for the Corning Traps. No. 2 fuel was used for all engine tests. Due to extremely low particulate and SOF emissions, no sampling was conducted at modes 5, 9 or 10 for chemical fractionation, which requires large amounts of SOF.

Table 3.2.21 Test Matrix for Corning Trap Evaluation

EPA Mode	3		4		5		9		10		11	
Speed (RPM)	1680		1680		1680		2800		2800		2800	
Load (N-M)	160		320		480		399		266		133	
BMEP (mPa)	192		383		575		485		322		161	
Trap	w/o	w	w/o	w	w/o	w	w/o	w	w/o	w	w/o	w
Total Particulate, SOF, and $SO_4^{=}$ mass emissions	x	x	x	x	x	x	x	x	x	x	x	x
HC, NO, and NO_x Mass Emissions	x	x	x	x	x	x	x	x	x	x	x	x
Chemical Characterization of SOF	x	x	x	x							x	x
Ames Mutagenicity Bioassay on SOF	x	x	x	x							x	x
Ames Mutagenicity Bioassay on Subfractions			x	x								

Effect of Corning Traps on Engine Operation and Mass Emissions - The results of the Corning trap tests must be viewed with caution because of the time-dependent behavior of the traps during the engine tests. Depending on the engine output of particulate matter and the exhaust temperature, the pressure drop across the traps varied with time. This is illustrated dramatically in Figure 3.2.49 with similar behavior among the intermediate speed modes (3, 4, 5) and vastly different behavior among the rated speed modes (9, 10, 11). The intermediate speed modes are characterized by fairly low particulate rates and exhaust temperatures below the temperature necessary for rapid oxidation of filtered particulate (i.e. fairly low but steady rates of trap pressure drop increase). The rated speed modes are characterized by high particulate rates and a range of exhaust temperatures bracketing the rapid particulate oxidation rate temperature. Mode 9 has an exhaust temperature of 625°C which apparently produced an oxidation rate equal to the high particulate filtration rate (zero increase in pressure drop with time). Mode 11 has an exhaust temperature below the rapid oxidation temperature and therefore suffered a high pressure drop increase rate due to its high particulate filtration rate. Mode 10 began its time dependent behavior similar to mode 11 but had an initial temperature much higher than mode 11, and the friction of increasing pressure drop gradually raised the temperature (Figure 3.2.50). When the mode 10 exhaust temperature reached 925°F (496°C) at time = 110 minutes, the pressure drop slowly decreased. This suggests that 925°F (496°C) is sufficient to produce rapid particulate oxidation in the Corning traps (at least for the oxygen and hydrocarbon concentrations of mode 10 and the heat transfer characteristics of the trap container system).

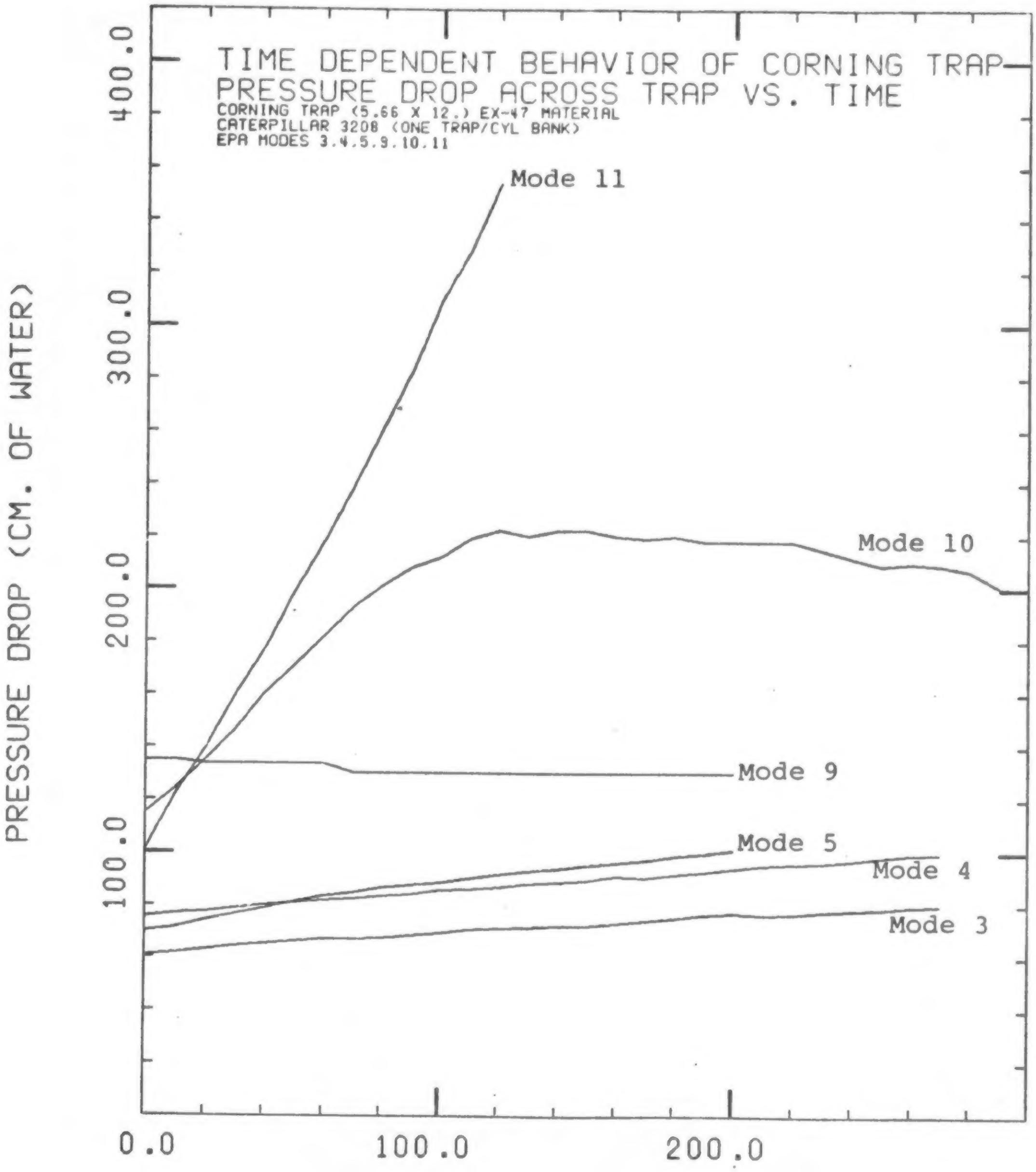

FIG.3.2.49 TIME DEPENDENT BEHAVIOR OF CORNING TRAP
CORNING TRAP (5.66 X 12.) EX-47 MATERIAL
CATERPILLAR 3208 (ONE TRAP/CYL BANK)
EPA MODES 3,4,5,9,10,11

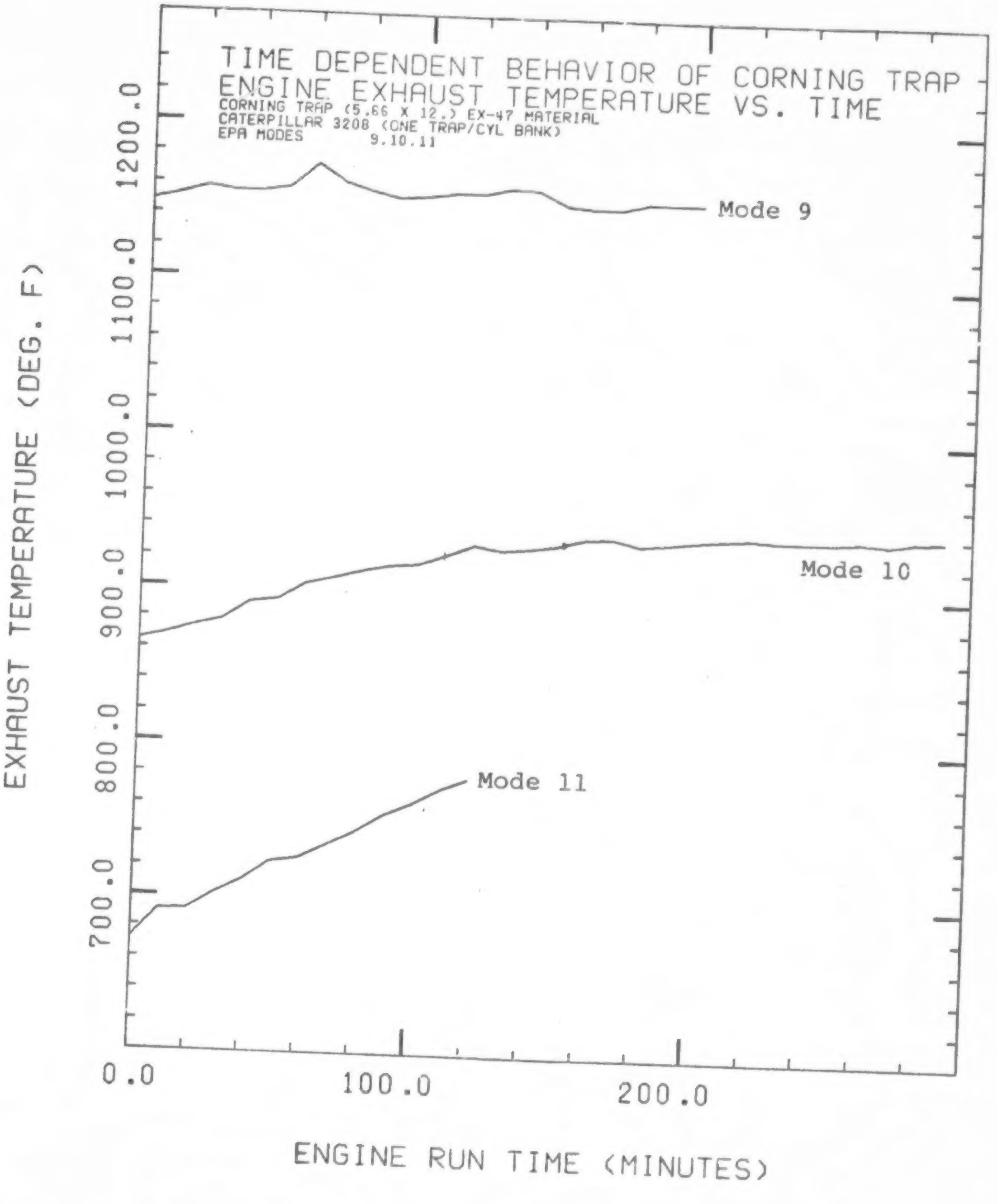

FIG. 3.2.50 TIME DEPENDENT BEHAVIOR OF CORNING TRAP
CORNING TRAP (5.66 X 12.) EX-47 MATERIAL
CATERPILLAR 3208 (ONE TRAP/CYL BANK)
EPA MODES 9.10.11

The time dependent pressure drop produced a time dependent fuel consumption as shown in Figure 3.2.51 for the rated speed modes. The average fuel consumption increase rates were: 0 for mode 9; +2.6 percent/hour for mode 10 (initial phase); and +3.4 percent/hour for mode 11.

In the remainder of the Corning trap results presented, the time dependent behavior has been eliminated by taking the average of the results of three sequential one hour tests.

The effect of the higher pressure drop in the exhaust system resulted in higher fuel consumption at all modes as shown in Figure 3.2.52 The greatest increase in fuel consumption was at mode 11 which corresponds to the highest average pressure drop mode.

The gas phase hydrocarbon emissions are shown with the baseline in Figure 3.2.53 Fairly significant reductions are observed at the rated speed modes with smaller reductions at intermediate speed. This reduction in hydrocarbons is consistent with past results reported where bare (uncatalyzed) ceramic catalytic converter monoliths produced reductions due to the catalytic effect of the large, hot surfaces. This effect should be even greater in the Corning traps due to the intimate gas-solid contact as the exhaust passes through the porous walls. The increase in hydrocarbons observed at mode 3 is due to an unanticipated upward shift in baseline hydrocarbon emissions at this mode rather than an increase through the traps. The reduction in hydrocarbons through the traps appears to be a function of load (temperature) as shown in Figure 3.2.54 which supports the hypothesis that oxidation of hydrocarbons is occurring through the trap rather than adsorption onto the trapped particulate.

The NO_x and NO emissions were not significantly changed as a result of installation of the traps. The BSNO emissions showed decreases through the traps under all conditions except mode 3 (see Figure 3.2.55). This is not

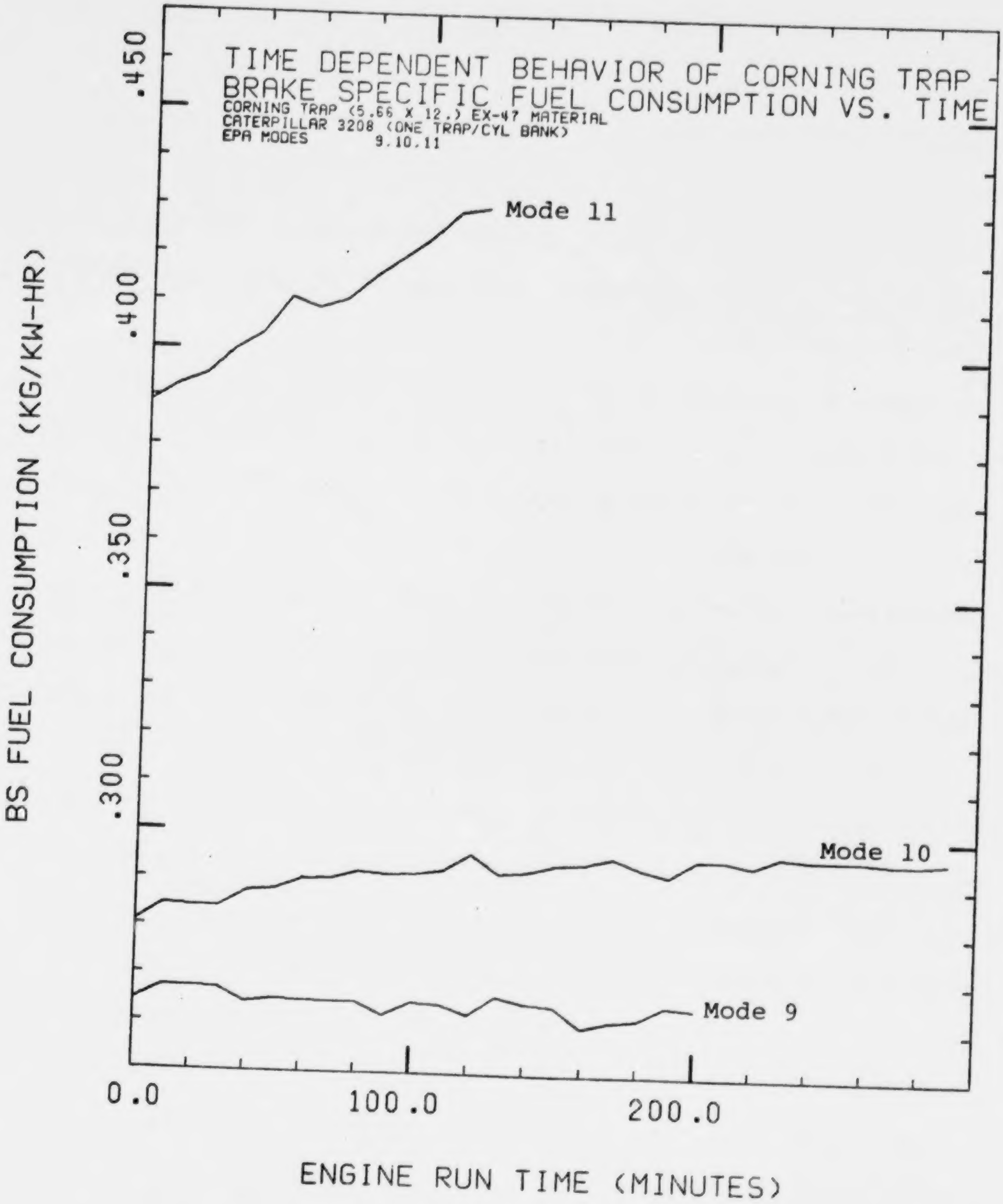

FIG.3.2.51 TIME DEPENDENT BEHAVIOR OF CORNING TRAP
CORNING TRAP (5.66 X 12.) EX-47 MATERIAL
CATERPILLAR 3208 (ONE TRAP/CYL BANK)
EPA MODES 9.10.11

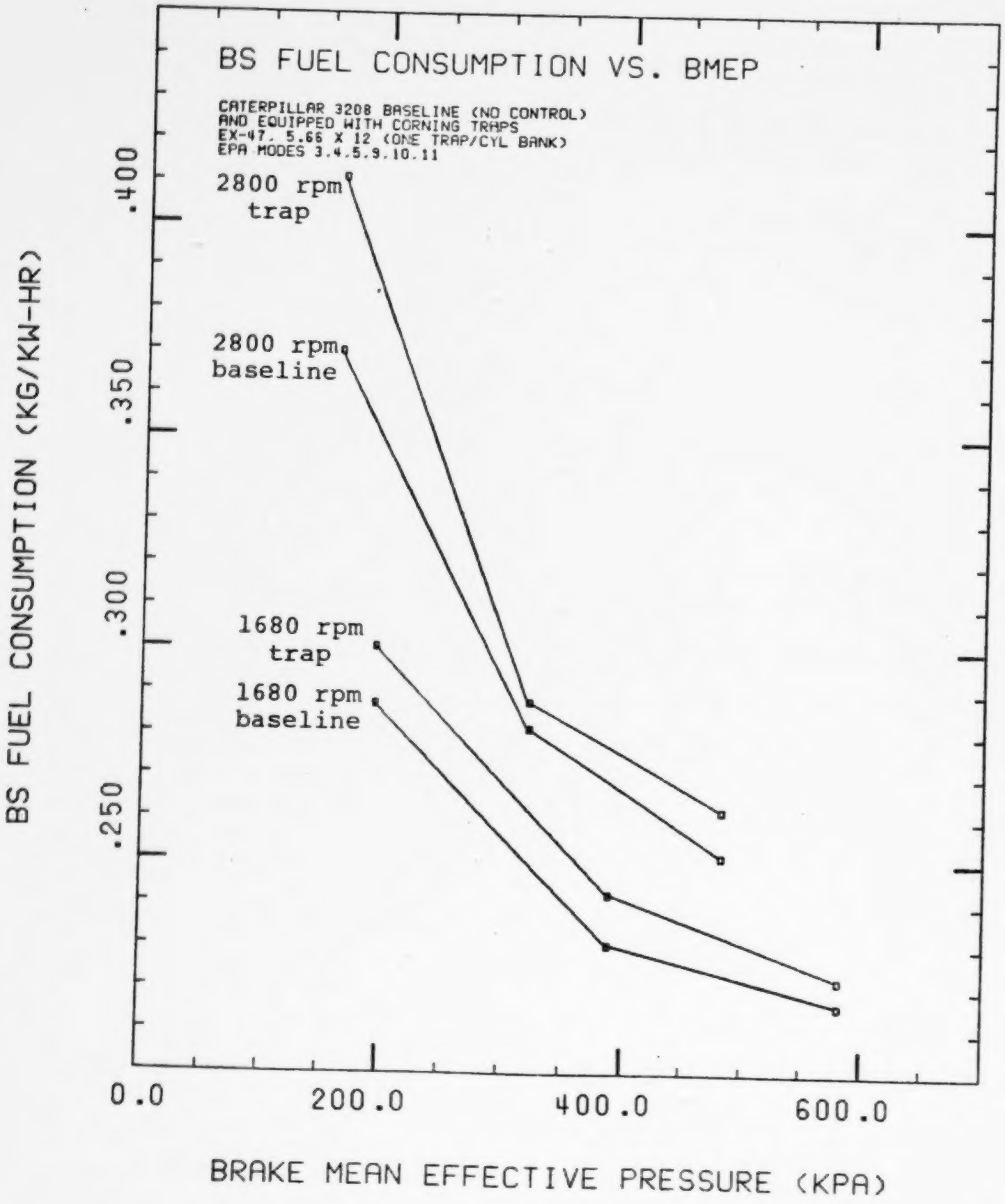

FIG.3.2.52 THE EFFECT OF CORNING PARTICULATE TRAPS ON BS FUEL CONSUMPTION OF THE CAT 3208. TRAPS: CORNING EX-47 DESIGNATION 5.66 INCH X 12 INCH (1 TRAP/CYL BANK)

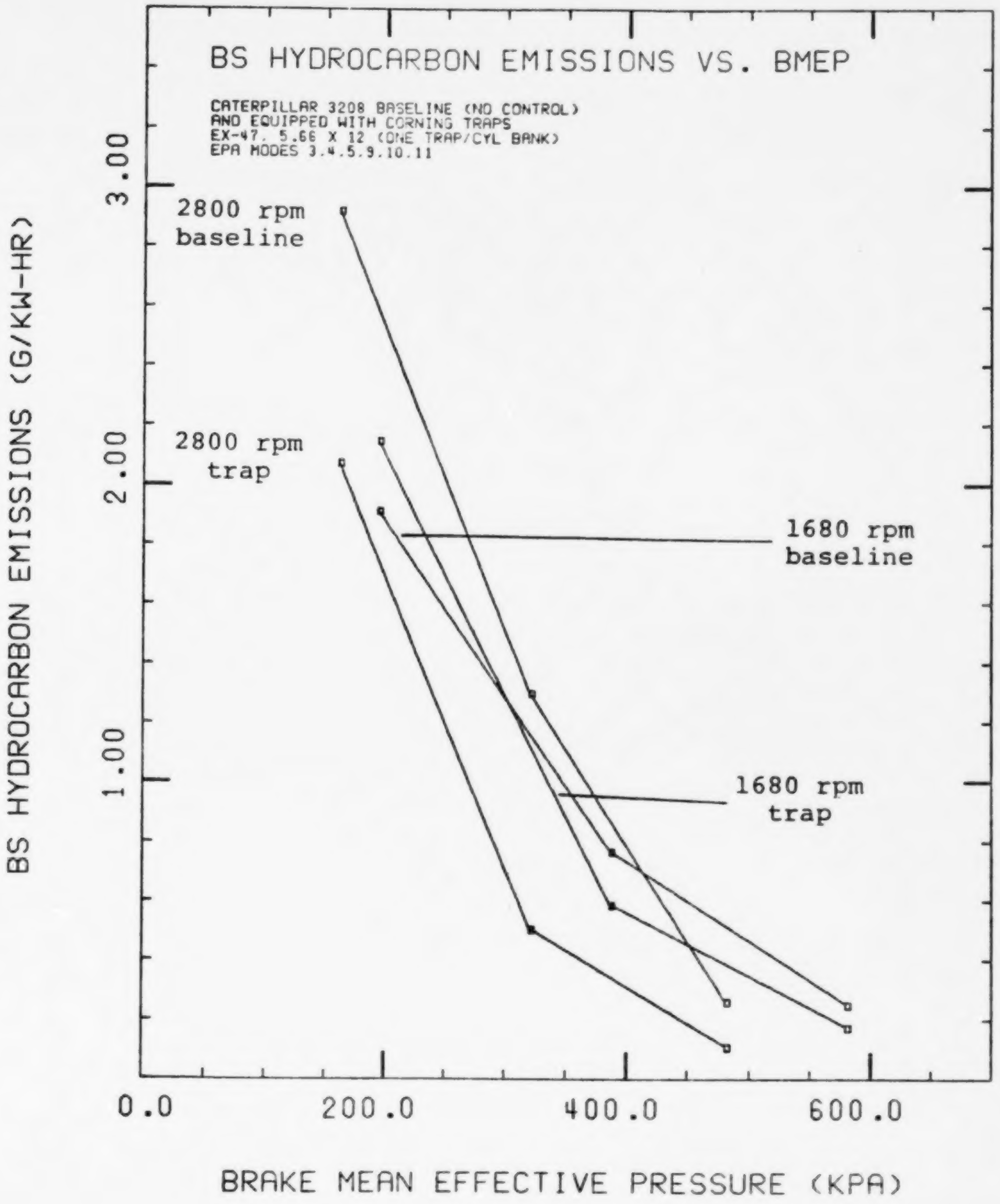

FIG.3.2.53 THE EFFECT OF CORNING PARTICULATE TRAPS ON HYDROCARBON EMISSIONS OF CAT 3208. TRAPS: CORNING EX-47 DESIGNATION 5.66 INCH X 12 INCH (1 TRAP/CYL BANK)

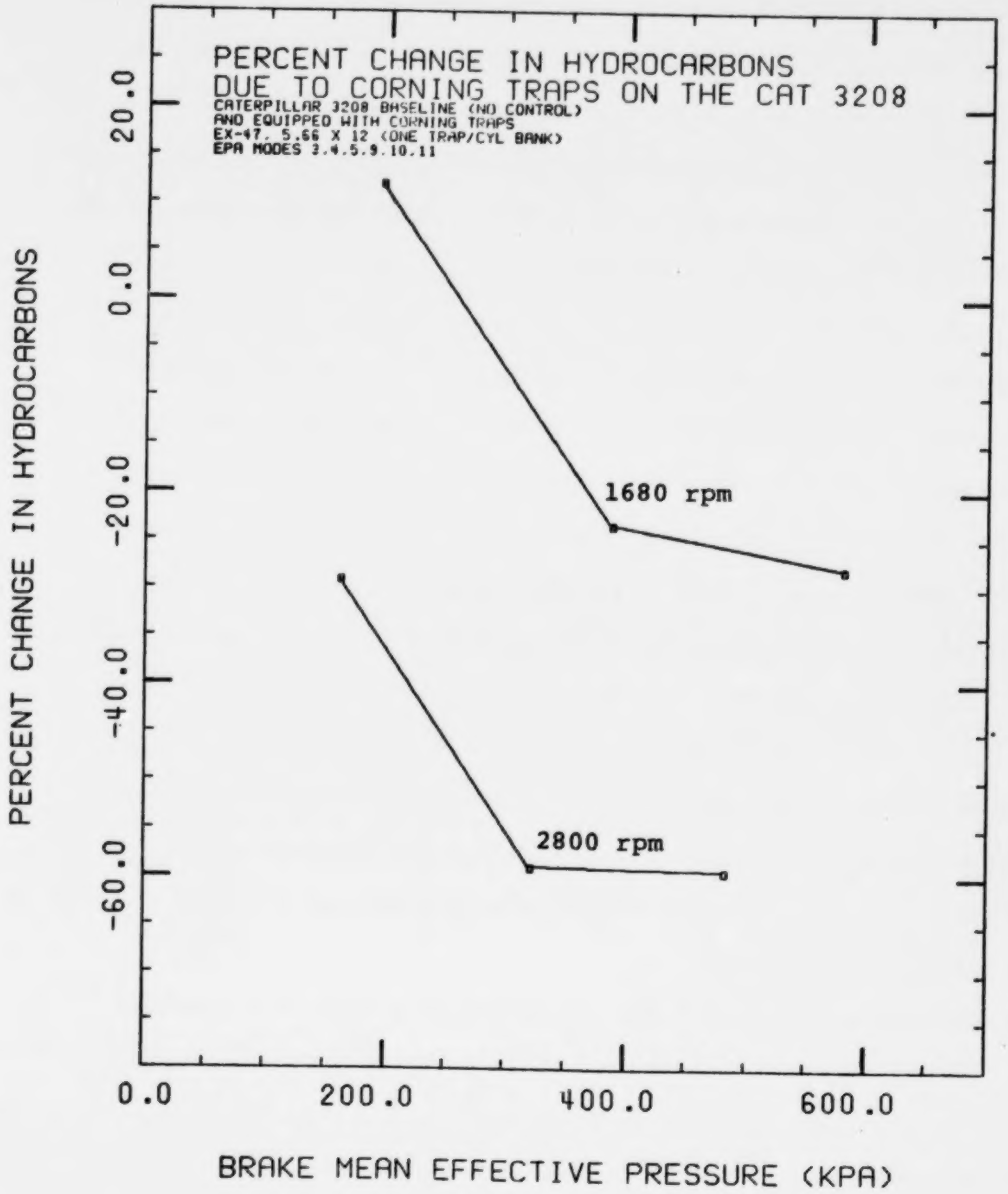

FIG.3.2.54 PERCENT CHANGE IN GASEOUS HYDROCARBONS
DUE TO CORNING TRAPS ON THE CAT 3208
TRAPS: CORNING EX-47 DESIGNATION
5.66 INCH X 12 INCH (1 TRAP/CYL BANK)

consistent with the observed oxidation of hydrocarbons through the traps. Since the hot trap surfaces lead to hydrocarbon oxidation, it is expected that they would also oxidize NO to NO_2. The increase in back pressure with time may cause an effect similar to EGR in that partial retention of oxygen-poor exhaust in the cylinder dilutes the incoming air charge and lowers peak combustion temperatures and NO_2 levels. A second possibility for reduction in NO_2 levels is possible physical or chemical adsorption of NO_2 onto the particulate, as evidenced by work of Gibson et. al. (73) and investigated by Ahmed (74) in the context of sampling errors. Ahmad found that the predicted activation energy for NO_x adsorption agreed with a measured activation energy of a physical adsorption process; however, these studies were conducted at room temperature. Greater adsorption of NO_x at higher temperatures should indicate the extent of NO_x chemisorption. Yet another possibility for lowered NO_2 levels using the trap is reaction of NO_2 with water vapor according to

$$3NO_2 + H_2O \rightarrow 2HNO_3 + NO.$$

The increase in exhaust back pressure and increase in mixing caused by abrupt flow changes through the trap walls could increase the residence time sufficiently to favor this reaction, which proceeds efficiently without a catalyst (75).

The particulate emission results are summarized in Figures 3.2.56a and 3.2.56b. The TPM emissions were reduced at every engine condition ranging from an essentially zero reduction of 0.7 percent at mode 3 to a 97.2 percent reduction at mode 9.

The solid fraction of the particulate was of most interest because it is the only component of the particulate which the trap is fundamentally capable of trapping. Some amounts of hydrocarbons could be adsorbed into the dead ended pores of the trap and the trapped particulate itself but this would be minimal

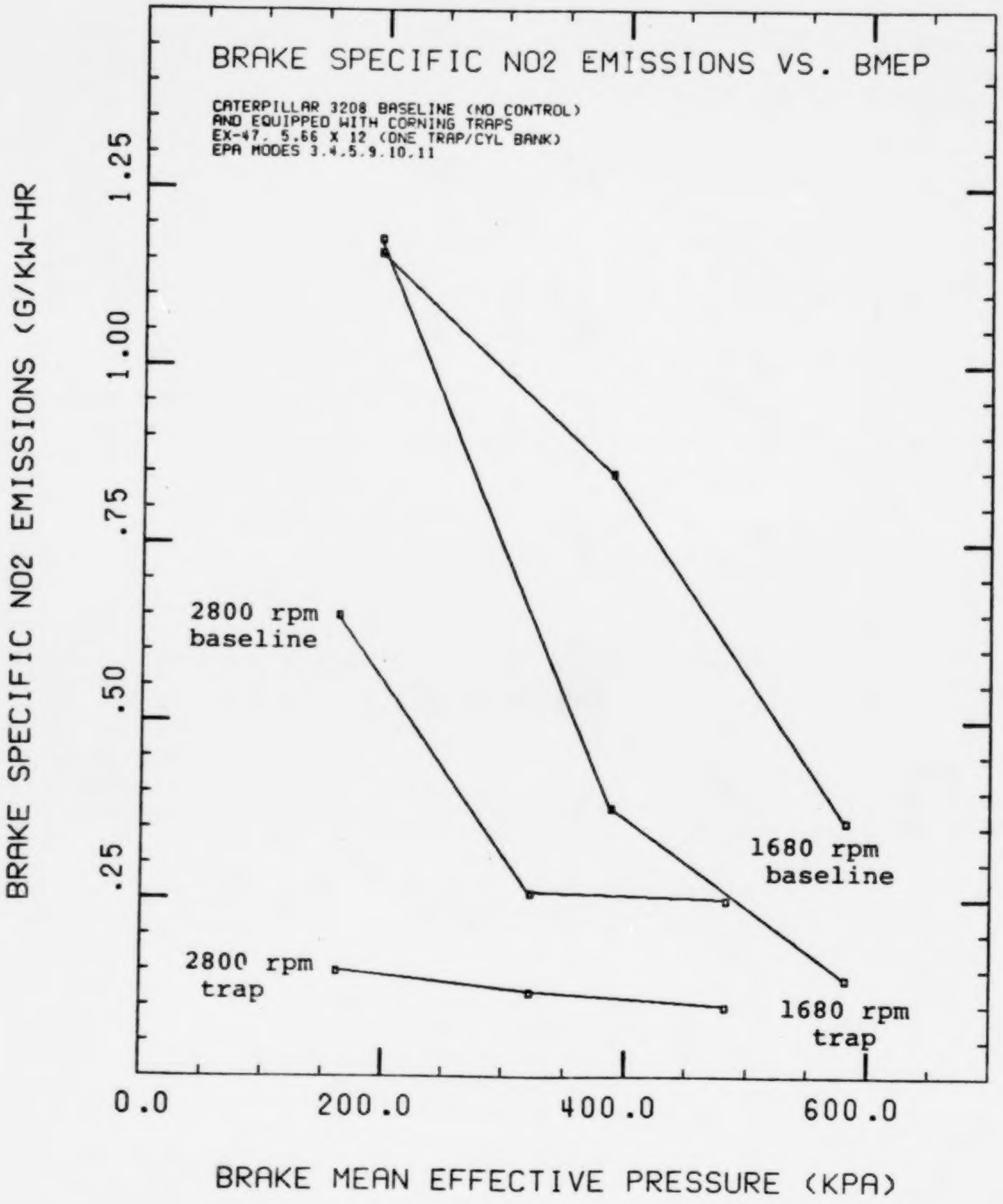

FIG.3.2.55 THE EFFECT OF CORNING PARTICULATE TRAPS ON NO2 EMISSIONS FROM THE CAT 3208. TRAPS: CORNING EX-47 DESIGNATION 5.66 INCH X 12 INCH (1 TRAP/CYL BANK)

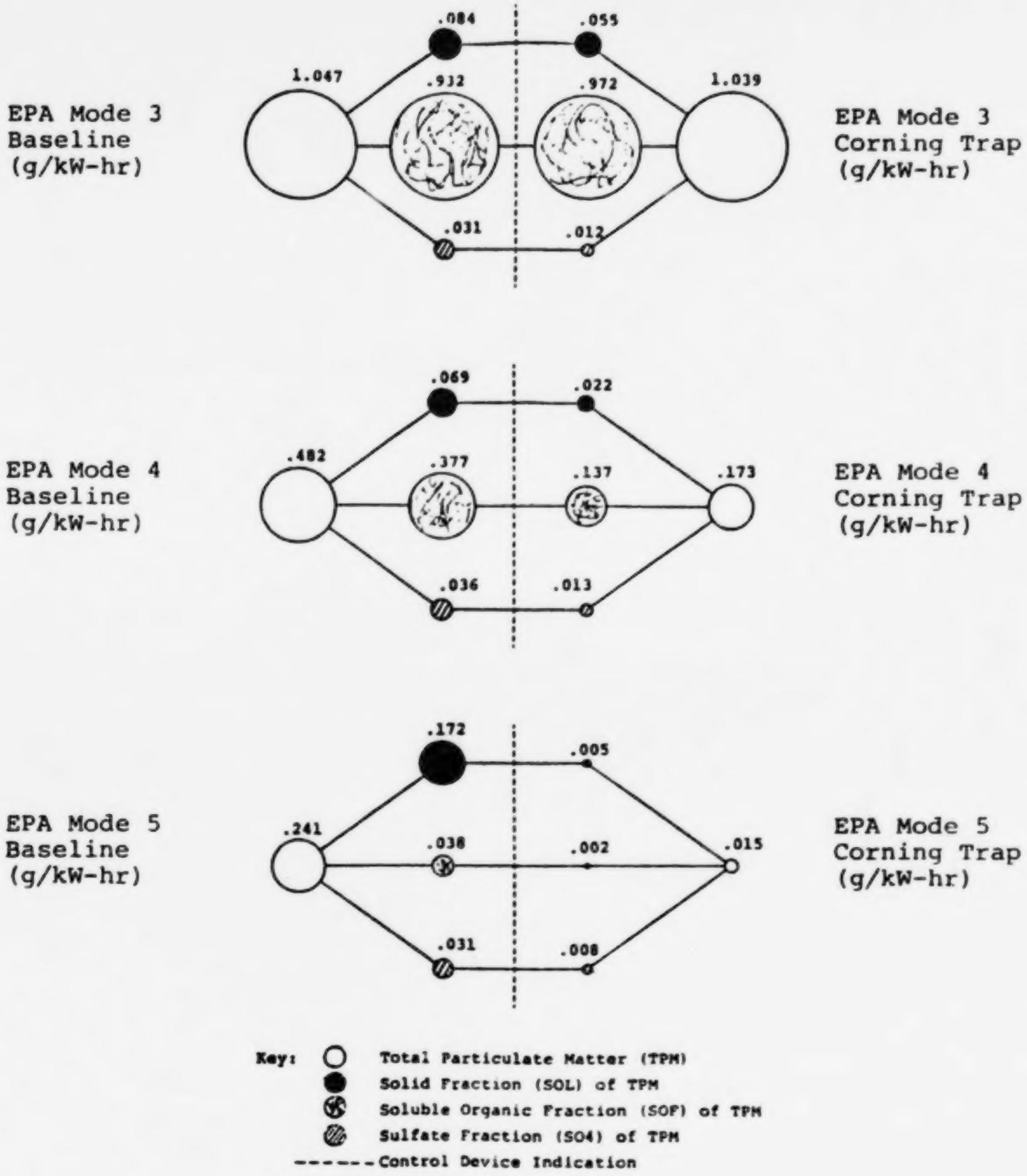
EPA Mode 3 Baseline (g/kW-hr)
1.047
.084
.932
.031
.055
.972
.012
1.039
EPA Mode 3 Corning Trap (g/kW-hr)
EPA Mode 4 Baseline (g/kW-hr)
.482
.069
.377
.036
.022
.137
.013
.173
EPA Mode 4 Corning Trap (g/kW-hr)
EPA Mode 5 Baseline (g/kW-hr)
.241
.172
.038
.031
.005
.002
.008
.015
EPA Mode 5 Corning Trap (g/kW-hr)
Key:
Total Particulate Matter (TPM)
Solid Fraction (SOL) of TPM
Soluble Organic Fraction (SOF) of TPM
Sulfate Fraction (SO4) of TPM
Control Device Indication

Fig.3.2.56a The Effect of Corning EX-47 Ceramic Particulate Traps on Caterpillar 3208 Particulate Emissions at 1680 rpm (1-5.66" X 12" Corning EX-47 trap per cylinder bank)

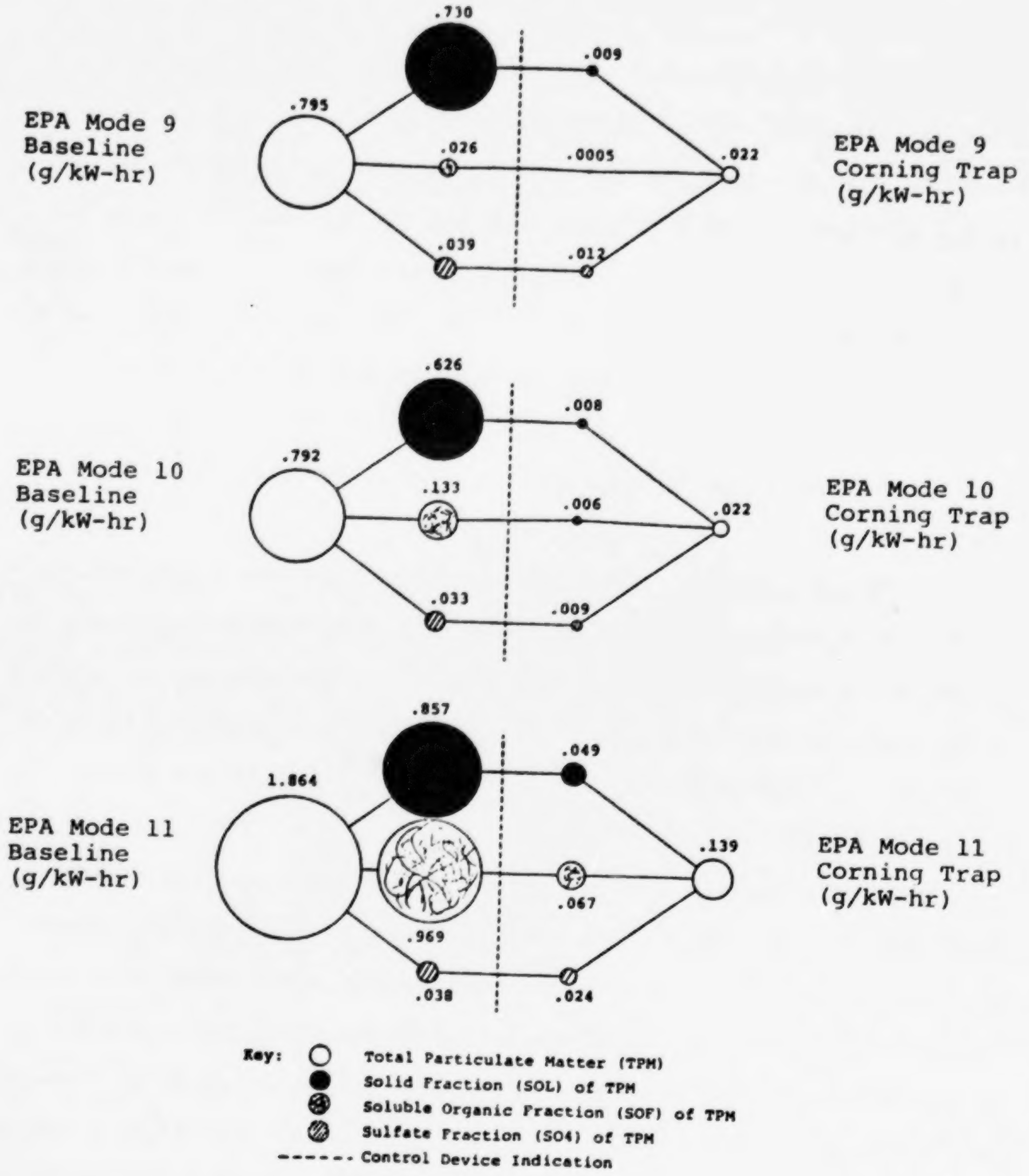
EPA Mode 9
Baseline
(g/kW-hr)
.795
.730
.026
.039
.009
.0005
.012
.022
EPA Mode 9
Corning Trap
(g/kW-hr)
EPA Mode 10
Baseline
(g/kW-hr)
.792
.626
.133
.033
.008
.006
.009
.022
EPA Mode 10
Corning Trap
(g/kW-hr)
EPA Mode 11
Baseline
(g/kW-hr)
1.864
.857
.969
.038
.049
.067
.024
.139
EPA Mode 11
Corning Trap
(g/kW-hr)
Key:
Total Particulate Matter (TPM)
Solid Fraction (SOL) of TPM
Soluble Organic Fraction (SOF) of TPM
Sulfate Fraction (SO4) of TPM
Control Device Indication

Fig3.2.56b The Effect of Corning EX-47 Ceramic Particulate Traps on Caterpillar 3208 Particulate Emissions at 2800 rpm (1-5.66" X 12" Corning EX-47 trap per cylinder bank)

at typical locations of the trap near the engine and at moderate to high loads. The trap would reach a steady state eventually when the adsorption capacity is reached. Likewise sulfates could become attached to the trapped solids. The percent reductions in SOL are plotted in Figure 3.2.57. The rated speed reductions are all greater than 95% while the reductions at intermediate speed are strongly a function of load, varying from 0.7% at mode 3 to 97% at mode 5. An effort at explaining this behavior was made by developing a model of the Corning trap based on membrane type filter theory. The development and application of the membrane filter model is covered in detail in a later section.

The SOF emissions were reduced at every mode except mode 3 (the same one where an increase in hydrocarbons was observed). The SOF reductions cannot be explained by the hydrocarbon reductions alone. The SOF reductions are parallel to the SOL reductions which tends to support the accepted adsorption theory of SOF formation. This adsorption theory application will b treated in the Discussion section.

The sulfate fraction ($SO_4^=$) was reduced at every mode from 42% to 76% (significant in every case). Some possible explanations for this observation are: sulfates becoming attached to the trapped solid particulates, lower sulfate conversion in the exhaust system/dilution tunnel due to the lower particle concentrations reducing the known catalytic effect of particles on $SO_4^=$ formation (48), or lower humidity during the trap test resulting in lower $SO_4^=$(48). It is likely that the observed sulfate reductions were the result of a combination of these factors. A summary of the effects of the Corning traps on fuel consumption and gaseous and particulate emissions is given in Table 3.2.22.

The effect of the Corning traps on the chemical composition of the SOF is illustrated in Fig. 3.2.58a and 3.2.58b and tabulated in Appendix C. From the

Table 3.2.22 - Summary of the Effects of Corning Ceramic Particulate Traps on Caterpillar 3208: Fuel Consumption and Emissions

PERCENT CHANGE (FROM BASELINE) IN
BRAKE SPECIFIC FUEL CONSUMPTION AND EMISSIONS

		Particulate				Gaseous			
EPA Mode	BSFC	Total	Solid	Soluble Organic	Sulfate	NO_x	NO_2	NO	Gas Phase Hydrocarbons
3	+4.9	-0.7	-34.5	+4.3	-61.3	+5.3	+1.7	+5.7	+12.0
4	+4.8	-64.1	-68.1	-63.7	-63.9	-6.5	-57.0	-2.3	-23.4
5	+2.8	-93.8	-97.0	-94.7	-75.5	-5.6	-61.1	-3.3	-28.0
9	+4.0	-97.2	-98.7	-98.0	-69.2	-12.2	-60.0	-10.7	-59.3
10	+2.1	-97.2	-98.8	-95.6	-73.3	-1.0	-52.0	-0.6	-58.9
11	+11.1	-93.1	-94.7	-93.6	-42.7	+6.6	-76.9	+12.5	-29.0

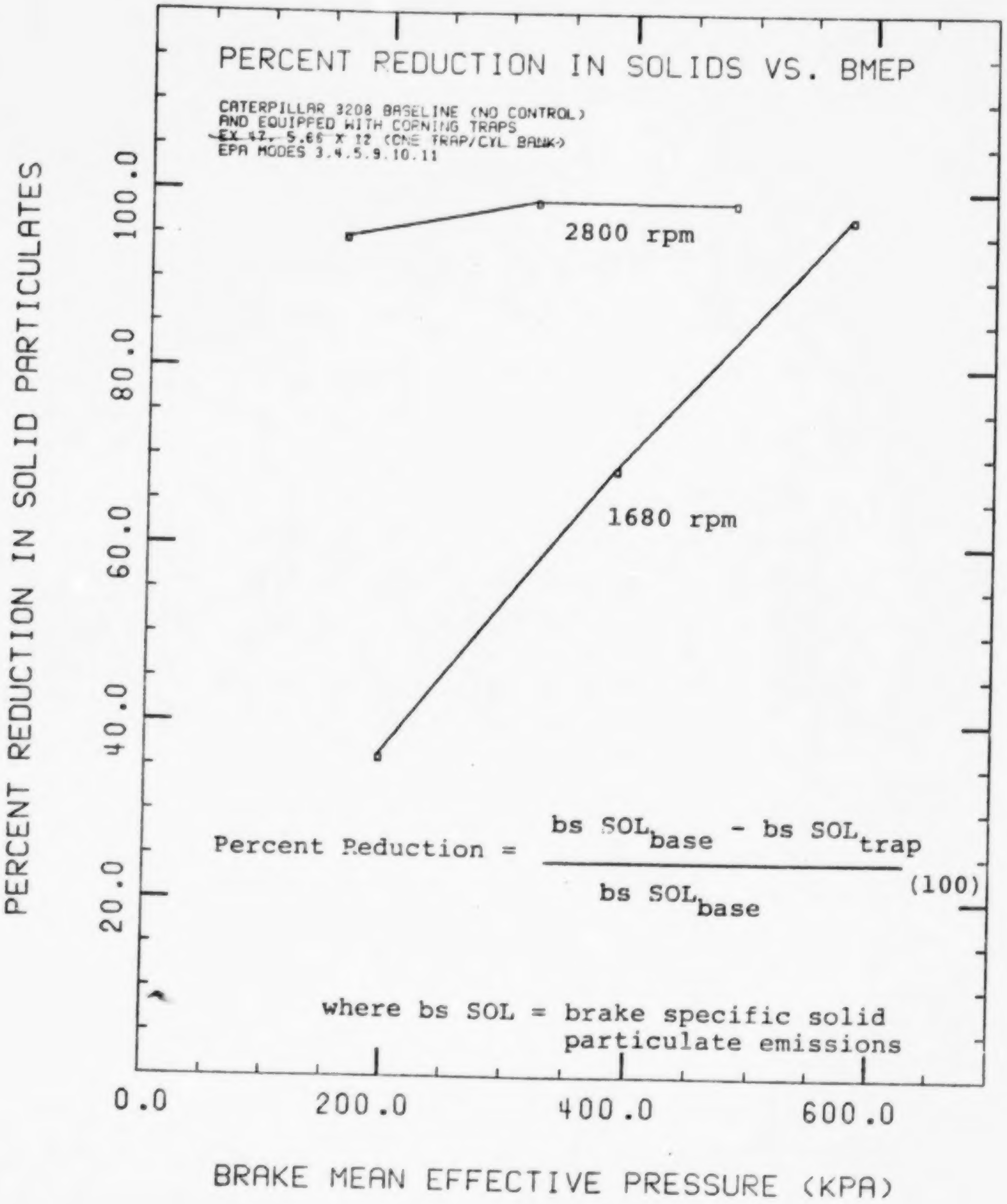

FIG.3.2.57 THE EFFECT OF CORNING PARTICULATE TRAPS ON CAT 3208 SOLID PARTICULATES.
TRAPS: CORNING EX-47 DESIGNATION
5.66 INCH X 12 INCH (1 TRAP/CYL BANK)

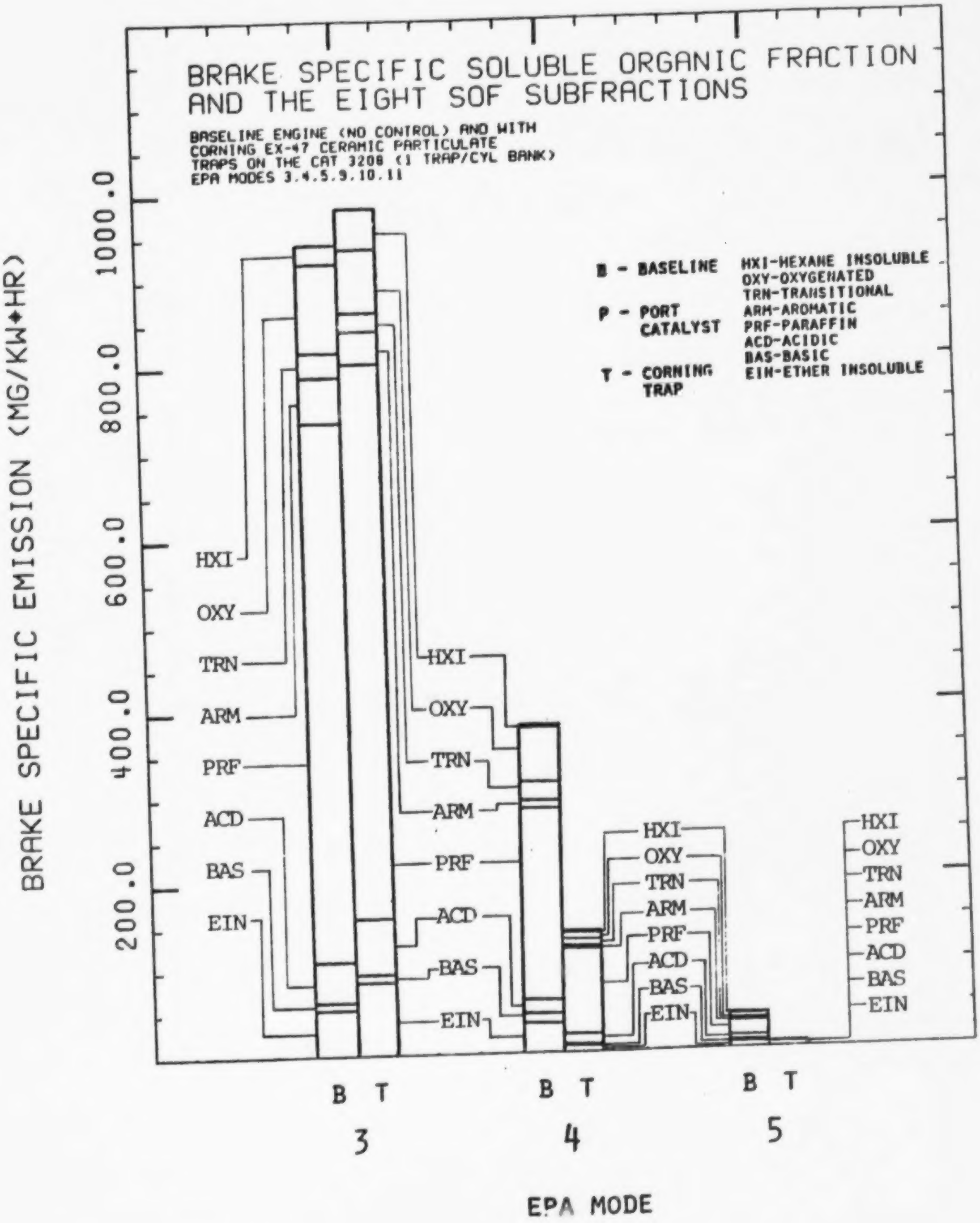

FIG.3.2.58a THE EFFECT OF CORNING CERAMIC TRAPS ON THE CHEMICAL COMPOSITION OF THE SOLUBLE ORGANIC FRACTION OF CAT 3208 PARTICULATE MATTER.

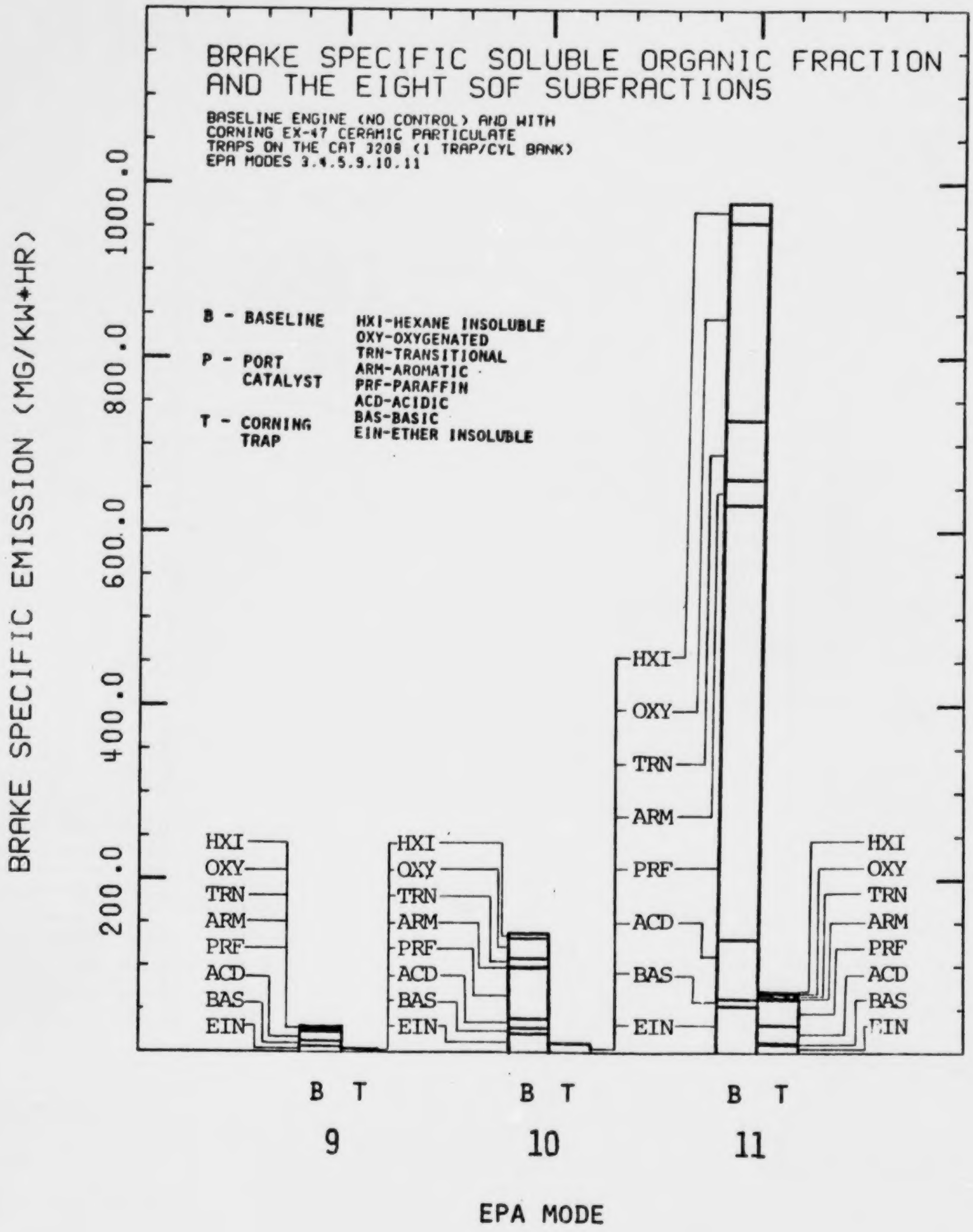

FIG.3.2.58b THE EFFECT OF CORNING CERAMIC TRAPS ON THE CHEMICAL COMPOSITION OF THE SOLUBLE ORGANIC FRACTION OF CAT 3208 PARTICULATE MATTER.

data present, it appears that there was some selectivity (different percent changes for different subfractions) due to preferential oxidation in the trap and/or selective adsorption/condensation in the dilution tunnel.

The results of the Ames bioassays on the total SOF are presented in Figure 3.2.59. The traps increased the SA of the SOF over the baseline significantly at all modes except mode 3. This is in contrast to the port catalysts which decreased the specific activity at the rated speed modes. The SA of the SOF for the baseline and the Corning traps are given in Table 3.2.23, and for mode 4 subfractions in Table 3.2.24. The SA of some of the trap subfractions are of unprecedented magnitude in the experience of the diesel SOF Ames testing at MTU. The SA of the Corning trap oxygenated subfraction actually approaches the activity of 2-nitrofluorene, a highly mutagenic pure compound used as a positive control in the Ames bioassay.

The BSSA was, however, significantly decreased at the rated speed modes with mixed results at the intermediate speed (see Figure 3.2.60). In both of the 75 percent load modes (5 and 9) the BSSA was reduced to essentially zero.

Discussion of Trap Behavior - Based upon the membrane filter theory reviewed in the Background section, a computer model was developed to explain the Corning trap behavior theoretically. Using the assumed properties of the trap materal (effective porosity, mean pore diamter) and the assumed flow conditions of exhaust flow rate, density, viscosity, and capillary conduit flow (76), this model predicted much higher pressure drops than the pressure drops measured across the traps during the engine tests. It was felt that the reported porosity of 50% represented total porosity, and that the effective porosity of 4.88% as calculated using the pressure-flow characteristics of Mogaka et al (34) for a clean trap represented the effective trap porosity, discounting dead-ended and isolated pores.

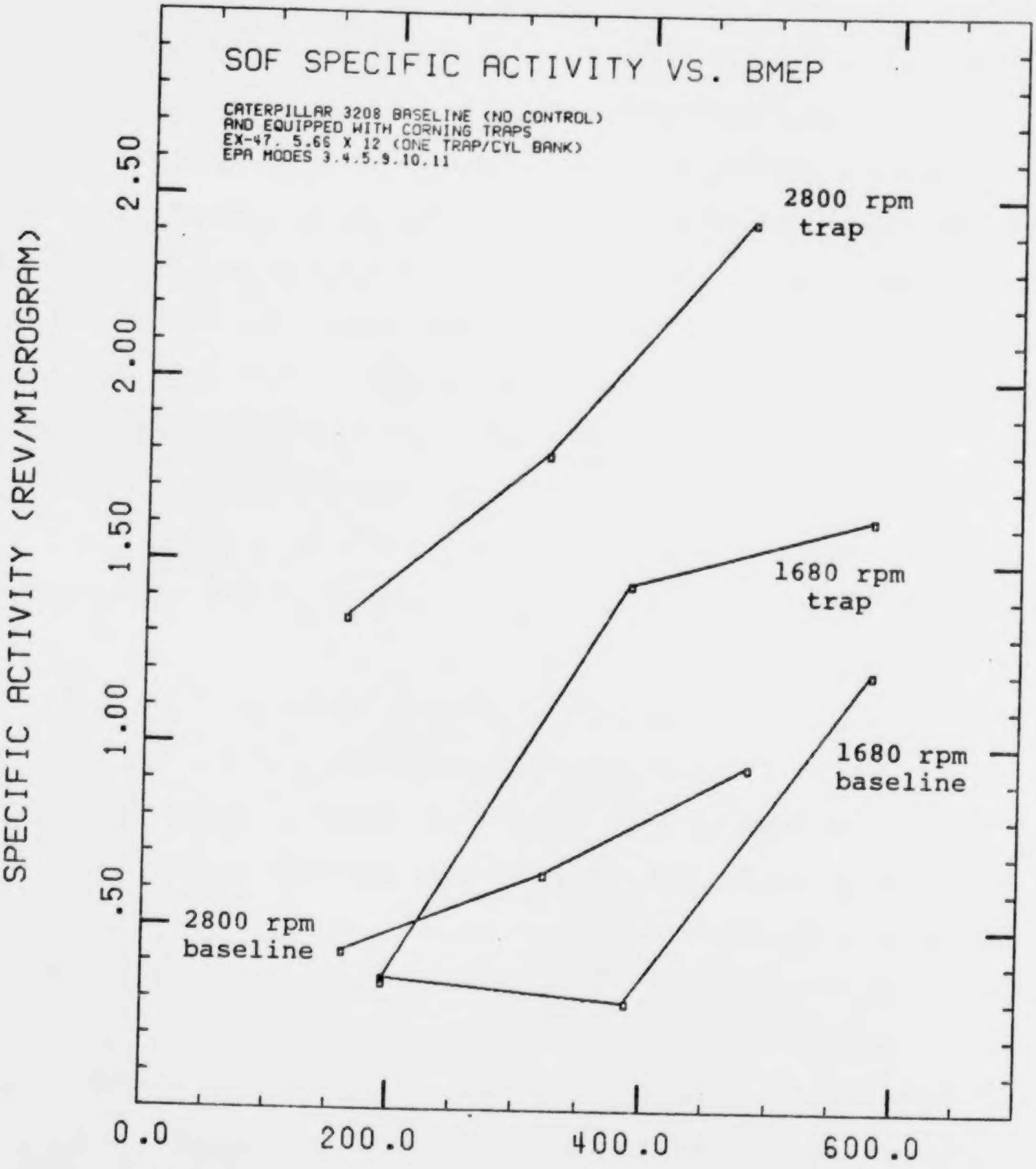

BRAKE MEAN EFFECTIVE PRESSURE (KPA)

FIG.3.2.59 THE EFFECT OF CORNING PARTICULATE TRAPS ON SPECIFIC ACTIVITY OF CAT 3208 SOF. TRAPS: CORNING EX-47 DESIGNATION 5.66 INCH X 12 INCH (1 TRAP/CYL BANK)

Table 3.2.23 Cat 3208 - Corning Trap (Uncatalyzed, EX-47) Ames Bioassay Results on Total SOF C_1 = 18.75 μg, C_2 = 600 μg Throughout Assayed on Same Day (TA98 w/o S-9)

EPA Mode Control Device	$SA_{SL(c)}$ (Rev/μg)	$SA_{LL(d)}$ (Rev/μg)	BSSOF (g/kw-hr)	$BSSA_{(e)}$ (kRev/kw-hr)
3 - B[(a)]	0.426	0.390	0.932	363
3 - T[(b)]	0.410	0.375	0.972	365
4 - B	0.257	0.245	0.377	92
4 - T	1.402	1.407	0.137	193
5 - B	1.212	1.426	0.038	54
5 - T	1.411	1.637	0.002	3.3
9 - B	0.842	0.860	0.026	22
9 - T	2.325	2.640	0.001	2.6
10 - B	0.725	0.799	0.127	101
10 - T	1.499	1.741	0.006	10.7
11 - B	0.378	0.336	0.969	325
11 - T	1.199	1.302	0.067	87

(a) B = Cat 3208 Baseline Engine (No Control)

(b) T = Cat 3208 with Corning Uncatalyzed Traps, Ex-47

(c) $SA_{SL} = \frac{b}{(c_2 - c_1)} \log_{10} \frac{c_2}{c_1}$, Model: Rev = a + b log (mass)

(d) $SA_{LL} = 10^a \frac{(c_2^b - c_1^b)}{(c_2 - c_1)}$, Model: Rev = a $(\text{mass})^b$

(e) $bsSA = (SA_{LL})\ (bsSOF)\ (10^6 \frac{\mu g}{g})\ (\frac{KRev}{1000\ Rev})$

Table 3.2.24 Caterpillar 3208, EPA Mode 4, SOF Subfractions, Ames Bioassay Results for Baseline and Corning Trap (Uncatalyzed). C_1, C_2 as shown Assayed on the Same Day (TA 98 w/o S-9)

Subfraction Device	C_1 (g)	C_2 (g)	SA_{SL} Rev/ g	SA_{LL} Rev/ g	% of Total SOF
EIN - B	18.75	600.	0.484	0.489	8.36
EIN - T	0.20	150.	22.64	32.41	3.25
BAS - B	18.75	37.5	0.373	0.372	2.63
BAS - T	2.34	75.	8.19	8.18	0.54
ACD - B	18.75	300.	0.657	0.672	4.10
ACD - T	18.75	600.	1.78	2.02	9.43
PRF - B	18.75	600.	0.09	0.07	56.61
PRF - T	18.75	600.	0.005	0.005	72.95
ARM - B	18.75	600.	0.503	0.592	2.33
ARM - T	18.75	300.	0.131	0.130	2.84
TRN - B	18.75	600.	0.066	0.065	5.50
TRN - T	18.75	600.	0.504	0.526	3.50
OXY - B	18.75	600.	0.362	0.329	16.21
OXY - T	0.05	18.75	153.4	190.6	6.50
HIN - B	18.75	150.	0.838	0.708	1.37
HIN - T	18.75	150.	0.598	0.595	0.99

B = Cat 3208 Baseline Engine (No Control)

T = Cat 3208 with Corning Uncatalyzed Traps, EX-47

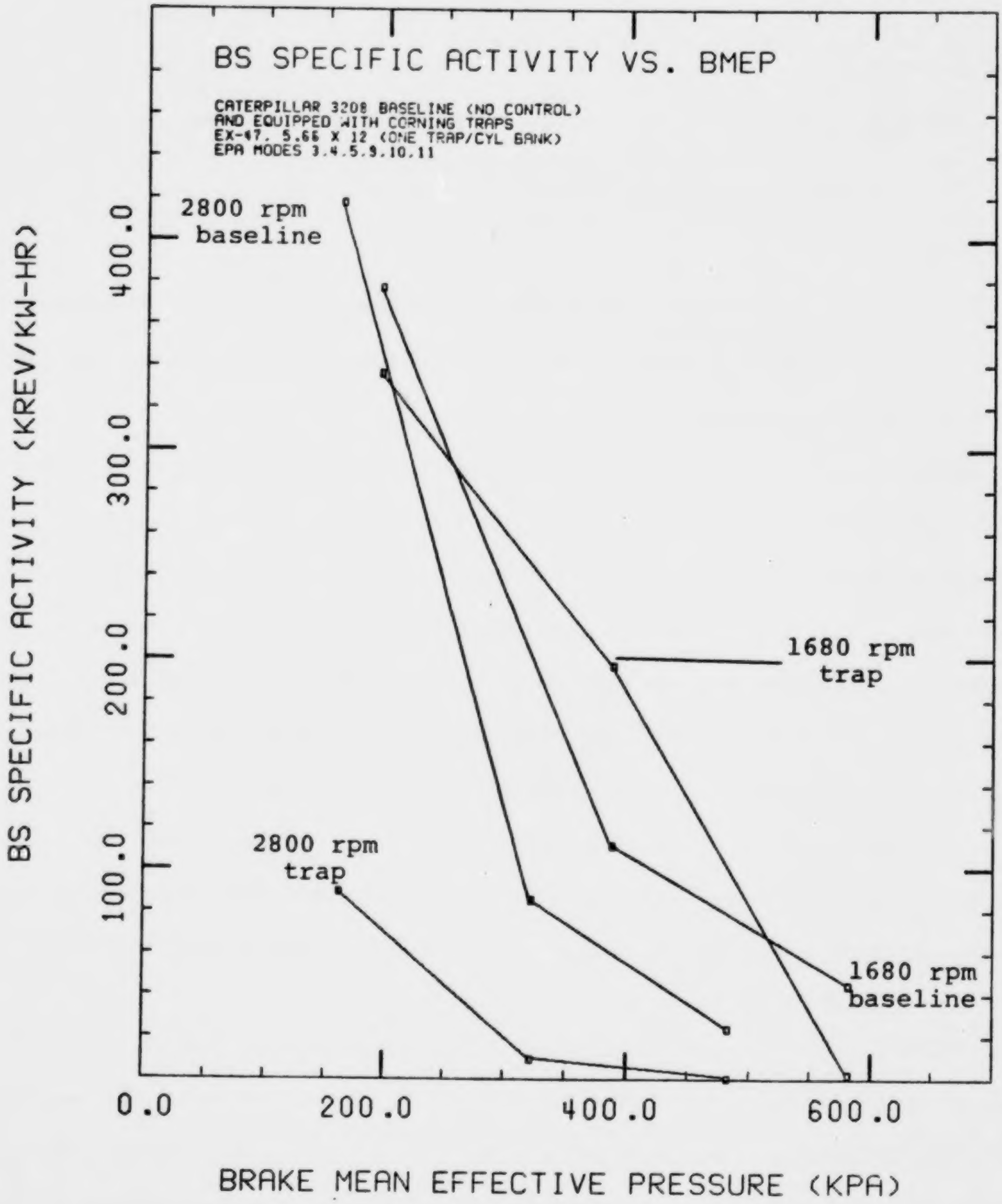

FIG.3.2.60 THE EFFECT OF CORNING PARTICULATE TRAPS ON BS SPECIFIC ACTIVITY OF CAT THE 3208. TRAPS: CORNING EX-47 DESIGNATION 5.66 INCH X 12 INCH (1 TRAP/CYL BANK)

Using the known functional relationship between porosity, mean pore diameter, and mean center-to-center pore spacing (39):

E = Effective porosity (%) derived as 4.88% for a clean trap

MPD = Mean Pore Diameter given as 12 μm (91) for a clean trap

B = Mean Pore Spacing (center-to-center) same units as MPD

$$B = MPD\sqrt{\frac{\pi}{2\sqrt{3}\ (E/100)}} = 51.73\ \mu m$$

the value of 51.73 micrometers was obtained, which was used in all computations since it should remain constant as the trap is loaded. The pores are much more widely spaced than originally thought.

Table 3.2.25 gives the porosity and mean pore diameter predicted for each particulate filter taken during the Corning trap tests, assuring that the measured pressure drop was accurately estimated by the model-predicted pressure drop. Each filter corresponds to a one-hour sampling period, and the traps were regenerated in an oven between each mode to establish baseline conditions. The porosity and mean pore diameter are seen to decrease for all modes but those for which continuous regeneration was observed (modes 9 and 10).

A parametric study of the membrane filter theory was implemented by approximating two standard conditions: EPA mode 4 and EPA mode 9 with the Caterpillar 3208. Material properties and flow conditions chosen for these conditions are shown in Table 3.2.26.

Figures 3.2.61 and 3.2.62 show the filtering efficiency for both sets of flow conditions. The total filtering efficiency as well as individual mechanism filtering efficiencies are plotted as a function of particle diameter. The diffusion mechanism, which, if 100% effective for particles smaller than about 0.4 micrometers, is slighty more efficient for SC/1, perhaps due to lower exhaust viscosity. Higher gas velocities cause slightly higher efficiencies for the inertial impaction mechanism for SC/2. The direct interception mechanism is predicted to be the same for both mechanisms because it depends only upon mean

Table 3.2.25 Predicted Properties for the Corning Trap Based on the Membrane Filter Theory Model

EPA Mode	Filter Number	Model Predicted Porosity (percent)	Mean Pore Diameter (micrometers)
3	3-T-1 (a)	3.40	10.02
3	3-T-2	3.28	9.84
3	3-T-3	3.18	9.69
3	3-T-4	3.11	9.58
4	4-T-1	3.55	10.23
4	4-T-2	3.43	10.06
4	4-T-3	3.33	9.91
4	4-T-4	3.23	9.76
5	5-T-1	4.12	11.03
5	5-T-2	3.94	10.78
5	5-T-3	3.70	10.45
9	9-T-1	4.42	11.42
9	9-T-2	4.47	11.48
9	9-T-3	4.50	11.52
10	10-T-1	3.20	9.72
10	10-T-2	3.04	9.74
10	10-T-3	3.33	9.91
11	11-T-1	3.33	9.91
11	11-T-2	2.72	8.96
11	11-T-3	2.35	8.33

(a) Each filter represents a one hour time period in the total sample time for the mode. Therefore the predicted porosities and mean pore diameters are the average predicted values for that one hour period.

Table 3.2.26 Standard Material and Flow Conditions Chosen for Parametric Study of Corning Trap using the Membrane Filter Theory Based Model Developed.

Parameter	SC/1 ∿ EPA Mode 4	SC/2 ∿ EPA Mode 9
Porosity (percent)	3.500	3.500
Pore Spacing (micrometers)	51.73	51.73
Mean Pore Diameter (micrometers)	10.16	10.16
Filter Wall Thickness (micrometers)	431.8	431.8
Total Filter Area (m^2)	4.75795	4.75795
Total Exhaust Flow (m^3/min)	16.39	34.44
Exhaust Temp. (deg K)	639	901
Exhaust Viscosity (N-s/m^2)	$.273(10^{-4})$	$.379(10^{-4})$
Exhaust Density (kg/m^3)	.648	.379
Exhaust Molecular Weight (kg/kg-mole)	28.80	28.82

pore diameter. Overall, the filtering efficiencies display a concave upward "droop" with a minimum of about 35% for both sets of standard conditions; but this minimum is shifted slightly to larger particle diameters for SC/1. The input particle size distribution is necessary for predicting which set of standard conditions would produce the better overall particle size filtration efficiency.

Figures 3.2.63 through 3.2.66 show independent effects of four trap properties using the flow conditions of SC/1. Although these plots are informative, one must have information on the particle size distribution to predict the optimum filter properties.

The best particle size distribution that could be found for this application was a log-normal distribution presented by Vuk et al (65). The data given by Vuk et al were based on Anderson inertial impactor results from the raw exhaust of Caterpillar 3150 Engine. The average of their data over the 13 mode cycle was taken as a starting point and the two parameters needed to define the log-normal distribution were determined using the mathematical procedures of Reference 77. The mass median diameter used was 0.075 micrometers with a standard geometric deviation of 8.10 micrometers.

Because a cumulative frequency is needed for a filter input model and the lognormal distribution is expressed by a non-integrable function (e^{-x^2}). The log-normal distribution was transformed into a cumulative distribution by integration of a fifth order polynomial fit of the normal distribution given in Reference 78; this is plotted in Figure 3.2.67. The model was modified to integrate the predicted efficiency using the cumulative distribution of Figure 3.2.67 to get overall efficiency. The model was then applied to the predicted porosities for the actual filter data (Table 3.2.25) and the actual flow conditions. The predicted overall efficiencies are compared with the actual

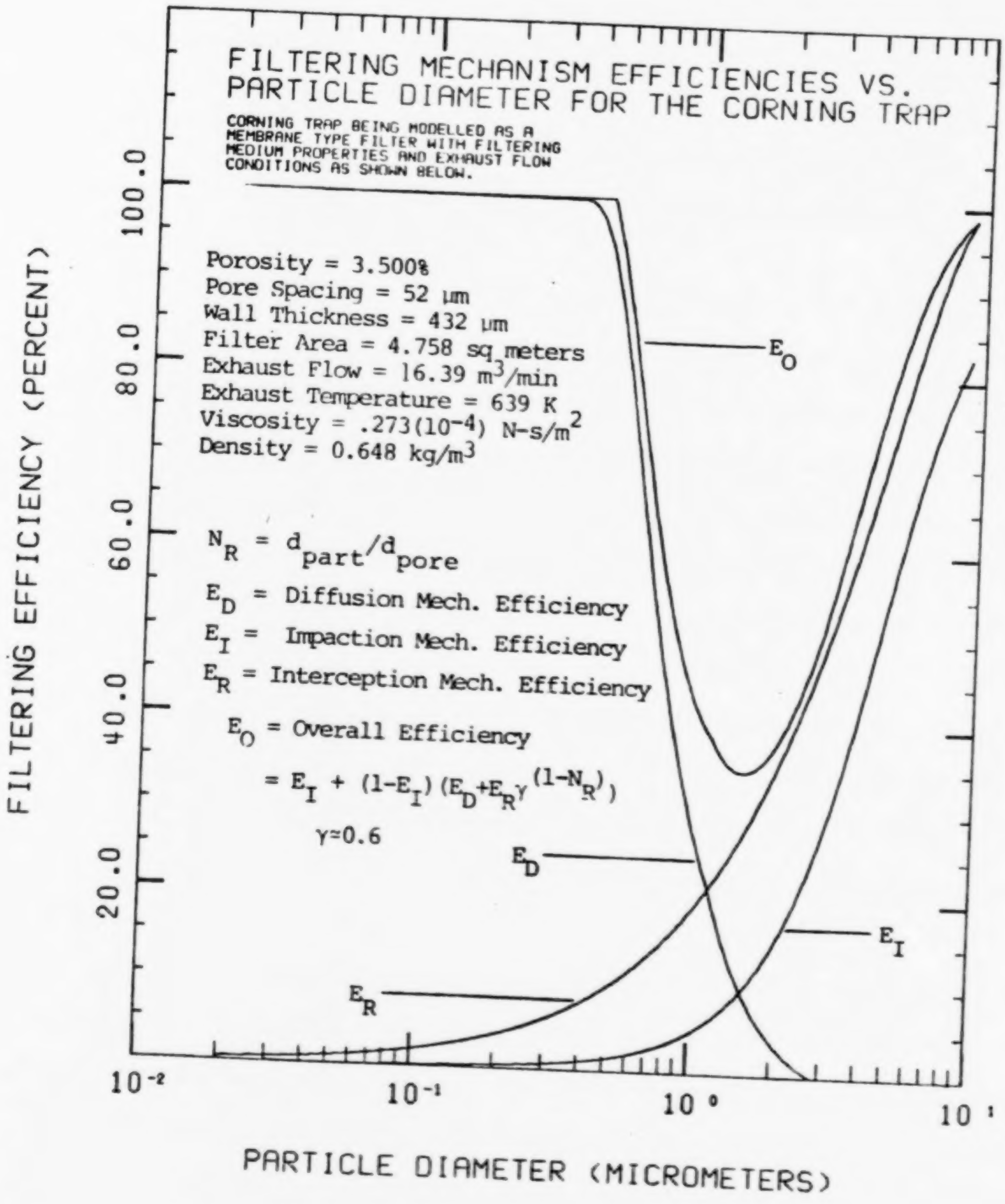

FIG.3.2.61 FILTERING MECHANISMS FOR CORNING TRAP MODELLED AS A MEMBRANE TYPE FILTER INCLUDING: DIFFUSION, INERTIAL IMPACTION, AND DIRECT INTERCEPTION

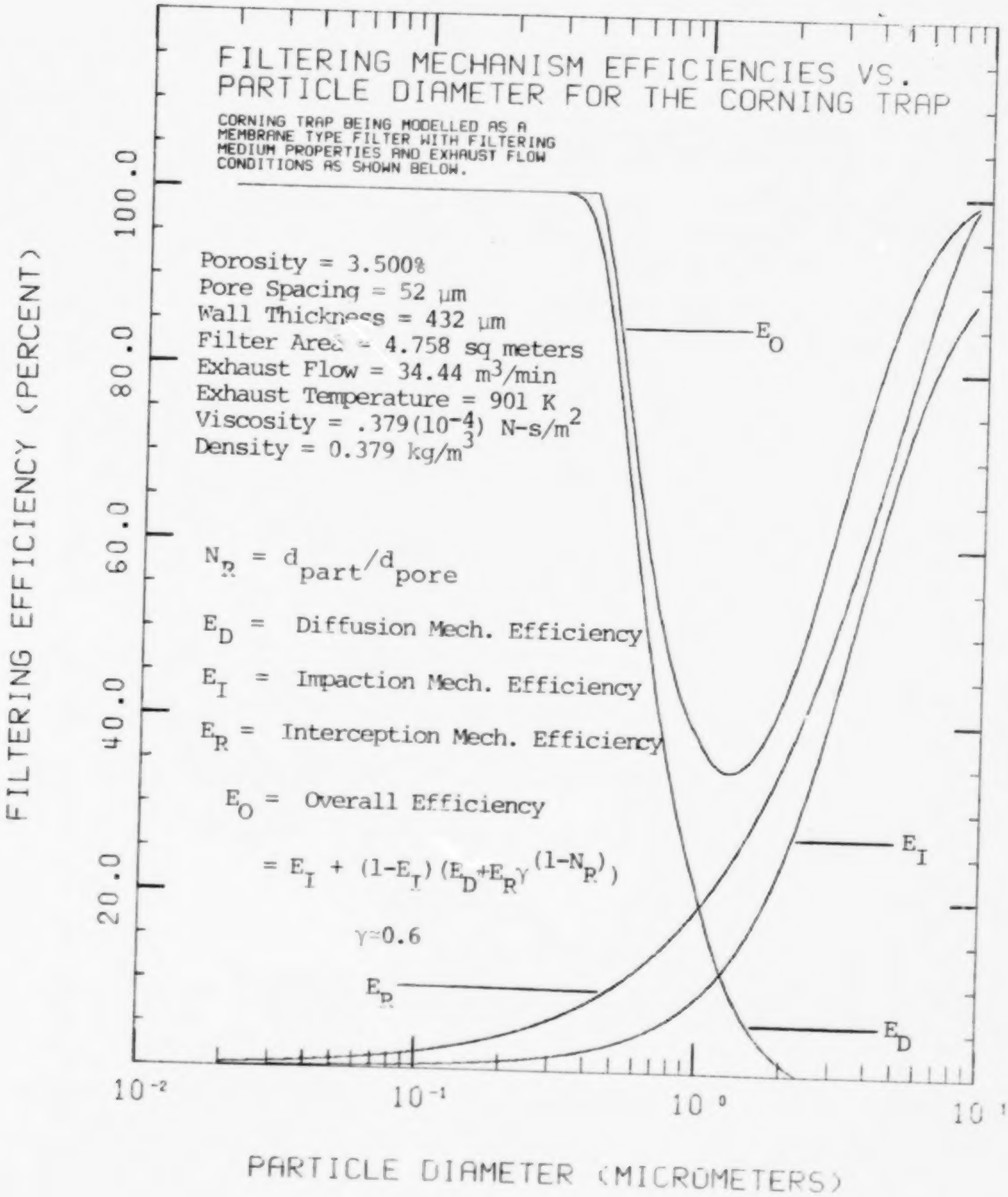

FIG.3.2.62 FILTERING MECHANISMS FOR CORNING TRAP MODELLED AS A MEMBRANE TYPE FILTER INCLUDING: DIFFUSION, INERTIAL IMPACTION, AND DIRECT INTERCEPTION

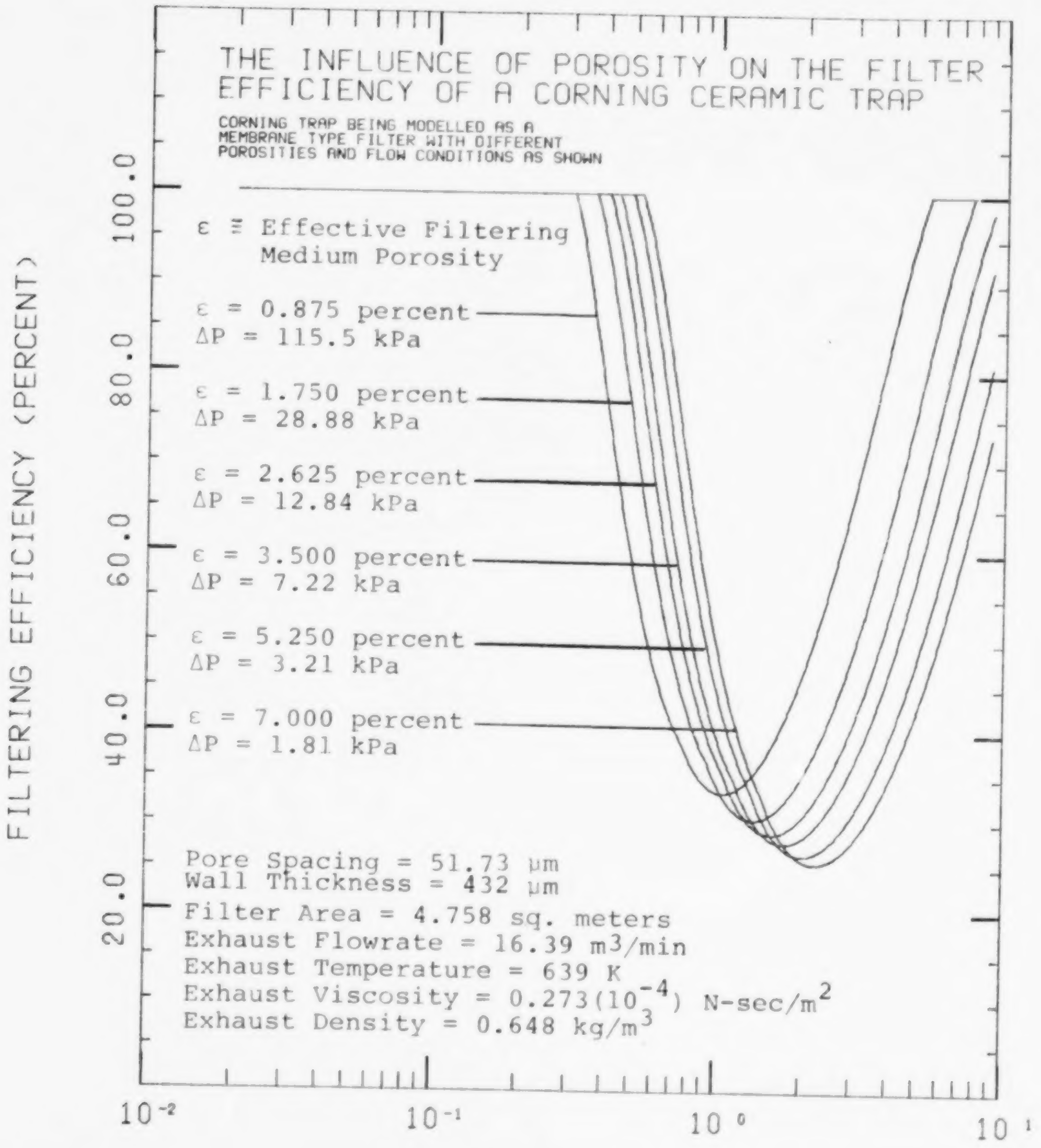

FIG.3.2.63 PARAMETRIC STUDY FOR CORNING TRAP MODELLED AS A MEMBRANE TYPE FILTER STUDYING THE INFLUENCE OF EFFECTIVE FILTERING MEDIUM POROSITY ON EFFICIENCY

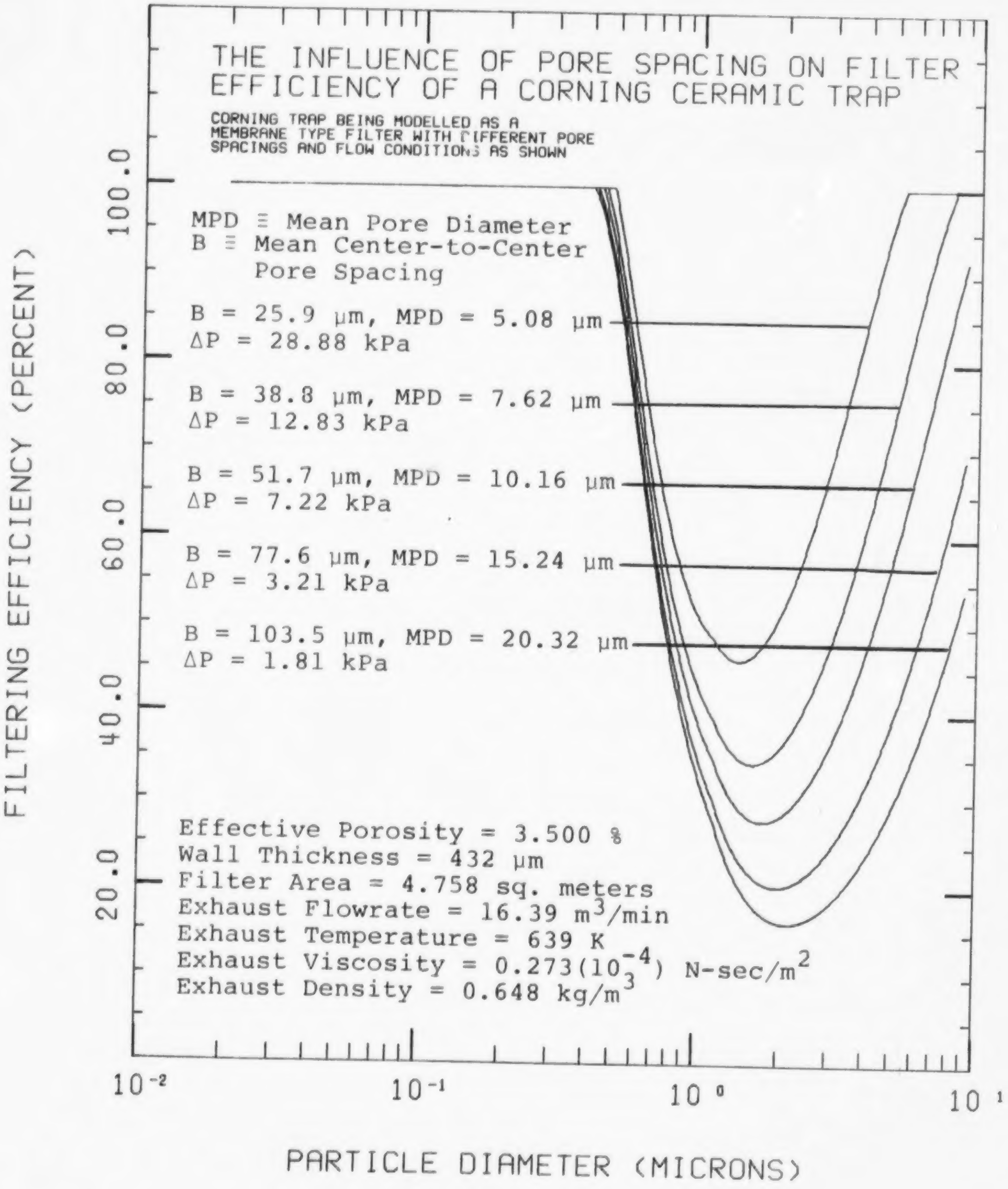

FIG.3.2.64 PARAMETRIC STUDY FOR CORNING TRAP MODELLED AS A MEMBRANE TYPE FILTER STUDYING THE INFLUENCE OF CENTER-TO-CENTER PORE SPACING ON FILTER EFFICIENCY

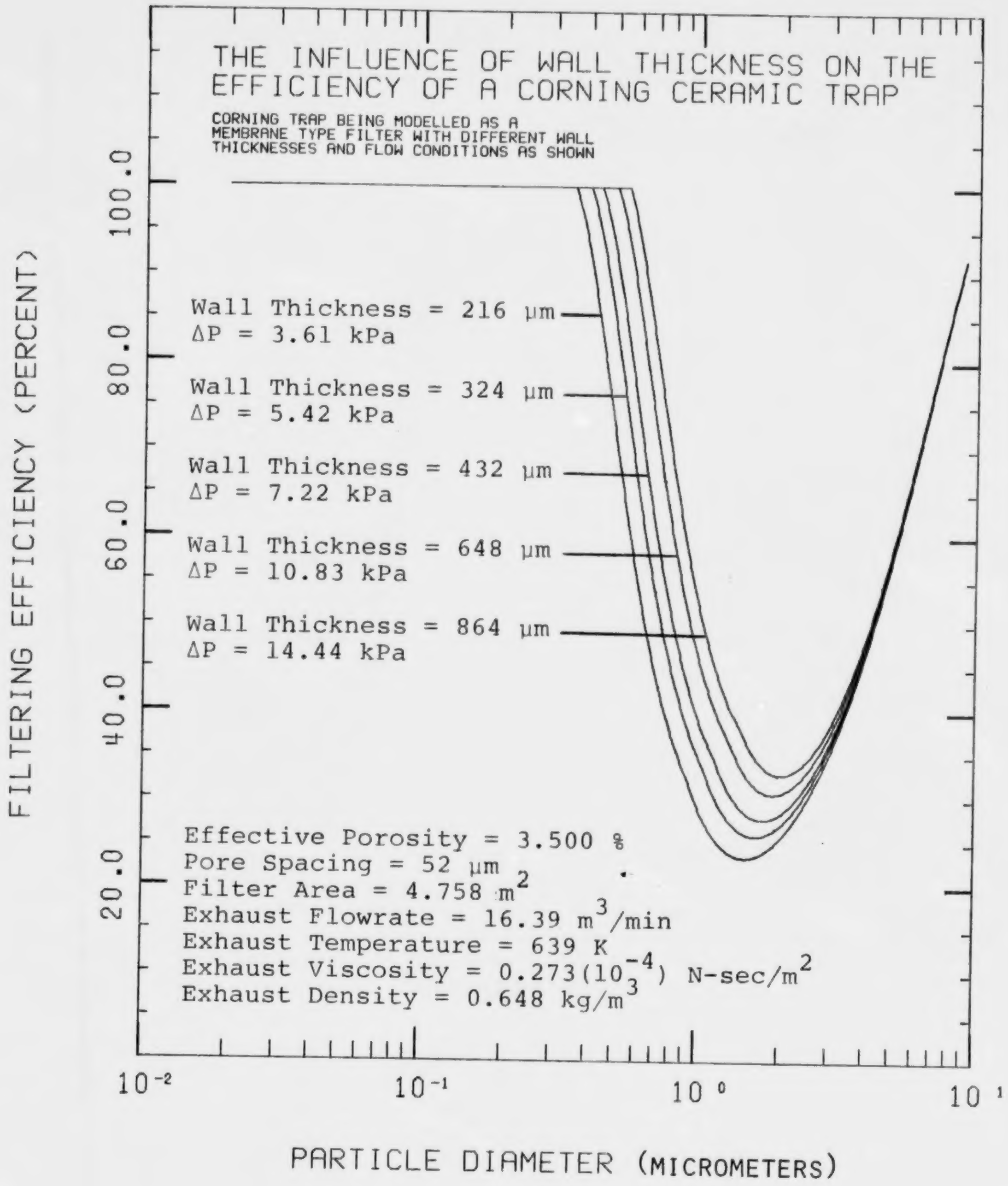

FIG. 3.2.65 PARAMETRIC STUDY FOR CORNING TRAP MODELLED AS A MEMBRANE TYPE FILTER STUDYING THE INFLUENCE OF FILTERING MEDIUM THICKNESS ON FILTER EFFICIENCY

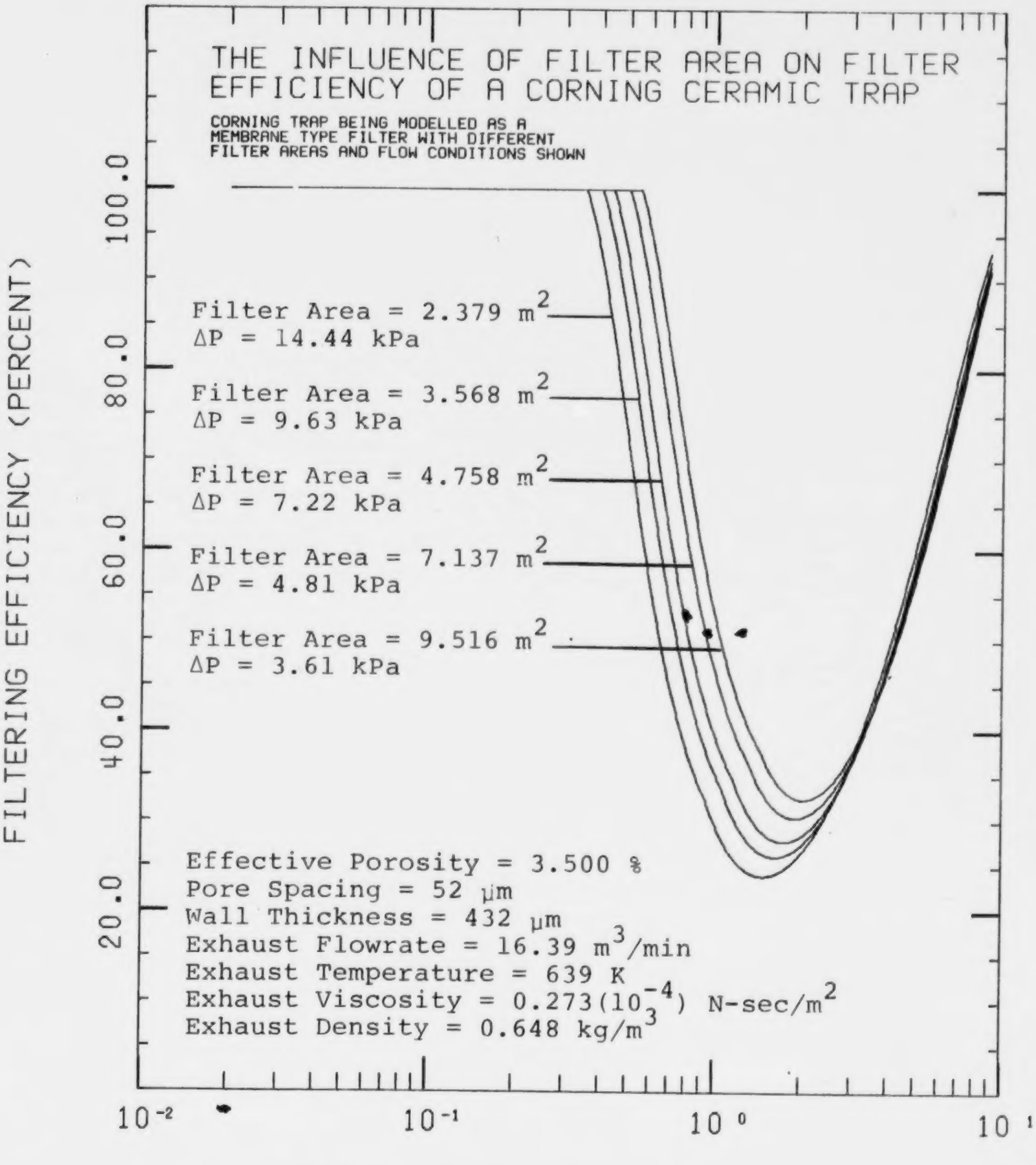

FIG.3.2.66 PARAMETRIC STUDY FOR CORNING TRAP MODELLED AS A MEMBRANE TYPE FILTER STUDYING THE INFLUENCE OF TOTAL FILTER MEDIUM AREA ON FILTERING EFFICIENCY

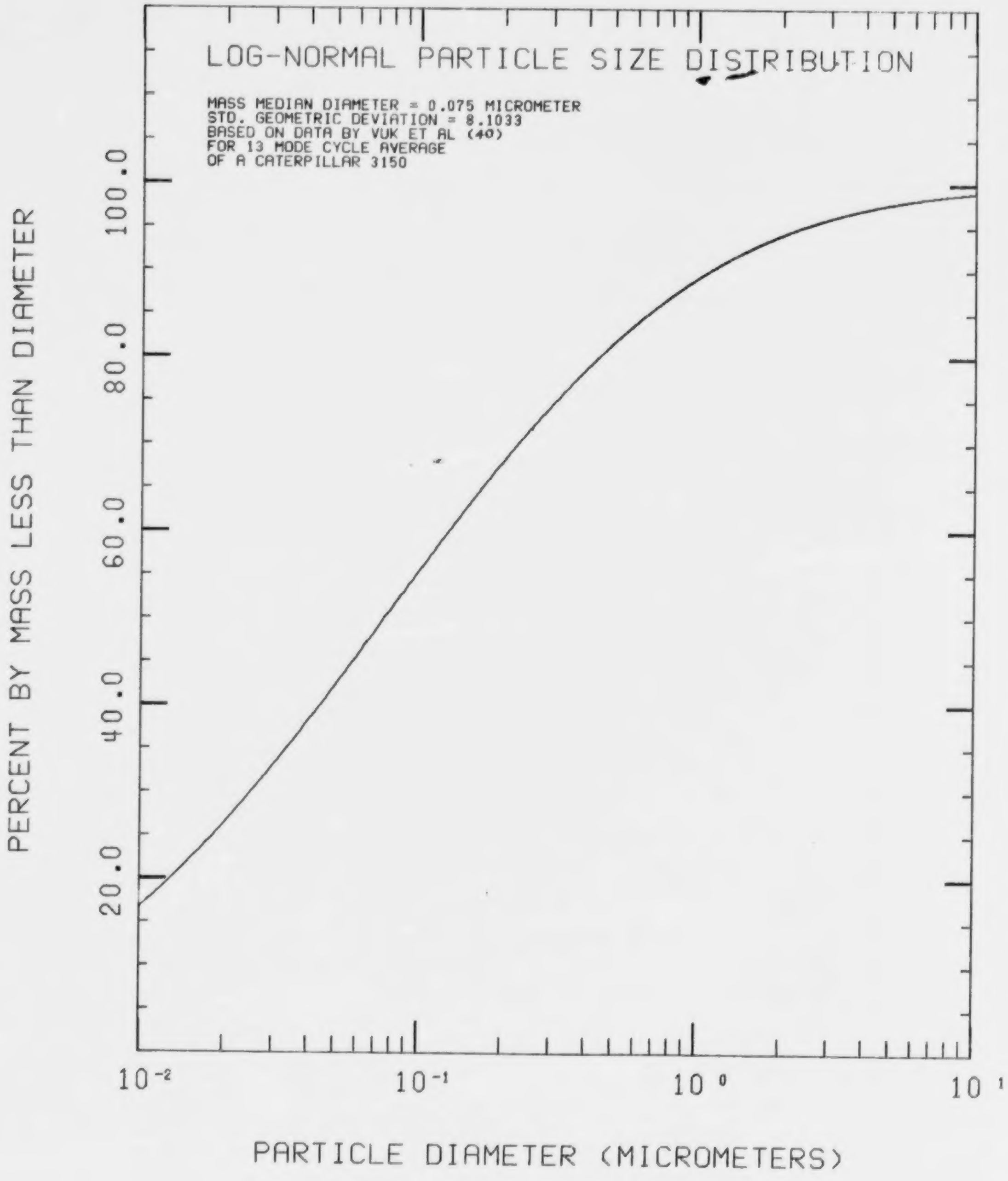

FIG. 3.2.67 LOG-NORMAL PARTICLE SIZE DISTRIBUTION ASSUMED FOR INTEGRATION OF THE MEMBRANE FILTER THEORY PREDICTED EFFICIENCY TO APPROXIMATE THE OVERALL EFFICIENCY

observed efficiencies in Table 3.2.27. The model predicts between 89 and 92 percent efficiency through the whole range of engine conditions. Obviously the original purpose of the model (explaining the load dependent efficiency at 1680 rpm) was not satisfied. Some inadequacies in the model which may account for the discrepancies are: 1) The model assumes a sticking probability of 100% (i.e. if a particle contacts a surface of the ceramic it will stick and not become re-entrained). This is probably not realistic and it is possible that the variables which affect the sticking probability (unknown are load-related. 2) The particulate bulk density was assumed to be 1 gram/cubic centimeter which is probably also a function of load. 3) A large fraction of the particles are actually not in the continuum (or Stokes) regime. Many particles are in the slip flow regime (where corrections can be applied) but many are also in the transition region between slip and free molecule flow. The various size regimes and the percent by mass of particles in these regimes are given in Fig. 3.2.68 for SC/1 and SC/2.It is likely that the theory is inadequate for many of the very small particles and the diffusion mechanism may be somewhate overestimated. 4) The particle size distribution used was an average over a wide range of conditions when in fact it is actually a function of load. There are some discrepancies among studies of load dependence of particle size but generally particle size distributions are shifted smaller with increased load. This would yield higher efficiency for increased load as was observed in this study. 5) There are many discrepancies between the idealized representation of the porous ceramic and the true structure (such as variable pore diameters and lengths). These variations could result in inertial effects which might be responsible for a load dependent efficiency (higher velocities at higher loads resulting in greater inertial impaction).

The model as it exists now is not of any quantitative use because of the inadequacies outlined above but it should be useful for predicting general

Table 3.2.27 Comparison of Model Predicted Efficiencies with Actual Measured Efficiencies of the Corning Trap on the Caterpillar 3208

EPA Mode	Filter Number	Model Predicted Efficiency (percent)	Average Predicted Efficiency (percent)	Average Measured Efficiency (percent)
3	3-T-1	91.42	91.37	34.5
3	3-T-2	91.38		
3	3-T-3	91.34		
3	3-T-4	91.32		
4	4-T-1	91.35	91.30	68.1
4	4-T-2	91.31		
4	4-T-3	91.28		
4	4-T-4	91.25		
5	5-T-1	91.48	91.42	97.0
5	5-T-2	91.43		
5	5-T-3	91.36		
9	9-T-1	90.50	90.50	98.7
9	9-T-2	90.50		
9	9-T-3	90.50		
10	10-T-1	90.14	90.12	98.8
10	10-T-2	90.08		
10	10-T-3	90.15		
11	11-T-1	90.13	89.92	94.7
11	11-T-2	89.89		
11	11-T-3	89.74		

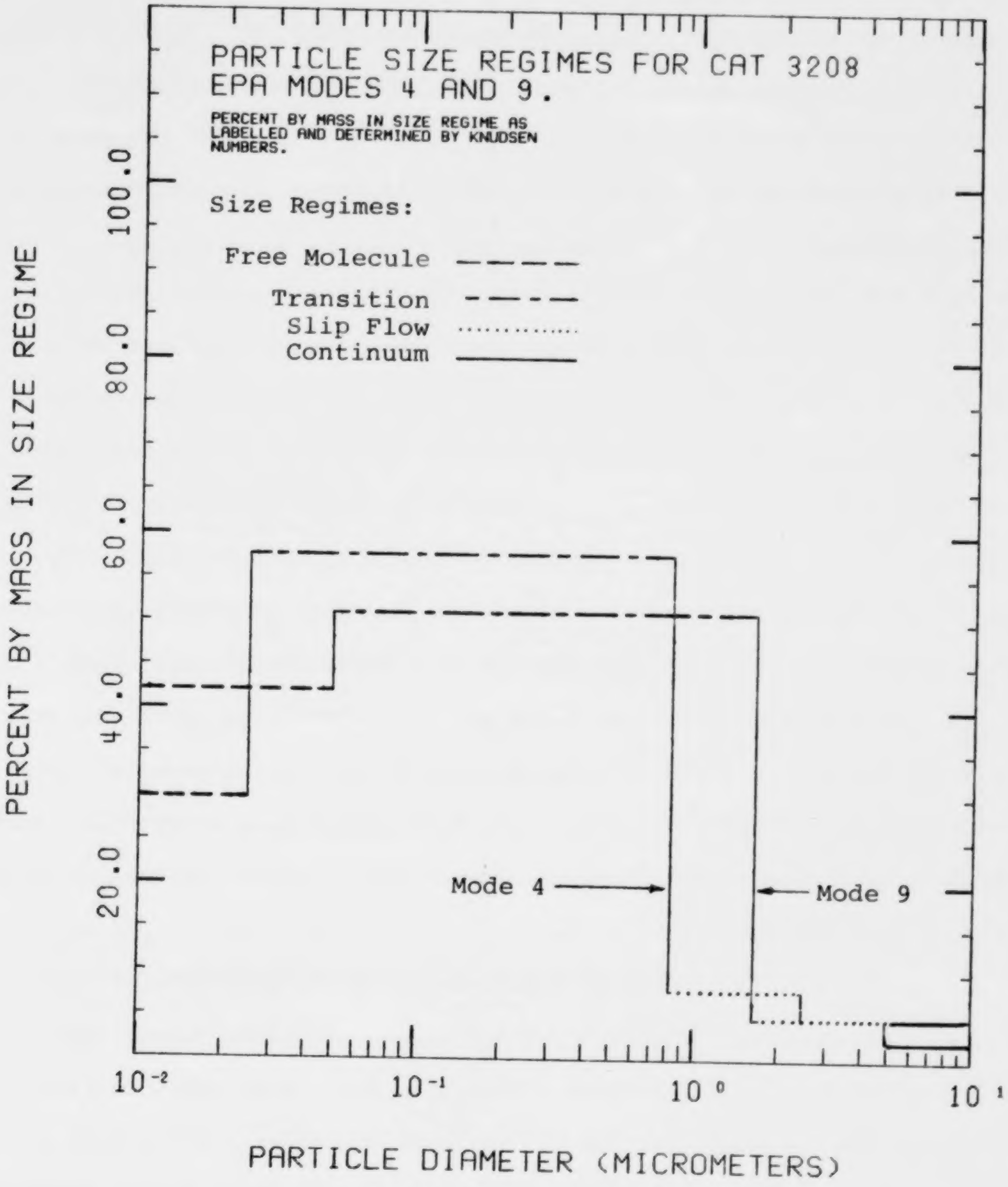

FIG.3.2.68 PARTICLE SIZE REGIMES FOR CAT 3208 FREE MOLECULE, TRANSITION, SLIP FLOW, AND CONTINUUM REGIMES FOR TWO ENGINE CONDITIONS: EPA MODE 4 AND 9 .

trends. A parametric study of the effects of certain variables on trap performance was carried out. The parameters varied independently were: porosity, pore spacing, filter thickness, total filter flow area, exhaust temperature, mass median particle diameter, and standard geometric deviation. The variables predicted were overall filtering efficiency, pressure drop, and a composite variable called filter quality. Filter quality considers both efficiency and pressure drop together such that high filter quality is desirable. The definition of filter quality is given at the bottom of the results of the parametric study, Table 3.2.28. The lack of precision of the model dictated the presentation of directions of change rather than magnitudes. It can be seen that all combinations of changes in efficiency and pressure drop are present but the filter quality parameter decides if the net effect is beneficial. Based on filter quality alone, the following conditions are desirable in the construction and operation of a porous ceramic trap: high porosity, large pore spacing (i.e., large pores relative to the 12 micrometers mean pore diameter used in the Corning material EX-47), thin cell walls, large filter area (i.e., largest trap practical), high exhaust temperature (i.e., close to engine), small mass median particle diameter, and standard geometric deviation (i.e., close to the engine).

The last step in the model development taken was the prediction of the output particle size distribution, given the assumed log-normal input. The output particle size distribution was expected to have a mass median diameter somewhere in the low efficiency region (0.4 to 10 micrometers) with a much smaller standard geometric deviation. The result of this final step is given in Fig. 3.2.69 and appears to match the expectation. The particle size distribution is not strictly log-normal because it does not extend to infinity in the negative and positive directions. However, it can be approximated as a log normal distribution with a very small standard geometric deviation. The

Table 3.2.28 Results of Parametric Study using the Corning Trap-Membrane Filter Theory-Based Computer Model

Increase In Independent Variable		Change in Dependent Variable		
		Overall Efficiency	Pressure Drop	Filter Quality
Effective Porosity	↑	↑	↓	↑
Mean Pore Spacing	↑	↓	↓	↑
Filter (wall) Thickness	↑	↑	↑	↓
Total Filter Flow Area	↑	↑	↓	↑
Exhaust Temperature	↑	↑	≃	↑
Mass Median Particle Dia.	↑	↓	≃	↓
Standard Geom. Dia. Deviation	↑	↓	≃	↓

Filter Quality is a composite of the effects of efficiency and pressure drop relating the desirability of high efficiency and low pressure drop in one parameter.

$$\text{Filter Quality} = \frac{-\ell n(1-E)}{\Delta P}$$

E = overall filtering efficiency (fraction)
ΔP = pressure drop across filter

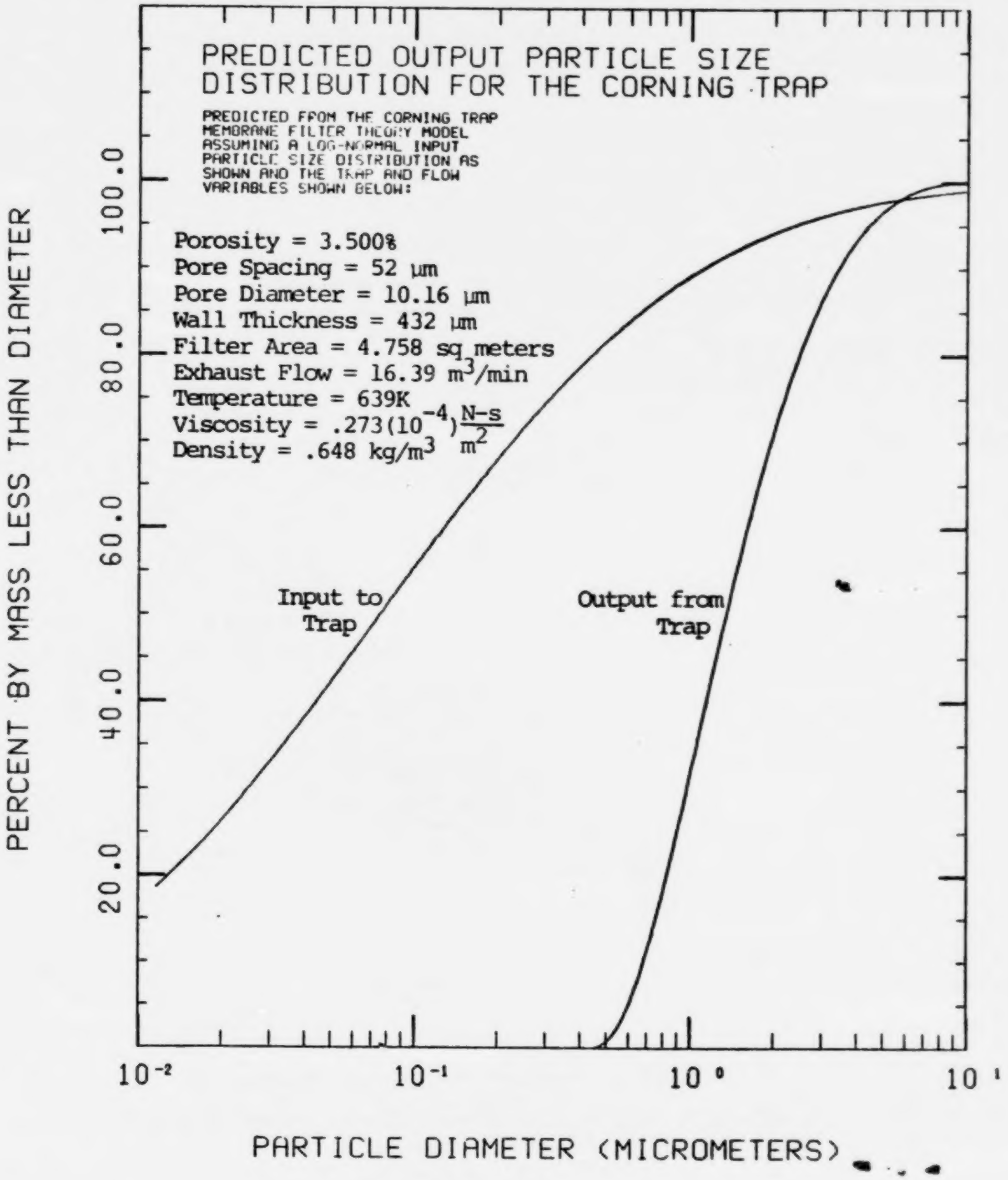

FIG.3.2.69 PREDICTED PARTICLE SIZE DISTRIBUTION OUTPUT FROM THE CORNING TRAP FOR THE ASSUMED LOG-NORM INPUT SIZE DISTRIBUTION MASS MEDIAN DIA = 0.075 MICROMETERS

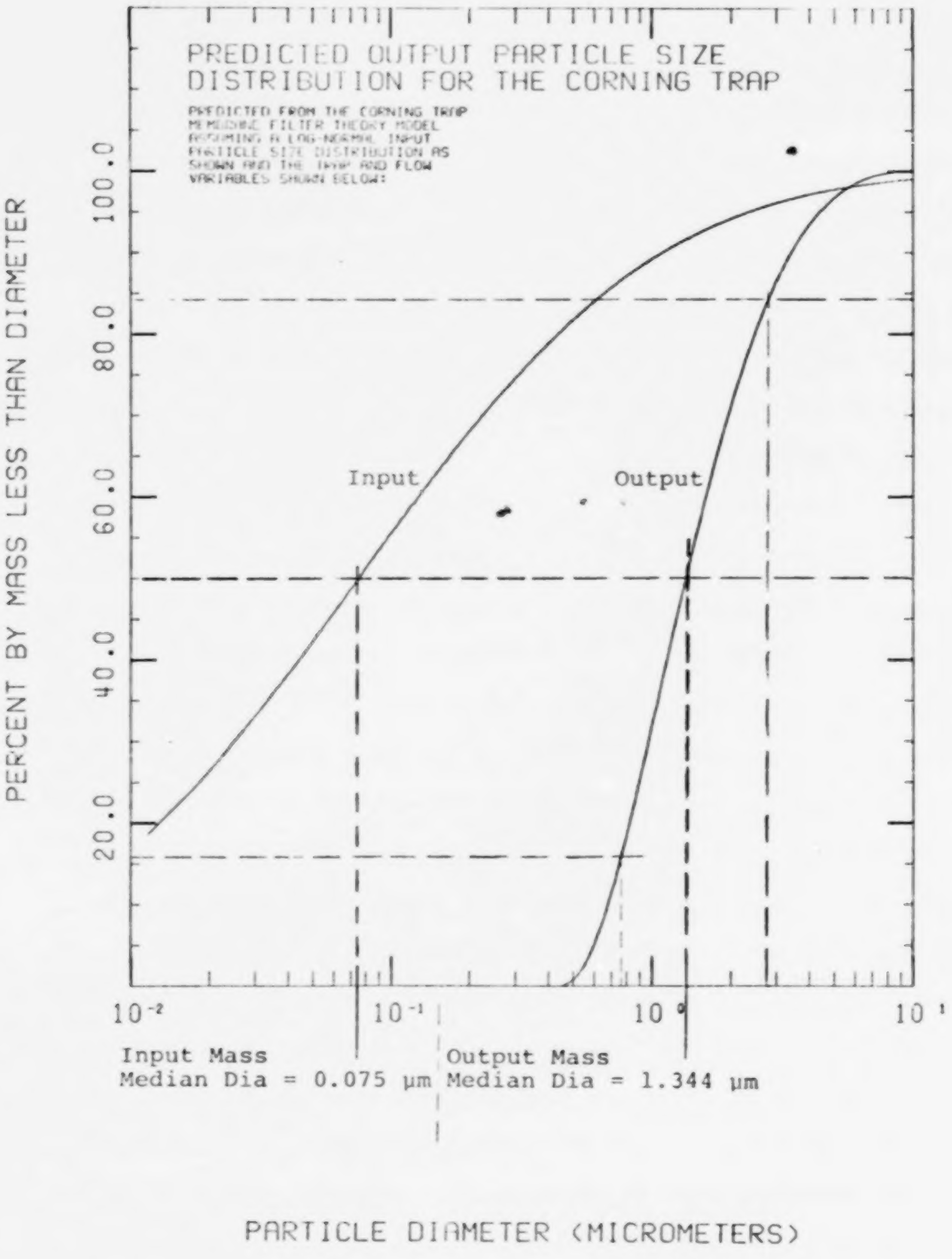

FIG.3.2.70 PREDICTED PARTICLE SIZE DISTRIBUTION OUTPUT FROM THE CORNING TRAP FOR THE ASSUMED LOG-NORM INPUT SIZE DISTRIBUTION MASS MEDIAN DIA = 0.075 MICROMETERS

parameters of the output distribution are derived from the diameters corresponding to the 50 and 84 cumulative mass percent. The mass median diameter is the diameter at 50% while the standard geometric deviation is the diameter at 84% divided by the mass median diameter = 1.34 micrometers and standard geometric deviation = 1.90 micrometers. The shift in mass median diameter is shown in Fig. 3.2.70. This observation is significant in terms of health effects because it appears that a large portion of the very fine particulates (which are capable of entering and being retained by the lungs) are effectively removed by the Corning trap.

Adsorption and SOF/Solids Ratio

Figure 3.2.71 plots the ratio of SOF/SOLID as a function of raw exhaust hydrocarbon concentration. Of the three aftertreatment devices thoroughly investigated during this project, the Corning traps produced the highest SOF/SOLID ratio. Despite the extreme reduction in solids, the exhaust hydrocarbons were sufficiently high to produce an SOF/SOLID ratio much higher than that of the port catalysts at modes 3 and 4, which are the two rightmost points in each 1680 rpm curve. The PTX and port catalysts always had enough solids emissions to establish an SOF/SOLIDS ratio below that of the baseline. Also, the mode 11 data point (rightmost point on the 2800 rpm curve) of the Corning trap lies above that of the baseline or either of the other aftertreatment devices, despite the extreme reduction in solids for the Corning trap tests at this mode. This finding supports the hypothesis of Clerc (79) who developed a semi-empirical computer model for predicting SOF concentrations based upon raw exhaust opacity, hydrocarbon concentration, and BET adsorption theory. The SOF/solids ratio is the fundamental adsorption parameter which should be a function of hydrocarbon concentration and filter temperature. Clerc saw the greatest difference between condensed hydrocarbon (SOF) as measured in the dilution tunnel and the SOF predicted by the semi-empirical model for mode 3

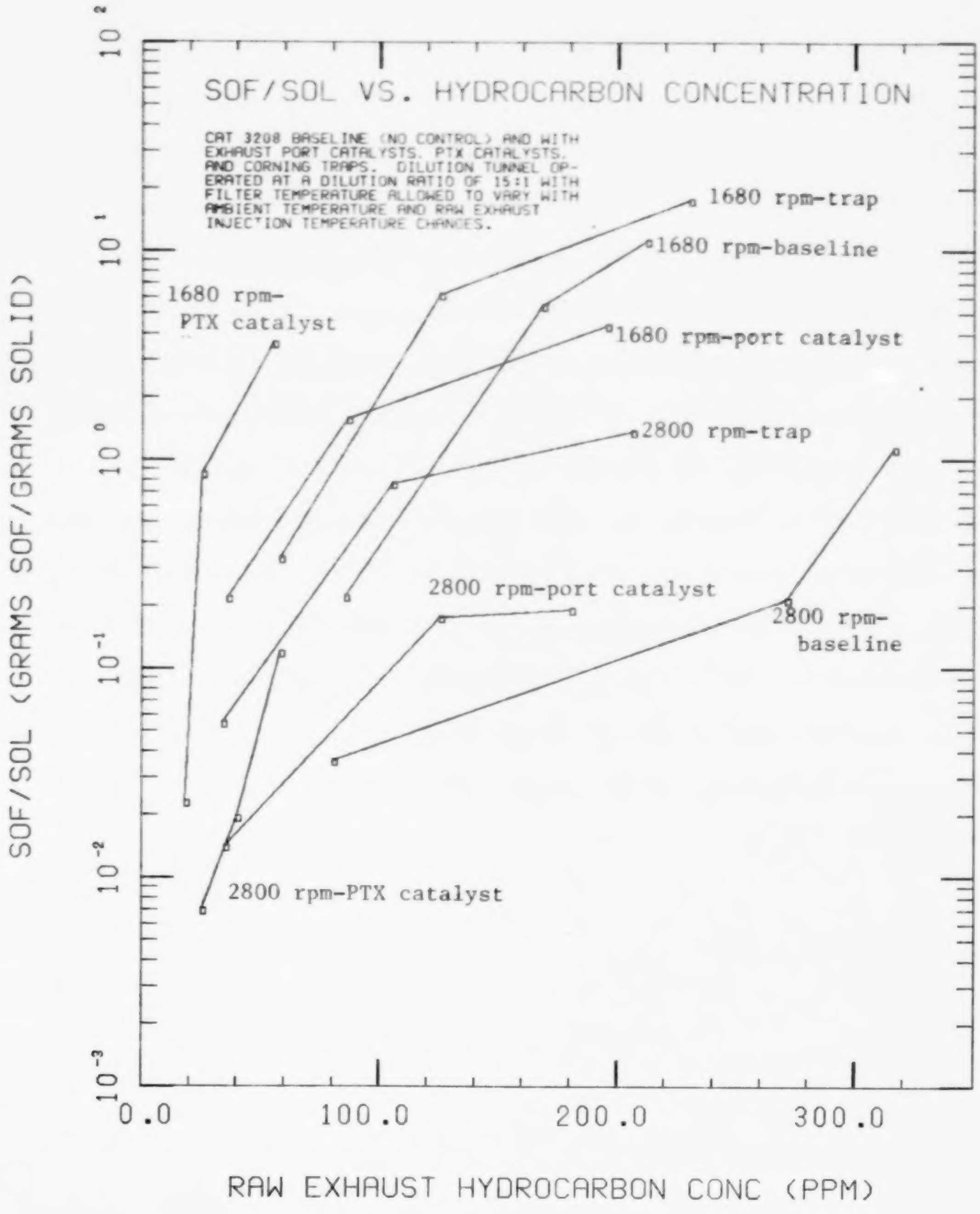

FIG.3.2.71SOLUBLE ORGANIC FRACTION TO SOLID RATIO: CAT 3208 BASELINE (NO CONTROL) AND WITH EXHAUST PORT CATALYSTS AND WITH CORNING TRAPS TESTED AT EPA MODES 3,4,5,9,10,11

on the Caterpillar engine, with lesser differences at modes 4 and 11. This difference was attributed to condensed high-molecular-weight hydrocarbons.

Dilution tunnel mixture (sample filter) temperature is not accounted for in the plot of Fig. 3.2.71 and could explain some of the other differences. Clerc showed that ambient temperature (which influences filter temperature) affects SOF/SOLID significantly (a 10°C ambient temperature decrease can cause a 70% increase in SOF). The effect of ambient temperature could be significant in these comparisons because of the different times of the year during which the tests were conducted. Clearly one needs either ambient condition controllability or a method for correcting to a standard ambient condition. Clerc recommends a constant filter temperature (filter temperature determined by running the engine at the various speeds and loads with dilution ratio = 15:1, and correcting the observed filter temperature vs. load curve as the basis for setting dilution ratio in all future experiments) as the best way of achieving repeatability between different ambient condition test days.

Johnson Matthey Cylindrical Mesh Trap

The fourth aftertreatment device tested was a trap designed by Johnson-Matthey Corporation. Table 3.2.29 gives specifications for this trap, which contains a proprietary catalyst and a washcoat formulated to minimize sulfate emission. The mesh material in this trap has been tested in the modified manifold of a 2-liter passenger car diesel with 52-76% reduction in emissions during a 50,000-mile test period (35), but has not received testing on a larger engine until now.

Table 3.2.29 Cylindrical Mesh Trap Specifications

Manufacturer	Johnson-Matthey
Catalytic Agent	Not specified
Substrate Material	310 Stainless Steel ribbon, knitted into mesh
Substrate Geometry	Compressed blocks of mesh with radially graduated bulk density and surface-to volume ratio; designed to trap gradually smaller particles in radial flow direction
Washcoat	Not specified
Trap dimensions	35cm dia x 101 cm long

Table 3.2.30 compares BSFC and emissions data for the baseline engine as well as for the Johnson-Matthey trap. Due to difficulties in obtaining stable filter weights, the particulate data is missing for many of these tests.

The first mode run after receipt of the trap was mode 11. Although only one test was obtained, the trap displayed higher fuel consumption and NO_2 and HC emissions; solid particulate was also increased as was sulfate, but SOF was greatly reduced. Modes 9, 4, 10, and 5 were then run in that order.

Table 3.2.30 - Comparison of Fuel Consumption and Emissions for the Johnson-Matthey Mesh Trap with Baseline Values, Before and After Reactivating Mesh Material. All values are Brake-Specific, in g/kw-hr, ± 1 Standard Deviation

EPA MODE	3			4			5			9	
Mesh Trap	W/O	W,as rec	W,react	W/O	W,as rec	W,react	W/O	W,as rec	W,react	W/O	W,as rec
Speed rpm	1680	1680	1680	1680	1680	1680	1680	1680	1680	2800	2800
Load, N-m	160	160	160	320	320	320	480	480	480	399	399
BS FC	287 0.00	N.A.	284 0.00	231± 0.00	229± 2	226± 2	217± 2	216± 2	N.A.	216± 0	251± 5
BS NO_x	10.24± 0.03	N.A.	10.10± 0.00	10.39± 0.13	9.33± 0.21	9.60± 0.09	9.69± 0.08	9.65± 0.19	N.A.	8.41± 0.08	7.81± 0.09
BS NO_2	1.16± 0.22	N.A.	0.31± 0.00	0.85± 0.05	2.17± 0.57	2.39± 0.01	0.36± 0.01	1.80± 0.20	N.A.	0.250± 0.033	0.173± 0.067
BS NO	5.91 0.16	N.A.	6.38± 0.00	6.22± 0.07	4.67± 0.24	4.70± 0.05	6.08± 0.05	5.13± 0.01	N.A.	5.32± 0.05	4.98± 0.08
BS HC	1.92± 0.21	N.A.	0.90± 0.00	0.77± 0.02	0.05± 0.02	0.05± 0.00	0.25± 0.00	0.04± 0.00	N.A.	0.26± 0.01	0.04± 0.00
BS TPM	1.047± 0.031	N.A.	(a)	0.482± 0.03	(a)	0.852± 0.014	0.241± 0.005	(a)	N.A	0.795± 0.064	2.121± 0.174 (b)
BS SOF	0.932± 0.030	N.A.	(a)	0.377± 0.024	(a)	0.013± 0.001	0.038± 0.001	(a)	N.A.	0.066± 0.007	0.012± 0.015
BS SO_4	0.031± 0.001	N.A.	(a)	0.036± 0.002	(a)	0.664± 0.005	0.031± 0.002	(a)	N.A	0.039± 0.009	1.842± 0.080
BS SOLIDS	0.084 -	N.A.	(a)	0.069 -	(a)	0.177 -	0.172 -	(a)	N.A.	0.730± 0.051	0.770± 0.210
Opacity(%)	0.3 -	N.A.	0.2 -	0.9± 0.05	1.1± 0.39	0.7± 0.0	1.9± 0.0	4.5± 0.35	N.A.	4.9± 0.2	5.6± 0.29

(a) Particulate data notavailable due to insufficient filter ammoniation and/or insufficient sampling times
N.A. Not available

(b) Particulate data at Mode 9 may be inaccurate, as sulfate values steadily increased with time and filters may have not been completely ammoniated

Table 3.2.30 - Comparison of Fuel Consumption and Emissions for the Johnson-Matthey Mesh Trap With Baseline Values, Before and After Reactivating Mesh Material. All values are Brake-Specific, in g/kw-hr, ± 1 Standard Deviation

EPA MODE	9	10			11		
Mesh Trap	W,reactivitated	W/O	W,as rec	W,reactivated	W/O	W,as rec	W,reactivated
Speed rpm	2800	2800	2800	2800	2800	2800	2800
Load, N-m	399	266	266	266	133	133	133
BS FC	N.A.	282 0	278± 2.191	275± 0	370 0	383 (c)	391± 0
BS NO_x	N.A.	9.02 0	8.49± 0.170	8.66± 0	10.09± 0.101±	9.78 (c)	10.81± 0
BS NO_2	N.A.	0.26± 0.026	1.416± 0.296	1.84± 0	0.65± 0.026	2.19 (c)	2.58± 0
BS NO	N.A.	5.72± 0	4.61± 0.301	4.45± 0	6.15± 0.062	4.45 (c)	5.36± 0
BS HC	N.A.	1.305± 0.052	0.100 0.055	0.15± 0	2.926± 0.117	0.18 (c)	0.15± 0
BS TPM	N.A.	0.792± 0.016	(a)	3.17± 0.025	1.864± 0.019	2.967 (c)	2.298 0.106
BS SOF	N.A.	0.133± 0.021	(a)	0.043± 0.018	0.969± 0.107	0.067 (c)	-.396± 0.052
BS SO_4	N.A.	0.033± 0.005	(a)	2.343± 0.001	0.857± 0.111	2.467 (c)	1.733± 0.066
BS SOLIDS	N.A.	0.626± 0.031	(a)	0.793± 0.042	0.038± 0.004	0.428 (c)	0.189± 0.069
Opacity(%)		3.8± 0.84	1.8± 0.05	5.2± 0.0	3.2± 0.10	1.4 (c)	2.0± 0.0

(c) One test value, only

Hydrocarbon emissions were reduced at all modes, but NO_2 was increased at all modes but mode 9. The most notable increase over baseline emissions was the sulfate, which dominated the total particulate to the extent that SOF and solids were difficult to measure. A series of six filters run at mode 9 gave steadily increasing sulfate levels, with 71 to 94 percent of the total particulate analyzed as sulfate.

Since sulfate conversion had been shown to be a problem in the development of this trap (79), Johnson-Matthey agreed to reactivate the trap mesh material with a washcoat designed to minimize this problem. After return of the trap to MTU, a re-run of mode 11 showed that the sulfate conversion had been reduced slightly but not to baseline levels. Subsequent running of modes 4 and 10 showed that the particulate was not now completely dominated by sulfate, but that sulfate (as well as solids) were still higher than baseline levels. Results from mode 3 as of this writing showed particulate values well below baseline emissions, but sulfate predominance made TPM measurements difficult; modes 5 and 9 have not been rerun since catalyst reactivation. It appears as if higher load conditions eliminate the trap's ability to reduce sulfate emissions.

The regeneration characteristics of the Johnson-Matthey trap were not completely investigated; however, modes 4 and 10 showed no increase in trap pressure drop after two hours of running, while mode 3 showed a pressure drop increase of less than 0.5kPa over 2 hours. Mode 11 showed a pressure drop increase of about 0.6 kPa per hour, based on a 30 minute run, and modes 5 and 9 were essentially stable over 30 minutes.

CUMMINS ADIABATIC ENGINE - ALTERNATE FUEL SAMPLES

This work by Michigan Tech involved collection of filter samples by Cummins Engine Company followed by extraction and mutagenicity testing on SOF obtained from the first build of a single-cylinder experimental adiabatic engine. This engine configuration was the non-adiabatic build of the engine. Two other builds of the engine were carried out on a DOE Cummins contract and the results are not reported here. Specifications of this engine are given in Table 3.3.1.

Table 3.3.1 Cummins Engine Specifications

Manufacturer and Model: Cummins NTC-400
Type : Single-cylinder, direct injection, turbocharged
Bore x Stroke : 140mm x 153 mm (5.52in x 6.02 in)
Displacement : 2.35 liter (143.4 in^3)
Compression Ratio: 14.5:1
Rated power : 49.8KW (67.0hp) @ 1900 rpm
Rated torque : 344 N-M (254Ft-lbf)

A mini-dilution tunnel system similar to the system described by MacDonald et al. was used for particle collection. Dilution ratios were established to dilute exhaust gases to 130°F. For modes 6 and 8, dilution ratio was typically 15:1, while mode 9 utilized a 10:1 dilution ratio and mode 11 used a 6.5:1 dilution ratio. Particulate samples were collected on 110 mm round Pallflex filters, and were extracted with DCM to give SOF samples, which were bioassayed as described in the experimental section of this report.

Table 3.3.2 lists the fuel properties of the No. 2 diesel fuel, shale fuel, and solvent-refined coal fuel used in this work. The most notable differences between these fuels are the low cetane number, H/C ratio, and percent saturates as well as the high viscosity, percent aromatics and percent nitrogen of the coal-derived SRC-II fuel.

Table 3.3.2 Fuels Analysis: Cummins Experimental Engine

FUEL PROPERTY	NO. 2	SRC II MIDDLE DISTILATE	SHALE
PHYSICAL AND CHEMICAL PROPERTIES			
Energy Content BTU/LB Gross	19,200	17,102	19,365
Gravity 60 °F	33	12.4	38.2
Specific Gravity 60/60, ° F	.86	.983	.834
Viscosity, cP	2.85	3.87	2.72
Pour Point,° F	-35	-65	-5
Flash Point, °F	167	175	178
Cetane Number	45-50	22	46
Hydrogen/Carbon Molar Ratio	1.75	1.24	1.86
% Aromatics	36	79.1	30.5
% Saturates	62	14.4	67.7
% Olefins	20	6.5	1.8
Elemental Analysis			
% Sulfur	.29	.31	.07
% Nitrogen	.4	1.0	.024

Sample collection was carried out at EPA modes 6, 8, 10, and 11. Due to unstable running conditions for SRC-II at mode 11, this fuel was run at 75% load and rated speed (mode 9) instead.

Effects of Operating Conditions on Ames Bioassay Results

Table 3.3.3 gives dose-response statistics from the thirteen samples assayed. Because of sample limitations, only three samples (mode 8, SRC-II fuel; mode 11, shale fuel; and mode 6, No. 2 fuel) showed evidence of toxicity, and a uniform dose-range analysis was not performed. All samples were assayed without metabolic activation, and those with sufficient concentration were also assayed with activation (S-9). The only sample demonstrating increased mutagenicity with S-9 was the mode 6 (peak torque) sample obtained with No.2 diesel fuel. This sample showed considerably higher activity than any other sample tested, but no explanation for this high activity can be offered.

Comparing fuels, it appears that SRC-II SOF is not appreciably more mutagenic than the shale fuel, and is similar to No. 2 fuel SOF if the mode 6 data point for No. 2 fuel is disregarded. However, it should be stressed that the effects of toxicity cannot always be discounted, and a toxic effect may suppress mutagenic activity at lower doses before manifesting itself at higher doses.

Comparing modes, the mode 8 (rated speed at full load) samples showed the greatest biological activity if the extremely active No. 2 fuel, mode 6 sample is disregarded. This mode also demonstrated slightly higher activity at the retarded timing of 24°BTC than at 27°BTC for SRC-II.

Table 3.3.3 Specific Activity Calculations for Cummins Test Data[(a)]

Sample[(b)] Fuel, Mode, Timing,°	S-9[c]	SA_{SL}^{d}	C_1	C_2	b	r
SRC-II, 6, 29°	−	1.43	18.75	300.00	334	.94
SRC-II, 8, 27°	−	3.05	4.69	150.00	294	.94
SRC-II, 8, 24°	−	4.19	4.69	300.00	685	.98
SRC-II, 9, 27°	−	3.54	4.69	300.00	578	.96
SRC-II, 10, 27°	−	1.63	9.38	600.00	534	.96
SRC-II, 8, 27°	+	3.19	9.38	75.00	232	.95
SRC-II, 8, 24°	+	3.79	9.38	150.00	443	.91
SF, 6, 27°	−	2.04	9.38	600.00	668	.96
SF, 8, 27°	−	5.99	9.38	600.00	699	.98
SF, 10, 27°	−	0.61	75.00	1200.00	573	.97
SF, 11, 27°	−	1.38	18.75	600.00	533	.96
SF, 6, 27°	+	2.51	18.75	300.00	587	.87
SF, 8, 27°	+	2.95	18.75	300.00	690	.95
SF, 10, 27°	+	0.70	37.50	600.00	328	.93
SF, 11, 27°	+	0.70	75.00	1200.00	654	.95
No.2, 6, 27°	−	29.09	1.17	37.50	702	.95
No.2, 8, 27°	−	3.59	9.38	300.00	692	.97
No.2, 10, 27°	−	2.97	18.85	300.00	694	.96
No.2, 11, 27°	−	0.82	18.75	1200.00	539	.96
No.2, 6, 27°	+	37.43	4.69	37.50	1360	.98
No.2, 10, 27°	+	2.05	18.75	300.00	478	.92
No.2, 11, 27°	+	1.02	18.75	300.00	237	.94

(a) Using Ames S. typhimurium tester strain TA100

(b) Fuel type (SRC-II - Solvent-Refined Coal-Derived Fuel, SF-Shale Fuel, No.2-Standard Lab Fuel); Mode; Timing in °BTC)

(c) Microsomal activation system

(d) SA_{SL} = Specific Activity (rev/μg)= $\frac{b}{C_2-C_1} \log_{10} (C_2/C_1)$

C_1 = Minimum dose (μg/plate) on linear portion of dose-response curve

C_2 = Maximum dose (μg/plate) on linear portion of dose response curve

b = Slope of dose-response curve in linear-log format, determined statistically

r = Coefficient of correlation

4

CONCLUSIONS

MACK ENDT-676 FUEL INJECTION PARAMETER STUDY

1) The effect of load at intermediate speed increased NO, NO_2, smoke, and solids emissions, while reducing BSFC and SOF emissions, primarily due to increased equivalence ratio and temperatures at higher load. At rated speed, increased mixing rates and temperatures above the solid-formation range kept solids emissions from increasing.

2) Increased engine speed reduced NO and NO_2 while increasing SOF and BSFC and made solids emissions less load-sensitive, all probably due to increased mixing rates and decreased residence times.

3) Increased fuel injection rates (at the same injection timing) reduced solids, SOF, and BSFC while increasing NO_2 and NO, primarily due to increased fuel-air mixing rates. The reduction in pumping efficiency with the ultra-high-rate shuttle pump increased BFSC. Excessive fuel accumulation during the premixed combustion period led to increased SOF with this pump. The overall biological activity and percentage of transitional, oxygenated, and acidic subfractions in the SOF generally increased with increased injection rates, because increased amounts of fuel in lean-limit regions underwent thermal decomposition. Reduced SOF at high rates failed to offset the increased SA; SOF increased with ultra-high rates. The result was a net increase in BSSA with increased injection rates at constant timing.

4) Retarded injection timing (at higher injection rates) increased solid particulates and BSFC, but decreased SOF, NO, and NO_2, as a result of shorter ignition delays and reduced peak cycle temperatures. Ultra-high rates

showed similar trends, for the same reasons and also due to a high-density air charge (which reduced over-penetration). Retarded timing at high rates increased acidic and decreased ether-insoluble subfractions in the SOF. The acidic, transitional, and oxygenated subfractions did not always decrease as expected from the amount of fuel undergoing thermal decomposition. This was true for mode 3 conditions for both high and ultra-high injection rates. At mode 9, retarded timings caused an increase in transitional and oxygenated subfractions, suggesting that monatomic oxygen is more available for production of these species due to lower combustion temperatures and reduced pyrolysis of N_2 to monatomic nitrogen.

5) Larger injector nozzle sac volume, as expected, increased HC, solids, and SOF with minimal reductions in NO_x. The increase in SOF was much less than the increase in solids or HC, and the composition of the SOF with large sac-volume nozzles showed extensive modification.

6) The combination parameter BSFC-BSTPM-$BSNO_x$ was improved by both increased injection rates and retarded timings, except for extremely retarded timings at the ultra-high rate. Moderately increased injection rate was more effective than injection timing in reducing the BS solids and $BSNO_2$, but greatly increased injection rates made most emissions more sensitive to injection timing. All emissions and the BSSA decreased with increased rates and retarded timings, but BSFC increased with the ultra-high-rate shuttle pump.

7) The biological activity of the particulate is related to at least three factors: 1) exhaust temperature, 2) relative amounts of acidic, oxygenated, and transitional subfractions, and 3) exhaust NO_2 concentration. Whether NO_2 concentration is an influential parameter in the real world or is merely a contributor to artifactual mutagenic compounds is unanswered.

8) Use of the ideal injection characteristics hypothesized could result in 1) reducing solids by as much as 70% and reducing SOF, 2) maintaining the BSFC

at levels similar to the 3.8-inch bowl, high-rate system, and 3) achieving $BSNO_x$ emissions of about 10 g/kw-hr. Although the overall rate of injection is important, the instantaneous rate (especially the beginning and ending) of injection is more important in controlling solids and SOF formation. The use of high-sulfur fuels with the ideal injection characteristics may result in the majority of the particulate being sulfate. This conclusion is warranted in light of the insensitivity of exhaust sulfate levels to injection parameter modifications.

CATERPILLAR 3208 AFTERTREATMENT DEVICE STUDY

The conclusions from the Caterpillar 3208 engine study will be subdivided according to control device tested, and the final section will summarize the advantages and disadvantages of all devices.

Englehard PTX Oxidation Catalysts

1) The effect of the oxidation catalysts on NO_x emissions was negligible for all fuels and modes tested, but NO_2 emissions increased at the expense of NO for all modes and fuels except mode 3 with No. 1 and No. 2 fuels. Mode 3 showed a decrease in NO_2, probably due to a net catalytic reduction of NO_2 to NO. Values of NO_x were highest for the No. 2 fuel, with No. 1 and shale fuel giving equivalent NO_x emissions both with and without the catalysts (mode 4 only).

2) The catalysts decreased both HC and SOF emissions for all fuels and modes tested. Percent reduction of HC was generally lower for No. 1 fuel than for No. 2 fuel.

3) The catalysts increased sulfate emissions for all fuels and modes tested. Conversion of fuel sulfur to sulfate ranged from 6% at mode 3 with No. 1 fuel to 89% at mode 9 with No. 2 fuel; the uncatalyzed exhaust typically contained less than 3% of the fuel sulfur as sulfate. Shale fuel sulfate emissions were extremely low due to the very low fuel sulfur content.

4) The catalysts increased solid particulates for all fuels and modes except mode 3 with both No. 1 and No. 2 fuels; solids emissions using shale fuel increased, but not significantly. Dehydrogenation of exhaust hydrocarbons on the catalyst are thought to account for this solids increase. A decrease in percentage paraffins in the catalyzed SOF supports the idea that dehydrogenation is occurring.

5) The catalysts increased total particulates more for the No. 2 than the

No. 1 fuel, due to higher fuel sulfur and higher aromatics content (leading to more solids).

6) Biological activity of the SOF is increased by use of the PTX catalyst and by the use of No. 2 fuel. Shale fuel gave SOF of higher SA, with and without the catalyst, than either of the other fuels (mode 4 only). BSSA was increased by use of the catalysts except at mode 3.

Johnson-Matthey Close-Coupled Port Catalysts

1) The exhaust port catalysts usually increased NO_x slightly, although NO_2 emissions were significantly higher than the baseline engine at the high-load modes (5 and 9). A significant reduction of NO_2 back to NO took place at the low-load modes (3 and 11), while NO_2 levels for intermediate-load modes (4 and 10) were not significantly different from baseline conditions.

2) The port catalysts decreased HC and SOF at all modes tested. Shale fuel increased HC emissions over No. 2 fuel (mode 4 only).

3) The port catalysts increased sulfate emissions at all modes tested, although the percent conversion of fuel sulfur to sulfate was lower than for the PTX catalyst (ranging from 2% at mode 3 to 32% at mode 5). For both catalysts, molar conversion of sulfur to sulfate peaked at near 500°C, which is close to the temperature used in manufacturing sulfuric acid.

4) The port catalysts did not significantly change solid particulates except for mode 11 (a large increase). Slight increases were noted at modes 3, 9, and 10, mode 4 was essentially unchanged, and mode 5 showed decreased solids emissions. For the intermediate speed modes, shale fuel showed a reduction in solids at mode 3, little change at mode 4, and a large increase at mode 5. This fuel-dependent behavior is probably due to more stable aromatics in the shale fuel, leading to a predominance of dehydrogenation (to solids) at the

same conditions for which oxidation (to CO_2 and H_2O) is predominant using the No. 2 fuel.

5) The port catalysts increased total particulate at rated-speed modes (due largely to increases in sulfate), and had mixed results at intermediate speed (due to lower sulfate and variable competition between dehydrogenation and oxidation).

6) The port catalysts increased SA at all intermediate-speed modes and decreased it at all rated-speed modes. The port catalysts reduced BSSA at all modes with greater reductions at rated speed.

Corning Particulate Trap

1) The Corning traps decreased NO_2 emissions with little change in total NO_x and NO emissions. The reduction in NO_2 may be due to either increased back pressure or reaction with trapped particulate, but is more likely due to reaction of NO_2 with water of combustion to form nitric acid. Mixing conditions in the traps could increase residence time sufficiently to favor the conversion of NO_2 to nitric acid.

2) The Corning traps decreased HC emissions considerably at rated speed with smaller reductions at intermediate speed.

3) The Corning traps reduced sulfates significantly at all speeds and loads, probably via sulfate trapping, lower conversions of SO_2 to sulfate at lower particulate levels (36), or lower ambient humidity (36). Since modes 9 and 10 showed continuous regeneration, the first possibility may be less important.

4) The Corning traps decreased solids emissions significantly, especially at rated-speed modes. The solids in particulate matter should, after all, be removed preferentially by the trap.

5) The Corning traps reduced total particulate, especially at rated-speed modes. Using porous wall filter theory, this control device

should be capable of completely trapping particulate less than 0.4 μm and greater than 10 μm with lesser trapping efficiencies for particles of intermediate size. The approximate particle input size distribution for the Caterpillar 3208 yields a predicted trapping efficiency quite different from that measured for 2 of the 6 modes tested. This difference was ascribed to particulate and trap characteristics not in the model. The deviation of the SOF/solid ratio from that expected from adsorption theory at certain modes can be explained by condensation of SOF onto the particulate after the traps.

6) The Corning traps increased SA of the SOF at all modes but mode 3. BSSA were drastically reduced for most modes, but very high SA of certain SOF subfractions suggests that production of certain compounds could negate the advantages of the trap as a particulate control device.

7) The Corning traps increased exhaust back pressure with time. The increase was mode-dependent with rated-speed modes showing the most difference; a trap temperature of about 500°C (achieved at modes 9 and 10) was necessary for continuous trap regeneration. These traps, without regeneration hardware, would require continuous operation at high-load, high-speed conditions.

Johnson-Matthey Trap

1) The Johnson-Matthey trap increased BSFC and NO_2 emissions at most modes with little change in NO_x emissions and a large reduction in HC emissions. Total particulate increased, due largely to higher sulfate emissions which dominated the particulate at most modes. Reactivation of the mesh trap material with a washcoat designed to minimize sulfate conversion (which Johnson-Matthey [J-M] believed was left off in the new trap) improved sulfate emissions slightly, but reduction of sulfate to baseline levels was not achieved.

2) The pressure drop across the Johnson-Matthey trap increased with time at mode 3 with a larger increase at mode 11. For modes 4, 5, 9, and 10, pressure drop increased only slightly during brief test periods.

Summary of All Aftertreatment Devices Tested

Table 4.1 gives the BSFC and emissions changes for all four aftertreatment devices. Disregarding time-dependent behavior, particulate traps are more effective overall in reducing the greater number of emissions. In this study, Corning traps are best overall except for their substantial fuel consumption penalty and SOF biological activity.

An important concern in a comparison such as this is the time-dependence of trap emissions. The Johnson-Matthey trap, particularly, was not investigated thoroughly enough to establish all pertinent specifics for regeneration. An effective and economical means of regeneration under highway or field conditions is needed, if continuous regeneration under normal operating conditions is not possible.

Also important is the relative change in particulate and gaseous emissions with a given control device. While all four devices were effective in reducing HC and SOF, only the Corning traps showed a net decrease in sulfate and NO_2 emissions.

Consideration for widespread use of any control device must include health effects assessment. Although the Corning traps were the most effective for overall emissions reduction, they produced a particulate SOF with subfractions of extremely high biological activity (measured as SA). The mode-averaged HC were reduced less with the Corning trap than with the other devices, and this gaseous phase could be as biologically active as the particulate phase. The gaseous phase HC could be significantly increased by the Corning traps. Short-term bioassay and inhalation studies should be done before widespread use of these or any other traps.

Table 4.1 Comparison of Four Aftertreatment Devices for Diesel Emissions Control, No. 2 fuel, six-mode weighted average (equal weighting)

Percent Change (from Baseline)
Brake-Specific Fuel Consumption and Emissions

DEVICE	Brake-Specific Fuel Consumption	Particulate Emissions				Gaseous Emissions			
		Total	Solid Fraction	Soluble Organic Fraction	Sulfate Fraction	NO_x	NO_2	NO	HC
Englehard PTX Oxidation Catalysts	-0.8	+254	+162	-75	+3626	+2	+398	-6	-83
Johnson-Matthey Exhaust Port Catalysts	+3.3	+41	+17	-49	+861	+16	+45	+17	-43
Corning Ceramic Trap(a)	+5.0	-63	-82	-73	-63	-2	-51	+0.4	-31
Johnson-Matthey Mesh Trap(b)	+0.3	+140	+36	-74	+3068	+1	+371	-19	-92

(a) Values are averages of consecutive 7-hour tests and do not consider the time-dependent behavior of the Corning traps.

(b) Values are equally weighted between modes 4, 10, and 11 only and do not consider any time-dependent behavior.

CUMMINS ADIABATIC ENGINE - ALTERNATE FUEL SAMPLES

Fuel change in the Cummins experimental engine in its cooled configuration slightly increased the SA of the particulate SOF from the use of No. 2 and solvent-refind, coal-derived fuel above that of shale fuel except at mode 8. Mode 6 SOF using No. 2 fuel showed much higher SA than SOF from other fuels and modes and was the only SOF whose SA was appreciably increased with metabolic activation. In this engine, there was a general increase in SA with increasing speed and load.

5

RECOMMENDATIONS FOR FUTURE RESEARCH

IN-CYLINDER MODIFICATIONS

1) The APE-6G pump should be further tested with additional instrumentation, specifically: pressure transducers in the injection lines and cylinder to monitor fuel injection pressure and rate, and a photomultiplier window in a cylinder for observing combustion temperature. Testing at selected modes and timings with a different-rate cam and the additional temperature and pressure information should provide a data base for an engine simulation program. Including chemical and biological information in this study would allow the effects of proposed injection/combustion systems to be screened without extensive testing.

2) The effect of spray geometry should be investigated using a larger piston bowl diameter and smaller orifice nozzles, which may limit the spray over-penetration anticipated from the use of higher injection pressures. Lower sac-volume nozzles (ideally, nozzles with plungers covering orifice holes) should be utilized to see if particulate can be reduced substantially.

3) The ideal injection characteristics discussed in this report should be investigated. This would be possible by obtaining the Universal Fuel Injection System or UFIS (80). Test procedures outlined in the first suggestion should be followed.

AFTERTREATMENT MODIFICATIONS

1) An uncatalyzed monolith similar to the PTX catalysts should be investigated. The results with the Corning traps suggest that SOF and HC reductions may be achieved without a metal catalyst, and the increase in solids seen with the catalyzed PTX could be reduced if platinum catalyst were excluded from the monolith. Regeneration

would be unnecessary with the uncatalyzed monoliths, and the effectiveness of the platinum catalyst would be determined

2) A ceramic, uncatalyzed port catalyst or other close-coupled trap should be investigated to determine the effect of increased temperature. Higher operating temperatures may enable continuous regeneration, and a smaller filter flow area may not degrade operating conditions at higher temperatures.

3) Limited testing of catalyzed Corning traps should determine whether the Pt catalyst improves trap effectiveness. Higher exhaust temperatures and continuous regeneration at more modes should result, but the Pt catalyst might cause dehydrogenation of hydrocarbons to solid and thereby negate the effect of higher temperatures.

4) Diesel particulate size distributions should be determined for those engines and running conditions expected to receive widespread trap applications. This information is necessary to determine the most effective pore structure for particulate traps. They would also help to determine the weaknesses of the membrane filter model and provide information on other particle retention factors.

GENERAL RECOMMENDATIONS

1) A chemical fractionation scheme should be developed to separate particulate SOF into classes of known chemical characteristics without modification. The scheme should be automated and be able to handle enough material to provide subfractions for biological testing. No present scheme is ideal in all these respects.

2) The effect of sampling time on SOF biological activity should be investigated. Use of a variety of nitroreductase-deficient strains of *Salmonella typhimurium* should disclose nitroaromatic compounds and establish how nitration (artifact formation) of polynuclear aromatic hydrocarbons relates to biological activity.

3) Widespread use of the Ames bioassay requires standardization of methods for dose-response data analysis. A standard method should be relatively simple, statistically sound, and usable with samples of widely varying mutagenic activities. Current analysis methods do not meet these requirements.

4) A closer look at the gaseous phase of diesel emissions is warranted, especially regarding biological activity. Unregulated gaseous emissions, especially nitric acid and vapor-phase organic nitro compounds, should be measured, since they may actually be more bioavailable than particulate, due to diffusion across cell membranes.

5) The rate constants for formation of mutagenic precursors in diesels should be determined experimentally. The nitro-aromatics are prime candidates: aromatic hydrocarbons should be exposed to various levels of NO_2 and nitric acid with and without exhaust. Polymer or carbon traps may be useful to investigate volatile compounds in similar experiments.

REFERENCES

1) South Coast Technology, Inc., 1979, An Initial Assessment of the Literature on the Measurement, Control, Transport, Transformation, and Health Effects of Unregulated Diesel Engine Emissions. Final Report, DOT Contract No. DOT-HS-7-01790.

2) National Research Council of the U.S., 1981, Health Effects of Exposure to Diesel Exhaust. National Academy Press, Washington, D.C.

3) Aaronson, A. E., and R. A. Matula, 1971, "Diesel Odor and Formation of Aromatic Hydrocarbons during the Heterogeneous Combustion of Pure Cetane in a Single-Cylinder Diesel Engine," Thirteenth International Symposium on Combustion, p. 421.

4) Ames, B. N.; J. McCann, and E. Yamasaki, 1975, "Methods for Detecting Carcinogens and Mutagens with the Salmonella Mammalian-Microsome Mutagenicity Test," Mutation Research, 31, p. 347.

5) Hollstein, M.; J. McCann, F. A. Angelsanto, and W. W. Nichols, 1979, "Short Term Tests for Carcinogens and Mutagens," Mutation Research, 65, p. 133.

6) Wright, A. S., 1980, "The Role of Metabolism in Chemical Mutagenesis and Chemical Carcinogenesis," Mutation Research, 75, p. 215.

7) Brooks, A. L.; C. R. Clark, and R. E. Royer, 1980, "Mutagenic Characterization of Particulate Materials in Diesel Exhaust," Inhalation Toxicology Research Institute Annual Report, Lovelace Biomedical and Environmental Research Institute.

8) Wang, Y. Y.; M. S. Lee, C. M. King, and P. O. Warner, 1980, "Evidence for Nitroaromatics as Direct-Acting Mutagens of Airborne Particulates," Chemosphere, 9, p. 83.

9) Wei, E. T.; Y. Y. Wang, and S. M. Rappaport, 1980, "Diesel Emissions and the Ames Test: A Commentary," J. Air Pollution Control Assoc., 30, p. 267.

10) Ames, B. N., 1979, "Identifying Environmental Chemicals Causing Mutations and Cancer," Science 204, 587.

11) Schuetzle, D.; F. S. C. Lee, T. J. Prater, and S. B. Tejada, 1980, "The Identification of Polynuclear Aromatic Hydrocarbon Derivatives in Mutagenic Fractions of Diesel Particulate Extract," Presented at the 10th Annual Symposium on the Analytical Chemistry of Pollutants, Dortmund, Germany.

12) Funkenbusch, E. F.; D. G. Leddy, and J. H. Johnson, 1979, "The Characterization of the Soluble Organic Fraction of Diesel Particulate Matter," SAE Paper No. 790418.

13) Mentser, M., and A. G. Sharkey, Jr., 1977, "Characterization of Diesel Exhaust Particulate," Pittsburgh Energy Research Center Publication Number RI-77/5.

14) Frisch, L. E.; J. H. Johnson, and D. G. Leddy, 1979, "Effect of Fuels and Dilution Ratio on Diesel Particulate Emissions," SAE Paper No.790417.

15) Schuetzle, D., L. M. Skewes, G. E. Fischer, S. P. Levine, and R. A. Gorse, Jr., 1981, "Determination of Sulfate in Diesel Particulate," Analyt. Chem., 53, p. 837.

16) Aoyagi, Y.; T. Kamimoto, Y. Matsui, and S. Matsuoka, 1980, "A Gas Sampling Study on the Formation Processes of Soot and NO in a DI Diesel Engine," SAE Paper 800254 (SAE Special Publication P-86).

17) Nielsen, T., 1981, "Nitro Derivatives of Polynuclear Aromatics: Formation Presence, and Transformation in Stack and Exhaust Gases, and in the Atmosphere," Risø National Laboratory Publication R-455, 43 pp.

18) Greeves, G., 1979, "Response of Diesel Combustion Systems to Increase of Fuel Injection Rate," SAE Paper No. 790037.

19) Henein, N. A., and D. S. Patterson, 1972, *Emissions from Combustion Engines and Their Control*, Chapter 8. Ann Arbor Science Publishers, p. 231.

20) Brysik, W., and C. O. Smith, 1977, "Relationships Between Exhaust Smoke and Operating Variables in Diesel Engines," SAE Paper No. 770718.

21) Khan, I. M., and C. H. T. Wang, 1971, "Factors Affecting Emissions of Smoke and Gaseous Pollutants from Direct Injection Engines," Institute of Mechanical Engineers, Paper C151.

22) Hiroyasu, H., and T. Kadota, 1976, "Models for Combustion and Formation of Nitric Oxide and Soot in Direct Injection Diesel Engines," SAE Paper No. 760129.

23) Khan, I. M.; G. Greeves, and D. M. Drobert, 1971, "Predictions of Soot and Nitric Oxide Concentrations in Diesel Engine Exhaust," Symposium on Pollution Control in Transport Engines, Inst. Mech. Engrs., London.

24) Shahed, S. M.; W. S. Chiu, and V. S. Yumlu, 1973, "A Preliminary Model for the Formation of Nitric Oxide in Direct Injection Diesel Engines and its Application to Parametric Studies, SAE Paper No. 730083.

25) Murphy, M. J.; L. J. Hillenbrand, and D. A. Trayser, 1979, "Oxidation of Diesel Particulate," EPA Report on Contract Number 68-02-2629, Battelle Memorial Institute.

26) Pierson, W. R.; R. H. Hammerle, and J. T. Kummer, 1974, "Sulfuric Acid Aerosol Emissions from Catalyst-Equipped Vehicles," SAE Paper 740287, SAE Transactions, V. 83.

27) Carpenter, K. A., 1979, "The Design and Development of a Dilution Tunnel for the Physical and Chemical Characterization of Diesel Particulate Material," M.S. Thesis, Michigan Technological University.

28) Society of Automotive Engineers, 1979, "Measurement of Carbon Dioxide, Carbon Monoxide, and Oxides of Nitrogen in Diesel Exhaust--SAEJ177," SAE Handbook, Part 2.

29) Matthews, R. D.; R. F. Sawyer, and R. W. Schafer, 1977, "Interferences in Chemiluminescent Measurements of NO and NO_2 Emissions from Combustion Systems," Environ. Science and Tech., 11, p. 1092.

30) EPA Draft Recommended Practice for Measurement of Gaseous and Particulate Emissions from Heavy-Duty Engines under Transient Conditions, 1979.

31) Hunter, G.; J. Scholl, F. Hibbler, S. Bagley, D. Leddy, D. Abata, and J. Johnson, 1981, "The Effects of Fuels on Diesel Oxidation Catalyst Performance and the Physical, Chemical, and Biological Character of Diesel Particulate Emissions," Society of Automotive Engineers, Publication SP-484, SAE Paper No. 810263.

32) Hillenbrand, L. J., and D. A. Trayser, 1981, "A Concept for Catalyzed Ignition of Diesel Soot," SAE Paper No. 811236.

33) Wade, W. R.; J. E. White, and J. J. Florek, 1981, "Diesel Particulate Trap Regeneration Techniques," SAE Paper No. 810118.

34) Mogaka, Z. N.; V. W. Wong, and S. M. Shahed, 1982, "Performance and Regeneration Characteristics of a Cellular Ceramic Diesel Particulate Trap," SAE Paper No. 820272.

35) Enga, B. E.; M. F. Buchman, and I. E. Lichtenstein, 1982, "Catalytic Control of Diesel Particulate," SAE Paper No. 820184.

36) Oh, S. H.; J. S. MacDonald, G. L. Vaneman, and L. L. Hegedus, 1981, "Mathematical Modeling of Fibrous Filters for Diesel Particulates--Theory and Experiment," SAE Paper No. 810113.

37) MacDonald, J. S., and G. L. Vaneman, 1981, "Experimental Evaluation of Fibrous Filters for Trapping Diesel Exhaust Particulates," SAE Paper No. 810956.

38) Howitt, J. S.; and M. R. Montierth, 1981, "Cellular Ceramic Diesel Particulate Filter SAE Paper No. 810114.

39) Orr, C., 1977, Filtration--Principles and Practices, Part I, New York and Basel: Marcel Dekker, Inc.

40) Orr, C., 1966, Particulate Technology, New York: The MacMillan Company.

41) Davies, C. N., 1973, Air Filtration, London and New York: Academic Press.

42) Davies, C. N. (Editor), 1966, Aerosol Science, London and New York: Academic Press.

43) Lipkea, W. H.; J. H. Johnson, and C. T. Vuk, 1978, "The Physical and Chemical Character of Diesel Particulate Emissions--Measurement Techniques and Fundamental Considerations," SAE Paper No. 780108, SAE Publication SP-430.

44) EPA Recommended Practice for Measurement of Exhaust Sulfate from Light-Duty Vehicles and Trucks, 1977.

45) Lee, F. S. C.; T. M. Harvey, T. J. Prater, M. C. Paputa, and D. Schuetzle, 1980, "Chemical Analysis of Diesel Particulate Matter and an Evaluation of Artifact Formation," ASTM STP-721, American Society for Testing and Materials, p. 92.

46) Killough, P.; J. Watson, and R. Bradow, 1979, "Filter Type, High Volume Particulate Sampler for Automotive Diesel Emission Studies," Environmental Protection Agency Report on Contract No. 68-02-2566.

47) Huisingh, J.; R. Bradow, R. Jungers, L. Claxton, R. Zweidinger, S. Tejada, J. Bumgarner, F. Duffield, M. Waters, V. F. Simmon, C. Hare, C. Rodriguez, and L. Snow, 1978, "Application of a Mutagenicity Bioassay to Monitoring Light-Duty Diesel Particle Emissions," in; Waters, M.D.; S. Nelnow, J. L. Huisingh, S. S. Sandhu, and L. Claxton (eds.), Applications of Short-term Bioassays in the Fractionation and Analysis of Complex Environmental Mixtures, New York: Plenum Press, pp. 383-418.

48) Khatri, N. J.; J. H. Johnson, and D. G. Leddy, 1978, "The Characterization of the Hydrocarbon and Sulfate Fraction of Diesel Particulate Matter," SAE Publication No. 780111, Society of Automotive Engineers Transactions, V. 87.

49) "Current Methods to Measure Atmospheric Nitric Acid and Nitrate Artifacts," 1979, EPA Report No. 600/2-79-051.

50) Ames, B. N.; J. McCann, and E. Yamasaki, 1975, "Methods for Detecting Carcinogens and Mutagens with the Salmonella/Mammalian-Microsome Mutagenicity Test," Mutation Research, V. 31, p. 374.

51) Belser, W.; S. D. Shaffer, R. D. Bliss, P. M. Hynds, L. Yamamoto, J. N. Pitts, and J. A. Winer, 1981, "A Standardized Procedure for Quantification of the Ames Salmonella/Mammalian-Microsome Mutagenicity Test," Environ. Mut., V. 3, p. 221.

52) Vois, J. R., and R. E. Vanderpoel, 1977, "The Shuttle Distributor for a Diesel Fuel Injection Pump," SAE Transactions Volume 86, SAE Paper No. 770083.

53) Kido, H.; Y. Wakuri, S. Ono, and E. Marase, 1980, "Prediction of In-Cylinder Gas Motion in Engines by an Energy Method," SAE Special Publication SD-468, SAE Paper No. 800985.

54) J. Kimberly, 1980, Personal Communication. American Bosch Diesel Products.

55) Parker, R. F., 1976, "Future Fuel Injection System Requirements of Diesel Engines for Mobile Power," SAE Transactions, V. 85, SAE Paper No. 760125.

56) Obert, E. O., 1973, Internal Combustion Engines and Air Pollution, New York, Intext Educational.

57) J. Hansel, Englehard Industries Division, 1979, Personal Communication.

58) AMOCO, 200 E. Randolph Dr., Chicago, IL.

59) Chevron Research Company, 576 Standard Ave., Richmond, CA.

60) "Diesel Fuel Oils--1974," Petroleum Products Survey, No. 87, Mineral Industry Surveys, Bureau of Mines, U.S. Dept. of Interior.

61) Culberson, S. F., and P. D. Rolniak, 1981, "Shale Oil--Likely Prospect for Refining," Technol. Oil and Gas J., V. 43.

62) Lin, Chieh-Shen, and D. E. Foster, 1981, "A Study of Fuel Nitrogen Conversion, Performance, and Emission Characteristics of Blended SRC-II in a High-Speed Diesel Engine," SAE Paper No. 810251, SAE Publication SP-480.

63) Tuteja, A. D., and D. W. Clar, 1980, "Comparative Performance and Emission Characteristics of Petroleum, Oil Shale, and Tar Sands Derived Diesel Fuels," SAE Paper No. 800331.

64) Muller, K., 1975, "Influence of Engine Design and Fuel Quality on Diesel Emissions--Part II, Fuel Quality," V. 6, Proceedings of the Ninth World Petroleum Congress, Tokyo.

65) Vuk, C. T.; M. A. Jones, and J. H. Johnson, 1976, "The Measurement and Analysis of the Physical Character of Diesel Particulate Emissions," SAE Paper No. 760131.

66) M. Skaates, MTU, 1980, Personal Communication.

67) Goodger, E. M., 1975, "Hydrocarbon Fuels," New York, NY, Halsted Press.

68) Marke, L. F., and D. A. Hahn, 1932, "The Catalytic Oxidation of Organic Compounds in the Vapor Phase," The Chemical Catalog Co., New York, NY.

69) Latimer, W. M., and J. H. Hildebrand, 1951, "Reference Book of Inorganic Chemistry, 3rd Ed.," New York, NY: The MacMillan Co.

70) Wang, Y. Y., S. M. Rappaport, R. F. Sawyer, F. E. Talcott, and F. T. Wei, 1978, "Direct-Acting Mutagens in Automobile Exhaust," Cancer Letters, V. 5, p. 39.

71) Allen, J. R., and J. M. Learn, 1971, "Regan 2: A Multiple Linear Regression Analysis," Academic Computing Center, University of Wisconsin-Madison.

72) Coates, P., 1981, 3M Company, Technical Ceramic Resources, Personal Communication.

73) Gibson, T.L.; A. I. Ricci, and R. L. Williams, 1980, "Measurement of Polynuclear Aromatic Hydrocarbons, Their Derivatives, and Their Reactivity in Diesel Automobile Exhaust," General Motors Research Laboratories, Publication GMR-3478, 11 pp.

74) Ahmad, T., 1980 "Effect of Particulate on the Measurement of Oxides of Nitrogen in Diesel Exhaust," SAE Transactions, v. 89, SAE Paper No. 800189.

75) Dean, David L., 1982, "Processing Pollution into Product", J. Chemical Education, v. 59 p. 639.

76) Roberson, J. A., and C. T. Crowe, 1975, "Engineering Fluid Mechanics," Boston" Houghton Mifflin Co.

77) Larsen, R. I., 1971 "A Mathematical Model for Relating Air Quality Measurements to Air Quality Standards," U.S. Government Printing Office, Office of Air Programs Publication No. AP-89.

78) Abramowitz and Stegun, 1964, "Handbook of Mathematical Functions," National Bureau of Standards.

79) Clerc, J. C., 1982, "A Computer Model for Predicting Temperature, Solids, Concentration, and Adsorbed Hydrocarbon Concentration for Dilute Diesel Particulate Emissions," M.S. Thesis, Michigan Technological University.

80) Kimberly, J. A. ; and R. A. DiDomenico, 1977, "UFIS - A New Diesel Injection System." SAE Paper 770084.

81) Campbell, J.; J. Scholl, F. Hibbler, S. Bagley, D. Leddy, D. Abata, and J. Johnson, 1981, "The Effect of Fuel Injection Rate and Timing on the Physical, Chemical, and Biological Character of Diesel Particulate Emissions," Society of Automotive Engineers, Publication SP-495, SAE Paper No. 810946.

82) Stead, A. G.; V. Hasselblad, J. Creason, and L. Claxton, 1980, "Modelling the Ames Test," Mutation Research, V. 85, p. 13.

83) Myers, L. E., N. H. Sexton, L. I. Southerland, and T. J. Wolff, 1981, "Regression Analysis of Ames Test Data," Environ. Mutagen., V. 3, p. 575.

84) Dent, J. C., 1980, "Turbulent Mixing Rate--Its Effect on Smoke and Hydrocarbon Emissions from Diesel Engines, Society of Automotive Engineers Special Publication P-86, SAE Paper No. 800092.

85) Hibbler F. 1982, "Quantification of Ames Salmonella Microsome System Variables", M.S. Thesis, Michigan Technological University.

86) Sokal, R. R., and F. J. Rolf, 1981, Biometry, W. H. Freeman & Co., San Francisco.

87) Zar, J. H., 1974, Biostatistical Analysis, Prentice-Hall Inc., Englewood Cliffs, NJ.

88) Schuetzle, D., and J. M. Perez, 1981, "A CRC Cooperative Comparison of Extraction and HPLC Techniques for Diesel Particulate Emissions, "Presented at the 74th Annual Meeting of the Air Pollution Control Association, Philadelphia.

89) Snyder, L. R., and J. J. Kirkland, 1979, Introduction to Modern Liquid Chromatography, 2nd Edition. New York: Wiley-Interscience, p. 106.

APPENDICES

TABLE A-1

MEAN

MACK ENDT-676 PARTICULATE CONTROL STUDY

C.V.

SEE EXPERIMENTAL TEST MATRIX (TABLE 3.1.3) FOR EXPLANATION OF TEST CODES

MODE	EPA MODE 3									
TEST NUMBER	3B	3.8-3	G-12-3	G-17-3	G-19-3	G-22-3	S-8-3	S-12-3	S-14-3	S-17-3
AMBIENT TEMP. (deg. C)	29 0%	32 0%	28 2%	23 15%	22 3%	24 0%	27 2%	22 3%	29 0%	25 4%
SPEC. HUM. (g_{H_2O}/g_{Air})	4.75 0%	16.41 1%	3.36 9%	5.62 28%	2.11 15	4.06 7%	2.15 41%	2.21 26%	3.94 8%	2.59 16%
BSFC (kg/kw-hr)	0.233 0%	0.231 2%	0.240 0%	0.231 1%	0.288 2%	0.233 0%	0.290 0%	0.254 0%	0.247 0%	0.242 3%
NO_x (ppm, corr.)	705. 1%	607. 7%	380. 1%	713. 3%	716. 0%	976. 1%	545. 4%	612. 1%	542. 3%	860. 1%
$BSNO_x$ (g/kw-hr)	10.13 1%	9.42 1%	5.42 2%	10.71 4%	10.12 4%	13.63 1%	7.99 5%	9.35 0%	7.75 3%	12.11 5%
NO_2 (ppm, corr.)	81.0 8%	26.1 31%	7.2 6%	55.4 11%	40.3 5%	86.5 14%	78.5 16%	60.2 4%	31.8 11%	49.0 1%
$BSNO_2$ (g/kw-hr)	1.19 8%	0.40 28%	0.10 10%	0.83 6%	0.57 7%	1.21 14%	1.15 17%	0.92 4%	0.45 11%	0.69 3%
NO (ppm, corr.)	624. 1%	581. 7%	373. 1%	658. 4%	675. 1%	889. 2%	466. 3%	552 1%	510. 3%	810. 1%
BSNO (g/kw-hr)	5.95 0%	5.88 1%	3.47 2%	6.44 5%	6.23 4%	8.10 1%	4.46 3%	5.50 1%	4.76 2%	7.45 5%
TPM (mg/m^3, std.)	47.9 5%	71.1 18%	65.0 7%	48.3 1%	51.6 1%	46.9 0%	33.1 8%	28.2 4%	35.5 8%	54.6 6%

MACK ENDT-676 PARTICULATE CONTROL STUDY

SEE EXPERIMENTAL TEST MATRIX (TABLE 3.1.3) FOR EXPLANATION OF TEST CODES

MEAN
C.V.

MODE	EPA MODE 3									
TEST NUMBER	3B	3.8-3	G-12-3	G-17-3	G-19-3	G-22-3	S-8-3	S-12-3	S-14-3	S-17-3
BSTPM (g/kw-hr)	0.41 5%	0.58 14%	0.55 6%	0.40 4%	0.43 5%	0.39 1%	0.29 9%	0.26 4%	0.30 9%	0.46 3%
$SO_4^=$ (mg/m^3, std.)	9.9 39%	3.7 14%	6.2 12%	6.3 3%	5.0 33%	6.0 7%	4.4 8%	5.2 3%	5.9 5%	6.1 2%
$BSSO_4^=$ (g/kw-hr)	0.08 41%	0.03 10%	0.05 12%	0.05 6%	0.04 38%	0.05 6%	0.04 8%	0.05 4%	0.05 6%	0.05 0%
SOF (mg/m^3, std.)	21.2 12%	10.1 33%	3.5 15%	7.2 2%	6.1 8%	15.1 4%	15.1 8%	11.1 5%	12.1 14%	14.5 2%
BSSOF (g/kw-hr)	0.18 12%	0.08 30%	0.03 13%	0.06 3%	0.05 6%	0.12 4%	0.13 92%	0.10 5%	0.10 14%	0.12 3%
INJECTION DURATION (°CA)	9.0	10.0	9.4	9.1	9.0	9.0	3.0	3.0	3.0	3.0
RATE PARAMETER (mm^3/°CA)	5.6	4.2	6.1	6.0	5.9	6.0	17.7	17.7	17.7	17.7
PEAK INJECTION PRESSURE (mPa)	40.0	41.4	46.5	46.5	46.5	46.5	65.5	65.5	65.5	65.5

MEAN
C.V.

TABLE A-1 (cont'd)
MACK ENDT-676 PARTICULATE CONTROL STUDY

SEE EXPERIMENTAL TEST MATRIX (TABLE 3.1.3) FOR EXPLANATION OF TEST CODES

MODE	EPA MODE 4						
TEST NUMBER	4B	3.8-4	G-12-4	G-17-4	G-19-4	G-22-4	S-17-4
AMBIENT TEMP. (deg. C)	33 0%	20 10%	18 3%	24 7%	22 3	19 0%	31 3%
SPEC. HUM. (g_{H_2O}/g_{Air})	5.47 0%	6.65 2%	1.77 36%	6.63 10%	1.56 0%	3.08 11%	10.16 4%
BSFC (kg/kw-hr)	0.209	0.213 1%	0.236 10%	0.209 0%	0.214 0%	0.213 0%	0.212 0%
NO_x (ppm, corr.)	1278 0%	1061.0 1%	746.0 1%	1284 0%	1444 1%	1768 1%	1396 1%
$BSNO_x$ (g/kw-hr)	10.74 0%	9.52 1%	7.04 11%	10.88 1%	11.71 3%	14.46 1%	12.27 3%
NO_2 (ppm, corr.)	133.7 4%	31.3 19%	15.6 24%	22.5 44%	93.3 2%	100.6 1%	69.1 27%
$BSNO_2$ (g/kw-hr)	1.12 4%	0.28 21%	0.15 33%	0.19 42%	0.76 1%	0.82 1%	0.61 26%
NO (ppm, corr.)	1144. 1%	1030. 1%	730. 2%	1261. 1%	1351. 1%	1668. 1%	1327. 2%
BSNO (g/kw-hr)	6.27 0%	6.03 0%	4.49 10%	6.97 2%	7.15 3%	8.89 0%	7.61 4%
TPM (mg/m^3, std.)	84.0 6%	79.1 3%	71.4 12%	63.0 7%	65.9 1%	57.0 4%	107.5 2%

TABLE A-1 (cont'd)

MACK ENDT - 676 PARTICULATE CONTROL STUDY — MEAN

SEE EXPERIMENTAL TEST MATRIX FOR EXPLANATION OF TEST CODES — C.V.

MODE	EPA MODE 4						
TEST NUMBER	4B	3.8-4	G-12-4	G-17-4	G-19-4	G-22-4	S-17-4
BSTPM (g/kw-hr)	0.40 6%	0.39 3%	0.39 13%	0.30 6%	0.31 4%	0.28 4%	0.50 3%
$SO_4^=$ (mg/m^3, std.)	7.5 2%	5.2 6%	7.0 5%	7.3 3%	6.6 32%	8.4 5%	9.4 5%
$BSSO_4^=$ (g/kw-hr)	0.04 3%	0.03 3%	0.04 13%	0.04 3%	0.03 37%	0.04 5%	.04 5%
SOF (mg/m^3, std.)	10.8 14%	6.9 12%	1.2 67%	2.1 23%	3.3 8%	7.3 14%	5.0 16%
BSSOF (g/kw-hr)	0.05 14%	0.03 13%	0.01 50%	0.01 20%	0.02 5%	0.04 13%	0.02 13%
INJECTION DURATION (°CA)	15.0	16.0	13.4	12.8	13.0	12.6	
RATE PARAMETER (mm^3/°CA)	4.2	4.2	5.4	5.3	5.3	5.3	
PEAK INJECTION PRESSURE (mPa)	46.5	48.3	51.7	51.7	51.7	51.7	

TABLE A-1 (cont'd)

MACK ENDT - 676 PARTICULATE CONTROL STUDY

SEE EXPERIMENTAL TEST MATRIX FOR EXPLANATION OF TEST CODES

MODE	EPA MODE 5						MEAN C.V.
TEST NUMBER	5B	3.8-5	G-12-5	G2-12-5	G-17-5	G2-17-5	
AMBIENT TEMP. (deg. C)	28 0%	21 0%	18 3%	14 8%	7 9%	31 8%	
SPEC. HUM. (g_{H_2O}/g_{Air})	10.64 0%	6.72 5%	2.77 12%	3.97 15%	4.40 0%	5.16 0%	
BSFC (kg/kw-hr)	0.212 0%	0.216 0%	0.222 0%	0.228 1%	0.211 0%	0.216 0%	
NO_x (ppm, corr.)	1247 5%	1170 2%	974. 1%	743 7%	1670 2%	1070 0%	
$BSNO_x$ (g/kw-hr)	8.67 6%	7.90 3%	6.52 2%	4.61 18%	9.10 25%	8.21 2%	
NO_2 (ppm, corr.)	55.9 63%	33.3 17%	14.1 30%	20.6 53%	93.6 20%	32.5 0%	
$BSNO_2$ (g/kw-hr)	0.39 62%	0.22 18%	0.09 33%	0.13 53%	0.50 18%	0.25 2%	
NO (ppm, corr.)	1190. 6%	1136. 2%	960. 1%	722. 6%	1576. 3%	1037 0%	
BSNO (g/kw-hr)	5.40 5%	5.01 3%	4.19 1%	2.91 16%	5.61 26%	5.19 2%	
TPM (mg/m^3, std.)	155.7 6%	166.2 9%	108.5 6%	8.62 9%	81.9 11%	179.4 7%	

TABLE A-1 (cont'd)

MACK ENDT - 676 PARTICULATE CONTROL STUDY

SEE EXPERIMENTAL TEST MATRIX FOR EXPLANATION OF TEST CODES

MEAN
C.V.

MODE	EPA MODE 5					
TEST NUMBER	5B	3.8-5	G-12-5	G2-12-5	G-17-5	G2-17-5
BSTPM (g/kw-hr)	0.62 2%	0.62 8%	0.42 7%	0.51 17%	0.26 17%	0.78 5%
$SO_4^=$ (mg/m^3, std.)	4.6 42%	3.6 3%	6.2 22%	0.376 14%	8.3 13%	5.4 6.5%
$BSSO_4^=$ (g/kw-hr)	0.02 35%	0.01 10%	0.02 25%	0.022 25%	0.03 17%	0.023 4%
SOF (mg/m^3, std.)	6.65 5%	4.7 12%	1.2 73%	0.22 12%	0.5 80%	3.87 19%
BSSOF (g/kw-hr)	0.028 18%	0.02 10%	0.00 0%	0.013 15%	0.00 0%	0.017 16%
INJECTION DURATION (°CA)	19.0	22.0	18.0	18.0	17.0	17.0
RATE PARAMETER (mm^3/°CA)	4.0	3.7	4.9	4.9	4.7	4.7
PEAK INJECTION PRESSURE (mPa)	51.9	58.6	51.7	51.7	51.7	51.7

TABLE A-1 (cont'd)

MACK ENDT-676 PARTICULATE CONTROL STUDY
SEE EXPERIMENTAL TEST MATRIX FOR EXPLANATION OF TEST CODES

MEAN
C.V.

MODE EPA MODE 5

TEST NUMBER	G-19-5	G-22-5	G2-22-5	S-12-5	S-14-5	S-17-5
AMBIENT TEMP. (deg. C)	19 0%	15 7.5%	29 2%	33 6%	32 5%	35 1%
SPEC. HUM. (g_{H_2O}/g_{Air})	1.3 89%	3.3 15%	10.8 0%	12.7 6%	12.1 4%	10.9 10%
BSFC (kg/kw-hr)	0.216	0.211	0.208	0.230	0.231	0.212
NO_x (ppm, corr.)	1809 0%	2078 0%	1751 0%	813 1%	900 1%	1723 1%
$BSNO_x$ (g/kw-hr)	11.50 2%	13.23 0%	14.36 0%	5.44 6%	5.76 12%	10.87 2%
NO_2 (ppm, corr.)	121.8 1%	115.2 12%	26.7 9%	21.9 15%	32.8 29%	83.0 6%
$BSNO_2$ (g/kw-hr)	0.77 1%	0.73 12%	0.22 8%	0.14 15%	0.23 25%	0.53 8%
NO (ppm, corr.)	1687. 0%	1963. 1%	1724. 0%	798. 1%	864. 2%	1639. 1%
BSNO (g/kw-hr)	6.99 2%	8.15 1%	9.22 0%	3.45 6%	3.61 12%	6.74 1%
TPM (mg/m^3, std.)	131.6	73.3	187.1	183.5	193.3	210.1

TABLE A-1 (cont'd)

MEAN

C.V.

MACK ENDT-676 PARTICULATE CONTROL STUDY

SEE EXPERIMENTAL TEST MATRIX FOR EXPLANATION OF TEST CODES

MODE	EPA MODE 5					
TEST NUMBER	G-19-5	G-22-5	G2-22-5	S-12-5	S-14-5	S-17-5
BSTPM (g/kw-hr)	0.50 4%	0.28 5%	0.81 3%	0.66 9%	0.65 3%	0.70 2%
$SO_4^=$ (mg/m^3, std.)	3.3 25%	7.6 4%	6.0 4%	8.6 11%	9.7 7%	7.4 11%
$BSSO_4^=$ (g/kw-hr)	0.01 30%	0.03 3%	0.03 4%	0.03 10%	0.03 15%	0.02 12%
SOF (mg/m^3, std.)	4.0 6%	2.4 21%	2.3 89%	4.9 46%	5.6 31%	3.6 32%
BSSOF (g/kw-hr)	0.02 5%	0.01 20%	0.01 87%	0.02 44%	0.02 42%	0.01 33%
INJECTION DURATION (°CA)	17.0	17.0	17.0			
RATE PARAMETER (mm^3/°CA)	4.8	4.8	4.8			
PEAK INJECTION PRESSURE (mPa)	51.7	51.7	51.7			

TABLE A-1 (cont'd)

MACK ENDT - 676 PARTICULATE CONTROL STUDY

SEE EXPERIMENTAL TEST MATRIX FOR EXPLANATION OF TEST CODES

MEAN

C.V.

MODE	EPA MODE 9					
TEST NUMBER	9B	3.8-9	G-12-9	G-17-9	G-19-9	G-22-9
AMBIENT TEMP. (deg. C)	31 0%	26 0%	7 14%	9 7%	15 7.5%	20 3%
SPEC. HUM. (g_{H_2O}/g_{Air})	9.45 0%	18.08 4%	2.46 10%	4.62 6%	0.0 0%	3.93 7%
BSFC (kg/kw-hr)	0.252 0%	0.261 2%	0.285 0%	0.255 0%	0.262 0%	0.248 0%
NO_x (ppm, corr.)	586.1 2%	503.1 1%	395.0 0%	665.7 1%	728.3 0%	897.7 4%
$BSNO_x$ (g/kw-hr)	6.14 4%	6.05 8%	4.34 1%	7.65 1%	7.66 2%	9.46 4%
NO_2 (ppm, corr.)	24.7 40%	12.9 11%	10.1 71%	45.9 5%	37.9 6%	62.9 28%
$BSNO_2$ (g/kw-hr)	0.26 38%	0.16 13%	0.11 73%	0.53 6%	0.40 5%	0.66 27%
NO (ppm, corr.)	561.4 2%	490.2 1%	384.9 2%	619.8 1%	690.4 0%	834.8 4%
BSNO (g/kw-hr)	3.84 5%	3.85 8%	2.76 2%	4.65 1%	4.74 2%	5.74 4%
TPM (mg/m^3, std.)	50.7 9%	152.3 9%	56.6 3%	62.8 1%	56.7 3%	59.1 6%

TABLE A-1 (cont'd)

MACK ENDT - 676 PARTICULATE CONTROL STUDY

SEE EXPERIMENTAL TEST MATRIX FOR EXPLANATION OF TEST CODES

MEAN
C.V.

MODE	EPA MODE 9					
TEST NUMBER	9B	3.8-9	G-12-9	G-17-9	G-19-9	G-22-9
BSTPM (g/kw-hr)	0.30 10%	0.89 10%	0.36 4%	0.39 1%	0.36 3%	0.36 6%
$SO_4^=$ (mg/m^3, std.)	3.0 7%	3.1 5%	7.4 2%	7.2 1%	9.0 28%	6.2 4%
$BSSO_4^=$ (g/kw-hr)	0.02 5%	0.02 5%	0.05 20%	0.04 0%	0.06 25%	0.04 5%
SOF (mg/m^3, std.)	7.2 13%	8.1 19%	5.8 16%	12.0 5%	9.5 17%	17.8 9%
BSSOF (g/kw-hr)	0.04 15%	0.05 18%	0.04 15%	0.07 6%	0.06 15%	0.11 9%
INJECTION DURATION (°CA)	25.0	28.0	22.0	20.0	20.0	19.0
RATE PARAMETER (mm^3/°CA)	3.0	2.9	4.2	4.1	3.8	4.0
PEAK INJECTION PRESSURE (mPa)	77.6	75.8	82.7	82.7	82.7	82.7

MACK ENDT - 676 PARTICULATE CONTROL STUDY

SEE EXPERIMENTAL TEST MATRIX FOR EXPLANATION OF TEST CODES

MEAN

C.V.

MODE	EPA MODE 10					
TEST NUMBER	10B	3.8-10	G-12-10	G-17-10	G-19-10	G-22-10
AMBIENT TEMP. (deg. C)	35 0%	26 2%	19 3%	21 0%	16 7%	28 6%
SPEC. HUM. (g_{H_2O}/g_{Air})	4.22 0%	4.27 35%	1.98 31%	7.31 3%	1.39 4%	2.87 5%
BSFC (kg/kw-hr)	0.269 1%	0.276 1%	0.299 0%	0.268 0%	0.278 7%	0.259 0%
NO_x (ppm, corr.)	426.8 1%	398.9 3%	307.3 0%	447.5 0%	515.3 1%	669.6 2%
$BSNO_x$ (g/kw-hr)	5.65 1%	5.45 3%	4.59 1%	6.59 0%	6.89 5%	8.02 2%
NO_2 (ppm, corr.)	17.5 15%	7.3 25%	2.9 14%	9.6 40%	20.2 4%	48.5 4%
$BSNO_2$ (g/kw-hr)	0.23 17%	0.10 30%	0.04 25%	0.14 43%	0.27 7%	0.58 2%
NO (ppm, corr.)	409.3 1%	391.6 4%	304.4 0%	437.9 1%	495.1 2%	621.0 2%
BSNO (g/kw-hr)	3.53 0%	3.49 3%	2.96 1%	4.20 1%	4.32 5%	4.85 2%
TPM (mg/m^3, std.)	56.9 3%	129.3 8%	56.4 2%	68.6 3%	68.9 4%	74.9 7%

TABLE A-1 (cont'd)

MACK ENDT - 676 PARTICULATE CONTROL STUDY — MEAN

SEE EXPERIMENTAL TEST MATRIX FOR EXPLANATION OF TEST CODES — C.V.

MODE	EPA MODE 10					
TEST NUMBER	10B	3.8-10	G-12-10	G-17-10	G-19-10	G-22-10
BSTPM (g/kw-hr)	0.45 3%	1.23 37%	0.50 2%	0.56 3%	0.56 5%	0.57 8%
$SO_4^=$ (mg/m^3, std.)	5.1 14%	2.0 89%	5.6 38%	5.7 1%	5.7 14%	5.6 4%
$BSSO_4^=$ (g/kw-hr)	0.04 15%	0.02 700%	0.05 38%	0.05 0%	0.05 16%	0.04 5%
SOF (mg/m^3, std.)	10.6 5%	14.6 10%	3.7 36%	12.0 14%	12.2 6%	27.6 12%
BSSOF (g/kw-hr)	0.08 5%	0.115 9%	0.03 40%	0.10 14%	0.10 9%	0.21 12%
INJECTION DURATION (°CA)	18.0	20.0	17.0	16.0	16.0	15.0
RATE PARAMETER (mm^3/°CA)	3.6	3.6	4.6	4.4	4.4	4.2
PEAK INJECTION PRESSURE (mPa)	56.9	68.9	68.9	68.9	68.9	68.9

TABLE A-1 (cont'd)

MACK ENDT - 676 PARTICULATE CONTROL STUDY

SEE EXPERIMENTAL TEST MATRIX FOR EXPLANATION OF TEST CODES

MEAN
C.V.

MODE	EPA MODE 11					
TEST NUMBER	11B	3.8-11	G-12-11	G2-12-11	G-17-11	G2-17-11
AMBIENT TEMP. (deg. C)	35 0%	26 2%	25 26%	19 11%	30 2%	23 2%
SPEC. HUM. (g_{H_2O}/g_{Air})	2.74 0%	3.62 15%	2.72 74%	1.72 31%	5.36 3%	9.38 0%
BSFC (kg/kw-hr)	0.337	0.356 1%	0.372 2%	0.395 1%	0.337 0%	.357 0%
NO_x (ppm, corr.)	255.8 0%	236.5 2%	179.3 3%	131 2%	284.0 1%	208 1%
$BSNO_x$ (g/kw-hr)	6.65 1%	5.68 1%	4.41 2%	4.41 6%	6.56 0%	7.04 1%
NO_2 (ppm, corr.)	1.8 28%	6.7 70%	2.3 52%	3.1 22%	8.4 38%	0.6 83%
$BSNO_2$ (g/kw-hr)	0.05 20%	0.16 69%	0.06 50%	0.10 20%	0.19 37%	0.02 100%
NO (ppm, corr.)	254.0 0%	229.8 3%	177.0 3%	128 2%	275.6 1%	207 1%
BSNO (g/kw-hr)	4.31 1%	3.63 2%	2.84 2%	4.31 6%	4.15 1%	4.58 0%
TPM (mg/m^3, std.)	54.4 5%	172.2 10%	82.2 2%	84.3 3%	106.2 6%	94.9 0.5%

TABLE A-1 (cont'd)

MACK ENDT - 676 PARTICULATE CONTROL STUDY

MEAN

SEE EXPERIMENTAL TEST MATRIX FOR EXPLANATION OF TEST CODES

C.V.

MODE	EPA MODE 11					
TEST NUMBER	11B	3.8-11	G-12-11	G2-12-11	G-17-11	G2-17-11
BSTPM (g/kw-hr)	0.78 6%	2.44 10%	1.21 7%	1.48 3%	1.44 7%	1.69 1%
$SO_4^=$ (mg/m^3, std.)	4.0 30%	2.3 13%	3.9 3%	4.6 15%	5.5 6%	5.0 3%
$BSSO_4^=$ (g/kw-hr)	0.06 28%	0.03 13%	0.06 2%	.082 17%	0.07 7%	0.09 2%
SOF (mg/m^3, std.)	17.6 10%	20.03 10%	5.7 39%	7.7 13%	17.7 9%	11.0 22%
BSSOF (g/kw-hr)	0.25 108%	0.28 9%	0.09 41%	0.14 14%	0.24 9%	0.20 22%
INJECTION DURATION (°CA)	13.0	14.0	13.1	13.1	12.0	12.0
RATE PARAMETER (mm^3/°CA)	4.2	4.2	5.1	5.1	4.7	4.7
PEAK INJECTION PRESSURE (mPa)	55.2	55.2	65.5	65.5	65.5	65.5

TABLE A-1 (cont'd)

MACK ENDT - 676 PARTICULATE CONTROL STUDY

SEE EXPERIMENTAL TEST MATRIX FOR EXPLANATION OF TEST CODES

MEAN

C.V.

MODE	EPA MODE 11				
TEST NUMBER	G-19-11	G-22-11	G2-22-11	G3-22-11	S-12-11
AMBIENT TEMP. (deg. C)	23 0%	30 8%	29 2%	30 4%	31 13%
SPEC. HUM. (g_{H_2O}/g_{Air})	1.66 12%	2.92 6%	12.73 0%	9.50 0%	13.68 10%
BSFC (kg/kw-hr)	0.346 0%	0.324 2%	0.324 0	0.338 0%	0.396 2%
NO_x (ppm, corr.)	302. 1%	373. 5%	319 1%	295. 1%	282. 1%
$BSNO_x$ (g/kw-hr)	7.07 1%	8.27 14%	10.1 1%	9.46 2%	7.42 4%
NO_2 (ppm, corr.)	11.8 8%	15.7 16%	19.4 0.5%	1.9 0%	35.4 1%
$BSNO_2$ (g/kw-hr)	0.28 7%	0.35 23%	0.62 1.6%	0.06 0%	0.93 4%
NO (ppm, corr.)	290. 1%	357. 6%	300. 1%	293. 1%	246. 1%
BSNO (g/kw-hr)	4.43 1%	5.16 14%	6.18 1%	6.13 2%	4.23 4%
TPM (mg/m^3, std.)	115.8 4%	88.0 2%	82.3 3%	107.9 3%	36.0 9%

TABLE A-1 (cont'd) MACK ENDT - 676 PARTICULATE CONTROL STUDY MEAN

SEE EXPERIMENTAL TEST MATRIX FOR EXPLANATION OF TEST CODES C.V.

MODE	EPA MODE 11				
TEST NUMBER	G-19-11	G-22-11	G2-22-11	G3-22-11	S-12-11
BSTPM (g/kw-hr)	1.63 4%	1.20 6%	1.37 4%	1.82 3%	0.50 11%
$SO_4^=$ (mg/m^3, std.)	5.05 10%	4.60 9%	5.70 4%	4.11 4%	4.34 8%
$BSSO_4^=$ (g/kw-hr)	0.080 9%	0.060 8%	0.095 4%	0.069 4%	0.060 5%
SOF (mg/m^3, std.)	17.2 3%	28.5 3%	15.3 2%	11.6 8%	18.1 14%
BSSOF (g/kw-hr)	0.24 3%	0.39 6%	0.25 3%	0.20 8%	0.25 16%
INJECTION DURATION (°CA)	12.0	11.5	11.5		
RATE PARAMETER (mm^3/°CA)	4.8	4.7	4.7		
PEAK INJECTION PRESSURE (mPa)	65.5	65.5	65.5		

TABLE A-2

CATERPILLAR 3208 PARTICULATE CONTROL STUDY
ENGLEHARD PTX CATALYST EVALUATION
INTERMEDIATE SPEED TEST SUMMARY

MEAN

C.V.

MODE	EPA MODE 3				EPA MODE 4						EPA MODE 5			
FUEL	NO.2		NO.1		NO.2		NO.1		SHALE		NO.2		NO.1	
PTX CATALYST	W/O	W	W/O	W	W/O	W	W/O	W	W/O	W	W/O	W	W/O	W
AMBIENT TEMP. (deg. C)	29 0%	30 1%	34 2%	28 3%	31 0%	32 1%	34 4%	31 3%	29 2%	30 3%	31 0%	31 3%	33 3%	31 0%
BAROMETRIC PRES. (kPa)	99 0%	100 0%	99 0%	100 0%	101 0%	100 0%	100 0%	100 0%	98 0%	98 0%	99 0%	100 0%	98 0%	99 0%
SPEC. HUM. (g_{H_2O}/g_{Air})	4.5 11%	3.0 6%	13.2 5%	9.1 5%	2.0 10%	2.7 29%	6.7 9%	9.5 6%	4.3 6%	5.1 4%	3.1 13%	2.4 25%	10.8 2%	10.4 3%
SPEED (rpm)	1680 --	1680 --	1680 --	1680 --	1680 --	1680 --	1680 --	1680 --	1680 --	1680 --	1680 --	1680 --	1680 --	1680 --
LOAD (N-m)	160 --	160 --	160 --	160 --	320 --	320 --	320 --	320 --	320 --	320 --	480 --	480 --	480 --	480 --
BMEP, Corr. (kPa)	193 0%	191 1%	197 0%	193 0%	385 0%	381 0%	389 0%	390 0%	388 0%	389 0%	580 0%	571 0%	594 0%	585 0%
BSFC (kg/kw-hr)	.286 1%	.293 1%	.280 4%	.280 2%	.233 0%	.236 1%	.243 6%	.235 3%	.229 0%	.231 0%	.217 1%	.214 1%	.219 0%	.215 1%

TABLE A-2 (cont'd)

CATERPILLAR 3208 PARTICULATE CONTROL STUDY
ENGLEHARD PTX CATALYST EVALUATION
INTERMEDIATE SPEED TEST SUMMARY

MEAN
C.V.

MODE	EPA MODE 3				EPA MODE 4						EPA MODE 5			
FUEL	NO.2		NO.1		NO.2		NO.1		SHALE		NO.2		NO.1	
PTX CATALYST	W/O	W	W/O	W	W/O	W	W/O	W	W/O	W	W/O	W	W/O	W
AIR/FUEL RATIO (kg_{Air}/kg_{Fuel})	67 1%	67 1%	64 3%	69 1%	41 2%	41 2%	37 5%	40 3%	40 0%	40 1%	30 3%	31 0%	26 0%	29 3%
MASS FLOW AIR (kg/hr)	536 0%	547 0%	514 1%	539 0%	530 0%	535 0%	514 1%	529 0%	522 0%	518 0%	539 2%	554 1%	495 1%	523 1%
MASS FLOW EXH. (kg/hr)	544 0%	555 0%	522 1%	546 0%	543 0%	546 0%	529 1%	542 0%	534 0%	531 0%	558 2%	571 0%	514 1%	541 0%
MASS FLOW EXH. (m^3/min., act.)	13.9 1%	14.2 0%	13.2 1%	14.0 1%	16.8 1%	17.0 1%	16.1 0%	16.9 0%	16.2 0%	16.4 0%	20.4 2%	20.6 1%	19.3 0%	20.4 0%
EXH. TEMP. (deg. C)	252 0%	258 1%	246 1%	254 0%	365 0%	372 1%	356 0%	367 0%	346 0%	358 0%	499 0%	481 0%	489 0%	500 1%
EXH. O_2 CONC. (%)	16.0 1%	16.1 1%	15.5 1%	16.0 1%	13.1 0%	13.1 0%	12.2 3%	12.6 1%	12.9 0%	12.7 0%	10.2 2%	10.8 2%	8.6 1%	9.6 1%
NO_x CONC. (ppm, corr.)	432 2%	429 1%	352 2%	398 2%	805 1%	765 1%	673 1%	701 2%	688 2%	691 2%	1119 1%	1019 2%	1027 1%	1062 4%
NO_2 CONC. (ppm, corr.)	28 10%	18 11%	29 7%	15 13%	16 12%	246 2%	12 8%	209 6%	40 10%	234 4%	17 29%	105 24%	14 71%	114 7%
NO CONC. (ppm, corr.)	405 2%	411 1%	352 2%	398 2%	788 1%	519 1%	673 1%	701 2%	647 2%	455 1%	1102 1%	914 5%	1027 1%	1062 4%

TABLE A-2 (cont'd)

CATERPILLAR 3208 PARTICULATE CONTROL STUDY
ENGLEHARD PTX CATALYST EVALUATION
RATED SPEED TEST SUMMARY

MEAN

C.V.

MODE	EPA MODE 3				EPA MODE 4						EPA MODE 5			
FUEL	NO.2		NO.1		NO.2		NO.1		SHALE		NO.2		NO.1	
PTX CATALYST	W/O	W	W/O	W	W/O	W	W/O	W	W/O	W	W/O	W	W/O	W
NO_2 CONC. (ppm, act.)	30 10%	21 10%	29 7%	15 13%	19 11%	286 1%	13 8%	215 7%	45 9%	262 4%	19 32%	120 21%	15 67%	115 9%
HC CONC. (ppm C)	210 5%	55 0%	220 0%	54 4%	150 7%	25 0%	85 8%	29 21%	152 0%	52 0%	97 3%	18 17%	52 4%	13 23%
$BSNO_x$ (g/kw-hr)	15.5 1%	16.2 1%	10.2 1%	13.0 2%	14.9 1%	14.2 1%	11.2 2%	11.3 3%	10.7 2%	10.7 2%	13.6 4%	12.9 3%	10.1 1%	11.2 4%
$BSNO_2$ (g/kw-hr)	1.0 10%	0.7 14%	0.9 11%	0.5 20%	0.3 0%	4.6 2%	0.2 0%	3.4 6%	0.6 10%	3.6 4%	0.2 50%	1.3 23%	0.2 50%	1.2 8%
BSNO (g/kw-hr)	9.5 2%	10.2 1%	6.1 2%	8.2 2%	9.5 1%	6.3 2%	7.2 1%	5.2 2%	6.6 2%	4.6 1%	8.7 5%	7.6 5%	6.5 0%	6.5 6%
BSHC (g/kw-hr)	2.05 5%	0.25 0%	2.30 0%	0.60 0%	0.73 7%	0.11 0%	0.50 0%	0.20 0%	0.71 0%	0.24 0%	0.31 3%	0.05 20%	0.20 0%	0.10 0%
EXH. OPACITY (%)	0.3 0%	0.4 0%	0.4 0%	0.3 0%	0.5 0%	1.2 0%	0.5 20%	0.7 14%	0.4 0%	0.8 0%	1.8 0%	1.9 0%	1.3 0%	1.7 6%

TABLE A-2 (cont'd)

CATERPILLAR 3208 PARTICULATE CONTROL STUDY
ENGLEHARD PTX CATALYST EVALUATION
INTERMEDIATE SPEED TEST SUMMARY

MEAN

C.V.

MODE	EPA MODE 3				EPA MODE 4						EPA MODE 5			
FUEL	NO.2		NO.1		NO.2		NO.1		SHALE		NO.2		NO.1	
PTX CATALYST	W/O	W	W/O	W	W/O	W	W/O	W	W/O	W	W/O	W	W/O	W
NO$_2$ @ FILTER FACE	2.0	1.4	2.0	1.0	1.3	19.2	0.9	14.7	2.8	17.4	1.3	8.4	1.0	7.8
(ppm)	10%	7%	10%	20%	15%	1%	11%	7%	17%	3%	31%	24%	60%	6%
TEMP. @ FILTER FA	39	40	44	41	48	47	50	49	44	47	51	51	50	48
(deg. C)	0%	3%	2%	2%	0%	4%	2%	4%	3%	1%	0%	2%	2%	0%
TPM CONC.	3.3	2.1	3.2	1.2	2.5	12.7	2.1	2.6	3.3	1.2	2.9	22.2	1.9	4.2
(mg/m^3, act.)	0%	5%	9%	0%	0%	1%	10%	4%	2%	3%	3%	3%	5%	7%
TPM CONC.	53	34	51	20	40	204	35	42	59	20	47	343	32	69
(mg/m^3, std.)	6%	0%	8%	5%	3%	2%	14%	5%	9%	2%	0%	2%	3%	7%
BSTPM	0.89	0.57	0.80	0.33	0.33	1.70	0.28	0.35	0.48	0.16	0.27	1.99	0.16	0.37
(g/kw-hr)	4%	0%	9%	3%	3%	2%	14%	6%	9%	2%	4%	3%	6%	5%
TPM E.F.	2.10	1.40	1.92	0.80	1.00	5.00	0.77	1.00	1.46	0.49	0.80	6.50	0.50	1.17
(g/1)	5%	7%	7%	0%	0%	2%	13%	0%	9%	2%	13%	5%	0%	8%
SOLID CONC.	7	5	6	4	10	70	9	15	8	9	35	87	26	30
(mg/m^3, std.)	--	--	--	--	--	--	--	--	--	--	--	--	--	--
SOF CONC.	2.8	1.1	2.8	0.9	1.6	0.4	1.6	0.4	2.8	0.5	0.4	0.1	0.3	0.1
(mg/m^3, act.)	0%	9%	11%	0%	0%	25%	13%	25%	2%	4%	25%	100%	33%	100%
SOF CONC.	45	18	45	15	26	6	26	7	50	8	6	2	5	2
(mg/m^3, std.)	4%	11%	9%	7%	0%	0%	15%	14%	8%	6%	17%	50%	20%	50%

TABLE A-2 (cont'd)

CATERPILLAR 3208 PARTICULATE CONTROL STUDY
ENGLEHARD PTX CATALYST EVALUATION
INTERMEDIATE SPEED TEST SUMMARY

MEAN
C.V.

MODE	EPA MODE 3				EPA MODE 4						EPA MODE 5			
FUEL	NO.2		NO.1		NO.2		NO.1		SHALE		NO.2		NO.1	
PTX CATALYST	W/O	W	W/O	W	W/O	W	W/O	W	W/O	W	W/O	W	W/O	W
BSSOF (g/kw-hr)	0.76 4%	0.31 16%	0.71 10%	0.24 4%	0.21 5%	0.5 0%	0.21 14%	0.06 17%	0.41 8%	0.61 6%	0.03 33%	0.01 0%	0.03 33%	0.01 100%
SOF E.F. (g/1)	1.53 4%	0.61 15%	1.54 10%	0.47 9%	0.72 1%	0.16 6%	0.73 15%	0.20 10%	1.24 8%	0.18 6%	0.13 15%	0.04 50%	0.12 33%	0.03 67%
$SO_4^=$ CONC. (mg/m^3, act.)	0.1 0%	0.7 14%	0.0 0%	0.1 0%	0.2 50%	7.6 8%	0.0 0%	1.2 25%	0.04 12%	0.2 11%	0.4 25%	16.5 5%	0.0 N.A.	2.3 17%
$SO_4^=$ CONC. (mg/m^3, std.)	1.0 0%	11.0 9%	0 0%	1 0%	4.0 25%	128 3%	0 0%	20 25%	0.8 12%	2.9 10%	5.7 37%	254 6%	1.0 N.A.	37 16%
$BSSO_4^=$ (g/kw-hr)	0.02 50%	0.18 11%	0.01 100%	0.02 0%	0.03 33%	1.08 5%	0.00 0%	0.17 24%	0.006 15%	0.02 9%	0.03 66%	1.48 6%	0.00 N.A.	0.20 20%
$SO_4^=$ E.F. (g/1)	0.04 25%	0.42 14%	0.02 50%	0.05 20%	0.10 20%	3.13 4%	0.01 0%	0.48 21%	0.02 13%	0.07 10%	0.10 40%	4.80 6%	0.01 N.A.	0.64 17%
CONV. FUEL S → $SO_4^=$ (%)	0.83 19%	7.82 13%	2.01 55%	5.6 14%	1.92 22%	58.0 4%	1.1 0%	58.9 22%	N.A.	N.A.	1.89 41%	89.0 6%	1.3 N.A.	78.8 18%
DEVICE OPER. TEMP. (deg. C)	269 0%		262 0%		383 0%		376 1%				498 0%		513 0%	
DEVICE SPACE VELOCITY (device vol./sec.)	167 0%		167 1%		200 1%		203 1%				242 1%		245 1%	

TABLE A-2 (cont'd)

CATERPILLAR 3208 PARTICULATE CONTROL STUDY
ENGLEHARD PTX CATALYST EVALUATION
RATED SPEED TEST SUMMARY

MODE	EPA MODE 9		EPA MODE 10		EPA MODE 11		MEAN C.V.
FUEL	NO.2		NO.2		NO.2		
PTX CATALYST	W/O	W	W/O	W	W/O	W	
AMBIENT TEMP. (deg. C)	37 3%	22 5%	25 4%	27 0%	32 3%	27 0%	
BAROMETRIC PRES. (kPa)	99 0%	99 0%	102 0%	99 0%	99 0%	99 0%	
SPEC. HUM. (g_{H_2O}/g_{Air})	6.2 6%	7.4 4%	2.1 10%	4.3 28%	9.8 29%	2.3 13%	
SPEED (rpm)	2800 --	2800 --	2800 --	2800 --	2800 --	2800 --	
LOAD (N-m)	399 --	399 --	266 --	266 --	133 --	133 --	
BMEP, Corr. (kPa)	489 0%	479 0%	308 0%	318 0%	162 1%	159 0%	
BSFC (kg/kw-hr)	.255 0%	.271 3%	.296 2%	.285 1%	.379 1%	.342 1%	
AIR-FUEL RATIO (kg_{Air}/kg_{Fuel})	24 4%	25 4%	36 3%	35 3%	50 2%	52 2%	

TABLE A-2 (cont'd)

MEAN

CATERPILLAR 3208 PARTICULATE CONTROL STUDY
ENGLEHARD PTX CATALYST EVALUATION
RATED SPEED TEST SUMMARY

C.V.

MODE	EPA MODE 9		EPA MODE 10		EPA MODE 11	
FUEL	NO.2		NO.2		NO.2	
PTX CATALYST	W/O	W	W/O	W	W/O	W
MASS FLOW AIR	738	803	795	777	754	780
(kg/hr)	1%	0%	0%	0%	2%	1%
MASS FLOW EXH.	768	834	817	799	769	795
(kg/hr)	1%	0%	0%	0%	2%	1%
MASS FLOW EXH.	34.1	38.3	29.0	29.7	24.3	25.1
(m^3/min., act.)	1%	1%	0%	0%	2%	1%
EXH. TEMP.	642	666	475	491	377	374
(deg. C)	0%	1%	1%	0%	1%	1%
EXH. O_2 CONC.	8.0	8.5	12.1	11.9	14.0	14.7
(%)	1%	4%	1%	1%	0%	0%
NO_x CONC.	904	1061	627	657	432	352
(ppm, corr.)	3%	2%	1%	3%	5%	1%
NO_2 CONC.	7	16	13	23	13	48
(ppm, corr.)	71%	69%	8%	13%	15%	6%
NO CONC.	897	1045	614	634	419	304
(ppm, corr.)	3%	2%	1%	3%	6%	2%

TABLE A-2 (cont'd)

MEAN

C.V.

CATERPILLAR 3208 PARTICULATE CONTROL STUDY
ENGLEHARD PTX CATALYST EVALUATION
RATED SPEED TEST SUMMARY

MODE	EPA MODE 9		EPA MODE 10		EPA MODE 11	
FUEL	NO.2		NO.2		NO.2	
PTX CATALYST	W/O	W	W/O	W	W/O	W
NO_2 CONC. (ppm, act.)	8 75%	16 69%	14 14%	26 12%	14 21%	56 7%
HC CONC. (ppm C)	113 13%	25 20%	320 0%	40 0%	310 3%	58 5%
$BSNO_x$ (g/kw-hr)	10.2 3%	13.0 2%	12.4 1%	12.3 2%	13.8 7%	13.8 1%
$BSNO_2$ (g/kw-hr)	0.1 100%	0.2 50%	0.3 0%	0.4 25%	0.4 25%	1.9 5%
BSNO (g/kw-hr)	6.6 3%	8.3 1%	7.9 1%	7.7 3%	8.7 7%	7.8 1%
BSHC (g/kw-hr)	0.38 13%	0.08 25%	1.61 0%	0.21 0%	3.14 3%	0.68 6%
EXH. OPACITY (%)	8.6 1%	8.8 6%	3.8 3%	4.4 2%	4.9 2%	4.8 0%

TABLE A-2 (cont'd)

CATERPILLAR 3208 PARTICULATE CONTROL STUDY
ENGLEHARD PTX CATALYST EVALUATION
RATED SPEED TEST SUMMARY

MEAN

C.V.

MODE	EPA MODE 9		EPA MODE 10		EPA MODE 11	
FUEL	NO.2		NO.2		NO.2	
PTX CATALYST	W/O	W	W/O	W	W/O	W
NO_2 @ FILTER FACE	0.5	1.1	1.0	1.7	0.9	3.9
(ppm)	60%	64%	10%	12%	22%	8%
TEMP. @ FILTER FACE						
(deg. C)	60	52	50	51	49	47
	2%	2%	0%	0%	2%	2%
TPM CONC.	11.6	25.3	5.8	23.4	8.5	15.5
(mg/m^3, act.)	3%	11%	5%	5%	5%	3%
TPM CONC.	187	397	92	368	138	235
(mg/m^3, std.)	5%	12%	2%	4%	5%	2%
BSTPM	1.04	2.46	0.84	3.27	2.32	4.15
(g/kw-hr)	5%	12%	2%	4%	5%	2%
TPM E.F.*	2.8	6.3	2.0	8.0	4.2	7.4
(g/1)	7%	11%	5%	4%	5%	3%
SOLID CONC.	170	285	65	206	78	84
(mg/m^3, std.)	--	--	--	--	--	--
SOF CONC.	0.4	0.1	1.4	0.2	3.6	0.6
(mg/m^3, act.)	25%	100%	0%	100%	3%	33%
SOF CONC.	7	2	23	4	58	10
(mg/m^3, std.)	29%	50%	4%	50%	5%	30%

---

*E.F. = Emission Factor

TABLE A-2 (cont'd)

CATERPILLAR 3208 PARTICULATE CONTROL STUDY
ENGLEHARD PTX CATALYST EVALUATION
RATED SPEED TEST SUMMARY

MODE	EPA MODE 9		EPA MODE 10		EPA MODE 11		MEAN C.V.
FUEL	NO.2		NO.2		NO.2		
PTX CATALYST	W/O	W	W/O	W	W/O	W	
BSSOF (g/kw-hr)	0.03 33%	0.01 100%	0.21 10%	0.03 67%	0.98 6%	0.17 29%	
SOF E.F. (g/l)	0.14 29%	0.03 67%	0.53 4%	0.09 56%	1.58 4%	0.27 30%	
$SO_4^=$ CONC. (mg/m^3, act.)	0.6 83%	7.0 24%	0.3 33%	10.1 17%	0.1 100%	9.3 4%	
$SO_4^=$ CONC. (mg/m^3, std.)	10.0 82%	110 24%	4.5 33%	158 17%	2.0 50%	141 6%	
$BSSO_4^=$ (g/kw-hr)	0.06 67%	0.68 24%	0.04 50%	1.41 17%	0.03 67%	2.48 6%	
$SO_4^=$ E.F. (g/l)	0.15 80%	1.74 26%	0.91 55%	3.44 17%	0.06 50%	4.40 6%	
CONV. FUEL $S \rightarrow SO_4^=$ (%)	2.80 82%	32.2 26%	1.69 54%	63.7 17%	1.09 43%	81.5 6%	
DEVICE OPER. TEMP. (deg. C)	--	695 1%	--	507 0%	--	391 1%	
DEVICE SPACE VELOCITY (device vol./sec.)		450 1%		349 0%		295 1%	

TABLE A-3

CATERPILLAR 3208 PARTICULATE CONTROL STUDY

INTERMEDIATE SPEED TEST SUMMARY

MEAN
C.V.

PARAMETER	EPA MODE 3 BASELINE NO CONTROL	EPA MODE 3 PORT CATALYST	EPA MODE 3 TRAP (UNCAT.)	EPA MODE 4 BASELINE NO CONTROL	EPA MODE 4 PORT CATALYST	EPA MODE 4 TRAP (UNCAT.)	EPA MODE 5 BASELINE NO CONTROL	EPA MODE 5 PORT CATALYST	EPA MODE 5 TRAP (UNCAT.)
AMBIENT TEMPERATURE (deg C)	31.7 0%	29.4 0%	23.9 0%	29.4 0%	31.1 0%	24.4 0%	32.2 0%	23.1 1%	30.0 0%
BAROMETRIC PRESSURE (kPa)	99.6 0%	97.6 0%	99.7 0%	99.9 0%	98.2 0%	100.5 0%	99.2 0%	98.5 0%	100.3 0%
SPECIFIC HUMIDITY (g H2O/kg AIR)	5.94 0%	7.47 0%	2.94 0%	8.21 0%	6.01 0%	2.12 0%	8.54 0%	3.68 20%	3.12 0%
SPEED (rpm)	1680. 0%	1680. 0%	1680. 0%	1680. 0%	1680. 0%	1680. 0%	1680. 0%	1680. 0%	1680. 0%
LOAD (N-m)	160. 0%	160. 0%	160. 0%	320. 0%	320. 0%	320. 0%	480. 0%	480. 0%	480. 0%
CORRECTED POWER (kW)	28.14 0%	28.62 0%	27.54 0%	56.00 0%	57.02 0%	54.67 0%	85.45 0%	83.46 0%	83.33 0%
CORRECTED BMEP (kPa)	193.0 0%	196.4 0%	188.5 0%	384.3 0%	390.9 0%	373.9 0%	584.8 0%	571.8 0%	570.0 0%
BSFC (kg/kW-hr)	.2874 0%	.2910 0%	.3007 0%	.2307 0%	.2293 0%	.2427 0%	.2167 0%	.2181 0%	.2227 0%
AIR-FUEL RATIO (kg AIR/kg FUEL)	63.13 0%	61.23 0%	62.67 0%	39.66 0%	38.87 0%	39.24 0%	26.71 0%	28.03 0%	27.43 0%
MASS FLOW AIR (kg/hr)	510.6 0%	509.9 0%	519.1 0%	512.5 0%	508.1 0%	520.6 0%	494.6 0%	510.0 0%	508.9 0%
MASS FLOW FUEL (kg/hr)	8.089 0%	8.328 0%	8.283 0%	12.921 0%	13.072 0%	13.269 0%	18.519 0%	18.199 0%	18.553 0%
MASS FLOW EXHAUST (kg/hr)	518.7 0%	518.2 0%	527.4	525.4 0%	521.2 0%	533.9 0%	513.1 0%	528.2 0%	527.5 0%
VOL. FLOW EXH. (ACTUAL) (cubic meters/min)	12.96 0%	14.04 0%	13.56 0%	15.90 0%	16.75 0%	16.39 0%	18.89 0%	19.44 0%	19.42 0%
DENSITY EXHAUST (kg/cubic meter)	.667 0%	.615 0%	.648 0%	.551 0%	.518 0%	.543 0%	.453 0%	.453 0%	.453 0%
MOL WT. EXHAUST (kg/mole)	28.75 0%	28.72 0%	28.80 0%	28.72 0%	28.76 0%	28.82 0%	28.72 0%	28.80 0%	28.81 0%
EXHAUST TEMP (MANIFOLD) (deg C)	242.9 0%	275.0 0%	259.5 0%	353.1 1%	381.9 0%	368.2 0%	483.2 0%	480.0 0%	494.8 0%
EXHAUST VISCOSITY (kg/m-sec)	.268-004 0%	.283-004 0%	.273-004 0%	.301-004 0%	.318-004 0%	.305-004 0%	.337-004 0%	.352-004 0%	.340-004 0%
EXH. OXYGEN CONC. (percent)	15.72 0%	15.52 0%	15.78 0%	12.73 0%	12.64 0%	12.82 0%	8.99 0%	9.65 0%	9.43 0%
NOx CONC. (corr) (ppm)	341.3 0%	399.6 0%	346.8 0%	681.5 1%	700.6 0%	617.9 0%	986.0 0%	1179.1 1%	897.0 0%
NO2 CONC. (corr) (ppm)	38.7 18%	22.7 6%	37.9 6%	56.0 5%	40.0 6%	24.1 6%	36.4 3%	100.3 1%	14.0 9%
NO CONC. (corr) (ppm)	302.6 2%	376.9 0%	308.9 0%	625.5 0%	660.6 0%	593.8 0%	949.7 0%	1078.8 1%	883.0 0%
NO2 CONC. (actual) (ppm)	43.2 18%	24.2 6%	43.0 6%	58.7 5%	43.8 6%	27.5 6%	37.7 3%	110.0 2%	15.7 9%
HC CONC. (ppm C)	212. 10%	195. 0%	230. 5%	168. 2%	86. 0%	125. 0%	85. 1%	36. 0%	58. 1%

TABLE A-3
(cont'd)

CATERPILLAR 3208 PARTICULATE CONTROL STUDY

INTERMEDIATE SPEED TEST SUMMARY

MEAN
C.V.

PARAMETER	EPA MODE 3			EPA MODE 4			EPA MODE 5		
	BASELINE NO CONTROL	PORT CATALYST	TRAP (UNCAT.)	BASELINE NO CONTROL	PORT CATALYST	TRAP (UNCAT.)	BASELINE NO CONTROL	PORT CATALYST	TRAP (UNCAT.)
bs NOx (g/kW-hr)	10.24 0%	12.02 0%	10.78 0%	10.39 1%	10.56 0%	9.71 0%	9.69 0%	12.26 1%	9.15 0%
bs NO2 (g/kW-hr)	1.16 18%	.68 6%	1.18 6%	.85 5%	.60 6%	.38 6%	.36 3%	1.04 1%	.14 9%
bs NO (g/kW-hr)	5.92 2%	7.40 0%	6.26 0%	6.22 1%	6.50 0%	6.08 0%	6.08 0%	7.31 1%	5.88 0%
bs HC (g/kW-hr)	1.917 10%	1.766 0%	2.152 5%	.771 2%	.390 0%	.591 0%	.253 1%	.113 0%	.178 1%
EXHAUST OPACITY (percent)	.3 0%	.3 0%	.3 23%	.9 6%	.5 0%	.1 0%	1.9 0%	1.4 0%	.1 0%
NO2 @ FILTER FACE (ppm)	2.81 17%	1.65 6%	3.00 5%	3.81 5%	2.99 5%	1.85 6%	2.50 3%	7.39 3%	1.07 9%
TEMP @ FILTER FACE (deg C)	37.2 0%	40.0 0%	31.7 1%	45.6 0%	47.2 0%	37.2 2%	50.4 0%	41.1 0%	45.9 1%
MASS FLOW TPM (g/hr)	29.461 3%	22.617 6%	28.617 6%	26.974 6%	26.902 2%	9.448 19%	20.594 2%	59.186 1%	1.269 17%
CONC. TPM (mg/m**3 act)	37.882 2%	26.844 6%	35.172 6%	28.272 5%	26.762 2%	9.618 20%	18.171 2%	50.751 1%	1.090 18%
CONC. TPM (mg/m**3 std)	66.419 2%	49.990 6%	63.638 6%	60.161 6%	59.559 2%	20.940 19%	46.689 2%	129.847 1%	2.841 17%
bs TPM (g/kW-hr)	1.047 3%	.790 6%	1.039 6%	.482 6%	.472 2%	.173 19%	.241 2%	.709 1%	.015 17%
TPM E.F. (g/l)	2.519 2%	1.878 6%	2.390 6%	1.444 6%	1.423 2%	.493 20%	.769 2%	2.249 1%	.047 18%
MASS FLOW SOLID (g/hr)	2.357 2%	3.979 13%	1.528 4%	3.875 12%	4.228 4%	1.223 5%	14.680 3%	9.331 13%	.453 26%
CONC. SOLID (mg/m**3 act)	3.031 1%	4.723 13%	1.877 4%	4.061 12%	4.206 4%	1.244 5%	12.953 3%	8.001 12%	.389 26%
CONC. SOLID (mg/m**3 std)	5.314 2%	8.795 13%	3.397 4%	8.643 12%	9.359 4%	2.710 5%	33.281 3%	20.471 13%	1.014 26%
bs SOLID (g/kW-hr)	.084 2%	.139 13%	.055 4%	.069 12%	.074 4%	.022 5%	.172 3%	.112 12%	.005 25%
SOLID E.F. (g/l)	.202 1%	.330 13%	.128 4%	.207 12%	.224 4%	.064 5%	.548 3%	.355 12%	.017 26%
MASS FLOW SOF (g/hr)	26.230 3%	17.431 5%	26.762 6%	21.106 6%	6.576 5%	7.512 24%	3.235 5%	2.021 25%	.152 8%
CONC. SOF (mg/m**3 act)	33.727 3%	20.689 5%	32.892 7%	22.121 5%	6.542 5%	7.648 25%	2.855 5%	1.733 25%	.130 8%
CONC. SOF (mg/m**3 std)	59.134 3%	38.528 5%	59.512 6%	47.073 6%	14.559 5%	16.647 24%	7.335 5%	4.433 25%	.340 8%
bs SOF (g/kW-hr)	.932 3%	.609 5%	.972 6%	.377 6%	.115 5%	.137 24%	.038 5%	.024 25%	.002 8%
SOF E.F. (g/l)	2.243 2%	1.448 5%	2.235 7%	1.130 6%	.348 5%	.392 25%	.121 5%	.077 25%	.006 8%

TABLE A-3 (cont'd)

CATERPILLAR 3208 PARTICULATE CONTROL STUDY

INTERMEDIATE SPEED TEST SUMMARY

MEAN
C.V.

	EPA MODE 3			EPA MODE 4			EPA MODE 5		
PARAMETER	BASELINE NO CONTROL	PORT CATALYST	TRAP (UNCAT.)	BASELINE NO CONTROL	PORT CATALYST	TRAP (UNCAT.)	BASELINE NO CONTROL	PORT CATALYST	TRAP (UNCAT.)
MASS FLOW SO4 (g/hr)	.874 4%	1.207 4%	.327 18%	1.993 6%	16.099 1%	.714 6%	2.679 5%	47.835 1%	.664 17%
CONC. SO4 (mg/m**3 act)	1.124 4%	1.432 4%	.403 19%	2.090 6%	16.015 1%	.726 5%	2.364 5%	41.017 1%	.570 18%
CONC. SO4 (mg/m**3 std)	1.971 4%	2.667 4%	.728 18%	4.445 6%	35.640 1%	1.582 6%	6.073 5%	104.943 1%	1.486 17%
bs SO4 (g/kW-hr)	.031 4%	.042 4%	.012 18%	.036 6%	.282 1%	.013 5%	.031 5%	.573 1%	.008 17%
SO4 E.F. (g/l)	.075 4%	.100 4%	.027 19%	.107 6%	.852 1%	.037 6%	.100 5%	1.818 1%	.025 18%
CONV. FUEL S to SO4 (percent)	1.33 4%	1.79 4%	.49 19%	1.90 6%	15.19 1%	.66 6%	1.78 5%	32.43 1%	.44 18%
DEVICE OPERATING TEMP. (deg C)	242.9 0%	288.9 0%	258.5 0%	353.1 1%	406.9 0%	365.9 0%	483.2 0%	530.4 0%	489.3 0%
DEVICE SPACE VELOCITY (device volumes/second)	.0 0%	404.0 0%	42.0 0%	.0 0%	488.1 0%	50.6 0%	.0 0%	581.9 0%	59.8 0%
DEVICE RESIDENCE TIME (msec)	.00 0%	2.48 0%	23.83 0%	.00 0%	2.05 0%	19.75 0%	.00 0%	1.72 0%	16.72 0%
TRAP PRESSURE DROP (kPa)	.000 0%	.000 0%	6.996 8%	.000 0%	.000 0%	8.616 9%	.000 0%	.000 0%	8.565 11%
TRAP LOADING PARAMETER (dimensionless)	0. 0%	0. 0%	1694. 7%	0. 0%	0. 0%	1548. 8%	0. 0%	0. 0%	1170. 11%

TABLE A-3
(cont'd)

CATERPILLAR 3208 PARTICULATE CONTROL STUDY
RATED SPEED TEST SUMMARY

MEAN
C.V.

	EPA MODE 9			EPA MODE 10			EPA MODE 11		
PARAMETER	BASELINE NO CONTROL	PORT CATALYST	TRAP (UNCAT.)	BASELINE NO CONTROL	PORT CATALYST	TRAP (UNCAT.)	BASELINE NO CONTROL	PORT CATALYST	TRAP (UNCAT.)
AMBIENT TEMPERATURE (deg C)	31.7 0%	26.1 2%	34.4 0%	37.8 0%	27.7 2%	33.3 0%	36.7 0%	31.1 0%	27.8 0%
BAROMETRIC PRESSURE (kPa)	98.5 0%	100.1 0%	99.0 0%	101.2 0%	98.7 0%	98.0 0%	97.6 0%	98.3 0%	99.9 0%
SPECIFIC HUMIDITY (g H2O/kg AIR)	11.56 0%	3.76 19%	2.90 0%	11.73 0%	6.44 3%	4.11 0%	12.02 0%	5.35 0%	3.52 0%
SPEED (rpm)	2800. 0%	2800. 0%	2800. 0%	2800. 0%	2800. 0%	2800. 0%	2800. 0%	2800. 0%	2800. 0%
LOAD (N-m)	399. 0%	399. 0%	399. 0%	266. 0%	266. 0%	266. 0%	133. 0%	133. 0%	133. 0%
CORRECTED POWER (kW)	119.29 0%	114.59 0%	118.02 0%	78.47 0%	78.05 0%	79.34 0%	40.63 0%	39.39 0%	38.90 2%
CORRECTED BMEP (kPa)	490.8 0%	470.9 0%	484.5 0%	323.1 0%	320.9 0%	326.1 0%	167.1 0%	162.1 0%	157.8 0%
BSFC (kg/kW-hr)	.2516 0%	.2718 0%	.2623 0%	.2816 0%	.2895 0%	.2879 0%	.3703 0%	.3988 0%	.4113 5%
AIR-FUEL RATIO (kg AIR/kg FUEL)	25.34 0%	25.97 0%	24.31 0%	34.36 0%	34.52 0%	32.94 0%	48.81 0%	48.79 0%	49.32 3%
MASS FLOW AIR (kg/hr)	760.4 0%	808.9 0%	752.5 0%	759.1 0%	780.0 0%	752.5 0%	734.4 0%	766.6 0%	788.0 0%
MASS FLOW FUEL (kg/hr)	30.009 0%	31.147 0%	30.955 0%	22.096 0%	22.595 0%	22.842 0%	15.047 0%	15.711 0%	15.992 3%
MASS FLOW EXHAUST (kg/hr)	790.4 0%	840.0 0%	783.5 0%	781.2 0%	802.6 0%	775.3 0%	749.5 0%	782.3 0%	804.0 0%
VOL. FLOW EXH. (ACTUAL) (cubic meters/min)	33.38 0%	36.52 0%	34.44 0%	28.02 0%	30.23 0%	29.46 1%	23.67 0%	25.89 0%	25.71 2%
DENSITY EXHAUST (kg/cubic meter)	.395 0%	.383 0%	.379 0%	.465 0%	.443 0%	.439 1%	.528 0%	.504 0%	.522 2%
MOL WT. EXHAUST (kg/mole)	28.68 0%	28.81 0%	28.82 0%	28.66 0%	28.75 0%	28.79 0%	28.65 0%	28.76 0%	28.79 0%
EXHAUST TEMP (MANIFOLD) (deg C)	587.2 0%	630.9 0%	631.8 0%	477.2 0%	497.7 0%	500.4 1%	363.7 0%	401.7 0%	390.4 4%
EXHAUST VISCOSITY (kg/m-sec)	.367-004 0%	.397-004 0%	.379-004 0%	.338-004 0%	.358-004 0%	.344-004 0%	.305-004 0%	.331-004 0%	.300-004 6%
EXH. OXYGEN CONC. (percent)	8.31 0%	8.79 0%	8.02 1%	11.44 0%	11.62 0%	11.26 0%	14.09 0%	14.28 0%	14.40 1%
NOx CONC. (corr) (ppm)	768.7 1%	857.6 1%	681.3 0%	564.0 0%	592.7 0%	527.7 1%	328.0 1%	349.2 0%	321.2 3%
NO2 CONC. (corr) (ppm)	23.2 13%	55.4 1%	9.6 28%	16.1 10%	19.0 3%	7.4 6%	21.3 4%	11.6 0%	4.4 0%
NO CONC. (corr) (ppm)	745.5 1%	802.2 1%	671.7 1%	548.0 0%	573.7 0%	520.3 1%	306.7 1%	337.6 0%	316.8 3%
NO2 CONC. (actual) (ppm)	23.0 13%	60.8 0%	10.7 28%	16.2 10%	20.3 3%	8.3 6%	21.5 4%	13.0 0%	5.0 0%
HC CONC. (ppm C)	80. 5%	35. 0%	34. 2%	271. 4%	125. 0%	105. 0%	316. 4%	180. 0%	206. 0%

TABLE A-3
(cont'd)

CATERPILLAR 3208 PARTICULATE CONTROL STUDY

RATED SPEED TEST SUMMARY

MEAN
C.V.

	EPA MODE 9			EPA MODE 10			EPA MODE 11		
PARAMETER	BASELINE NO CONTROL	PORT CATALYST	TRAP (UNCAT.)	BASELINE NO CONTROL	PORT CATALYST	TRAP (UNCAT.)	BASELINE NO CONTROL	PORT CATALYST	TRAP (UNCAT.)
bs NOx (g/kW-hr)	8.41 1%	10.16 0%	7.38 0%	9.02 0%	10.01 0%	8.52 1%	10.09 1%	11.43 0%	10.76 4%
bs NO2 (g/kW-hr)	.25 13%	.66 1%	.10 28%	.26 10%	.32 3%	.12 6%	.65 4%	.38 0%	.15 2%
bs NO (g/kW-hr)	5.32 1%	6.20 0%	4.75 0%	5.72 0%	6.32 0%	5.48 2%	6.15 1%	7.21 0%	6.92 4%
bs HC (g/kW-hr)	.265 5%	.125 0%	.111 2%	1.305 4%	.634 0%	.510 1%	2.926 4%	1.774 0%	2.077 2%
EXHAUST OPACITY (percent)	4.9 4%	5.5 2%	.1 0%	3.8 22%	3.5 4%	.1 0%	3.2 3%	4.6 0%	.1 0%
NO2 @ FILTER FACE (ppm)	1.55 13%	4.12 1%	.72 27%	1.11 8%	1.38 3%	.58 7%	1.43 5%	.87 0%	.36 1%
TEMP @ FILTER FACE (deg C)	61.7 1%	50.6 1%	57.4 0%	58.1 1%	47.0 1%	50.2 3%	51.1 0%	45.0 0%	42.8 4%
MASS FLOW TPM (g/hr)	94.669 8%	136.534 3%	2.547 19%	62.144 2%	98.025 1%	1.777 19%	75,717 1%	81.875 0%	5.442 28%
CONC. TPM (mg/m**3 act)	47.363 7%	62.303 3%	1.233 20%	36.961 2%	54.049 1%	1.008 20%	53.315 1%	52.710 0%	3.549 30%
CONC. TPM (mg/m**3 std)	138.429 8%	191.344 3%	3.791 20%	94.203 2%	141.527 1%	2.643 19%	115.341 1%	120.836 0%	7.952 28%
bs TPM (g/kW-hr)	.795 6%	1.192 4%	.022 19%	.792 2%	1.256 1%	.022 19%	1.864 1%	2.079 0%	.139 26%
TPM E.F. (g/l)	2.186 7%	3.031 3%	.057 19%	1.945 2%	3.001 1%	.054 20%	3.480 1%	3.604 0%	.237 31%
MASS FLOW SOLID (g/hr)	87.066 7%	90.019 4%	1.071 46%	49.113 5%	54.119 6%	.612 42%	34.823 13%	58.032 2%	1.915 22%
CONC. SOLID (mg/m**3 act)	43.467 7%	41.076 4%	.519 46%	29.214 5%	29.841 6%	.347 42%	24.523 13%	37.360 2%	1.248 25%
CONC. SOLID (mg/m**3 std)	127.042 7%	126.155 4%	1.594 46%	74.457 5%	78.128 6%	.909 42%	53.043 13%	85.646 2%	2.798 22%
bs SOLID (g/kW-hr)	.730 7%	.786 4%	.009 46%	.626 5%	.693 7%	.008 42%	.857 13%	1.473 2%	.049 20%
SOLID E.F. (g/l)	2.006 7%	1.999 4%	.024 46%	1.537 5%	1.657 7%	.019 42%	1.601 13%	2.555 2%	.083 25%
MASS FLOW SOF (g/hr)	3.110 27%	1.258 46%	.059 51%	10.463 16%	9.400 9%	.465 38%	39.357 11%	11.056 8%	2.609 39%
CONC. SOF (mg/m**3 act)	1.554 27%	.575 46%	.029 51%	6.219 15%	5.183 9%	.264 38%	27.709 11%	7.117 8%	1.705 41%
CONC. SOF (mg/m**3 std)	4.538 27%	1.763 46%	.088 51%	15.854 15%	13.571 9%	.693 38%	59.956 11%	16.316 8%	3.812 39%
bs SOF (g/kW-hr)	.026 27%	.011 45%	.001 51%	.133 16%	.120 9%	.006 37%	.969 11%	.281 8%	.067 37%
SOF E.F. (g/l)	.072 27%	.028 46%	.001 50%	.328 16%	.288 9%	.014 38%	1.809 11%	.487 8%	.114 42%

TABLE A-3 (cont'd)

CATERPILLAR 3208 PARTICULATE CONTROL STUDY

RATED SPEED TEST SUMMARY

MEAN
C.V.

PARAMETER	EPA MODE 9 BASELINE NO CONTROL	EPA MODE 9 PORT CATALYST	EPA MODE 9 TRAP (UNCAT.)	EPA MODE 10 BASELINE NO CONTROL	EPA MODE 10 PORT CATALYST	EPA MODE 10 TRAP (UNCAT.)	EPA MODE 11 BASELINE NO CONTROL	EPA MODE 11 PORT CATALYST	EPA MODE 11 TRAP (UNCAT.)
MASS FLOW SO4 (g/hr)	4.693 23%	45.257 3%	1.418 2%	2.567 15%	34.506 8%	.700 10%	1.538 11%	12.788 2%	.918 10%
CONC. SO4 (mg/m**3 act)	2.343 23%	20.652 3%	.686 2%	1.528 15%	19.025 8%	.397 11%	1.083 11%	8.233 2%	.597 12%
CONC. SO4 (mg/m**3 std)	6.848 23%	63.426 3%	2.109 2%	3.893 15%	49.827 9%	1.041 10%	2.342 11%	18.873 2%	1.342 10%
bs SO4 (g/kW-hr)	.039 23%	.395 3%	.012 2%	.033 15%	.442 8%	.009 10%	.038 11%	.325 2%	.024 10%
SO4 E.F. (g/l)	.108 23%	1.005 3%	.032 3%	.080 15%	1.056 8%	.021 11%	.071 11%	.563 2%	.040 13%
CONV. FUEL S to SO4 (percent)	1.93 23%	17.93 3%	.57 3%	1.43 15%	18.84 8%	.38 11%	1.26 11%	10.04 2%	.71 13%
DEVICE OPERATING TEMP. (deg C)	587.2 0%	690.9 0%	627.9 0%	477.2 0%	545.5 0%	498.1 1%	363.7 0%	445.0 0%	344.7 17%
DEVICE SPACE VELOCITY (device volumes/second)	.0 0%	1092.9 0%	106.3 0%	.0 0%	900.8 0%	91.1 1%	.0 0%	773.1 0%	74.2 9%
DEVICE RESIDENCE TIME (msec)	.00 0%	.92 0%	9.40 0%	.00 0%	1.11 0%	10.98 1%	.00 0%	1.29 0%	13.56 10%
TRAP PRESSURE DROP (kPa)	.000 0%	.000 0%	12.902 1%	.000 0%	.000 0%	20.617 6%	.000 0%	.000 0%	21.726 37%
TRAP LOADING PARAMETER (dimensionless)	0. 0%	0. 0%	889. 1%	0. 0%	0. 0%	1825. 4%	0. 0%	0. 0%	2848. 53%

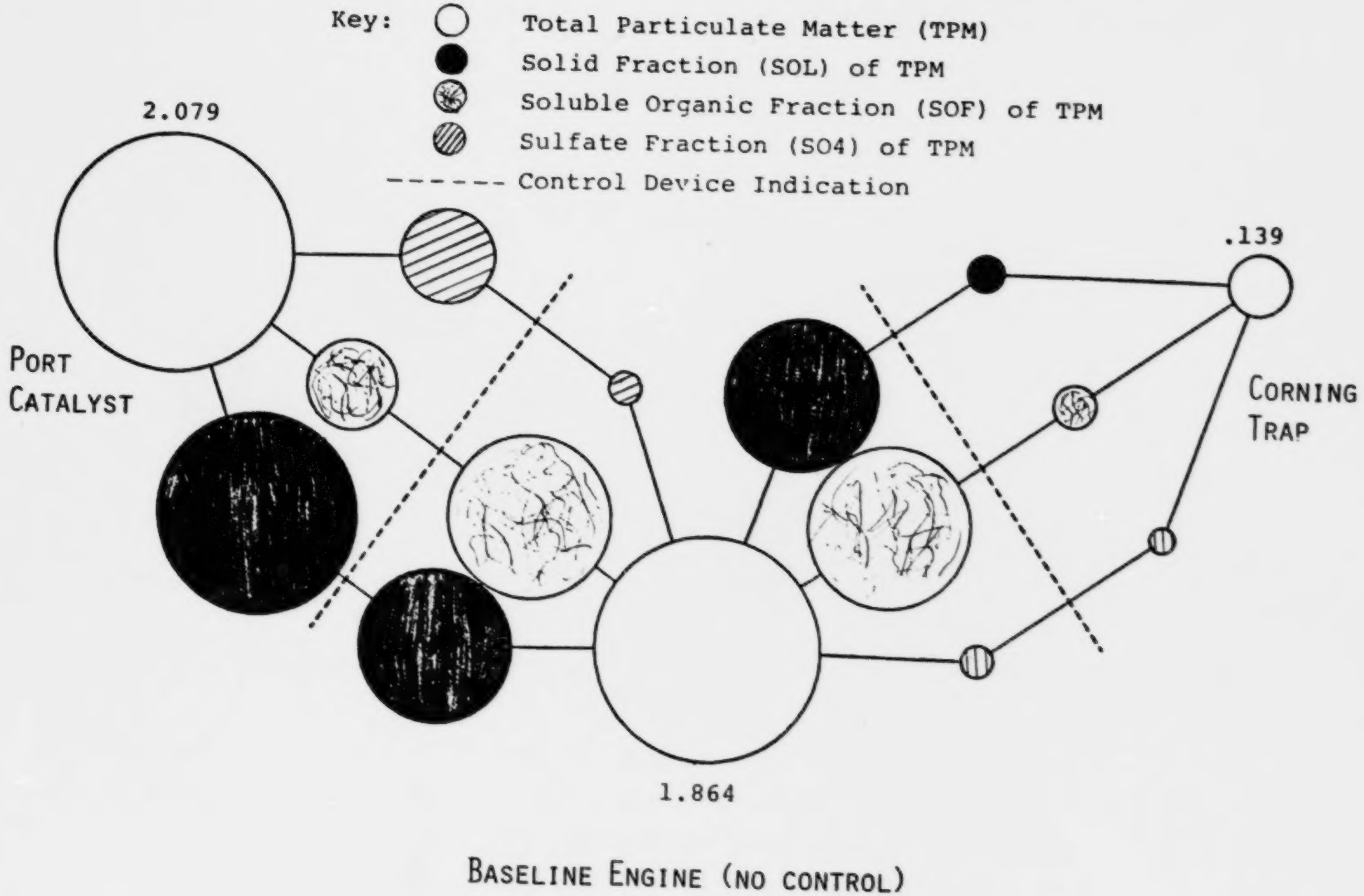
Key:
○ Total Particulate Matter (TPM)
● Solid Fraction (SOL) of TPM
Soluble Organic Fraction (SOF) of TPM
▨ Sulfate Fraction (SO4) of TPM
------ Control Device Indication
2.079
PORT CATALYST
.139
CORNING TRAP
1.864
BASELINE ENGINE (NO CONTROL)

Fig. A6 The Effect of Aftertreatment Devices on Caterpillar 3208 Particulate Emissions: Johnson-Matthey Close-Coupled Exhaust Port Catalysts and Corning Ceramic Traps. EPA Mode 11 (2800 rpm and 25% load = 133 N-m) (numbers indicate bsTPM in g/kW-hr)

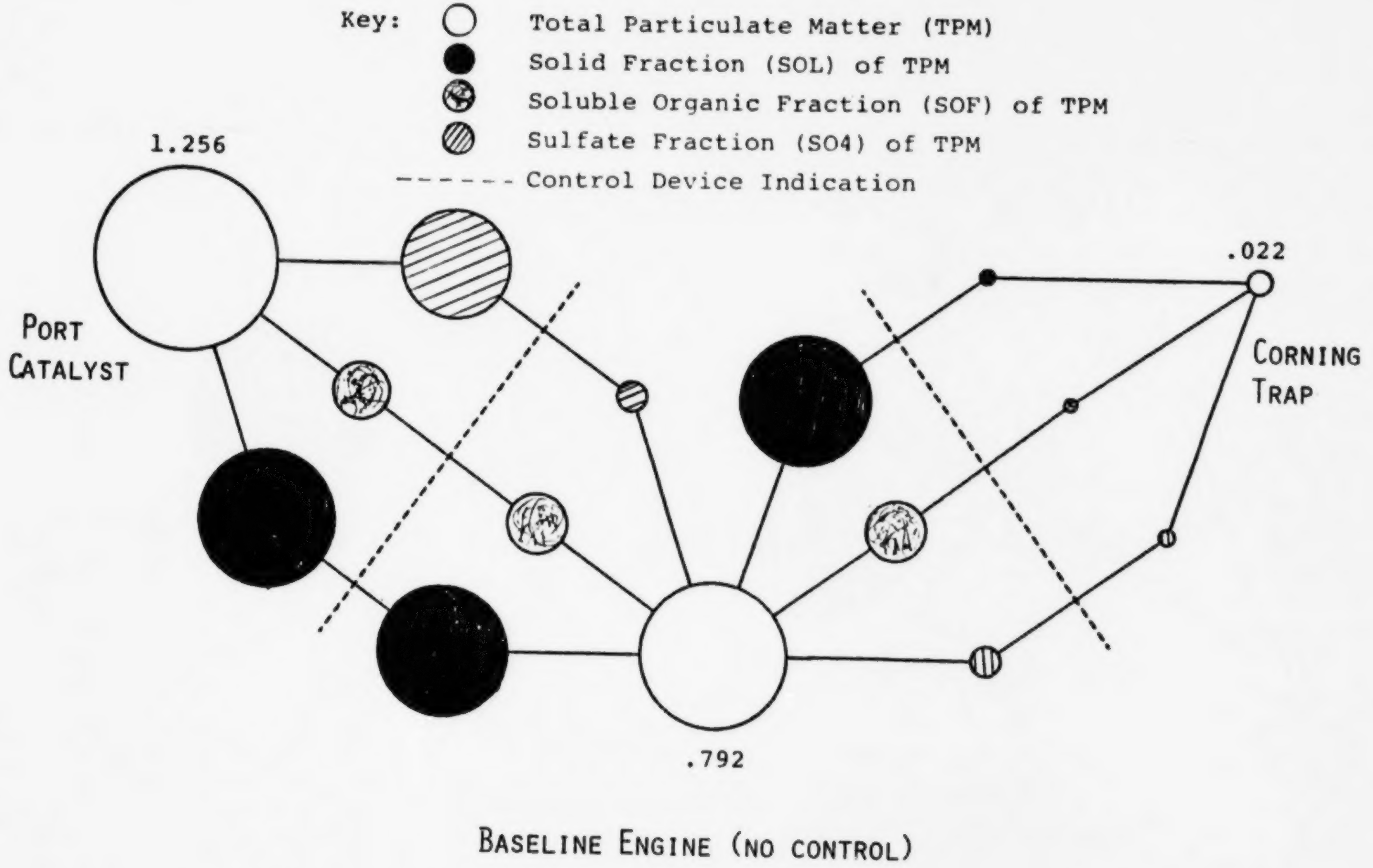
Key:
○ Total Particulate Matter (TPM)
● Solid Fraction (SOL) of TPM
Soluble Organic Fraction (SOF) of TPM
▨ Sulfate Fraction (SO4) of TPM
------ Control Device Indication
1.256
Port Catalyst
.022
Corning Trap
.792
Baseline Engine (no control)

Fig. A5 The Effect of Aftertreatment Devices on Caterpillar 3208 Particulate Emissions: Johnson-Matthey Close-Coupled Exhaust Port Catalysts and Corning Ceramic Traps. EPA Mode 10 (2800 rpm and 50% load = 266 N-m) (numbers indicate bsTPM in g/kW-hr)

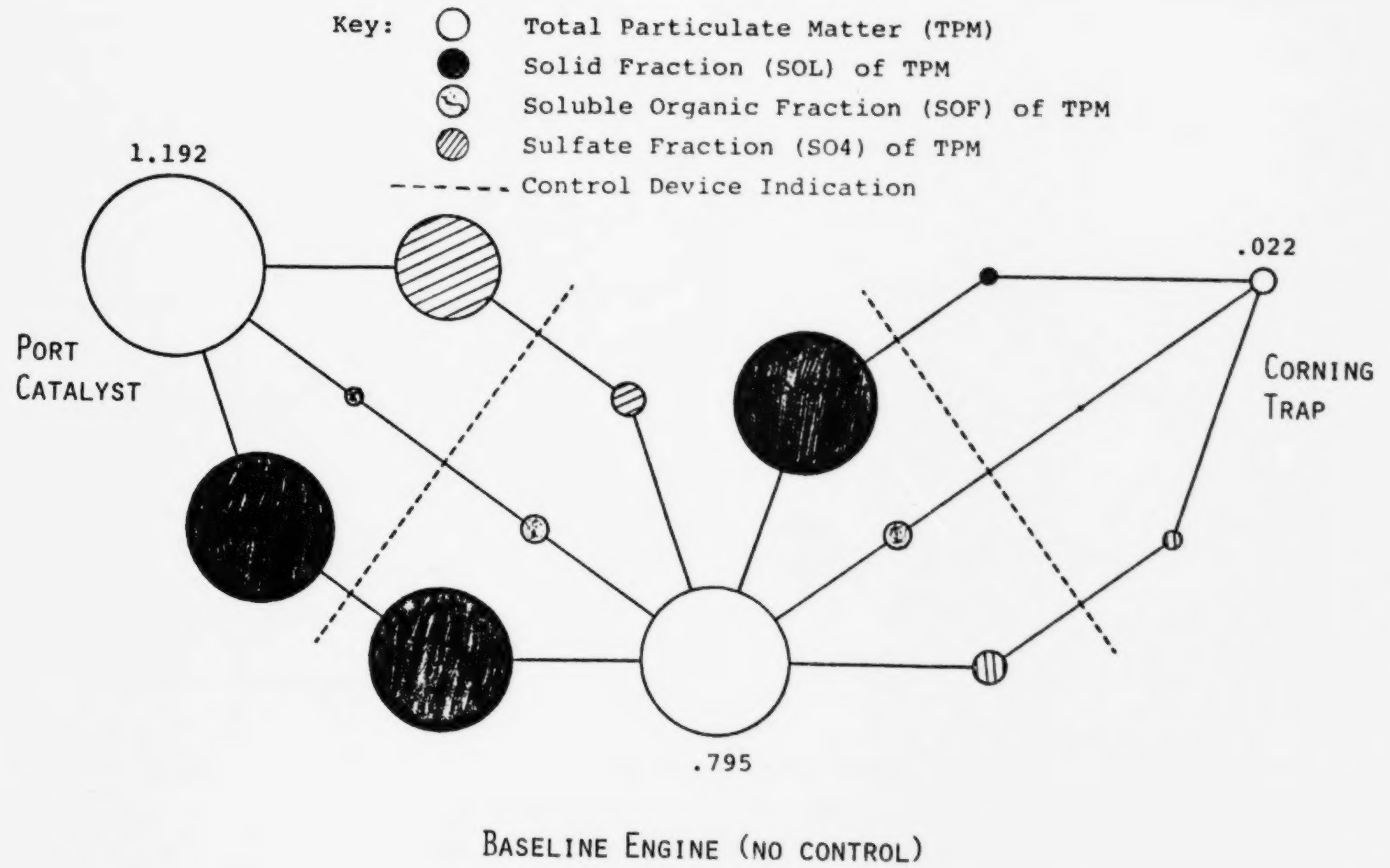
Key:
○ Total Particulate Matter (TPM)
● Solid Fraction (SOL) of TPM
Soluble Organic Fraction (SOF) of TPM
▨ Sulfate Fraction (SO4) of TPM
------ Control Device Indication
1.192
PORT CATALYST
.022
CORNING TRAP
.795
BASELINE ENGINE (NO CONTROL)

Fig. A4 The Effect of Aftertreatment Devices on Caterpillar 3208 Particulate Emissions: Johnson-Matthey Close-Coupled Exhaust Port Catalysts and Corning Ceramic Traps. EPA Mode 9 (2800 rpm and 75% load = 399 N-m) (numbers indicate bsTPM in g/kW-hr)
]

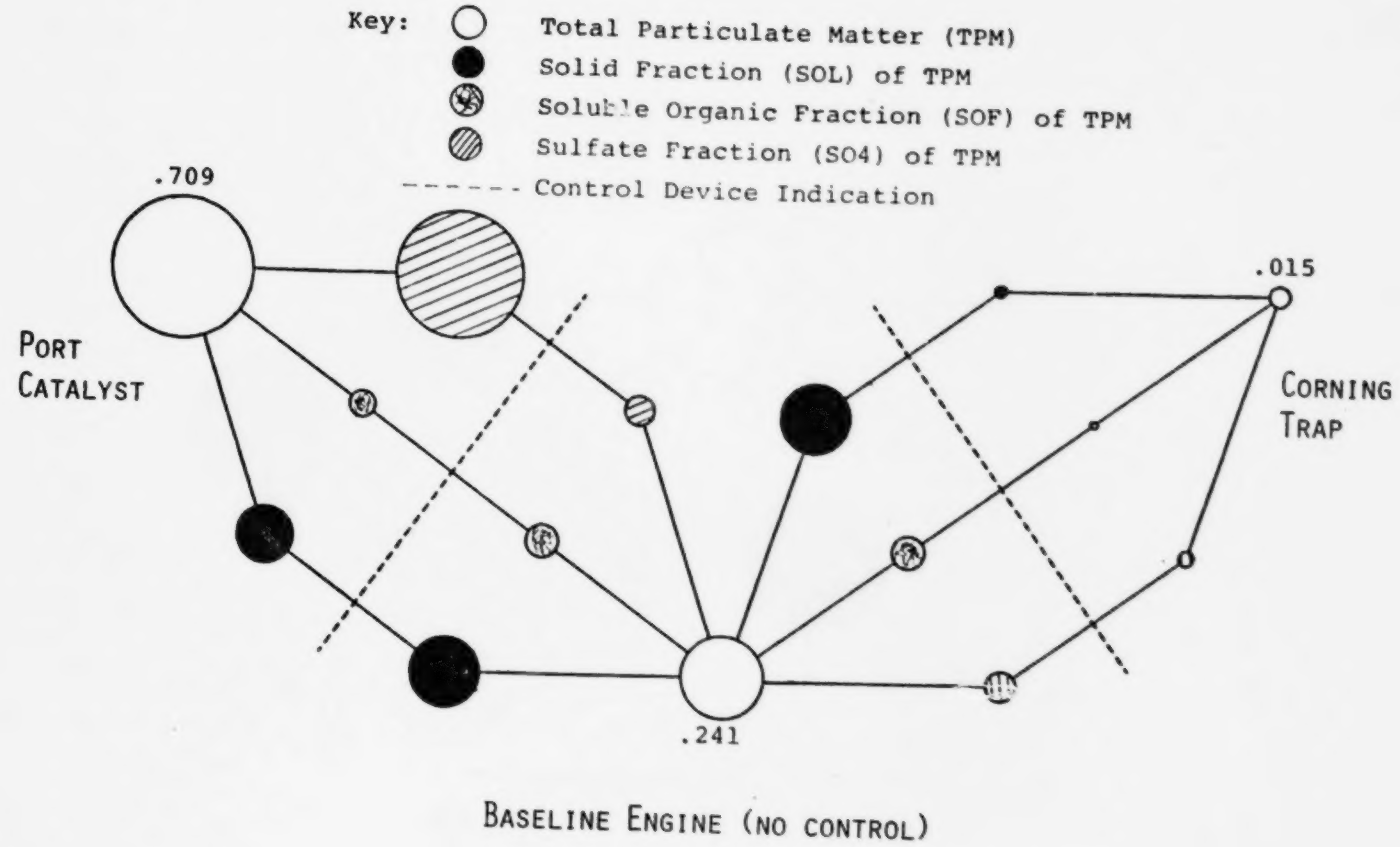

Fig. A3 The Effect of Aftertreatment Devices on Caterpillar 3208 Particulate Emissions: Johnson-Matthey Close-Coupled Exhaust Port Catalysts and Corning Ceramic Traps. EPA Mode 5 (1680 rpm and 75% load = 480 N-m)
(numbers indicate bsTPM in g/kW-hr)

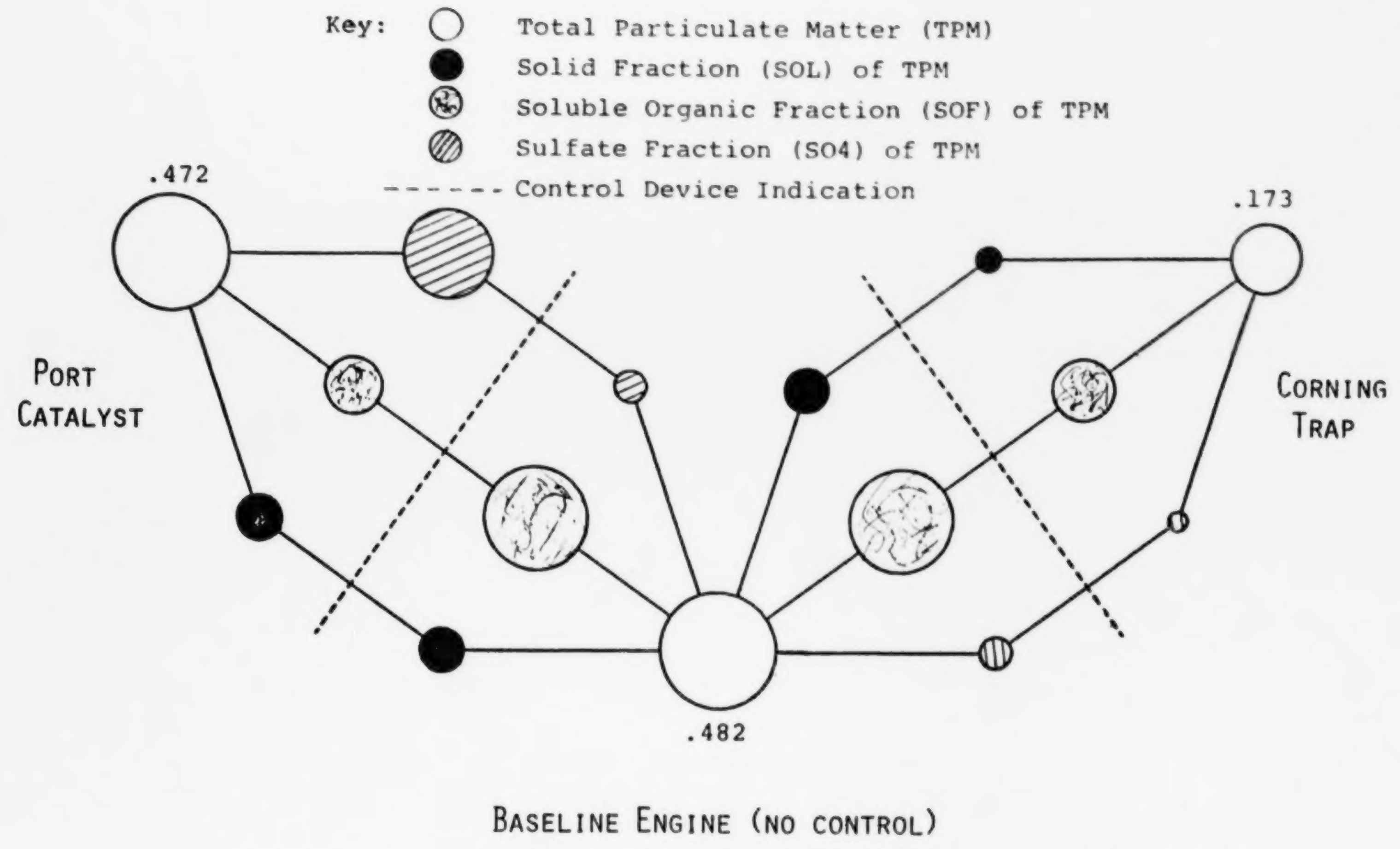
Key:
○ Total Particulate Matter (TPM)
● Solid Fraction (SOL) of TPM
Soluble Organic Fraction (SOF) of TPM
▨ Sulfate Fraction (SO4) of TPM
------ Control Device Indication
.472
Port Catalyst
.173
Corning Trap
.482
Baseline Engine (no control)

Fig. A2 The Effect of Aftertreatment Devices on Caterpillar 3208 Particulate Emissions: Johnson-Matthey Close-Coupled Exhaust Port Catalysts and Corning Ceramic Traps. EPA Mode 4 (1680 rpm and 50% load = 320 N-m)
(numbers indicate bsTPM in g/kW-hr)

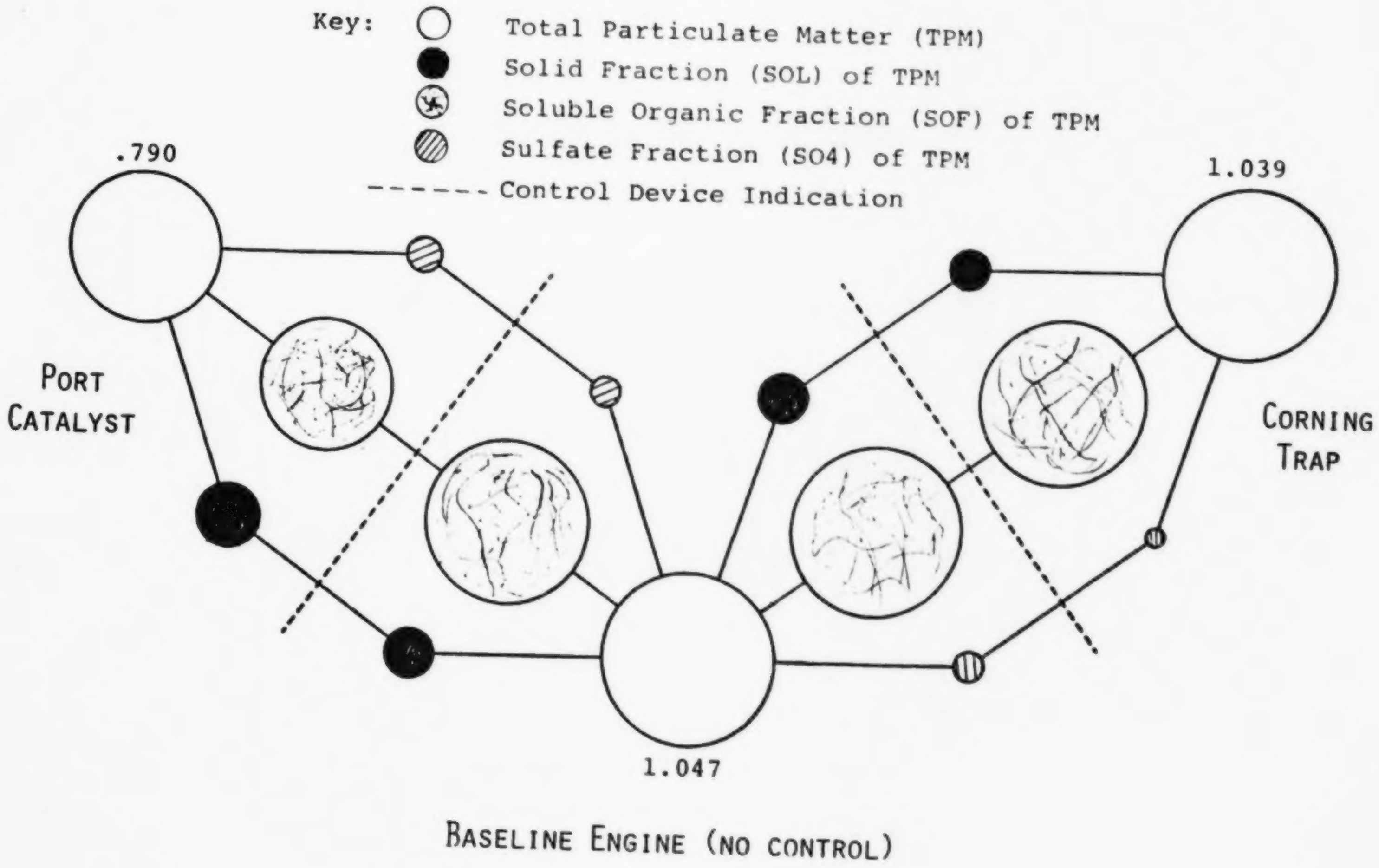
Key:
○ Total Particulate Matter (TPM)
● Solid Fraction (SOL) of TPM
Soluble Organic Fraction (SOF) of TPM
▨ Sulfate Fraction (SO4) of TPM
------ Control Device Indication
.790
Port Catalyst
1.039
Corning Trap
1.047
Baseline Engine (no control)

Fig. A1 The Effect of Aftertreatment Devices on Caterpillar 3208 Particulate Emissions: Johnson-Matthey Close-Coupled Exhaust Port Catalysts and Corning Ceramic Traps. EPA Mode 3 (1680 rpm and 25% load = 160 N-m) (numbers indicate bsTPM in g/kW-hr)

APPENDIX B

AMES BIOASSAY VARIABILITY AND DATA QUANTIFICATION

Sensitivity Analysis Experiments

Preliminary research in this laboratory has shown that a number of system variables can influence the Ames bioassay dose-response curve of a sample. The observed dose-response curve, as depicted in Figure B1.1, is influenced by many variables in addition to the sample concentration. Although a nominal value of 10^8 cells is used on each plate, this value is influenced by harvesting time, incubation temperature, medium variability, and strain idiosyncrasies. Small variations in nutrient levels may cause wide variability in bacteria capable of reverting. Space restrictions on the Petri plate limit the number of colonies; resolution of automatic colony counters is well below the saturation point of the agar surface. For meaningful laboratory or sample comparisons, these system variables must be considered and controlled.

A series of pilot experiments was performed to enable us to construct a model delineating the interactions of Ames test variables including initial cell concentration, histidine concentration, and presence of trace histidine from overnight growth broth. Although these experiments were performed without rigid statistical analysis and offer no proof of any theories set forth in this section, the data are still valuable, as they comprise a solid base from which a model of the Ames system can be obtained.

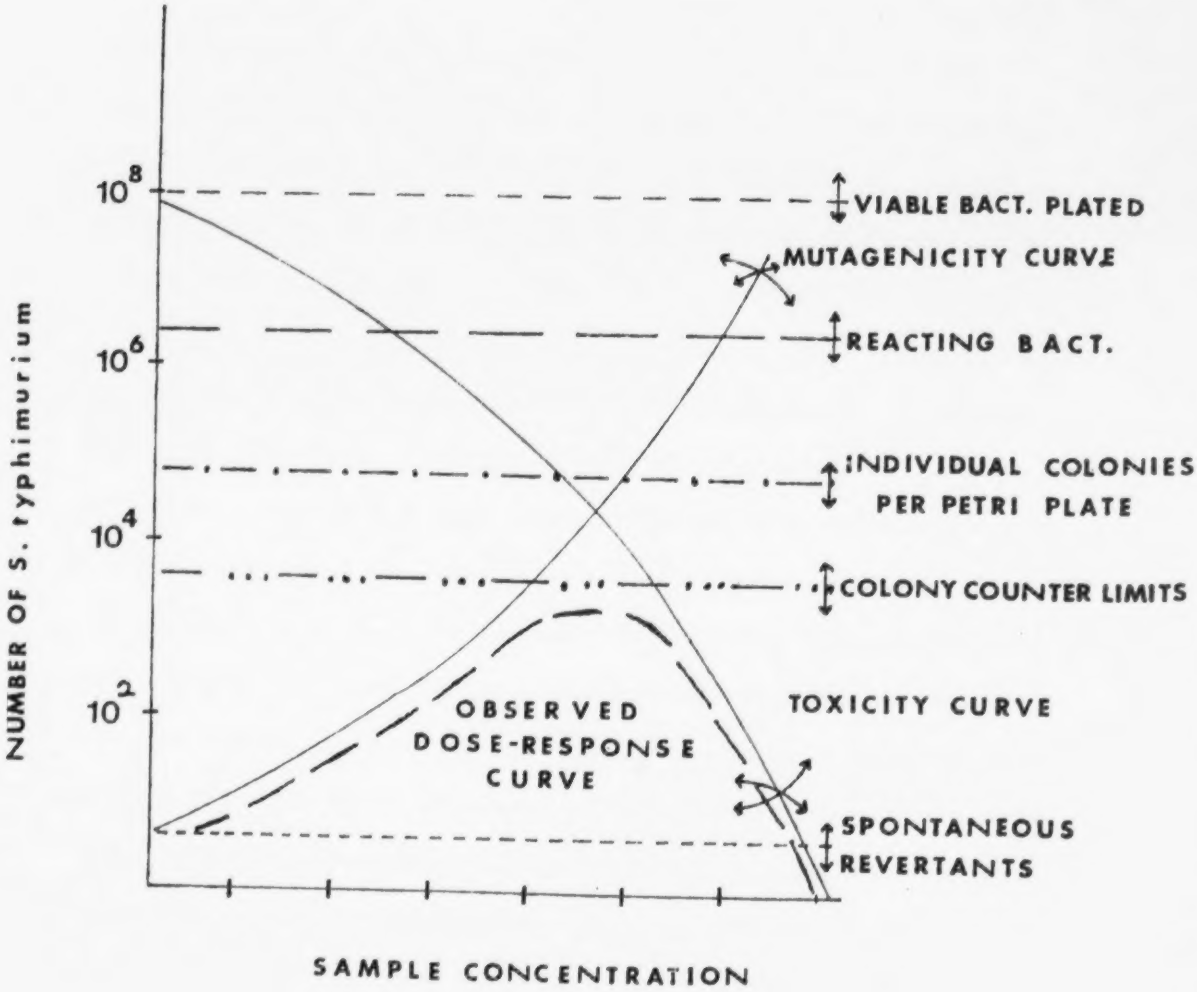

Figure B1.1 Theoretical relationships between Ames test system variables.

The Ames genotypic strain TA98, a frame-shift mutagen indicator, was used in these experiments. The standard Ames plate incorporation assay (50) as modified by Belser et al. (51) was followed. A direct-acting, known frameshift mutagen, 2-nitrofluorene (2-NF) was used as the test compound, without S-9 mammalian microsomal activation. The spontaneous mutation rate was estimated without addition of 2-NF. For determining the influence of residual histidine in the overnight growth broth, cells were washed and resuspended in sterile 0.001 M tris-(hydroxy methyl) amino methane buffer (Tris) at pH 7. This was accomplished by centrifuging the growth broth, discarding the supernate, and resuspending the cells in Tris. This procedure was repeated three times.

Figure B1.2 shows the effects of cell washing and initial cell and histidine concentration on the number of spontaneous revertants per plate. Unless exogenous histidine was added washed cells did not spontaneously revert with cell inocula between 10^2 and 10^6 cells. With 10^7 cells, one spontaneous revertant formed, and with 10^8 cells, two spontaneous revertants formed. Washed cells responded similarly to unwashed cells when exogenous histidine was added.

Figure B1.2 also shows the dependence of spontaneous revertants/plate on cell density and exogenous histidine concentration. Histidine remaining in the overnight growth broth allowed 10^2 but not 10^3 cells to grow into countable colonies, and 0.5mM histidine allowed growth of 10^3 cells into countable colonies. Due to colony counter limitations, the number of cells counted with 10^4 cells/plate was deceptive. At all three histidine concentrations, there were visible colonies too small to be detected by the colony counter. The histidine

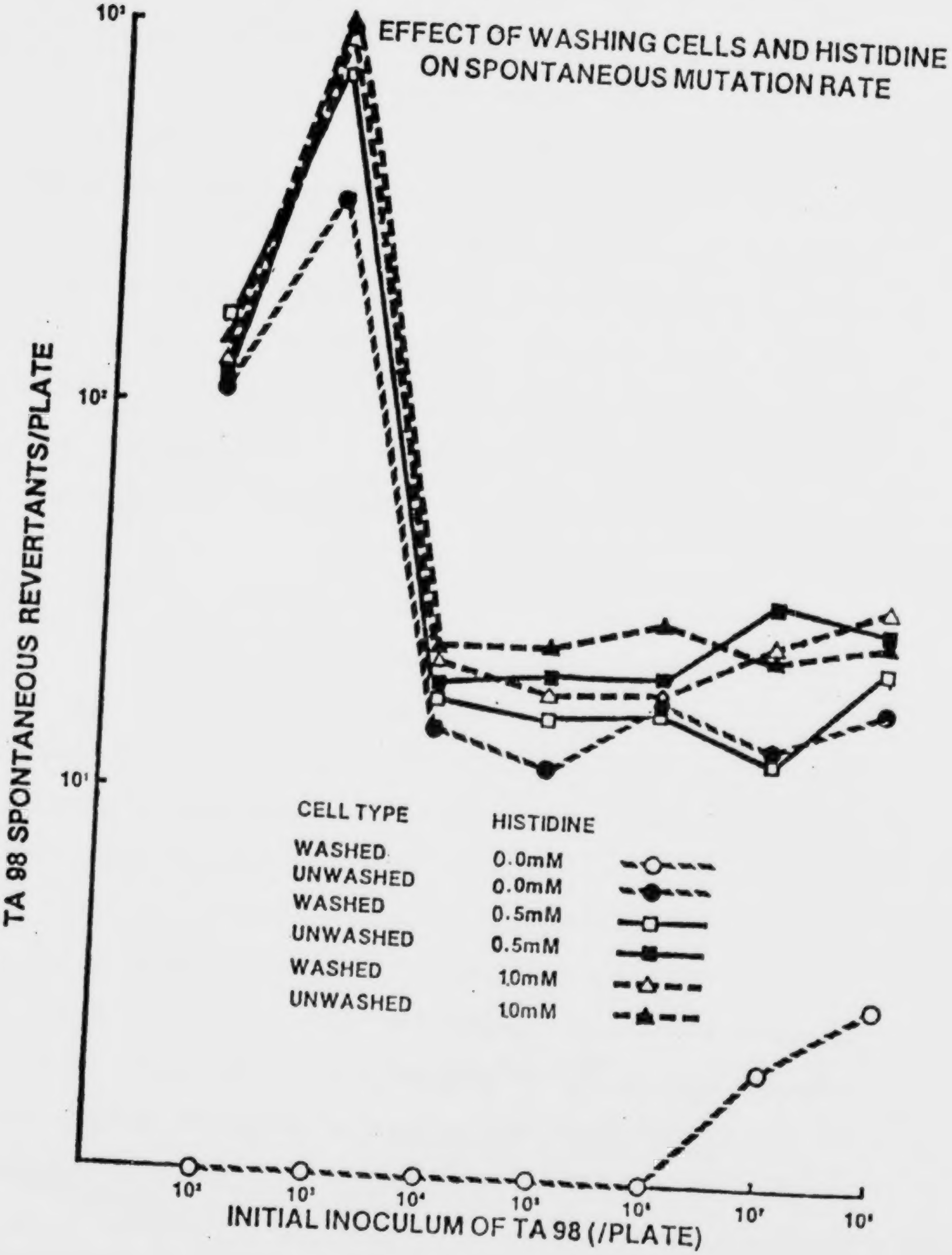

Fig. B1.2 SYSTEM VARIABLES INFLUENCING AMES DATA

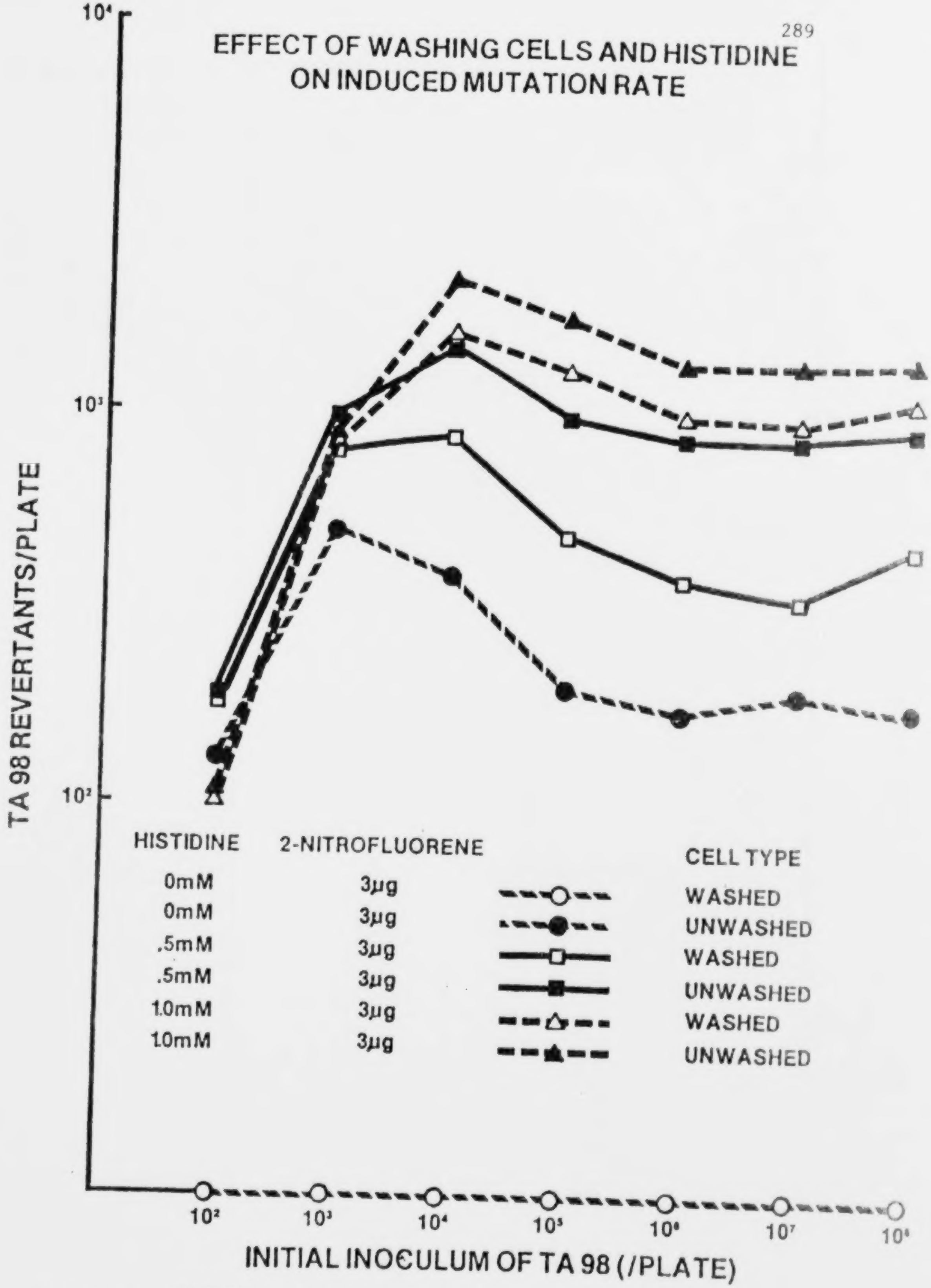

Fig. B1.3 SYSTEM VARIABLES INFLUENCING AMES DATA

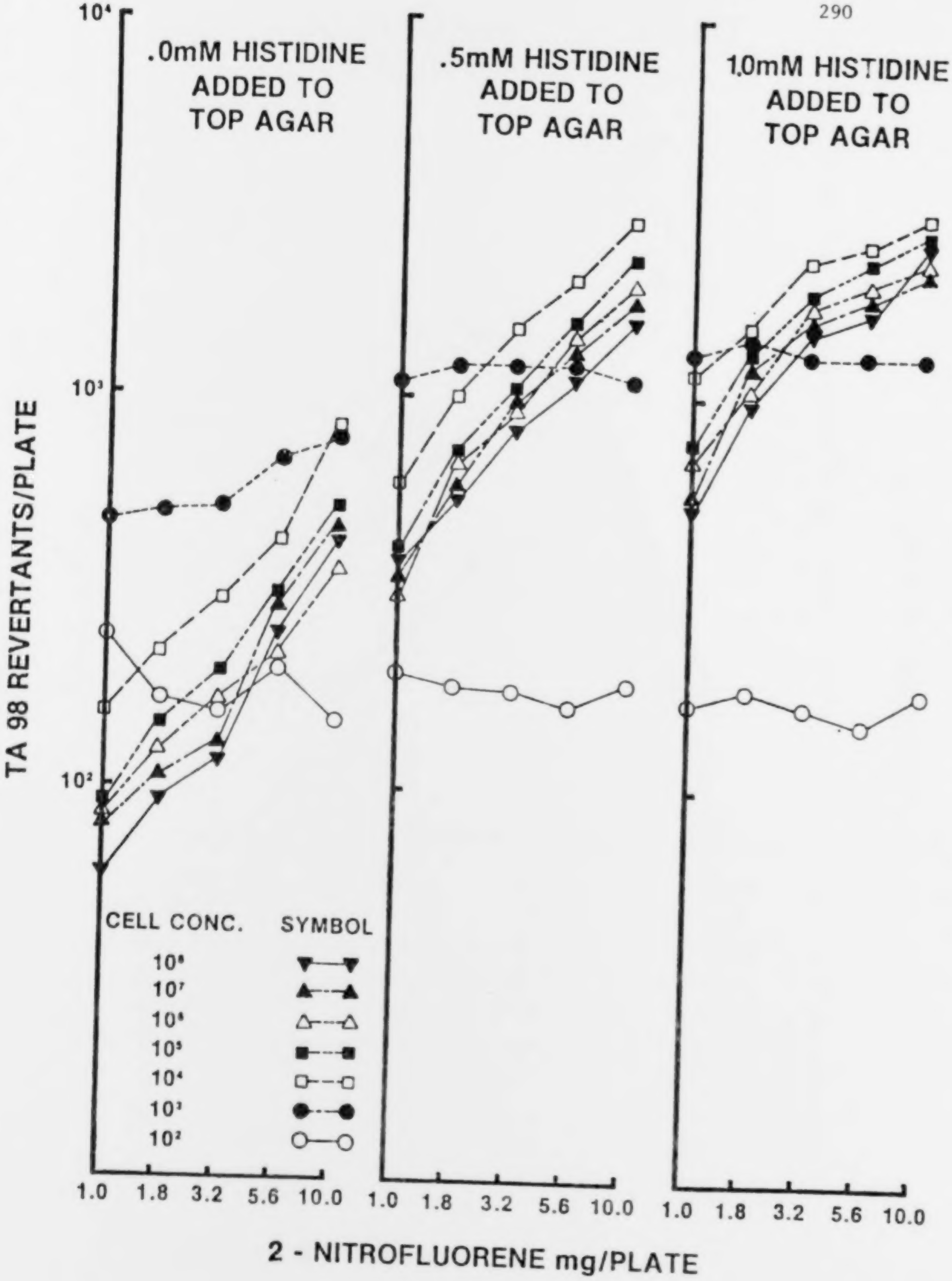

Fig. B1.4 Influence of histidine and cell concentration.

concentration limited the number of spontaneous revertants between 10^4 and 10^8 cells/inoculum. Varying the histidine concentration affected the number of revertants within a cell concentration, but the number of revertants remained constant between concentrations. This supports the thesis that a given histidine level allows a constant fraction of cells to grow and be counted as spontaneous revertants above 10^4 cells/inoculum.

Figure B1.3 shows the effects of cell washing, histidine concentration, and cell concentration on the induced revertant rate of TA98 with 3μg/plate of 2-NF. Washed cells showed no revertants at any concentration, indicated that the cellular DNA must be replicating (with the histidine) before 2-NF can be effective. The influence of washing and histidine concentration is more pronounced with induced mutations than with spontaneous mutations.

Figure B1.4 shows the effect of histidine and initial cell inoculum concentration of the dose-response curve of TA98 to 2-NF. Increasing histidine concentration changes the y-intercept of the curves but has little effect upon their slopes. Colony counter limitations make the slopes of the 1.0mM histidine curves appear lower at high 2-NF concentrations. From 10^4 to 10^8 cells/inoculum, dose curves showed a higher y-intercept for lower cell concentration. This indicates that at lower inoculum concentration there was more histidine and sample per bacterium, allowing a greater opportunity for reversion.

The model derived from these results is not yet complete, but can be described by:

$$\text{Log (Revertants)} = a + b1 \times (\text{Wash}) + b2 \times (\text{Hist } .5) + b3 \times (\text{Hist } 1.) + b4 \times (10^2 \text{ cells}) +$$

$$b5 \times (10^3 \text{ cells}) + b6 \times (10^4 \text{ cells}) +$$
$$b7 \times (10^5 \text{ cells}) + b8 \times (10^6 \text{ cells}) +$$
$$b9 \times (10^7 \text{ cells}) + b10 \times (10^8 \text{ cells}) + \text{error}.$$

This model utilizes the variables Wash, Hist .5, Hist 1., and seven cell concentrations as indicator variables with values of 1 or 0. The use of indicators allow one to quantify the effect of within-variable changes on the regression sum of squares. For instance, if the cells were not washed and 1.0mM histidine were added to an inoculum of 10^4 cells, the model reduces to

$$\text{Log (Revertants)} = a + b1 \times (\text{Wash}) + (\text{Hist 1.}) + b6 \times (10^4 \text{ cells}) + \text{error}$$

because all the variables were zero, except those specified.

Applying this model to the data of Figure B1.3 shows that washing has little effect on the spontaneous revertant rate of TA98 with addition of exogenous histidine. Raising the histidine concentration had little effect on the histidine regression coefficient; likewise 10^6 to 10^8 cells/inoculum showed insignificant regression coefficients, but significant coefficients resulted from use of 10^3 or 10^4 cells/inoculum, attributable to all the cells growing when histidine was added.

When the model was applied to induced revertant data, the results were quite different. Washing had a greater influence on the level of induced revertants than on the level of spontaneous revertants, and doubling of histidine concentration significantly increased its regression coefficient. The induced revertant data showed that all of the cell concentrations had an equal and significant influence.

This model enables us to conclude that:

1) Washing affects induced revertants more than spontaneous revertants;
2) histidine concentration has a greater affect on induced revertants than on spontaneous revertants; and
3) changes in cell inoculum concentration affect induced revertants more than spontaneous revertants.

Quantification of Ames Data

Originally, the Ames test was developed as a qualitative model for evaluating the mutagenic activity of both pure compounds and complex mixtures. When the link between bacterial mutagenicity and mammalian carcinogenicity was realized, the widespread use of the Ames test made its results useful in the regulatory decision-making process. This placed an increasing emphasis on quantifying Ames test data. Simple positive or negative results were no longer sufficient.

A direct method of dose-response curve quantification is a simple linear regression analysis for calculating the specific activity (SA) of sample, as used by Hunter et al. (31) and Campbell et al. (81).

Analysis of the dose-response curve was done as follows:

1) Statistically determine the curve fit for the dose-response data by least squares;

$$R = a + b\ (\log_{10} C)$$

where R = Number of revertants/plate;
C = Dose concentration (μg), and
a and b are determined statistically

2) the slope at any point is given by:

$$\frac{dR}{dC} = \frac{1}{\ln 10} \left(\frac{b}{C}\right)$$

3) the average slope of the dose-response curve in Cartesian coordinates is found from:

$$\overline{\frac{dR}{dC}} = \frac{\int_{C_1}^{C_2} \frac{dR}{dC} dC}{C_2 - C_1} = \frac{b}{C_2 - C_1} \log_{10} \frac{C_2}{C_1}$$

where C_1 = minimum dose (μg) observed on linear portion of dose-response curve and

C_2 = maximum dose (μg) observed on linear portion of dose-response curve; and

4) the value $\overline{\frac{dR}{dC}}$ is then the SA_{SL} (specific activity) of the dose-response curve, in semi-log coordinates.

The brake-specific revertants are obtained by taking brake-specific SOF (rate of SOF emissions per rate of work done by engine) and multiplying this by SA_{SL}:

$$\text{bsREV} = \frac{dR}{dC} \times \text{bsSOF} \times 10^6 \left(\frac{\mu g}{g}\right)$$

This linear regression method suffers from the inability to consistently choose a linear portion of the dose curve, and some data are always discarded.

Stead et al. (82) and Myers et al. (83) used non-linear regression techniques to quantify Ames data. This method offers no bias in choosing a linear portion of the dose curve, and little data are discarded. However, when the functional relationship between variables is not known, a non-linear analysis gives confusing and misleading results. There is also no assurance that the calculated parameters are the best estimates of the population parameters. For this reason, simple linear regression methods should be preferred if certain statistical assumptions can be met (84):

1) The independent variable, X (dosage for Ames data), is measured without error;
2) For any given value of X, corresponding Y values are independent and normally distributed;
3) Independent variable values are not autocorrelated;
4) The variance around the regression line is constant and independent of the magnitude of X and Y;
5) There are no extraneous variables which influence the relationship between X and Y; and
6) The expected value for the dependent variable, Y (revertants/plate for Ames data), is described by the linear function:

$$Y = a + bX$$

Unfortunately, none of these assumptions is rigorously met for data obtained from the Ames test as implemented at MTU and elsewhere (85). A transformation of the data, however, may enable some of these assumptions to be met. Additionally, if a statistically sound method for determining the beginning and ending of a dose-response curve's mutagenic region is utilized, simple linear regression may be useful in Ames data quantification.

A linear regression analysis provides a regression coefficient which describes the "goodness of fit" of the observed data to a calculated regression line. In addition, an analysis of variance table provides sum of squares data known as the residual, or unexplained, sum of squares:

Source of Variation	degrees of freedom	sum of Squares	mean square
Total			
Regression			
Residual			
Within Groups			
Deviation from Linearity			

The residual (unexplained) sum of squares is divided into within-group sum of squares (true experimental deviation of the data) and deviation from linearity sum of squares (bias of the regression from a simple linear model).

In addition to a non-transformed linear dose-revertant model, two transformations of this model (y = a + bX) were examined for within-group and deviation from linearity sum of squares as well as y-intercept and slope variability. The other transformations of this model were the log dose-revertant transformation (colonies/plate regressed on the common logarithm of concentration/plate) and the log dose-log revertant transformation (common logarithm of colonies/plate regressed on common logarithm of concentration/plate). Tables B1.1 thru B1.4 of this appendix display the four aforementioned regression statistics for every combination of three or more doses. The dose-revertant model and its log dose-revertant, and log dose-log revertant transformations are compared for data obtained with TA-98 and 2-NF assayed on July 8, 1981.

Tables B1.1 and B1.2 show that, given three or more doses, the slope and y-intercept is most stable if the log dose-log revertant transformation is used. Perhaps more importantly, Tables B1.3 and B1.4 show that the log dose-log revertant transformation offers the lowest variation in both the sum of squares due to deviation from linearity, and that due to random error in the data. Minimization of the deviation from linearity sum of squares helps satisfy statistical assumption number 4 pertaining to data subjected to linear regression analysis, which asserts that the variance around the regression line should be constant and independent of the magnitude of X and Y. Minimization of the random error sum of squares gives a regression line that is less sensitive to variation in choosing minimum and maximum doses on the mutagenic portion of the dose-response curve. This eliminates much of the bias in estimating the beginning of mutagenicity and the beginning of toxicity; however, a sound statistical method should be employed to choose these points consistently.

Table B1.1 Comparison of the slopes from the three Linear models describing Ames data collected on July 8, 1982.

LOG DOSE - LOG REVERTANT MODEL

MIN. DOSE (μg)	MAX. DOSE (μg)							
	.56	1.0	1.8	3.2	5.6	10.	18.	32.
10.								.0139
5.6							.4822	.2671
3.2						.6979	.5430	.3776
1.8					.9261	.8567	.6990	.5355
1.0				.9272	.8595	.8359	.7299	.5999
.56			.6235	.8102	.8033	.8025	.7317	.6303
.32		.8639	.7614	.8413	.8276	.8210	.7617	.6743
.18	.9088	.8464	.7839	.8347	.8260	.8212	.7737	.6999

LOG DOSE - REVERTANT MODEL

MIN. DOSE (μg)	MAX. DOSE (μg)							
	.56	1.0	1.8	3.2	5.6	10.	18.	32.
10.								57.
5.6							1446.	785.
3.2						1721.	1433.	992.
1.8					1267.	1570.	1429.	1114.
1.0				912.	1018.	1301.	1279.	1081.
.56			355.	678.	825.	1081.	1120.	1002.
.32		302.	336.	560.	698.	923.	989.	920.
.18	214.	249.	289.	463.	591.	790.	869.	835.

DOSE - REVERTANT MODEL

MIN. DOSE (μg)	MAX. DOSE (μg)							
	.56	1.0	1.8	3.2	5.6	10.	18.	32.
10.								5.
5.6							54.	17.
3.2						126.	67.	27.
1.8					159.	140.	81.	37.
1.0				215.	163.	145.	88.	43.
.56			144.	203.	165.	147.	93.	47.
.32		214.	165.	204.	169.	150.	97.	51.
.18	282.	223.	175.	204.	172.	152.	100.	53.

Table B1.2 Comparison of the Y-intercepts from the three Linear models describing Ames data collected on July 8, 1981.

LOG DOSE - LOG REVERTANT MODEL

MIN. DOSE (µg)	MAX. DOSE (µg)							
	.56	1.0	1.8	3.2	5.6	10.	18.	32.
10.								3.174
5.6							2.170	2.582
3.2						1.784	2.043	2.333
1.8					1.395	1.493	1.731	1.990
1.0				1.421	1.500	1.530	1.671	1.856
.56			1.749	1.578	1.585	1.585	1.668	1.795
.32		1.530	1.599	1.539	1.550	1.556	1.616	1.710
.18	1.518	1.545	1.576	1.546	1.552	1.556	1.596	1.663

LOG DOSE - REVERTANT MODEL

MIN. DOSE (µg)	MAX. DOSE (µg)							
	.56	1.0	1.8	3.2	5.6	10.	18.	32.
10.								1482.
5.6							-1487.	-221.
3.2						-1940.	-1460.	-686.
1.8					-1233.	-1664.	-1452.	-951.
1.0				-716.	-840.	-1194.	-1165.	-883.
.56			-107.	-402.	-549.	-827.	-872.	-724.
.32		-63.	-86.	-254.	-370.	-576.	-642.	-567.
.18	-4.	-18.	-39.	-141.	-227.	-376.	-443.	-411.

DOSE - REVERTANT MODEL

MIN. DOSE (µg)	MAX. DOSE (µg)							
	.56	1.0	1.8	3.2	5.6	10.	18.	32.
10.								1608.
5.6							798.	1167.
3.2						284.	612.	923.
1.8					111.	168.	430.	707.
1.0				-2.	89.	135.	337.	572.
.56			88.	29.	81.	117.	277.	479.
.32		30.	57.	27.	66.	97.	230.	406.
.18	4.	23.	44.	25.	56.	83.	196.	352.

Table B1.3 Comparison of the deviation from Linearity sum of squares for Ames data collected on July 8, 1982.

LOG DOSE - LOG REVERTANT MODEL

MAX. DOSE (μg)

		.56	1.0	1.8	3.2	5.6	10.	18.	32.
	10.								.0027
	5.6							.0137	.0436
	3.2						.0017	.0162	.0674
MIN.	1.8					.0142	.0171	.0622	.1780
DOSE	1.0				.0138	.0168	.0179	.0663	.2140
(μg)	.56			.0001	.0226	.0227	.0227	.0664	.2286
	.32		.0062	.0125	.0245	.0253	.0257	.0806	.2801
	.18	.0040	.0063	.0135	.0247	.0253	.0257	.0844	.3073

LOG DOSE - REVERTANT MODEL

MAX. DOSE (μg)

		.56	1.0	1.8	3.2	5.6	10.	18.	32.
	10.								38281
	5.6							94470	376747
	3.2						44777	94580	459602
MIN.	1.8					3203	58664	94613	525655
DOSE	1.0				32749	40074	189769	191872	534986
(μg)	.56			433	67742	109618	399508	412859	634165
	.32		4	677	94752	179995	619826	687636	810818
	.18	1049	1774	4772	136129	280562	898293	1062860	1111451

DOSE - REVERTANT MODEL

MAX. DOSE (μg)

		.56	1.0	1.8	3.2	5.6	10.	18.	32.
	10.								39503
	5.6							200988	606642
	3.2						2017	304343	1091694
MIN.	1.8					31252	40366	574505	1900261
DOSE.	1.0				7635	32525	49002	726370	2470475
(μg)	.56			227	10533	33018	54572	836463	2913128
	.32		956	3070	10582	37190	67204	949273	3318391
	.18	133	1095	4533	10639	40372	77403	1037988	3642705

Table B1.4 Comparison of the random error of the three models describing Ames data collected on July 8, 1981.

LOG DOSE - LOG REVERTANT MODEL

		MAX. DOSE (µg)							
		.56	1.0	1.8	3.2	5.6	10.	18.	32.
	10.								.0042
	5.6							.0019	.0046
	3.2						.0010	.0022	.0049
MIN.	1.8					.0183	.0186	.0198	.0225
DOSE	1.0				.0221	.0225	.0228	.0239	.0267
(µg)	.56			.0245	.0248	.0252	.0255	.0267	.0294
	.32		.0104	.0281	.0284	.0288	.0291	.0302	.0329
	.18	.0076	.0118	.0294	.0297	.0301	.0304	.0316	.0343

LOG DOSE - REVERTANT MODEL

		MAX. DOSE (µg)							
		.56	1.0	1.8	3.2	5.6	10.	18.	32.
	10.								59181.
	5.6							23755.	61197.
	3.2						6541.	24575.	62018.
MIN.	1.8					12931.	16635.	34669.	72112.
DOSE	1.0				12165.	14181.	17885.	35920.	73363.
(µg)	.56			11747.	12567.	14583.	18287.	36322.	73765.
	.32		1799.	11893.	12713.	14729.	18433.	36468.	73911.
	.18	573.	1823.	11917.	12738.	14754.	18459.	36493.	73936.

DOSE - REVERTANT MODEL

		MAX. DOSE (µg)							
		.56	1.0	1.8	3.2	5.6	10.	18.	32.
	10.								59181.
	5.6							23755.	61197.
	3.2						6541.	24575.	62018.
MIN.	1.8					12931.	16635.	34669.	72112.
DOSE	1.0				12165.	14181.	17885.	35920.	73363.
(µg)	.56			11747.	12567.	14583.	18287.	36322.	73765.
	.32		1799.	11893.	12713.	14729.	18433.	36468.	73911.
	.18	573.	1823.	11917.	12738.	14754.	18458.	36493.	73936.

The Student-Newman-Keuls (S-N-K) multiple comparison test (86) was applied to the data examined in Tables B1.1 through B1.4, and six doses were obtained which were neither significantly non-mutagenic nor toxic. Figure B1.5 shows the log-log transform of the dose-response curve of this data and that from the same test compound and bacterial strain assayed on eight other dates. Figure B1.6 shows the linear portion of eight of these curves, after applying the S-N-K multiple comparison test to obtain the linear region.

To obtain an unbiased estimate of any sample's regression coefficient, the data from several dates should be pooled after eliminating any statistically significant outliers. An analysis of covariance ($\alpha = 0.05$) performed on the dose-response curves of Figure B1.5 showed that the slopes of all these curves were not statistically different, while the y-intercepts for all curves except that obtained from the March 16, 1982 data, were not statistically different.

To demonstrate blocking of assay dates using diesel SOF samples, two samples were analyzed simultaneously on four different dates. Figure B1.7 shows the dose-response curve of these samples in log-log format; sample 4-B is the SOF from the baseline Caterpillar 3208 engine without exhaust aftertreatment, while sample 4-P is SOF from the same engine with Johnson-Matthey close-coupled port catalysts installed. To choose the mutagenic section of each curve, the S-N-K test yielded the points between C_1 and C_2, as listed in Table B1.5.

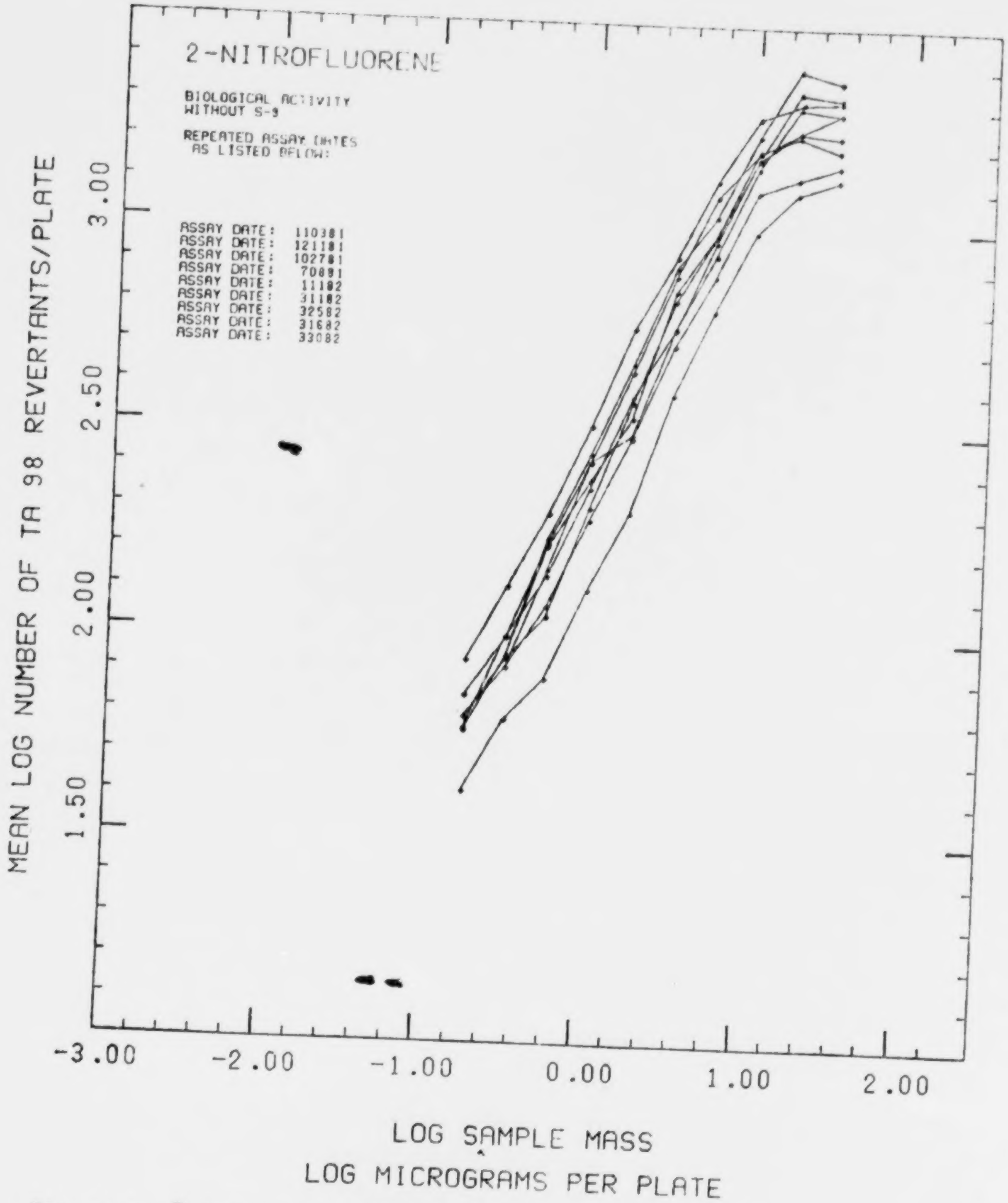

Fig. B1.5 **2-NF Dose-Response Curve with TA 98.**

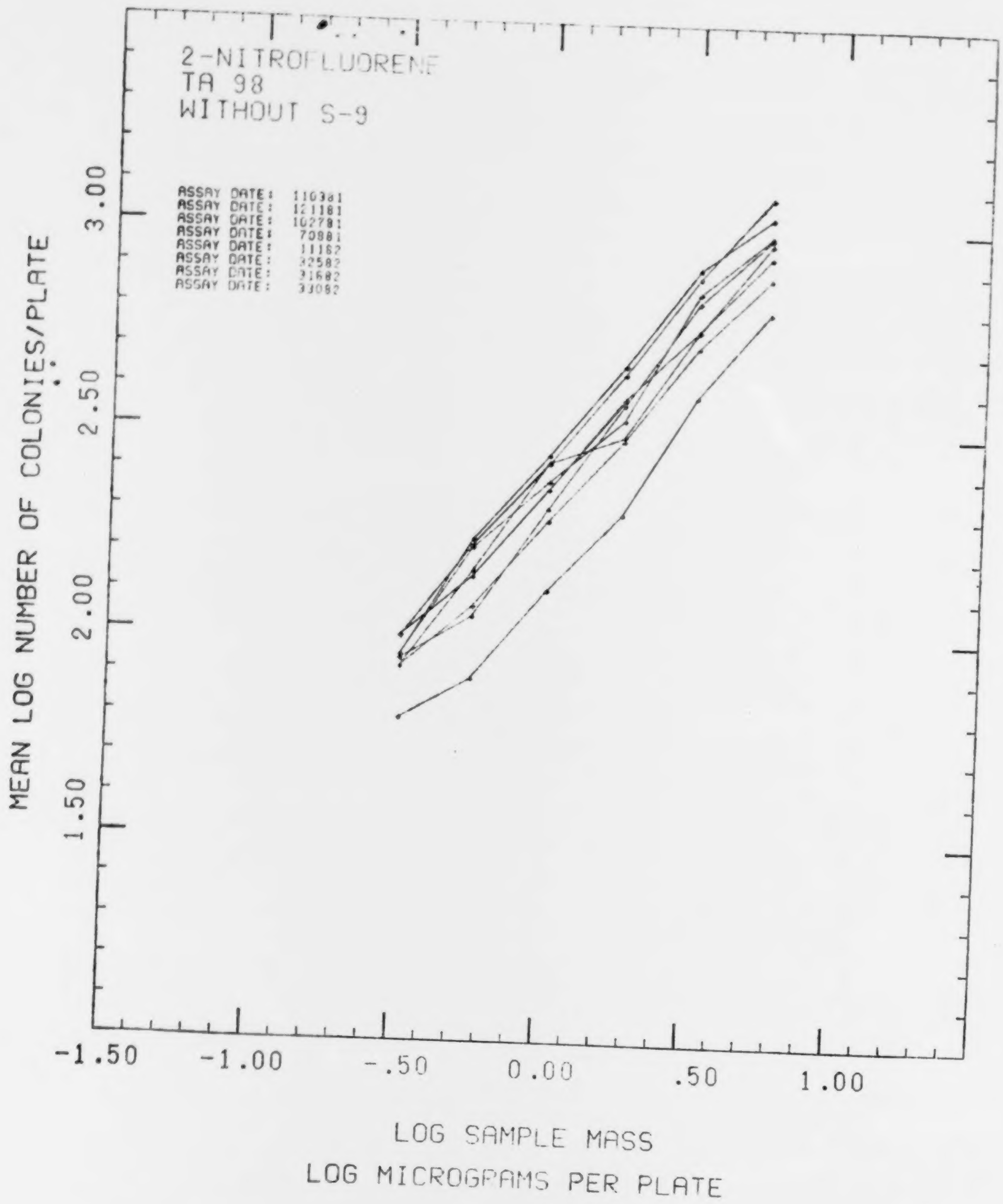

Fig. B1.6 **Linear section of 2-NF curve.**

Table B1.5: Summary Statistics of Dose-Response curves for Samples 4-B and 4-P chosen by the Student-Newman-Keuls test with an alpha level of 0.001

Sample	Degrees of freedom	C_1	C_2	a	σ_a	$\%C_{va}$	b	σ_b	$\%C_{vb}$
4-P	18	37.5	1200	0.5779	0.0559	9.677	0.7862	0.0235	2.99
4-B	15	75	1200	0.3484	0.0719	20.61	0.7312	0.0285	3.90

The slopes (b-values) in this table appear to be similar and have low variability, while y-intercepts (a-values) seem quite different, despite their relatively higher variabilities. To test the equality or non-equality of both values, an analysis of covariance was performed by calculating a t-statistic for each group of data (87). Comparison of the calculated t-statistic with the critical t-value for slope and y-intercept showed that slopes, but not y-intercepts, were equal at the 0.05 significance level.

In practical terms, this means that the slopes of dose-response curves may have little meaning when the log dose-log revertant transformation of a simple linear model is used. Instead, one could use the y-intercept as a predictor for the dose required to obtain a predefined mutagenic effect, similar to the use of LD-50 values for mortality data. If one chooses the spontaneous revertant level (shown to be stable for constant experimental parameters), one can define the Order of Magnitude Mutagenic Potential (OMMP) dose as the dose level exhibiting a 10-fold increase in mutagenicity over background levels on the regression line described by the dose-response curve. Application of this potential to the data for 4-B and 4-P diesel SOF discussed previously, the value giving ten-fold increase over background revertants with 4-B SOF is 2.806 μg/plate, while the same value for 4-P SOF is 2.318 μg/plate. As seen in Figure B1.7, the leftward shift of the dose-response curve for the catalyzed (4-P) SOF yields a lower figure for the Order of Magnitude Mutagenic Potential.

This OMMP is derived from the y-intercept of the log-dose-log revertant transformation of the linear regression model. Table B1.6 compares the standard SA (semi-log) parameter with the y-intercepts obtained from this log-log transformation for three compounds and nine different assay dates. The coefficient of variation was only slightly better for the 2-NF data, while it was either worse for the y-intercept value (baseline engine SOF) or essentially the same (port catalyst SOF), for diesel SOF samples. The improvement in variability expected by using the OMMP was not realized; so a closer look at the definition of slope was made.

Table B1.6 Ames Data Parameter Comparisons on Repeat Assays, 3 Different Samples, 9 Different Assays Each

Model	$Rev = a + b \log_{10} X$		$\log Rev = a + b \log_{10} X$ or $Rev = 10^a * X^b$	
Characteristic Activity Parameter	$SA = \frac{b}{C_2 - C_1} \ell og \frac{C_2}{C_1}$		10^a	
	mean	C.V.,%	mean	C.V.,%
2-NF	89.6	32	221	25
Baseline Engine	0.211	33	5.28	42
Port Catalyst	1.513	40	8.71	39

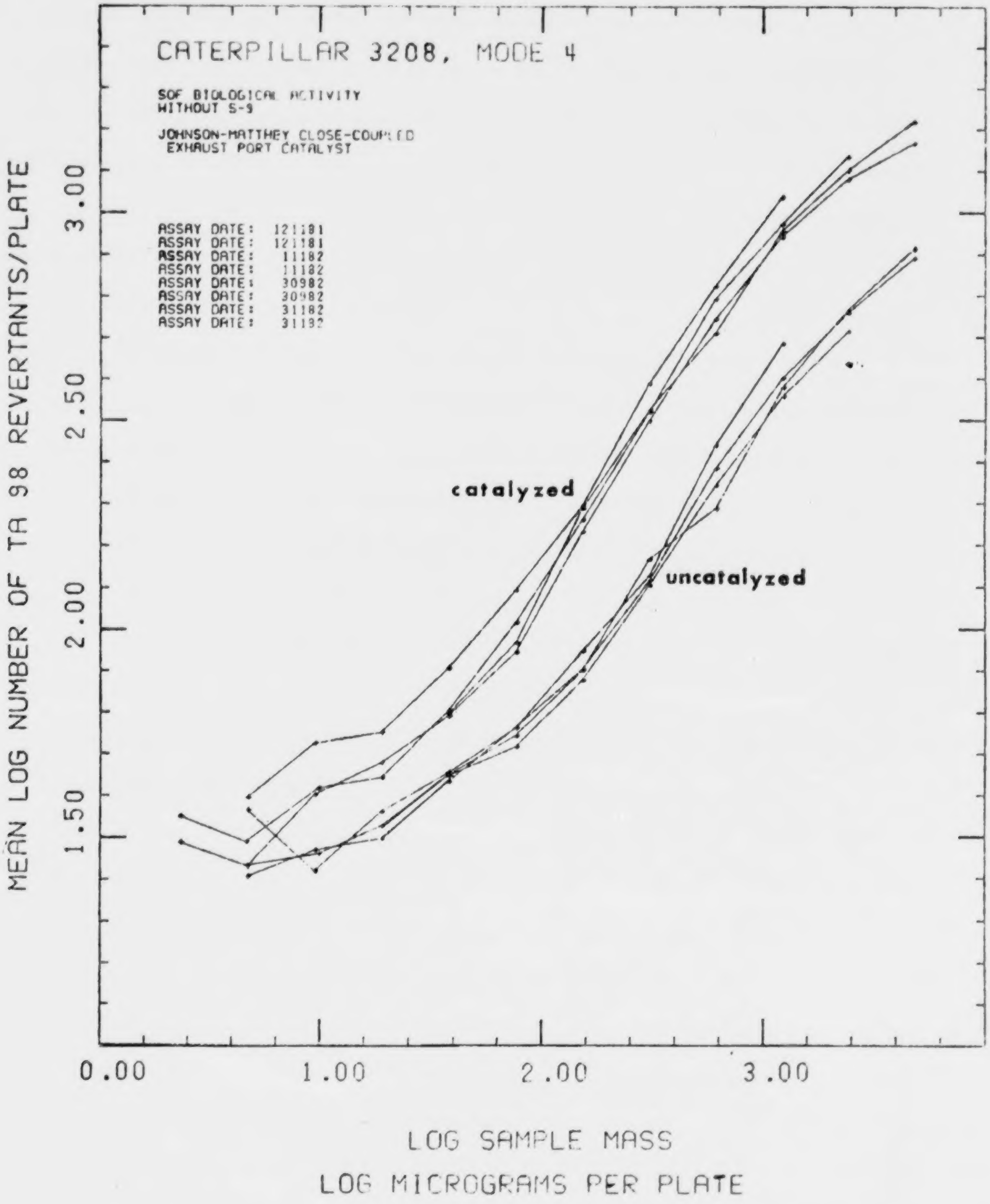

Fig. B1.7 **Two diesel SOF samples assayed on four dates.**

Figure B1.8 shows the wide variety of values for specific activity obtainable from one assay depending upon the units of dose range chosen; this demonstrates the sensitivity of an assay to non-uniform dose ranges. The S-N-K multiple comparison test cannot be effectively utilized for samples not reaching toxicity because of mass limitations, so a uniform dose range may be a more accurate method to use for calculating specific activity. The Caterpillar 3208 data base showed no SOF samples toxic at 600 µg/plate, while 18.75 µg/plate was always into the linear portion of the responding region. Using these values as the C_1 and C_2 values for 4-B and 4-P SOF yielded nearly equal coefficients of variation for SA values (Table B1.7) This shows that the SA figure can be made repeatable if replicate assays demonstrate that major linear portions of different samples' dose-response curves are confined to identical dose levels. This may not always be the case, however. The optimum parameter for measuring a sample's mutagenicity may not be the same for different groups of data.

Table B1.7 Results of 9 Repeat Assays, C_1 = 18.75 µg/pl.
C_2 = 600 µg/pl.

CATERPILLAR 3208, EPA MODE 4

	SA		C.V.
	(rev/µg)	(rev/µg)	(%)
Baseline	0.317	0.041	12.8
Close-Coupled Catalyst	1.028	0.113	11.0

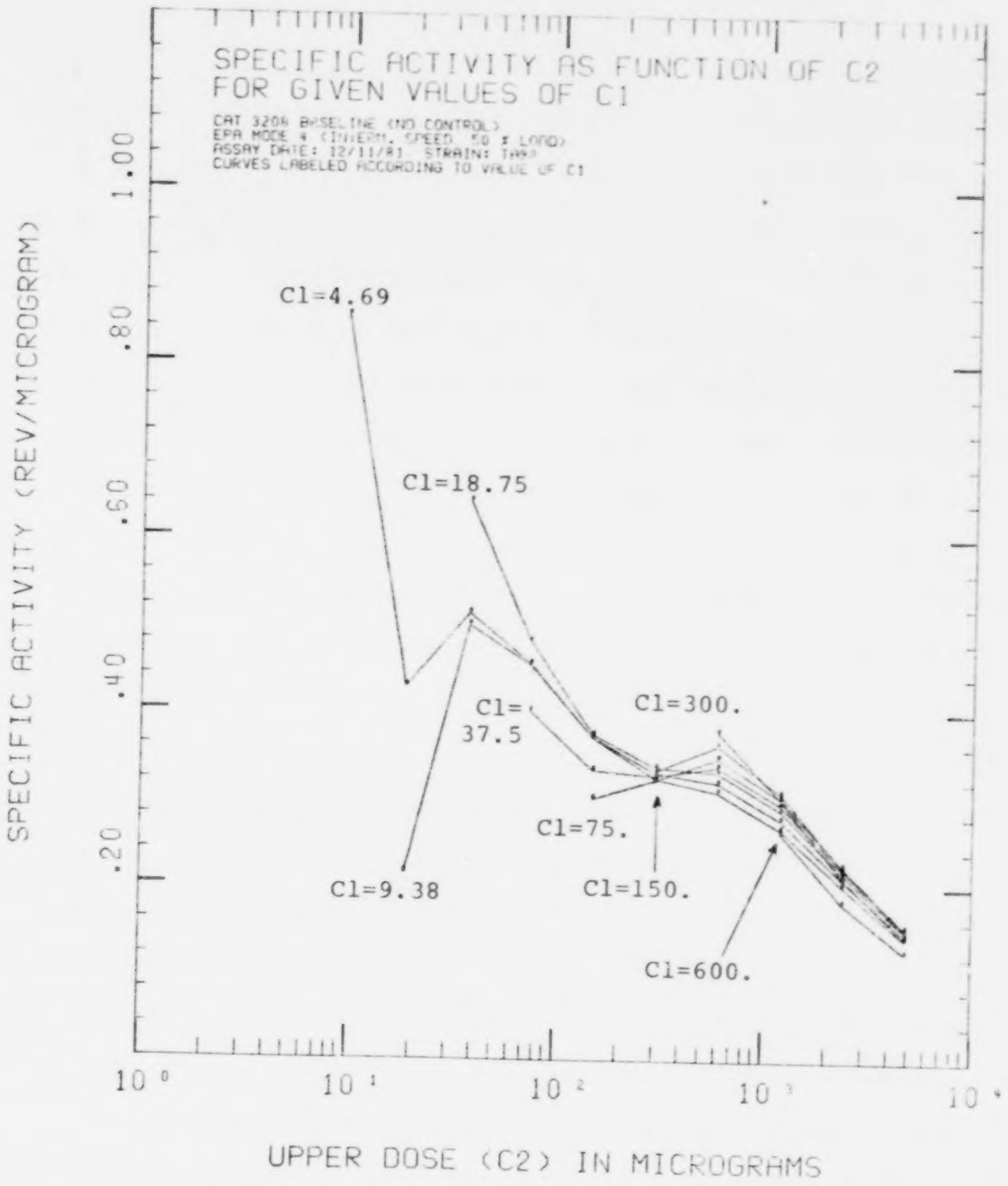

FIG. B1.8 SPECIFIC ACTIVITY AS A FUNCTION OF C2
FOR VARIOUS VALUES OF C1
CAT 3208 BASELINE (NO CONTROL)
EPA MODE 4 (INTERM. SPEED, 50 % LOAD)

It can be concluded that quantification of Ames test data is a very difficult task, mainly due to the complex nature of the interaction between sample and bacteria and also due to the fact that convenient implementation of the Ames test and limitations in counting methodology interfere with many of the statistical assumptions necessary for a reliable data analysis. However, if certain practices are followed, the data are usually amenable to reliable, statistically sound quantification. These practices include the following:

1) Use of the log dose-log revertant transformation of a simple linear regression model, which reduces bias in estimating the regression line.

2) Use of a multiple comparison test such as the Student-Newman-Keuls test, if the sample is sufficiently concentrated to allow demonstration of a toxic effect. This reduces bias in estimating the extremes of mutagenic potential. If toxicity is not reached, use of a uniform dose region for the regression line may give more accurate results for samples with similar activities. Comparison of samples with widely differing activities may not be accurate unless sufficient sample is available to demonstrate toxicity.

3) Use of an SA parameter calculated from the log dose-log revertant transformation of a simple linear model (85, 86), although it may not reduce variability significantly. This transformation can be expressed as a power function, since the equation upon which it is based ($\log_{10}R = a + b \log_{10}C$) is equivalent to $R = 10^a*C^b$, when antilogs of both sides are taken. The advantage of this transformation is the inclusion of the y-intercept in calculation of the specific activity parameter, since slopes of different samples have been shown to be similar, while y-intercepts are quite different. The SA value from this transformation (SA_{LL}) may be calculated as:

$$SA_{LL} = \frac{10^a \, (C_2{}^b - C_1{}^b)}{C_2 - C_1}$$

where a, b, C_1, and C_2 are defined as before and SA_{LL} is the average specific activity (revertants/μg) between C_1 and C_2.

Reproducibility of Ames Data

Intralaboratory and interlaboratory reproducibility is crucial to any attempt to quantify Ames data. The intralaboratory reproducibility of Ames data was examined at MTU by collecting numerous data sets over time, using tester strain TA98. The first data set of TA 98 spontaneous revertants (without S-9 activation) was collected from experiments performed between March 31, 1980 and November 16, 1981. The statistics presented in Table B1.8 confirm that no trends existed over this time period. This indicated the spontaneous background reversion rate of TA 98 was consistent and reproducible throughout this time period. The second data set is the response of TA 98 to 10 μg/plate of 2-NF (without S-9 activiation). These data were collected from various experiments between June 6, 1980 and November 12, 1981. Table B1.9 gives the mean, standard deviation and 98% confidence interval for the response of TA 98 to 10 μg/plate 2-NF over this time period. Since no trends appear in the data, TA 98's response to 10 μg/plate 2-NF is considered to be stable.

Table B1.8 Statistics describing TA 98 spontaneous revertants/plate as a function of time.

TA 98 SPONTANEOUS REVERTANTS/PLATE STATISTICS

THE REGRESSION EQUATION IS

REVERTANTS = 27.8 - .0387 * DATE

R-SQUARED = .6 PERCENT

MEAN NUMBER OF REVERTANTS/PLATE M = 26.971

STD. DEV. = 7.23

90% C.I. IS 26.05 $\leq$ u $\leq$ 27.88

WITH (172- 2) = 170 DEGREES OF FREEDOM

ANALYSIS OF VARIANCE

DUE TO	DF	SS	MS=SS/DF	CALC. F
REGRESSION	1	54.87	54.87	1.05
RESIDUAL	170	8873.98	52.20	
TOTAL	171	8928.85		

F .05(1) 1,170 = 3.84

Table B1.9 Statistics describing revertants/plate induced by 2-NF as a function of time.

INDUCED REVERTANTS/PLATE WITH 10 μg/PLATE 2-NF

THE REGRESSION EQUATION IS

REVERTANTS = 1577. - 3.15 * 2NF CONC

MEAN NUMBER OF REVERTANTS/PLATE M = 1555.6

STD. DEV. = 366.0

R-SQUARED = .1 PERCENT

90% C.I. IS $1504.27 \leq u \leq 1608.69$

WITH (37- 2) = 35 DEGREES OF FREEDOM

ANALYSIS OF VARIANCE

DUE TO	DF	SS	MS=SS/DF	CALC. F
REGRESSION	1	4887	4887	0.036
RESIDUAL	35	4813335	137524	
TOTAL	36	4818222		

F .05(1) 1,35 = 4.13

Interlaboratory variability was assessed at MTU by participation in two sets of round-robin sample analyses with EPA-RTP and EG&G Mason laboratories. Due to lack of dilution instructions for the sample and positive controls in the first round robin, only spontaneous revertants and 2-nitrofluorene induced revertant statistics are available. Although five tester strains were utilized for both round-robins, only the results of strain TA100 will be discussed here.

Figure B1.9 shows the spontaneous revertant rate and Figure B1.10 shows the revertants induced by 3 μg/plate of 2-NF, as assayed in the three laboratories (in both tests). A nested analysis of variance showed that neither set of data demonstrated any significant variability between laboratories, at a 5% alpha level. There were significant differences for different assay dates, at the same 5% alpha level, for spontaneous revertants, but not for mutants induced by 3 μg of 2-NF.

For the second round robin, two diesel SOF samples generated at MTU using the Caterpillar 3208 Engine at mode 4, with and without an oxidation catalyst, were assayed using strain TA100 without S-9 activation. Figure B1.11 shows the dose-response curve in log dose-revertant format. Although statistics were not applied to these data, inspection of the curves shows similar trends. Some of the differences may have been due to differences in automatic colony counter setting with the MTU counter being able to detect smaller and therefore more colonies.

In summary, intralaboratory variability of Ames data was shown to be less than random experimental error while interlaboratory variability was shown to be less than experimental error in most cases. The number of spontaneous revertants varied significantly between assay dates, but not between laboratories. Interlaboratory experimental error was found to be

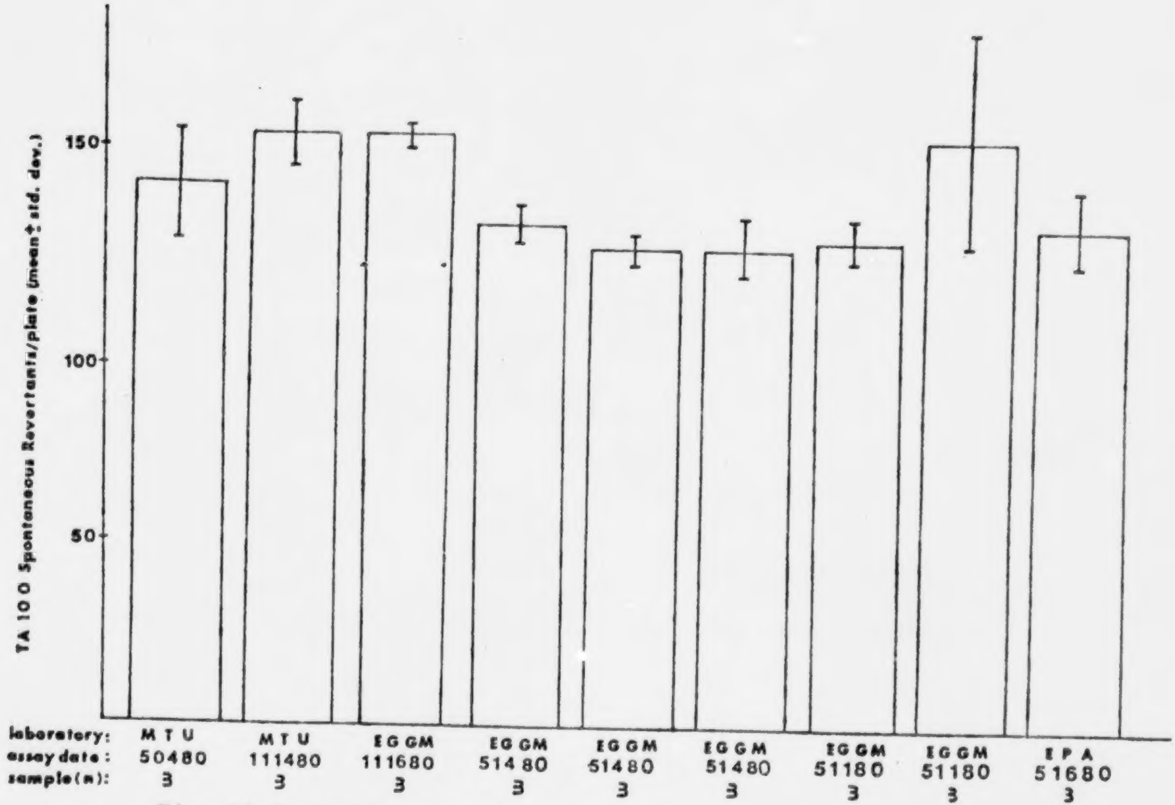

Fig. B1.9 TA 100 Spontaneous Revertants/plate in three Ames laboratories.

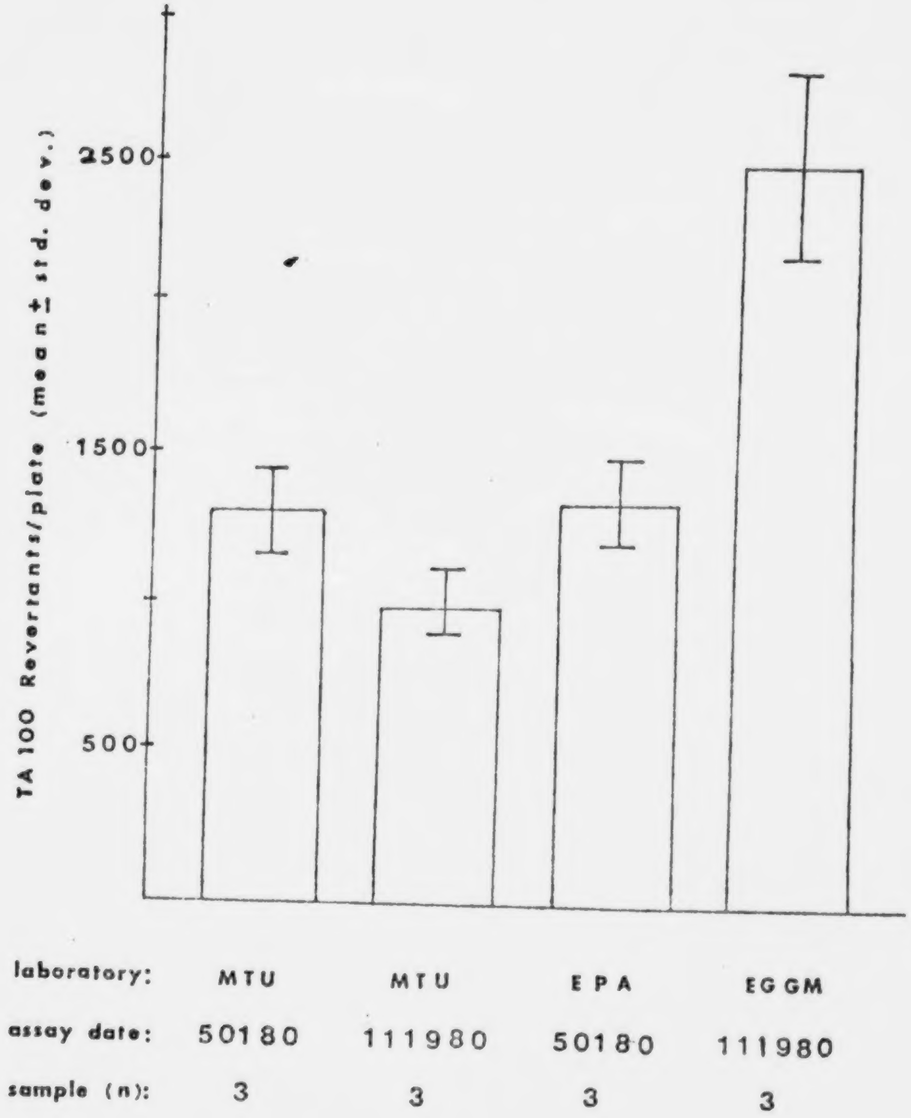

Fig. B1.10 Response of TA 100 to 3μg 2-NF.

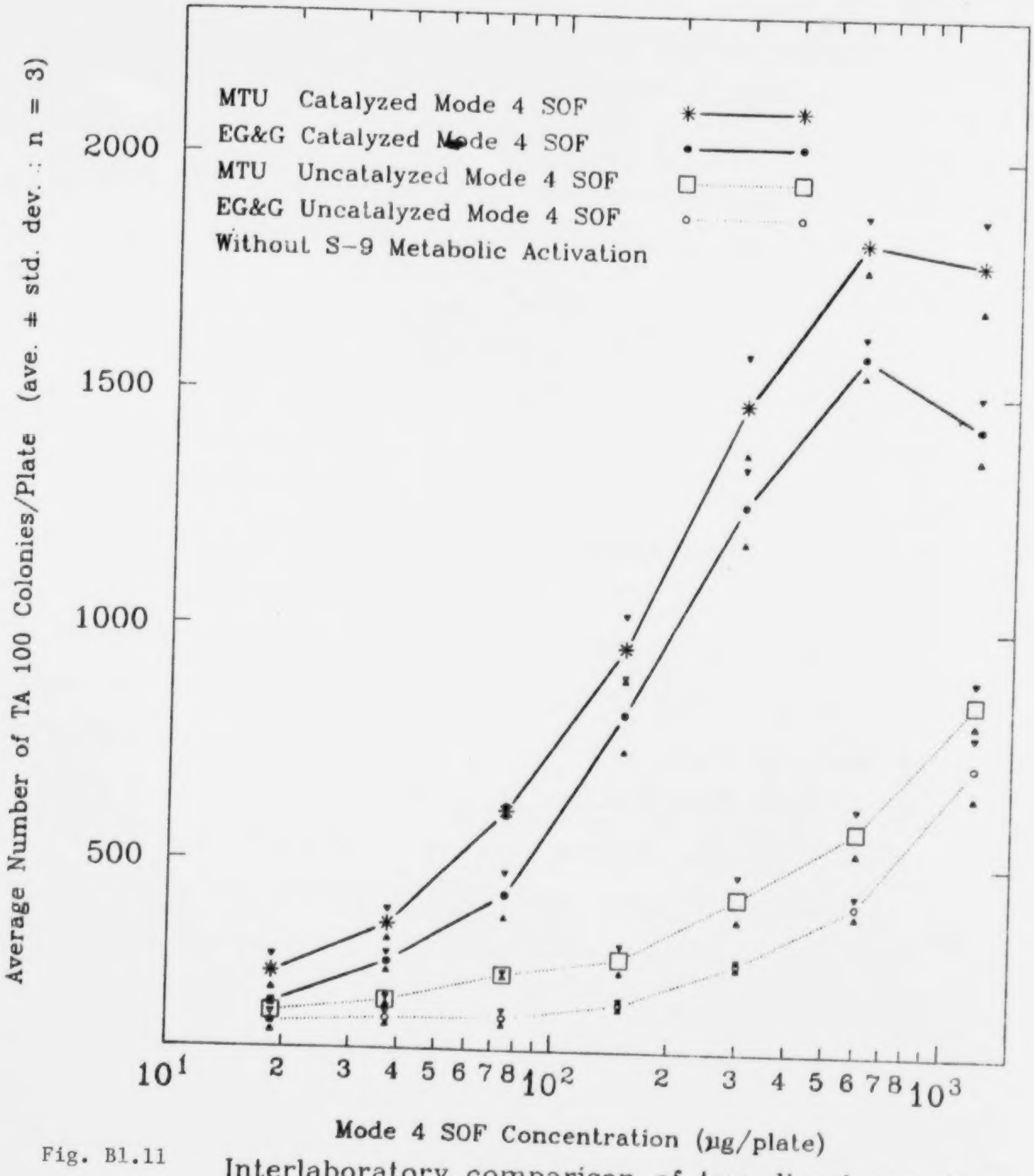

Fig. B1.11 Interlaboratory comparison of two diesel samples.

greater than the experimental random error, although similar trends were seen in the data.

Ames Bioassay Results for Selected Data

The Caterpillar 3208 provided the greatest number of SOF samples for repeat bioassays of any of the engine systems tested during this study. A detailed analysis of Ames bioassay results from SOF collected using No.2 fuel and this engine, after replacement of its injection pump, was performed.

Figures B1.12 through B1.20 plot the Ames dose-response curves of twelve assay dates between July 1981 and April 1982, using SOF from the Caterpillar 3208 engine in its baseline configuration as well as with close-coupled port catalysts and Corning ceramic traps. Triangles placed above and below data points designate standard deviation for all plate replicates.

Figures B1.12 through B1.17 compare the three test conditions on a modal basis, and show that the Corning traps yielded SOF with the highest mutagenic activity at all modes but mode 3. Additionally the Corning trap SOF exhibited signs of toxicity at all modes (including mode 3) and was significantly toxic at 1200μg/plate for all modes but mode 3.

Figures B1.18 through B1.20 show the same data plotted as a function of aftertreatment configuration. Mode 9 was the only mode exhibiting significant toxicity for the baseline engine, while mode 10 displayed a slight indication of toxicity. The port catalyst SOF was noticeably toxic at modes 5 and 10, while the Corning trap SOF showed toxicity for all modes.

As discussed in the section on Ames bioassay variability and data quantification, the mutagenic response is often marked by toxicity. The most significant example of this is shown in Figure B1.21, which is a plot

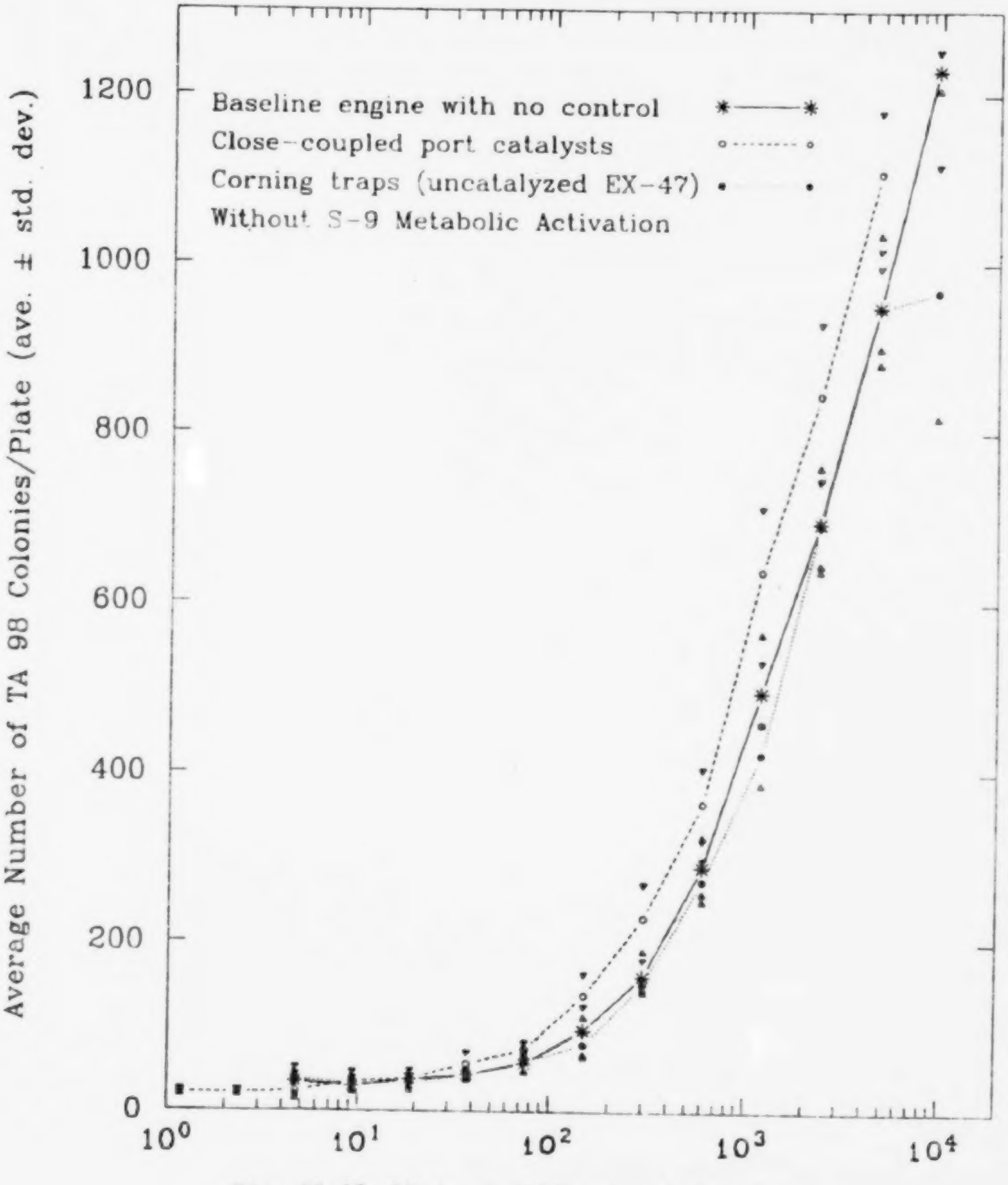

Fig. B1.12 Summary of Caterpillar 3208 Data from July 1981 to April 1982

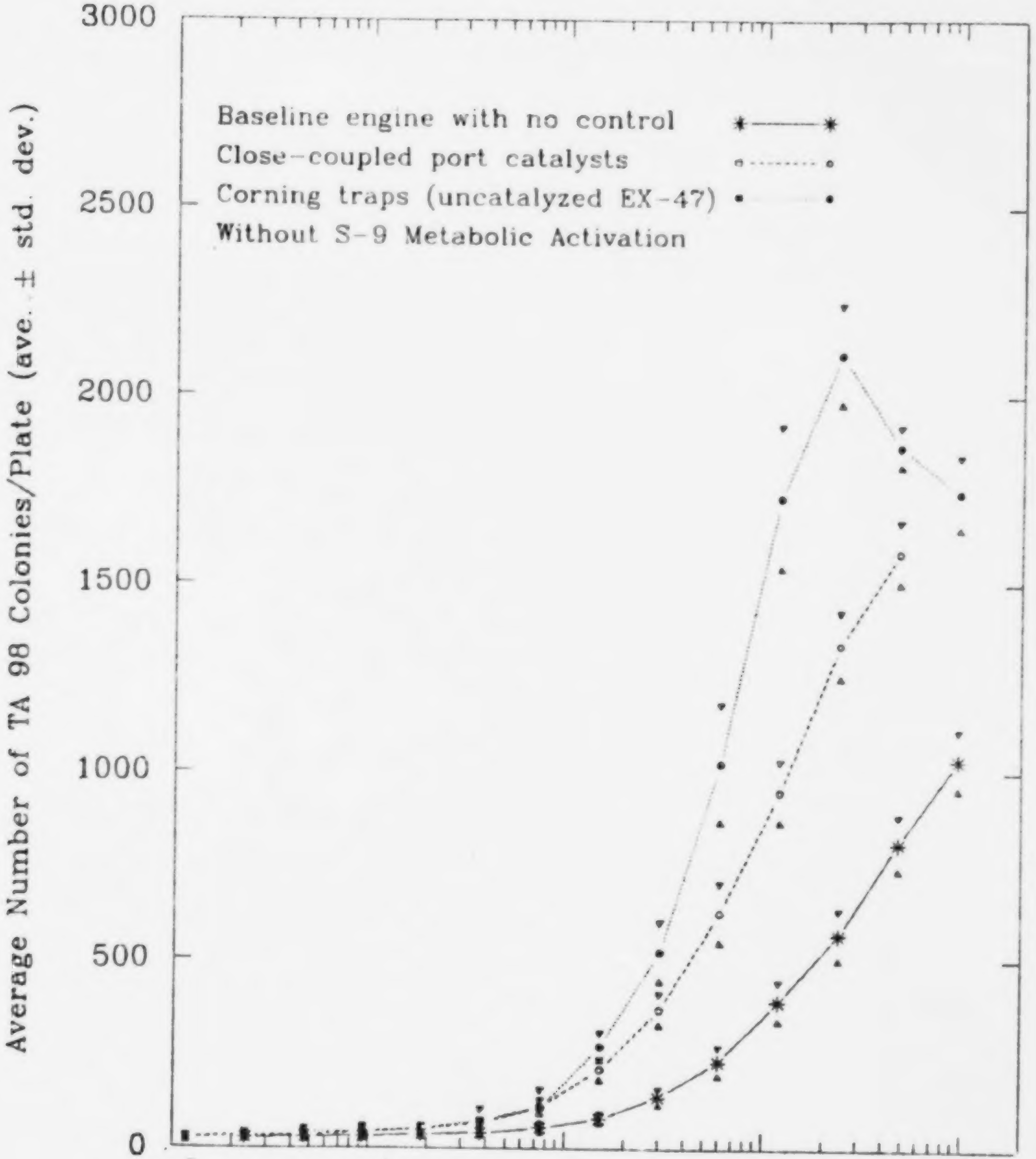

Fig. B1.13 Mode 4 SOF (µg/plate)

Summary of Caterpillar 3208 Data from July 1981 to April 1982

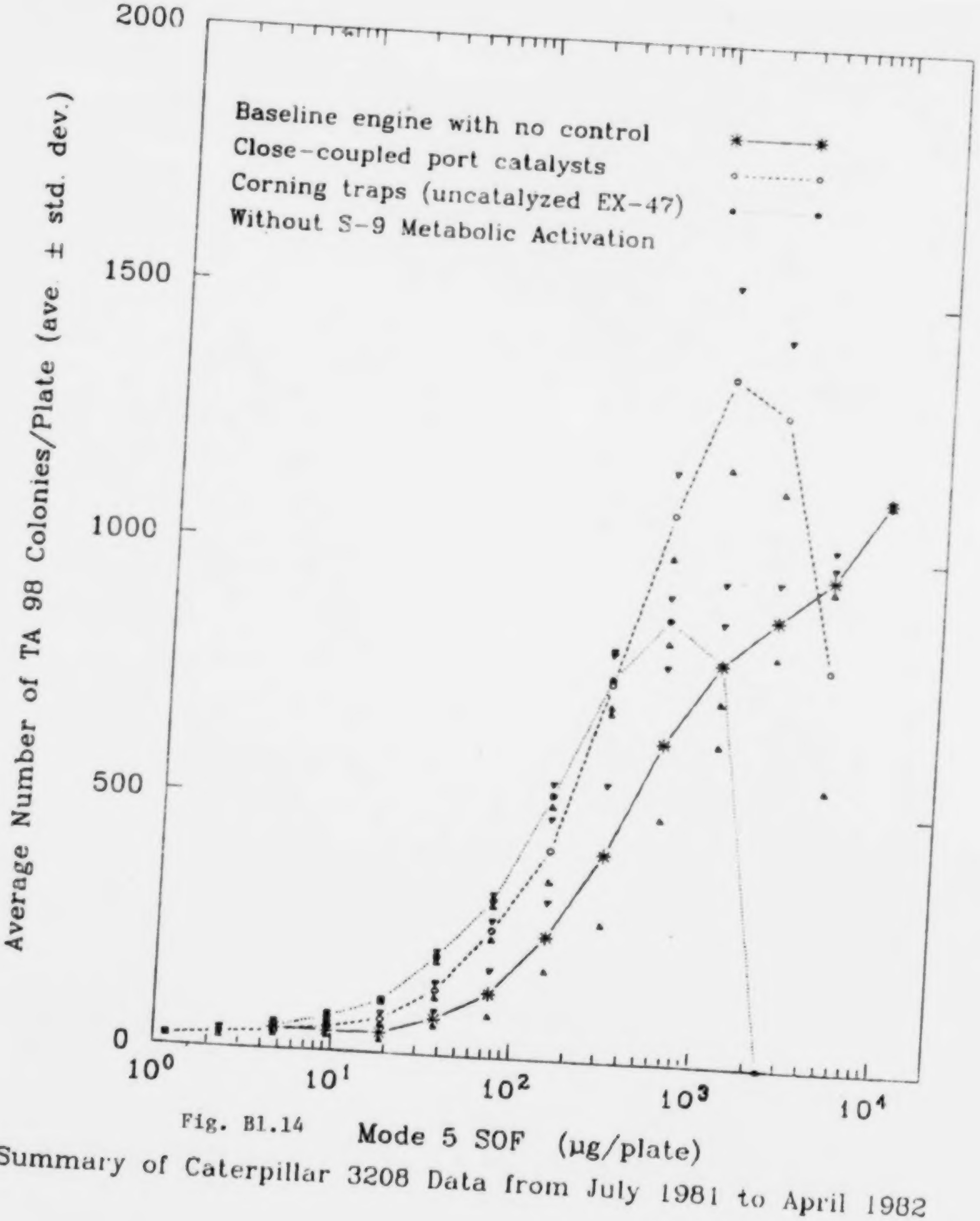

Fig. B1.14

Summary of Caterpillar 3208 Data from July 1981 to April 1982

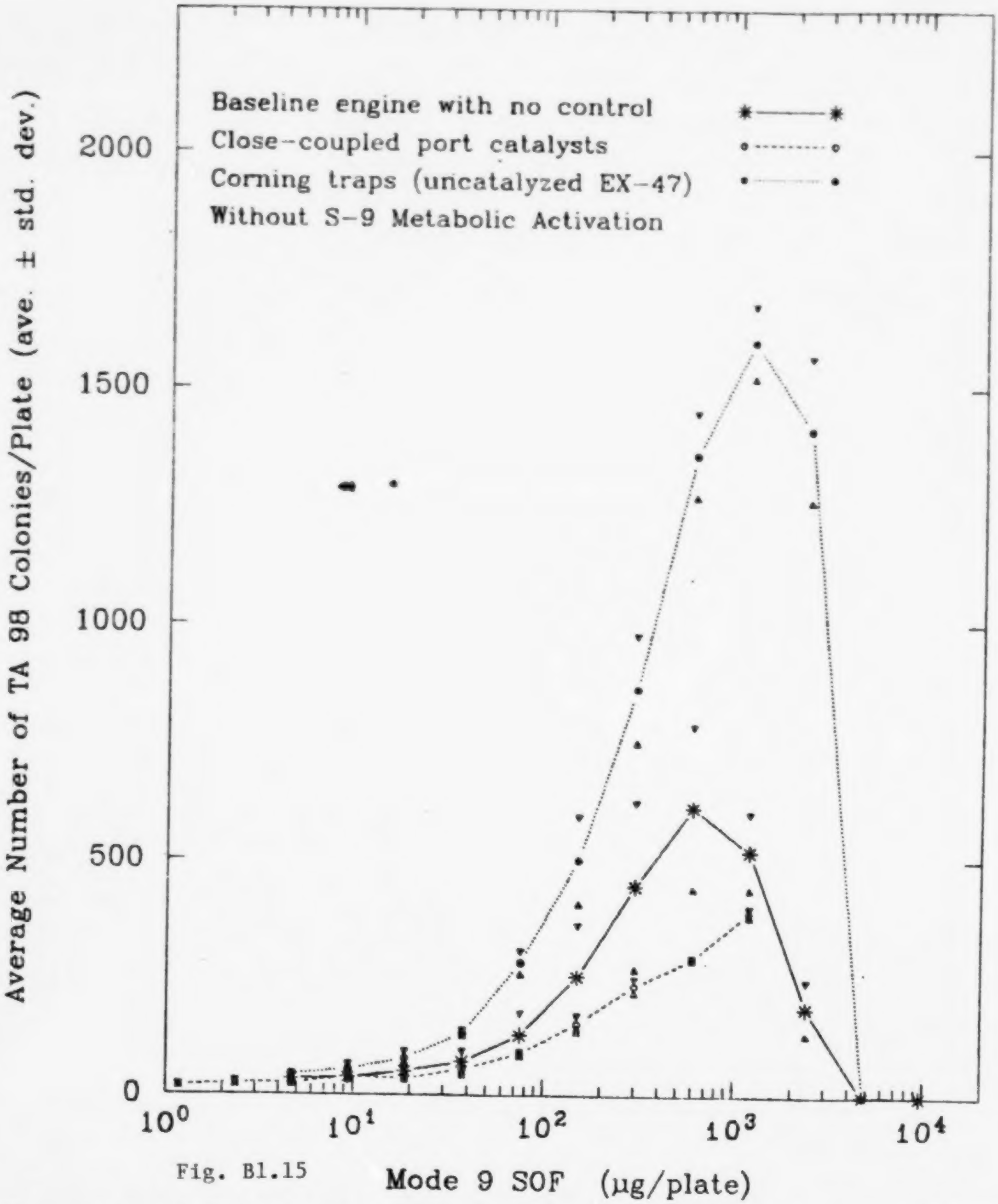

Fig. B1.15

Summary of Caterpillar 3208 Data from July 1981 to April 1982

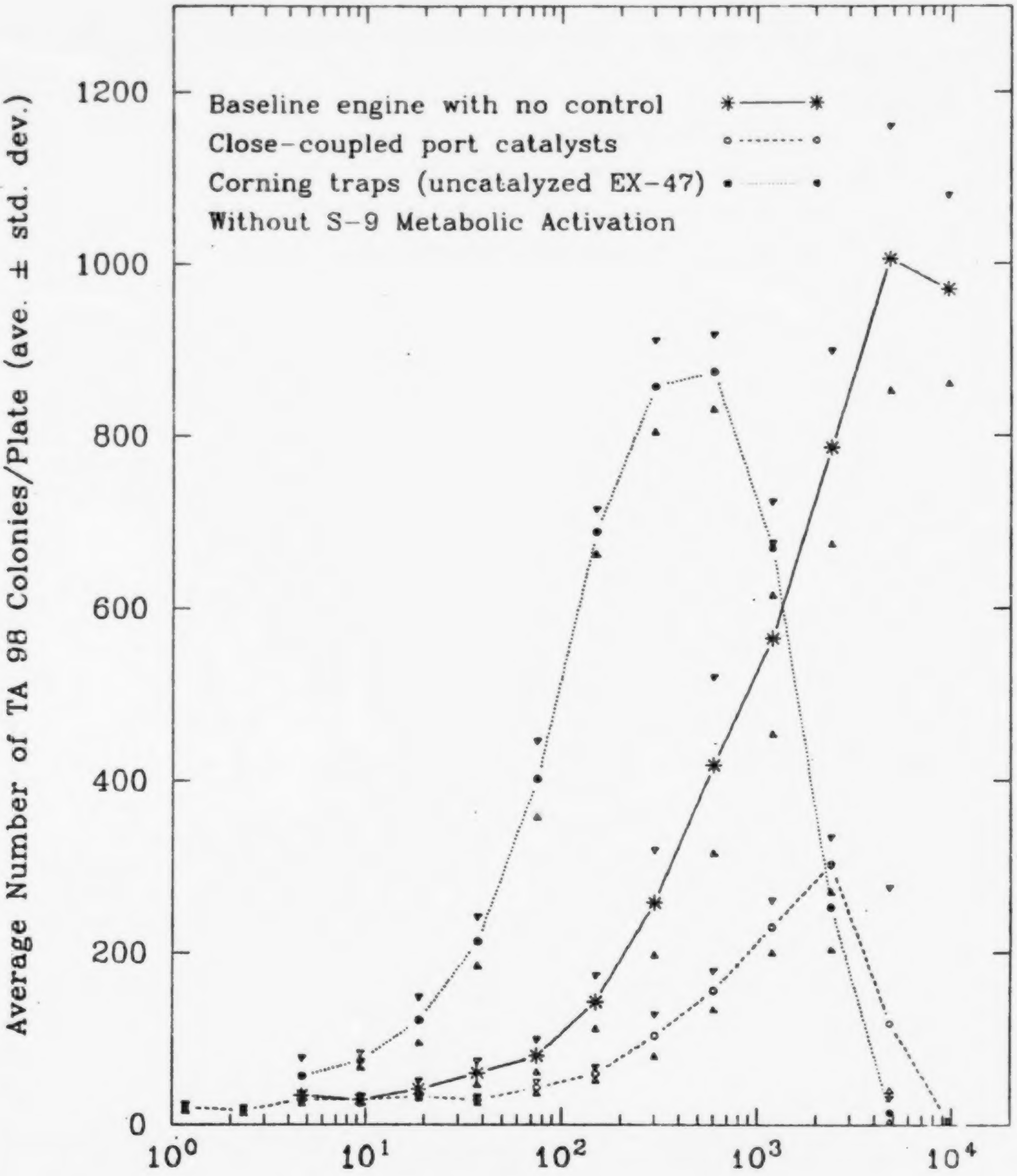

Fig. B1.16 Mode 10 SOF (µg/plate)

Summary of Caterpillar 3208 Data from July 1981 to April 1982

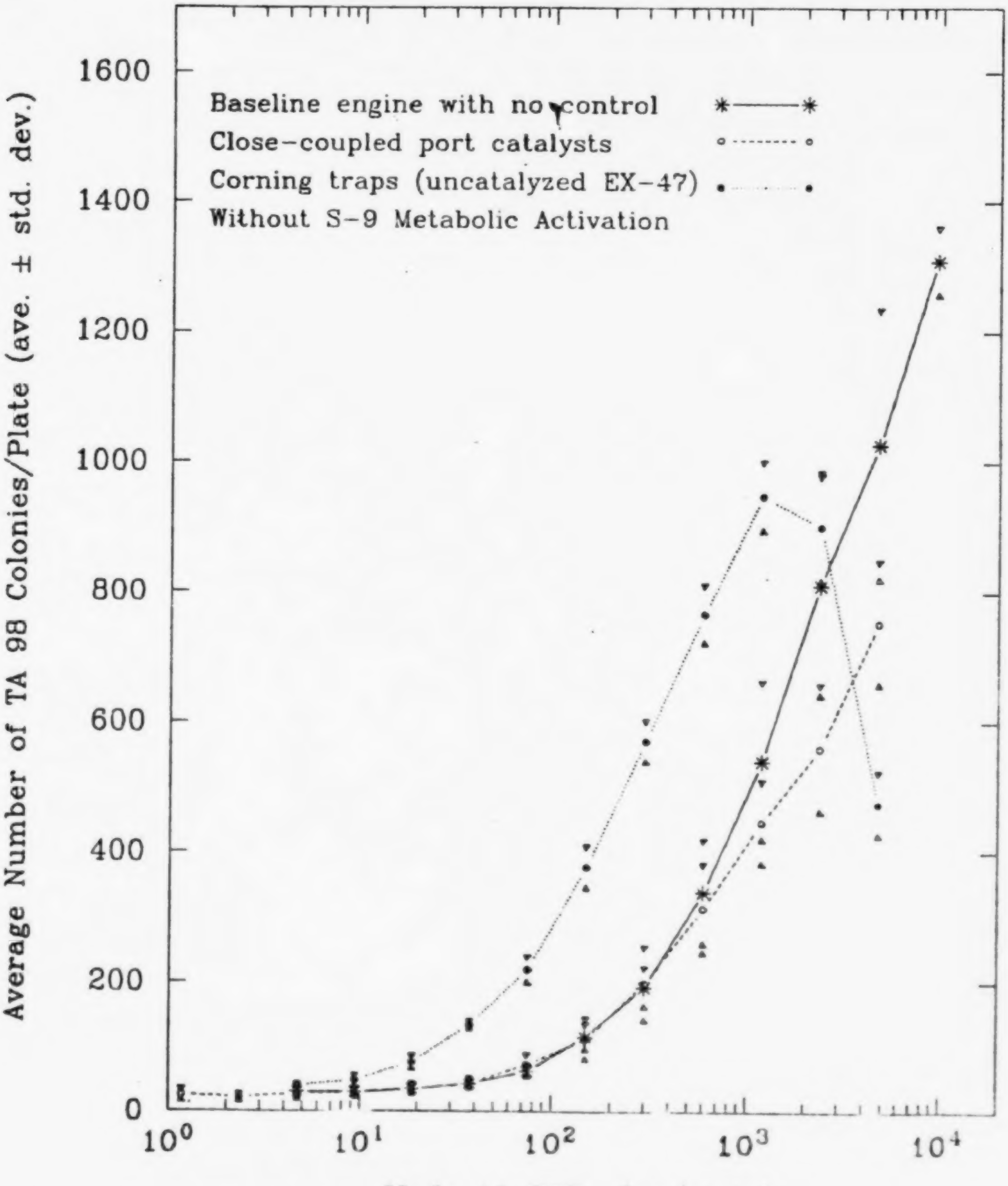

Fig. B1.17

Summary of Caterpillar 3208 Data from July 1981 to April 1982

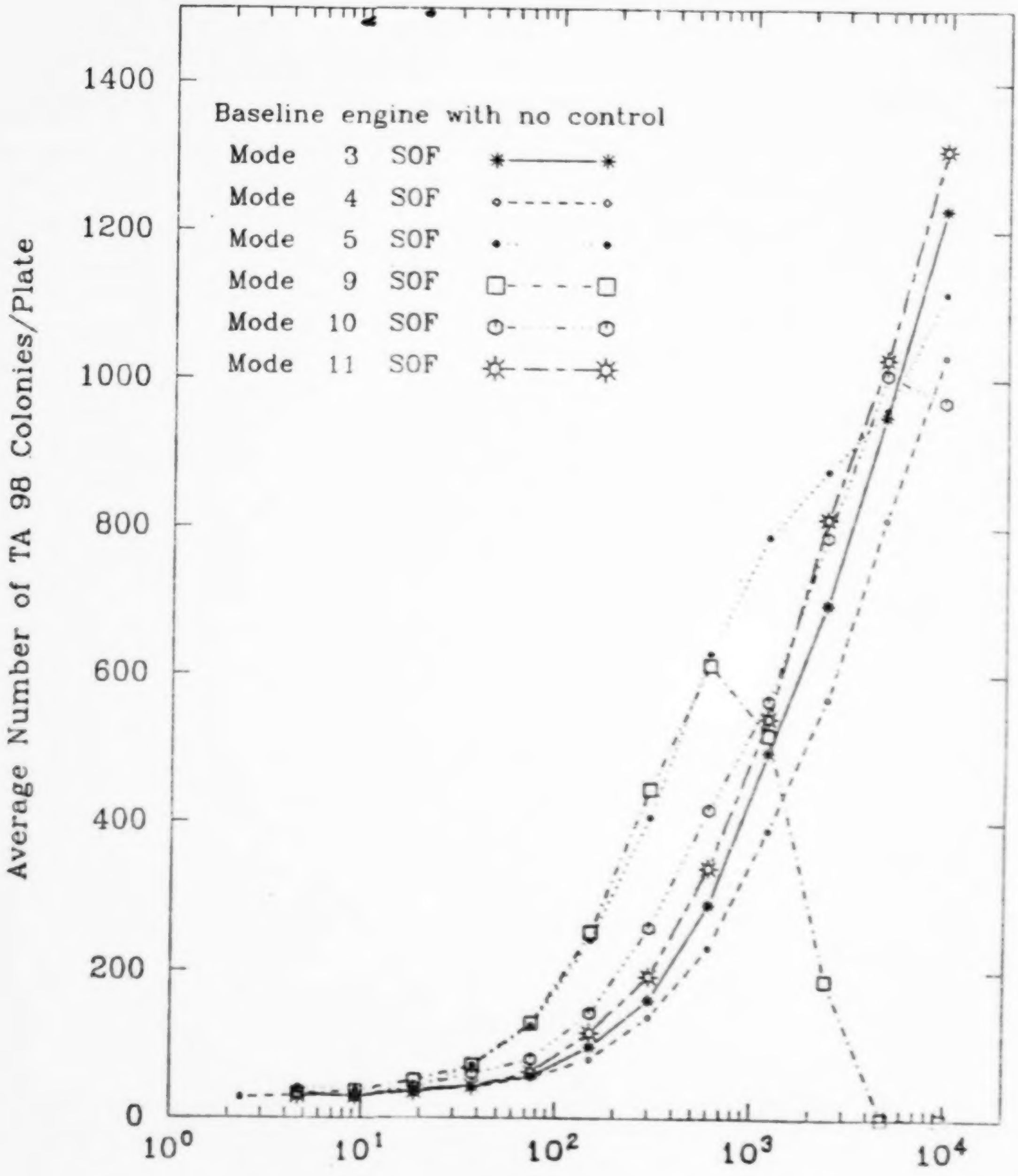

Fig. B1.18

Summary of Caterpillar 3208 Data from July 1981 to April 1982

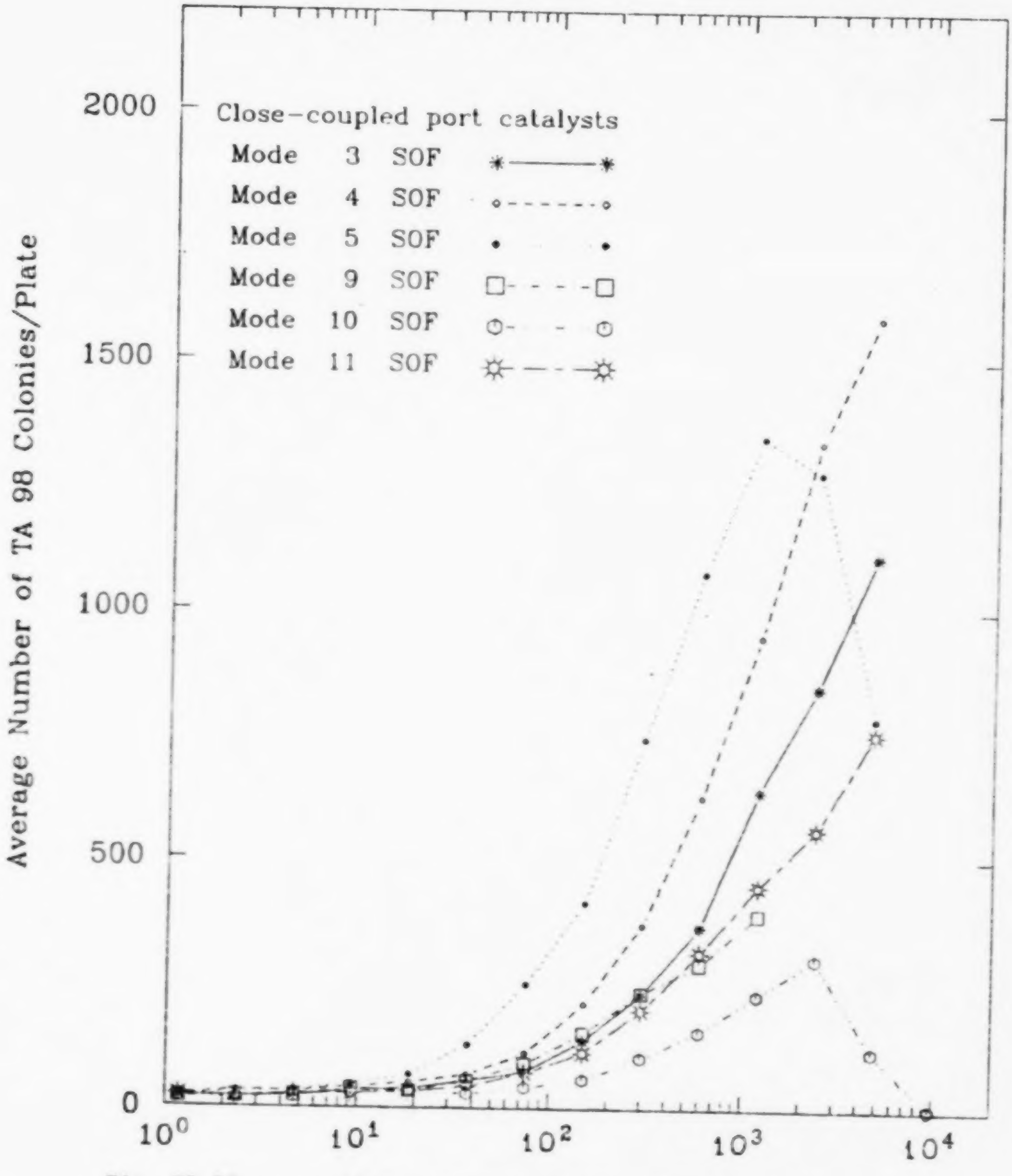

Fig. B1.19

Summary of Caterpillar 3208 Data from July 1981 to April 1982

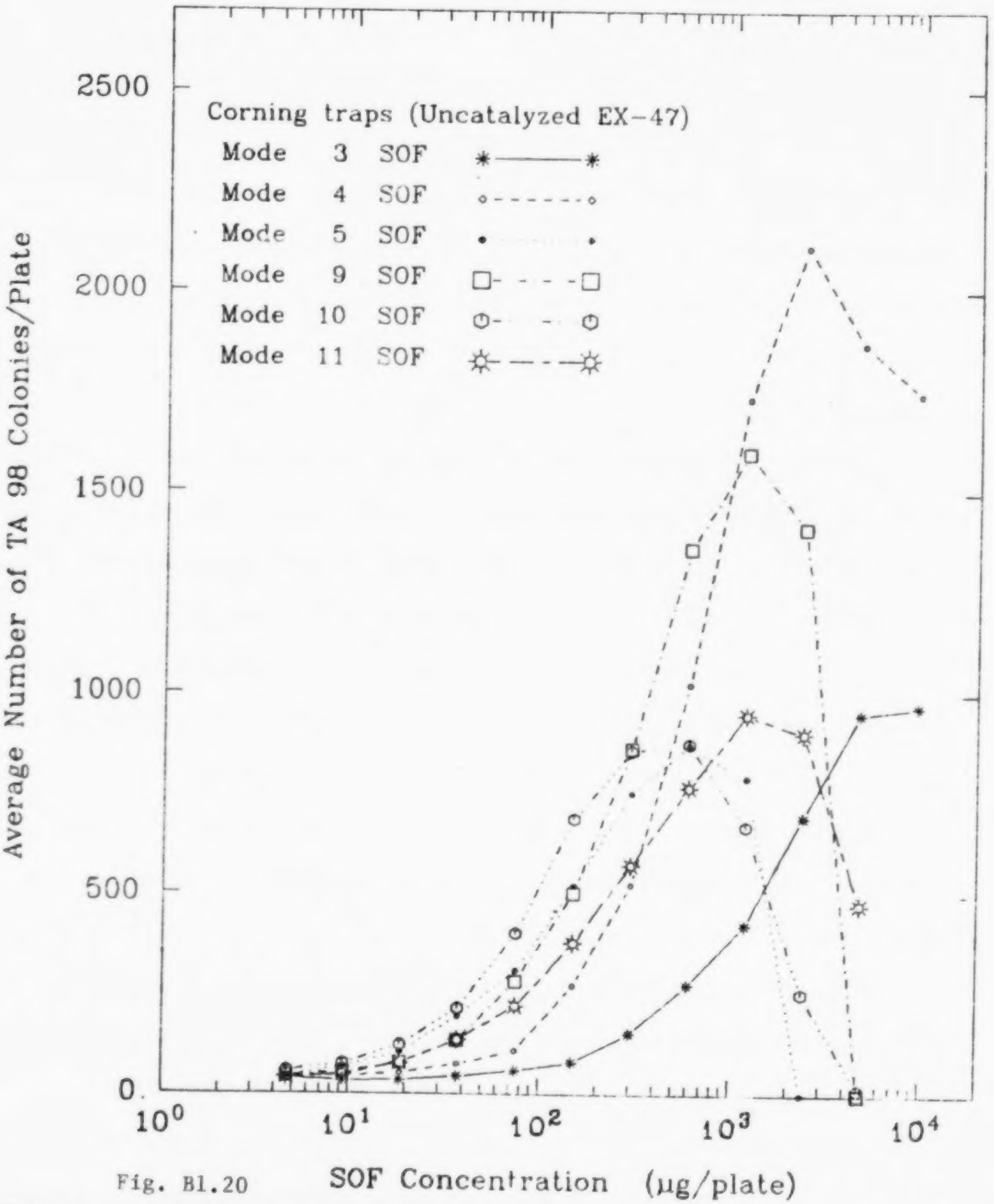

Fig. B1.20

Summary of Caterpillar 3208 Data from July 1981 to April 1982

of all subfraction dose-response curves from the Caterpillar Engine between July 1981 and April 1982, in log-log format. The Corning trap mode 4 oxygenated, ether insoluble, and basic subfractions (each assayed twice) stand out as more mutagenic than any other samples run in this laboratory. The shape of the theoretical toxicity curve may not allow direct observation of a toxic effect for a composite sample, and the extremely active oxygenated subfraction (toxic at 18.75 μg/plate), which constitutes only 6.5% of the SOF mass, does not raise the total SOF activity as significantly as expected. This suggests that hazardous compounds may be obscured if one observes the total SOF mutagenic activity.

The SOF subfractions obtained from the Caterpillar engine during this study are ranked in decreasing order of specific activity in Table B1.10. Despite the lack of specific activity data for three subfractions from the PTX catalyst, it can be seen that the ether insoluble, acidic, and oxygenated subfractions are the most active of the eight subfractions tested. While more limited data are available from the Mack engine, the general trend shows transitionals to be somewhat more and hexane insolubles somewhat less active, in a relative sense. Acidic, ether insoluble, and basic subfractions are still quite active, as shown in Figure 3.1.9 in the discussion of the Mack engine emissions.

The effect of sample storage on mutagenic specific activity was investigated using mode 11 SOF from the Caterpillar 3208 engine equipped with port catalysts. The SOF was stored on four different filters and extracted on three separate assay dates, with storage in either DMSO, on the particulate filter, as a dry residue, or in dichloromethane. Although not all storage conditions were utilized for all assay dates, a uniform dose

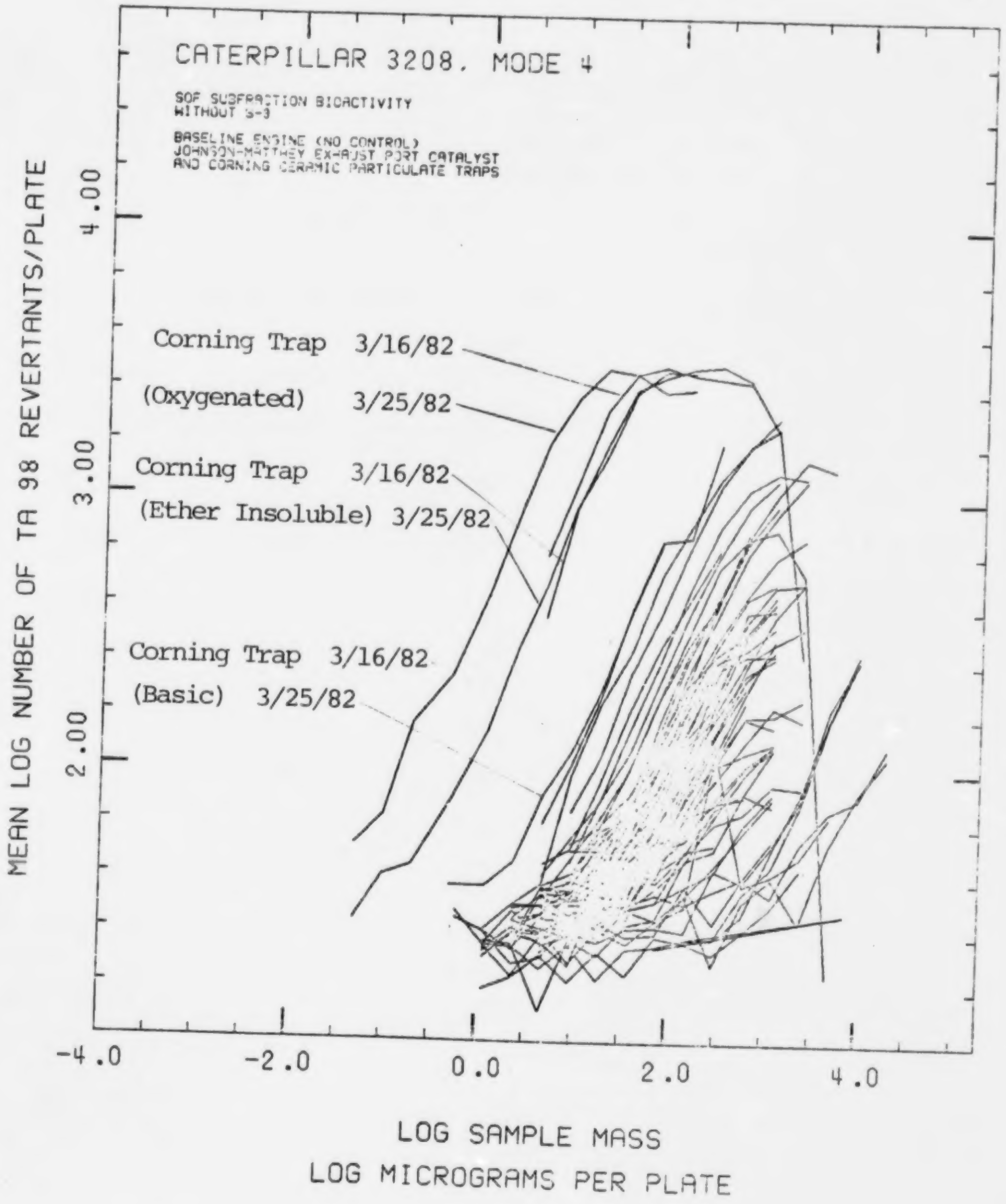

FIG. B1.21 CATERPILLAR 3208 SOF SUBFRACTION DOSE RESPONSE CURVES BASELINE, J-M PORT CATALYST, AND CORNING TRAP REPEAT ASSAYS FOR EACH SUBFRACTION, EPA MODE 4

Table B1.10 Ranking of SOF Subfractions According to Specific Activity for the Baseline, PTX Catalyst, Port Catalyst, and Corning Trap tests at Mode 4 with the Caterpillar 3208 and an Overall Ranking Considering all Three. (Highest Specific Activity on Top Decreasing Down)

Baseline	* PTX Catalyst	Port Catalyst	Corning Trap	Overall
ACD	OXY	ACD	OXY	EIN,ACD
EIN	ACD	EIN	EIN	OXY
OXY	TRN	OXY	BAS	HXI,BAS
HXI	BAS	BAS	ACD	TRN
ARM	ARM	HXI	HXI	ARM
TRN		TRN	TRN	PRF
BAS		ARM	ARM	
PRF		PRF	PRF	

EIN - Ether Insoluble
BAS - Basic
ACD - Acidic
PRF - Paraffin
ARM - Aromatic
TRN - Transitional
OXY - Oxygenated
HXI - Hexane Insoluble

* PTX Subfractions not assayed were EIN, PRF, HXI

range analysis of the resultant Ames data showed no clear pattern of sample gain or loss of mutagenic activity. This suggests that the practice of holding samples for testing on the same date is acceptable.

Tables B1.11 and B1.12 give SA data calculated using the log dose-revertant and log dose-log revertant tranformation of the linear regression model. The use of the power function (log-log) transformation generally results in a coefficient of variation for SA values somewhat higher than that for the semilog transformation. This is expected, as the log-log tranformation utilizes the y-intercept as well as the slope coefficient of the linear regression model, and y-intercepts of repeat assays in log-log coordinates are more variable than slopes.

The results in Tables B1.11 and B1.12 also show that the variability due to repeat engine runs and extractions may not contribute significantly to the total variability in SA, since C.V. values for all tests are not consistently higher or lower than C.V. values for repeat tests of identical samples.

Table B1.11 Summary of specific activity (SA) from model: Revertants = A + B * log (Sample Concentration) SOF Concentration range: 18.75 - 600.00 μg/plate. Caterpillar 3208 data July 1981 to April 1982.

Assay	Mode 3			Mode 4			Mode 5			Mode 9			Mode 10			Mode 11		
Date	B	P	T	B	P	T	B	P	T	B	P	T	B	P	T	B	P	T
7/10/81		0.564			1.117			1.639			0.460			0.252			0.597	
11/03/81				0.367	1.156													
12/11/81	0.358	0.456		0.332	0.835		1.176	1.690		0.588			0.637	0.171		0.449		0.344
1/11/82	0.452	0.578		0.276 0.369	1.096 0.997		1.224	1.912		0.837			0.827	0.184		0.443		0.396
3/09/82				0.377 0.341	0.989 1.167													
3/11/82				0.287 0.299	0.963 0.930													
3/16/82			0.348	0.295		1.380			1.402			2.005			1.442			1.217
(a) 3/16/82				0.360														
3/25/82				0.456		1.418												
3/30/82	0.426		0.409	0.267		1.798	0.670		1.411	1.269		2.234	0.413		1.499	0.529		1.199
(a) 3/30/82	0.355			0.256		1.401	1.212			0.842			0.725			0.378		
4/13/82				0.384														
(a) 4/13/82				0.299														

Table B1.11 Summary of specific activity (SA) from model: Revertants = A + B * log (Sample Concentration) SOF Concentration range: 18.75 - 600.00 µg/plate. Caterpillar 3208 data July 1981 to April 1982.

Assay	Mode 3			Mode 4			Mode 5			Mode 9			Mode 10			Mode 11		
Date	B	P	T	B	P	T	B	P	T	B	P	T	B	P	T	B	P	T
4/15/82				0.415														
(a) 4/15/82				0.314														
(a) 4/27/82	0.446					1.817	0.717			1.449			0.483			0.683		
n	3	3	2	13	9	3	3	3	2	3	1	2	3	3	2	3	3	2
average	0.388	0.533	0.379	0.343	1.028	1.532	1.023	1.747	1.407	1.898	0.460	2.119	0.626	0.202	1.471	0.474	0.446	1.208
C.V.(%)	14	12	11	17	11	15	30	8	0.4	38		8	33	21	3	10	30	1
n (a)	5			17		5	5			5			5			5		
average	0.407			0.335		1.563	1.000			0.997			0.617			0.496		
C.V.%	12			17		14	28			35			28			24		

(a) Indicates repeat engine run (sample) and/or extraction (therefore includes the variation of the engine, sample collection, and extraction process) Two numbers in the same box indicate separate extractions from the same engine run.

B = baseline engine with no control
P = with close-coupled port catalysts
T = with Corning traps (uncatalyzed EX-47)

Table B1.12 Summary of specific activity (SA) from model: log (Revertants)= a + b * log (Sample Concentration)
SOF Concentration range:18.75 - 600.00 g/plate. Caterpillar 3208 data July 1981 to April 1982.

Assay	Mode 3			Mode 4			Mode 5			Mode 9			Mode 10			Mode 11		
Date	B	P	T	B	P	T	B	P	T	B	P	T	B	P	T	B	P	T
7/01/81		0.643			1.143			1.828			0.509			0.224			0.643	
11/01/81				0.283	1.135													
12/11/81	0.308	0.429		0.307	0.802		1.368	1.966		0.614			0.649	0.154	0.451	0.305		
1/11/82	0.411	0.537		0.266 0.330	1.100 0.971		1.322	2.174		0.821			0.737	0.173	0.445	0.387		
3/09/82				0.293 0.275	0.860 1.023													
3/11/82				0.256 0.272	0.957 0.917													
3/16/28			0.318	0.277		1.368			1.603			2.231			1.794			1.390
(a) 3/16/82				0.304														
3/25/82						1.281												
3/30/82	0.390		0.375	0.245		1.407	1.426		1.637	0.860		2.640	0.799		1.791	0.336		1.302
(a) 3/30/82	0.341			0.243		1.708	0.684			1.477			0.406			0.496		
4/13/82				0.351														

Table B1.12 Summary of specific activity (SA) from model: log (Revertants) = a + b * log (Sample Concentration) SOF Concentration range:18.75 - 600.00 μg/plate. Caterpillar 3208 data July 1981 to April 1982.

Assay	Mode 3			Mode 4			Mode 5			Mode 9			Mode 10			Mode 11		
Date	B	P	T	B	P	T	B	P	T	B	P	T	B	P	T	B	P	T
(a) 4/13/82				0.267														
4/15/82				0.395														
(a) 4/15/82				0.274														
4/27/82	0.400					1.803	0.749			1.670			0.426			0.664		
n	3	3	2	12	9	3	4	3	2	3	1	2	3	3	2	3	3	2
average	0.310	0.536	0.346	0.296	0.990	1.352	1.216	1.989	1.620	0.765	0.509	2.436	0.528	0.184	1.793	0.411	0.445	1.346
C.V.(%)	15	20	12	15	12	5	26	9	1	17		12	10	20	0	18	40	5
n (a)	5			17		5	5			5			4			5		
average	0.370			0.300		1.513	1.110			1.088			0.603			0.478		
C.V.(%)	12			19		15	33			42			30			25		

(a) Indicates Repeat Engine Run (Sample) and/or Extraction (therefore includes the variation of the engine, sample collection, and extraction process)

B = baseline engine with no control
P = with close-coupled port catalyst
T = with Corning traps (uncatalyzed EX-47)

Two numbers in the same box indicate separate extraction from the same engine run.

Table B-2- Mack ENDT-676 SOF: Biological Activity Data for Tester Strain TA100 without S-9 Metabolic Activation [(a)]

Test [(b)]	C_1 (μg/plate)	C_2 (μg/plate)	a	b	r	SA_{SL} [(d)] (rev/μg)	BSSA (rev/kw-hr)
3B	75	1200	-1825	1039	0.97	1.112	202,000
4B	NA [(c)]	NA	NA	NA	NA	NA	NA
5B	75	600	0557	436	0.98	0.75	21,000
9B	75	1200	-1834	1095	0.97	1.17	46,800
10B	75	600	-687	485	0.95	0.835	67,000
11B	75	1200	-1136	647	0.98	0.692	173,000
3.803	150	1200	-407	364	0.98	0.313	25,000
3.8-9	37.5	1200	-631	382	0.95	0.494	25.000
G-19-3	37.5	1200	-1226	816	0.95	1.06	53,000
G-19-9	75	1200	-1199	644	0.98	0.690	41,000
G-12-13	37.5	1200	-1096	700	0.92	0.907	27,000
G-12-9	150	1200	-609	348	0.95	0.299	12,000
G-17-3	37.5	2400	-1063	664	0.95	0.507	30,000
G-17-9	150	1200	-880	480	0.98	0.413	29,000
G-22-3	37.5	1200	-880	480	0.98	0.621	75,000
G-22-9	37.5	1200	-541	316	0.95	0.409	45,000
S-8-3	9.4	600	-1584	1072	0.99	3.28	426,400
S-12-3	9.4	2400	-1690	944	0.99	1.00	100,000
S-14-3	9.4	600	-1915	1280	1.0	3.91	391,000
S-17-3	4.7	2400	-1730	965	0.98	1.09	130,800

(a) Calculations explained in Appendix B, "Quantification of Ames Data"
(b) An explanation of the test code is given in Tables 3.1.1 and 3.1.3
(c) Not Available
(d) SA_{SL} was used rather than SA_{LL} because data analysis was performed before the SA_{LL} parameter was developed

Table B-3. Caterpillar 3208 With and Without Englehard PTX Oxidation Catalysts: Biological Activity for SOF from Modes 3, 4 and 5 Using Ames Tester Strain TA98 Without S-9 Metabolic Activation

	EPA MODE	3		4		5	
	PTX Catalyst	Without	With	Without	With	Without	With
No. 2 Fuel	c_1	37.5	37.5	37.5	37.5	37.5	37.5
	c_2	600.	600.	600.	600.	600.	600.
	a	-508.05	-340.42	-374.15	-2279.22	-354.92	-1585.79
	b	337.51	232.53	247.48	1533.40	244.16	1557.65
	r	.96	.96	.96	.99	.97	.98
	SA_{SL}	.72	.50	.53	3.28	.52	3.33
No. 1 Fuel	c_1	37.5	37.5	37.5	37.5	37.5	37.5
	c_2	600.	600.	600.	600.	600.	600.
	a	-362.87	-141.02	-196.09	-2311.40	-334.72	-1063.91
	b	239.18	98.99	139.19	1521.44	248.54	750.76
	r	.94	.91	.91	.98	.95	.99
	SA_{SL}	.51	.21	.30	3.26	.53	1.61
Shale Fuel	c_1	N.A.	N.A.	37.5	37.5	N.A.	N.A.
	c_2			600.	600.		
	a			-714.56	-2431.43		
	b			461.08	1736.70		
	r			.94	.99		
	SA			.99	3.72		

SA_{SL} = specific activity (REV/μg) (average slope of dose-response curve, semi-log transformation of linear model)
c_1 = minimum dose in linear portion of dose-response curve
c_2 = maximum dose on linear portion of dose-response curve
a = response intercept of dose-response curve, determined statistically
b = slope of dose-response curve in linear-log format, determined statistically
r = coefficient of correlation
N.A. = data not available

Calculations are explained in Appendix B.
SA_{SL} was used, rather than SA_{LL}, because data analysis was performed before the SA_{LL} parameter was developed.

Table B-4. Caterpillar 3208 With and Without Englehard PTX Oxidation Catalysts: Biological Activity for Mode 4 SOF Subfractions, Using Ames Tester Strain TA98 Without S-9 Metabolic Activation

Fraction		ACD*[(a)]		ARO		BAS		EIN	
PTX Catalyst		-	+	-	+	-	+	-	+
#2 Fuel	c_1	18.75	18.75	18.75	18.75	18.75	18.75	18.75	N.A.
	c_2	600.	300.	600.	1200.	300.	300.	600.	
	a	-404.0	-1186.2	-145.0	-45.20	-1.02	-1058.6	-246.4	
	b	306.0	1812.11	125.66	49.98	23.59	813.20	198.18	
	r	.93	.99	.94	.88	.98	.95	.94	
	SA_{SL}[(b)]	.79	7.76	.33	.08	.10	3.48	.51	
#1 Fuel	c_1	18.75	18.75	18.75	18.75	18.75	4.69	18.75	18.75
	c_2	2400.	1200.	2400.	1200.	300.	75.	600.	600.
	a	-621.33	-2019.2	22.77	20.17	18.12	-34.73	-17.75	-1189.38
	b	420.60	1657.0	6.92	20.4	18.60	112.28	34.93	878.13
	r	.95	.98	.78	.88	.97	.91	.93	.94
	SA_{SL}	.37	2.53	<.01	.03	.08	1.92	.09	2.27
Shale Fuel	c_1	18.75	18.75	18.75	18.75	18.75	18.75	18.75	18.75
	c_2	4800.	600.	2400.	2400.	600.	300.	2400.	1200.
	a	-882.6	-1836.6	-43.90	-198.3	-112.04	-808.7	-698.97	-1000.3
	b	564.23	1552.8	45.68	141.70	99.09	840.8	457.36	727.74
	r	.95	.99	.88	.93	.89	.96	.94	.98
	SA_{SL}	.28	4.02	.04	.13	.26	2.74	.40	1.11

Symbols and calculations are explained in Appendix B.

(a) ACD-Acidic, ARO-Aromatic, BAS-Basic, EIN-Ether Insoluble

(b) SA_{SL} was used, rather than SS_{LL}, because data analysis was performed before the SA_{LL} parameter was developed

Table B-4 Continued

Fraction		HIN		OXY		PAR		TRN	
PTX									
Catalyst		-	+	-	+	-	+	-	+
#2 Fuel	c_1	18.75	N.A.	18.75	18.75	N.A.	N.A.	18.75	18.75
	c_2	300.		1200.	300.			1200.00	300.
	a	-11.98		-581.25	-2076.5			-52.68	-1634.5
	b	34.55		473.97	1986.85			91.82	1413.14
	r	.97		.98	.99			.99	.99
	$SA_{SL}^{(b)}$	.15		.72	8.51			.14	6.05
#1 Fuel	c_1	18.75	18.75	18.75	18.75	300.	600.	18.75	9.375
	c_2	300.	1200.	4800.	2400.	19200.	9600.	2400.	150.
	a	-3.27	-1132.08	-114.70	-1755.6	22.39	.06	-21.88	-95.0
	b	32.89	796.55	105.69	1229.55	4.15	16.61	40.30	184.36
	r	.99	.94	.98	.97	.49	.84	.98	.99
	SA_{SL}	.14	1.22	.05	1.08	2.01	2.01	.04	1.58
Shale Fuel	c_1	18.75	18.75	18.75	18.75	1200.	1200.00	18.75	18.75
	c_2	600.	4800.	2400.	1200.	4800.	9600.	1200.	600.
	a	-8.18	-584.7	-164.86	-1289.2	15.76	-46.06	-114.3	-469.8
	b	30.37	353.18	138.01	1271.11	18.27	25.58	117.45	435.93
	r	.91	.89	.97	.99	.90	.99	.94	.99
	SA_{SL}	.09	.18	.12	1.94	$<.01$	$<.01$	.18	1.13

Symbols and calculations are explained in Appendix B.

(a) HIN-Hexane Insoluble, OXY-Oxygenated, PAR-Paraffinic, TRN-Transitional

(b) SA_{SL} was used, rather than SA_{LL}, because data analysis was performed before the SA_{LL} parameter was developed

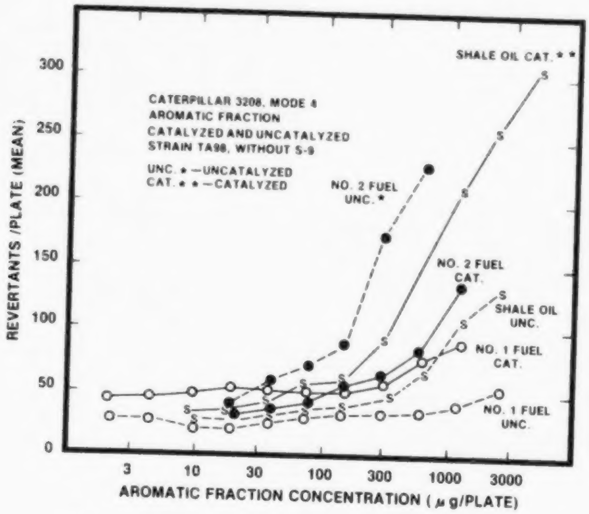

Fig. B2 - Fuel effects on dose-response curves for Ames tester strain TA98 without S-9 activation for aromatic fraction of SOF, with and without PTX oxidation catalysts

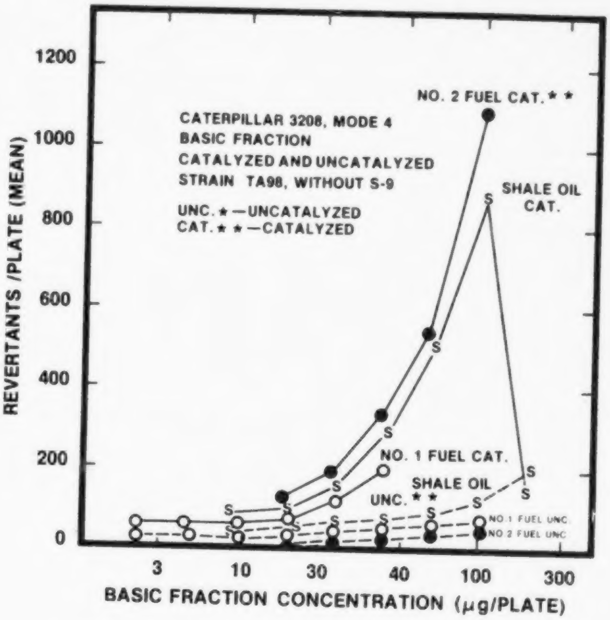

Fig. B3 - Fuel effects on dose-response curves for Ames tester strain TA98 without S-9 activation for basic fraction of SOF, with and without PTX oxidation catalysts

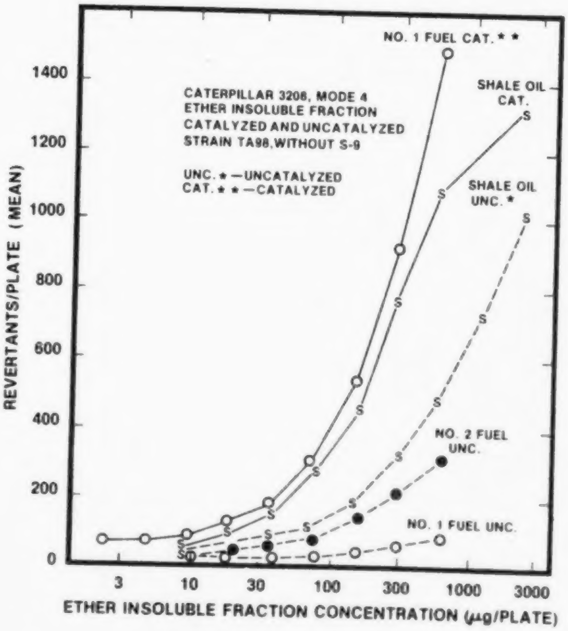

Fig. B4 - Fuel effects on dose-response curves for Ames tester strain TA98 without S-9 activation. for ether-insoluble fraction of SOF, with and without PTX oxidation catalysts

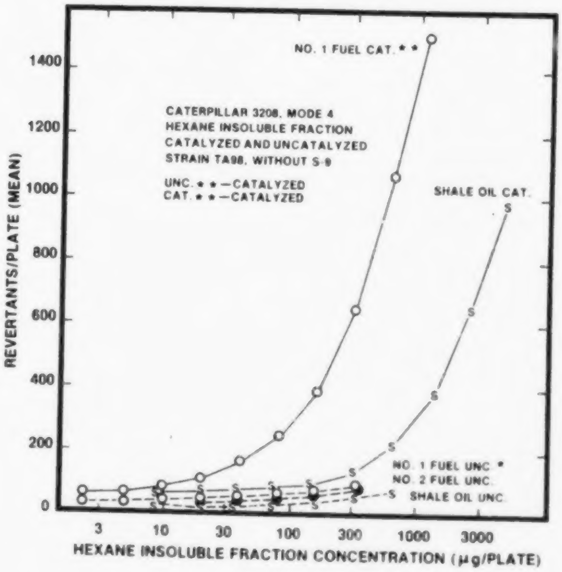

Fig. B5 - Fuel effects on dose -response curves for Ames tester strain TA98 without S-9 activation for hexane-insoluble fraction of SOF, with and without PTX oxidation catalysts

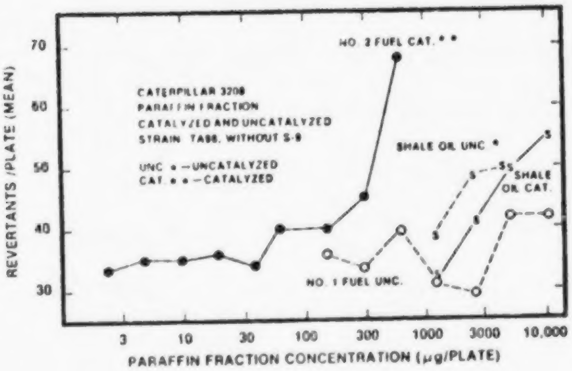

Fig. B6 - Fuel effects on dose-response curves for Ames tester strain TA98 without S-9 activation for paraffin fraction of SOF, with and without PTX oxidation catalysts

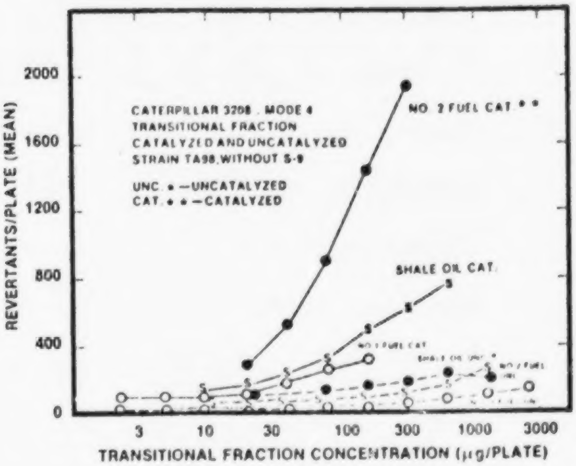

Fig. B7 - Fuel effects on dose-response curves for Ames tester strain TA 98 without S-9 activation for transitional fraction of SOF, with and without PTX oxidation catalysts

APPENDIX C

NON-ROUTINE CHEMICAL INVESTIGATIONS

CRC Round Robin

In 1980, the Coordinating Research Council (CRC) Chemical Charactization panel conducted an interlaboratory round robin to investigate an automated (HPLC) method for diesel SOF characterization. MTU participated in that round robin, and the results are presented here.

Table C1.1 shows retention time values and relative areas of compound classes from Nissan and Cummins Engine particulate as determined by the microparticulate silica gel HPLC method. Figures C1.1 and C1.2 are HPLC chromatograms for these two extracts. Four replicate runs were taken, and the best reproducibility was obtained on both samples for the α_1 and α_2 peaks. The α_1 and α_2 peaks are polynuclear aromatic hydrocarbons, and the β peak (not always seen in our runs) consists of larger (higher molecular weight) polynuclear aromatic hydrocarbons. The γ_1 and γ_2 peaks consist mainly of quinone and hydroxy derivatives of polynuclear aromatic hydrocarbons, while acid, acid anhydride, and aldehyde derivatives of polynuclear aromatic hydrocarbons comprise the δ peak.

Table C1.2 is a pool of data collected by the CRC from ten laboratories for this HPLC round robin (88). Since a 3 mm-i.d. HPLC column (not available in time for MTU to participate) and solvent flow rate of 1.0 ml/min was prescribed in the experimental section of this round robin, the data generated by MTU was not included in this data set. Retention times were earlier for MTU analyses than the CRC round robin analyses, due to

Table C1.1: Retention Time Values and Area Percentages of Compound Classes from Nissan and Cummins Engine Extracts for Four Replicate HPLC Runs using a Silica Gel Column, MTU Data only.

	Retention Time, Minutes					
Nissan Extract	α_1	α_2	β	γ_1	γ_2	δ
$\bar{X}\pm\sigma$	6.43±0.82	9.69±1.26	21.03±0.50	28.34±0.85	37.60±.06	66.11±0.42*
%C_v	12.7	13.0	2.4	3.0	2.8	0.6*
Cummins Extract						
$\bar{X}\pm\sigma$	1.83±0.26	6.92±0.47	21.66±0.52	28.56±0.76	37.36±0.69	65.92±0.05*
%C_v	14.4	6.8	2.4	1.8	1.8	0.08*

	Relative Peak Areas				
Nissan Extract	$\alpha_1 + \alpha_2$	β	γ_1	γ_2	δ
$\bar{X}\pm\sigma$	1.00	0.01±0.013	0.67±0.073	0.699±0.074	0.446±0.07
%C_v	--	134	10.8	10.5	15.7
Cummins Extract					
$\bar{X}\pm\sigma$	0.059±0.005	0.024±0.038	1.00	0.150±0.045	1.24±0.26
%C_v	9.0	158	--	30.6	20.7

---

*Standard deviation and %C_v for retention time of δ peak was this low only because this peak required acetonitrile injection to elute.

Table C1.2

Summary of Coordinating Research Council HPLC Round-Robin Results (n = 10, ref. 88).

Retention Time (Minutes)

Sample	α_1	α_2	β	γ_1	γ_2	δ
Nissan						
$\bar{X}\pm\sigma$	10.0±1.3	15.4±2.1	24.4±3.0	35.1±2.7	50.6±3.8	56.7±3.6
$\%C_v$	13.0	13.6	12.3	7.7	7.5	6.3
Cummins						
$\bar{X}\pm\sigma$	9.3±1.8	14.7±2.7	26.0±2.7	34.4±4.5	49.3±5.1	56.5±0.5
$\%C_v$	19.4	18.4	10.4	13.1	10.3	0.9

Relative Peak Areas

	$\alpha_1 + \alpha_2$	β	γ_1	γ_2	δ
Nissan					
$\bar{X}\pm\sigma$	1.00	0.21±0.06	0.77±0.14	0.70±0.11	0.66±0.18
$\%C_v$	-	28.5	18.2	15.7	27.3
Cummins					
$\bar{X}\pm\sigma$	0.07±0.01	0.14±0.03	1.00	0.20±0.05	1.43±0.19
$\%C_v$	14.3	21.4	-	25.0	13.3

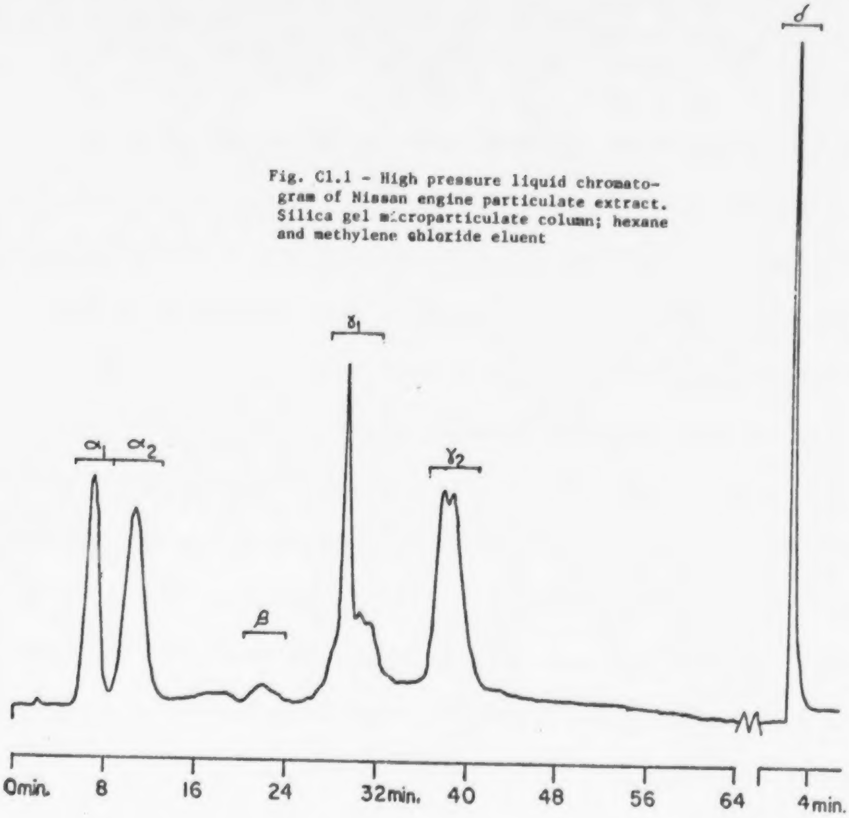

Fig. C1.1 - High pressure liquid chromatogram of Nissan engine particulate extract. Silica gel microparticulate column; hexane and methylene chloride eluent

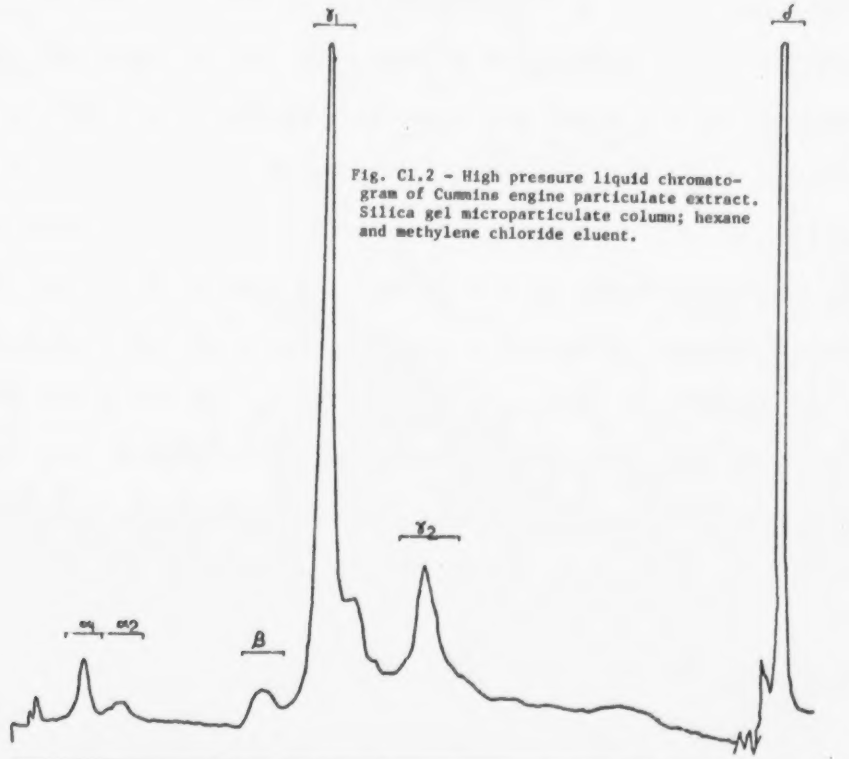

Fig. C1.2 - High pressure liquid chromatogram of Cummins engine particulate extract. Silica gel microparticulate column; hexane and methylene chloride eluent.

different column size and flow rate as well as initial solvent composition which may have varied significantly from that prescribed by the round robin. Solvent was not pre-mixed by MTU, but was formed by the gradient system of the liquid chromatograph. Because of the imprecision of such systems at low percentage composition of one solvent (89), the prescribed 5% hexane in DCM composition may have been somewhat different from that actually delivered by the HPLC pumps. Although retention times were less than those observed by most investigators, relative peak areas (except for the β peak) were similar to those of other investigators. The discrepancy in β peak areas could also be due to difference in solvent composition from that of others since this was not always observed by MTU, and actually belongs to the α peaks in chemical character.

Sephadex LH-20 Lipophilic Gel

Table C1.3 is the acid-base-neutral fractionation data for SOF from the baseline Caterpillar engine run at mode 3 (25% rated load, 1680 RPM) using No.1 fuel and an air volume dilution ratio of 5:1. The same SOF was fractionated using LH-20 lipophilic gel; results of this fractionation are shown in Table C1.4. Recoveries of material in both cases were 90% or better; relative standard deviation was less than 10% for major fractions and total recovery. Dose-response curves for LH-20 separated fractions are shown in Figure C1.3. The curve labeled "E" is unfractionated SOF, and that labeled "BHT" is butylated hydroxytoluene, the solvent preservative in THF. The majority of biological activity resides in fractions 4 thru 7, which consititutes approximately 11% of the SOF mass.

TABLE C1.3 ACID-BASE-NEUTRAL FRACTIONATION RESULTS

PERCENTAGES OF TOTAL SAMPLE

(AVERAGE SAMPLE SIZE 146 MG)

FRACTION NAME	1-3D5-1	1-3D5-2	1-3D5-3	$\bar{X}$	σ
ETHER INSOLUBLE	5.1	1.2	3.0	3.1	1.6
BASIC	3.4	0.6	1.3	1.8	1.2
ACIDIC	3.4	5.0	9.0	5.8	2.4
PARAFFIN	65.6	59.7	61.3	62.2	2.5
AROMATIC	0.8	4.5	4.6	3.3	1.8
TRANSITIONAL	4.2	6.3	4.3	4.9	1.0
OXYGENATED	11.2	13.5	11.9	12.2	1.0
HEXANE INSOLUBLE	0.9	0.3	0.4	0.5	0.3
PERCENT RECOVERY	94.6	83.4	91.5	90.0	5.5

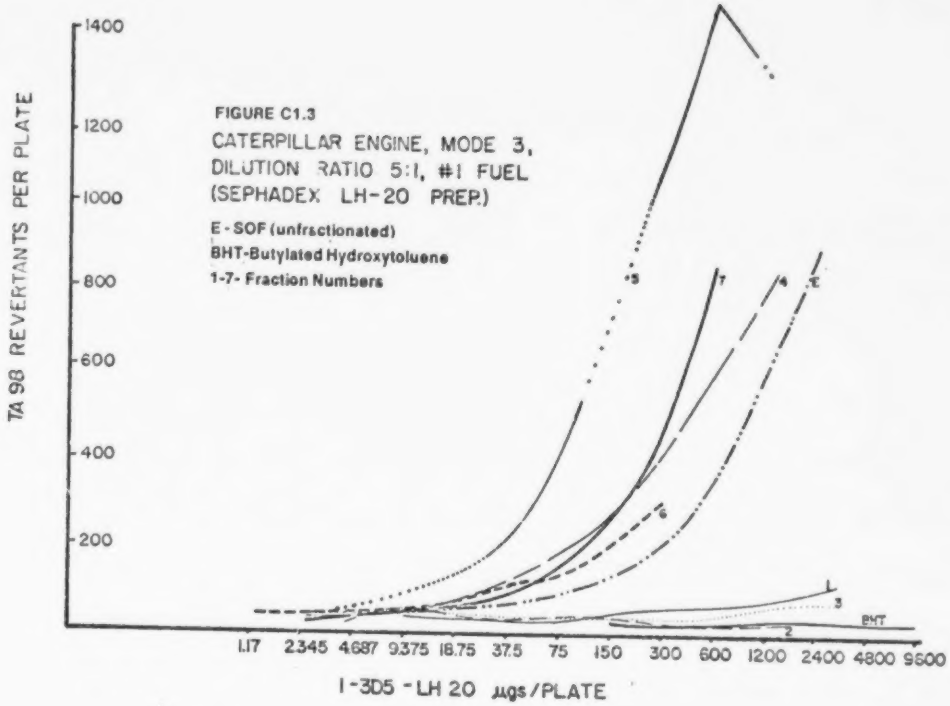

FIGURE C1.3

CATERPILLAR ENGINE, MODE 3,
DILUTION RATIO 5:1, #1 FUEL
(SEPHADEX LH-20 PREP.)

E - SOF (unfractionated)
BHT-Butylated Hydroxytoluene
1-7- Fraction Numbers

FIGURE C1.4

SUBFRACTIONATION OF SAMPLE 1-3D5
FRACTION 5
VYDAC 501TP10
CYANOPROPYL POLAR BONDED PHASE
10mm I.D. HPLC COLUMN
6mg SAMPLE INJECTED
HEXANE - ISOPROPANOL GRADIENT
ATTENUATION 256
UV DETECTION, 350nm

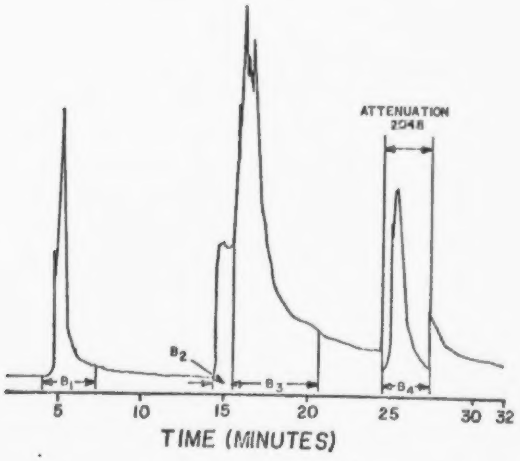

Table C1.4 SEPHADEX LH-20 GEL CHROMATOGRAPHY RESULTS

PERCENTAGES OF TOTAL SAMPLES

AVERAGE SAMPLE SIZE 195 MG FOR TRIALS 1-3;

420 MG FOR TRIALS 4 and 5

FRACTION	1-3D5-1	-2	-3	-4	-5	$\bar{X}$	$\pm\sigma$
1	4.9	5.2	4.4	6.3	4.7	5.1	0.7
2	57.1	52.7	61.9	54.2	64.0	58.0	4.3
3	25.1	16.1	20.5	25.0	18.4	20.7	3.1
4	3.7	4.1	2.7	3.1	2.3	3.2	0.6
5	2.9	3.3	2.5	2.8	3.2	3.9	0.3
6	6.1(a)	3.4	4.0	3.7	3.1	3.6(b)	0.3(b)
7		0.8	3.0	0.8	1.2	1.4(b)	0.9(b)
PERCENT RECOVERY	99.5	84.5	97.8	93.3	97.3	94.5	5.4

(a) FRACTIONS 6 & 7 WERE COMBINED IN RUN #1.

(b) FOUR DETERMINATIONS

Subfractionation of the most active LH-20 separated fraction (A5) from this SOF was accomplished using a Vydac cyanopropyl polar bonded phase semi-preparative HPLC column (10 mm I.D.). Figure C1.4 shows the resultant chromatogram. Capillary gas chromatography of subfractions B1 and B2 of this fraction is shown in Figures C1.5 and C1.6. These fractions were subjected to GC/MS analysis using the Hewlett-Packard 5985 GC/MS - data system; subfraction A5-B1 was also analyzed using the Kratos MS-50 GC/MS at the Midwest Center for Mass Spectrometry in Lincoln, Nebraska. Due largely to high background levels, no identifications of compounds in these subfractions could be made.

FIGURE C1.5

SAMPLE 1-3D5

FRACTION A5-B1

SE-54, 30 METER
FUSED SILICA CAPILLARY COLUMN

SPLITLESS INJECTION IN TOLUENE

ATTENUATION 8 (AFTER 6 MINUTES)

120°C ISOTHERMAL, 5 MINUTES

3°/MINUTE TO 280°; 10 MINUTE HOLD

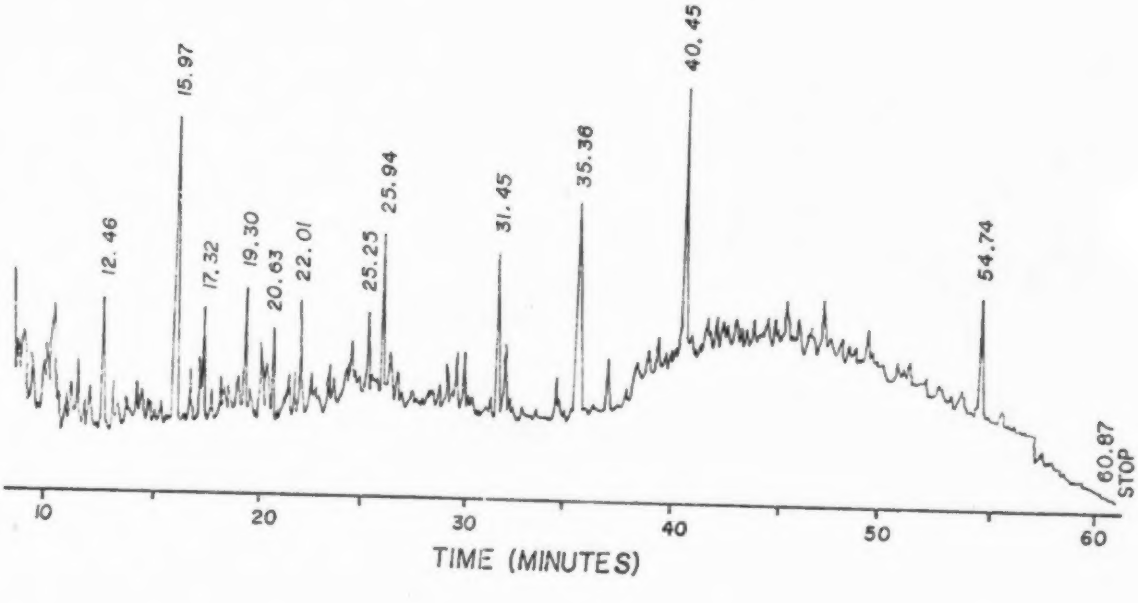

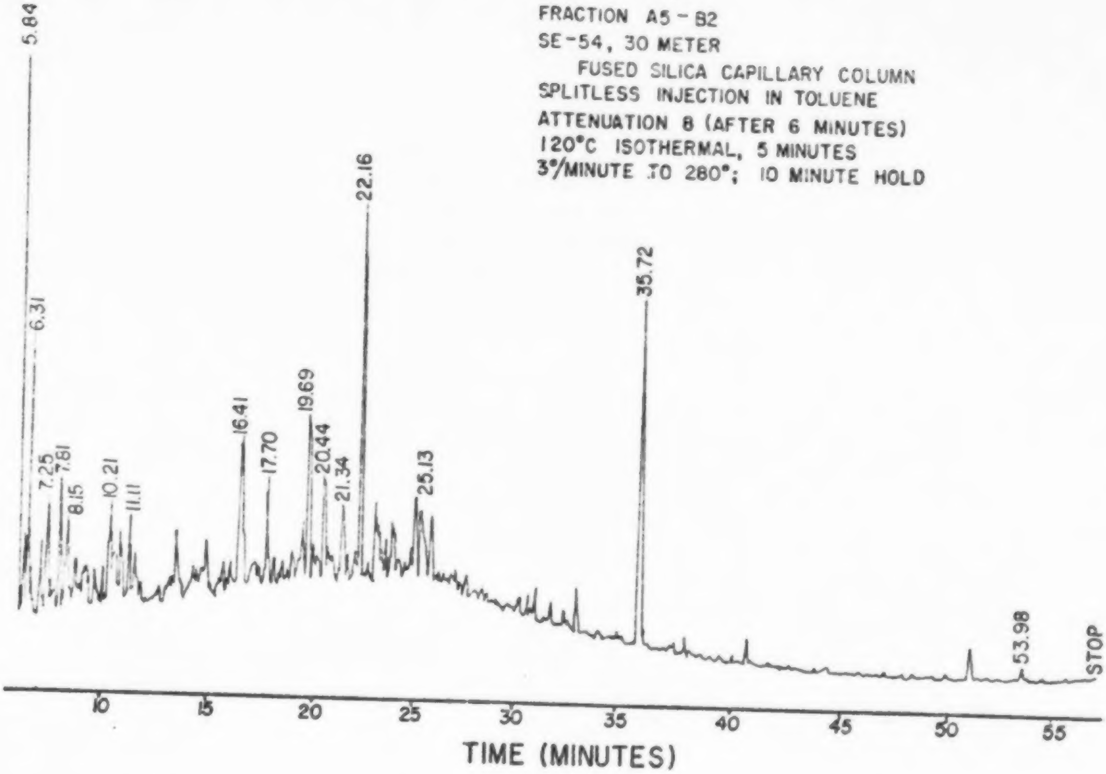

FIGURE C1.6
SAMPLE I-305
FRACTION A5 - B2
SE-54, 30 METER
FUSED SILICA CAPILLARY COLUMN
SPLITLESS INJECTION IN TOLUENE
ATTENUATION 8 (AFTER 6 MINUTES)
120°C ISOTHERMAL, 5 MINUTES
3°/MINUTE TO 280°; 10 MINUTE HOLD

Sulfate Analysis By Ion Chromatography Versus the Barium Chloranilate Method

Table C1.5 shows comparative values for four pairs of filters collected for sulfate analysis by the EPA barium chloranilate method, as well as by ion chromatography using a Dionex Model 10 Ion Chromatograph. Each pair of filters was run for identical length of time in parallel sampling probes and collected similar amounts of particulate and SOF from the Caterpillar 3208 engine with close-coupled port catalysts installed. Although the reproducibility of each method is good, it appears from these data that the barium chloranilate method gives a consistently higher sulfate value than ion chromatography. To investigate the possibility that extraction efficiency for isopropanol-water 60:40 (used in the barium chloranilate method) is higher than that of deionized water (used in ion chromatography), a series of samples were extracted using both deionized water and IPA: H_2O, 60:40, to

Table C1.5 Comparison of the Barium Chloranilate Colorimetric Method with the Dionex Ion Chromatographic Method for Sulfate Analysis

(n = 4 determinations per filter)

Ion Chromatography				Barium Chloranilate			
Sample	mg $SO_4^=$	mg TPM	%$SO_4^=$	Sample	mg $SO_4^=$	mg TPM	%$SO_4^=$
4-P-3	5.12±0.±09 %C_v = 2.1	7.61	67.3	4-P-4	6.28±0.084 1.3%	8.84	71.1
4-P-5	5.38±0.157 2.9%	7.27	74.0	4-P-6	6.42±0.23 3.5%	8.46	75.9
4-P-7	12.14±0.209 1.7%	16.92	71.8	4-P-8	14.60±0.73 5.0%	17.37	84.0
4-P-11	12.00±0.136 1.5%	17.95	66.8	4-P-12	14.08±0.54 3.8%	18.67	75.4

analyze by ion chromatography. Table C1.6 shows that filters extracted with IPA: H_2O, 60:40 are not extracted more efficiently than those extracted with deionized water.

Table C1.6: Effect of Solvent on Sulfate Ion Analysis Using Dionex Model 10 Ion Chromatograph. Caterpillar 3208, Close-Coupled Port Catalyst, EPA Mode 4

Sample	Solvent	mg TPM	mg $SO_4^=$	%$SO_4^=$
20	IPA: H_2O	6.24	4.05	65.0
22	IPA: H_2O	6.13	3.62	59.0
15	D.I. H_2O	8.75	6.16	70.4
14	D.I. H_2O	12.70	8.74	68.8

Extraction volume as a possible factor in extraction efficiency was investigated for the barium chloranilate method, with results shown in Table C1.7. Smaller volumes than the 25 ml normally employed do not show consistent effects on the percentage sulfate removable from filters. Likewise, reducing the particulate loading demonstrates no consistent solvent effect except perhaps the greater efficiency of the larger extraction volume (Table C1.8).

Recoveries of sulfate solution added to aliquots of various filter extracts are shown in Table C1.9. Recoveries ranged from 92.9 to 105.9%. Similarly, recoveries for sulfate added as extract to filters whose original sulfate loading was calculated from most similarly-loaded, non-spiked filters varied between 97.0 and 102.1 percent (Table C1.10), well within the statistical variability of the method.

Table C1.7: Effect of Solvent Volume on Percentage Sulfate Measured using the Barium Chloranilate Method. Caterpillar 3208, Close-Coupled Port Catalysts, EPA Mode 4

Sample	Solvent	mg TPM	mg $SO_4^=$	%$SO_4^=$
21	IPA: H_2O, 10 ml	3.192	2.43	76.1
24	IPA: H_2O, 10 ml	6.204	3.69	59.5
13	IPA: H_2O, 25 ml	8.89	5.88	66.2
17	IPA: H_2O, 25 ml	8.43	5.84	69.3

Table C1.8: Effects of Solvent Volume and Composition on Percentage Sulfate Measured with Light Particulate Loadings, Caterpiller 3208, Close-Coupled Port Catalyst, EPA Mode 4

		Barium Chloranilate		
Sample	Solvent	mg TPM	mg $SO_4^=$	%$SO_4^=$
32	IPA: H_2O 10 ml	0.309	0.198	63.9
30	IPA: H_2O 25 ml	0.312	0.250	80.2
		Ion Chromatography		
27	IPA: H_2O 10 ml	0.328	0.203	61.9
29	D.I. H_2O 25 ml	0.401	0.306	76.2

The precision and true chromatographic nature of ion chromatography, as well as its simplicity of execution relative to the barium chloranilate method convinced us to adopt the method in March, 1981.

Table C1.9: Recoveries of Sulfate Added to Aliquots of Filter Extract Using Both Sulfate Analysis Methods. Caterpillar 3208, Close-Coupled Port Catalysts, EPA Mode 4

Sample	Method	PPM $SO_4^=$ in Extract	PPM $SO_4^=$ Added	% Recovery
17	BCA	233.4	250	92.9
21	BCA	97.2	125	98.4
20	IC	162.0	250	105.9
14	IC	349.6	250	104.0

Table C1.10: Recoveries of Sulfate Added to Filters Whose Sulfate Levels Were Estimated from the Loading of Other, Similarly Loaded, Filters: Extracted With Standard Sulfate Before Analysis, Caterpillar 3208, Close-Coupled Port Catalysts, EPA Mode 4.

Sample	Method	PPM $SO_4^=$ on filter	mg $SO_4^=$ Added	% Recovery
23	BCA	3.13	2.50	98.8
16	BCA	8.15	6.25	102.1
19	IC	3.11	2.50	97.0
18	IC	7.90	6.25	99.6

TABLE C-2

MACK ENDT-676 SOF CHEMICAL FRACTIONATION DATA

TEST[a]	3B	G-19-3	G-12-3	G-17-3	G-22-3	G-19-9	G-12-9
ACD (% of SOF)	5.7	7.5	14.4	9.5	3.5	8.6	8.3
BSACD (mg/kw-hr)	10.3	3.76	4.26	5.66	4.39	5.19	3.06
ARM (% of SOF)	3.5	4.0	3.8	2.9	2.8	4.5	3.6
BSARM (mg/kw-hr)	6.35	2.03	1.13	1.73	3.52	2.71	1.33
BAS (% of SOF)	2.7	2.1	2.4	4.3	0.7	2.1	1.7
BSBAS (mg/kw-hr)	4.90	1.07	0.71	2.56	0.88	1.27	0.62
EIN (% of SOF)	13.3	5.9	6.1	7.0	8.0	15.5	6.3
BSEIN (mg/kw-hr)	2.41	3.0	1.81	4.17	10.05	9.35	2.32
HIN (% of SOF)	4.2	2.4	3.2	3.7	1.7	3.3	3.2
BSHIN (mg/kw-hr)	7.62	1.22	0.95	2.21	2.13	1.99	1.18
OXY (% of SOF)	13.6	19.4	13.4	13.9	12.3	26.1	27.9
BSOXY (mg/kw-hr)	24.7	9.86	3.97	8.29	15.4	15.7	10.3
PRF (% of SOF)	49.2	55.1	52.3	52.7	65.9	36.0	43.3
BSPRF (mg/kw-hr)	89.3	28.0	15.5	31.4	82.7	21.7	16.0
TRN (% of SOF)	7.8	3.8	4.5	6.1	5.2	3.3	5.7
BSTRN (mg/kw-hr)	14.2	1.93	1.33	3.64	6.53	1.99	2.10

[a] A complete description of engine and fuel injection components corresponding to the test numbers is given in Tables 3.1.2 and 3.1.3

TABLE C-2 (cont'd)

MACK ENDT-676 CHEMICAL FRACTIONATION DATA

TEST[(a)]	G-17-9	G-22-9	G2-12-5	G2-17-5	G2-22-5	G2-12-11	G2-17-11
ACD (% of SOF)	3.9	4.3	10.6	12.0	23.9	19.7	17.2
BSACD (mg/kw-hr)	2.91	4.66	1.38	2.04	3.56	27.0	33.5
ARM (% of SOF)	2.2	10.6(b)	6.2	7.5	10.1	4.1	4.8
BSARM (mg/kw-hr)	1.64	11.56(b)	0.81	1.28	1.51	5.6	9.3
BAS (% of SOF)	6.8	1.3	0.95	0.87	2.17	2.32	1.53
BSBAS (mg/kw-hr)	5.07	1.41	0.12	0.15	0.32	3.20	3.00
EIN (% of SOF)	5.8	7.6	4.5	7.7	8.9	9.3	7.0
BSEIN (mg/kw-hr)	4.32	8.24	0.58	1.31	1.32	12.7	13.7
HIN (% of SOF)	3.2	4.5	4.4	8.3	7.6	4.2	11.9
BSHIN (mg/kw-hr)	3.35	4.79	1.07	1.30	0.62	16.3	11.5
OXY (%of SOF)	27.5	18.4	5.0	6.1	7.1	16.8	16.4
BSOXY (mg/kw-hr)	20.49	19.91	0.65	1.04	1.06	23.1	31.9
PRF (% of SOF)	46.1	53.5	64.0	62.8	49.4	34.1	46.0
BSPRF (mg/kw-hr)	34.4	58.0	8.32	10.7	7.35	46.8	89.7
TRN (% of SOF)	3.2	(b)	0.41	1.59	0.28	3.77	2.41
BSTRN (mg/kw-hr)	2.38	(b)	0.05	0.27	0.04	5.20	4.70

(a) A complete description of engine and fuel injection components corresponding to the test numbers is given in Tables 3.1.2 and 3.1.3

(b) ARM and TRN combined due to lack of distinct ARM band

TABLE C-2 (cont'd)

MACK ENDT-676 CHEMICAL FRACTIONATION DATA

TEST[a]	G2-22-11	G3-22-11	S-8-3	S-12-3	S-14-3	S-17-3
ACD (% of SOF)	14.7	17.3	16.9	4.8	5.1	6.2
BSACD (mg/kw-hr)	26.1	33.8	21.9	4.8	5.1	7.4
ARM (% of SOF)	4.0	4.9	4.7	27.7	14.1	5.7
BSARM (mg/kw-hr)	7.0	9.6	6.1	27.3	14.1	6.8
BAS (% of SOF)	1.6	1.6	1.9	2.5	1.6	2.8
BSBAS (mg/kw-hr)	2.9	3.1	2.5	2.5	1.6	3.4
EIN (% of SOF)	7.5	6.6	46.6	16.6	4.5	11.6
BSEIN (mg/kw-hr)	13.3	12.9	60.6	16.6	4.5	13.9
HIN (% of SOF)	5.0	5.9	4.5	3.0	1.7	1.2
BSHIN (mg/kw-hr)	8.9	11.5	5.9	3.0	1.7	1.4
OXY (% of SOF)	12.4	16.3	11.1	16.5	18.1	16.9
BSOXY (mg/kw-hr)	21.9	31.7	14.4	16.5	18.1	20.3
PRF (% of SOF)	53.8	44.5	11.5	25.1	52.4	46.3
BSPRF (mg/kw-hr)	95.2	86.8	15.0	25.1	52.4	55.6
TRN (% of SOF)	1.19	2.87	2.80	4.30	3.00	9.40
BSTRN (mg/kw-hr)	2.1	5.6	3.6	4.3	3.0	11.3

[a] A complete description of engine and fuel injection components corresponding to the test numbers is given in Tables 3.1.2 and 3.1.3

TABLE C-3

CATERPILLAR 3208 SOF CHEMICAL FRACTIONATION

DATA: ENGLEHARD PTX CATALYST EVALUATION

MODE	EPA MODE 3				EPA MODE 4					
FUEL	NO.2		NO.1		NO.2		NO.1		SHALE	
PTX CATALYST	W/O	W	W/O	W	W/O	W	W/O	W	W/O	W
ACD (% of SOF)	10.5	3.9	11.0	11.5	4.5	7.1	8.5	13.4	18.8	7.4
BSACD (mg/kw-hr)	79.8	11.7	82.9	34.2	9.5	3.6	18.2	7.5	76.3	4.5
ARM (% of SOF)	3.7	6.3	3.1	3.5	4.2	1.2	5.5	2.9	8.9	18.9
BSARM (mg/kw-hr)	28.1	18.9	23.4	10.4	8.8	0.6	11.8	1.6	36.1	11.5
BAS (% of SOF)	3.3	2.1	1.9	2.4	1.0	1.7	1.9	2.9	2.9	2.8
BSBAS (mg/kw-hr)	25.1	6.3	14.3	7.1	2.1	0.9	4.1	1.6	11.8	1.7
EIN (% of SOF)	7.5	9.0	3.1	4.6	9.4	14.2	3.1	7.9	12.7	6.1
BSEIN(mg/kw-hr)	57.0	27.0	23.4	13.7	10.7	7.1	6.6	4.4	51.6	3.7
HIN (% of SOF)	2.3	1.8	3.7	0	0.6	1.4	0	6.7	1.8	3.3
BSHIN(mg/kw-hr)	17.5	5.4	27.9	0	1.3	0.7	0	3.8	7.3	2.0
OXY (% of SOF)	11.8	13.0	13.1	15.9	12.2	24.8	13.0	13.0	17.0	12.4
BSOXY(mg/kw-hr)	89.7	39.0	98.8	47.2	25.6	12.4	27.8	7.3	69.0	7.6
PRF(% of SOF)	55.3	60.0	61.6	59.2	63.3	45.2	60.8	46.7	33.2	45.7
BSPRF(mg/kw-hr)	420.3	180.0	464.4	175.8	132.9	22.6	130.1	26.2	134.8	27.9
TRN(% of SOF)	5.6	4.0	2.4	2.9	4.9	4.4	5.8	6.6	4.6	3.3
BSTRN(mg/kw-hr)	42.6	1.2	18.1	8.6	10.3	2.2	12.6	3.7	18.7	2.0

TABLE C-3(continued)

CATERPILLAR 3208 SOF CHEMICAL FRACTIONATION DATA

ENGLEHARD PTX CATALYST EVALUATION

MODE	EPA MODE 5				EPA MODE 9		EPA MODE 10		EPA MODE 11	
FUEL	NO.2		NO.1		NO.2		NO.2		NO.2	
PTX CATALYST	W/O	W	W/O	W	W/O	W	W/O	W	W/O	W
ACD (% of SOF)	12.6	28.5	10.4	12.5	21.1	24.2	9.6	26.9	15.5	8.9
BSACD (mg/kw-hr)	3.8	2.9	2.7	1.1	8.4	2.4	23.0	8.1	152.0	14.2
ARM (% of SOF)	0.6	2.4	2.1	8.4	1.6	3.6	3.6	3.2	3.3	4.2
BSARM (mg/kw-hr)	0.2	0.2	0.5	0.8	0.6	0.4	8.6	1.0	32.3	6.7
BAS (% of SOF)	1.5	4.5	2.3	1.3	1.8	1.7	2.6	4.6	2.7	1.7
BSBAS (mg/kw-hr)	0.5	0.5	0.6	0.1	0.7	0.2	6.2	1.4	26.5	2.7
EIN (% of SOF)	14.7	13.3	4.9	25.2	3.0	29.7	17.8	2.3	6.6	11.8
BSEIN(mg/kw-hr)	4.4	1.3	1.3	2.3	1.2	3.0	42.7	0.7	64.7	18.9
HIN (% of SOF)	1.7	1.8	1.3	1.2	5.4	0.9	3.7	4.8	1.7	4.6
BSHIN(mg/kw-hr)	0.5	0.1	0.3	0.1	2.2	0.1	8.9	1.4	16.7	7.4
OXY (% of SOF)	14.4	28.7	14.1	23.8	53.5	17.9	20.1	23.8	19.2	24.1
BSOXY(mg/kw-hr)	4.3	2.9	3.7	2.1	21.4	1.8	48.2	7.1	188.2	38.6
PRF(% of SOF)	49.7	14.5	55.3	22.8	10.6	17.6	34.6	29.7	44.6	39.6
BSPRF(mg/kw-hr)	14.9	1.5	14.4	2.1	4.2	1.8	83.0	8.9	437.1	63.4
TRN(% of SOF)	4.7	6.3	9.6	6.1	3.1	17.9	8.0	3.2	6.4	5.3
BTRN(mg/kw-hr)	1.4	0.6	2.5	0.5	1.2	1.8	19.2	1.0	62.7	8.5

Table C-4 CATERPILLAR 3208 SOF CHEMICAL FRACTIONATION DATA: JOHNSON-MATTHEY CLOSE-COUPLED PORT CATALYST AND CORNING TRAP EVALUATION, NO.2 FUEL

EPA MODE	3			4			5		
AFTERTREATMENT	NONE	PORT CATALYST	TRAP	NONE	PORT CATALYST	TRAP	NONE	PORT CATALYST	TRAP[(a)]
ACD (% of SOF)	5.0	6.1	6.3	4.2	6.5	9.4	9.4	20.4	-
BSACD (mg/kw-hr)	46.	37.	62.	16.	7.	13.	4.	5.	-
ARM (% of SOF)	5.5	4.9	3.6	2.4	8.7	2.8	3.4	10.5	-
BSARM (mg/kw-hr)	51.	30.	35.	9.	10.	4.	1.	3.	-
BAS (% of SOF)	0.8	1.3	0.9	2.7	0.7	0.5	2.4	0.6	-
BSBAS (mg/kw-hr)	7.	8.	9.	10.	1.	1.	1.	0	-
EIN (% of SOF)	5.1	12.2	7.7	8.6	15.1	3.2	6.9	8.2	-
BSEIN(mg/kw-hr)	48.	74.	77.	32.	17.	4.	3.	2.	-
HIN (% of SOF)	3.1	5.2	5.5	1.4	3.4	1.0	5.6	1.3	-
BSHIN(mg/kw-hr)	28.	32.	53.	5.	4.	1.	2.	0.	-
OXY (% of SOF)	10.8	12.9	7.5	16.7	13.1	6.5	16.4	11.6	-
BSOXY(mg/kw-hr)	100.	78.	73.	63.	15.	9.	6.	3.	-
PRF(% of SOF)	66.7	54.1	66.2	58.5	48.5	73.0	50.0	44.3	-
PRF(mg/kw-hr)	622.	330.	643.	220.	56.	100.	19.	11.	-
TRN(% of SOF)	3.1	3.2	2.0	5.7	4.0	3.5	5.9	3.2	-
BSTRN(mg/kw-hr)	29.	20.	20.	21.	5.	5.	2.	1.	-

(a) No SOF samples obtained due to extremely low levels.

Table C-4 CATERPILLAR 3208 SOF CHEMICAL FRACTIONATION DATA: JOHNSON-MATTHEY CLOSE-COUPLED PORT CATALYST AND CORNING TRAP EVALUATION, NO.2 FUEL

EPA MODE	9			10			11		
AFTERTREATMENT	NONE	PORT CATALYST	TRAP	NONE	PORT CATALYST	TRAP	NONE	PORT CATALYST	TRAP
ACD (% of SOF)	18.0	7.7	-(a)	8.6	14.3	-(a)	7.0	6.4	33.6
BSACD (mg/kw-hr)	5.	1.	-	11.	17	-	67.	18.	22.
ARM (% of SOF)	7.9	8.1	-	0.5	3.4	-	3.0	5.8	1.0
BSARM (mg/kw-hr)	2.	1.	-	1.	4.	-	29.	16.	1.
BAS (% of SOF)	1.7	5.1	-	3.7	1.2	-	1.1	0.4	1.3
BSBAS (mg/kw-hr)	0.	1.	-	5.	1.	-	10.	1.	1.
EIN (% of SOF)	10.7	37.7	-	11.6	18.4	-	5.2	20.9	10.0
BSEIN(mg/kw-hr)	3.	4.	-	15.	22.	-	50.	59.	7.
HIN (% of SOF)	3.9	1.1	-	7.6	4.8	-	2.4	5.0	1.7
BSHIN(mg/kw-hr)	1.	0.	-	10.	6.	-	23.	14.	1.
OXY (% of SOF)	12.3	14.3	-	19.9	24.0	-	23.0	17.2	7.6
BSOXY(mg/kw-hr)	3.	2.	-	27.	9.	-	223.	48.	5.
PRF(% of SOF)	41.6	21.3	-	41.8	30.7	-	51.7	39.2	43.3
PRF(mg/kw-hr)	11.	2.	-	56.	37.	-	500.	110.	29.
TRN(% of SOF)	3.9	5.3	-	6.4	3.3	-	6.9	5.1	1.4
BSTRN(mg/kw-hr)	1.	1.	-	9.	4.	-	67.	14.	1.

(a) No SOF samples obtained due to extremely low levels.

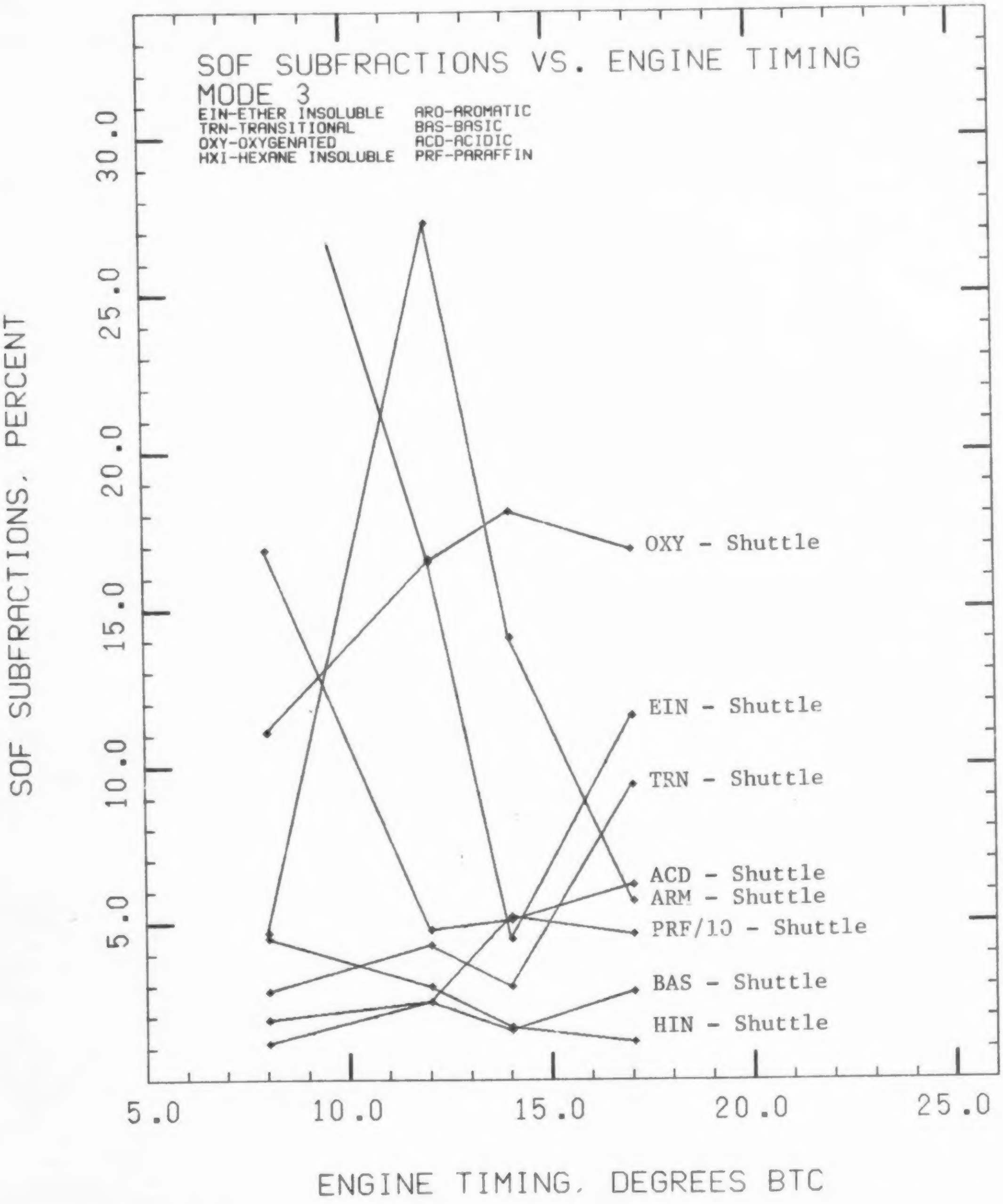

Fig. C2 - Trend in chemical subfractions as a percent of total SOF with engine timing, Mack ENDT-676 equipped with APS "ultra-high rate" shuttle pump, mode 3

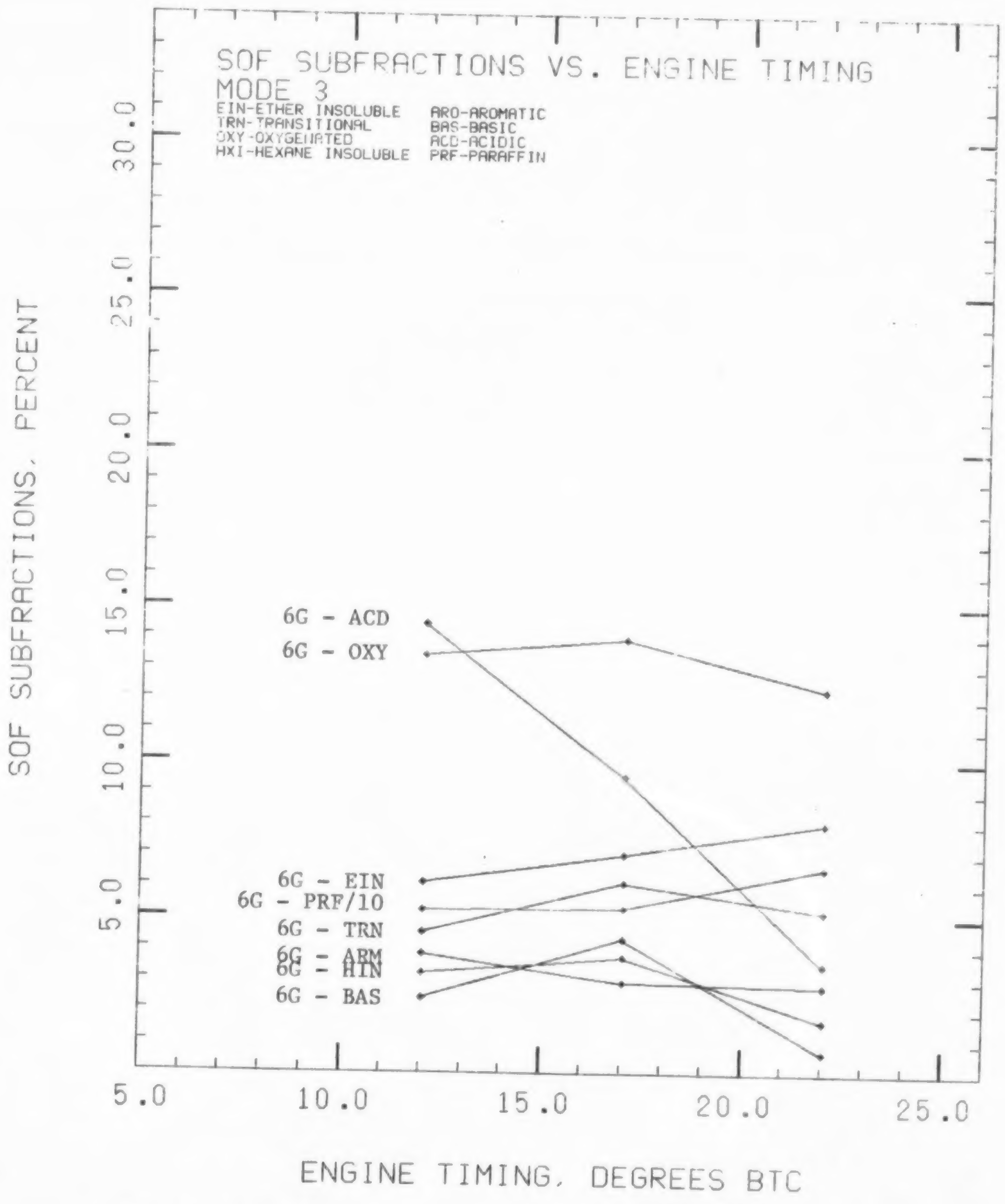

Fig. C3 - Trend in chemical subfractions as a percent of total SOF with engine timing, Mack ENDT-676 equipped with APE-6G "high rate" pump, mode 3

Reproduced from
best available copy.

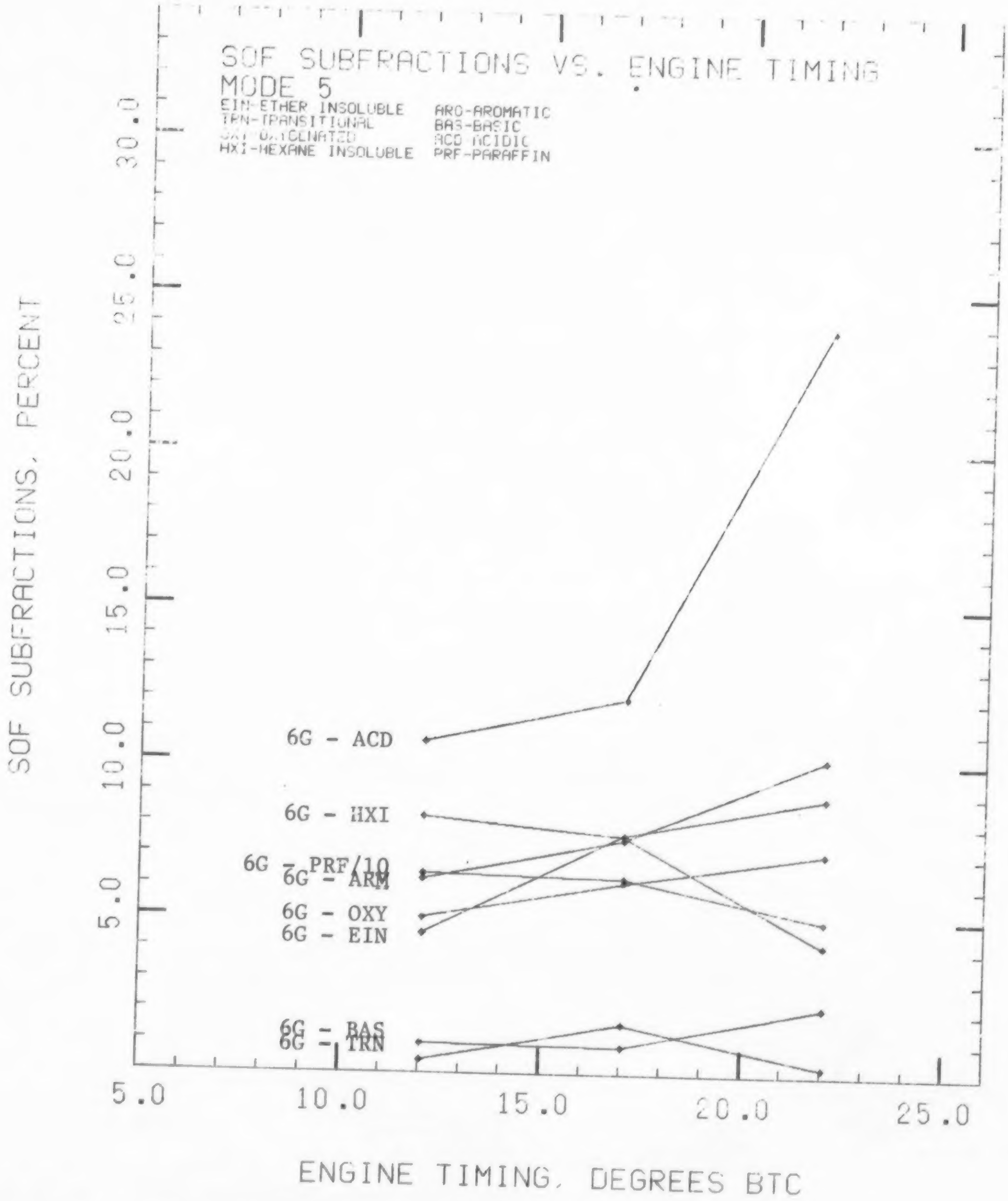

Fig. C4 - Trend in chemical subfractions as a percent of total SOF with engine timing, Mack ENDT-676 equipped with APE-6G "high rate" pump, mode 5

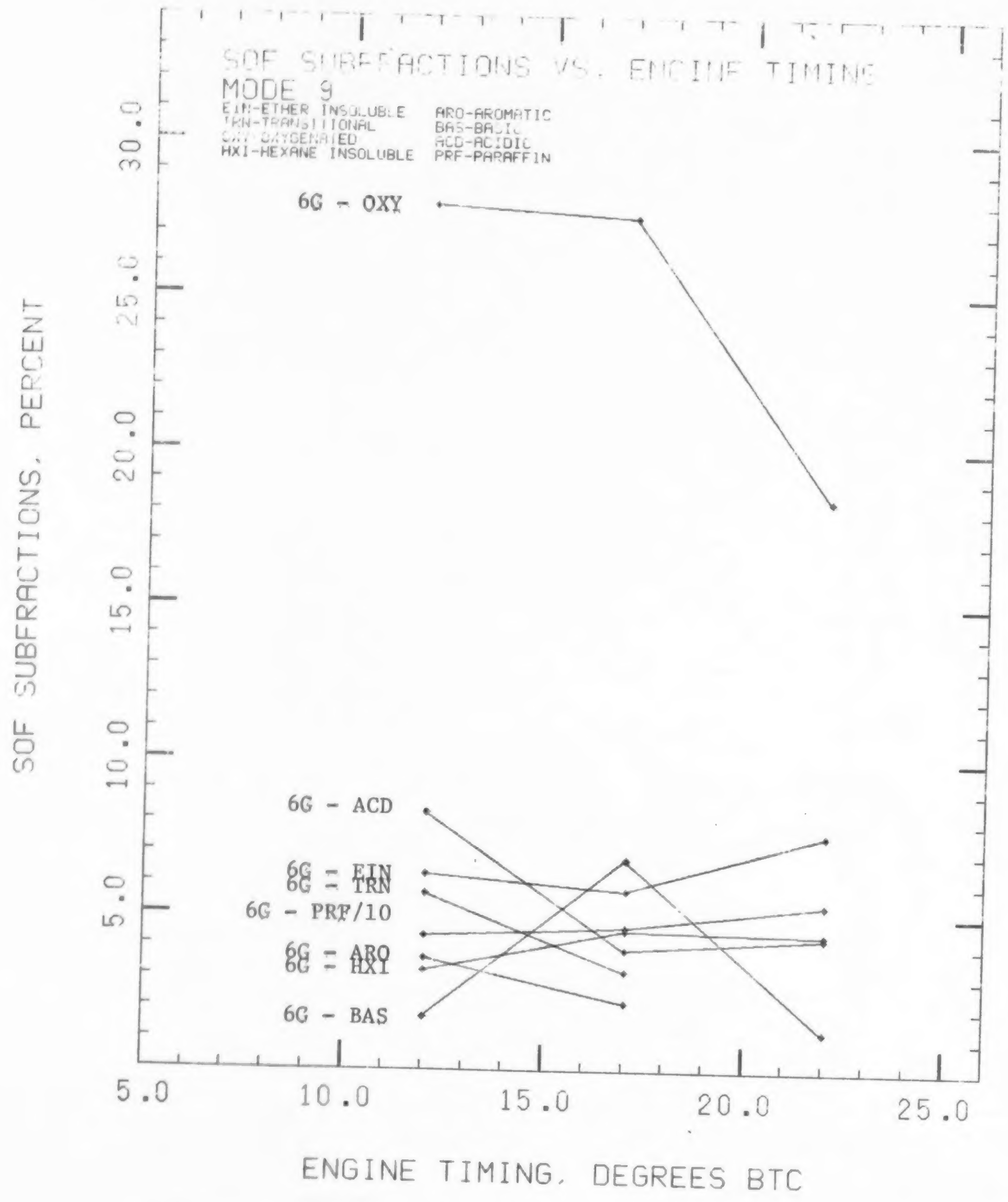

Fig. C5 - Trend in chemical subfractions as a percent of total SOF with engine timing, Mack ENDT-676 equipped with APE-6G "high rate" pump, mode 9

Reproduced from best available copy.

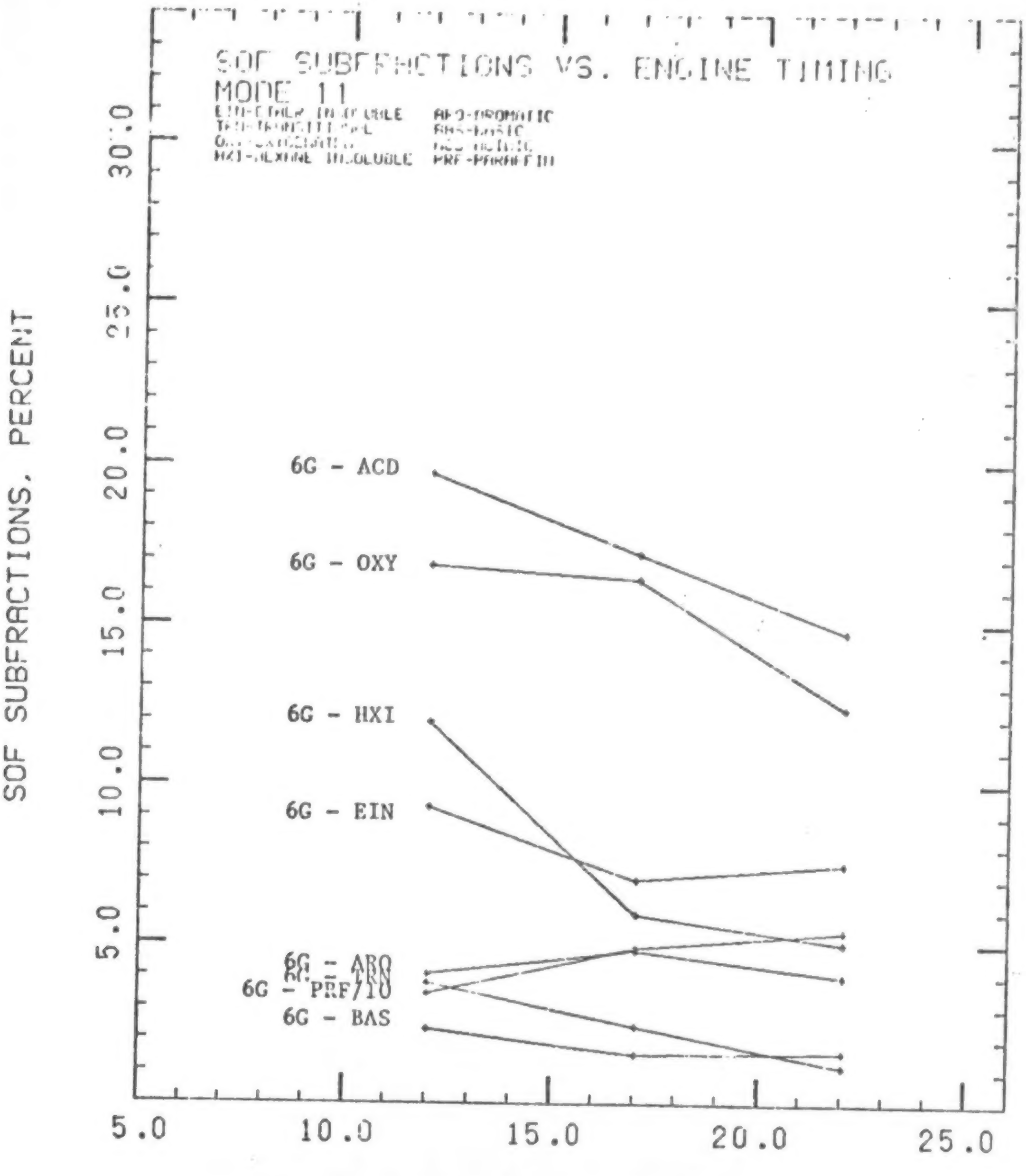

Fig. C6 - Trend in chemical subfractions as a percent of total SOF with engine timing, Mack ENDT-676 equipped with APE-6G "high rate" pump, mode 11

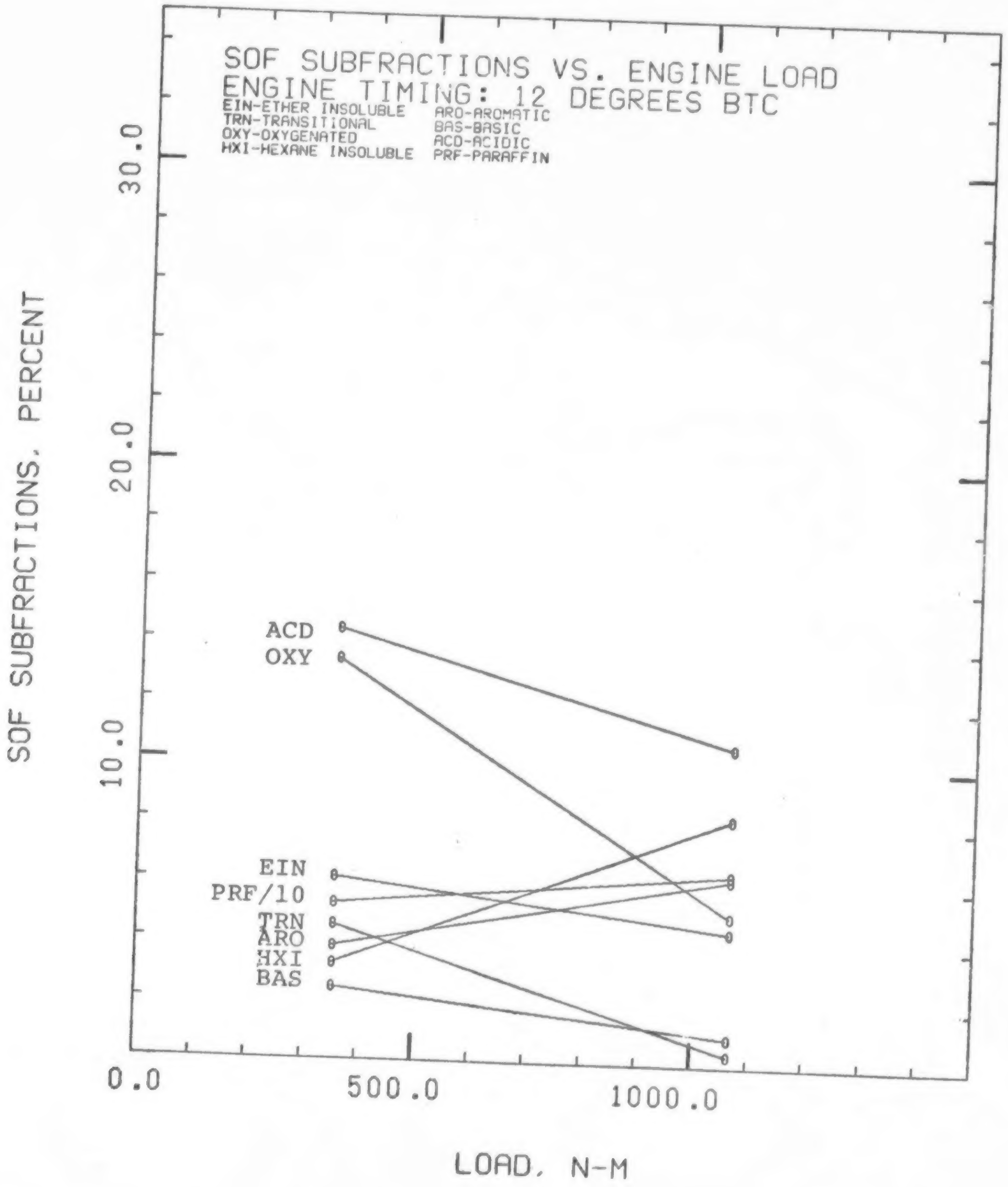

Fig. C7 - Trend in chemical subfractions as a percent of total SOF with engine load, Mack Endt-676 equipped with APE-6G "high rate" pump, modes 3 and 5, 12°BTC

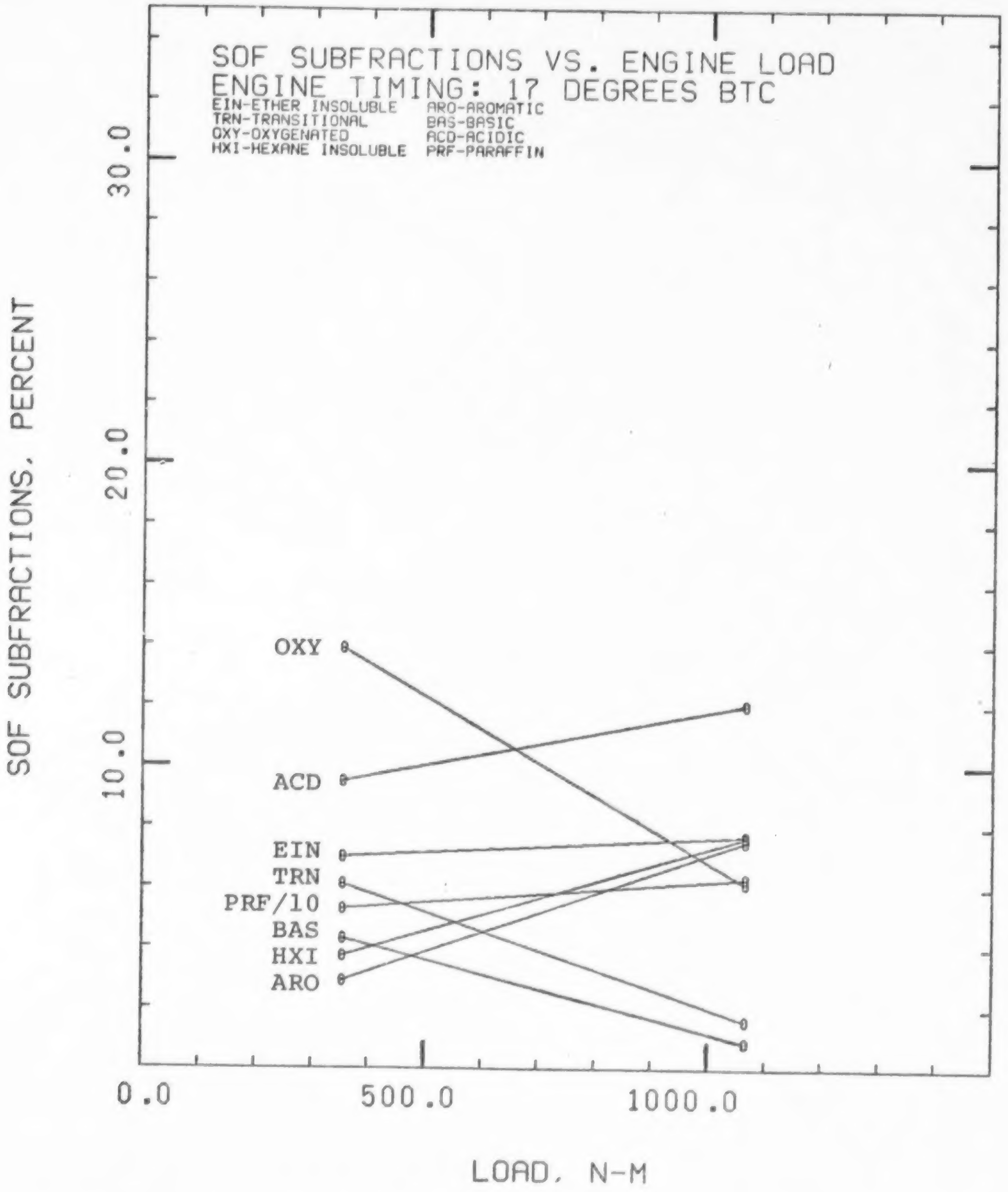

Fig. C8 - Trend in chemical subfractions as a percent of total SOF with engine load, Mack ENDT-676 equipped with APE-6G "high rate" pump, modes 3 and 5, 17°BTC

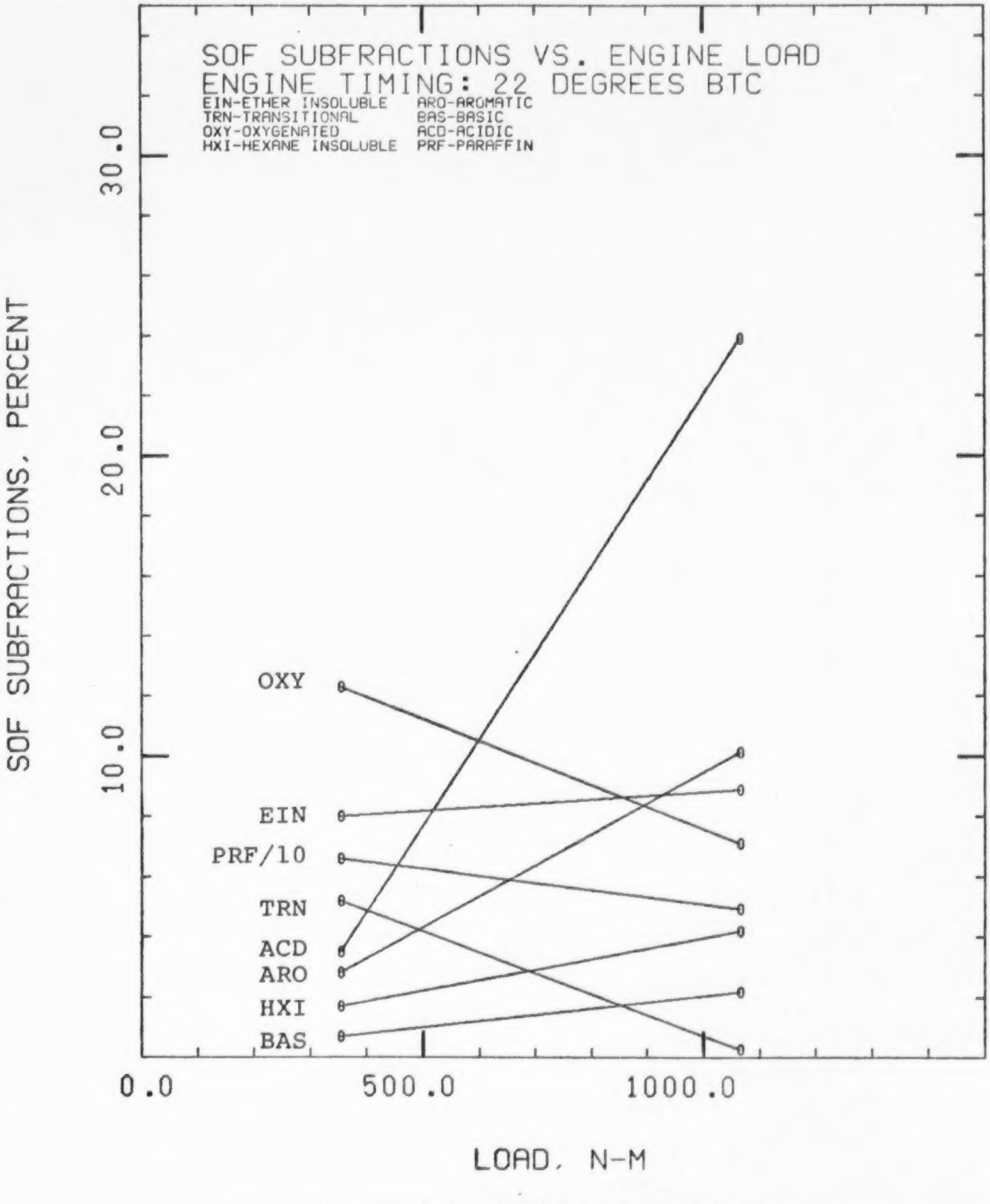

Fig. C9 - Trend in chemical subfractions as a percent of total SOF with engine load, Mack ENDT-676 equipped with APE-6G "high rate" pump, modes 3 and 5, 22°BTC

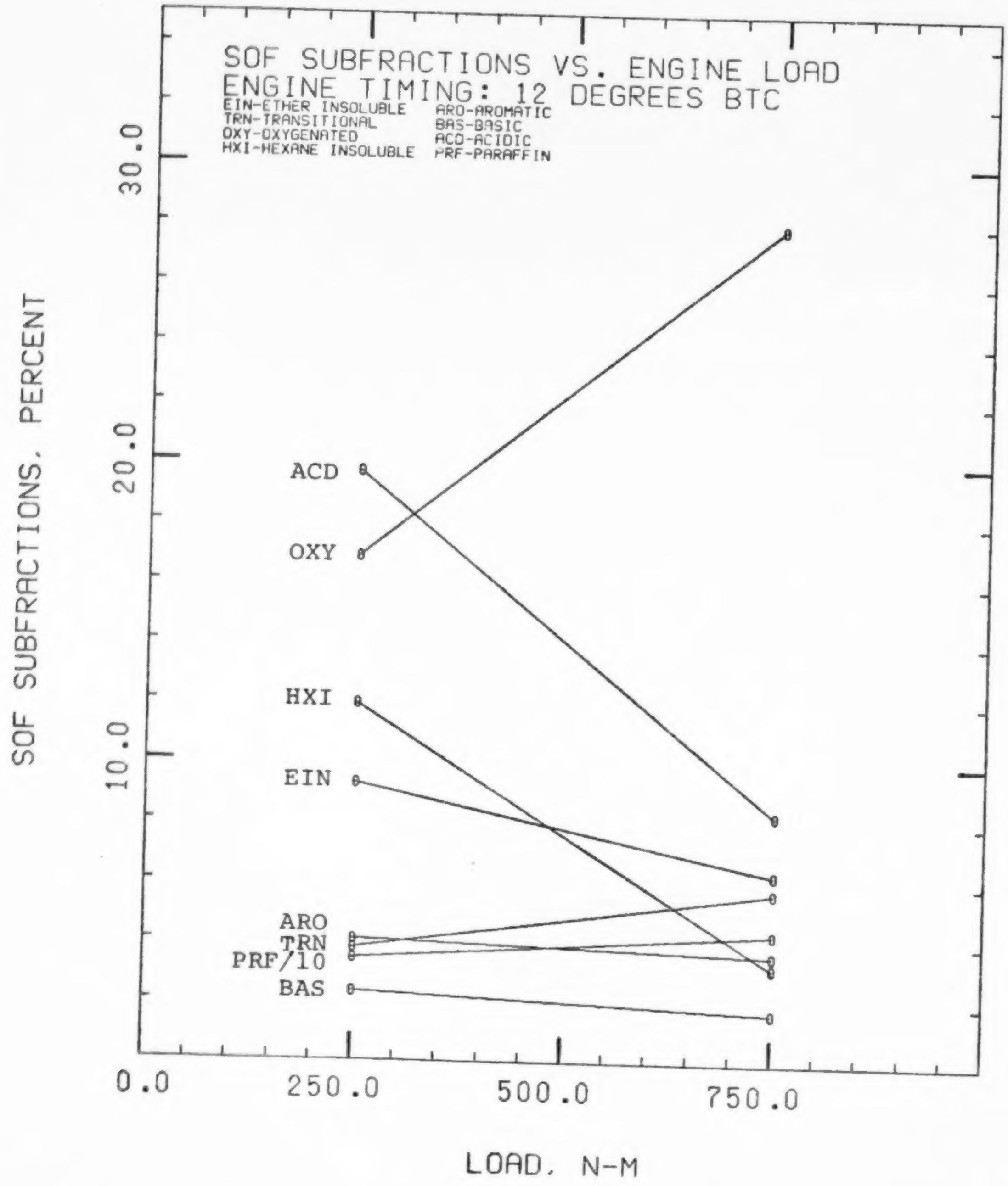

Fig. C10 - Trend in chemical subfractions as a percent of total SOF with engine load, Mack ENDT-676 equipped with APE-6G "high rate" pump, modes 11 and 9, 12°BTC

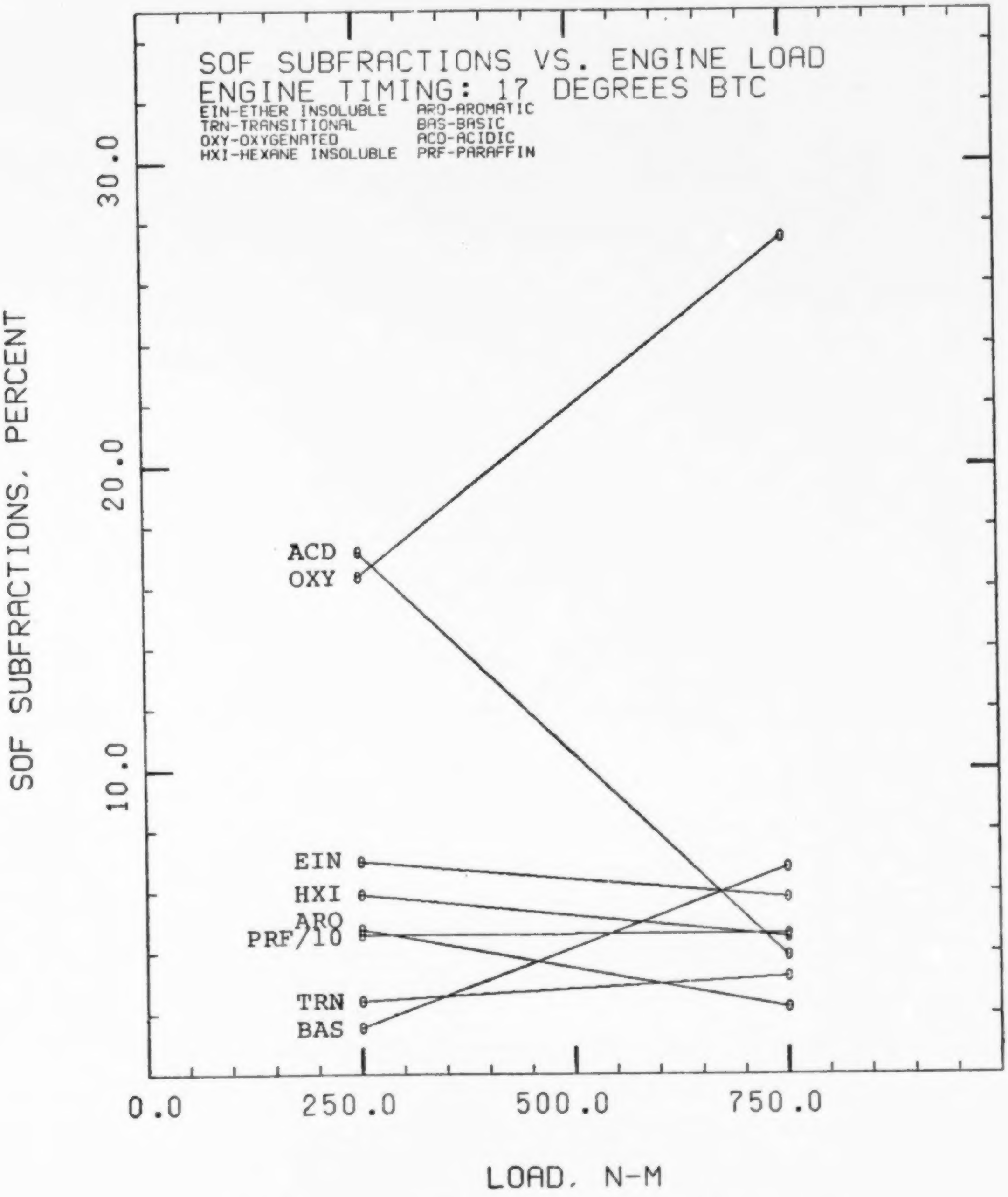

Fig. C11 - Trend in chemical subfractions as a percent of total SOF with engine load, Mack ENDT-676 equipped with APE-6G "high rate" pump, modes 11 and 9, 17°BTC

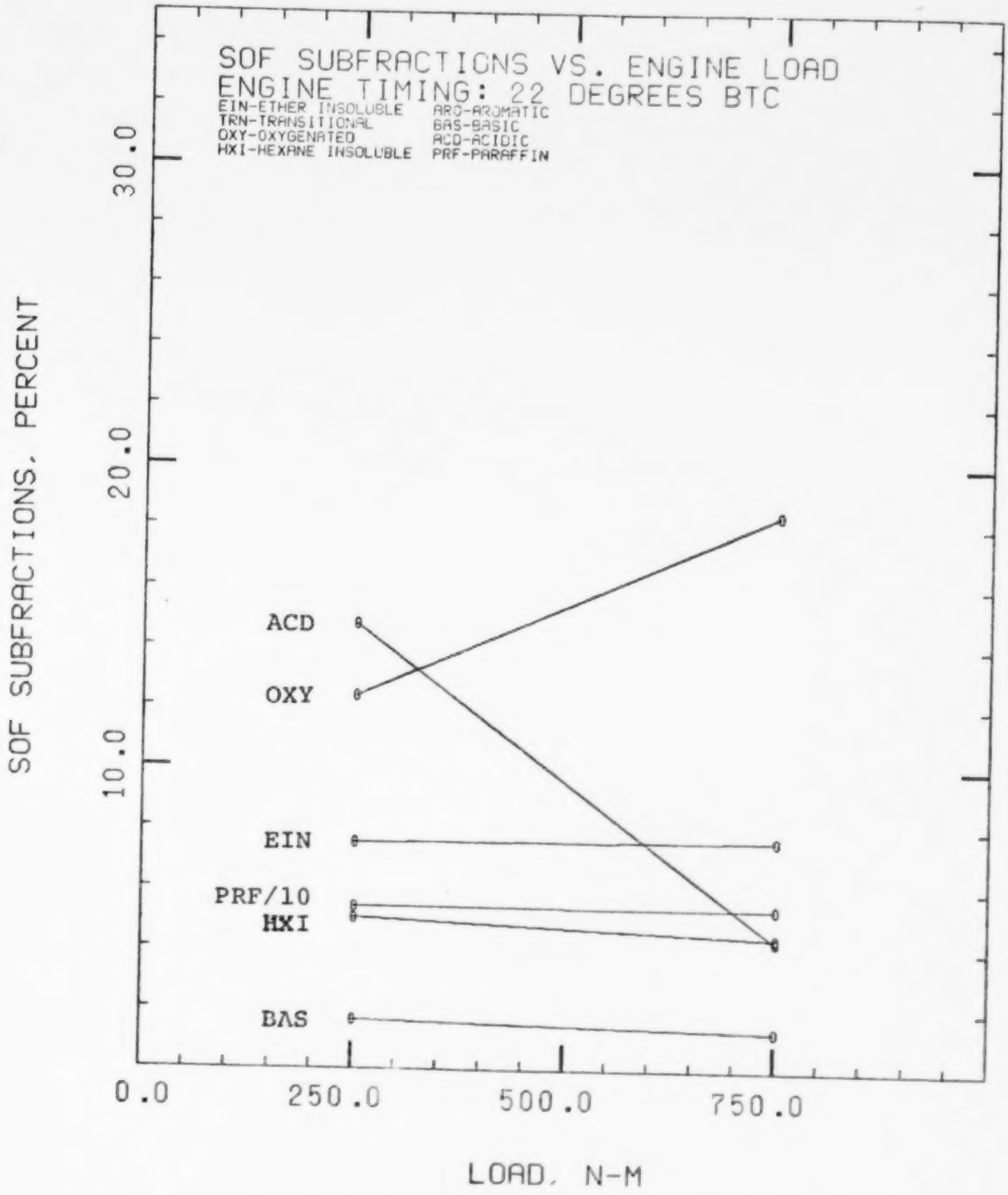

Fig. C12 - Trend in chemical subfractions as a percent of total SOF with engine load, Mack ENDT-676 equipped with APE-6G "high rate" pump, modes 11 and 9, 22°BTC